Journal of Applied Mechanics

(Formerly part of the ASME Applied Mechanics Division)

F. [illegible] 1

G. A. G. [illegible] 7

J. W. [illegible] 11

E. G. [illegible] 17

R. A. Di [illegible] 21

M. J. [illegible] 28

B. A. Boley and Ch[illegible] Chao 31

W. A. Benali and R. [illegible] 37

E. R. [illegible] 47

R. K. Kaul and [illegible] 53

R. A. [illegible] 57

W. Johnson and [illegible] Yu 64

E. [illegible] 69

[illegible] 75

W. S. Hodge, Jr., and [illegible] 79

Brahtz[illegible] 86

R. [illegible] 89

I. Nivsky and [illegible] 97

Shaloh and M. [illegible] 105

R. [illegible] 109

[illegible] 119

[illegible] 123

Leif Bergwall and J. [illegible] 125

R. [illegible] 129

[illegible] 135

A. C. Hagg and [illegible] 141

Kinn[illegible]

[illegible] B. Pa[illegible]

[illegible] and H. N. [illegible]

[illegible] and J. W. Bo[illegible]

[illegible]

[illegible] Mechanical E[illegible]

Journal of Applied Mechanics

Papers Contributed to the Transactions by the ASME Applied Mechanics Division

[illegible]

[illegible]

W. Prager, Secretary

[illegible]

S. C. Hunter and J. Kestin, Technical Editors

Published Quarterly by

The American Society of Mechanical Engineers

Publication Office, 20th and Northampton Streets, Easton, Pa.

[illegible] of the Society, 29 West Thirty-Ninth Street, New York 18, N. Y.

[illegible] to the Technical Editors, Journal of Applied Mechanics, ASME, [illegible] of Engineering, Brown University, Providence 12, R. I.

OFFICERS OF THE SOCIETY

J. N. Lycan, President

[illegible]

C. E. Davies, Secretary

[illegible]

[illegible]

J. J. Eyanson, Jr., Editor

[illegible]

[illegible]

[illegible] prized in its publications (30), Par. 4)

[illegible]

Velocity and Acceleration Analysis of Plane and Space Mechanisms by Means of Independent-Position Equations[1]

By FRANCIS H. RAVEN,[2] ITHACA, N. Y.

This paper presents a generalized analytical method for the determination of velocities and accelerations in mechanisms having motion in either two or three dimensions. In this method of analysis, one first obtains independent-position equations for a particular point or for a particular link. The first derivative with respect to time of these position equations yields equations for obtaining the velocity of the point or the angular velocity of the link of interest; and the second derivative with respect to time furnishes new equations from which the desired accelerations may be found. Position vectors are expressed as complex numbers in exponential form because of the ease with which they may be differentiated, and also because numerical results are readily obtainable from the real and imaginary parts of the complex numbers.

Introduction

A POSITION equation is a vector equation which expresses the position of a point on a mechanism as a function of the geometry of the mechanism. There are only two position equations which are mathematically independent for mechanisms other than complex[3] mechanisms which have three. Successive differentiation of these independent-position equations for a point on a mechanism will yield independent equations for the velocity and acceleration of that point. The desired kinematic quantities may be determined from the simultaneous solution of these independent equations. Therefore the method presented in this paper is called the method of independent-position equations.

Kinematic analysis by using independent-position equations is fundamentally different from those methods of analysis which are based upon the equations of relative motion. These include the familiar method of graphical analysis by polygons (1)[4] and the method of generalized co-ordinate systems (2), and also the more recent method presented by Martin and Spotts (3).[5] Some of the major distinctions between a kinematic analysis based on independent-position equations and one based upon the equations of relative motion are as follows:

From the independent-position equations, one obtains the desired kinematic quantities directly by a purely mathematical means in which the need for interpreting the kinematic process is eliminated. On the other hand, a solution by equations of relative motion requires a detailed knowledge of the motion of paths of particles and the directions of velocity and acceleration vectors in order to evaluate each quantity of a generalized expression which includes all possible terms. The directness of the method of independent-position equations eliminates the danger of inadvertently including or excluding terms, such as the Coriolis expression. Also, because of the mathematical directness of the method, complex linkages and space mechanisms are handled more readily.

Procedure for Determining Independent-Position Equations

The procedure for determining independent-position equations for a point on a mechanism having plane or spatial motion may be summarized as follows:

1 A ground point is the point in common between a link and ground at which there is no relative motion; i.e., a fixed center. Starting from any ground point of the mechanism (the ground point chosen to be known as the original ground point) and using the links as paths, trace all independent routes to the point of interest. For two routes to be independent, there must be at least one link not in common to the two routes. Write the vector equation for each route in complex exponential form.[6]

2 From the original ground point go to each other ground point in turn and trace all independent routes to the point of interest. In complex exponential form, write vector equations for these new routes which start from the original ground point.

The foregoing principles will now be illustrated for a variety of mechanisms.

Crank-Shaper Mechanism

For the quick-return crank-shaper mechanism shown in Fig. 1, link r_2 is the driving link. Assuming that O_2O_4, r_2, r_B, θ_2, $\dot{\theta}_2$, and $\ddot{\theta}_2$ are known, let it be required to find equations for the velocity and the acceleration of B, the point of interest. (θ_4 and r_4 may be calculated from the known geometry.)

To determine the velocity and acceleration of B, proceed in the following manner: Arbitrarily selecting O_4 as the original

---

[1] From a dissertation submitted by the author in partial fulfillment of the requirements for the degree of Doctor of Philosophy, Cornell University.

[2] Instructor, Department of Machine Design, Sibley School of Mechanical Engineering, College of Engineering, Cornell University.

[3] Complex mechanisms are those mechanisms which require trial solutions in the construction of velocity and acceleration polygons.

[4] Numbers in parentheses refer to the Bibliography at the end of the paper.

[5] Martin and Spotts analyze mechanisms having plane motion by using complex geometry to solve the equations of relative motion.

Contributed by the Applied Mechanics Division and presented at the Annual Meeting, New York, N. Y., December 1-6, 1957, of The American Society of Mechanical Engineers.

Discussion of this paper should be addressed to the Secretary, ASME, 29 West 39th Street, New York, N. Y., and will be accepted until April 10, 1958, for publication at a later date. Discussion received after the closing date will be returned.

Note: Statements and opinions advanced in papers are to be understood as individual expressions of their authors and not those of the Society. Manuscript received by ASME Applied Mechanics Division, August 21, 1956. Paper No. 57—A-2.

[6] Position vectors are expressed in complex exponential form because of the ease with which they lend themselves to the necessary mathematical operations. The earliest applications of complex numbers to mechanisms (4, 5, 6), were in the field of kinematic synthesis. The only feature in common between the work in synthesis of these references and the present paper which is concerned with analysis is the mathematical tool of the complex exponential representation of a vector.

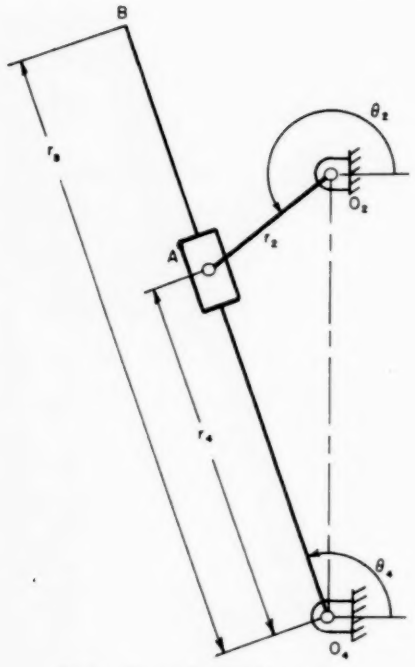

FIG. 1 CRANK-SHAPER MECHANISM

ground point, and going directly from O_4 to B, the first independent-position equation is

$$\mathbf{r}_B = r_B e^{i\theta_4} \quad \ldots\ldots\ldots\ldots\ldots\ldots [1a]$$

A second route may be traced to B by proceeding from O_4 to O_2 to A to B. Thus the second position equation is

$$\mathbf{r}_B = (O_4O_2)e^{i(\pi/2)} + r_2 e^{i\theta_2} + (r_B - r_4)e^{i\theta_4} \ldots\ldots [2a]$$

Equating the right-hand sides of Equations [1a] and [2a], we see that

$$\mathbf{r}_B = r_B e^{i\theta_4} = (O_4O_2)e^{i(\pi/2)} + r_2 e^{i\theta_2} + (r_B - r_4)e^{i\theta_4} \ldots [3a]$$

To obtain the velocity of point B, first differentiate the independent-position Equations [3a]. Thus

$$\mathbf{v}_B = \frac{d\mathbf{r}_B}{dt} = ir_B\dot{\theta}_4 e^{i\theta_4} = ir_2\dot{\theta}_2 e^{i\theta_2} + i(r_B - r_4)\dot{\theta}_4 e^{i\theta_4} - \dot{r}_4 e^{i\theta_4} \ldots\ldots [4a]$$

Each term in Equation [4a] may be distinguished as follows:

$ir_2\dot{\theta}_2 e^{i\theta_2}$ is the absolute velocity of the point A considered to be on link O_2A. This may be written in the form $r_2\dot{\theta}_2 e^{i(\theta_2+90°)}$, where $r_2\dot{\theta}_2$ is the magnitude of the velocity and $e^{i(\theta_2+90°)}$ is the direction. Since the direction is perpendicular to link r_2, the foregoing term represents a tangential velocity.

$i(r_B - r_4)\dot{\theta}_4 e^{i\theta_4}$ is the relative velocity of B with respect to the point A considered to be on link O_4B. We may write this in the form $(r_B - r_4)\dot{\theta}_4 e^{i(\theta_4+90°)}$. The magnitude is represented by $(r_B - r_4)\dot{\theta}_4$ and the direction is indicated by $e^{i(\theta_4+90°)}$.

$-\dot{r}_4 e^{i\theta_4}$ is the velocity of the slider with respect to the point A fixed on link O_4B. The term $\dot{r}_4$ is the magnitude and $-e^{i\theta_4} = e^{i(\theta_4+180°)}$ represents the direction.

Separating Equation [4a] into its real and imaginary parts, and solving for $\dot{\theta}_4$ and $\dot{r}_4$, we obtain

$$\left.\begin{aligned}\dot{\theta}_4 &= \frac{r_2\dot{\theta}_2}{r_4}\cos(\theta_4 - \theta_2)\\ \dot{r}_4 &= r_2\dot{\theta}_2 \sin(\theta_4 - \theta_2)\end{aligned}\right\} \ldots\ldots\ldots\ldots [5a]$$

Substituting $\dot{\theta}_4$ from Equations [5a] into [4a], we find

$$\mathbf{V}_B = \frac{r_B r_2\dot{\theta}_2}{r_4}\cos(\theta_4 - \theta_2)e^{i(\theta_4+90°)} \ldots\ldots\ldots [6a]$$

The acceleration of point B is found by differentiating Equation [4a] with respect to time. Thus

$$\mathbf{a}_B = \frac{d\mathbf{v}_B}{dt} = r_B(i\ddot{\theta}_4 - \dot{\theta}_4^2)e^{i\theta_4} = r_2(i\ddot{\theta}_2 - \dot{\theta}_2^2)e^{i\theta_2} - \ddot{r}_4 e^{i\theta_4} - 2i\dot{r}_4\dot{\theta}_4 e^{i\theta_4} + (r_B - r_4)(i\ddot{\theta}_4 - \dot{\theta}_4^2)e^{i\theta_4} \ldots\ldots [7a]$$

Each acceleration term in Equation [7a] may be recognized as follows:

$ir_B\ddot{\theta}_4 e^{i\theta_4}$ is the tangential acceleration of the point B.

$-r_B\dot{\theta}_4^2 e^{i\theta_4}$ is the normal acceleration of B.

$r_2(i\ddot{\theta}_2 - \dot{\theta}_2^2)e^{i\theta_2}$ represents the tangential and normal accelerations respectively of a point A considered to be on link O_2A.

$-\ddot{r}_4 e^{i\theta_4}$ is the acceleration of the slider with respect to link O_4B.

$-2i\dot{r}_4\dot{\theta}_4 e^{i\theta_4}$ is the Coriolis component of acceleration.

$(r_B - r_4)(i\ddot{\theta}_4 - \dot{\theta}_4^2)e^{i\theta_4}$ represents the tangential and normal accelerations respectively of point B relative to point A considered to be on link O_4B.

Separating Equation [7a] into its real and imaginary parts, solving for $\ddot{\theta}_4$ and substituting $\ddot{\theta}_4$ into Equation [7a], we find

$$\mathbf{a}_B = \frac{r_B}{r_4}[r_2\ddot{\theta}_2\cos(\theta_4 - \theta_2) + r_2\dot{\theta}_2^2\sin(\theta_4 - \theta_2) - 2\dot{r}_4\dot{\theta}_4]e^{i(\theta_4+90°)} - r_B\dot{\theta}_4^2 e^{i\theta_4} \ldots\ldots [8a]$$

It should be noted that the equations developed for the velocity Equation [6a] and acceleration Equation [8a] are general in that they apply for any phase of the mechanism and for any length of the various links.

As illustrated by the preceding analysis, the procedure for determining the velocity and acceleration of the point of interest on a mechanism may be generalized as follows:[7]

1 Differentiate the position equations with respect to time. Because this yields two independent expressions for the velocity, we may

2 Equate the two expressions. Thus we obtain one equation in complex exponential form which we may

3 Separate into real and imaginary parts (for space mechanisms, there is also a z-component), thereby obtaining two algebraic equations (three, in space). These we may now

4 Solve simultaneously for the unknown quantities. We then

5 Substitute these values in either of the original expressions for the velocity.

6 The acceleration of the point of interest may be determined by taking the second derivative of the position equations and proceeding as described in the foregoing.

For complex mechanisms which have three independent-position equations, the method parallels that just given, with the exception that two equations are obtained rather than one, as was found in step 2.

[7] As is later shown, slight variations of this procedure may be used for simplification of the analysis of direct contact mechanisms.

Direct-Contact Mechanisms

For the two members in direct contact shown in Fig. 2, link 2 is the driving member. Q is a point on link 2 at the point of contact of the two bodies, while P is considered to be on link 3.

In Fig. 2, $r_{2c}e^{i\theta_{2c}}$ is the radius of curvature of the cam surface of link 2 at the point of contact, and $r_{3c}e^{i\theta_{3c}}$, which may be written in the form $-r_{3c}e^{i\theta_{3c}}$, is the radius of curvature of link 3. $r_2e^{i\theta_2}$ is the vector from O_2 to A, where A is the center of curvature of link 2. Similarly, $r_3e^{i\theta_3}$ connects O_3 to B, where B is the center of curvature of link 3. Assuming that θ_2, $\dot{\theta}_2$, $\ddot{\theta}_2$, O_2O_3 and the four preceding radii vectors are known, let it be required to find the velocity and acceleration of P.

It should be noticed that in Fig. 2 (also Fig. 3), the vectors O_2 to A, A to B, B to O_3, and O_3 to O_2 may be regarded as forming a four-bar linkage. In each of these figures, we also see that for a small angular rotation of the driver, the lengths r_{2c} and r_{3c} will remain constant. Thus the angular velocity and acceleration, $\dot{\theta}_2$ and $\ddot{\theta}_2$, of the driving cam will be the same as for link O_2A. Similarly, the angular velocity and acceleration of the driven member, $\dot{\theta}_3$ and $\ddot{\theta}_3$, will be the same as for link O_3B. A formal proof for the validity of the equivalent linkage for direct-contact mechanisms is presented by Hinkle, Ip, and Frame (7).

For members in direct contact, the path to follow in going from one link to another is by way of the radius of curvature of the surfaces at the point of contact. (An advantage of using the paths of the radii of curvature is that, when these radii vectors are differentiated, their magnitudes remain constant.)

Thus in Fig. 2, with O_2 as the original ground point, the first independent-position equation is obtained by going from O_2 to A to the point of contact, and the second, by going from O_2 to O_3 to B to the point of contact. Thus

$$r_2e^{i\theta_2} + r_{2c}e^{i\theta_{2c}} = O_2O_3 + r_3e^{i\theta_3} - r_{3c}e^{i\theta_{3c}} \quad [1b]$$

Since P is a fixed point on body 3, we may write

$$\mathbf{r}_P = r_pe^{i\theta_P} \quad [2b]$$

Differentiating Equation [2b] with respect to time, we find that the velocity of P is

$$\mathbf{v}_P = ir_p\dot{\theta}_2e^{i\theta_P} \quad [3b]$$

Differentiating Equation [1b], and solving for $\dot{\theta}_3$ and $\dot{\theta}_{2c}$, we obtain

$$\dot{\theta}_3 = \frac{r_2\dot{\theta}_2 \sin(\theta_{2c} - \theta_2)}{r_3 \sin(\theta_{2c} - \theta_3)}; \quad \dot{\theta}_{2c} = \frac{r_2\dot{\theta}_2}{(r_{2c} + r_{3c})} \frac{\sin(\theta_3 - \theta_2)}{\sin(\theta_{2c} - \theta_3)} \quad [4b]$$

Substituting $\dot{\theta}_2$ from Equation [4b] into [3b], we obtain for the velocity of P

$$\mathbf{v}_P = \frac{r_2r_p\dot{\theta}_2}{r_3} \frac{\sin(\theta_{2c} - \theta_2)}{\sin(\theta_{2c} - \theta_3)} e^{i(\theta_P + 90°)} \quad [5b]$$

To determine the acceleration of point P, first differentiate Equation [3b] with respect to time. Thus

$$\mathbf{a}_P = r_P(i\ddot{\theta}_3 - \dot{\theta}_3^2)e^{i\theta_P} \quad [6b]$$

By solving for $\ddot{\theta}_3$ from the second derivative with respect to time of Equation [1b], and substituting this value into Equation [6b], we obtain for the acceleration of the point P

$$\mathbf{a}_P = \frac{r_P[r_3\ddot{\theta}_3 \sin(\theta_{2c} - \theta_3) - r_2\dot{\theta}_2^2 \cos(\theta_{2c} - \theta_2) + r_3\dot{\theta}_3^2 \cos(\theta_{2c} - \theta_3) - (r_{2c} + r_{3c})\dot{\theta}_{2c}^2]}{r_3 \sin(\theta_{2c} - \theta_3)} e^{i(\theta_P + 90°)} - r_P\dot{\theta}_2^2e^{i\theta_P}$$

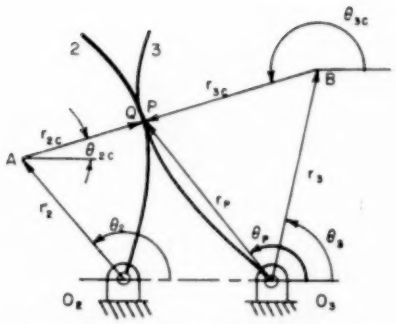

Fig. 2 Two Members in Direct Contact

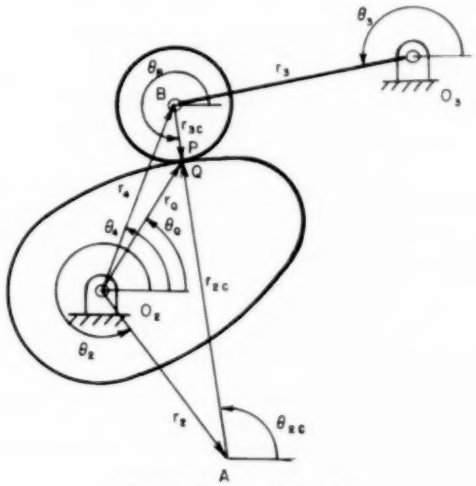

Fig. 3 Cam and Follower

Cams and Followers

For the oscillating cam shown in Fig. 3, let r_2, r_{2c}, r_{3c}, r_3, θ_2, θ_{2c}, θ_3, $\dot{\theta}_2$, and $\ddot{\theta}_2$ be known quantities. Suppose that it is desired to determine the velocity and acceleration of B, the center of the follower.

Selecting O_3 as the original ground point and going from O_3 to A to B, the first position equation to B, the point of interest, is

$$\mathbf{r}_B = r_2e^{i\theta_2} + (r_{3c} + r_{2c})e^{i\theta_{3c}} \quad [1c]$$

The second position equation is obtained by going from O_2 to O_3 to B. Thus

$$\mathbf{r}_B = O_2O_3e^{i\theta_{O_2O_3}} + r_3e^{i\theta_3} \quad [2c]$$

where $\theta_{O_2O_3}$ is the angle between the line joining O_2O_3 and the horizontal.

Equating [1c] and [2c], we find that

$$\mathbf{r}_B = r_3e^{i\theta_3} + (r_{3c} + r_{3c})e^{i\theta_{3c}} = O_2O_3e^{i\theta_{O_2O_3}} + r_3e^{i\theta_3} \quad [3c]$$

An equation for the velocity of B is obtained by differentiating Equation [3c] as follows

$$\mathbf{v}_B = ir_3\dot{\theta}_3e^{i\theta_3} + i(r_{3c} + r_{3c})\dot{\theta}_{3c}e^{i\theta_{3c}} = ir_3\dot{\theta}_3e^{i\theta_3} \quad [4c]$$

Solving for $\dot{\theta}_3$ and $\dot{\theta}_{2c}$, we see that

$$\dot{\theta}_3 = \frac{r_2\dot{\theta}_2}{r_3} \frac{\sin(\theta_{2c} - \theta_2)}{\sin(\theta_{2c} - \theta_3)}; \quad \dot{\theta}_{2c} = \frac{r_2\dot{\theta}_2}{(r_{2c} + r_{3c})} \frac{\sin(\theta_3 - \theta_2)}{\sin(\theta_{2c} - \theta_3)} \quad [5c]$$

Thus the velocity of B is

$$\mathbf{v}_B = r_3\dot{\theta}_3 \frac{\sin(\theta_{3c} - \theta_2)}{\sin(\theta_{2c} - \theta_3)} e^{i(\theta_3+90°)} \quad \ldots\ldots\ldots [6c]$$

It should be noted that Equation [6c] is also valid for the case of a reciprocating follower (i.e., $r_3 = \infty$) as well as for an oscillating follower.

To determine the acceleration of B, first differentiate Equation [4c] with respect to time; therefore

$$\mathbf{a}_B = r_2(i\ddot{\theta}_2 - \dot{\theta}_2^2)e^{i\theta_2} + (r_{2c} + r_{3c})(i\ddot{\theta}_{2c} - \dot{\theta}_{2c}^2)\, e^{i\theta_{2c}}$$
$$= r_3(i\ddot{\theta}_3 - \dot{\theta}_3^2)e^{i\theta_3} \quad \ldots\ldots [7c]$$

Separating Equation [7c] into its real and imaginary parts and then solving for $\ddot{\theta}_3$ and $\ddot{\theta}_{2c}$, we obtain

$$\left.\begin{aligned} \ddot{\theta}_3 &= \frac{r_2\ddot{\theta}_2 \sin(\theta_{2c} - \theta_2) - r_2\dot{\theta}_2^2 \cos(\theta_{2c} - \theta_2) + r_3\dot{\theta}_3^2 \cos(\theta_{2c} - \theta_3) - (r_{2c} + r_{3c})\dot{\theta}_{2c}^2}{r_3 \sin(\theta_{2c} - \theta_2)} \\ \ddot{\theta}_{2c} &= \frac{-r_2\ddot{\theta}_2 \sin(\theta_3 - \theta_2) + r_2\dot{\theta}_2^2 \cos(\theta_3 - \theta_2) + (r_{2c} + r_{3c})\dot{\theta}_{2c}^2 \cos(\theta_3 - \theta_{2c}) - r_3\dot{\theta}_3^2}{(r_{2c} + r_{3c}) \sin(\theta_3 - \theta_{2c})} \end{aligned}\right\} \ldots [8c]$$

Thus we find for the acceleration of the point B

$$\mathbf{a}_B = \frac{[r_2\ddot{\theta}_2 \sin(\theta_{2c} - \theta_2) - r_2\dot{\theta}_2^2 \cos(\theta_{2c} - \theta_2) + r_3\dot{\theta}_3^2 \cos(\theta_{2c} - \theta_3) - (r_{2c} + r_{3c})\dot{\theta}_{2c}^2]}{\sin(\theta_{2c} - \theta_3)} e^{i(\theta_3+90°)}$$
$$- r_3\dot{\theta}_3^2 e^{i\theta_3} \quad \ldots\ldots [9c]$$

For the case of a reciprocating follower, the terms in [9c] containing $r_3\dot{\theta}_3^2$ are zero.

Velocity and Acceleration of a Point on the Roller. Assuming that there is pure rolling between the follower and the cam, let it be desired to determine the velocity and acceleration of P, the point on the follower at the point of contact.

Considering Q as a point on the cam at the point of contact, we may write

$$\mathbf{r}_Q = r_Q e^{i\theta_Q}$$

and differentiating

$$\mathbf{v}_Q = ir_Q\dot{\theta}_2 e^{i\theta_Q} \quad \ldots\ldots\ldots\ldots\ldots [10c]$$

Similarly, we may write for the position of P

$$\mathbf{r}_P = O_2O_3e^{i\theta_{O_2O_3}} + r_3e^{i\theta_3} + r_{BP}e^{i\theta_R} \quad \ldots\ldots [11c]$$

where θ_R is the angle defining the direction of BP, the radius of the roller.

Differentiating Equation [11c], we obtain the following equation for the velocity of P

$$\mathbf{v}_P = ir_3\dot{\theta}_2 e^{i\theta_3} + ir_{BP}\dot{\theta}_R e^{i\theta_R} \quad \ldots\ldots\ldots\ldots [12c]$$

where $\dot{\theta}_R$ = angular velocity of the roller.

Since there is pure rolling between the cam and the follower, we may equate [10c] and [12c], thus obtaining

$$ir_Q\dot{\theta}_2 e^{i\theta_Q} = ir_3\dot{\theta}_2 e^{i\theta_3} + ir_{BP}\dot{\theta}_R e^{i\theta_R}$$

Solving for $\dot{\theta}_3$ and $\dot{\theta}_R$, we find

$$\left.\begin{aligned} \dot{\theta}_3 &= \frac{r_Q\dot{\theta}_2 \sin(\theta_R - \theta_Q)}{r_3 \sin(\theta_R - \theta_3)} \\ \dot{\theta}_R &= \frac{r_Q\dot{\theta}_2 \sin(\theta_3 - \theta_Q)}{r_{BP} \sin(\theta_3 - \theta_R)} \end{aligned}\right\} \quad \ldots\ldots\ldots [13c]$$

Since $\dot{\theta}_3$ is not affected by whether or not the follower has pure rolling, then $\dot{\theta}_3$ could have been obtained from Equation [5c] as well as from the foregoing expression.

Differentiating Equation [12c], we obtain the following equation for the total acceleration of P

$$\mathbf{a}_P = r_3(i\ddot{\theta}_3 - \dot{\theta}_3^2)e^{i\theta_3} + r_{BP}(i\ddot{\theta}_R - \dot{\theta}_R^2)e^{i\theta_R} \quad \ldots\ldots [14c]$$

To obtain $\ddot{\theta}_R$, we note that the tangential accelerations of both P and Q with respect to the point of contact must be equal for pure rolling to continue.

The position of P with respect to the point of contact is

$$\mathbf{r}_{Pc} = r_{BP}e^{i\theta_R} - r_{BP}e^{i(\theta_{3c}+\pi)}$$

Taking the second derivative of the foregoing expression, we see that the tangential component may be written as follows

$$\overrightarrow{a}_{Pc} = r_{BP}(\ddot{\theta}_R - \ddot{\theta}_{3c})\, e^{i(\theta_R+90°)} \quad \ldots\ldots\ldots [15c]$$

Similarly, the position of Q with respect to the point of contact is

$$\mathbf{r}_{Qc} = r_Qe^{i\theta_Q} - [r_2e^{i\theta_2} + r_{3c}e^{i\theta_{3c}}]$$

and taking the second time derivative, we find the tangential component of a_{Qc} is

$$\overrightarrow{a}_{Qc} = -r_{3c}(\ddot{\theta}_2 - \ddot{\theta}_{3c})e^{i(\theta_R+90°)} \quad \ldots\ldots\ldots [16c]$$

Equating [15c] and [16c] and solving for $\ddot{\theta}_R$, we find

$$\ddot{\theta}_R = \frac{(r_{3c} + r_{BP})\ddot{\theta}_{3c} - r_{3c}\ddot{\theta}_2}{r_{BP}}$$

Obtaining $\ddot{\theta}_R$ from the foregoing expression, we may then find the acceleration of P from Equation [14c].

As in the preceding case of two members in direct contact, we see that this method of analysis eliminates the need for determining relative paths of motion.

Complex Mechanisms

For the complex mechanism shown in Fig. 4, link r_2 is the driver. Assuming that $\dot{\theta}_2$, $\ddot{\theta}_2$, and the various angles and the lengths of the links are known, let it be desired to find the velocity and acceleration of point A.

By noting that $\mathbf{r}_A = r_2e^{i\theta_2}$

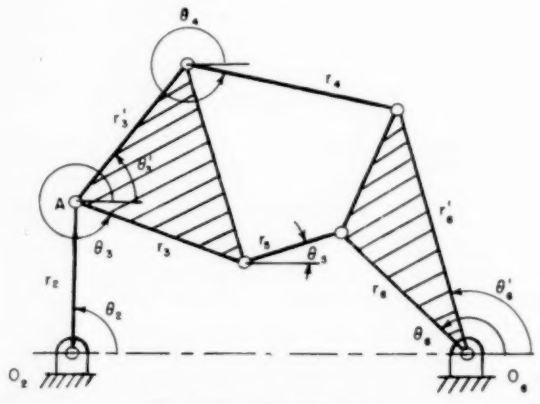

Fig. 4 Complex Mechanism

and thus

$$v_A = ir_2\dot{\theta}_2 e^{i\theta_2}; \quad a_A = r_2(i\ddot{\theta}_2 - \dot{\theta}_2^2)e^{i\theta_2}$$

it is seen that this problem may be solved readily by finding the angular velocity $\dot{\theta}_2$, and acceleration, $\ddot{\theta}_2$. Although angular velocities and accelerations for the various links may be determined from the independent-position equations for a point of interest, the following method is more direct:

1 Taking the ground points in pairs, select any two ground points and trace all independent routes starting from one of the ground points, and proceeding through the links to the other ground point of the pair, and then back to the first.

2 Taking the other pairs of ground points in turn, proceed as before until all pairs are used. Write vector equations in complex exponential form for these closed paths or loops.

3 The angular velocities and accelerations are determined by differentiation, and so on, of these loop equations. Because there is one less loop equation for a link than there were position equations for a point of interest, the mathematical operations are simplified.

Since O_2 and O_6 are the only two ground points, our loop equations are

$$\left.\begin{aligned} r_2e^{i\theta_2} + r_3e^{i\theta_3} + 0 + r_6e^{i\theta_6} &= O_2O_6 + r_6e^{i\theta_6} \\ r_2e^{i\theta_2} + r_3'e^{i\theta_3'} + r_4e^{i\theta_4} + 0 &= O_2O_6 + r_6'e^{i\theta_6'} \end{aligned}\right\} \quad ..[1d]$$

Differentiating the independent-position equations with respect to time, and putting the real and imaginary parts of these equations in determinant form to solve for $\dot{\theta}_2$, we find

$$\dot{\theta}_2 = \frac{\begin{vmatrix} -r_6\dot{\theta}_6\sin\theta_6 & -r_3\sin\theta_3 & 0 & -r_6\sin\theta_6 \\ r_6\dot{\theta}_6\cos\theta_6 & r_3\cos\theta_3 & 0 & r_6\cos\theta_6 \\ -r_6'\dot{\theta}_6\sin\theta_6' & -r_3'\sin\theta_3' & -r_4\sin\theta_4 & 0 \\ r_6'\dot{\theta}_6\cos\theta_6' & r_3'\cos\theta_3' & r_4\cos\theta_4 & 0 \end{vmatrix}}{\begin{vmatrix} -r_2\sin\theta_2 & -r_3\sin\theta_3 & 0 & -r_6\sin\theta_6 \\ r_2\cos\theta_2 & r_3\cos\theta_3 & 0 & r_6\cos\theta_6 \\ -r_2\sin\theta_2 & -r_3'\sin\theta_3' & -r_4\sin\theta_4 & 0 \\ r_2\cos\theta_2 & r_3'\cos\theta_3' & r_4\cos\theta_4 & 0 \end{vmatrix}} \quad ...[2d]$$

The above fourth-order determinants may rapidly be reduced to second-order determinants because of the many zeros. It should be noticed that the zeros occur because a link is not traversed in writing the position equations. In general, determinants for complex mechanisms will have numerous zeros.

By dividing the top row of both the numerator and the denominator determinants by $\tan\theta_6$ and adding each top row to its respective second row, we obtain third-order determinants. Similarly, dividing the second rows of the resulting third-order determinants by $\tan\theta_4$ and adding each second row to its respective third row, we obtain

$$\dot{\theta}_2 = \frac{\dot{\theta}_6\begin{vmatrix} r_6\sin(\theta_6-\theta_6) & r_3\sin(\theta_6-\theta_3) \\ r_6'\sin(\theta_4-\theta_6') & r_3'\sin(\theta_4-\theta_3') \end{vmatrix}}{r_2\begin{vmatrix} \sin(\theta_6-\theta_2) & r_3\sin(\theta_6-\theta_3) \\ \sin(\theta_4-\theta_2) & r_3'\sin(\theta_4-\theta_3') \end{vmatrix}}$$

Thus

$$\dot{\theta}_2 = \frac{\dot{\theta}_6[r_6r_3'\sin(\theta_6-\theta_6)\sin(\theta_4-\theta_3') - r_6'r_3\sin(\theta_6-\theta_3)\sin(\theta_4-\theta_6')]}{r_2[r_3'\sin(\theta_6-\theta_2)\sin(\theta_4-\theta_3') - r_3\sin(\theta_6-\theta_3)\sin(\theta_4-\theta_2)]}$$

By taking the second derivative of Equation [1d] with respect to time, a set of equations is obtained from which the angular acceleration of any link may be determined. These acceleration equations will be the same type of equations as were obtained for angular velocities; thus one may follow the same procedures or their solution.

Space Mechanisms

Designation of a Vector in Space. Referring to Fig. 5, we see that a vector $\mathbf{r}_P$ may be designated as follows

$$\mathbf{r}_P = (r_P\sin\phi)e^{i\theta} + j(r_P\cos\phi) = r_P[e^{i\theta}\sin\phi + j\cos\phi]$$

where θ is the angle between the real axis and the projection of $\mathbf{r}_P$ on the complex plane, and ϕ is the angle between j, the vertical axis, and $\mathbf{r}_P$.

To convert a vector, $\mathbf{r}_P = (x_1, y_1, z_1)$, from rectangular co-ordinates to the foregoing system, we note

$$\theta = \tan^{-1}(y_1/x_1)$$

$$\phi = \tan^{-1}(x_1^2 + y_1^2)^{1/2}/z_1$$

$$r_P = (x_1^2 + y_1^2 + z_1^2)^{1/2}$$

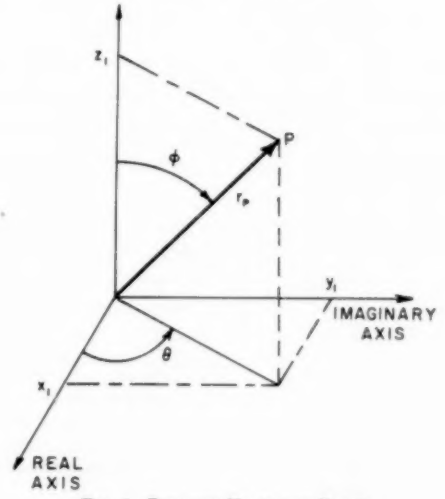

Fig. 5 Position Vector in Space

By designating positions in space by means of spherical co-ordinates, as just shown, then the method of independent-position equations also becomes applicable for the analysis of space mechanisms.

Space Linkage. For the space linkage shown in Fig. 6, link r_2 is the driver. As may be seen from Fig. 6, link r_3 is rotating in the plane defined by the i-axis and the j-axis, while link r_4 is constrained to rotate in the plane of the real axis and the j-axis. Knowing $\dot{\phi}_2$, $\ddot{\phi}_2$, and the various angles and the lengths of the links, let it be desired to find the angular velocity and acceleration of the driven link r_4.

The independent-position equation for the links may be written as follows

$$r_2(e^{i\theta_2}\sin\phi_2 + j\cos\phi_2) + r_3(e^{i\theta_3}\sin\phi_3 + j\cos\phi_3) = a + ib + jc + r_4(e^{i\theta_4}\sin\phi_4 + j\cos\phi_4)$$

Differentiating the preceding equation with respect to time, we find

$$\begin{aligned} r_2[(\dot{\phi}_2\cos\phi_2 + i\dot{\theta}_2\sin\phi_2)e^{i\theta_2} - j\dot{\phi}_2\sin\phi_2] \\ + r_3[(\dot{\phi}_3\cos\phi_3 + i\dot{\theta}_3\sin\phi_3)e^{i\theta_3} - j\dot{\phi}_3\sin\phi_3] \\ = r_4[(\dot{\phi}_4\cos\phi_4 + i\dot{\theta}_4\sin\phi_4)e^{i\theta_4} - j\dot{\phi}_4\sin\phi_4] \quad .....[1e] \end{aligned}$$

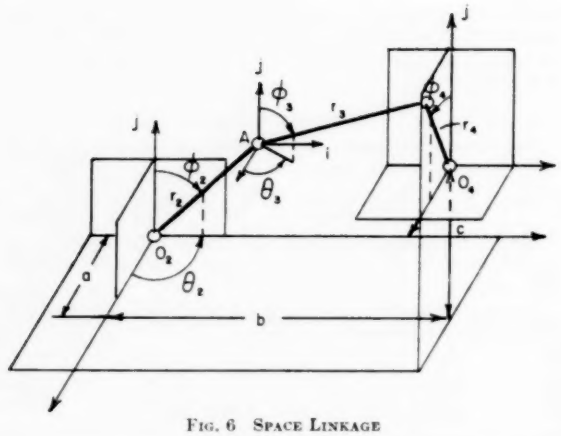

FIG. 6 SPACE LINKAGE

Separating the foregoing into its real, imaginary, and vertical components and noting that $\dot{\theta}_2 = \dot{\theta}_4 = 0$, we obtain

$$\left.\begin{aligned} r_2 \cos\phi_2 \cos\theta_2\dot{\phi}_2 + r_3 \cos\phi_3 \cos\theta_3\dot{\phi}_3 - r_3 \sin\phi_3 \sin\theta_3\dot{\theta}_3 &= r_4 \cos\phi_4 \cos\theta_4\dot{\phi}_4 \\ r_2 \cos\phi_2 \sin\theta_2\dot{\phi}_2 + r_3 \cos\phi_3 \sin\theta_3\dot{\phi}_3 + r_3 \sin\phi_3 \cos\theta_3\dot{\theta}_3 &= r_4 \cos\phi_4 \sin\theta_4\dot{\phi}_4 \\ -r_2 \sin\phi_2\dot{\phi}_2 \qquad -r_3 \sin\phi_3\dot{\phi}_3 \qquad + 0\,\dot{\theta}_3 &= -r_4 \sin\phi_4\dot{\phi}_4 \end{aligned}\right\} \quad \ldots [2e]$$

From the preceding equations, we see that the determinant for $\dot{\phi}_4$ is

$$\dot{\phi}_4 = \frac{\begin{vmatrix} r_2 \cos\phi_2 \cos\theta_2\,\dot{\phi}_2 & -r_3 \cos\phi_3 \cos\theta_3 & r_3 \sin\phi_3 \sin\theta_3 \\ r_2 \cos\phi_2 \sin\theta_2\,\dot{\phi}_2 & -r_3 \cos\phi_3 \sin\theta_3 & -r_3 \sin\phi_3 \cos\theta_3 \\ -r_2 \sin\phi_2\,\dot{\phi}_2 & r_3 \sin\phi_3 & 0 \end{vmatrix}}{\begin{vmatrix} r_4 \cos\phi_4 \cos\theta_4 & -r_3 \cos\phi_3 \cos\theta_3 & r_3 \sin\phi_3 \sin\theta_3 \\ r_4 \cos\phi_4 \sin\theta_4 & -r_3 \cos\phi_3 \sin\theta_3 & -r_3 \sin\phi_3 \cos\theta_3 \\ -r_4 \sin\phi_4 & r_3 \sin\phi_3 & 0 \end{vmatrix}} \quad [3e]$$

We see that r_2, r_4, and $\dot{\phi}_2$ may be factored out of the foregoing determinants, and that r_3 cancels when factored out. Dividing the first row of each determinant by $\tan\theta_3$, and adding the first row to the second, the foregoing determinants are reduced to the second order, as follows

$$\dot{\phi}_4 = \frac{r_2\dot{\phi}_2}{r_4} \frac{\begin{vmatrix} \cos\phi_2\left(\sin\theta_2 + \dfrac{\cos\theta_2}{\tan\theta_3}\right) & -\cos\phi_3\left(\sin\theta_3 + \dfrac{\cos\theta_3}{\tan\theta_3}\right) \\ -\sin\phi_2 & \sin\phi_3 \end{vmatrix}}{\begin{vmatrix} \cos\phi_4\left(\sin\theta_4 + \dfrac{\cos\theta_4}{\tan\theta_3}\right) & -\cos\phi_3\left(\sin\theta_3 + \dfrac{\cos\theta_3}{\tan\theta_3}\right) \\ -\sin\phi_4 & \sin\phi_3 \end{vmatrix}} \quad \ldots [4e]$$

By expanding the trigonometric terms in the parentheses, [4e] may be simplified as follows

$$\dot{\phi}_4 = \frac{r_2\dot{\phi}_2}{r_4} \frac{\begin{vmatrix} \cos\phi_2 \cos(\theta_2 - \theta_3) & -\cos\phi_3 \\ -\sin\phi_2 & \sin\phi_3 \end{vmatrix}}{\begin{vmatrix} \cos\phi_4 \cos(\theta_4 - \theta_3) & -\cos\phi_3 \\ -\sin\phi_4 & \sin\phi_3 \end{vmatrix}}$$

Thus

$$\dot{\phi}_4 = \frac{r_2\dot{\phi}_2 [\sin\phi_2 \cos\phi_2 - \cos\phi_2 \sin\phi_3 \cos(\theta_2 - \theta_3)]}{r_4 [\sin\phi_4 \cos\phi_2 - \cos\phi_4 \sin\phi_2 \cos(\theta_4 - \theta_3)]}$$

Either of the other unknown angular velocities, $\dot{\phi}_3$ or $\dot{\theta}_3$, could similarly have been obtained from [2e]. It would only be necessary to compute the determinant for the numerator, since the denominator remains the same.

By differentiating Equation [1e] and obtaining the real, imaginary, and vertical components, as was done for angular velocities in [2e], we can then solve for any of the desired unknown angular accelerations.

ACKNOWLEDGMENT

The author expresses his appreciation to his thesis advisor, Prof. H. H. Mabie, for his helpful suggestions and constant encouragement throughout the preparation of this paper. He also wishes to thank Prof. A. H. Burr, Head of the Machine Design Department; and Prof. F. W. Ocvirk for their fine comments.

BIBLIOGRAPHY

1 "Mechanisms and Dynamics of Machinery," by H. H. Mabie and F. W. Ocvirk, John Wiley & Sons, Inc., New York, N. Y., 1957, pp. 209–237.

2 "Mechanism," by J. Beggs, McGraw-Hill Book Company, Inc., New York, N. Y., 1955, pp. 24–31.

3 "An Application of Complex Geometry to Relative Velocities and Accelerations in Mechanisms," by G. H. Martin and M. F. Spotts, Trans. ASME, vol. 79, 1957, pp. 687–693.

4 "Kinematische Getriebesynthese," by R. Beyer, Springer-Verlag, Berlin, Germany, 1953, pp. 189–191.

5 "Syntheses of Four-Link Mechanisms," by Z. S. Bloch, *Izvestiya Academiya Nauk USSR Otdeleniye Technicheskikh Nauk*, No. 1, 1940, pp. 47–54.

6 "Gelenkvierecke mit vorgeshriebenen Groesst- und Kleinstwerten der Abtriebswinkelgeschwindigkeit," by N. Rosenauer, *Werkstattstechnik*, vol. 38, 1944, pp. 25–27.

7 "Acceleration in Mechanisms," by R. T. Hinkle, C. Ip, and J. S. Frame, JOURNAL OF APPLIED MECHANICS, Trans. ASME, vol. 77, 1955, pp. 222–226.

Some Basic Properties of Shoe Brakes

By G. A. G. FAZEKAS,[1] BROOKLYN, N. Y.

In a previous paper, the author has shown how performance of a fixed anchor shoe is affected by its geometry. The present paper refines and extends the treatment to brake shoes that have two degrees of freedom of movement, showing also how their geometry may be optimized.

Introduction

FIG. 1 shows diagrammatically a floating shoe brake, the analysis[2] of which indicates that its geometry can be defined uniquely by R, a, Z, α, φ, θ, γ, direction of drum rotation, and nominal friction angle ($\rho = \tan^{-1} \mu$). When designing a brake, any of these independent parameters may be selected almost arbitrarily. The purpose of this paper is to show quite generally, for any kind of brake-shoe construction, how geometry affects performance, and how performance may be optimized.

On considering now the torque generated to remain constant, brake performance can be defined uniquely, and measured experimentally in terms of (a) actuating (pedal) load; (b) travel of the actuator (pedal); (c) tendency to fade; and (d) tendency to shudder. Of these four items, only the first three will be discussed here. It has been shown[3] that (a) is assessed by the "shoe factor" K; (b) by (actuator travel)/(shoe center lift) = A, which is significant for heat expansion of the drum + elastic distortion of the assembly; and for (c) the fade-sensitivity factor f = (per cent change of torque)/(1 per cent change of friction) is an appropriate yardstick at the design stage. It is also expeditious to combine K and A into a

$$\text{Work factor} = w = \frac{K}{A} = \frac{\text{torque/in. drum radius}}{\text{in-lb work done by actuating force}} \quad [1]$$

which is introduced here as a single criterion of torque output.

In what follows, the general equation connecting performance with geometry will be derived first. The fixed-anchor shoe will be considered next, followed by the treatment of brake shoes that have two degrees of freedom of movement.

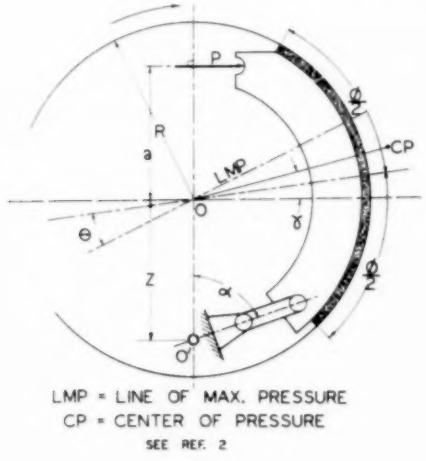

FIG. 1

General Performance Equations

Fig. 2 is intended to show any kind of a brake shoe, with actuating force P, drum reaction Q, and anchor reaction S acting thereon.[2] If the shoe is of the fixed-anchor type, its anchor is to be at O'; if it is a "floating shoe" some linkage may be arranged anywhere along $O'H$, as sketched in broken line. A "sliding shoe" can be considered to have an abutment anywhere on and perpendicular to $O'H$. Pressure pattern on the lining is not specified, only the center of pressure (C)[2], which is defined here by radius vector ($L = OC$), and argument γ to be taken as positive above the horizontal center line.

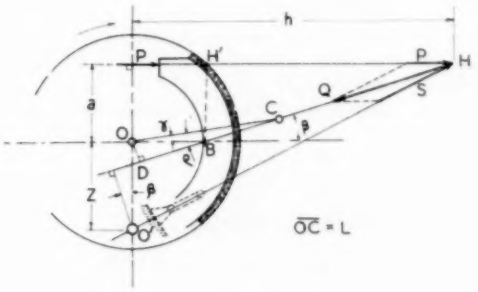

FIG. 2

On considering equilibrium of the shoe, and taking moments about O' we have

$$P(a + Z) = Q(Z \cos \beta - L \sin \rho) \quad [2]$$

From the equilibrium of the drum it follows that the brake torque T is compensated by

$$T = QL \sin \rho \quad [3]$$

The shoe factor K is therefore, from Equations [2] and [3]

$$K = \frac{T}{PR} = \frac{a + Z}{R} \frac{1}{\frac{Z}{L} \frac{\cos \beta}{\sin \rho} - 1} \quad [4]$$

To obtain the fade-sensitivity factor f, the foregoing equation is put into a logarithmic form and differentiated

---

[1] Associate Professor of Mechanical Engineering, Polytechnic Institute of Brooklyn. Mem. ASME.

[2] "Graphical Shoe-Brake Analysis," by G. A. G. Fazekas, TRANS. ASME, vol. 79, 1957, pp. 1322–1328.

[3] "Brake Fade," by G. A. G. Fazekas, *Automobile Engineer*, vol. 41, no. 534, 1951, p. 53.

Contributed by the Applied Mechanics Division and presented at the Annual Meeting, New York, N. Y., December 1–6, 1957, of THE AMERICAN SOCIETY OF MECHANICAL ENGINEERS.

Discussion of this paper should be addressed to the Secretary, ASME, 29 West 39th Street, New York, N. Y., and will be accepted until April 10, 1958, for publication at a later date. Discussion received after the closing date will be returned.

NOTE: Statements and opinions advanced in papers are to be understood as individual expressions of their authors and not those of the Society. Manuscript received by ASME Applied Mechanics Division, August 28, 1956. Paper No. 57—A-6.

$$\frac{dK}{K} = \frac{\frac{Z}{L}}{\frac{Z}{L}\frac{\cos\beta}{\sin\rho} - 1}$$

$$\left[\frac{\sin\beta\sin\rho\,d\beta + \cos\rho\cos\beta\,d\rho + \cos\beta\sin\rho\,dL/L}{\sin^2\rho}\right] \ldots [5]$$

with $\rho = \tan^{-1}\mu$, we have also

$$\frac{d\rho}{\sin^2\rho} = \frac{d\mu}{\mu^2} \ldots [6]$$

so that on combining Equation [5] with [4] the general expression for the fade factor f is

$$f = \frac{dK/K}{d\mu/\mu} = \frac{K}{\mu}\frac{R}{L}\frac{Z}{a+Z}\left[\cos\beta\cos\rho + \sin\beta\sin\rho\frac{d\beta}{d\rho} + \frac{\cos\beta\sin\rho}{L}\frac{dL}{d\rho}\right] \ldots [7]$$

These equations refer to a "leading shoe" with the drum rotating in the direction indicated in Figs. 1 and 2. If the rotation is reversed, we have a "trailing shoe" for which all the foregoing equations remain valid if ρ is given a negative sign. The torque T being in the opposite direction, becomes of course negative too. These equations are quite general, apply for any pressure pattern, but they are physically significant only if L and γ are independent of P. This is usually the case, and also may be defined as $T \propto P$.

As mentioned, the foregoing is valid for any shoe design. If the shoe has a fixed anchor, the center of pressure C is fixed; for shoes with two degrees of freedom of movement, the point H is fixed, L, γ, and β being some functions of ρ.

Fixed-Anchor Shoe

As explained earlier, in this case the dotted link in Fig. 2 is absent, the shoe being positively fulcrumed at O'. Also it is well known[4] that the LMP lies at right angle to OO', and the position of C may be found readily,[2] it being independent of ρ. Consequently

$$\frac{d\beta}{d\rho} = 0 \quad \text{and} \quad \frac{dL}{d\rho} = 0 \ldots [8]$$

From ΔBOC it follows further that

$$\gamma + \rho = \beta \text{ and hence } d\beta = d\rho \ldots [9]$$

In Equation [7], the expression in the parentheses becomes therefore

$$[\ ] = \cos\beta\cos\rho + \sin\beta\sin\rho = \cos(\beta - \rho) = \cos\gamma \ldots [10]$$

so that we have

$$f = \frac{K}{\mu}\frac{R}{L}\frac{Z}{a+Z}\cos\gamma \ldots [11]$$

In this equation

$$\frac{a+Z}{Z} = \frac{\text{movement of } P}{\text{movement of } O} = A \ldots [12]$$

Ultimately, in terms of the work factor we obtain thus

$$f = \frac{w}{\mu}\frac{R}{L}\cos\gamma \ldots [13]$$

[4] "Machine Design," by A. Vallance and V. L. Doughtie, third edition, McGraw-Hill Book Company, Inc., New York, N. Y., 1951, p. 281.

Referring to Fig. 1, the lining offset θ is in practice limited to 10 deg or so, since otherwise maximum pressure is unduly increased.[3] Consequently, γ is in the order of a few degrees, so that C has to lie close to the diameter of the CP-circle and L is then virtually a function of the lining arc ϕ alone. As in practice $90° < \phi < 130°$, it also follows that $1.120 < L/R < 1.17$.[3] The effects of L and γ are thus insignificant. This leads to two important conclusions; namely (a) a highly self-energized brake shoe, producing a lot of torque for a little application effort must needs be very sensitive to fade; and (b) high-friction linings are generally preferable.

Often fixed-anchor shoes are designed with a configuration indicated in Fig. 3; this case evidently can be equated to the one in Fig. 4, merely by making $a = a' - Z(1 - \cos\delta)$.

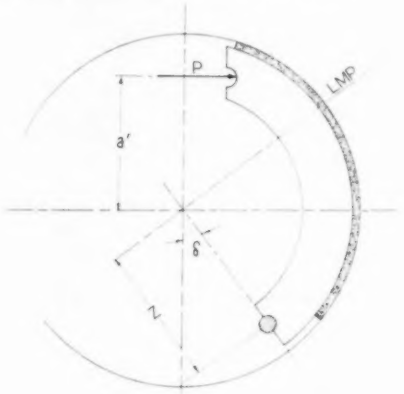

Fig. 3

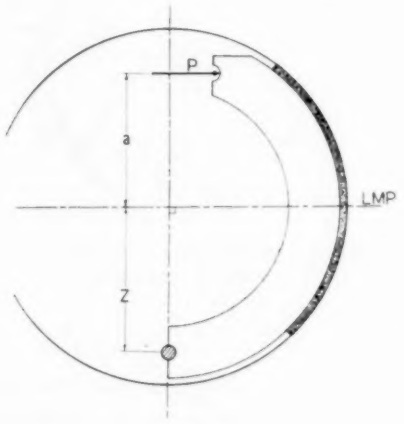

Fig. 4

Floating Shoes

By what has been stated earlier, it is self-evident that floating shoes or the like are so designed that for the nominal coefficient of friction the LMP virtually coincides with the bisector of the lining arc. Referring to Fig. 5, which shows a sliding shoe, it will be seen that in this case C moves over the flat arc of the CP-circle,[2] so that for a few degrees movement L remains constant to the second order of small quantities. We may write, thus, with good approximation

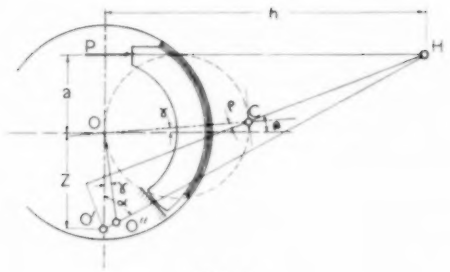

FIG. 5

$$dL/d\rho = 0 \quad \ldots\ldots [14]$$

Also when engaged, the shoe has a virtual anchor at O^* which is so situated that $Z' = O^*O$ is perpendicular to OC within a degree or so. Movement of P may be defined, therefore, by

$$A = \frac{a + Z' \cos \gamma}{Z'} \quad \ldots\ldots [15]$$

In turn, Z' may be obtained from

$$Z' \sin (\alpha + \gamma) = Z \sin \alpha \quad \ldots\ldots [16]$$

so that

$$A = \cos \gamma + \frac{a \sin (\alpha + \gamma)}{Z \sin \alpha}$$

$$= \cos \gamma + \frac{a}{Z} (\cos \gamma + \cot \alpha \sin \gamma) \quad \ldots\ldots [17]$$

A further criterion is that for floating shoes the point H and hence h remain fixed. From $\Delta BH'H$ and ΔBOD in Fig. 2, we have then

$$h = (a + Z) \tan \alpha = a \cot \beta + L \sin \rho \operatorname{cosec} \beta \ldots [18]$$

On eliminating $\tan \alpha$ from Equations [17] and [18], ultimately we obtain

$$A = \frac{a + Z}{Z} \left[\cos \gamma + \frac{a \sin \beta \sin \gamma}{a \cos \beta + L \sin \rho} \right] \ldots\ldots [19]$$

Next, to evaluate the expression in the parentheses of Equation [7], on differentiating Equation [18], we have

$$\frac{d\beta}{d\rho} = \frac{L \cos \rho}{h \cos \beta + a \sin \beta} \quad \ldots\ldots [20]$$

or if h is eliminated with the aid of Equation [18], we have

$$\frac{d\beta}{d\rho} = \frac{L \sin \beta \cos \rho}{a + L \sin \rho \cos \beta} \quad \ldots\ldots [21]$$

With Equations [14] and [21] the expression in parentheses of Equation [7] becomes

$$[\ ] = \cos \beta \cos \rho + \sin \beta \sin \rho \frac{L \sin \beta \cos \rho}{a + L \sin \rho \cos \beta} \ldots [22]$$

and after some manipulation we obtain

$$f = \frac{K}{\mu} \frac{R}{L} \frac{Z}{a + Z} \left[\frac{a \cos \beta + L \sin \rho}{a + L \sin \rho \cos \beta} \right] \cos \rho \ldots [23]$$

To express f in terms of w, Equations [19] and [23] may be now combined to give

$$f = \frac{w}{\mu} \frac{R}{L} \left[\frac{(a \cos \beta + L \sin \rho) \cos \gamma}{a + L \sin \rho \cos \beta} + \frac{a \sin \beta \sin \gamma}{a + L \sin \rho \cos \beta} \right] \cos \rho \ldots [24]$$

Considering further that $\beta = \gamma + \rho$, the foregoing may be simplified to

$$f = \frac{w}{\mu} \frac{R}{L} \left[\frac{a \cos^2 \rho + L \sin \rho \cos \rho \cos \gamma}{a + L \sin \rho \cos (\gamma + \rho)} \right] \ldots [25]$$

or in more conventional terms, with $\rho = \tan^{-1} \mu$, the final result is

$$f = \frac{w}{\mu} \frac{R}{L} \left[1 - \frac{\mu^2 (a/L - \sin \gamma)}{a/L(1 + \mu^2) + \mu \cos \gamma - \mu^2 \sin \gamma} \right] \ldots [26]$$

A comparison of Equations [13] and [26] shows much resemblance. But whereas in Equation [13] the angle γ is a measure of the lining offset θ, in Equation [26], γ indicates merely the lining disposition for a ($\theta \sim 0$) offset. For a fixed-anchor shoe $\gamma \leqslant 4°$ but for shoes with two degrees of freedom of movement $-30° \leqslant \gamma \leqslant 20°$. Consequently, γ may be neglected in Equation [13], and we may write

$$f_0 = \frac{w}{\mu} \frac{R}{L} \quad \ldots\ldots [27]$$

which we may use as a yardstick to evaluate the difference between fixed and floating shoes. From Equations [26] and [27] it follows then that

$$f/f_0 = 1 - \frac{\mu^2 \left(\frac{a}{L} - \sin \gamma \right)}{\frac{a}{L}(1 + \mu^2) + \mu \cos \mu - \mu^2 \sin \gamma} \quad \ldots\ldots [28]$$

This equation is plotted in Fig. 6 and shows that in practice floating shoes or the like are functionally quite superior to those of the fixed-anchor type. It also shows that negative values of γ seem preferable from the present point of view.

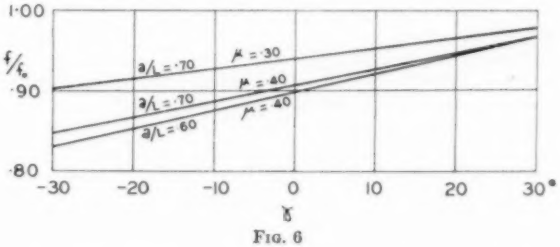

FIG. 6

Once again Equations [15] to [28] were derived for a leading shoe, but are equally valid for a trailing one if the signs of ρ or μ are changed.

CONCLUSIONS

The foregoing leads to some quite basic concepts in shoe-brake design. Perhaps the most important point is that sensitivity to fade f directly increases with w, and conversely. This explains why brake fade is such an acute problem on current American motor cars. The demand for a light pedal load necessitates high w which increases f automatically to such a level that secondary effects cannot possibly correct it. Conversely, the relationship between f and w has been realized intuitively long ago by the designers of certain foreign cars who used brakes with $f \leqslant 1$.

Naturally, for such brakes a power boost is unavoidable; on a famous make it has been standard equipment for the past 20 years. This shows indeed that the full advantage of some power-braking system consists not only in light application load, but also in the use of such fade-resistant brakes which could not otherwise be employed at all. Unfortunately, this point seems to have been overlooked hitherto on American motor vehicles.

The next important point concerns the use of floating versus fixed anchor shoes. Floating shoes or the like, being self-aligning, tolerate much wider production limits and are thus much more economical to produce than those of the fixed-anchor type. The foregoing has shown that, far from having to sacrifice some functional advantages for ease of production, floating shoes have an over-all superiority.

Tensor Flexibility Analysis of Closed-Loop Piping Systems

By J. W. SOULE,[1] SWARTHMORE, PA.

A technique is presented for applying Kirchhoff's laws to the more complex structures, using the tensor method of analysis presented in previous papers by the author. Tensor formulas are used to solve a typical closed-loop piping system containing inclined branches.

Introduction

THE author developed in two previous papers (1, 2)[2] a general procedure by means of which the basic tensor concepts and transformation formulas derived by Kron (3) could be used for the flexibility analysis of highly complex systems. Experience has shown that there are two troublesome complicating factors which frequently occur in applying either the tensor method or any of the various other methods of flexibility analysis:

1 Closed-loop systems, or systems which contain branches connected in parallel. (It is hoped that, after reading the theory to follow, the reader will recognize all piping systems as closed-loop systems.)

2 Branches inclined with respect to the co-ordinate axes.

The present paper will show in detail how each of these difficulties can be overcome by use of the proper techniques in applying the general tensor method which was developed previously. However, before proceeding with a specific problem, a few remarks are in order, to help the reader form the proper concept of the piping system as an elastic structure, and so help him visualize what actually happens in a structure subjected to given deflections. It is assumed, in the theory to follow, that the reader has familiarized himself with the fundamentals, by following through the discussion and the examples for constructing the basic **A** flexibility matrix, the **B**-matrix expressing the conditions of static equilibrium in the structure, and the **C** connection tensor, as given in the author's previous papers (1, 2). A detailed discussion of the role played by the connection tensor and of tensor mathematics in general would be valuable to the reader, but is beyond the scope of this paper and may be found in reference (3).

Theory

Although the tensor method has been commonly thought of as a method for analyzing electrical networks, it is important to note that if force is substituted for current and deflection for voltage drop, the elastic structure obeys Kirchhoff's laws just as an electric circuit does. With proper regard for sign, the sum of the forces leaving a point in the structure equals the sum of those entering it. This statement follows from the conditions of static equilibrium: $\Sigma F = 0$; and $\Sigma M = 0$. Also, if we include the connected equipment and building as part of the structure, we see that, with proper regard for sign, the sum of the deflections around any loop is identically zero. This is simply another way of saying that the mismatch due to differences in expansion around any complete circuit is corrected by the deflection, so that the structure does not come apart. The mismatch plays the same role in the elastic circuit as the battery does in applying Kirchhoff's law for voltage drop around various loops in an electric circuit. This concept can be of great help in visualizing the physical meaning of the tensor equations.

It now becomes apparent why a tensor method of analysis which was valid for electric circuits can be used for the analysis of an elastic structure as well. Tensor transformations, which were derived from the fact that the product **EI**, current times voltage, or instantaneous power, was invariant in changing from one reference frame to another, are true for structures because the tensor product **DF**, deflection times force, or total work, is invariant for the same system in all reference frames.

In order to apply tensor concepts to an elastic structure we must visualize a tensor force as flowing through the system, making a complete loop so as to complete a circuit, the components of the tensor changing value at each point of the circuit. However, the operators which determine these values, instead of being resistance, inductance, capacitance, as in the electrical network, are simply the laws of static equilibrium: $\Sigma F = 0$; $\Sigma M = 0$. Using these relations, we can always write the components of a tensor force at one point in the structure in terms of its components at any other point by the use of an appropriate matrix, which we call the **B**-matrix. In certain cases the **B**-matrix may happen to be a unit matrix, in which case we denote it as **I**. A little reflection will show the reader that, starting at any given point, the forces in the system actually do travel complete circuits through the connected equipment and back to the starting point. This is the *only* way a system *can* satisfy the conditions of static equilibrium. The use of the **B**-matrix to express the relationships between the components of the force tensor as it flows through the structure is a valuable technique, since it enables us to write out the elements of the connection tensor by inspection of the diagram.

Before applying the theory to an actual system, it is desirable to outline a general procedure which may be used to solve any flexibility problem. The procedure was described in reference (1) but is repeated here in greater detail for the reader's convenience.

1 Analyze and write the equation of performance for each component system as if the other component systems were nonexistent. The coefficients of the forces and moments in these equations form the flexibility matrixes of the system, and are carried through the analysis as $\mathbf{A}_1$, $\mathbf{A}_2$, and so on, the subscripts indicating which branch is referred to. Of course, it makes no difference whether these matrixes are obtained by the dummy-load method, moment areas, or any other applicable method.

2 Write the equation of the primitive system consisting of the several isolated systems in matrix notation, in the form $\mathbf{ZF} = \mathbf{D}$. The **Z**-matrix simply consists of the flexibility matrixes of all

[1] Designer, United Engineers and Constructors, Inc., Philadelphia, Pa.

[2] Numbers in parentheses refer to the Bibliography at the end of the paper.

Contributed by the Applied Mechanics Division and presented at the Fall Meeting, Hartford, Conn., September 23–25, 1957, of The American Society of Mechanical Engineers.

Discussion of this paper should be addressed to the Secretary, ASME, 29 West 39th Street, New York, N. Y., and will be accepted until April 10, 1958, for publication at a later date. Discussion received after the closing date will be returned.

Note: Statements and opinions advanced in papers are to be understood as individual expressions of their authors and not those of the Society. Manuscript received by ASME Applied Mechanics Division, January 24, 1956. Paper No. 57—F-3.

the component systems arranged on the main diagonal of a larger matrix.

3 Draw the force-flow diagram showing how the component systems are interconnected.

4 Denoting the variables of the interconnected system by a prime, write out by inspection of the diagram the old tensor forces in terms of the new, thus establishing the elements of the connection tensor $\mathbf{C}$ by means of the relation $\mathbf{F} = \mathbf{CF}'$. Of course, the variables of the interconnected system must be chosen by the analyst so that the number of final equations will equal the number of unknowns. However, this choice is usually a quite obvious one.

5 Transform the original $\mathbf{Z}$-tensor to the new reference frame by the formula $\mathbf{Z}' = \mathbf{C}_t\mathbf{ZC}$.

6 The equation of the interconnected system can now be written as $\mathbf{Z}'\mathbf{F}' = \mathbf{D}'$. Once the equation of the system has been obtained, it can be expanded by the rules of matrix multiplication and the resulting simultaneous equations solved by standard procedures such as Cramer's rule, Crout's method, or by electronic computer.

We can now proceed to show how the foregoing general method of procedure can be adapted to the solution of a problem containing closed loops or inclined branches, as shown in Fig. 1.

If we draw a diagram of the primitive system, showing the force tensor for each branch before the system is interconnected, we obtain the diagram shown in Fig. 2. It should be noted that, since the tensor $\mathbf{F}_j$ is shown at point d, the $\mathbf{A}_j$ flexibility matrix must be computed using the co-ordinates at the same point d. Similarly, $\mathbf{A}_m$ and $\mathbf{F}_m$ are at point c. $\mathbf{A}_i$ and $\mathbf{F}_i$ are also at point c, but $\mathbf{A}_n$ and $\mathbf{F}_n$ are at e, and so on. The equation of the primitive system is $\mathbf{ZF} = \mathbf{D}$, and the elements are shown in Fig. 3.

The diagram of the interconnected system can now be drawn, as shown in Fig. 4. Since there appear to be several paths available through the system, the question arises as to which paths the force tensors will follow. The trick in solving such complex problems is arbitrarily to select enough variables to determine the system completely, remembering that each branch in the interconnected system must be traversed at least once. It must be realized that there is no single set of paths which is the only correct one, but several choices are possible, any one of which will lead to a proper set of equations provided the deflections, when summed algebraically around the loops, follow the same paths as the corresponding forces. In the present case, the minimum number of loops to determine the system completely is three (Appendix). With this in mind, we can choose a set of variables and mark them on the diagram as shown in Fig. 4. The reader should notice that the $\mathbf{F}_j'$ tensor has been routed around the loop starting and finishing at point d. We have chosen to refer to this tensor as $\mathbf{F}_j'$ but we could just as easily have labeled it $\mathbf{F}_k'$, or we might have used some other subscript, since its relation to the old (unprimed) variables will be taken care of automatically by the connection tensor $\mathbf{C}$. The $\mathbf{B}$-matrixes can be constructed from the conditions of static equilibrium as explained in reference (1), except for $\mathbf{B}_1$ and $\mathbf{B}_2$ which relate the forces and moments in the auxiliary co-ordinate systems of branches i and l to the co-ordinate systems shown in Fig. 1. A method for constructing matrixes such as $\mathbf{B}_1$ and $\mathbf{B}_2$ will be shown later. The elements of the $\mathbf{B}$-matrixes need not be shown in order to analyze the problem, since we can insert the symbols $\mathbf{B}_1$ and $\mathbf{B}_2$ into the connection tensor and carry on with the analysis, leaving the arithmetic until later.

Writing out the old forces in terms of the new by inspection of Figs. 2 and 4, we obtain

$$\left.\begin{aligned}
\mathbf{F}_i &= \mathbf{IF}_i' \\
\mathbf{F}_j &= \mathbf{IF}_j' + \mathbf{B}_2\mathbf{F}_l' \\
\mathbf{F}_k &= \mathbf{IF}_j' \\
\mathbf{F}_l &= \mathbf{IF}_l' \\
\mathbf{F}_m &= \mathbf{B}_1\mathbf{F}_i' + \mathbf{B}_2\mathbf{F}_j' + \mathbf{B}_2\mathbf{B}_2\mathbf{F}_l' \\
\mathbf{F}_n &= \mathbf{B}_4\mathbf{B}_1\mathbf{F}_i' + \mathbf{B}_2\mathbf{B}_2\mathbf{F}_l'
\end{aligned}\right\} \quad \ldots\ldots\ldots [1]$$

The coefficients of the variables in Equations [1] form the $\mathbf{C}$ connection tensor in accordance with the relation $\mathbf{F} = \mathbf{CF}'$ and the $\mathbf{C}$-tensor is shown in Fig. 5.

Since $\mathbf{C}$ and $\mathbf{Z}$ are known, we can now proceed to find $\mathbf{Z}'$ using

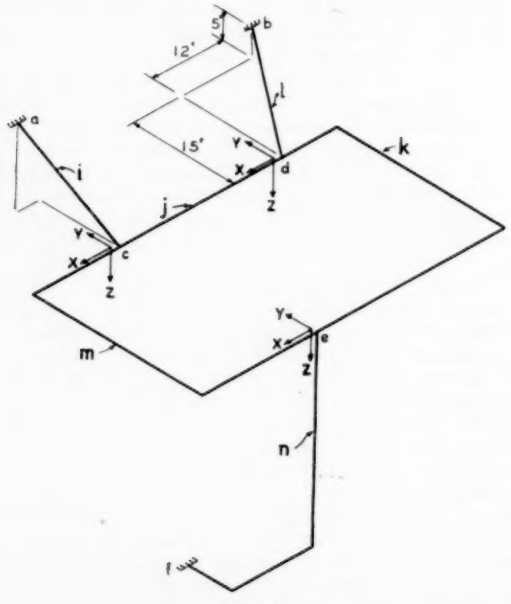

FIG. 1

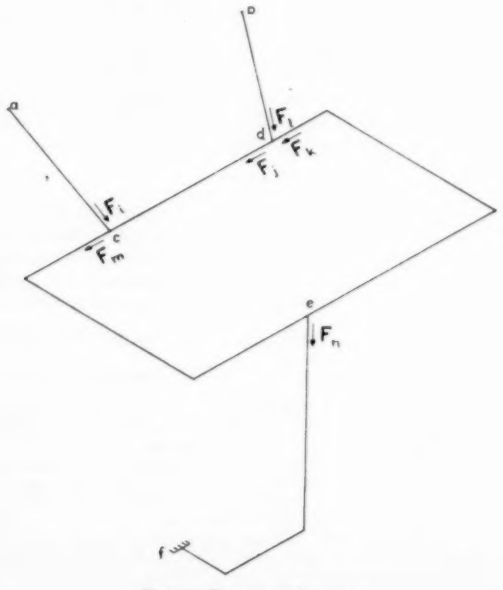

FIG. 2 PRIMITIVE SYSTEM

the formula $\mathbf{Z}' = \mathbf{C}_t\mathbf{Z}\mathbf{C}$, and $\mathbf{Z}'$ turns out as shown in Fig. 6. The equation of the interconnected system is $\mathbf{Z}'\mathbf{F}' = \mathbf{D}'$, in which

$$\mathbf{F}' = \begin{bmatrix} \mathbf{F}_i' \\ \mathbf{F}_j' \\ \mathbf{F}_l' \end{bmatrix} \quad \text{and} \quad \mathbf{D}' = \begin{bmatrix} \mathbf{D}_i' \\ \mathbf{D}_j' \\ \mathbf{D}_l' \end{bmatrix}$$

The equation $\mathbf{Z}'\mathbf{F}' = \mathbf{D}'$ can be expanded by the rules of matrix multiplication into a system of 18 simultaneous equations, which form the equations of performance of the given piping system. The **A**-matrixes and the **B**-matrixes, which must be known in order to carry out the multiplications, are constructed as described in reference (1) except for matrixes such as $\mathbf{B}_1$ and $\mathbf{B}_2$, which express the forces and moments in the x, y, z-co-ordinate system in terms of a u, v, w, auxiliary co-ordinate system in which the axes are all oriented either parallel or perpendicular to the branch under consideration. (The **A** flexibility matrixes of the inclined branches are computed relative to the auxiliary u, v, w-systems.)

We will now consider the case of matrix $\mathbf{B}_2$ as an example of the way in which such matrixes can be constructed. The only additional mathematical tools needed are the fundamental formulas of vector analysis, which may be obtained from any one of several texts, two of which are references (4) and (5).

Branch l is shown in Fig. 7 in its relation to both the u, v, w, and the x, y, z-systems. For problems which contain inclined branches it is best to use only right-hand co-ordinate systems,

$$\mathbf{Z} = \begin{bmatrix} \mathbf{A}_i & & & & & \\ & \mathbf{A}_j & & & & \\ & & \mathbf{A}_k & & & \\ & & & \mathbf{A}_l & & \\ & & & & \mathbf{A}_m & \\ & & & & & \mathbf{A}_n \end{bmatrix}$$

$$\mathbf{F} = \begin{bmatrix} \mathbf{F}_i \\ \mathbf{F}_j \\ \mathbf{F}_k \\ \mathbf{F}_l \\ \mathbf{F}_m \\ \mathbf{F}_n \end{bmatrix} \qquad \mathbf{D} = \begin{bmatrix} \mathbf{D}_i \\ \mathbf{D}_j \\ \mathbf{D}_k \\ \mathbf{D}_l \\ \mathbf{D}_m \\ \mathbf{D}_n \end{bmatrix}$$

FIG. 3 MATRIX ELEMENTS FOR PRIMITIVE SYSTEM

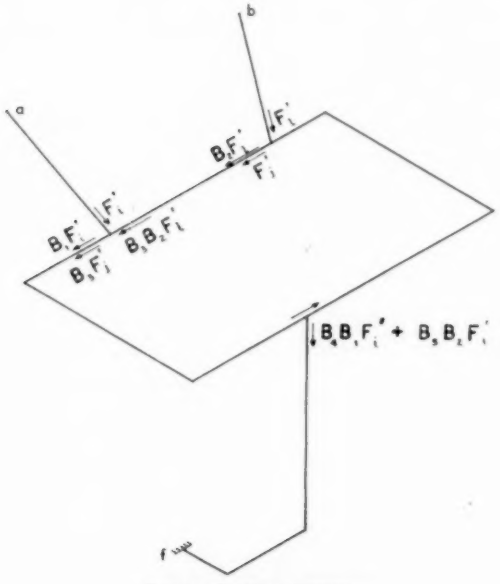

FIG. 4 DERIVED SYSTEM

$$\mathbf{C} = \begin{array}{c|ccc} & i' & j' & l' \\ \hline i & \mathbf{I} & & \\ j & & \mathbf{I} & \mathbf{B}_2 \\ k & & \mathbf{I} & \\ l & & & \mathbf{I} \\ m & \mathbf{B}_1 & \mathbf{B}_3 & \mathbf{B}_3\mathbf{B}_2 \\ n & \mathbf{B}_4\mathbf{B}_1 & & \mathbf{B}_5\mathbf{B}_2 \end{array}$$

FIG. 5 C CONNECTION TENSOR

$$\mathbf{Z}' = \mathbf{C}_t\,\mathbf{Z}\,\mathbf{C} =$$

$\mathbf{A}_i + \widetilde{\mathbf{B}}_1\mathbf{A}_m\mathbf{B}_1 + \widetilde{\mathbf{B}}_4\widetilde{\mathbf{B}}_1\mathbf{A}_n\mathbf{B}_4\mathbf{B}_1$	$\widetilde{\mathbf{B}}_1\mathbf{A}_m\mathbf{B}_3$	$\widetilde{\mathbf{B}}_1\mathbf{A}_m\mathbf{B}_3\mathbf{B}_2 + \widetilde{\mathbf{B}}_4\widetilde{\mathbf{B}}_1\mathbf{A}_n\mathbf{B}_3\mathbf{B}_2$
$\widetilde{\mathbf{B}}_3\mathbf{A}_m\mathbf{B}_1$	$\mathbf{A}_j + \mathbf{A}_k + \widetilde{\mathbf{B}}_3\mathbf{A}_m\mathbf{B}_3$	$\mathbf{A}_j\mathbf{B}_2 + \widetilde{\mathbf{B}}_3\mathbf{A}_m\mathbf{B}_3\mathbf{B}_2$
$\widetilde{\mathbf{B}_3\mathbf{B}_2}\mathbf{A}_m\mathbf{B}_1 + \widetilde{\mathbf{B}_3\mathbf{B}_2}\mathbf{A}_n\mathbf{B}_4\mathbf{B}_1$	$\widetilde{\mathbf{B}_2}\mathbf{A}_j + \widetilde{\mathbf{B}_3\mathbf{B}_2}\mathbf{A}_m\mathbf{B}_3$	$\widetilde{\mathbf{B}_2}\mathbf{A}_j\mathbf{B}_2 + \mathbf{A}_l + \widetilde{\mathbf{B}_3\mathbf{B}_2}\mathbf{A}_m\mathbf{B}_3\mathbf{B}_2 + \widetilde{\mathbf{B}_3\mathbf{B}_2}\mathbf{A}_n\mathbf{B}_3\mathbf{B}_2$

FIG. 6 $\mathbf{Z}'$-TENSOR OF THE DERIVED SYSTEM. TILDE INDICATES A TRANSPOSED MATRIX

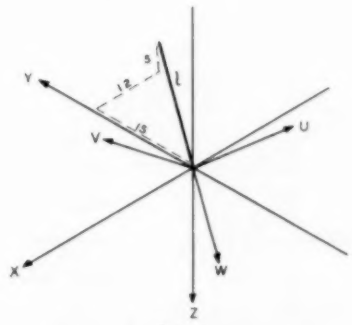

FIG. 7

that is, systems such that $\mathbf{x} \times \mathbf{y} = \mathbf{z}$; $\mathbf{y} \times \mathbf{z} = \mathbf{x}$; and $\mathbf{z} \times \mathbf{x} = \mathbf{y}$ (in cyclic permutation), since this will eliminate confusion in using the vector formulas. The co-ordinate systems used in this sample problem were purposely drawn as right-hand systems for this very reason. In the theory to follow, scalars will be shown plain face and unit vectors will appear in bold lower case, as $\mathbf{x}$, $\mathbf{y}$, $\mathbf{z}$, or $\mathbf{u}$, $\mathbf{v}$, $\mathbf{w}$.

For branch l, $\mathbf{F}_{xyz} = \mathbf{B}_2\mathbf{F}_{uvw}$ and the u, v, w-axes are mutually perpendicular. The u, v, w-system may be oriented so that one axis, say v, lies in the xz-plane. (This is convenient but not mandatory.) Let w coincide with branch l, and to complete the system, draw u perpendicular to both v and w. Since the $\mathbf{A}$ flexibility matrix for branch l is computed in the u, v ,w-system, u should always be regarded as abscissa and w always as ordinate to conform with the conventions adopted in reference (1).

Moments in the uv-plane can be represented by vectors parallel to w; in the uw-plane by vectors parallel to v; and in the vw-plane by vectors parallel to u, according to the right-hand rule for cross products of vectors. Similar rules will hold in the x, y, z-system; so, with this understanding we can write (referring to Fig. 7)

$$\left.\begin{aligned} F_x &= \cos\theta_{ux}F_u + \cos\theta_{vx}F_v + \cos\theta_{wx}F_w \\ F_y &= \cos\theta_{uy}F_u + \cos\theta_{vy}F_v + \cos\theta_{wy}F_w \\ F_z &= \cos\theta_{uz}F_u + \cos\theta_{vz}F_v + \cos\theta_{wz}F_w \\ M_{xy} &= \cos\theta_{wx}M_{uv} - \cos\theta_{vx}M_{uw} + \cos\theta_{ux}M_{vw} \\ M_{xz} &= -\cos\theta_{wy}M_{uv} + \cos\theta_{vy}M_{uw} - \cos\theta_{uy}M_{vw} \\ M_{yz} &= \cos\theta_{wz}M_{uv} - \cos\theta_{vz}M_{uw} + \cos\theta_{uz}M_{vw} \end{aligned}\right\} \quad \ldots [2]$$

In the foregoing equations θ_{ux} = the angle between positive directions of z and w; θ_{vz} = the angle between positive directions of z and v, and so on. M_{uv} = magnitude of the vector representing a moment in the uv-plane; M_{uw} = magnitude of the vector representing a moment in the uw-plane, and so on. (Note that the vector $\mathbf{M}_{uv}$ is parallel to w; the vector $\mathbf{M}_{uw}$ is parallel to v; and $\mathbf{M}_{vw}$ is parallel to u.)

The coefficients in Equations [2] form the $\mathbf{B}_2$-matrix. Since the development was based on standard vector formulas and conventions, it may be adopted for the general case as well as this specific problem, the only restriction being that the sign conventions mentioned previously regarding forces, moments, and angles which were used throughout, must be adhered to. So far, then, the $\mathbf{B}_1$ and $\mathbf{B}_2$-matrixes are derived in general form and appear as shown in Fig. 8. For some problems it may be useful to have the $\mathbf{B}_1$ and $\mathbf{B}_2$-matrixes in the inverse form where $\mathbf{F}_{uvw} = \mathbf{B}\mathbf{F}_{xyz}$, and for that reason the inverse $\mathbf{B}$ has been derived in a similar manner, and is shown in Fig. 9.

All that remains is to show how the elements $\cos\theta_{ux}$, $\cos\theta_{vz}$, and so on, are obtained and substituted with proper sign into the $\mathbf{B}$-matrix. Referring to Fig. 7, we see that since the unit vector $\mathbf{w}$ is parallel to l and the length of l is $(5^2 + 12^2 + 15^2)^{1/2} = \sqrt{394}$, we have $\cos\theta_{wz} = 12/\sqrt{394}$. (This value will supply elements B_{13} and B_{64} in Fig. 8.) Also $\cos\theta_{wy} = -15/\sqrt{394}$ (elements B_{23} and B_{54} become $-15/\sqrt{394}$ and $+15/\sqrt{394}$, respectively). Also, $\cos\theta_{wx} = +5/\sqrt{394}$ (elements B_{33} and B_{44}). Using the foregoing direction cosines we can write

$$\mathbf{w} = \frac{12}{\sqrt{394}}\mathbf{x} - \frac{15}{\sqrt{394}}\mathbf{y} + \frac{5}{\sqrt{394}}\mathbf{z} \quad \ldots [3]$$

$$\mathbf{v} = \cos\theta_{vx}\mathbf{x} + \cos\theta_{vz}\mathbf{z} \quad \ldots [4]$$

Since $\mathbf{v}$ is perpendicular to $\mathbf{w}$

$$\mathbf{v} \cdot \mathbf{w} = \frac{12}{\sqrt{394}}\cos\theta_{vx} + \frac{5}{\sqrt{394}}\cos\theta_{vz} = 0$$

and therefore

$$\cos\theta_{vx} = -\frac{5}{12}\cos\theta_{vz} \quad \ldots [5]$$

Since $\mathbf{v}$ is a unit vector its length is 1.0, and

$$1 = (\cos^2\theta_{vx} + \cos^2\theta_{vz})^{1/2}$$

Squaring both sides

$$1 = \cos^2\theta_{vx} + \cos^2\theta_{vz} \quad \ldots [6]$$

Substituting Equation [5] into [6] we obtain

$$1 = \frac{25}{144}\cos^2\theta_{vz} + \cos^2\theta_{vz} = \frac{169}{144}\cos^2\theta_{vz}$$

and therefore

$$\cos\theta_{vz} = -\frac{12}{13}, \quad \text{and} \quad \cos\theta_{vx} = \left(-\frac{5}{12}\right)\left(-\frac{12}{13}\right) = \frac{5}{13}$$

We know that $\mathbf{u} \times \mathbf{v} = \mathbf{w}$
and

$\mathbf{B} =$

$\cos\theta_{ux}$	$\cos\theta_{vx}$	$\cos\theta_{wx}$			
$\cos\theta_{uy}$	$\cos\theta_{vy}$	$\cos\theta_{wy}$			
$\cos\theta_{uz}$	$\cos\theta_{vz}$	$\cos\theta_{wz}$			
			$\cos\theta_{wz}$	$-\cos\theta_{vz}$	$\cos\theta_{uz}$
			$-\cos\theta_{wy}$	$\cos\theta_{vy}$	$-\cos\theta_{uy}$
			$\cos\theta_{wx}$	$-\cos\theta_{vx}$	$\cos\theta_{ux}$

FIG. 8 $\mathbf{B}$-MATRIX FOR $\mathbf{F}_{xyz} = \mathbf{B}\mathbf{F}_{uvw}$

$\mathbf{B} =$

$\cos\theta_{ux}$	$\cos\theta_{uy}$	$\cos\theta_{uz}$			
$\cos\theta_{vx}$	$\cos\theta_{vy}$	$\cos\theta_{vz}$			
$\cos\theta_{wx}$	$\cos\theta_{wy}$	$\cos\theta_{wz}$			
			$\cos\theta_{wz}$	$-\cos\theta_{wy}$	$\cos\theta_{wx}$
			$-\cos\theta_{vz}$	$\cos\theta_{vy}$	$-\cos\theta_{vx}$
			$\cos\theta_{uz}$	$-\cos\theta_{uy}$	$\cos\theta_{ux}$

FIG. 9 $\mathbf{B}$-Matrix for $\mathbf{F}_{uvw} = \mathbf{B}\mathbf{F}_{xyz}$

$$\mathbf{u} \times \mathbf{v} = \begin{vmatrix} \mathbf{x} & \mathbf{y} & \mathbf{z} \\ \cos\theta_{ux} & \cos\theta_{uy} & \cos\theta_{uz} \\ \frac{5}{13} & 0 & -\frac{12}{13} \end{vmatrix}$$

Expanding the determinant, we obtain

$$-\frac{12}{13}\cos\theta_{uy}\mathbf{x} + \left(\frac{5}{13}\cos\theta_{uz} + \frac{12}{13}\cos\theta_{ux}\right)\mathbf{y} - \frac{5}{13}\cos\theta_{uy}\,\mathbf{z} = \mathbf{w}$$

Setting this value of $\mathbf{w}$ equal to the value in Equation [3]

$$-\frac{12}{13}\cos\theta_{uy} = \frac{12}{\sqrt{394}}, \quad \text{so} \quad \cos\theta_{uy} = -\frac{13}{\sqrt{394}}$$

and

$$\frac{5}{13}\cos\theta_{uz} + \frac{12}{13}\cos\theta_{ux} = -\frac{15}{\sqrt{394}} \quad \ldots\ldots\ldots [7]$$

But we also know that $\mathbf{u}\cdot\mathbf{v} = 0$, and this yields

$$\cos\theta_{vz}\cos\theta_{ux} + \cos\theta_{vx}\cos\theta_{uz} = 0$$

Substituting the values already found for $\cos\theta_{vz}$ and $\cos\theta_{vx}$ in the foregoing, we obtain

$$\frac{5}{13}\cos\theta_{ux} - \frac{12}{13}\cos\theta_{uz} = 0$$

and therefore

$$\cos\theta_{uz} = \left(\frac{13}{12}\right)\left(\frac{5}{13}\right)\cos\theta_{ux} = \frac{5}{12}\cos\theta_{ux}$$

Substituting this value in Equation [7], we obtain

$$\frac{25}{156}\cos\theta_{ux} + \frac{12}{13}\cos\theta_{ux} = -\frac{15}{\sqrt{394}}$$

Solving for $\cos\theta_{ux}$, we obtain

$$\cos\theta_{ux} = -\frac{15}{\sqrt{394}}\left(\frac{156}{169}\right) = -\frac{180}{13\sqrt{394}}$$

$$\mathbf{B}_2 = \begin{array}{|c|c|c|c|c|c|} \hline -\frac{180}{13\sqrt{394}} & \frac{5}{13} & \frac{12}{\sqrt{394}} & & & \\ \hline -\frac{13}{\sqrt{394}} & & -\frac{15}{\sqrt{394}} & & & \\ \hline -\frac{75}{13\sqrt{394}} & -\frac{12}{13} & \frac{5}{\sqrt{394}} & & & \\ \hline & & & \frac{5}{\sqrt{394}} & \frac{12}{13} & -\frac{75}{13\sqrt{394}} \\ \hline & & & \frac{15}{\sqrt{394}} & & \frac{13}{\sqrt{394}} \\ \hline & & & \frac{12}{\sqrt{394}} & -\frac{5}{13} & -\frac{180}{13\sqrt{394}} \\ \hline \end{array}$$

FIG. 10

and

$$\cos\theta_{uz} = \frac{5}{12}\cos\theta_{ux} = \left(-\frac{15}{\sqrt{394}}\right)\left(\frac{156}{169}\right)\left(\frac{5}{12}\right) = -\frac{75}{13\sqrt{394}}$$

Substituting the values just found into Fig. 8, we obtain all the elements of $\mathbf{B}_2$ for the interconnected system shown in Fig. 4, and the matrix $\mathbf{B}_2$ appears as shown in Fig. 10. The elements of $\mathbf{B}_i$ for branch i could be found by a similar procedure.

Conclusion

For closed-loop systems such as the one considered here, an interesting problem can arise when computing the elements of the deflection matrix $\mathbf{D}_j'$. Suppose, for example, that the operating temperatures for branches j, m, and k were different from each other. The deflections can be computed by noting that, in accordance with the principles enumerated earlier in the paper, all that is necessary is to imagine the structure cut apart just to the right or left of point d and compute the mismatch due to thermal expansion around the j, m, k-loop alone. The proper deflections are the amounts needed to correct the mismatch. Since the $\mathbf{F}_j'$-tensor traverses the loop in the order j, m, k (that is, from point d_j to point d_k in Fig. 11), the deflection will be measured as the distance point d_j must be deflected to meet point d_k. For example, element D_a' would be negative in Fig. 11(a), but positive for the case shown in Fig. 11(b). It will be noted that the mismatch is opposite in sign to the deflection, so that their sum is zero (Kirchhoff's law). For the case where the temperatures do not vary around the loop and the pipe material also is constant, so that there is no mismatch, the matrix $\mathbf{D}_j' = \mathbf{O}$.

A cautionary note should be added concerning the deflections for points such as a and b which lie on inclined branches. The important thing to remember is that the deflection matrixes $\mathbf{D}_i'$ and $\mathbf{D}_l'$ which represent the deflections of points a and b, respectively, must be compatible with the chosen reference frame as expressed in the $\mathbf{C}$ connection tensor. Consequently, the $\mathbf{D}_i'$ and $\mathbf{D}_l'$-matrixes for the present case should be expressed in terms of

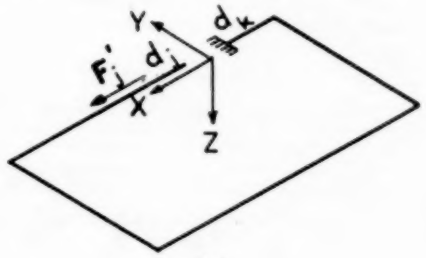

(a)

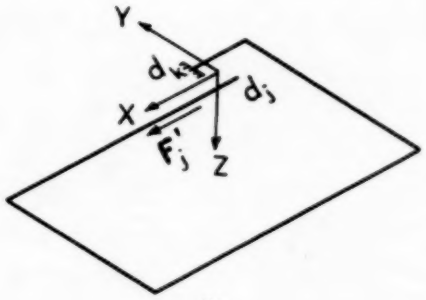

(b)

FIG. 11

the u, v, w-system, since referring to the **C** connection tensor as shown in Fig. 5, we see that $\mathbf{F}_i = \mathbf{IF}_i'$, and $\mathbf{F}_l = \mathbf{IF}_l'$. For many problems it will be convenient to use one of the **B** transformation matrixes of Fig. 8 or Fig. 9 to convert deflections from one coordinate system to the other, since it can be seen readily that, in general, at any single point of the system $\mathbf{D}_{xyz} = \mathbf{BD}_{uvw}$ and $\mathbf{D}_{uvw} = \mathbf{BD}_{xyz}$ in which the **B**-matrixes are obtained from Figs. 8 and 9, respectively.

Systems such as the one considered here also serve as a good example of the power of the tensor method as an analytical tool, serving automatically to derive the equations of performance of extremely complex systems by considering them as a collection of smaller systems whose equations are already known by fundamental theory. The connection tensor serves the analyst as a convenient "plug-in switchboard," since he can fill in its elements by inspection of the diagram, using simple symbols such as **I**, or $\mathbf{B}_1$, $\mathbf{B}_2$, and so on, to represent the complex relationships in the system. The "pick-and-shovel work" of carrying out the large number of additions, subtractions, and so on, if desired, can be performed by an electronic computer programmed to perform the multiplication **C**$_i$**ZC**, since all the necessary information describing the system is contained in the **Z**-matrix and the **C** connection tensor. It is believed that the method here presented will lend itself readily to being programmed. For the computer with a large memory storage, the **Z**-tensor and the **C**-tensor may be exhibited *in extensio;* that is, the operational forms **A** and **B** may be replaced by arrays of numbers which are their elements. For the computer having a small memory storage relative to the amount of data, the operational form of notation used throughout the paper can be used, thus reducing the size of matrix to be handled by the computer, at the expense of a slight amount of additional work to be performed by the analyst. In this connection, it is worthy of note that the tensor method as developed in the previous papers (1, 2) as well as the present paper, requires no matrix inversion other than the solution of the final equations.

Those who care to, should have no trouble adapting the methods presented here to other types of elastic structure as well. The reader who desires to experiment with tensor methods also may be interested in Kron's recent work on interconnecting highly complex structures (6, 7).

BIBLIOGRAPHY

1 "The Solution of Multiple-Branch Piping-Flexibility Problems by Tensor Analysis," by J. W. Soule, JOURNAL OF APPLIED MECHANICS, Trans. ASME, vol. 78, 1956, pp. 176–180.

2 "Tensor-Flexibility Analysis of Pipe-Supporting Systems," by J. W. Soule, JOURNAL OF APPLIED MECHANICS, Trans. ASME, vol. 78, 1956, pp. 181–184.

3 "Tensor Analysis of Networks," by Gabriel Kron, John Wiley & Sons, Inc., New York, N. Y., 1939, pp. 1–49, 62–86, 94–104, and 196–241.

4 "Advanced Calculus for Engineers," by F. B. Hildebrand, Prentice-Hall, Inc., New York, N. Y., 1949, pp. 281–288.

5 "Higher Mathematics," by R. C. Burington and C. C. Torrance, McGraw-Hill Book Company, Inc., New York, N. Y., 1939, pp. 677–688.

6 "Solving Highly Complex Elastic Structures in Easy Stages," by Gabriel Kron, JOURNAL OF APPLIED MECHANICS, Trans. ASME, vol. 77, 1955, pp. 235–244.

7 "Tensorial Analysis and Equivalent Circuits of Elastic Structures," by Gabriel Kron, *Journal of the Franklin Institute*, vol. 238, December, 1944, pp. 400–452.

Appendix

It is necessary to have some criterion by which to judge when a given system has been defined adequately by a set of chosen force tensors. The method to follow has been found useful by the author.

Consider the junction of four branches illustrated diagrammatically in Fig. 12(a). At first inspection, it might be deemed

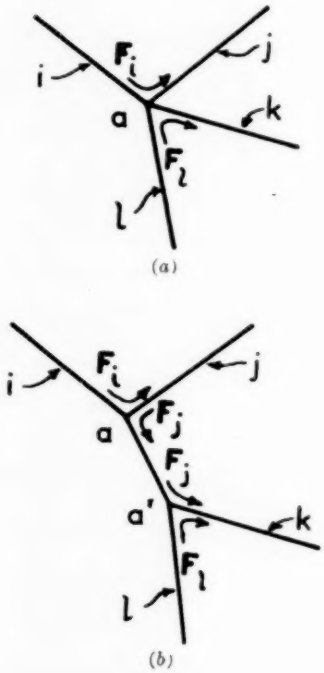

FIG. 12

adequate to solve the system by setting up the two tensors $\mathbf{F}_i$ and $\mathbf{F}_l$ as shown, since each branch would seem to have been traversed at least once. However, it may be seen by inspection of Fig. 12(b) that the system actually may be considered as containing five branches, one of which has zero length. This would not be important except for the fact that there is actually one more path necessary to describe the system than was at first supposed. Mistakes such as this can be avoided at the beginning of a problem by checking the diagram to make certain that at each junction of n-branches, at least $(n - 1)$ separate and distinct paths have been traversed.

High Order Accuracy in the Solution of Partial Differential Equations by Resistor Networks

By H. G. LANDAU,[1] NEW YORK N. Y.

In the practical solution of partial differential equations, very high accuracy is sometimes needed, particularly when the derivatives of the solution are the quantities in which we are interested. A procedure is given here for obtaining this high accuracy by a combined numerical and electric resistor-network method. The equation is first solved approximately on the resistor network; then the residuals in the corresponding finite-difference equation are evaluated numerically. These residuals are used as current inputs to the nodes of the network to obtain a correction to the first solution. If the errors in the first solution (including both experimental and lumping errors) are of the order of a few per cent, then the errors in the corrected solution will be of the order of a few hundredths of 1 per cent. The method makes possible accurate solutions without very stringent requirements on the precision of the resistors and other components of the electric circuit.

Introduction

THE numerical value of the solution of a partial differential equation must sometimes be known very exactly. This is true, for example, in solving the equations of elasticity where the solution gives the stress function, although we are interested in the stresses which must be obtained by calculating derivatives of the stress function. To obtain a given accuracy in the numerical computation of derivatives from values of a function, it is, of course, necessary that the function be known to a much higher degree of accuracy. Roughly, if second derivatives are to be calculated with an error of not more than a few per cent, then the function itself will need to be known within an error of a few hundredths of 1 per cent. In general, whenever the values of the solution of the partial differential equation are not themselves the final answer but are to be used in a further calculation, it will be necessary to know these values rather accurately.

In addition, there occur problems in which the requirements on accuracy are not very stringent, but it is necessary that we be certain that the error is within given limits. For example, in a two-dimensional steady-state heat-conduction problem in this laboratory, it was required that the temperatures at certain critical points be determined within 2 per cent. Ordinarily, the errors in resistor-network solutions of this type of problem can be expected to be somewhat smaller than this, but it is very difficult to be certain that the error in a particular value does not exceed the required limit. The method proposed here does, however, make it possible to determine bounds on the error and hence to achieve a guaranteed accuracy.

As was pointed out in a previous publication,[2] the solution of a partial differential equation by a resistor network corresponds to solving this equation numerically by replacing partial derivatives by finite differences.[3] There are two types of errors; namely, (*a*) the lumping errors and (*b*) the experimental errors.[4] The present procedure is most simply applicable to reducing the experimental errors, but also can be used to reduce the lumping errors.

As was shown before,[2] in solving the two-dimensional Poisson equation

$$\frac{\partial^2 u}{\partial x^2} + \frac{\partial^2 u}{\partial y^2} = f(x, y) \quad \ldots\ldots\ldots\ldots [1]$$

the lumping error at interior points can be made very small by the addition of diagonal resistors to the usual network. For a great many engineering problems this will be enough to bring the lumping error within the required limits. However, if still smaller errors are needed, or if the lumping errors at the boundary are the important ones, then the present method can be used to reduce simultaneously both lumping errors and experimental errors.

Procedure for Correcting Experimental Errors

To describe the procedure we must distinguish between u, the desired solution of the differential equation with its boundary conditions, v, the approximation to u which is the solution of the difference equation corresponding to the network used, and V, the voltage at a node of the resistance network. We have

$$v = cV \quad \ldots\ldots\ldots\ldots [2]$$

where c is a scale factor. Also we use V_i to indicate the voltage at the i-th node.

The equations for the network form a set of linear equations. The ith equation is the Kirchhoff equation for the currents at the ith node. These can be represented as[5]

---

[1] Research Associate in Mechanical Engineering, Columbia University.

Contributed by the Applied Mechanics Division and presented at the Fall Meeting, Hartford, Conn., September 23–25, 1957, of The American Society of Mechanical Engineers.

Discussion of this paper should be addressed to the Secretary, ASME, 29 West 39th Street, New York, N. Y., and will be accepted until April 10, 1958, for publication at a later date. Discussion received after the closing date will be returned.

Note: Statements and opinions advanced in papers are to be understood as individual expressions of their authors and not those of the Society. Manuscript received by ASME Applied Mechanics Division, October 25, 1956. Paper No. 57—F-1.

[2] "A Simple Procedure for Improved Accuracy in the Resistor-Network Solution of Laplace's and Poisson's Equation," by H. G. Landau, Journal of Applied Mechanics, Trans. ASME, vol. 79, March, 1957, pp. 93–97.

[3] This is true for the heat conduction equation when the resistor-network procedure proposed by Liebmann is used. "A New Electrical Analog Method for the Solution of Transient Heat-Conduction Problems," by G. Liebmann, Trans. ASME, vol. 78, 1956, pp. 655–665.

[4] The corresponding terms in numerical analysis are truncation errors and round-off errors.

[5] In carrying out the procedure it is not necessary to write down the equations.

$$\left.\begin{aligned} a_{11}V_1 + a_{12}V_2 + \ldots + a_{1n}V_n + g_1 &= 0 \\ a_{21}V_1 + a_{22}V_2 + \ldots + a_{2n}V_n + g_2 &= 0 \\ \ldots\ldots\ldots\ldots\ldots\ldots\ldots\ldots & \\ a_{n1}V_1 + a_{n2}V_2 + \ldots + a_{nn}V_n + g_n &= 0 \end{aligned}\right\} \quad \ldots\ldots [3]$$

For $i \neq j$, the coefficient a_{ij} here is proportional to $1/r_{ij}$, where r_{ij} is the resistance between the ith node and jth node; and

$$a_{ii} = -\sum_{j=1}^{n} a_{ij}$$

Most of the a_{ij} are, of course, zero in any large network. The g_i result from boundary values, sources, and so on; electrically they represent input currents.

Suppose we have solved the Equations [3] on the resistor network. Then we have values for V_i, $i = 1, \ldots, n$, which satisfy Equations [3] approximately. Let these observed values be V_{i0}, and let V_{i1} be the necessary corrections

$$V_i = V_{i0} + V_{i1} \ldots\ldots\ldots\ldots\ldots\ldots [4]$$

since the V_i are the exact (unknown) values.

Now if we define the residuals by

$$\rho_i = a_{i1}V_{10} + a_{i2}V_{20} + \ldots + a_{in}V_{n0} + g_i \ldots\ldots [5]$$

and substitute $V_i = V_{i0} + V_{i1}$ into Equations [3], we get

$$\left.\begin{aligned} a_{11}V_{11} + a_{12}V_{21} + \ldots + a_{1n}V_{n1} + \rho_1 &= 0 \\ a_{21}V_{11} + a_{22}V_{21} + \ldots + a_{2n}V_{n1} + \rho_2 &= 0 \\ \ldots\ldots\ldots\ldots\ldots\ldots\ldots\ldots & \\ a_{n1}V_{n1} + a_{n2}V_{21} + \ldots + a_{nn}V_{n1} + \rho_n &= 0 \end{aligned}\right\} \quad \ldots\ldots [6]$$

These equations show that the corrections V_{i1}, must satisfy the same equations as the V_i except that the input currents are now the residuals ρ_i. Hence the corrections can be found with the same network by feeding in properly adjusted input currents.

Now the ρ_i will be small quantities since the V_{i0} differ from the correct V_i by only a few per cent. In fact, if the ρ_i are not small some blunder is indicated, and the procedure up to this point should be checked carefully.

The fact that the ρ_i are small quantities means that we can introduce another scale factor and still stay within allowable voltages. Suppose this new scale factor is c_1, and V_{i1}' is the voltage actually obtained at the ith node, so that

$$V_{i1} = c_1 V_{i1}' \ldots\ldots\ldots\ldots\ldots\ldots [7]$$

and the equation for the ith node is now

$$a_{i1}V_{11}' + a_{i2}V_{21}' + \ldots + a_{in}V_{n1}' + \frac{\rho_i}{c_1} = 0 \ldots\ldots [8]$$

If the errors in the first solution are, say, 1 per cent, so that the V_{i1} are 1 per cent of V_i, the factor c_1 can be about $^1/_{100}$. The errors in the V_{i1}' as determined from a second run based on Equation [8] should also be about 1 per cent so that V_{i1}, and consequently V_i, will now be determined with an error of 0.01 per cent. This increased accuracy is made possible by the introduction of the new scale factor c_1 which is an essential point of the method.

Obviously, the process could be repeated if still higher accuracy were needed, or if the error at each stage is larger.

Example of Experimental Error Correction

As an example of this procedure, it was used to correct the experimental error in the resistor-network solution of the problem of the elastic torsion of a square section.[2] The differential equation is

$$\frac{\partial^2 u}{\partial x^2} + \frac{\partial^2 u}{\partial y^2} = -2 \ldots\ldots\ldots\ldots\ldots\ldots [9]$$

in the unit square with $u = 0$ on the boundary. This was solved using an interval of $h = {}^1/_8$, and because of symmetry only one eighth of the square need actually be set up. Two nets were used as shown in Figs. 1 and 2; the net in Fig. 1 is the usual one consisting of a square mesh. The corresponding finite-difference equation is based on the use of the H or 5-point operator at each point (see Equation [12]). The second net uses the diagonal resistors introduced[2] to reduce lumping error; this is the K or 9-point operator.

The equations for the first case (5-point operator) with $R = 1000$ ohms, $I = 15$ microamp, $c = {}^1/_{270}$, V in millivolts, are

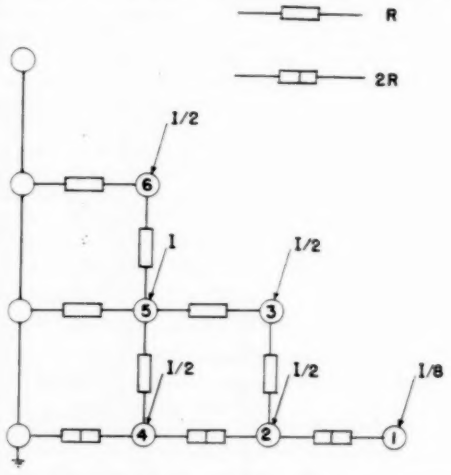

Fig. 1 Usual Network for Elastic-Torsion Problem, Based on H or 5-Point Difference Operator

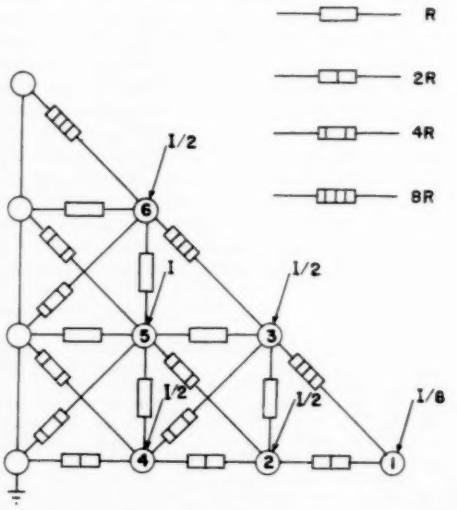

Fig. 2 Diagonal Resistor Network for Elastic-Torsion Problem, Based on K or 9-Point Difference Operator

$$\left.\begin{aligned}
-4V_1 + 4V_2 \qquad\qquad\qquad\qquad + 15 &= 0 \\
V_1 - 4V_2 + 2V_3 + V_4 \qquad\qquad + 15 &= 0 \\
2V_2 - 4V_3 \qquad + 2V_5 \qquad + 15 &= 0 \\
V_2 \qquad - 4V_4 + 2V_5 \qquad + 15 &= 0 \\
V_3 + V_4 - 4V_5 + V_6 + 15 &= 0 \\
2V_5 - 4V_6 + 15 &= 0
\end{aligned}\right\} \quad \ldots [10]$$

The voltages obtained from the resistor network V_{i0}, are shown in line 1 of Table 1. Using these values, the residuals ρ_i are calculated and are given in line 2; they range from -0.15 to $+0.5$. For the second run it is necessary to choose a scale factor c_1, so that with input currents of ρ_i/c_1, the measured voltage will fall in the desired range—in this case 1 to 50 millivolts. By comparison with the first run where 15 microamp was the input to each node, $c_1 = {}^1/_{100}$ seems about right. The resistors from the voltage source to each node were then adjusted to give an input current of $100\rho_i$ in microamp. The resulting voltages which were measured in a second run, V_{i1}', are given in line 3.

To check whether the process has been carried out correctly and whether a significant reduction of error has been obtained, the new residuals, ρ_{i1}, were calculated using the corrected voltages, $V_{i0} + c_1V_{i1}'$

$$\rho_{i1} = a_{i1}(V_{10} + c_1V_{11}') + a_{i2}(V_{20} + c_1V_{21}') + \ldots + a_{in}(V_{n0} + c_1V_{n1}') + g_i \quad \ldots [11]$$

These values are given in line 4; comparison with line 2 shows that a very great reduction in the residuals has been effected.

In general, the actual errors in the solution cannot be determined, although estimates can be obtained from the residuals as mentioned later. In the simple example discussed here, it is easy to solve the finite-difference equations exactly, and then the comparison of this solution with the values obtained from the electric network gives the experimental error. The network and finite-difference solutions are given in lines 5 and 6, using the units of the original problem. The per cent error of the corrected solution is given in line 7; it averages 0.006 per cent in absolute value. The per cent error from the first solution, cV_{i0}, is given in line 8 and averages 0.67 per cent in absolute value. Thus the experimental error has been reduced by a factor of 100.

In lines 9 to 16 of Table 1 the same data have been given for the solution of this problem on a network using diagonal resistors. Here the present method is applied to reduce the experimental error which in the first solution averaged 0.18 per cent in absolute value. The correction run brought the experimental error down to an average of 0.003 per cent.

Procedure for Correcting Both Lumping and Experimental Errors

Lumping errors can arise from three sources: (1) At interior points of the resistor network the voltages satisfy a difference equation which is an approximation to the partial differential equation; (2) on the boundary the solution must satisfy conditions specifying the values of certain derivatives, but the resistor network approximates to those derivatives by finite differences; (3) the boundary of the region has a complicated shape which does not intersect a square mesh at nodal points, so that an approximation to the true shape is necessary. In all cases, the application of the present procedure to reducing lumping errors is based on the calculation of a correction term to the finite-difference approximation. The correction term is the term needed to give the next higher order approximation to the partial differential equation or to the boundary conditions.

To evaluate the correction terms exactly would, of course, require having the solution u, which is unknown; but for this purpose it is quite adequate to use the values from the first solution, V_{i0}. This is possible because the first solution given by the resistor network, even for a rather coarse net, should not be in error by more than a few per cent.

As an example of these correction terms, for finite-difference approximation to the differential equation, suppose we have to solve the Poisson Equation [1] and use the H or 5-point operator; so that we are using the equation

$$Hv - h^2f = 0$$

$$H = \begin{array}{|c|c|c|}\hline 0 & 1 & 0 \\ \hline 1 & -4 & 1 \\ \hline 0 & 1 & 0 \\ \hline \end{array} \quad \ldots [12]$$

and h is the mesh size. It is known[6] that a closer approximation is given by

$$Hv - h^2f - \frac{1}{12}(\delta_x^4 + \delta_y^4)v = 0 \quad \ldots [13]$$

where δ_x^4, δ_y^4 are the fourth-order central difference operators.

[6] "Numerical Solution of Differential Equations," by W. E. Milne, John Wiley & Sons, Inc., New York, N. Y., 1953.

Table 1 Correction Method for Experimental Error Applied to Elastic-Torsion Problem

Node No., i		1	2	3	4	5	6
5-Point Operator (Fig. 1): $c = {}^1/_{270}$, $c_1 = {}^1/_{100}$							
1	First network solution, V_{i0}	38.5	34.8	31.6	23.0	21.0	14.25
2	Residual, ρ_i	0.2	0.5	0.2	−0.2	−0.15	0
3	Correction, V_{i1}'	44.0	39.1	27.5	7.5	5.6	2.8
4	Residual after correction, ρ_{i1}	0.004	0.001	−0.006	−0.008	−0.009	−0.008
5	Network solution, $v_i = c(V_{i0} + c_1V_{i1}')$	0.144222	0.130337	0.118056	0.085463	0.077985	0.052881
6	Finite-difference solution	0.144230	0.130342	0.118056	0.085470	0.077992	0.052885
7	Per cent error	−0.006	−0.004	0	−0.008	−0.009	−0.008
8	Per cent error from first solution	−1.1	−1.1	−0.9	−0.4	−0.3	−0.2
9-Point Operator (Fig. 2): $c = {}^1/_{180}$, $c_1 = {}^1/_{100}$							
9	First network solutions, V_{i0}	26.5	23.9	21.7	15.7	14.4	9.85
10	Residual, ρ_i	−0.8	1.2	0.25	−0.8	−0.5	−0.1
11	Correction, V_{i1}'	2.68	7.58	3.0	−3.28	−2.62	−1.42
12	Residual after correction, ρ_{i1}	−0.0032	−0.0008	−0.0062	0.0096	0.0056	0.0044
13	Network solution, $v_i = c(V_{i0} + c_1V_{i1}')$	0.147371	0.133199	0.120722	0.087318	0.079854	0.054643
14	Finite-difference solution	0.147372	0.133200	0.120723	0.087322	0.079858	0.054646
15	Per cent error	−0.001	−0.001	−0.001	−0.004	−0.005	−0.005
16	Per cent error from first solution	−0.14	−0.30	−0.08	0.23	0.13	0.18

TABLE 2 CORRECTION METHOD FOR LUMPING AND EXPERIMENTAL ERROR APPLIED TO ELASTIC-TORSION PROBLEM

Node No., i		1	2	3	4	5	6
5-Point Operator (Fig. 1): $c = {}^1/_{270}$, $c_1 = {}^2/_{100}$							
1	First network solution, V_{i0}	38.5	34.8	31.6	23.0	21.0	14.25
2	Residual, ρ_i	0.2	0.5	0.2	−0.2	−0.15	0
3	Lumping error, μ_i	0.333	0.233	0.325	0.267	0.350	0.767
4	Correction, V_{i1}'	41.8	37.7	32.6	19.2	18.5	15.6
5	Network solution, $v_i = c(V_{i0} + c_1 V_{i1}')$	0.147237	0.133078	0.120659	0.087319	0.079833	0.054511
6	Analytical solution, u	0.147343	0.133172	0.120692	0.087303	0.079829	0.054560
7	Per cent error	−0.07	−0.07	−0.03	+0.02	+0.005	−0.09

Also if $$\frac{\partial^2 f}{\partial x^2} + \frac{\partial^2 f}{\partial y^2} = 0$$

Equation [12] can be written, to the same order of approximation, as

$$Hv - h^2 f + \frac{1}{6}\,\delta_x^2\delta_y^2\, v = 0 \qquad [14]$$

where $\delta_x^2\delta_y^2$ (called N^2 by Milne[6]) is the operator

$$\delta_x^2\delta_y^2 = \begin{array}{|c|c|c|}\hline 1 & -2 & 1 \\ \hline -2 & 4 & -2 \\ \hline 1 & -2 & 1 \\ \hline \end{array} \qquad [15]$$

The application of such a correction for lumping simultaneously with the correction for experimental error is easy to see. Suppose μ_i is the lumping correction at the ith node, in the same units as the V_i. Then the V_{i0} give an approximate solution of [3]

$$a_{i1}V_1 + a_{i2}V_2 + \ldots + a_{in}V_n + g_i = 0$$

whereas with the lumping-error correction we wish to solve

$$a_{i1}V_1 + a_{i2}V_2 + \ldots + a_{in}V_n + g_i + \mu_i = 0$$

Hence, it is only necessary to add the lumping-error term to the residual from the first run to obtain a correction for both simultaneously.

In Table 2, we give the results of such a correction applied to the same problem as before, where the 5-point operator was used.[7] The lumping error, μ_i, in line 3 was computed from

$$\mu_i = \frac{1}{6}\,\delta_x^2\delta_y^2 V_{i0}$$

Line 4 gives the readings (in millivolts) obtained from the network when the input currents were $(\rho_i + \mu_i)/c_1$. The corrected network solution on Line 5 compared to the analytic solution on Line 6 shows an average absolute error of 0.05 per cent.

REMARKS

The method proposed here can be regarded as the electric counterpart of a process which is used in relaxation calculations and in other methods for numerical solution of differential equations. As applied to resistor networks it derives its usefulness from the combination of the advantages of the resistor network and numerical calculation. The resistor network, once set up, solves the equation rapidly and with fair accuracy; the numerical calculation gives the residuals precisely, so that when they are put back in the net with a suitable scale factor, we obtain a corrected solution of very high accuracy. At the same time we avoid the really lengthy and difficult part of the work in all purely numerical methods; that is, the actual solution of the equations.

The calculation of the residuals requires only the evaluation of linear expressions, each of which has only a few terms. These expressions do not even need to be written out; instead the V_{i0} are written on a sheet in the proper relative position, and then a transparent template carrying the coefficients of the finite-difference operator is placed over each node in succession. The calculation of the lumping-error correction can be reduced in a like manner to an operator applied to each node in succession; both residual and lumping error can be calculated simultaneously.

From the point of view of the design and operation of resistor-network calculators, our correction procedure has the advantage of reducing the requirements on the precision of the physical components and of the measurements. Errors of a few per cent in the resistors, input currents, and measured voltages easily can be tolerated, thus reducing the expense for equipment and operating time. The whole design sometimes can be simplified because of these more lenient tolerances.

As an example, the solution of the biharmonic by a pair of coupled networks (equivalent to replacing it by a pair of Poisson equations) was under consideration in this laboratory. The input current to each node of one network must be proportional to the voltage at the corresponding node of the second network. An accurate method for obtaining this coupling would be to use an electronic "voltage-dependent current source" between each pair of corresponding nodes; but this would involve considerable expense for a large number of nodes. The simple method is to use a resistance between the nodes, but this involves an error resulting from back emf because it is not possible to have the voltage on one network extremely large compared to the other. By using the correction method, the error due to the simpler and cheaper method can, however, easily be tolerated.

The correction method, because it requires the calculation of residuals, makes immediately apparent any gross errors in circuit design, setup, or operation. The method has the feature, in common with other effective successive-approximation methods, of being automatically self-correcting; that is, if there are errors in the first solution which are large, but not recognized as such from examining the residuals, they should be eliminated when the solution is run again with adjusted inputs. If the residuals do not decrease significantly, this means that there has been a mistake which needs to be eliminated.

The calculation of the residuals also makes it possible to obtain an estimate of the experimental error. Some formulas for this purpose are given by Milne.[8] These give an upper bound for the experimental error, based on the maximum residual, and are overestimates of the actual error. However, such estimates, even if too high, are very useful in increasing confidence in the results of resistor-network solutions of differential equations, and make it possible to guarantee that the error is within specified limits.

ACKNOWLEDGMENTS

The resistor-network experiments were performed by Mr. Paul Calcaterra of the Heat and Mass Flow Analyzer Laboratory, Columbia University.

This work was made possible by a grant from the Higgins Fund and is part of a continuing study of the solution of engineering problems on electric network computers.

[7] When the diagonal resistor network is used, correction for lumping error is not necessary, if accuracy of 0.03 per cent is enough. This can be seen by comparing the diagonal resistor network solution (Table 1, Line 13) with the analytic solution (Table 2, Line 6).

A Blade-Vibration-Damping Device—Its Testing and a Preliminary Theory of Its Operation

By R. A. DI TARANTO,[1] CAMDEN, N. J.

Presented herein is a report on a wire-damping device[2] which has shown considerable damping ability when placed in a hollow rotor blade. A series of tests is reported which have all shown the damping ability of this device at nonrotating and rotating conditions. Two theories are postulated and expressions derived to explain the mechanism of damping by the wires for nonrotating-type damping and rotating-type damping. The postulated mechanism for damping in the nonrotating rotor blade considers that the wires absorb energy by rubbing around one another as a result of the motion imparted by the vibratory motion of the blade. The postulated mechanism for damping in the rotating rotor blade considers that a component of centrifugal force holds the wires against the side of the blade and the vibratory bending motion of the blade causes relative motion between the blade wall and the adjacent wires to absorb energy. Criteria are set forth for determining which mechanism is operative. Good correlation was obtained between test and theory.

Nomenclature

The following nomenclature is used in the paper:

- y = lateral displacement of blade, in.
- n = number of rows of wire
- N = number of wires in a row
- l = length of wire, in.
- R_1 = ineffective length of wire which does not slide around adjacent wire in stationary-type damping
- r = radius of wire, in.
- θ = angle through which wire slides around adjacent wire in stationary type damping, radians (rad)
- ρ = mass per unit length of wire, $\frac{\text{lb-sec}^2}{\text{in.}}\Big/\text{in.}$
- ρ_m = mass per unit length of blade envelope, $\frac{\text{lb-sec}^2}{\text{in.}}\Big/\text{in.}$
- ω = natural frequency of blade, rad/sec
- Ω = angular rotor speed, rad/sec
- α = lean angle, rad
- μ = coefficient of friction
- L = length of blade, in.
- R = distance from center of rotation to base of blade, in.
- c = average normal distance from neutral axis to fiber on internal surface of blade, in.

Introduction

In present-day aviation gas turbines it is found that under certain conditions the rotor blades undergo large vibratory stresses which may cause rupture. These stresses may be caused by resonant effects, a stall-flutter condition, or a rotating-stall condition. In an effort to alleviate this large stress condition, much thought is being given to this problem from a mechanical design standpoint. Present approaches to the design of rotor blades, in order to alleviate the high stresses, are to design the blades to a given natural frequency, or to increase the damping in the blade. The investigation of the latter method for reducing the blade stresses, among others, has considered the following:

1 Insertion of particles of different sizes and kinds of materials into a hollow blade. This method yields damping for stationary (nonrotating) blades, but when the blade is rotated the particles pile together giving but slight relative particle motion and therefore little damping.

2 The use of two flat cantilevered plates under normal force, rubbing against one another when vibrating. Damping is obtained for this device, but the damping is dependent upon the difficult-to-control normal force.

3 Root damping of the vibrating blade. Here, as before, the normal force is the critical factor. Too great a normal force prevents relative blade-root motion and too small a normal force reduces the energy-absorption ability.

4 Tuned dampers in the tip of blades also have been tried. They are relatively effective but only in a narrow frequency band.

Literature and/or experimental investigation of the foregoing methods for obtaining damping has shown that all of these have their limitations and have not solved the problem of high vibratory stresses in blades. It is the purpose of this paper to present the experimental and analytical investigations of a method for obtaining high damping in rotor blades which shows promise of alleviating this problem.

Discussion

Early in the investigation of this problem, calculations were made to determine the damping potentials of two flat cantilevered plates rubbing over one another when vibrating.

Analysis of the damping provided by the rubbing plates showed that the plates could give damping if the inertia force of their mass could be used as the normal force. This suggested that a device was required which had mass, but little shear-carrying capacity and which would allow the inertia force of its mass to be used as a normal force. Wire strands fit this requirement. A series of tests, which we shall call Series I, showed that the wires

[1] Engineer, Defense Electronic Products Division of the Radio Corporation of America; formerly, Mechanical Engineer, Westinghouse Electric Corporation, Aviation Gas Turbine Division. Assoc. Mem. ASME.

[2] Patent applied for in the names of R. A. Di Taranto and S. Ackerman by Westinghouse Electric Corporation, Aviation Gas Turbine Division.

Contributed by Applied Mechanics Division and presented at the Annual Meeting, New York, N. Y., December 1–6, 1957, of The American Society of Mechanical Engineers.

Discussion of this paper should be addressed to the Secretary, ASME, 29 West 39th Street, New York, N. Y., and will be accepted until April 10, 1958, for publication at a later date. Discussion received after the closing date will be returned.

Note: Statements and opinions advanced in papers are to be understood as individual expressions of their authors and not those of the Society. Manuscript received by ASME Applied Mechanics Division, February 27, 1956. Paper No. 57—A-10.

did in fact give high damping. A theory for this damping was postulated and expressions were derived for an ideal case of a rectangular hollow blade. Good correlation was obtained. This series of tests showed that, for stationary components (stator vanes), this wire-damper device could give appreciable damping.

The next series of tests (Series II) was run to determine the effect of centrifugal force on the damping ability of the wires. It was not known how stiff the wires would become, so that they would become shear carrying and tend to decrease the normal force between wires and reduce the damping. A low-speed 1175-rpm test rig was designed and built to ascertain the centrifugal-force effect on the wires, Fig. 1.

After preliminary tests in the low-speed rig, it became apparent that two conditions could occur in the rotating wire damper. This results from the blades having a lean angle which is used to alleviate the gas bending stresses. This lean angle creates a component of centrifugal force of the wires normal to the blade. If this component of force is greater than that due to the accelerative force of the blade vibratory motion, the wires would remain against the side of the blade and the stationary-type damping first postulated would not come into effect. The criteria for obtaining this latter condition are shown in the Appendix. A theory to explain this behavior is postulated herein, considering the wires to remain against the side of the blade. Good correlation with test results was obtained for both postulated theories and the damping was seen to remain large.

To insure that the damping still occurred at near normally existing centrifugal accelerations, a series of tests (Series III) was run at high rotating speeds (8000 rpm) in an air-evacuated spin pit.[1] A simulated blade of proportions closer to an actual blade was designed, fabricated, and used, Fig. 2. The results showed high damping and good correlation with theory.

These series of tests have shown that a device is available for increasing damping in stationary components and which remains effective under centrifugal accelerations.

Analysis

Stationary Damping Mechanism. The mechanism of damping postulated for the stationary-type damping is as follows: Ideally, the wires are arranged in a row shown in Fig. 3(*a*). As the envelope enclosing them vibrates, it causes the wires to try to follow, and a "squeezing" action as shown in Fig. 3(*b*) takes place. The squeezing action causes rubbing of the wires about one another. The force acting between the wires is due to the vibratory acceleration caused by the envelope. This normal force, which varies from row to row of wires in the direction of vibration along with the rubbing action, dissipates the vibratory energy of the envelope. The wires undergo a "squeezing," then "unsqueezing" to a "squeezing" action as the blade accelerates, reaches its maximum velocity, then decelerates in that order. In this preliminary analysis, the following assumptions are made:

1 The blade deflection is approximated by $y = Kx^2$.

2 All wires move through the same deflection as the free end of the wires, through an effective length $(l - R_1)$. (Wires are not tightly packed.)

3 Rubbing motion of wire is $r\theta$.

4 A rectangular-cross-section hollow blade is considered.

The work is done by two wires moving around one another, where the normal force between wires is F; the coefficient of friction μ and the displacement δ. This can be written as

$$W = \int F\mu\delta \ldots\ldots\ldots\ldots\ldots\ldots [1]$$

[1] "Hot Spin Tests of Bladed Jet-Engine Rotors," by H. Saldin and P. G. DeHuff, Trans. ASME, vol. 71, 1949, pp. 605–612.

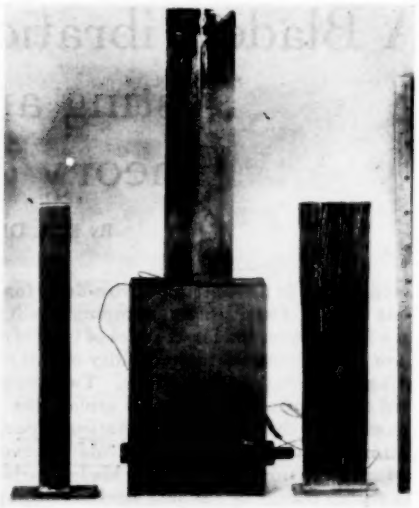

Fig. 1 Simulated Hollow Rotor Blade Used in Low-Speed Testing
(Left to right—solid insert, blade, wire insert.)

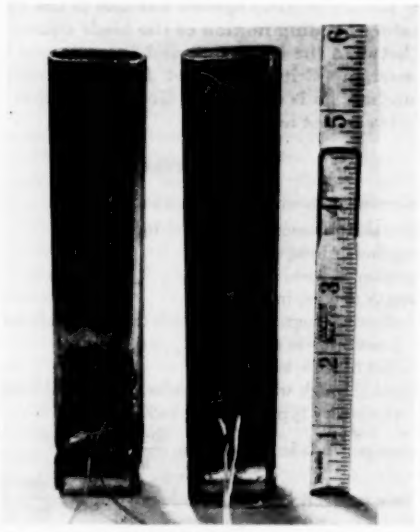

Fig. 2 Simulated Hollow Rotor Blade Used in High-Speed Testing
(Left to right—hollow control blade, wire-filled blade.)

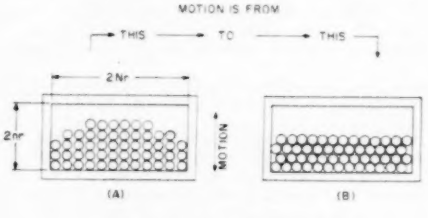

NON-ROTATING DAMPING MECHANISM
(A) WIRES CONSIDERED IN NORMAL POSITION
(B) WIRES 'SQUEEZED' TOGETHER AFTER HAVING RUBBED OVER ONE ANOTHER TO DISSIPATE ENERGY

Fig. 3 End View of Blade With Wires

If we take the top row alone, the work done by friction is W_1

$$W_1 = \int_{R_1}^{l} N\rho y_0\omega^2 r\theta\mu \cos^2 \omega\, t\, dx \quad [2]$$

where

N = number of wires in a row

$$\left.\begin{aligned} F &= \int \rho y_0\omega^2 \cos \omega\, t\, dx \\ \delta &= r\theta \cos \omega t \end{aligned}\right\} \quad [3]$$

The work done by the second row is

$$W_2 = \int_{R_1}^{l} N(2)\rho y_0\omega^2 r\theta\mu \cos^2 \omega\, t\, dx \quad [4]$$

and the third row does work W_3

$$W_3 = \int_{R_1}^{l} N(3)\rho y_0\omega^2 r\theta\, \mu \cos^2 \omega\, t\, dx \quad [5]$$

The total work due to friction is

$$W_T = W_1 + W_2 + W_3 + \ldots + \ldots$$

This yields

$$W_T = \int_{R_1}^{l} N\left[\sum_1^n S\right]\rho y_0\omega^2 r\theta\, \mu \cos^2 \omega\, t\, dx \quad [6]$$

where n = number of rows of N wires or

$$W_T = N\int_{R_1}^{l} \rho\left[\frac{n^2+n}{2}\right] y_0\omega^2 r\theta\mu \cos^2 \omega\, t\, dx \quad [7]$$

Assuming $y_0 = y_l = Kl^2$

i.e., the effective portion of the wire $(l - R_1)$ all moves the same distance as the blade tip

$$W_T = N\left[\frac{n^2+n}{2}\right]\rho K l^2\omega^2\theta\mu r[l - R_1]\cos^2 \omega t \quad [8]$$

The energy of dissipation per cycle is

$$\frac{W_T}{\text{Cycle}} = \int_0^{2\pi/\omega} W_T dt$$

which yields

$$\frac{W_T}{\text{Cycle}} = N\left[\frac{n^2+n}{2}\right]\rho\pi K l^2\omega r\theta\mu[l - R_1] \quad [9]$$

To obtain the change in kinetic energy per cycle, we proceed as follows:

The kinetic energy (KE) of the blade is

T = KE of wires + KE of blade envelope

then

$$T_1 = \frac{Nn}{2}\int_{R_1}^{l} \rho dx[Kl^2]^2\omega^2 \sin^2 \omega t + 1/2\int_0^L \rho_m \dot{y}^2 dx \quad [10]$$

where

$$\dot{y} = -\omega K x^2 \sin \omega t$$

so that

$$T_1 = \left[\omega^2\frac{Nn}{2}\rho l^4[l - R_1]K^2 + \frac{\rho_m}{10}\omega^2 K^2 L^5\right]\sin^2 \omega t \quad [11]$$

The kinetic energy per cycle is

$$\frac{T_1}{\text{Cycle}} = \left[\frac{Nn}{2}\rho\omega^2 l^4[l - R_1]K^2 + \frac{\rho_m}{10}\omega^2 K^2 L^5\right]\int_0^{2\pi/\omega} \sin^2 \omega t\, dt \quad [12]$$

or

$$\frac{T_1}{\text{Cycle}} = \frac{Nn}{2}\rho\omega l^4(l - R_1)K^2 + \frac{\rho_m}{10}\pi\omega K^2 L^5 \quad [12a]$$

After one cycle the kinetic energy is decreased with a decrease in the deflection y

$$y_1 = (y - \Delta y) = (K - \Delta K)x^2 \cos \omega t \quad [13]$$

and

$$T_2 = \frac{Nn}{2}\int_{R_1} \rho dx l^4(K - \Delta K)^2\omega^2 \sin^2\omega t + 1/2\int_0^L \rho_m\, dx\, \dot{y}_1^2 \quad [14]$$

whereupon

$$\frac{T_2}{\text{Cycle}} = \frac{Nn\pi}{2}\omega\rho l^4(l - R_1)(K - \Delta K)^2 + \frac{\rho_m\omega L^5}{10}\pi(K - \Delta K)^2 \quad [15]$$

Neglecting $(\Delta K)^2$ terms we find

$$\frac{T_1 - T_2}{\text{Cycle}} = 2K\Delta K\left[\frac{nN\pi}{2}\omega\rho l^4(l - R_1) + \frac{\rho_m}{10}\omega L^5\pi\right] \quad [16]$$

Now the change in kinetic energy per cycle is equal to the energy dissipated per cycle or

$$\frac{T_2 - T_1}{\text{Cycle}} = \frac{\Delta W}{\text{cycle}}$$

so that

$$\left.\begin{aligned} 2K\Delta K\left[\frac{nN\pi}{2}\rho\omega l^4(l - R_1) + \frac{\rho_m\omega}{10}L^5\pi\right] \\ = N\left(\frac{n^2+n}{2}\right)\pi\rho K l^2 r\theta\mu(l - R_1)\omega \end{aligned}\right\} \quad [17]$$

Then

$$\Delta K = \frac{N\rho(n^2+n)l^2(l - R_1)r\theta\mu}{4\left[\frac{nN}{2}\rho l^4(l - R_1) + \frac{\rho_m}{10}L^5\right]} \quad [18]$$

and finally we obtain

$$\frac{(\Delta K)x^2}{Kx^2} = \frac{\Delta y}{y} = \frac{N\rho(n^2+n)l^2(l - R_1)r\theta\mu}{40K[5nN\rho l^4(l - R_1) + \rho_m L^5]} \quad [19]$$

Rotating-Blade-Damping Theory. For this case, the wires are considered to remain against the side of the blade under a component of centrifugal force. The energy is considered dissipated between the blade wall and adjacent wires. The normal force is that of the component of centrifugal force due to all the wires, and the relative motion is the difference in movement of the blade due to bending, and the movement of the adjacent wire strands due to the force created by the normal force and coefficient of friction tending to elongate the wire. In the following, the assumptions made are:

1 The wire is the same length as the blade.

2 The blade is leaned sufficiently to hold all wires against one side at all times.

3 A rectangular-cross-section hollow blade is considered.

The blade-bending displacement, at the wall, is equal to $c(dy/dx)$, where c = distance from neutral axis to the inside blade wall.

The wire displacement at any x, due to forces along the wire is

$$\Delta = \int_0^x \frac{Fx}{AE}\, dx \cos \omega t \ldots\ldots\ldots\ldots [20]$$

where

A = wire area
E = modulus of elasticity

Where the force along the wire is due to the centrifugal force acting along the lean angle α and is

$$F = n(R + x)\Omega^2 \rho\mu \sin \alpha \ldots\ldots\ldots\ldots [21]$$

i.e., for one row of n wires. The incremental friction work due to N columns of wires is ΔW

ΔW = (normal force between blade wall and adjacent wire) × (relative displacement of blade wall and adjacent wires) . . . . [22]

$$\Delta W = \int_0^L N[n(R + x)\Omega^2 \rho\mu \sin \alpha] \left[c \frac{dy}{dx} - \int_0^x \frac{Fx}{AE}\, dx \cos \omega t \right] dx \ldots . [22a]$$

Assuming $y = Kx^3 \cos \omega t$

$$\Delta W = N\rho n\Omega^2 \mu \sin \alpha \left[Rcy_l + \frac{2}{3} cLy_l - G \right] \cos \omega t \ldots [23]$$

where

$$G = \frac{n\Omega^2 \rho\mu \sin \alpha}{AE} \left[\frac{R^2 L^3}{6} + \frac{RL^4}{4} + \frac{L^5}{5} \right]$$

or

$$\frac{\Delta W}{\text{Cycle}} = \frac{4Nn}{\omega} \rho\Omega^2 \mu \sin \alpha \left[cy_l \left(R + \frac{2L}{3} \right) - G \right] \ldots . [24]$$

The change in kinetic energy per cycle is given in the foregoing and is

$$\frac{\Delta T}{\text{Cycle}} = 2K(\Delta K) \left[\frac{nN\pi\omega\rho L^5}{10} + \frac{\rho_m L^5 \omega\pi}{10} \right] \ldots\ldots [25]$$

For one cycle

$$\Delta W = \Delta T$$

$$\Delta K = \frac{4nN\rho\Omega^2 \mu \sin \alpha \left[cy_l \left(R + \frac{2L}{3} \right) - G \right]}{\pi K\omega^2 \left[\frac{nN\rho L^5 + \rho_m L^5}{10} \right]} \ldots . [26]$$

and finally

$$\frac{\Delta y}{y} = \frac{(\Delta K)x^3}{Kx^3} = \frac{40\, nN\rho\Omega^2 \mu \sin \alpha \left[cy_l \left(R + \frac{2L}{3} \right) - G \right]}{\pi K^2 \omega^2 L^5 (Nn\rho + \rho_m)} \ldots [27]$$

Test Series I—Nonrotating

Procedure. A hollow stator vane was filled with 0.005-in-diam copper wires. One end of the stator was welded to a plate which in turn was fastened to a large fixed mass to approximate a cantilevered beam. An electric strain gage was fastened to the base of the vane and its leads were connected to a Wheatstone-bridge circuit, the resulting signal being displayed on the face of an oscilloscope. The blade was plucked by hand and the resulting decay wave on the face of oscilloscope was photographed by a Polaroid Land camera.

The log decrement was measured from this photograph. For small damping, the relation which exists is $\Delta y/y$ = log decrement (see Appendix for relationship at large values of damping).

Results. Using 946 strands of 0.005-in-diam copper wire in the stator vane whose dimensions were 3.1 in. long and 1.75 in. wide, 0.156 in. maximum thickness, and weighing 0.0815 lb, it was found that the measured damping ability $\Delta y/y$ was 0.67 for a 20,000-psi stress at the base of the blade. This compared well with the calculated value of 0.61 for $\theta = \pi/6$, $\mu = 0.69$, and $\rho_m = 0.51 \times 10^{-4}$ lb sec²/sq in. The value for the coefficient of friction is high, but values of $\mu = 0.57$ have been obtained.[4]

The plot of the length of wire versus damping ability ($\Delta y/y$) was made of the test results and that calculated on the basis of Expression [19] is superimposed. This plot is shown in Fig. 4. Good correlation was obtained.

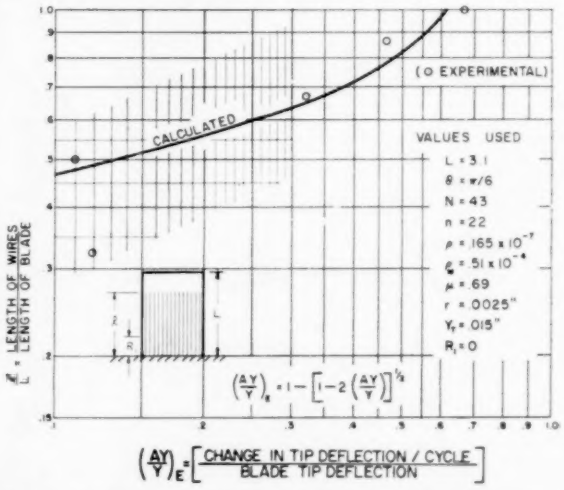

Fig. 4 Comparison of Calculated and Experimental Damping Characteristics for Variation in Length of Wires in Nonrotating Vane

Test Series II—Low-Speed Rig (1175 Rpm)

Procedure. This series of tests was run to ascertain the effect of centrifugal force and lean angle of the blade on the damping ability of the wire damper. A simulated blade was made which would yield measurable amounts of damping based on the derived damping Expressions [27], Fig. 1. The simulated blade was instrumented with an electric strain gage and the signal led through slip rings to the same recording setup as was used in Test Series I.

Tests were run in the following manner: The blade was brought to a rotative speed of 1125 rpm. At this speed a kind of inverted guillotine with a number of thicknesses of masking tape at the open end was abruptly raised into the path of the rotating blade. This supplied a single impact by breaking the tape on the blade. The decay records of the stresses at the base of the blade were photographed from the oscilloscope screen. Tests were run for 0, 3, 6, and 9-deg lean angle.

[4] "Frictional Phenomena," by Andrew Gemant, Chemical Publishing Company, Brooklyn, N. Y., 1950.

To obtain a control on the tests, the following were performed:

1 Empty blade.
2 Full of wires—Insert I.
3 Half full of wires—Insert II.
4 Solid bar equal in weight to the full wires of run 2.

Results. Test data showed a certain amount of scatter of the log decrement for a given lean angle. The data obtained indicated the order of magnitude of the log decrement. A plot of the average value of log decrement for each lean angle showed small variations of log decrement with the lean angle. For the wire damper, this curve indicates a slight decrease in damping ability with increasing lean angle, which is contrary to the formulated rotating damping Expression [27], which type of damping was expected to be acting. Expression [27] is based on having the wires remain against the side of the blade if the tip deflection y_t satisfies the following expression

$$y_t > \alpha L \frac{\Omega^2}{\omega^2}$$

The tip deflections, at the stress levels obtained in the tests, were on the order of 0.1 in. This value would allow for the wires to leave the side of the blade for the lean angles used. These facts when analyzed indicate a stationary damping mechanism to be taking place. This appears to be substantiated by the good agreement between the values calculated by use of stationary damping Expression [19] and the measured values. A comparison of these values follows:

Calculated	$\Delta y/y = 0.71$
Measured	$\Delta y/y = 0.81$

This shows that, for the amplitude of vibration encountered, the calculated damping for stationary wire dampers agrees well with that observed. Values observed are higher than that calculated on the basis of a coefficient of friction of 1 and $\theta = \pi/6$. In order to agree fully with the observed data, a product of the coefficient of friction and θ of 1.4 is required.

Tests using wire Insert II showed an over-all average damping of $\Delta y/y = 0.38$. This value agrees well with the calculated value of $\Delta y/y = 0.30$ using the stationary-mechanism relationship.

The tests of the empty blade and the blade with a solid insert of the same weight as wire Insert I were run to show a comparison of wire-damping ability. From an over-all standpoint, the damping ability of the empty blade was $\Delta y/y = 0.06$, and the damping ability of the solid insert was $\Delta y/y = 0.22$. This showed the wire damper to yield the largest amount of damping. Typical decay records are shown in Fig. 5.

The recorded damping ability of wire Insert I at a lean angle of 9 deg showed high damping at high amplitudes and then a lower damping at small amplitudes. An explanation advanced is as follows: At the high amplitudes the vibratory acceleration is greater than the component of centrifugal force normal to the blade; thus it is free of the blade and acts in damping by the stationary mechanism. When the amplitude of vibration falls to a low value, the wires stay against the side of the blade and the rotating damping mechanism takes over. The values of damping measured and that calculated by the formulated rotating mechanism agree:

Calculated	$\Delta y/y = 0.28$
Measured	$\Delta y/y = 0.22$

Test Series III—High-Speed Spin Test

Procedure. The high-speed spin pit[3] was used to obtain the necessary centrifugal force. The blade used was a simulated blade made by squeezing a $^3/_4$-in. OD × 0.049-in-wall stainless-steel tube as seen in Fig. 2. An empty blade and a blade filled with approximately 525 of 0.015-in-diam stainless-steel wires were tested. The blade was set at a 3-deg lean angle for all tests and the speed varied. The blades were instrumented and the same recording means was used as in the Series II tests. The impactor was an oversize mousetrap-type device which was

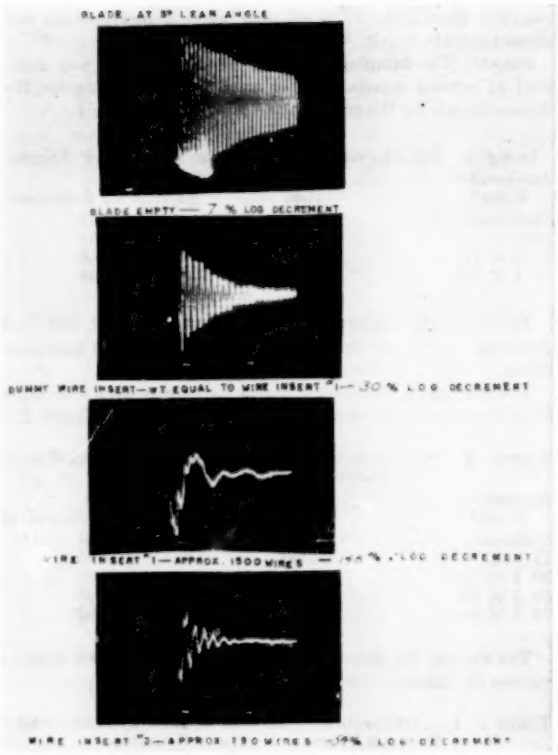
BLADE AT 3° LEAN ANGLE
BLADE EMPTY — .7 % LOG DECREMENT
DUMMY WIRE INSERT—WT EQUAL TO WIRE INSERT #1— .30 % LOG DECREMENT
WIRE INSERT #1—APPROX. 1500 WIRES
WIRE INSERT #2—APPROX. 750 WIRES

Fig. 5 Typical Decay Records
(Rotating speed = 1175 rpm; distance from center of rotation to center of gravity of blade = 18 in.)

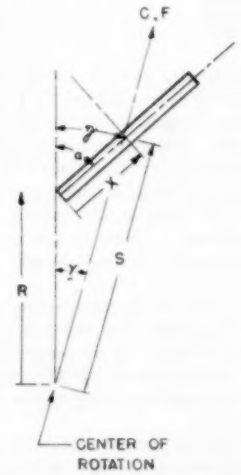

Fig. 6 Rotating Blade Set at a Lean Angle

triggered electrically by a solenoid when a push button was pressed outside the pit.

Results. The damping ability of the hollow blades was measured at several speeds. The average log decrements for the various speeds for the empty blade are given in Table 1.

TABLE 1 LOG-DECREMENT AVERAGES FOR EMPTY BLADE

Acceleration, ft/sec²	Speed, rpm	Average log decrement
Stationary	Stationary	0.057
39.4×10^4	6000	0.051
53.5×10^4	7000	0.056
70.4×10^4	8000	0.048

The foregoing represents essentially the material and root damping. There was small variation of damping with maximum stress.

The average log decrements for the various speeds for the wire-filled blade at maximum stress of 7000 psi are given in Table 2.

TABLE 2 LOG-DECREMENT AVERAGES FOR WIRE-FILLED BLADE AT 7000 PSI STRESS

Acceleration, ft/sec²	Speed, rpm	Average log decrement
Stationary	Stationary	0.50
17.6×10^4	4000	0.95
39.4×10^4	6000	0.90
53.5×10^4	7000	0.98
70.4×10^4	8000	0.92

The average log decrements at a rotor speed of 8000 rpm for various maximum stresses are given in Table 3.

TABLE 3 LOG-DECREMENT AVERAGES AT ROTOR SPEED OF 8000 RPM FOR VARIOUS MAXIMUM STRESSES

Maximum stress, psi	Average log decrement
6000	0.86
7000	0.92
8000	0.84
10000	0.95
12000	1.00
15000	1.05

It is to be noted that the stress (tip deflection) log-decrement variation is contrary to that predicted by Expression [27]. In this series of tests the readings under the same conditions varied as much as 40 per cent. The reason for this discrepancy was not evident. In view of this, the results of this series of tests are to be viewed from a qualitative sense and only show orders of damping possible. In every case, with the wire insert, and when rotating, the logarithmic damping exceeded 66 per cent, which is most significant when compared to the empty-blade damping measured of 6 per cent.

Calculations show that for the speeds run, stresses measured, and at the 3-deg lean angle, the wires should have remained against the side of the blade and rotating-type damping should have been acting. For the 5000 to 10,000-psi stress range at 8000 rpm the calculated log-decrement damping is critical damping to 50 per cent, respectively.

The agreement of theory and test is in order of magnitude only. A more consistent reproducible set of data on this phase of testing is needed. The over-all importance of the results of these series of tests is that they show that high damping may be obtained under near normally encountered accelerations and near the stall speeds normally encountered in jet engines.

Additional Remarks. High-speed moving pictures of wires in a vibratory blade which had its end open, exposing the ends of the wire, showed the rubbing, squeezing, and unsqueezing action of the wires to be taking place.

CONCLUSIONS AND RECOMMENDATIONS

These series of tests have shown that a device for alleviating the high vibratory stresses set up in blades by such phenomena as stall flutter and rotating stall is available in the form of a wire damper. The use of wires as the means for damping is not limited to blades alone, but may be used in other vibrating components.

In order to understand this device better, more refined experimentation is required to obtain more consistent data in the high-rotating-speed damping ability of blades so as better to check the correlation to the theory herein developed, or to indicate the path to another theory.

Laboratory testing of the effect of wire diameter and material of the wire on damping ability should be carried out.

Appendix

Relationship Showing Angle of Lean at Which Wires Can Vibrate Freely From the Side of a Blade When in a Centrifugal-Force Field

Let

a_n = acceleration normal to blade due to vibratory motion

$$a_n = y\omega^2 \quad [28]$$

a_{CFN} = acceleration normal to blade due to centripetal acceleration

The angular relations for small angles are seen to be, from Fig. 6

$$\gamma = \frac{\zeta}{R + X} \quad [29]$$

$$\alpha = \frac{\zeta}{X} \quad [30]$$

$$\gamma - \alpha = -\frac{\zeta R}{XS} \quad [31]$$

No motion of wires will occur when

$$a_n < a_{CFN}$$

or

$$y\omega^2 < \frac{\zeta R}{X}\Omega^2 \quad [32]$$

Where Ω is the rotating speed. This can be written as

$$y_1 < \alpha R \frac{\Omega^2}{\omega^2} \text{ (using largest } y) \quad [33]$$

Comparison of $(\Delta y/y)$, $(\Delta y/y)_E$ and Log Decrement

In obtaining $(\Delta y/y)$ in the analysis, the term $(\Delta K)^2$ was neglected as a second-order term. For large values of damping this leads to an appreciable error. Keeping this term leads to a true value $(\Delta y/y)_E$ in terms of the approximate $(\Delta y/y)$.

Equating Energies

$$\Delta T = \Delta W$$

$$\Delta T = T_1 - T_2 = \frac{1}{2} m y_1^2 \omega^2 - \frac{1}{2} m y_2^2 \omega^2 \quad [34]$$

$$\Delta T = \frac{1}{2} m\omega^2 [y_1^2 - (y_1 - \Delta y)^2] \quad [35]$$

1 If $(\Delta y)^2$ is neglected we obtain

$$m\omega^2(\Delta y)y = \Delta W \quad [36]$$

Then

$$\frac{\Delta y}{y} = \frac{\Delta W}{my^2\omega^2} \quad [37]$$

2 Considering $(\Delta y)^2$ we have

$$\frac{1}{2}m\omega^2[2(\Delta y)y - (\Delta y)^2] = \Delta W \quad [38]$$

or

$$(\Delta y)^2 - 2(\Delta y)y + \frac{2\Delta W}{m\omega^2} = 0 \quad [39]$$

from which

$$\Delta y = y \pm \left[y^2 - \frac{2\Delta W}{m\omega^2}\right]^{1/2} \quad [40]$$

or

$$\left(\frac{\Delta y}{y}\right)_E = 1 \pm \left[1 - 2\frac{\Delta W}{my^2\omega^2}\right]^{1/2} \quad [41]$$

and using Equation [37]

$$\left(\frac{\Delta y}{y}\right)_E = 1 \pm \left[1 - 2\frac{\Delta y}{y}\right]^{1/2} \quad [42]$$

It is known that $(\Delta y/y)_E = 0$ for $(\Delta y/y) = 0$, whereupon the minus sign is retained. Also it is noted that only values of $(\Delta y/y) < 0.5$ have meaning, so

$$\left(\frac{\Delta y}{y}\right)_E = 1 - \left[1 - 2\frac{\Delta y}{y}\right]^{1/2} \quad [43]$$

The log decrement is defined as

$$\log \frac{y_1}{y_2} = \delta \quad [44]$$

or

$$\delta = \log \frac{y_1}{y_1 - \Delta y} = \log \frac{1}{1 - \frac{\Delta y}{y}} \quad [45]$$

Letting $q = (\Delta y/y)$ and expanding the foregoing in a series

$$\delta = 2\left[\frac{q}{2} + \frac{1}{3}\left(\frac{q}{2-q}\right)^3 + \ldots\ldots\right] \quad [46]$$

for $(\Delta y/y) \ll 1$

$$\delta = \frac{\Delta y}{y} + \frac{1}{12}\left(\frac{\Delta y}{y}\right)^2 + \ldots\ldots \quad [47]$$

or

$$\delta = \frac{\Delta y}{y} \quad [48]$$

Thus for small damping, the log decrement is equal to

$$\frac{\Delta y}{y} = \delta$$

Bending Frequency of a Rotating Cantilever Beam

By M. J. SCHILHANSL,[1] PROVIDENCE, R. I.

The stiffening effect of the centrifugal forces on the first-mode bending frequency of a rotating cantilever beam of uniform cross section is investigated by means of the method of successive approximations. It depends upon the angle made by the minor axis of inertia with the direction of the circumferential velocity.

Nomenclature

The following nomenclature is used in the paper:

x = radial co-ordinate
y = tangential co-ordinate
z = axial co-ordinate
e = axis of the minor moment of inertia I_{min}
ψ = angle made by y and e-axes
f = deflection perpendicular to axis e
r_i = radius of hub
L = length of beam
F = cross section of beam
γ = specific weight of material of which blade is made
g = acceleration of gravity
E = modulus of elasticity
ω = angular velocity
ν = bending frequency of rotating beam
$\nu_{\omega=0}$ = bending frequency of nonrotating beam
t = time
M = bending moment
$\xi = x/L$ = dimensionless abscissa
$\rho_i = r_i/L$ = ratio of hub radius to blade length
$\eta(\xi) = f(x)\frac{1}{L}$ = dimensionless deflection
$I = I_{min}$ = minor moment of inertia

Introduction

The following investigation on vibrations of a blade of an axial-flow turbomachine is a contribution to the so-called classical theory of natural frequencies of spring-mass systems, in which a time-wise variation of the forces exerted by the flow is not accounted for as it is in the flutter theory. It is restricted to the analysis of pure bending. This means that the shear center of each cross section is assumed to coincide with the center of gravity and that the torsional rigidity is very high. If, in addition to that, it is assumed that the length L of the blade in the radial direction is large compared with the chord of the blade sections, the blade can be considered as a beam. Furthermore, it will be assumed that the major moment of inertia I_{max} is much larger than the minor moment of inertia I_{min}; thus the deflection perpendicular to the major principal axis of inertia can be neglected. Finally, it will be assumed that the blade is not twisted; thus the angle ψ made by the minor principal axis of inertia with the direction of the circumferential velocity is a constant; see Fig. 1.

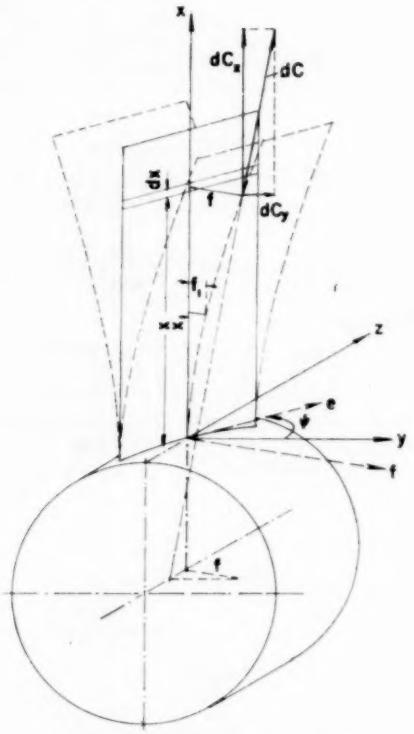

Fig. 1 Cantilever Beam Attached to a Hub

The goal of the following investigation is to find the effect of this angle ψ on the first-mode bending frequency of the rotating beam. This effect is not negligibly small. The bending frequency ν of the rotating beam is usually brought into relation with the bending frequency $\nu_{\omega=0}$ of the nonrotating beam and the angular velocity by

$$\nu^2 = \nu_{\omega=0}^2 + \varphi\omega^2$$

The factor φ is a function of the ratio of the hub radius to the blade length and of the angle ψ as shown in Fig. 2.

For simplicity, it is assumed that F and I are constant. This, however, is not an essential assumption. If F and I are functions of x or ξ, the amount of computing work is larger than for F and I independent of x.

---

[1] Professor of Engineering, Brown University.

Contributed by the Applied Mechanics Division and presented at the Fall Meeting, Hartford, Conn., September 23–25, 1957, of The American Society of Mechanical Engineers.

Discussion of this paper should be addressed to the Secretary, ASME, 29 West 39th Street, New York, N. Y., and will be accepted until April 10, 1958, for publication at a later date. Discussion received after the closing date will be returned.

Note: Statements and opinions advanced in papers are to be understood as individual expressions of their authors and not those of the Society. Manuscript received by ASME Applied Mechanics Division, January 4, 1957. Paper No. 57—F-6.

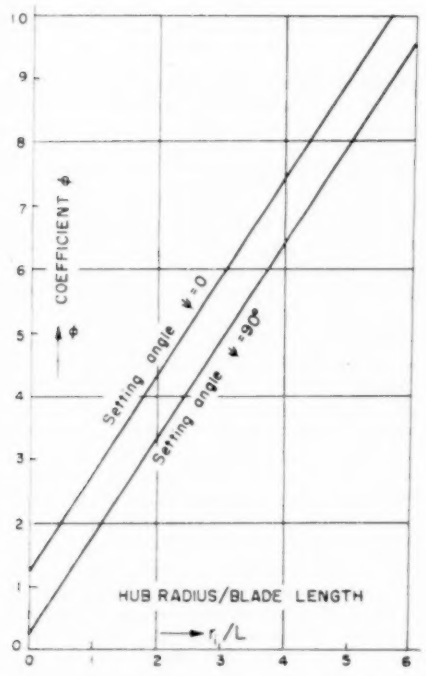

FIG. 2 COEFFICIENT φ AS FUNCTION OF RATIO OF HUB RADIUS r_i TO BLADE LENGTH L FOR TWO EXTREME SETTING ANGLES ψ

THE DIFFERENTIAL EQUATION

The centrifugal force dC exerted by a mass element of the radial length dx located at the abscissa x is

$$dC = \frac{\gamma\omega^2}{g} F(r_i + x)dx \quad \ldots\ldots [1]$$

If the deflection of the beam at any time t is $f(x, t)$, the radial and tangential components of dC are

$$dC_x = dC\left[1 - \left(\frac{f(x, t)\sin\psi}{r_i + x}\right)^2\right]^{1/2} \quad \ldots\ldots [2]$$

and

$$dC_y = dC\frac{f(x, t)\sin\psi}{r_i + x} \quad \ldots\ldots [3]$$

Obviously, dC_x can be equated to dC without any appreciable error. The components C_x and C_y applied at the abscissa x follow by integrating from $x = x$ to $x = L$ as to

$$C_x = \frac{\gamma\omega^2}{g} F\left[r_i(L - x) + \frac{1}{2}(L^2 - x^2)\right] \quad \ldots\ldots [4]$$

and

$$C_y = \frac{\gamma\omega^2}{g} F\sin\psi \int_x^L f(x, t)dx \quad \ldots\ldots [5]$$

The component C_x has a moment arm $df(x, t)$ with respect to the abscissa $(x - dx)$. The component C_y has a moment arm dx with respect to the abscissa $(x - dx)$. Thus the moment dM about the minor principal axis of inertia is

$$dM = C_x df(x, t) - C_y \sin\psi dx \quad \ldots\ldots [6]$$

The component C_y is small compared with the component C_x and the moment arm $df(x, t)$ is small compared to dx; thus both moments are of the same order of magnitude. It does not seem to be permissible to neglect the second term on the right-hand side of Equation [6] in spite of the fact that it is done in several investigations.

By introducing Equations [4] and [5] into Equation [6] and by differentiating partially with respect to dx, it follows that

$$\frac{\partial^2 M}{\partial x^2} = \frac{\gamma\omega^2}{g} F\left\{\left[r_i(L - x) + \frac{1}{2}(L^2 - x^2)\right]\frac{\partial^2 f(x, t)}{\partial x^2} - (r_i + x)\frac{\partial f(x, t)}{\partial x} + \sin^2\psi f(x, t)\right\} \quad \ldots\ldots [7]$$

The second derivative of the moment M with respect to the abscissa x can be comprehended as a lateral load depending upon the centrifugal effect.

The differential equation of a nonrotating beam is

$$EI\frac{\partial^4 f(x, t)}{\partial x^4} + \frac{\gamma F}{g}\frac{\partial^2 f(x, t)}{\partial t^2} = 0 \quad \ldots\ldots [8]$$

where the second term represents d'Alembert's forces. In the case of the rotating beam, the lateral load $-(\partial^2 M)/(\partial x^2)$ must be added. Thus with I = const

$$EI\frac{\partial^4 f(x, t)}{\partial x^4} = \frac{\gamma}{g} F\left\langle -\frac{\partial^2 f(x, t)}{\partial t^2} + \omega^2\left\{\left[r_i(L - x) + \frac{1}{2}(L^2 - x^2)\right]\frac{\partial^2 f(x, t)}{\partial x^2} - (r_i + x)\frac{\partial f(x, t)}{\partial x} + f(x, t)\sin^2\psi\right\}\right\rangle \quad \ldots\ldots [9]$$

Let

$$f(x, t) = f(x)\sin\nu t \quad \ldots\ldots [10]$$

Thence with the dimensionless co-ordinates

$$\frac{d^4\eta(\xi)}{d\xi^4} = \frac{\gamma F L^4}{gEI}\left\langle \nu^2\eta(\xi) + \omega^2\left\{\left[\rho_i(1 - \xi) + \frac{1}{2}(1 - \xi^2)\right]\frac{d^2\eta(\xi)}{d\xi^2} - (\rho_i + \xi)\frac{d\eta(\xi)}{d\xi} + \eta(\xi)\sin^2\psi\right\}\right\rangle \quad \ldots\ldots [11]$$

THE SOLUTION

If the elastic line $\eta(\xi)$ were known, it would be possible to introduce the function $\eta(\xi)$ into the right side of Equation [11], to integrate four times with respect to ξ, and to satisfy the boundary conditions. The function $\bar{\eta}(\xi)$ obtained by this procedure must be equal to the function $\eta(\xi)$ introduced into the right side. Then the frequency ν can be calculated from the equality $\bar{\eta}(\xi) = \eta(\xi)$.

If only an approximate function $\eta_0(\xi)$ is known, the procedure just described yields a function $\eta_1(\xi)$ which is closer to the actual elastic line than $\eta_0(\xi)$, and a frequency ν which is the closer to the actual frequency the better the approximation $\eta_0(\xi)$. The procedure must be iterated until the $(n + 1)$th approximation agrees with the nth approximation.

As a first approximation, the function

$$\eta_{(0)}(\xi) = \xi^2 \quad \ldots\ldots [12]$$

will be selected. It satisfies the geometrical boundary conditions—clamping in at one end—but not the dynamical boundary conditions—no bending moments and no shear forces at the other end.

Introducing Equation [12] into Equation [11] yields

$$\frac{d^4\eta_{(1)}(\xi)}{d\xi^4} = \frac{\gamma F L_1^4}{gEI}\left\{\nu_{(0)}{}^2\xi^2 + \omega^2\left[(\xi^2\sin^2\psi - 3\xi^2 + 1) + 2\rho_i(1 - 2\xi)\right]\right\} \quad [13]$$

By integrating and satisfying the boundary conditions

$$\left.\begin{aligned} &\text{at} \quad \xi = 0\text{:}\ \eta_{(1)} = 0 \quad \text{and} \quad \frac{d\eta_{(1)}}{d\xi} = 0 \\ &\text{at} \quad \xi = 1\text{:}\ \frac{d^2\eta_{(1)}}{d\xi^2} = 0 \quad \text{and} \quad \frac{d^3\eta_{(1)}}{d\xi^3} = 0 \end{aligned}\right\} \quad [14]$$

it follows that

$$\eta_{(1)}(\xi) = \frac{\gamma F L^4}{gEI}\left\{\frac{\nu_{(0)}{}^2}{360}(\xi^5 - 20\xi^3 + 45\xi^2) + \omega^2\left[\frac{\sin^2\psi}{360}(\xi^5 - 20\xi^3 + 45\xi^2) - \frac{1}{120}(\xi^5 - 5\xi^4 + 15\xi^2) + \frac{1}{60}\rho_i(5\xi^4 - 2\xi^3 - 10\xi^2)\right]\right\} \quad [15]$$

The best agreement of the elastic lines $\eta_0(\xi)$ and $\eta_1(\xi)$ is reached by the requirement that

$$\int_0^1 \eta_{(0)}(\xi)d\xi = \int_0^1 \eta_{(1)}(\xi)d\xi \quad [16]$$

Thence

$$\frac{1}{3} = \frac{\gamma F L^4}{gEI}\left\{\frac{71}{2520}\nu_{(0)}{}^2 + \omega^2\left[\frac{71}{2520}\sin^2\psi - \frac{29}{840} - \frac{2}{45}\rho_i\right]\right\} \quad [17]$$

Solving for the first approximation $\nu_{(0)}{}^2$ yields

$$\nu_{(0)}{}^2 = \frac{2520}{213}\frac{gEI}{\gamma F L^4} + \omega^2\left[\frac{(29)(2520)}{(840)(71)} + \frac{(2)(2520)}{(71)(45)}\rho_i - \sin^2\psi\right] \quad [18]$$

The first term on the right side of Equation [18] is the square of the frequency of the nonrotating blade $\nu_{\omega=0(0)}$. With the abbreviation

$$\varphi_{(0)} = 1.225 + 1.577\rho_i - \sin^2\psi \quad [19]$$

Equation [18] can be written as

$$\nu_{(0)}{}^2 = \nu_{\omega=0(0)}{}^2 + \varphi_{(0)}\omega^2 \quad [20]$$

For the purpose of iteration, Equation [18] must be introduced into Equation [15] and then the function $\eta_1(\xi)$ into the right side of Equation [11]. It is self-evident that now terms with ω^4 appear. Provided that ω is small compared with $\nu_{\omega=0}$, the terms with ω^4 may be neglected. Then it follows that

$$\nu_{(1)}{}^2 = \frac{1{,}686{,}960}{136{,}623}\frac{EI}{FL^4} + \omega^2\left[\frac{53{,}921}{45{,}541} + \rho_i\frac{(1{,}686{,}960)(1619)}{(38{,}340)(45{,}541)} - \sin^2\psi\right] \quad [21]$$

or

$$\nu_{(1)}{}^2 = \nu_{\omega=0(1)}{}^2 + \varphi_{(1)}\omega^2 \quad [22]$$

with

$$\varphi_{(1)} = 1.184 + 1.564\rho_i - \sin^2\psi \quad [23]$$

The comparison of the first and second approximations of the frequency of the nonrotating blade with the result of a rigorous theory[3] shows

$\nu_{\omega=0(0)}$ is 2.17 per cent smaller than $(\nu_{\omega=0})_{\text{rigorous}}$
$\nu_{\omega=0(1)}$ is 0.06 per cent smaller than $(\nu_{\omega=0})_{\text{rigorous}}$

The comparison of the first and second approximations of the coefficient φ shows that the difference in the absolute term is 3.5 per cent and in the factor of the ratio ρ_i of the hub radius to the blade length is merely 0.85 per cent.

It might seem objectionable to use such a simple function as represented in Equation [12] for a first approximation, not because it does not satisfy the dynamical boundary conditions, but because the first and the second derivatives of this function appear on the right side of Equation [11]. The differences between the first or second derivatives of an approximate function and the first or second derivatives of the correct function are larger than the differences between the approximate and correct functions. Thus the error caused by these differences might be unbearably large. This error, however, is diminished in each subsequent step and disappears gradually in the same manner as the error caused by the fact that the dynamical boundary conditions are not satisfied by the first approximate function. The second approximation $\eta_{(1)}(\xi)$ satisfies all boundary conditions as Equations [14] and [15] show. The approximation $\eta_{(0)}(\xi) = \xi^2$ would be really a questionable choice if the discrepancies between $\varphi_{(0)}$ and $\varphi_{(1)}$ would be larger than the differences between $\nu_{\omega=0(0)}{}^2$ and $\nu_{\omega=0(1)}{}^2$.

Of course, it is true that the first step already yields numerical values of $\nu_{\omega=0}$ and φ which are very close to the truth, if all boundary conditions are satisfied at the first approximation. If the function

$$\bar{\eta}_{(0)}(\xi) = 2\xi^2 - \frac{4}{3}\xi^3 + \frac{1}{3}\xi^4 \quad [24]$$

is selected instead of Equation [12] it can be found that

$$\nu_{\omega=0(0)} = \frac{1134}{91}\frac{gEI}{\gamma F L^4} \quad [25]$$

and

$$\bar{\varphi}_{(0)} = 1.173 + 1.558\rho_i - \sin^2\psi \quad [26]$$

This result agrees very well with the previous ones.

Conclusion

The stiffening effect of the centrifugal forces on the lowest bending frequency of a cantilever beam depends upon the ratio ρ_i of the hub radius to the blade length, and upon the setting angle ψ made by the blade chord and the rotational velocity. The latter effect is more significant at lower ratios ρ_i as Fig. 2 shows. It cannot be discovered if the component C_z of the centrifugal force is neglected.

---

[3] See, for instance, "Vibration Problems in Engineering," by S. Timoshenko, D. Van Nostrand Company, Inc., New York, N. Y., third edition, 1955, pp. 326, 338; or Biezeno-Grammel, "Technische Dynamik," first edition, Julius Springer, Berlin, Germany, 1939, p. 745.

An Approximate Analysis of Timoshenko Beams Under Dynamic Loads[1]

By B. A. BOLEY[2] and CHI-CHANG CHAO,[3] NEW YORK, N. Y.

An approximate method for the analysis of Timoshenko beams under impact is presented; it is based on a "traveling-wave" approach and on the principle of virtual work. Displacement functions are assumed in terms of several time-dependent parameters; the latter are found as the solution of a set of ordinary differential equations. Some of the characteristics of the propagation of disturbances are analyzed in the Appendix. Illustrative numerical results pertaining to semi-infinite and finite beams also are presented.

Introduction

SEVERAL exact solutions for the behavior of Timoshenko beams under dynamic loads have appeared recently in the literature; these solutions have been derived with the aid of integral-transform techniques leading to results in terms of definite integrals. The numerical evaluation of these integrals must be performed separately for any particular values of the space and time co-ordinates and is therefore very cumbersome. In an attempt to circumvent these drawbacks an approximate theory was developed[4] on the basis of a traveling-wave approach and of the principle of virtual work. The basic theory presented there is of general validity; its application to specific examples was however restricted to a very short portion of the beam near the point of impact and to very short times because of the introduction of additional simplifying assumptions. A method of solution which is free of these shortcomings is described in this paper; its basic theoretical foundation is the same as that of Boley.[4] The method is described in general terms in the next section; some numerical examples, and comparisons with the corresponding exact solutions, may be found later in the paper.

Basic Theory

Let $w = w(x, t)$ and $w_b = w_b(x, t)$ denote, respectively, the total displacement and that portion of it which is due to bending, at any distance x from the point of loading and at a time t. Let $L_1(t)$ be the distance traveled along the beam by the disturbance caused by the loading in a time t; then $L_1(0) = 0$ and

$$w(x, t) = w_b(x, t) = w_b'(x, t) = 0 \quad \text{for} \quad x \geqslant L_1(t) \ldots [1]$$

The principle of virtual work then requires that the displacements w and w_b satisfy the following relation for any arbitrary variations $\delta w_b'$ and δw (for derivation see footnote[4])

$$\int_0^{L_1(t)} [(EIw_b'')' + (GA/N)(w' - w_b') - \rho I w_b''']\delta w_b' dx + \int_0^{L_1(t)} \{[(GA/N)(w' - w_b')]' - \rho A w''\}\delta w \, dx = 0 \ldots [2]$$

where primes and dots indicate differentiation with respect to x and t, respectively, N is the shear-strain-energy correction coefficient, and the other symbols have the usual meanings. The differential equations of Timoshenko beams of nonuniform cross section and properties follow immediately from Equation [2] by setting each integrand equal to zero. The bending moment M, the shear force Q, the angular velocity ω and the velocity v are as follows

$$\left.\begin{aligned} M(x, t) &= -EIw_b'' \\ Q(x, t) &= -(GA/N)(w' - w_b') \\ \omega(x, t) &= w_b'' \\ v(x, t) &= w^{\cdot} \end{aligned}\right\} \ldots [3]$$

The boundary conditions at the loading point $x = 0$ are

$$\left.\begin{aligned} (EIw_b'' + M_0)\delta w_b' &= 0 \\ [(GA/N)(w' - w_b') + Q_0]\delta w &= 0 \end{aligned}\right\} \ldots [4]$$

where $M_0(t) = M(0, t)$ and $Q_0(t) = Q(0, t)$ are the applied moment and force, respectively. The boundary conditions at $x = L_1(t)$ given by Equations [1] must be supplemented by the following requirement which arises from the variational formulation

$$\{c_1^2 - [L_1^{\cdot}(t)]^2\}(w_b'')^2 = \{[L_1^{\cdot}(t)]^2 - c_2^2\}(w'/r)^2 \ldots [5]$$

with the notation

$$c_1 = (E/\rho)^{1/2}; \quad c_2 = [G/(\rho N)]^{1/2}; \quad r = (I/A)^{1/2} \ldots [5a]$$

Equation [5] leads to the conclusion that the disturbance exhibits two wave fronts, traveling with velocities c_1 and c_2, respectively. It is therefore convenient to write

$$\left.\begin{aligned} w &= w_1(x, t) + w_2(x, t) \\ w_b &= w_{b1}(x, t) + w_{b2}(x, t) \end{aligned}\right\} \ldots [6]$$

where, from Equations [1] and [5]

$$w_1 = w_{b1} = w_{b1}' = w_1' = 0 \quad \text{at } x = c_1 t \ldots [6a]$$

$$w_2 = w_{b2} = w_{b2}' = w_{b2}'' = 0 \quad \text{at } x = c_2 t \ldots [6b]$$

Displacements with subscript 1 are zero for $x > c_1 t$ and those with subscript 2 for $x > c_2 t$.

The foregoing formulation suggests a method of solution consisting of the following steps:

1 Assume expressions for the four functions w_1, w_{b1}', w_2, w_{b2}'

---

[1] The work reported here was part of a research project sponsored by the Office of Naval Research.

[2] Associate Professor of Civil Engineering, Institute of Flight Structures, Columbia University.

[3] Research Assistant, Institute of Flight Structures, Columbia University.

[4] "An Approximate Theory of Lateral Impact on Beams," by B. A. Boley, Journal of Applied Mechanics, Trans. ASME, vol. 77, 1955, pp. 69–76.

Contributed by the Applied Mechanics Division and presented at the Annual Meeting, New York, N. Y., December 1–6, 1957, of The American Society of Mechanical Engineers.

Discussion of this paper should be addressed to the Secretary, ASME, 29 West 39th Street, New York, N. Y., and will be accepted until April 10, 1958, for publication at a later date. Discussion received after the closing date will be returned.

Note: Statements and opinions advanced in papers are to be understood as individual expressions of their authors and not those of the Society. Manuscript received by ASME Applied Mechanics Division, August 23, 1956. Paper No. 57—A-17.

satisfying Equations [6a], [6b], and [4] in terms of several (say n) arbitrary parameters $p_1(t), \ldots, p_i(t), \ldots, p_n(t)$. Note that w_b does not appear in the integrands of Equation [2], but only its derivatives; it is therefore sufficient to work with the functions w_{b1}' and w_{b2}' rather than w_{b1} and w_{b2}.

In order to reduce the necessary number of these parameters, it was found desirable to choose the displacement functions so as to satisfy exactly, at the wave fronts, the governing differential equations, in addition to the requirements of Equations [6a] and [6b]. It is shown in the Appendix that the corresponding additional conditions are

$$w_{b1}''(c_1t, t) = w_{b1}''(0, 0)\left[\frac{(EIc_1)_{x=0}}{(EIc_1)_{x=c_1t}}\right]^{1/3} \quad \ldots\ldots [7a]$$

$$w_{b1}'''(c_1t, t) = w_{b1}'''(0, 0)\left[\frac{(EI/c_1)_{x=0}}{(EI/c_1)_{x=c_1t}}\right]^{1/3} \quad \ldots\ldots [7b]$$

$$w_2'(c_2t, t) = w_2'(0, 0)\left[\frac{(GAc_2/N)_{x=0}}{(GAc_2/N)_{x=c_2t}}\right]^{1/3} \quad \ldots\ldots [7c]$$

$$w_2^{\cdot}(c_2t, t) = w_2^{\cdot}(0, 0)\left[\frac{(GA/Nc_2)_{x=0}}{(GA/Nc_2)_{x=c_2t}}\right]^{1/3} \quad \ldots\ldots [7d]$$

These formulas prescribe the manner in which an initial jump in bending moment, angular velocity, shear force, and linear velocity, respectively, is propagated along the beam. For beams of uniform properties and cross section the magnitude of these jumps at the appropriate wave fronts is then clearly unchanged. Note that the quantities $w_{b1}''(0, 0)$, $w_{b1}'''(0, 0)$, $w_2'(0, 0)$, and $w_2^{\cdot}(0, 0)$ appearing in the foregoing are known in terms of the initial values of the applied moment $M_0(0)$, angular velocity $\omega_0(0)$, shear force $Q_0(0)$, and velocity $v_0(0)$ because of the relations (see footnote[4] and Appendix)

$$-w_{b1}''(0, 0) = [w_b'^{\cdot}(0, 0)/c_1] = [M_0(0)/EI] = [\omega_0(0)/c_1] \ldots [8a]$$

$$-w_2'(0, 0) = [w_2^{\cdot}(0, 0)/c_2] = [Q_0(0)N/GA] = [v_0(0)/c_2] \ldots [8b]$$

2 Substitute the assumed displacement functions in Equation [2] and perform the indicated operations. Note that in the region of integration $c_2t \leqslant x \leqslant c_1t$ the displacement with subscript 2 is zero, and therefore Equations [6] reduce to $w = w_1$ and $w_b = w_{b1}$; all displacement functions must of course be taken into account in the region $0 \leqslant x \leqslant c_2t$. Note also that the quantity

$$\delta w = \sum_{i=1}^{n} (\partial w/\partial p_i)\delta p_i \quad \ldots\ldots [9]$$

and similarly for $\delta w_b'$. The result of this step is of the form

$$\sum_{i=1}^{n} F_i(t, p_1, p_1^{\cdot}, p_1^{\cdot\cdot}, \ldots, p_n, p_n^{\cdot}, p_n^{\cdot\cdot})\delta p_i = 0 \quad \ldots\ldots [9a]$$

Since the δp_i quantities are arbitrary, Equation [9a] requires that

$$F_i = 0, \quad i = 1, 2, \ldots, n \quad \ldots\ldots [9b]$$

3 Equations [9b] represent a system of n simultaneous second-order ordinary linear differential equations, which in general have variable coefficients. These equations must now be solved for the n parameters $p_i(t)$ under the condition that at $t = 0$ the displacements conform with Equations [8] and be finite. The displacements, bending moment, and shear force now can be found readily by substitution in the appropriate equations.

Illustrative Examples for Semi-Infinite Beams

The method of solution just discussed will now be applied to a uniform semi-infinite beam ($x \geq 0$), under step inputs of velocity and moment at $x = 0$. The end conditions, for $t \geq 0$, are then

$$\left.\begin{aligned} w(0, t) &= v_0t \\ w_b''(0, t) &= -(M_0/EI) \end{aligned}\right\} \quad \ldots\ldots [10]$$

where v_0 and M_0 are prescribed constants.

Step 1. Functions w_1, w_2, w_{b1}', and w_{b2}' must be chosen so as to satisfy the following conditions (see Equations [6], [7], and [8])

At $x = 0$

$$\left.\begin{aligned} w_1 + w_2 &= v_0t \\ w_{b1}'' + w_{b2}'' &= -(M_0/EI) \end{aligned}\right\} \quad \ldots\ldots [11a]$$

At $x = c_2t$

$$\left.\begin{aligned} w_2 = w_{b2}' = w_{b2}'' &= 0 \\ w_2^{\cdot} = -c_2w_2' &= v_0 \end{aligned}\right\} \quad \ldots\ldots [11b]$$

At $x = c_1t$

$$\left.\begin{aligned} w_1 = w_{b1}' = w_1' &= 0 \\ w_{b1}'' = -(w_{b1}'''/c_1) &= -(M_0/EI) \end{aligned}\right\} \quad \ldots\ldots [11c]$$

The following displacement functions were selected

$$\left.\begin{aligned} w_1(x, t) &= \alpha(t)(x - c_1t)^3; \quad 0 \leqslant x \leqslant c_1t \\ w_2(x, t) &= -(v_0/c_2)(x - c_2t) - \alpha(t)(c_1/c_2)^2(x - c_2t)^3; \\ &\qquad 0 \leqslant x \leqslant c_2t \\ w_{b1}'(x, t) &= \beta(t)(x - c_1t)^3 - (M_0/EI)(x - c_1t); \\ &\qquad 0 \leqslant x \leqslant c_1t \\ w_{b2}'(x, t) &= -\beta(t)(c_1/c_2)(x - c_2t)^3; \quad 0 \leqslant x \leqslant c_2t \end{aligned}\right\} \quad \ldots [12]$$

Note that two parameter functions, α and β, are employed in the assumed deflections.

Step 2. Substitution of Equations [12] in Equation [2] gives the following result

$$\begin{aligned} \int_0^{c_2t} \Bigg[\Bigg[\Bigg\{ \frac{GA}{N}\left[2\alpha\left(1 - \frac{c_1^3}{c_2^3}\right) + \frac{M_0}{EI} - 2\beta x\left(1 - \frac{c_1}{c_2}\right)\right] \\ - \rho A\left[\ddot{\alpha}(x - c_1t)^3 - \ddot{\alpha}\left(\frac{c_1}{c_2}\right)^3(x - c_2t)^3 \right. \\ \left. - 4\dot{\alpha}c_1x\left(1 - \frac{c_1}{c_2}\right)\right]\Bigg\}\left[(x - c_1t)^3 - \left(\frac{c_1}{c_2}\right)^3(x - c_2t)^3\right]\delta\alpha \\ + \Bigg\{\frac{GA}{N}\left[2\alpha x\left(1 - \frac{c_1}{c_2}\right) - \beta(x - c_1t)^3 + \beta\frac{c_1}{c_2}(x - c_2t)^3 \right. \\ \left. + \frac{M_0}{EI}(x - c_1t) - \frac{V_0}{c_2}\right] - \rho I\left[2\beta\frac{c_1}{c_2}(c_1^3 - c_2^3) \right. \\ \left. + 4\dot{\beta}t(c_1^3 - c_1c_2) + \ddot{\beta}(x - c_1t)^3 - \ddot{\beta}\frac{c_1}{c_2}(x - c_2t)^3\right]\Bigg\} \\ \left[(x - c_1t)^3 - \frac{c_1}{c_2}(x - c_2t)^3\right]\delta\beta\Bigg]\Bigg] dx \\ + \int_{c_2t}^{c_1t} \Bigg[\Bigg[\Bigg\{\left[\frac{GA}{N}\left(2\alpha + \frac{M_0}{EI}\right) + \frac{\rho I}{c_1}4\dot{\beta}\right](x - c_1t)^3 \\ - \left[\frac{GA}{N}\beta + \rho I\ddot{\beta}\right](x - c_1t)^4\Bigg\}\delta\beta \\ + \delta\alpha\Bigg\{\left[\frac{GA}{N}\left(2\alpha + \frac{M_0}{EI}\right) - 2\rho Ac_1^2\alpha\right](x - c_1t)^3 \\ - \left[\frac{2GA}{N}\beta - 4\rho Ac_1\dot{\alpha}\right](x - c_1t)^4 - \rho A\ddot{\alpha}(x - c_1t)^4\Bigg\}\Bigg]\Bigg] dx \quad \ldots [13] \end{aligned}$$

Performing the indicated integrations, and setting the coefficients

of $\delta\alpha$ and $\delta\beta$ equal to zero, one obtains the following two differential equations (corresponding to Equations [9b])

$$\left.\begin{aligned}&\ddot{A}\tau^2 + 5\dot{A}\tau + AR_1 + BR_2\tau + (M_0/EI)R_3 = 0\\&\ddot{B}\tau^2 + 5\dot{B}\tau + B(R^2\tau^2 + R_4) + R_5A\tau + (V_0/c_1)R_6\\&\qquad + (M_0/EI)R_7\tau = 0\end{aligned}\right\} \quad [14]$$

The unknowns α and β appear in these equations in the nondimensional forms

$$A(\tau) = r\alpha(t);\quad B(\tau) = r^2\beta(t) \quad [14a]$$

The independent variable, time, is represented nondimensionally by the quantity

$$\tau = c_1 t/r \quad [14b]$$

where $r = (I/A)^{1/2}$ is the radius of gyration of the beam cross section. Dots represent here differentiation with respect to τ. The constants R_i are functions of the ratio R of the speeds of propagation c_1 and c_2 and are defined later. The numerical values listed in brackets are those corresponding to $N = 1.2$ and $G/E = {}^3/_8$ (i.e., Poisson's ratio $\nu = 1/3$); all numerical results presented in this paper were obtained on this basis

$$\left.\begin{aligned}R &= c_2/c_1 = [\sqrt{5/4} = 0.559017]\\R_1 &= \frac{10(1+R)}{3-R} = [6.386841]\\R_2 &= -\frac{5R^2}{2} = [-0.781250]\\R_3 &= -\frac{5R^2}{(3-R)(1-R)} = [1.451555]\\R_4 &= \frac{10(3-R)(1-R^2)}{3-7R^2+R^3} = [6.298882]\\R_5 &= -\frac{5(3-R)(1-R)R^2}{2(3-7R^2+R^3)} = [-0.315648]\\R_6 &= \frac{5(3-R)R^2}{3-7R^2+R^3} = [1.431564]\\R_7 &= +\frac{5(3+3R-R^2)R^2}{4(3-7R^2+R^3)} = [+0.639920]\end{aligned}\right\} \quad [14c]$$

The solution of Equations [14] must now be obtained under the initial conditions that $A(0)$, $\dot{A}(0)$, $B(0)$, and $\dot{B}(0)$ be finite, and can therefore be expressed in terms of series of non-negative powers of τ.

Let then $$A(\tau) = \sum_{i=0}^{\infty} a_i\tau^i;\quad B(\tau) = \sum_{i=0}^{\infty} b_i\tau^i \quad [15]$$

After substitution into Equations [14], the coefficients of each power of τ may be equated to give the coefficients a_i and b_i in the following form

$$\left.\begin{aligned}(EI/M_0)a_0 &= -(R_2/R_1) = -(R^2/2)/(1-R^2)\\(c_1/v_0)b_0 &= -(R_6/R_4) = -(R^2/2)/(1-R^2)\\(EI/M_0)b_1 &= -[R_7 + R_5(a_0EI/M_0)]/(R_4+5)\\a_i(i^2+4i+R_1) + b_{i-1}R_2 &= 0 \quad \text{for} \quad i = 1, 2, 3, \ldots\\b_i(i^2+4i+R_4)&\\+ b_{i-2}R^2 + a_{i-1}R_5 &= 0 \quad \text{for} \quad i = 2, 3, 4, \ldots\end{aligned}\right\} \quad [15a]$$

Numerical calculations can be carried out without difficulty from Equations [15a] and [14c] for $N = 1.2$ and $\nu = 1/3$; the results are as follows

$$\left.\begin{aligned}A(\tau) = (M_0/EI)[&0.227273 - 0.213666\times10^{-3}\tau^2\\&+ 0.112128\times10^{-4}\tau^4 - 0.386844\times10^{-7}\tau^6\\&+ 0.929803\times10^{-10}\tau^8 - 0.163555\times10^{-12}\tau^{10}\\&+ 0.218978\times10^{-15}\tau^{12} - 0.230232\times10^{-18}\tau^{14}\\&+ 0.194933\times10^{-21}\tau^{16} - 0.136678\times10^{-24}\tau^{18}\\&+ 0.801101\times10^{-28}\tau^{20} - 0.395601\times10^{-31}\tau^{22}\\&+ 0.167796\times10^{-34}\tau^{24}\ldots]\\+ (v_0/c_1)[&-0.155932\times10^{-1}\tau + 0.103046\times10^{-3}\tau^3\\&- 0.435198\times10^{-6}\tau^5 + 0.124470\times10^{-8}\tau^7\\&- 0.254532\times10^{-11}\tau^9 + 0.388916\times10^{-14}\tau^{11}\\&- 0.459826\times10^{-17}\tau^{13} + 0.432620\times10^{-20}\tau^{15}\\&- 0.331333\times10^{-23}\tau^{17} + 0.210479\times10^{-26}\tau^{19}\\&- 0.112656\times10^{-29}\tau^{21}\ldots]\end{aligned}\right\} \quad [16a]$$

$$\left.\begin{aligned}B(\tau) = (M_0/EI)[&-0.502866\times10^{-1}\tau + 0.550943\times10^{-3}\tau^3\\&- 0.328721\times10^{-5}\tau^5 + 0.121856\times10^{-7}\tau^7\\&- 0.306462\times10^{-10}\tau^9 + 0.556063\times10^{-13}\tau^{11}\\&- 0.761458\times10^{-16}\tau^{13} + 0.814383\times10^{-19}\tau^{15}\\&- 0.698817\times10^{-22}\tau^{17} + 0.498746\times10^{-25}\tau^{19}\\&- 0.292877\times10^{-28}\tau^{21} + 0.145703\times10^{-31}\tau^{23}\\&- 0.621896\times10^{-35}\tau^{25}\ldots]\\+ (v_0/c_1)[&-0.227273 + 0.361229\times10^{-2}\tau^2\\&- 0.286252\times10^{-4}\tau^4 + 0.132853\times10^{-6}\tau^6\\&- 0.401995\times10^{-9}\tau^8 + 0.853186\times10^{-12}\tau^{10}\\&- 0.133835\times10^{-14}\tau^{12} + 0.161357\times10^{-17}\tau^{14}\\&- 0.154115\times10^{-20}\tau^{16} + 0.119454\times10^{-23}\tau^{18}\\&- 0.766256\times10^{-27}\tau^{20} + 0.413453\times10^{-30}\tau^{22}\ldots]\end{aligned}\right\} \quad [16b]$$

Four series appear in Equations [16]; their convergence is quite rapid for $0 < \tau < 5$ approximately, and becomes slower as τ increases. For an accurate third significant figure, for example, $\tau = 10$ requires about 8 terms, while $\tau = 20$ requires approximately all the terms listed. For larger values of τ additional terms should be computed; the behavior of the solution in this case, however, may be studied as described later.

Numerical results showing the behavior of semi-infinite beams at comparatively short times are presented in Figs. 1, 2, 3, and 4. The loading conditions for these examples were chosen so as to permit a direct comparison with the pertinent exact results[5]; for convenience, these are reproduced in the figures. It may be seen that, although only two parameters were used, good agreement between the exact and the present approximate solution is obtained in Figs. 1 and 2. The agreement in Fig. 3 is less satisfactory, principally because the assumed deflections constrain the bending-moment distribution to be composed exclusively of straight-line segments. No exact results were available for comparison with Fig. 4.

Note that an additional check on the accuracy of the present solution may be obtained without reference to an exact solution, by making use of the reciprocal relations discussed previously.[5] Thus the variation of the velocity due to an applied end moment (with $v = 0$) should be the same as that of the moment due to an applied end velocity (with $M = 0$); the curves in Fig. 1 showing these variations are in fact quite close.

It is of interest to note that considerably less computational

[5] "Some Solutions of the Timoshenko-Beam Equations," by B. A. Boley and Chi-Chang Chao, JOURNAL OF APPLIED MECHANICS, Trans. ASME, vol. 77, 1955, pp. 579–586.

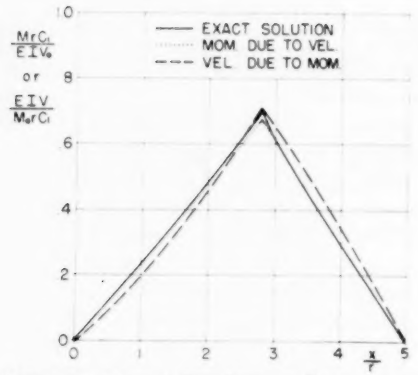

FIG. 1 VARIATION ALONG A SEMI-INFINITE BEAM, AT $\tau = 5$, OF VELOCITY DUE TO AN APPLIED END MOMENT (WITH $v_0 = 0$) AND OF MOMENT DUE TO AN APPLIED END VELOCITY (WITH $M_0 = 0$)

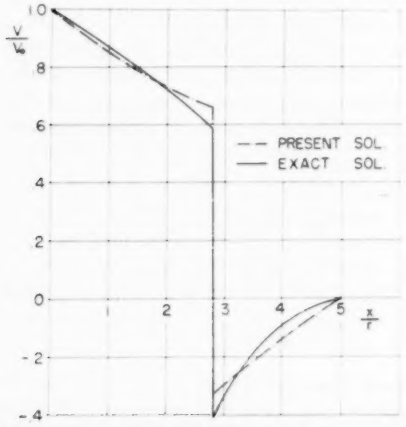

FIG. 2 VARIATION ALONG A SEMI-INFINITE BEAM, AT $\tau = 5$, OF VELOCITY DUE TO AN APPLIED END VELOCITY (WITH $M_0 = 0$)

labor is required to obtain the present results than the exact ones.[5] Roughly speaking, one may perhaps state that the work necessary to obtain only one exact point on a curve such as that of Fig. 1 will give the entire approximate curve by the present method.

The behavior of the coefficients a_i and b_i for large i, which is needed for analyses at long times, may be determined on the basis of Equations [15a], in the following manner: For simplicity, consider the case of $M_0 = 0$; then all even a_i and all odd b_i are zero. The coefficient b_0 is the same as before, and the remaining coefficients are obtained from the last two equations of Set [15a], which may be simplified as follows

$$\left.\begin{aligned} a_{2i+1}(4i^2 + 12i + 5 + R_1) \\ + b_{2i}R_2 = 0; \quad i = 0, 1, 2, \ldots \\ b_{2i}(4i^2 + 8i + R_4) \\ + b_{2i-2}R^2 + a_{2i-1}R_5 = 0; \quad i = 1, 2, 3, \ldots \end{aligned}\right\} \quad [17]$$

For large i, these equations can clearly be approximated by

$$\left.\begin{aligned} 4a_{2i+1}(i + 1)(i + 2) + R_2 b_{2i} = 0 \\ 4b_{2i}(i + 1)^2 + b_{2i-2}R^2 = 0 \end{aligned}\right\} \quad [17a]$$

The second of these gives

$$(b_{2i}/b_{2i-2}) = -R^2/[4(i + 1)^2] \quad [17b]$$

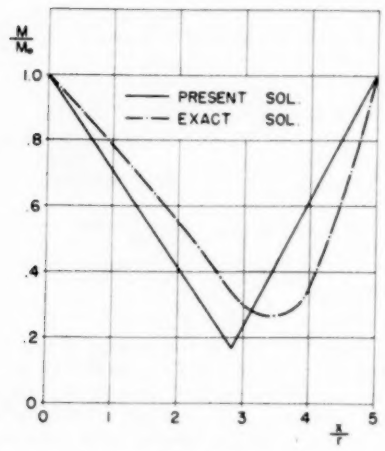

FIG. 3 VARIATION ALONG A SEMI-INFINITE BEAM, AT $\tau = 5$, OF BENDING MOMENT DUE TO AN APPLIED END MOMENT (WITH $v_0 = 0$)

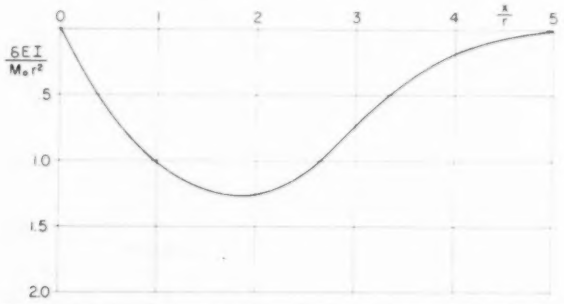

FIG. 4 VARIATION ALONG A SEMI-INFINITE BEAM, AT $\tau = 5$, OF DISPLACEMENT DUE TO AN APPLIED END MOMENT (WITH $v_0 = 0$)

For $i = 11$, for example, this ratio equals 1843.2, and agrees within about $\frac{1}{2}$ per cent with the correct value of 1853.3, obtained from Equation [16b]. Recalling now the series expansion for the Bessel function of order zero, one may write

$$\frac{1 - J_0(R\tau)}{\tau^2} = \sum_{i=0}^{\infty} c_{2i}\tau^{2i} \quad \text{with}$$

$$c_{2i} = (-1)^i R^{2(i+1)}/[2^{i+1}(i + 1)!]^2 \quad [18]$$

so that

$$(c_{2i}/c_{2i-2}) = -R^2/[4(i + 1)^2] \quad [18a]$$

which is identical with Equation [17b]. For any integer N sufficiently large (and $N = 11$ has been seen to be satisfactory) one may then write

$$(c_{2i}/c_{2N}) = (b_{2i}/b_{2N}) \quad [18b]$$

The function $B(\tau)$ may now be written as

$$B(\tau) = \sum_{i=0}^{N-1} b_{2i}\tau^{2i} + b_{2N} \sum_{i=N}^{\infty} (b_{2i}/b_{2N})\tau^{2i} \quad [18c]$$

Approximating the second summation in accordance with Equation [18b], adding and subtracting the quantity

$$b_{2N} \sum_{i=0}^{N-1} (c_{2i}/c_{2N})\tau^{2i}$$

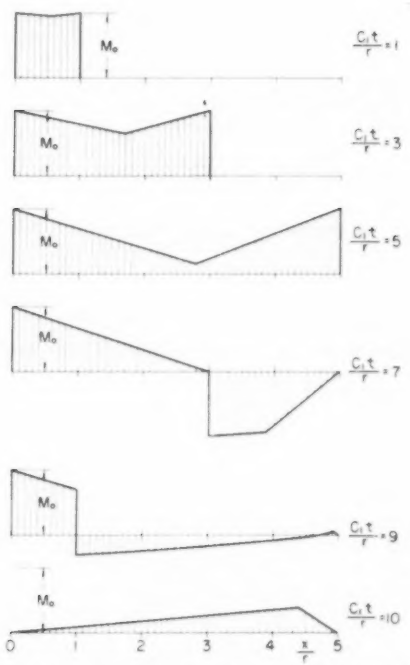

FIG. 5 DISTRIBUTION OF BENDING MOMENT AT VARIOUS TIMES IN A SIMPLY SUPPORTED FINITE BEAM DUE TO AN APPLIED END MOMENT

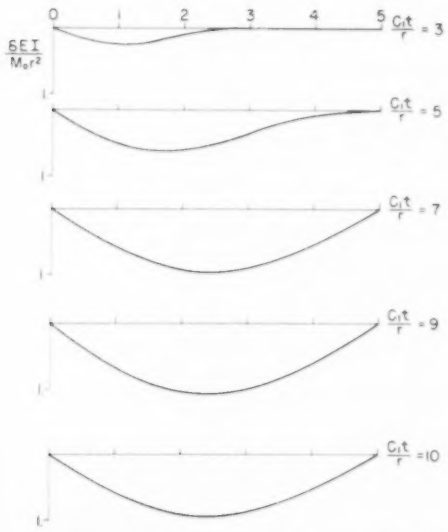

FIG. 6 DISTRIBUTION OF DISPLACEMENT AT VARIOUS TIMES IN A SIMPLY SUPPORTED FINITE BEAM DUE TO AN APPLIED END MOMENT

and finally using Equation [18], one arrives at the following approximate representation of $B(\tau)$

$$B(\tau) = \sum_{i=0}^{N-1} [b_{2i} - b_{2N}(c_{2i}/c_{2N})]\tau^{2i} + (b_{2N}/c_{2N})\left[\frac{1 - J_0(R\tau)}{\tau^2}\right] \quad [18d]$$

Equation [18] is very convenient for purposes of numerical computations. Similar results may be obtained for the other series of Equations [16]. The oscillatory nature of the exact solution of the Timoshenko beam equations is clearly shown by the presence of J_0 in Equation [18*d*]. Furthermore, the period T of these oscillations approaches, for long times, the value

$$(c_1 T/r) = (2\pi/R) \text{ or } T = 2\pi r/c_2 \quad [19]$$

namely, the period of thickness-shear vibrations accounted for by the Timoshenko theory.

FINITE-BEAM EXAMPLES

Solutions for simply supported finite beams can be constructed readily by superposition of semi-infinite beam results according to the method of images.[6] Some illustrative results are shown in Figs. 5 and 6, for the case of a simply supported beam one end of which is subjected to a step bending moment M_0.

Appendix

DERIVATION OF EQUATIONS [7] AND [8]

Let the symbols D_1 and D_2 denote total differentiation with respect to time along the wave fronts moving with velocities c_1 and c_2, respectively; thus for any function $F(x, t)$

$$D_1 F = F'c_1 + \dot{F};\ D_2 F = F'c_2 + \dot{F} \quad [20]$$

In particular it follows from Equations [6*a*] that at $x = c_1 t$

$$D_1 w_1 = D_1 w_{b1} = D_1 w_{b1}' = D_1 w_1' = D_1^2 w_1 = D_1^2 w_{b1} = D_1^2 w_{b1}' = D_1^2 w_1' = \ldots = 0 \quad [21a]$$

and from Equation [6*b*] that at $x = c_2 t$

$$D_2 w_2 = D_2 w_{b2} = D_2 w_{b2}' = D_2 w_{b2}'' = D_2^2 w_2 = D_2^2 w_{b2} = D_2^2 w_{b2}' = D_2^2 w_{b2}'' = \ldots = 0 \quad [21b]$$

Equations [8] follow immediately from the definitions of Equations [3], and from Relations [6*a*], [6*b*], [21*a*], and [21*b*].

The additional conditions of Equations [7*a*] and [7*b*], namely, those pertaining to the wave front moving with a velocity c_1, will now be derived. At this wave front

$$D_1\omega = w_{b1}''c_1 + w_{b1}''' \quad [22]$$

and the differential equation corresponding to the first integral in Equation [2], combined with Equation [6*a*], requires that

$$(EIw_{b1}'')' - \rho I w_{b1}''' = 0 \quad [23]$$

Elimination of w_{b1}''' from Equations [22] and [23] gives

$$(EI/c_1)D_1\omega = (EIw_{b1}'')'c_1 + (EIw_{b1}'')' = -D_1 M \quad [24]$$

Note that EI is a function of x alone. The condition that at this wave front $D_1^2 w_{b1}' = 0$ reduces to

$$D_1(D_1 w_{b1}') = D_1[\omega - (Mc_1/EI)] = D_1\omega - (c_1/EI)D_1 M - M D_1(c_1/EI) = 0 \quad [25]$$

With the expression for $D_1\omega$ given by Equation [24], the following differential equation is obtained

$$\frac{D_1 M}{M} = -\frac{1}{2}\frac{D_1(c_1/EI)}{(c_1/EI)} \quad [26]$$

Integration of this equation gives the relation between the initial

[6] "On Traveling Waves in Beams," by R. W. Leonard and B. Budiansky, NACA TN 2874, January, 1953.

applied bending moment $M_0(0)$ and the bending moment $M(c_1t, t)$ at any position of the wave front moving with velocity c_1 as

$$\frac{M(c_1t, t)}{M_0(0)} = \left[\frac{(EI/c_1)_{x=c_1t}}{(EI/c_1)_{x=0}}\right]^{1/2} \quad [26a]$$

From $D_1w_{b1}' = 0$ at $x = c_1t$ and from Equation [26a] it follows that

$$\frac{\omega(c_1t, t)}{\omega_0(0)} = \frac{M_0(0)}{M(c_1t, t)} \quad [26b]$$

Relations [7a] and [7b] follow directly from Equations [26a] and [26b], respectively, with the aid of Equations [3].

The derivation of Equations [7c] and [7d], pertaining to the wave front moving with a velocity c_2, is carried out in a manner analogous to that just outlined for Equations [7a] and [7b]. At this wave front

$$D_2w_2^{\cdot} = w_2''c_2 + w_2^{\cdot\cdot} \quad [27]$$

and the differential equation corresponding to the second integral in Equation [2], combined with Equations [6b], requires that

$$Q_2' + \rho A w_2^{\cdot\cdot} = 0; \quad Q_2 = -(GA/N)w_2' \quad [28]$$

Elimination of $w_2^{\cdot\cdot}$ from Equations [27] and [28] gives

$$(GA/Nc_2)D_2w_2^{\cdot} = -D_2Q_2 \quad [29]$$

Note that (GA/N) is a function of x alone. The condition that at this wave front $D_2^2w_2 = 0$ reduces to

$$\begin{aligned} D_2(D_2w_2) &= D_2[-Q_2(Nc_2/GA) + w_2^{\cdot}] \\ &= D_2w_2^{\cdot} - (Nc_2/GA)D_2Q_2 - Q_2D_2(Nc_2/GA) \end{aligned} \quad [30]$$

With the expression for $D_2w_2^{\cdot}$ given by Equation [29], the following differential equation is obtained

$$\frac{D_2Q_2}{Q_2} = -\frac{1}{2}\frac{D_2(Nc_2/GA)}{(Nc_2/GA)} \quad [31]$$

Integration of this equation gives the relation between the initial applied shear force $Q_0(0)$ and the shear force $Q_2(c_2t, t)$ carried by the wave which travels with a velocity c_2 as

$$\frac{Q_2(c_2t, t)}{Q_0(0)} = \left[\frac{(GA/Nc_2)_{x=c_2t}}{(GA/Nc_2)_{x=0}}\right]^{1/2} \quad [31a]$$

Note that the denominator of the left-hand side is obtained from the relation

$$\begin{aligned} Q_0(0) = Q(0,0) &= -(GA/N)(w_1' + w_2' - w_{b1}' - w_{b2}')_{x=t=0} \\ &= -(GAw_2'/N)_{x=t=0} = Q_2(0, 0) \end{aligned} \quad [31b]$$

From $D_2w_2 = 0$ at $x = c_2t$ and from Equation [31a] it follows that

$$\frac{w_2^{\cdot}(c_2t, t)}{v_0(0)} = \frac{Q_0(0)}{Q_2(c_2t, t)} \quad [31c]$$

Relations [7c] and [7d] follow directly from Equations [31a] and [31c], respectively, with the aid of Equations [3].

Relation such as Equations [26a], [26b], [31a], [31c], or [7], which describes the variation of certain quantities along the appropriate wave fronts, is usually derived either by studying the properties of the governing differential equations by the method of characteristics,[8] or by investigating the nature of the solution of these differential equations in the transformed domain.[5] It is interesting to note they were derived here from considerations arising entirely from the principle of virtual work and from the kinematic conditions [6]. Furthermore, the present derivation emphasizes the physical aspects of the propagation of disturbances.

Bending of an Elastically Restrained Circular Plate Under Normal Loading Over a Sector

By W. A. BASSALI,[1] ALEXANDRIA, EGYPT, AND R. H. DAWOUD,[2] CAIRO, EGYPT

The complex variable method is used to find the deflection, bending and twisting moments, and shearing forces at any point of a thin circular plate normally loaded over a sector and supported at its edge under a general boundary condition including the usual clamped and simply supported boundaries. In this way separate treatments for these two cases are avoided and a single treatment is available.

Nomenclature

The following nomenclature is used in the paper:

C = boundary of plate
w = deflection of plate in Z-direction
D = flexural rigidity
p = transverse load intensity
h = thickness of plate
s, n = arcs of orthogonal curves in mid-plane of plate
M_n, M_s = bending moments per unit length of sections of a plate perpendicular to n and s-directions
M_{ns} = twisting moment per unit length of a section of a plate perpendicular to n-direction
Q_n = shearing force parallel to Z-axis per unit length of section of a plate perpendicular to n-direction
$V_n = Q_n - \partial M_{ns}/\partial s$ = intensity of vertical reaction at boundary of plate per unit length of arc
K_s, K_n = curvatures of mid-surface of plate
$z = x + iy$ = complex variable in mid-plane of plate
c = radius of circular plate
$t = z/c$
r, θ = polar co-ordinates in mid-plane of plate
$\rho = r/c$
$-\mu$ = ratio between bending moments at any point on $C = M_n/M_s$
η = Poisson's ratio
$\beta = (1 - \eta)/(1 + \eta)$
λ = restraining parameter defining the type of constraint at boundary of plate
$\lambda = (\mu - 1)\beta/(\mu + 1)$
$\nu = (1 + \lambda)/(1 - \lambda) = (\mu + \eta)/(1 + \mu\eta)$
m, n, s, k = positive integers, $s' = s + 2$
$K; \delta_1, \delta_2, \delta_3; \gamma_1, \gamma_2, \gamma_3$ = dimensionless quantities defining deflection, bending and twisting moments, shearing forces, and vertical reaction at any point of plate

Other symbols are defined in the text.

Introduction

Methods of complex-function theory to solve boundary-value problems of two-dimensional elasticity were introduced originally by Kolossoff and developed later by him in collaboration with Muskhelishvili (1).[3] These methods were then applied to isotropic and anisotropic plate problems by Lechnitzky, Sherman, Stevenson, Lurie, Morris, and several others.[4] An English exposition of Lechnitzky's results is given in Sokolnikoff's notes (3).

A general form of the boundary condition defining certain types of constraint at the boundary of a thin plate has been introduced by the authors (4). This assumes the constancy of the ratio between the boundary bending moments M_n, M_s, and has the advantage of including the usual clamped and hinged boundaries as well as other special cases. The introduction of this boundary condition is of practical importance since neither rigidly clamped nor simply supported conditions can be realized exactly under actual physical conditions, and thus any case met in practice must lie somewhere between these two limiting cases. A short account of this boundary condition will be given in this paper.

Solutions of the problems of thin circular plates bent by uniformly distributed normal pressures or concentrated loads have been known for a long time (5, 6). When the plate is concentrically and symmetrically loaded the solutions also are found easily,[5] but the problem of a thin circular plate under an arbitrary distribution of normal thrust has not received much attention. It is clear that this problem is not without practical interest since we may have various nonuniform distribution of thrusts at points of contact when heavy bodies of different shapes are placed on the plate. For nonsymmetrical loadings there are the solutions of Flügge (7) for a linearly varying load over the whole simply supported circular plate and of Schmidt (8) for a clamped circular plate uniformly loaded over an eccentric circle. The complex-variable method was applied by the authors (4) to obtain solutions for a circular plate with an eccentric circular patch sym-

[1] Assistant Professor of Applied Mathematics, Faculty of Science, University of Alexandria.

[2] Assistant Professor, Department of Mathematics, Faculty of Engineering, Cairo University.

Contributed by the Applied Mechanics Division and presented at the Annual Meeting, New York, N. Y., December 1–6, 1957, of The American Society of Mechanical Engineers.

Discussion of this paper should be addressed to the Secretary, ASME, 29 West 39th Street, New York, N. Y., and will be accepted until April 10, 1958, for publication at a later date. Discussion received after the closing date will be returned.

Note: Statements and opinions advanced in papers are to be understood as individual expressions of their authors and not those of the Society. Manuscript received by ASME Applied Mechanics Division, February 13, 1956. Paper No. 57—A-8.

[3] Numbers in parentheses refer to the Bibliography at the end of the paper.

[4] References to the work of some of these authors and others are given at the end of (1). Other references for aeolotropic and isotropic materials are given in (2).

[5] Reference (5), p. 68.

metrically loaded with respect to its center and subjected to the general boundary condition introduced. The authors (9) also found the solutions for loading of the type $p_0 r^m \begin{matrix}\cos \\ \sin\end{matrix} n\theta$ over the whole plate or over a concentric circle under the same boundary condition. A summary of these solutions when the load is distributed over the complete plate will be given in this paper. By the principle of superposition we can thus obtain the solution corresponding to any loading over the whole plate, which can be expressed as the sum of a finite or infinite number of terms such as $p_0 r^m \begin{matrix}\cos \\ \sin\end{matrix} n\theta$. In this paper we use this method to obtain the solution for a circular plate under the boundary condition mentioned before (4) and normally loaded over a sector. Expressions for the bending and twisting moments, the shearing forces, and vertical reaction at any point on the boundary and at the center of the plate are obtained. We also give tables for the numerical values of the deflections at various points on the diameter of symmetry of the plate and for the bending moments, shearing forces, and vertical reaction at one end of this diameter. All these values were calculated for different types of boundary constraint and various angles of the loaded sector in the case of a uniform load over the sector, and curves showing these results are given.

Preliminary Results

Consider an isotropic homogeneous thin plate of thickness h and flexural rigidity D, bounded by a closed curve C. The transverse displacement w, measured positively downward, of the middle surface of the plate at any point $z = x + iy = re^{i\theta}$ satisfies the biharmonic equation

$$D\nabla^4 w = p(r, \theta) \quad [1]$$

where

$$\nabla^2 = \frac{\partial^2}{\partial x^2} + \frac{\partial^2}{\partial y^2} = \frac{\partial^2}{\partial r^2} + \frac{1}{r}\frac{\partial}{\partial r} + \frac{1}{r^2}\frac{\partial^2}{\partial \theta^2} = 4\frac{\partial^2}{\partial z \partial \bar{z}}$$

and $p(r, \theta)$ is the transverse load intensity at the point (r, θ).

The general solution of Equation [1] may be represented in terms of two analytic functions $\phi(z)$, $\psi(z)$ of the complex variable z and a particular integral $W(z, \bar{z})$

$$w = \bar{z}\phi(z) + z\bar{\phi}(\bar{z}) + \psi(z) + \bar{\psi}(\bar{z}) + W(z, \bar{z}) \quad [2]$$

where bars are used to denote conjugate complex quantities.

If s and n are arcs of orthogonal curves in the mid-plane of the plate, then the bending and twisting moments per unit length M_n, M_s, M_{ns}, and the shearing forces Q_n, Q_s per unit length at any point z may conveniently be expressed (10, 11) in terms of w as follows[6]

$$M_n + M_s = -4(1 + \eta)D\frac{\partial^2 w}{\partial z \partial \bar{z}} = -(1 + \eta)D\nabla^2 w \quad [3a]$$

$$M_n - M_s + 2iM_{ns} = -4(1 - \eta)De^{2i\alpha}\frac{\partial^2 w}{\partial z^2} \quad [3b]$$

$$Q_n - iQ_s = -8De^{i\alpha}\frac{\partial^3 w}{\partial z^2 \partial \bar{z}} = -D\left(\frac{\partial}{\partial n} - i\frac{\partial}{\partial s}\right)\nabla^2 w \quad [3c]$$

[6] The relations between the notations used here and those of A. C. Stevenson (10, 11) are $M_n = -h.n\bar{n}$, $M_s = h.s\bar{s}$, $M_{ns} = h.s\bar{n} = -h.n\bar{s}$; $Q_n = -h.n\bar{Z}$, $Q_s = -h.s\bar{Z}$, h being the thickness of the plate. Notice that in Stevenson's work w is measured positively upward and $2h$ is the thickness of the plate.

where α is the angle which the normal n at the point considered makes with the x-axis, and η is Poisson's ratio. Using Equations [1.18]–[1.23] of Stevenson[7] and noticing the difference in notation we easily find

$$M_n + M_s = -(1 + \eta)D\left(\frac{\partial^2 w}{\partial s^2} + K_s\frac{\partial w}{\partial n} + \frac{\partial^2 w}{\partial n^2} + K_n\frac{\partial w}{\partial s}\right) \quad [4a]$$

$$M_n - M_s = (1 - \eta)D\left(\frac{\partial^2 w}{\partial s^2} + K_s\frac{\partial w}{\partial n} - \frac{\partial^2 w}{\partial n^2} - K_n\frac{\partial w}{\partial s}\right) \quad [4b]$$

$$M_{ns} = (1 - \eta)D\left(\frac{\partial^2 w}{\partial s \partial n} - K_s\frac{\partial w}{\partial s}\right) \quad [4c]$$

where

$$K_s = \frac{\partial \alpha}{\partial s}, \quad K_n = -\frac{\partial \alpha}{\partial n} \quad [5]$$

Equating the real and imaginary parts of Equation [3c] we obtain

$$Q_n = -D\frac{\partial}{\partial n}(\nabla^2 w) \quad [6a]$$

$$Q_s = -D\frac{\partial}{\partial s}(\nabla^2 w) \quad [6b]$$

Using polar co-ordinates (r, θ) we have

$$K_s = \frac{1}{r}, \quad K_n = 0, \quad \alpha = \theta, \quad e^{i\alpha} = z/r \quad [7]$$

Equations [4] and [6] now reduce to the known equations in polar co-ordinates.[8] Substituting from [2] in [3], using [7] we get

$$M_r + M_\theta = -4(1 + \eta)D\left[\phi'(z) + \bar{\phi}'(\bar{z}) + \frac{\partial^2 W}{\partial z \partial \bar{z}}\right] \quad [8a]$$

$$M_r - M_\theta + 2iM_{r\theta} = -4(1 - \eta)D[z\phi''(z) + z^2(\bar{\psi}'' + W'')/r^2] \quad [8b]$$

$$Q_r - iQ_\theta = -8Dz\left(\phi'' + \frac{\partial^3 W}{\partial z^2 \partial \bar{z}}\right)\Big/ r \quad [8c]$$

where the accents on ϕ, ψ, and W denote derivatives with respect to z.

General Boundary Condition

The boundary conditions used in this paper were discussed by the authors in a previous paper (4), but it is helpful to give here a short account of these conditions as they were obtained in a different notation and as we need to refer to them frequently.

We shall assume that the plate is supported so that $w = 0$ along C and we take the second boundary condition along C as

$$M_n/M_s = \text{const}, -\mu \text{ say} \quad [9]$$

and hence

$$(M_n + M_s)/(M_n - M_s) = (\mu - 1)/(\mu + 1) \text{ along } C \quad [10]$$

Since $w = 0$ along C, we have

[7] Reference (11), pp. 107, 108.

[8] Reference (5), p. 259.

$$\partial w/\partial s = \partial^2 w/\partial s^2 = 0, \quad \nabla^2 w = \frac{\partial^2 w}{\partial n^2} + K_s \frac{\partial w}{\partial n} \quad \text{along } C \ldots [11]$$

Substituting from Equation [11] in [4a], [4b] we get

$$\left.\begin{aligned} M_n + M_s &= -(1+\eta)D\left(\frac{\partial^2 w}{\partial n^2} + K_s \frac{\partial w}{\partial n}\right) \\ M_n - M_s &= -(1-\eta)D\left(\frac{\partial^2 w}{\partial n^2} - K_s \frac{\partial w}{\partial n}\right) \end{aligned}\right\} \text{ along } C \ldots [12]$$

From Equations [10] and [12] we now obtain

$$\left(\frac{\partial^2 w}{\partial n^2} + K_s \frac{\partial w}{\partial n}\right) \Big/ \left(\frac{\partial^2 w}{\partial n^2} - K_s \frac{\partial w}{\partial n}\right) = \lambda \quad \ldots [13]$$

where

$$\lambda = \beta(\mu - 1)/(\mu + 1), \quad \beta = (1-\eta)/(1+\eta) \ldots [14]$$

Equation [13] can be written in the form

$$\partial^2 w/\partial n^2 + \nu K_s \partial w/\partial n = 0 \ldots [15]$$

where

$$\nu = (1+\lambda)/(1-\lambda) = (\mu+\eta)/(1+\mu\eta) \ldots [16]$$

and hence along C we have

$$\nabla^2 w = (1-\nu)K_s \partial w/\partial n \ldots [17]$$

From Equations [12] and [15] we now find that along C

$$\frac{M_n}{\eta - \nu} = \frac{M_s}{1-\eta\nu} = \frac{D}{\nu}\frac{\partial^2 w}{\partial n^2} = -DK_s \frac{\partial w}{\partial n} \ldots [18]$$

Substituting from Equations [11] and [17] in [4c] and [6b] we get

$$\left.\begin{aligned} M_{ns} &= (1-\eta)D \frac{\partial^2 w}{\partial s \partial n} \\ Q_s &= (\nu - 1)D \frac{\partial}{\partial s}\left(K_s \frac{\partial w}{\partial n}\right) \end{aligned}\right\} \text{ along } C \ldots [19]$$

Substituting from Equations [3a] and [3b] in [10] we find that the Boundary Condition [9] takes the forms

$$\mathrm{Re}\left[-\lambda e^{2i\alpha}\frac{\partial^2 w}{\partial z^2} + \frac{\partial^2 w}{\partial z \partial \bar{z}}\right] = 0 \ldots [20a]$$

or

$$\mathrm{Re}\left[-\lambda e^{2i\alpha}\{\bar{z}\phi''(z) + \psi''(z) + W''(z,\bar{z})\} + 2\phi'(z) + \frac{\partial^2 W}{\partial z \partial \bar{z}}\right] = 0 \ldots [20b]$$

where primes mean derivatives with respect to z.

It is now easily seen from Equations [15], [16], and [18] that the boundary C is clamped or simply supported according as the restraining parameter λ equals 1 or $-\beta$, respectively. For $\lambda = \beta$, $M_s = 0$, and for $\lambda = 0$ we have $M_n + M_s = 0$.

Along a circular boundary of radius c, subjected to the Boundary Condition [9], Equations [15], [18], [19], and [20] give

$$\frac{\partial^2 w}{\partial r^2} + \frac{\nu}{c}\frac{\partial w}{\partial r} = 0 \ldots [21a]$$

$$\frac{M_r}{\eta - \nu} = \frac{M_\theta}{1-\eta\nu} = -\frac{D}{c}\frac{\partial w}{\partial r} \ldots [21b]$$

$$\frac{M_{r\theta}}{1-\eta} = \frac{cQ_\theta}{\nu - 1} = \frac{D}{c}\frac{\partial^2 w}{\partial \theta \partial r} \ldots [21c]$$

$$\mathrm{Re}\left[-\lambda\left\{z\phi'' + \frac{z^2}{c^2}(\psi'' + W'')\right\} + 2\phi' + \frac{\partial^2 W}{\partial z \partial \bar{z}}\right] = 0 \quad \text{along } C \ldots [21d]$$

Circular Plate Under General Loading Over Entire Plate

Let C denote the boundary of a thin circular plate of center O and radius c. Let $p(r, \theta)$ be the normal load intensity at the point (r, θ), $0 \leqslant r \leqslant c$, $-\pi < \theta \leqslant \pi$. We assume that $p(r, \theta)$ can be expressed as the sum of a finite or infinite number of terms of the type $p_0 r^m \begin{matrix}\cos \\ \sin\end{matrix} n\theta$ and let us determine the particular integral $W(z, \bar{z})$ and the analytic functions $\phi(z)$, $\psi(z)$ corresponding to the load $p_0 r^{s-2} \cos n\theta$, $(s \geqslant 2)$ distributed over the entire plate where for the sake of later convenience we have written $s-2$ instead of m. Solutions corresponding to the load $p_0 r^{s-2} \sin n\theta$ can then be obtained by putting $\pi/2n - \theta$ instead of θ.

With the abbreviations $s' = s + 2$, $t = z/c$, $\rho = r/c$, the particular integral $W(z, \bar{z})$, the analytic functions ϕ, ψ, and deflection w under the load $p_0 r^{s-2} \cos n\theta$ over the complete plate are given by (9)

$$\left.\begin{aligned} W_{ss} &= \frac{p_0}{2D}\frac{(z\bar{z})^{(s'-n)/2}(z^n + \bar{z}^n)}{(n^2 - s^2)(n^2 - s'^2)} \\ &= \frac{p_0}{D}\frac{r^{s'}\cos n\theta}{(n^2 - s^2)(n^2 - s'^2)}, \quad n \neq s, s' \\ \phi_{ss} &= \frac{p_0 c^{s+1}}{4D}\frac{(n+s+\nu+1)t^{n+1}}{(n^2 - s^2)(n+s')(2n+\nu+1)}, \quad n \neq s \\ \psi_{ss} &= -\frac{p_0 c^{s'}}{4D}\frac{(n+s+\nu+3)t^n}{(n^2 - s'^2)(n+s)(2n+\nu+1)}, \quad n \neq s' \end{aligned}\right\} \ldots [22]$$

$$w_{ss} = \frac{p_0 c^{s'}\cos n\theta}{(n^2 - s^2)(n^2 - s'^2)D}\left[\rho^2(\rho^s - \rho^n) - \frac{(n-s)(n+s+\nu+3)}{2(2n+\nu+1)}\rho^n(1-\rho^2)\right], \quad n \neq s, s' \ldots [23]$$

$$\left.\begin{aligned} W_{ss} &= \frac{p_0 z\bar{z}}{32s(s+1)D}(z^s \log l + \bar{z}^s \log t) \\ \phi_{ss} &= -\frac{p_0 z^{s+1}}{32s(s+1)D}\left(\frac{2s+\nu+3}{2s+\nu+1} - \log t\right) \end{aligned}\right\} \ldots [24]$$

$$w_{ss} = \frac{p_0 c^s \rho^s \cos s\theta}{16s(s+1)D}\left[\frac{2s+\nu+3}{2s+\nu+1}(1-\rho^2) + 2\rho^2 \log \rho\right] \ldots [25]$$

$$\left.\begin{aligned} W_{s's} &= -\frac{p_0}{32s'(s'-1)D}(z^{s'} \log l + \bar{z}^{s'} \log t) \\ \psi_{s's} &= -\frac{p_0 z^{s'}}{32s'(s'-1)D}\left(\frac{2s'+\nu-1}{2s'+\nu+1} + \log t\right) \end{aligned}\right\} \ldots [26]$$

$$w_{s's} = -\frac{p_0 r^{s'}\cos s'\theta}{16s'(s'-1)D}\left[\frac{2s'+\nu-1}{2s'+\nu+1}(1-\rho^2) + 2\log\rho\right] \ldots [27]$$

where the principal value of the function $\log t$ is taken. It can be checked easily that the Solutions [23], [25], and [27] satisfy the biharmonic Equation [1] corresponding to the loadings

$p_0 r^{s-2} \cos n\theta$, $p_0 r^{s-2} \cos s\theta$, and $p_0 r^{s-2} \cos s'\theta$; and also satisfy the boundary conditions $w = 0$ and Equation [21a] along C.

Substituting from Equations [23], [25], and [27] in [21b], [21c] and using Equation [8c] we find that, for the load $p_0 r^{s-2} \cos n\theta$ over the entire plate, the bending and twisting moments and the shearing forces at any point on the boundary are given by

$$\frac{M_r}{(\eta - \nu)\cos n\theta} = \frac{M_\theta}{(1 - \eta\nu)\cos n\theta} = \frac{M_{r\theta}}{n(1 - \eta)\sin n\theta}$$

$$= \frac{cQ_\theta}{n(\nu - 1)\sin n\theta} = \frac{p_0 c^s}{(n + s)(n + s')(2n + \nu + 1)} \quad \ldots\ldots [28]$$

while the intensity of the vertical reaction on the boundary is

$$V_r = Q_r - \frac{1}{c}\frac{\partial M_{r\theta}}{\partial \theta} =$$

$$-\frac{p_0 c^{s-1} \cos n\theta}{n + s}\left[1 + \frac{n(n - n\eta + \nu - 1)}{(n + s')(2n + \nu + 1)}\right] \quad \ldots\ldots [29]$$

Circular Plate Under Normal Loading Over a Sector

Let us now find the small deflection w of a thin circular plate with center O, radius c, and boundary C when it is subjected to the boundary conditions $w = 0$ and the Condition [9] along C, and is acted upon by the load whose normal intensity is

$$\left.\begin{aligned} &p(r, \theta) = p_0 r^{s-2} \cos k\theta,\ s \geqslant 2 \\ &\qquad\qquad \text{over the sector } -\alpha \leqslant \theta \leqslant \alpha \\ &p(r, \theta) = 0 \text{ over the rest of the plate} \end{aligned}\right\} \quad \ldots [30]$$

where s and k are positive integers. The solution corresponding to the load intensity $p_0 r^{s-2} \sin k\theta$ over the sector can then be obtained by changing θ to $\pi/2k - \theta$.

For reasons of symmetry it is sufficient to obtain the solution in regions 1 and 2 defined by $0 \leqslant \theta < \alpha$, $\alpha < \theta \leqslant \pi$, respectively,

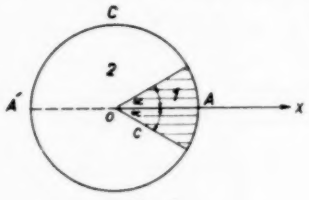

FIG. 1

Fig. 1. It can be shown easily that the function $p(r, \theta)$ defined by Equations [30] has the Fourier series expansion

$$p(r, \theta) = \frac{1}{\pi} p_0 r^{s-2}\left[a_{0k} + 2\sum_{n=1}^{\infty} a_{nk} \cos n\theta\right] \quad \ldots\ldots [31]$$

where

$$a_{0k} = \frac{\sin k\alpha}{k}, \quad 2a_{nk} = \frac{\sin (n + k)\alpha}{n + k} + \frac{\sin (n - k)\alpha}{n - k} \quad \ldots [32]$$

and hence

$$a_{00} = \alpha, \quad a_{n0} = \frac{\sin n\alpha}{n}$$

Applying the principle of superposition we see, using Equations [22]–[27], that for the supported circular plate loaded as in Equation [30] and subjected to the Boundary Condition [9] we have

$$W = \frac{p_0}{2\pi D}\left[\frac{2 \sin k\alpha}{ks^2 s'^2} + 4r^{s'} S^k(1, \theta)\right.$$

$$+ \frac{a_{sk}}{4s(s + s')}\, z\bar{z}(z^s \log l + \bar{z}^s \log l)$$

$$\left. - \frac{a_{s'k}}{4s'(s + s')}(z^{s'} \log l + \bar{z}^{s'} \log l)\right] \quad \ldots\ldots [33a]$$

$$\phi = -\frac{p_0 c^s z}{2\pi D}\left[\frac{(s' - s\lambda)\sin k\alpha}{4ks'^2} + N^k(l) - P_{ss'}{}^k(l)\right.$$

$$\left. + \frac{a_{sk} l^s}{4s(s + s')}(1 - \log l)\right] \quad \ldots\ldots [33b]$$

$$\psi = \frac{p_0 c^{s'}}{2\pi D}\left[\frac{(s' + 2 - s'\lambda)\sin k\alpha}{4kss'^2} + N^k(l) - P_{s's}{}^k(l)\right.$$

$$\left. - \frac{a_{s'k} l^{s'}}{4s'(s + s')}(1 + \log l)\right] \quad \ldots\ldots [33c]$$

$$w = \frac{p_0 c^{s'}}{\pi D}\left[\frac{\sin k\alpha}{ks^2 s'^2}\left\{\frac{1}{4}s(s' + 2 - s'\lambda)(1 - \rho^2)\right.\right.$$

$$\left.\left. - \rho^2(1 - \rho^s)\right\} + 2\rho^{s'} S^k(1, \theta) + (1 - \rho^2)N^k(\rho, \theta)\right.$$

$$+ \rho^2 P_{ss'}{}^k(\rho, \theta) - P_{s's}{}^k(\rho, \theta) - \frac{\rho^{s'}}{4(s + s')} \times$$

$$\left.\left\{\frac{1 - 2\log \rho}{s} a_{sk} \cos s\theta + \frac{1 + 2\log \rho}{s'} a_{s'k} \cos s'\theta\right\}\right] \quad \ldots\ldots [33d]$$

where

$$\left.\begin{aligned} N^k(l) &= \sum_{n=1}^{\infty} \frac{a_{nk} l^n}{(n + s)(n + s')(2n + \nu + 1)} \\ &\qquad N^k(\rho, \theta) = \text{Re } N^k(l) \\ P_{ss'}{}^k(l) &= \sum_{n=1}^{\infty}{}' \frac{a_{nk} l^n}{(n^2 - s^2)(n + s')} \\ &\qquad P_{ss'}{}^k(\rho, \theta) = \text{Re } P_{ss'}{}^k(l) \\ S^k(l) &= \sum_{n=1}^{\infty}{}' \frac{a_{nk} l^n}{(n^2 - s^2)(n^2 - s'^2)} \\ &\qquad S^k(\rho, \theta) = \text{Re } S^k(l) \end{aligned}\right\} \quad \ldots [34]$$

and the prime on Σ means that the terms corresponding to $n = s$ or $n = s'$ or both are not included in the summation.

We shall now study in more details the case $k = 0$, i.e., $p = p_0 r^{s-2}$ over the sector $-\alpha \leqslant \theta \leqslant \alpha$. In this case we have

$$S^0(1, \theta) = \sum_{n=1}^{\infty}{}' \frac{\sin n\alpha \cos n\theta}{n(n^2 - s^2)(n^2 - s'^2)}$$

and it is shown in Appendix 1 that $S^0(1, \theta)$ can be put in the closed form

$$\left.\begin{aligned} &S^0(1, \theta) = F_{ss'}(\theta) + F_{s's}(\theta) + G_{ss'}(\theta) - G_{s's}(\theta) \\ &\text{where} \\ &8s's^2(s + s')F_{ss'}(\theta) = s' \sin s\alpha \cos s\theta - 4\alpha \\ &4s^2(s + s')G_{ss'}(\theta) = \alpha \cos s\alpha \cos s\theta - \theta \sin s\alpha \sin s\theta \\ &\qquad - \left(\frac{1}{s + s'} + \frac{3}{2s}\right)\sin s\alpha \cos s\theta \\ &\qquad + \frac{\pi(1 - \cos s\alpha \cos s\theta)}{\pi \sin s\alpha \sin s\theta} \end{aligned}\right\} \quad \ldots [35]$$

according as θ lies in regions 1 or 2.

Putting $k = 0$ in Equations [33] and then substituting from Equations [32] and [35] we find that the particular integral $W(z, \bar{z})$ can be put in the form

$$W(z, \bar{z}) = \bar{z}f(z) + z\bar{f}(\bar{z}) + g(z) + \bar{g}(\bar{z}) + \frac{W_1(z, \bar{z})}{W_2(z, \bar{z})}$$

where

$$W_1(z, \bar{z}) = \frac{p_0}{s^2 s'^2 D}(z\bar{z})^{s'/2}, \quad W_2(z, \bar{z}) = 0$$

$$f(z) = \frac{p_0}{8\pi D}\frac{z^{s+1}}{s^2(s+s')}\left[\left(\log t + 1 - \frac{2}{s+s'} - \frac{3}{s}\right)\sin s\alpha + 2\alpha\cos s\alpha - \frac{2\pi\cos s\alpha}{2\pi i \sin s\alpha}\right]$$

$$g(z) = \frac{p_0}{8\pi D}\frac{z^{s'}}{s'^2(s+s')}\left[\left(\log t - 1 - \frac{2}{s+s'} - \frac{3}{s'}\right)\sin s'\alpha + 2\alpha\cos s'\alpha - \frac{2\pi\cos s'\alpha}{2\pi i \sin s'\alpha}\right]$$

It is now clear that the functions $f(z)$ and $g(z)$ may be added to $\phi(z)$ and $\psi(z)$, respectively, so that the particular integrals and analytic functions ϕ and ψ in the case $k = 0$ take the forms

$$\left.\begin{aligned} W_1(z, \bar{z}) &= \frac{p_0}{s^2 s'^2 D}(z\bar{z})^{s'/2}, \quad W_2(z, \bar{z}) = 0 \\ \phi(z) &= -zU_{ss'}(t), \qquad \psi(z) = U_{s's}(t) \end{aligned}\right\} \quad \ldots [36]$$

where

$$U_{ss'}(t) = \frac{p_0 c^s}{2\pi D}\left[\frac{s' - s\lambda}{4s^2 s'}\alpha + N^0(t) - P_{ss'}{}^0(t) + \frac{t^s}{2s^2(s+s')}\left\{\left(\frac{3}{2s} + \frac{1}{s+s'} - \log t\right)\sin s\alpha - \alpha\cos s\alpha + \frac{\pi\cos s\alpha}{\pi i \sin s\alpha}\right\}\right] \quad \ldots [37]$$

Substituting from Equations [36] and [37] in [2] or from Equations [35] and [32] in [33d] after putting $k = 0$ we obtain

$$w = \frac{p_0 c^{s'}}{\pi D}\left[(1-\rho^2)\left\{\frac{\alpha}{4ss'}(1-\lambda) + N^0(\rho, \theta)\right\} + \frac{\alpha}{2ss'}\left(\frac{1}{s'} - \frac{\rho^2}{s}\right) + \rho^2 P_{ss'}{}^0(\rho, \theta) - P_{s's}{}^0(\rho, \theta) + \rho^{s'}\{Q_{ss'}(\rho, \theta) - Q_{s's}(\rho, \theta)\}\right] \quad \ldots [38]$$

where

$$Q_{ss'}(\rho, \theta) = 2G_{ss'}(\theta) + \frac{\sin s\alpha \cos s\theta}{2s^2(s+s')}\log\rho$$

and the functions $N^0(\rho, \theta)$, $P_{ss'}{}^0(\rho, \theta)$, $P_{s's}{}^0(\rho, \theta)$ are given by Equations [34] while $G_{ss'}(\theta)$ is given by Equations [35]. Equation [38] can now be written in the form

$$\left.\begin{aligned} &w = Kp_0 c^{s'}/D, \quad K = K_1 + K_2 \\ &\text{where} \\ &\pi K_1 = \frac{\alpha}{2ss'}\left(\frac{1}{s'} - \frac{\rho^2}{s}\right) + \rho^2 P_{ss'}{}^0(\rho, \theta) - P_{s's}{}^0(\rho, \theta) \end{aligned}\right\} \quad \ldots [39]$$

$$\left.\begin{aligned} &+ \rho^{s'}\{Q_{ss'}(\rho, \theta) - Q_{s's}(\rho, \theta)\} \\ &\pi K_2 = (1-\rho^2)\left\{\frac{\alpha}{4ss'}(1-\lambda) + N^0(\rho, \theta)\right\} \end{aligned}\right\} \quad \ldots [39] \text{ (Cont.)}$$

and it is to be noticed that only the part K_2 depends on the type of constraint at the boundary and that, when $\lambda = 1$, $\nu = \infty$ and $N = 0$ so that $K_2 = 0$ for a clamped boundary.

The deflection at the center of the plate is obtained by putting $\rho = 0$ in Equation [38] and we get

$$w_{\rho=0} = \frac{\alpha}{\pi}\frac{p_0 c^{s'}}{4ss'^2 D}[s'(1-\lambda) + 2] \quad \ldots [40]$$

which equals α/π of the deflection at the center had the plate been completely loaded.

In Tables 1 to 5 we give for the case of uniform loading over the sector ($s = 2, s' = 4$) the numerical values of the coefficient K at different points of the diameter of symmetry of the plate ($\theta = 0$, $\theta = \pi$). Computations were carried out for different values of the angle α, and for the values 1, $^1/_2$, 0, $-^1/_2$, -1 of the restraining parameter λ, Poisson's ratio being taken as 1/3.

We also give in Figs. 2 and 3 systems of curves with λ as abscissa and the deflections at the center of the plate and at the point $\rho = {}^1/_2$, $\theta = 0$ as ordinates. The value of the deflection at the same points can therefore be estimated for other cases of

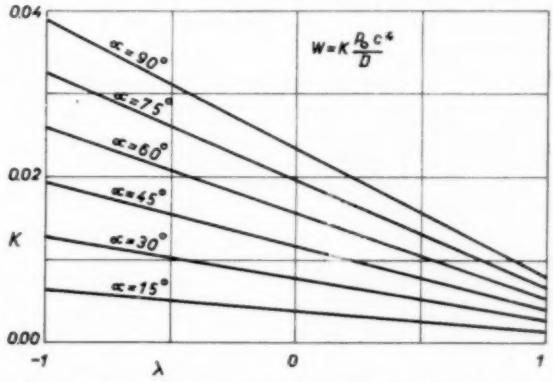

FIG. 2 DEFLECTION FACTOR K AT CENTER OF A CIRCULAR PLATE UNIFORMLY LOADED OVER A SECTOR OF ANGLE 2α; POISSON'S RATIO $\eta = 1/3$

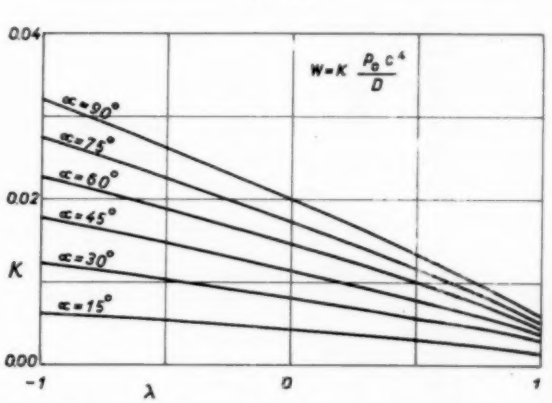

FIG. 3 DEFLECTION FACTOR K AT POINT $\theta = 0$, $\rho = 1/2$ OF A CIRCULAR PLATE UNIFORMLY LOADED OVER A SECTOR OF ANGLE 2α; POISSON'S RATIO $\eta = 1/3$

TABLE 1

VALUES OF $10^4 K$ ACROSS DIAMETER OF SYMMETRY IN THE CASE $\eta = \frac{1}{3}, \lambda = 1$ (Clamped Boundary)

	$\theta = \pi$				$\theta = 0$		
α \ ρ	0.75	0.50	0.25	0	0.25	0.50	0.75
15	1	4	8	13	16	15	7
30	2	8	17	26	32	28	12
45	3	12	25	39	47	38	16
60	4	17	34	52	60	47	19
75	6	22	44	65	72	54	21
90	7	27	54	78	83	61	23

TABLE 2

VALUES OF $10^4 K$ ACROSS DIAMETER OF SYMMETRY IN THE CASE $\eta = \frac{1}{3}, \lambda = \frac{1}{2}$

	$\theta = \pi$				$\theta = 0$		
α \ ρ	0.75	0.50	0.25	0	0.25	0.50	0.75
15	4	11	18	26	31	29	17
30	9	22	37	52	61	55	32
45	14	33	56	78	90	78	43
60	19	45	76	104	116	99	53
75	24	59	97	130	141	117	61
90	30	73	119	156	165	132	68

TABLE 3

VALUES OF $10^4 K$ ACROSS DIAMETER OF SYMMETRY IN THE CASE $\eta = \frac{1}{3}, \lambda = 0$

	$\theta = \pi$				$\theta = 0$		
α \ ρ	0.75	0.50	0.25	0	0.25	0.50	0.75
15	9	19	29	39	44	41	25
30	18	39	60	78	88	79	47
45	27	59	90	117	129	113	65
60	37	79	122	156	169	144	81
75	48	101	154	195	206	172	95
90	59	116	188	234	242	198	108

TABLE 4

VALUES OF $10^4 K$ ACROSS DIAMETER OF SYMMETRY IN THE CASE $\eta = \frac{1}{3}, \lambda = -\frac{1}{2}$ (Hinged Boundary)

	$\theta = \pi$				$\theta = 0$		
α \ ρ	0.75	0.50	0.25	0	0.25	0.50	0.75
15	14	28	41	52	57	52	32
30	28	56	83	104	113	101	60
45	42	85	125	156	168	146	85
60	57	115	168	208	220	187	107
75	73	146	213	260	270	225	127
90	90	179	259	312	318	260	145

TABLE 5

VALUES OF $10^4 K$ ACROSS DIAMETER OF SYMMETRY IN THE CASE $\eta = \frac{1}{3}, \lambda = -1$

	$\theta = \pi$				$\theta = 0$		
α \ ρ	0.75	0.50	0.25	0	0.25	0.50	0.75
15	19	37	53	65	70	62	38
30	38	75	107	130	139	122	73
45	58	113	161	195	206	177	104
60	78	152	216	260	270	228	132
75	99	193	272	325	331	276	158
90	121	235	330	391	393	321	182

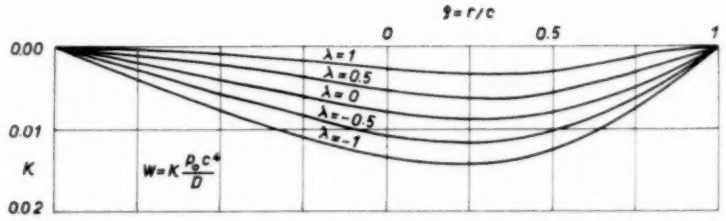

FIG. 4 DEFLECTION PROFILE ALONG DIAMETER OF SYMMETRY OF A CIRCULAR PLATE UNIFORMLY LOADED OVER A SECTOR OF ANGLE $2\alpha = 60$ DEG; POISSON'S RATIO = 1/3

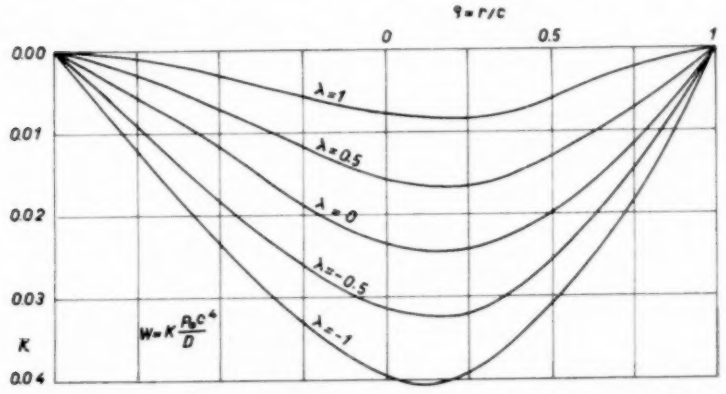

FIG. 5 DEFLECTION PROFILE ALONG DIAMETER OF SYMMETRY OF A CIRCULAR PLATE UNIFORMLY LOADED OVER HALF ITS SURFACE ($\alpha = 90$ DEG); POISSON'S RATIO = 1/3

partial fixation corresponding to other values of the restraining parameter λ. Similar curves may be drawn for any other point.

Figs. 4 and 5 show the deflection profile along the diameter of symmetry of the plate corresponding to the angles $\alpha = 30$ deg and $\alpha = 90$ deg of the loaded sector.

The bending and twisting moments and shearing forces at any point $z = re^{i\theta}$ of the plate are obtained either by substituting from Equations [36] and [37] in [8] or by substituting from Equation [38] in the well-known formulas in polar co-ordinates,[9] and the results may be expressed in the forms

$$\left.\begin{aligned} M_r &= -\delta_1 p_0 c^s, \qquad M_\theta = \delta_2 p_0 c^s, \qquad M_{r\theta} = \delta_3 p_0 c^s \\ Q_r &= -\gamma_1 p_0 c^{s-1}, \quad V_r = -\gamma_2 p_0 c^{s-1}, \quad Q_\theta = -\gamma_3 p_0 c^{s-1} \end{aligned}\right\} \ldots [41]$$

where $\delta_1, \delta_2, \delta_3$; γ_1, γ_2, and γ_3 are dimensionless quantities. Using the Fourier Series Expansion [31] and the results, Equations [28] and [29], for the boundary values due to a load $p_0 r^{s-2} \cos n\theta$ over the whole plate we obtain the following results for the boundary values due to the load $p_0 r^{s-2}$ over the sector $-\alpha \leqslant \theta \leqslant \alpha$

$$\left.\begin{aligned} \frac{\pi\delta_1}{\nu - \eta} &= \frac{\pi\delta_2}{1 - \eta\nu} = \frac{(1-\lambda)\alpha}{2ss'} + 2N^0(1,\theta) \\ \pi\gamma_1 &= \frac{\alpha}{s} + 2\sum_{n=1}^{\infty} \frac{\sin n\alpha \cos n\theta}{n(n+s)} + 2(\nu - 1) \sum_{n=1}^{\infty} \frac{\sin n\alpha \cos n\theta}{(n+s)(n+s')(2n+\nu+1)} \\ \pi\gamma_2 &= \pi\gamma_1 + 2(1-\eta) \sum_{n=1}^{\infty} \frac{n \sin n\alpha \cos n\theta}{(n+s)(n+s')(2n+\nu+1)} \\ \frac{\pi\delta_3}{1-\eta} &= \frac{\pi\gamma_3}{1-\nu} = 2\sum_{n=1}^{\infty} \frac{\sin n\alpha \sin n\theta}{(n+s)(n+s')(2n+\nu+1)} \end{aligned}\right\} \ldots [42]$$

and we notice that $-\int_0^{2\pi} V_r \cdot cd\theta = 2\alpha p_0 c^s/s =$ total load on the sector as it should. It may be useful to note that, since $\nu = (1+\lambda)/(1-\lambda)$ and $\beta = (1-\eta)/(1+\eta)$, the first of Equation [42] takes the form

$$\frac{\pi\delta_1}{\lambda + \beta} = \frac{-\pi\delta_2}{\lambda - \beta} = (1+\eta)\left[\frac{\alpha}{2ss'} + \sum_{n=1}^{\infty} \frac{\sin n\alpha \cos n\theta}{n(n+s)(n+s')(n - n\lambda + 1)}\right] \ldots [43]$$

The summation of the series appearing in Equations [42] and [43] will be dealt with in Appendix 2.

From Equation [21b] and the first of Equations [41] and [42] we find that the normal slope over the boundary is given by

$$\partial w/\partial r = -p_0 c^{s+1}\delta_1/(\nu - \eta)D = -(p_0 c^{s+1}/\pi D)[(1-\lambda)\alpha/2ss' + 2N^0(1,\theta)] \ldots [44]$$

Substituting from Equations [36] and [37] in [8] we find that at the center of the plate ($z = 0$)

[9] Reference (5), p. 259.

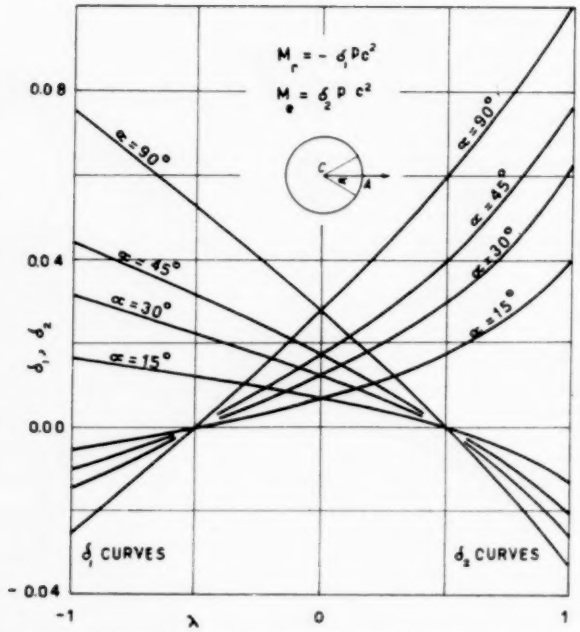

FIG. 6 BENDING-MOMENT FACTORS AT POINT A ($\theta = 0$, $\rho = 1$); POISSON'S RATIO = 1/3

$$\left.\begin{aligned}\frac{\delta_1}{\delta_2} &= \frac{1}{\pi s s'}\left[\mp\frac{\alpha}{2s}(1+\eta)(s'-s\lambda) + \frac{(1-\eta)(s+\nu+5)}{(s+4)(\nu+5)}\sin 2\alpha\cos 2\theta\right]\\ \delta_3 &= -\frac{1}{2\pi s s'}\frac{(1-\eta)(s+\nu+5)}{(s+4)(\nu+5)}\sin 2\alpha\sin 2\theta\\ \frac{-\gamma_1}{\cos\theta} &= \frac{\gamma_2}{\sin\theta} = \frac{8(s'+\nu)\sin\alpha}{\pi(s^2-1)(s+3)(\nu+3)}\end{aligned}\right\}\quad\ldots[45]$$

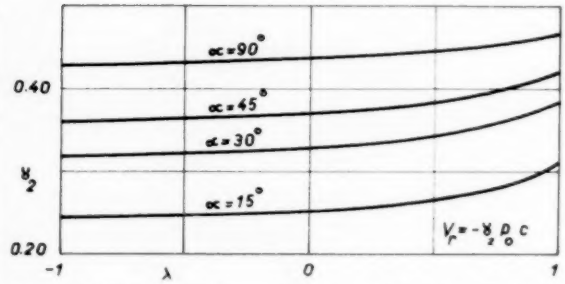

FIG. 7 VALUES OF THE VERTICAL REACTION FACTOR AT POINT A; POISSON'S RATIO = 1/3

Putting $\theta = 0$ in Equations [45] we get at the center of the plate

$$\left.\begin{aligned}\frac{M_x}{M_y} &= \frac{p_0 c^2}{\pi s s'}\left[\frac{\alpha}{2s}(1+\eta)(s'-s\lambda) \mp \frac{(1-\eta)(s+\nu+5)}{(s+4)(\nu+5)}\sin 2\alpha\right]\\ Q_x &= \frac{8 p_0 c^{s-1}}{\pi}\frac{(s'+\nu)\sin\alpha}{(s^2-1)(s+3)(\nu+3)}\\ M_{xy} &= 0 \qquad\qquad Q_y = 0\end{aligned}\right\}\quad\ldots[46]$$

The values of δ_1, δ_2, γ_1, and γ_2 at the point A (one end of the diameter of symmetry of the plate) for the case of uniform pressure over the sector ($s = 2$, $s' = 4$) are listed in Tables 6 and 7, Poisson's ratio being taken as 1/3.

Fig. 6 shows the bending moments at A as functions of the restraining parameter λ. Curves showing the intensity of the vertical reaction at A are plotted in Fig. 7.

BIBLIOGRAPHY

1 "Some Basic Problems of the Mathematical Theory of Elasticity," by N. I. Muskhelishvili, translated by M. Radok, P. Noordhoff, Editor, Groningen, Holland, 1953.

2 "Some New Methods of Solution of Two-Dimensional Problems in Elasticity," by I. S. Sokolnikoff, *Bulletin of the American Mathematical Society*, vol. 48, 1942, p. 539.

3 "Mathematical Theory of Elasticity," by I. S. Sokolnikoff, mimeographed lecture notes, Brown University, Providence, R. I., 1941, pp. 382–386.

TABLE 6

VALUES OF $10^4\delta_1$ AND $10^4\delta_2$ AT THE POINT A ($\rho = 1$, $\theta = 0$), $\eta = \frac{1}{3}$

	$10^4\delta_1$					$10^4\delta_2$				
α \ λ	-1	-0.5	0	0.5	1	-1	-0.5	0	0.5	1
15	- 56	0	68	166	400	167	121	68	0	-133
30	-105	0	124	294	619	314	225	124	0	-206
45	-148	0	171	392	761	443	314	171	0	-254
60	-186	0	210	471	863	558	391	210	0	-286
75	-221	0	245	536	940	663	461	245	0	-313
90	-253	0	275	592	1003	759	524	275	0	-334

TABLE 7

VALUES OF $10^4\gamma_1$ AND $10^4\gamma_2$ AT THE POINT A ($\rho = 1$, $\theta = 0$), $\eta = \frac{1}{3}$

	$10^4\gamma_1$					$10^4\gamma_2$				
α \ λ	-1	-0.5	0	0.5	1	-1	-0.5	0	0.5	1
15	2228	2272	2344	2494	3089	2438	2470	2528	2641	3089
30	2988	3046	3140	3318	3807	3159	3205	3281	3421	3807
45	3441	3504	3600	3773	4157	3573	3624	3703	3843	4157
60	3758	3818	3910	4066	4369	3860	3910	3986	4115	4369
75	3999	4055	4138	4274	4514	4078	4125	4195	4308	4514
90	4195	4244	4317	4432	4622	4256	4298	4359	4457	4622

4 "Bending of a Circular Plate With an Eccentric Circular Patch Symmetrically Loaded With Respect to Its Centre," by W. A. Bassali and R. H. Dawoud, Proceedings of the Cambridge Philosophical Society, vol. 52, 1956, pp. 584–598.

5 "Theory of Plates and Shells," by S. Timoshenko, McGraw-Hill Book Company, Inc., New York, N. Y., 1940, pp. 58 and 266.

6 "A Treatise on the Mathematical Theory of Elasticity," by A. E. H. Love, Cambridge University Press, fourth edition, 1927; reprinted by Dover Publications, New York, N. Y., 1944, pp. 489–491.

7 "Circular Plates Under a Linearly Varying Load," by W. Flügge; see reference (5), p. 260.

8 "Ein Beitrag zur Theorie der Biegung homogener Kreisplatten," by H. Schmidt, *Ingenieur-Archiv*, vol. 1, 1930, p. 147.

9 "Bending of a Thin Circular Plate Concentrically Loaded under a General Boundary Condition," by W. A. Bassali and R. H. Dawoud, to be published in Proceedings of the Mathematical and Physical Society of Egypt.

10 "On the Equilibrium of Plates," by A. C. Stevenson, *Philosophical Magazine*, vol. 33, 1942, pp. 639–661.

11 "The Boundary Couples in Thin Plates," by A. C. Stevenson, *Philosophical Magazine*, vol. 34, 1943, pp. 105–114.

Appendix 1

To sum the series

$$S^0(1,\theta) = \sum_{n=1}^{\infty}{}' \frac{\sin n\alpha \cos n\theta}{n(n^2 - s^2)(n^2 - s'^2)}$$

where the prime on Σ indicates that $n = s$ and $n = s'$ are omitted, we write it in the form

$$S^0(1,\theta) = \frac{1}{4s^2s'^2(s+s')} \sum_{n=1}^{\infty}{}' \left\{ \frac{2ns^2}{n^2 - s'^2} + \frac{4(s+s')}{n} - \frac{2ns'^2}{n^2 - s^2} \right\} \sin n\alpha \cos n\theta \quad \ldots\ldots [47]$$

and it can be verified easily by Fourier analysis that

$$\frac{\sin m\phi}{2m} + \sum_{n=1}^{\infty}{}' \frac{2n}{n^2 - m^2} \sin n\phi = (\pi - \phi) \cos m\phi, \quad 0 < \phi < 2\pi \quad \ldots\ldots [48]$$

where m is an integer different from zero, while

$$\sum_{n=1}^{\infty} \frac{\sin n\phi}{n} = \frac{1}{2}(\pi - \phi), \quad 0 < \phi < 2\pi \quad \ldots\ldots [49]$$

Putting $\phi = \alpha + \theta$ and $\alpha - \theta$ successively in Equation [48] and adding we get

$$\frac{\sin m\alpha \cos m\theta}{2m} + \sum_{n=1}^{\infty}{}' \frac{2n}{n^2 - m^2} \sin n\alpha \cos n\theta = (\pi - \alpha) \cos m\alpha \cos m\theta + \theta \sin m\alpha \sin m\theta, \quad 0 \leq \theta < \alpha \quad \ldots\ldots [50]$$

Again putting $\phi = \theta + \alpha$ and $\theta - \alpha$ in Equation [48] and subtracting we get

$$\frac{\sin m\alpha \cos m\theta}{2m} + \sum_{n=1}^{\infty}{}' \frac{2n}{n^2 - m^2} \sin n\alpha \cos n\theta = (\theta - \pi) \sin m\alpha \sin m\theta - \alpha \cos m\alpha \cos m\theta, \quad \alpha < \theta \leq \pi \quad [51]$$

When $\theta = \alpha$

$$\sum_{n=1}^{\infty}{}' \frac{2n}{n^2 - m^2} \sin n\alpha \cos n\theta = \sum_{n=1}^{\infty}{}' \frac{n}{n^2 - m^2} \sin 2n\alpha$$

whose sum is obtained from Equation [48] by putting $\phi = 2\alpha$, $0 < \alpha < \pi$. Treating Equation [49] in a similar way we get

$$\left.\begin{aligned} \sum_{n=1}^{\infty} \frac{\sin n\alpha \cos n\theta}{n} &= \frac{1}{2}(\pi - \alpha), \quad 0 \leq \theta < \alpha \\ &= -\frac{1}{2}\alpha, \quad \alpha < \theta \leq \pi \\ &= \frac{1}{4}(\pi - 2\alpha) \quad \text{if} \quad \theta = \alpha \end{aligned}\right\} \quad \ldots [52]$$

Substituting from Equations [50], [51], [52] in [47], noting that Σ' means $n = s$ and $n = s'$ are both omitted and that

$$2(s' + s) = s'^2 - s^2$$

we see that $S^0(1,\theta)$ may be written in the closed form given by Equation [35].

Appendix 2

To facilitate numerical evaluation of the bending and twisting moments and shearing forces on the boundary from Equations [42] we require the summation of series of the form

$$C_m(\theta) = \sum_{n=1}^{\infty} \frac{\sin n\alpha \cos n\theta}{n+m}$$

and

$$S_m(\theta) = \sum_{n=1}^{\infty} \frac{\sin n\alpha \sin n\theta}{n+m}, \quad m \geq 0$$

Now

$$\sum_{n=1}^{\infty} \frac{\xi^n}{n+m} = \xi^{-m} \int_0^{\xi} \frac{t^m}{1-t}\,dt, \quad m \geq 0, \quad \xi = e^{i\phi} \quad \ldots [53]$$

so that if m is an integer greater than zero we have

$$\sum_{n=1}^{\infty} \frac{\sin n\phi}{n+m} = \frac{1}{2}(\pi - \phi) \cos m\phi + \sin m\phi \log\left(2 \sin \frac{1}{2}\phi\right) + \sum_{n=1}^{m} \frac{\sin (m-n)\phi}{n}, \quad 0 < \phi < 2\pi \quad \ldots\ldots [54]$$

$$\sum_{n=1}^{\infty} \frac{\cos n\phi}{n+m} = \frac{1}{2}(\pi - \phi) \sin m\phi - \cos m\phi \log\left(2 \sin \frac{1}{2}\phi\right) - \sum_{n=1}^{m} \frac{\cos (m-n)\phi}{n}, \quad 0 < \phi < 2\pi \quad \ldots\ldots [55]$$

Following similar lines as in Appendix 1, and introducing the function δ_θ defined by $\delta_\theta = 1$ if $0 \leq \theta < \alpha$ and $\delta_\theta = -1$ if $\alpha < \theta \leq \pi$, we finally obtain

$$2C_m(\theta) = \left\{\theta - \frac{1}{2}(1 - \delta_\theta)\pi\right\} \sin m\alpha \sin m\theta - \left\{\alpha - \frac{1}{2}(1 + \delta_\theta)\pi\right\} \cos m\alpha \cos m\theta + 2\sum_{n=0}^{m-1} \frac{\sin n\alpha \cos n\theta}{m-n} + \sin m\alpha \cos m\theta \log 2\delta_\theta (\cos\theta - \cos\alpha) + \cos m\alpha \sin m\theta \log \delta_\theta \frac{\sin \frac{1}{2}(\alpha + \theta)}{\sin \frac{1}{2}(\alpha - \theta)} \quad \ldots\ldots [56]$$

$$2S_m(\theta) = \left\{\theta - \frac{1}{2}(1 - \delta_\theta)\pi\right\} \sin m\alpha \cos m\theta + \left\{\alpha - \frac{1}{2}(1 + \delta_\theta)\pi\right\} \cos m\alpha \sin m\theta - 2\sum_{n=0}^{m-1} \frac{\sin n\alpha \sin n\theta}{m - n}$$

$$- \sin m\alpha \sin m\theta \log 2\delta_\theta (\cos\theta - \cos\alpha)$$

$$+ \cos m\alpha \cos m\theta \log \delta_\theta \frac{\sin \frac{1}{2}(\alpha + \theta)}{\sin \frac{1}{2}(\alpha - \theta)} \quad \ldots\ldots [57]$$

If $m = 0$, then

$$2C_0(\theta) = \frac{1}{2}(1 + \delta_\theta)\pi - \alpha \quad \ldots\ldots [58]$$

(see Appendix 1)

$$2S_0(\theta) = \log \delta_\theta \frac{\sin \frac{1}{2}(\alpha + \theta)}{\sin \frac{1}{2}(\alpha - \theta)} \quad \ldots\ldots [59]$$

In particular we have

$$C_m(0) = \frac{1}{2}(\pi - \alpha) \cos m\alpha + \sin m\alpha \log\left(2 \sin \frac{1}{2}\alpha\right) + \sum_{n=0}^{m-1} \frac{\sin n\alpha}{m - n}$$

$$C_m(\pi) = (-1)^{m+1}\left\{\frac{1}{2}\alpha \cos m\alpha - \sin m\alpha \log\left(2 \cos \frac{1}{2}\alpha\right)\right\} + \sum_{n=0}^{m-1} \frac{(-1)^n \sin n\alpha}{m - n} \quad \ldots\ldots [60]$$

$$C_0(0) = \frac{1}{2}(\pi - \alpha), \quad C_0(\pi) = -\frac{1}{2}\alpha$$

If m is not an integer, the integral in Equation [53] can be evaluated in certain cases. If, for example, $m = 1/2$ we find

$$2C_{1/2}(\theta) = \frac{1}{2}\pi(\delta_\theta \cos B + \cos A) + \sin A \log \tan \frac{1}{2}A + \sin B \log\left(\delta_\theta \tan \frac{1}{2}B\right) \quad \ldots\ldots [61]$$

$$2S_{1/2}(\theta) = \frac{1}{2}\pi(\delta_\theta \sin B - \sin A) + \cos A \log \tan \frac{1}{2}A - \cos B \log\left(\delta_\theta \tan \frac{1}{2}B\right) \quad \ldots\ldots [62]$$

where $2A = \alpha + \theta$, $2B = \alpha - \theta$. In particular we have

$$C_{1/2}(0) = \frac{1}{2}\pi \cos \frac{1}{2}\alpha + \sin \frac{1}{2}\alpha \log \tan \frac{\alpha}{4}$$

$$C_{1/2}(\pi) = -\frac{1}{2}\pi \sin \frac{1}{2}\alpha - \cos \frac{1}{2}\alpha \log \tan \frac{\pi - \alpha}{4} \quad \ldots\ldots [63]$$

The series appearing in Equation [42] can be expressed in terms of $C_m(\theta)$ or $S_m(\theta)$ where $m = 0$, s, s', $\frac{1}{2}(1 + \nu)$ and $\frac{1}{2}(1 + \nu) \mp s, s'$.

On the Dynamical Behavior of Rotating Shafts Driven by Universal (Hooke) Couplings

By R. M. ROSENBERG,[1] TOLEDO, OHIO

The system considered here is a massless, uniform elastic shaft carrying at its mid-point a disk (having mass) and supported at the ends by universal (Hooke) joints. The purpose of this investigation is to examine the effect of Hooke-joint angularity (as obtained by design, or from faulty alignment) on the bending stability of the rotating shaft. It is found that separate investigations are required for shafts not transmitting axial torques and for those required to transmit torques. Each gives rise to instabilities which are absent when the Hooke joint is straight. In the absence of axial torques, the shaft develops unsuspected mild critical speeds at odd integer submultiples of the "familiar" critical speed found with a straight Hooke joint. When the shaft is required to transmit moderate axial torques, the joint angularity produces true instabilities near all integer submultiples of the familiar critical speed. Surprisingly, these instabilities vanish for sufficiently large axial torques.

Nomenclature

The following nomenclature is used in the paper:

$A = A(t)$, $B = B(t)$ = functions of time
C = constant of integration
EI = shaft bending stiffness
$G = G(t)$ = function of time
K_1, K_2 = constants
$P_r = P_r(\gamma^2)$, $Q_r = Q_r(\gamma^2)$ = polynomials in γ^2
T_i = torque applied to Hooke-joint driver end
T_0 = torque at Hooke-joint driven end
$T_{cr} = 2\frac{\pi}{l} EI$ = Greenhill's critical torque
a, b = constants in Mathieu's equation
e = distance between shaft center and disk mass center
k = shaft spring rate measured at mid-point
l = shaft length
m = disk mass
n, r = sequence of integers
t = time
x = co-ordinate along shaft
y, z = co-ordinates of shaft at mid-point normal to x-axis
$\alpha = T \Big/ \left(\frac{1}{l} EI\right)$ = nondimensional torque
$\alpha_0 = T_0 \Big/ \left(\frac{1}{l} EI\right)$
$\beta = m \Big/ \left[\left(\frac{1}{l}\right)^3 EI\right]$ = nondimensional disk mass
γ = Hooke-joint angularity
$\hat{\delta} = \hat{\delta}(\gamma^2)$ = polynomial in γ^2
$\epsilon = \hat{\delta} \Big/ \left(\frac{1}{l} EI\right)$
ζ, η = disk mass center co-ordinates normal to x,ξ-axis
$\theta = \theta(\gamma, t)$ = perturbation on φ
ν = shaft critical speed with straight Hooke joint
$\xi = x/l$ = nondimensional co-ordinate along shaft
ρ = radial shaft displacement at mid-point
$\rho_0 = \alpha_0/2$
$\tau = \tau(t)$ = a transformation of $G(t)$
$\varphi = \varphi(t)$ = angular displacement of driven shaft
ψ = phase angle
ω, ω_i = angular velocity of driver end of Hooke joint
ω_o = angular velocity of driven end of Hooke joint

Introduction

When it is desired to transmit rotational motion from one shaft (the driving shaft) to another (the driven shaft) and the axis of rotation of the driven shaft is tilted by moderate amounts with respect to the driving shaft, the coupling used to connect these two shafts is frequently a so-called Hooke or universal joint. Two such joints in series may be used to achieve a combination of tilt and translation of one rotating shaft with respect to another. A common example of the use of universal joints to transmit rotational motion and torque from one shaft to another is found in the "drive line" of the conventional automobile.

As is well known, the universal joint is not a "constant-velocity" device. Expressed more precisely, the angular velocity ω_i of the driving shaft is not at every instant equal to ω_0, that of the driven shaft. In fact, these two quantities are connected by a relation of the type

$$\frac{\omega_0}{\omega_i} = f(\gamma, t)$$

where γ is the angle subtended by the projection of the center lines of the shafts on the plane common to both. We shall call this angle the "joint angularity."

---

[1] Chairman, Department of Engineering Mechanics, University of Toledo. Now Professor of Engineering Mechanics, University of California, Berkeley, Calif.

Contributed by the Applied Mechanics Division and presented at the Annual Meeting, New York, N. Y., December 1–6, 1957, of The American Society of Mechanical Engineers.

Discussion of this paper should be addressed to the Secretary, ASME, 29 West 39th Street, New York, N. Y., and will be accepted until April 10, 1958, for publication at a later date. Discussion received after the closing date will be returned.

Note: Statements and opinions advanced in papers are to be understood as individual expressions of their authors and not those of the Society. Manuscript received by ASME Applied Mechanics Division, November 14, 1956. Paper No. 57—A-1.

Similarly, the universal joint is not a "constant-torque" device. If the torque on the driving shaft is denoted by T_i, and that on the driven shaft by T_0, these two quantities are connected by

$$\frac{T_0}{T_i} = g(\gamma, t)$$

If the velocity ω_i is constant, the functions $f(\gamma, t)$ and $g(\gamma, t)$ are periodic functions of time and both tend to unity as $\gamma \to 0$.

These are well-known properties of the universal joint which can be deduced from the kinematic relations governing the mechanism, and their derivation is easily accessible (1, 2).[2] Since relatively long shafts are frequently driven through universal joints, it becomes of interest to inquire into the effect which the nonuniformity of velocity and torque transmission through the universal joint has on the dynamical behavior of the shaft. This is the subject of our discussion. In particular, we should like to disclose the mechanism of a one-half order instability observed with nonvanishing joint angularity, but absent otherwise.

The System

We shall discuss in this paper a massless shaft of uniform bending stiffness EI. It is of length l, and it carries at the mid-point a thin disk of mass m. The distance between the shaft center and the mass center of the disk is e. The x-axis lies in the center line of the undeflected shaft, and at $x = 0$ and $x = l$ the shaft is supported in universal (Hooke) joints of joint angularity $\gamma \neq 0$. The y and z-axes are orthogonal to each other and to the x-axis, and they intersect the latter at $x = 0$. A constant torque T_0 is applied at the driving end of the joints. This system is illustrated in Fig. 1.

The nonuniform velocity transmission may be deduced from the well-known relation

$$\tan \varphi = \cos \gamma \tan \omega t \quad \ldots\ldots\ldots\ldots\ldots\ldots [1]$$

where $\varphi(t)$ is the angular displacement of the driven shaft, ωt is the angular displacement of the driving shaft under constant angular velocity ω, and γ is the joint angularity. Equation [1] is a valid relation connecting the angular displacements of driving and driven shafts provided the orientation of the y and z-axes with respect to the universal joint fork has been suitably chosen (1). We may write

$$\varphi(t) = \omega t + \theta(\gamma, t) \quad \ldots\ldots\ldots\ldots\ldots\ldots [2]$$

[2] Numbers in parentheses refer to the Bibliography at the end of the paper.

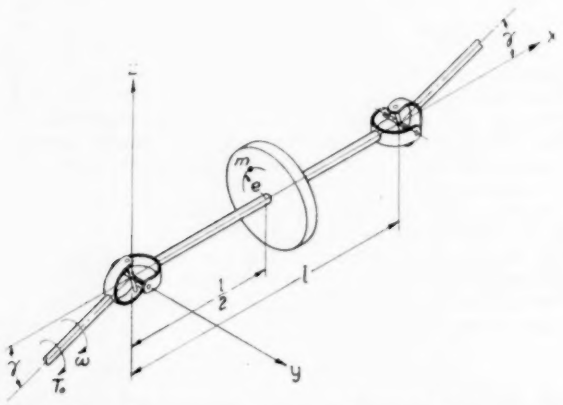

Fig. 1 Shaft Supported in Universal Joints of Nonvanishing Joint Angularity γ Subjected to a Torque, and Carrying a Disk of Mass m at the Mid-Point

and for sufficiently small $|\gamma|$, the quantity $\theta(\gamma, t)$ is of perturbation magnitude since φ is everywhere continuous in γ, and $\varphi \to \omega t$ as $\gamma \to 0$.

Combining Equations [1] and [2]

$$\tan (\omega t + \theta) = \cos \gamma \tan \omega t$$

in which both sides may be expanded in Taylor series. Now, it is evident from this equation that $\theta(\gamma, t)$ must be even in γ, and it follows from

$$\lim_{\gamma \to 0} \theta(\gamma, t) = 0$$

that when θ is expanded in a power series in γ, there is no term independent of γ; in other words, this series begins with a term in γ^2. Therefore retaining linear terms in θ when expanding the left-hand side of the foregoing equation must be accompanied by the retention, at least, of a term in γ^2 when expanding the right-hand side. Accordingly

$$\tan \omega t + \theta \sec^2 \omega t + \ldots = \left(1 - \frac{\gamma^2}{2!} + \ldots\right) \tan \omega t$$

which yields after some trigonometric manipulations

$$\theta(\gamma, t) = -\frac{1}{4} \gamma^2 \sin 2\omega t \quad \ldots\ldots\ldots\ldots\ldots\ldots [3]$$

Retention of more terms in the expansion would have resulted in a Fourier series of fundamental frequency 2ω, but containing more terms than one. The reason why only Fourier terms of frequency $2n\omega$, $(n = 1, 2, \ldots)$ occur is that the Hooke joint is so constructed that every event repeats itself after one half of a shaft revolution.

Shaft Stability Without Torque

In this section we examine the question to what extent nonvanishing joint angularity influences the shaft critical-speed phenomenon when no torque is transmitted by the shaft.

Consider the system of Fig. 1 with $T_0 = 0$ and denote by (η, ζ) the co-ordinates of the disk mass center measured parallel to the y and z-axes, respectively. Let it require a force of magnitude $k\rho$, applied to the disk in a plane normal to the x-axis, to deflect the shaft center by ρ. Then, if the distance between mass center and shaft center is denoted by e, and the angle of the line connecting mass and shaft centers with respect to the horizontal by φ, the equations of motion of the disk are given by (3)

$$\left.\begin{aligned} \ddot{\eta} + \nu^2 \eta &= \nu^2 e \cos \varphi \\ \ddot{\zeta} + \nu^2 \zeta &= \nu^2 e \sin \varphi \end{aligned}\right\} \quad \ldots\ldots\ldots\ldots [4]$$

where $\nu^2 = k/m$.

Since φ in Equations [4] has, clearly, the same meaning as in Equation [1] we find for the equations of motion

$$\left.\begin{aligned} \ddot{\eta} + \nu^2 \eta &= \nu^2 e \cos [\omega t + \theta(\gamma, t)] \\ \ddot{\zeta} + \nu^2 \zeta &= \nu^2 e \sin [\omega t + \theta(\gamma, t)] \end{aligned}\right\} \quad \ldots\ldots\ldots [5]$$

where $\theta(\gamma, t)$ is defined by Equation [3]. When the trigonometric terms in Equations [5] are expanded in powers of γ and powers higher than γ^2 are rejected, there results

$$\left.\begin{aligned} \cos [\omega t + \theta(\gamma, t)] &= \left(1 + \frac{\gamma^2}{8}\right) \cos \omega t - \frac{\gamma^2}{8} \cos 3\omega t \\ \sin [\omega t + \theta(\gamma, t)] &= \left(1 - \frac{\gamma^2}{8}\right) \sin \omega t - \frac{\gamma^2}{8} \sin 3\omega t \end{aligned}\right\} \quad \ldots [6]$$

If higher order terms in γ^2 are retained, it can be shown that

$$\left.\begin{aligned}\cos(\omega t+\theta) &= \sum_{r=1,3,\ldots} P_r \cos r\omega t\\ \sin(\omega t+\theta) &= \sum_{r=1,3,\ldots} Q_r \sin r\omega t\end{aligned}\right\} \quad \ldots\ldots [7]$$

where the P_r and Q_r are polynomials in γ^2. It is evident then that the equations of motion are

$$\left.\begin{aligned}\ddot{\eta}+\nu^2\eta &= \nu^2 e \sum_{r=1,3,\ldots} P_r \cos r\omega t\\ \ddot{\zeta}+\nu^2\zeta &= \nu^2 e \sum_{r=1,3,\ldots} Q_r \sin r\omega t\end{aligned}\right\} \quad \ldots\ldots [8]$$

and when $\nu^2 \neq \omega^2$, the steady-state solutions are

$$\left.\begin{aligned}\eta &= e \sum_{r=1,3,\ldots} \frac{P_r \cos r\omega t}{1-r^2\left(\frac{\omega}{\nu}\right)^2}\\ \zeta &= e \sum_{r=1,3,\ldots} \frac{Q_r \sin r\omega t}{1-r^2\left(\frac{\omega}{\nu}\right)^2}\end{aligned}\right\} \quad \ldots\ldots [9]$$

Thus the shaft becomes unstable whenever the driving speed is

$$\omega = \pm\nu/r, \qquad (r = 1, 3, \ldots) \ldots\ldots [10]$$

The effect of nonvanishing joint angularity γ is, therefore, to produce shaft instability whenever the driving speed is an odd-integer submultiple of the critical speed, found when the joint angularity vanishes.

It can be shown, however, that the new instabilities, i.e., those given by Equation [10] with $r = 3, 5, \ldots$, are very mild compared to the critical speed when $\omega = \pm\nu$.

In order to demonstrate this, we make use of Equation [6] by writing the equations of motion as

$$\ddot{\eta}+\nu^2\eta = \nu^2 e(P_1 \cos\omega t + P_3 \cos 3\omega t)$$
$$\ddot{\zeta}+\nu^2\zeta = \nu^2 e\,(Q_1 \sin\omega t + Q_3 \sin 3\omega t)$$

with

$$P_1 = 1+\gamma^2/8$$
$$Q_1 = 1-\gamma^2/8$$
$$P_3 = Q_3 = -\gamma^2/8$$

and we solve these equations for the two cases $\omega = \nu/3$ and $\omega = \nu$, resulting in solutions $\eta_{1/3}$, $\zeta_{1/3}$ and η_1, ζ_1, respectively. A measure of the violence of the instability of each is, then, the time derivative of $|\rho| = (\eta^2+\zeta^2)^{1/2}$. Carrying out these steps it is found that

$$\dot{\rho}_{1/3} = e\nu\gamma^2/16$$
$$\dot{\rho}_1 = e\nu/2$$

From these results, it is evident that the rate of amplitude increase at the new instability is only $\gamma^2/8$ that of the "resonant" instability which occurs when $\omega = \pm\nu$. In interpreting this result, it must be remembered that γ^2 is so small that its higher orders may be ignored.

We conclude that joint angularity produces mild instabilities at angular velocities $\omega = \pm\nu/r$, $(r = 3, 5, \ldots)$ where ν is the critical speed with zero joint angularity.

Shaft Stability in the Presence of Torque

We consider now the dynamics of the shaft described in the foregoing when a torque of constant magnitude T_0 is applied on the driving shaft, and the joint angularity is $\gamma \neq 0$.

The equations of equilibrium are similar to those given by (4) and are, in terms of our nomenclature

$$\left.\begin{aligned}EI\frac{\partial^2 y}{\partial x^2}+T\frac{\partial z}{\partial x} &= \frac{1}{2}mx\left.\frac{\partial^2 y}{\partial t^2}\right|_{x=\frac{l}{2}}\\ EI\frac{\partial^2 z}{\partial x^2}-T\frac{\partial y}{\partial x} &= 0\end{aligned}\right\} \quad \ldots\ldots [11]$$

where T is the torque on the driven shaft.

If we introduce the transformations

$$\left.\begin{aligned}\xi &= x/l\\ \alpha &= T\Big/\left(\frac{1}{l}EI\right)\\ \beta &= m\Big/\left[\left(\frac{1}{l}\right)^3 EI\right]\end{aligned}\right\} \quad \ldots\ldots [12]$$

the equations of motion become

$$\left.\begin{aligned}\frac{\partial^2 y}{\partial\xi^2}+\alpha\frac{\partial z}{\partial x} &= \frac{1}{2}\beta\xi\left.\frac{\partial^2 y}{\partial t^2}\right|_{\xi=1/2}\\ \frac{\partial^2 z}{\partial\xi^2}-\alpha\frac{\partial y}{\partial\xi} &= 0\end{aligned}\right\} \quad \ldots\ldots [13]$$

It is of interest to note that we are compelled to write the partial differential equations of the problem, while Grammel (4) was able to start from the ordinary differential equations which result when a product solution is introduced. The reason for the increased complication is that the torque T, or the parameter α, is a function of time. In fact, it is known (2) that the torque on the driven shaft is of the form

$$T = T_0 + \delta\cos(2\omega t+\psi) \ldots\ldots [14]$$

where the phase angle ψ can be made to vanish through proper choice of the co-ordinate axes orientation, and $\delta = \delta(\gamma^2)$ is a function of γ^2 which is continuous at zero and vanishes with γ^2. If Equation [14] is substituted in the second of Equations [12] and the axis orientation has been so chosen that $\psi = 0$, there results

$$\alpha(t) = \alpha_0 + \epsilon\cos 2\omega t \ldots\ldots [15]$$

where

$$\alpha_0 = T_0\Big/\left(\frac{1}{l}EI\right)$$
$$\epsilon = \delta\Big/\left(\frac{1}{l}EI\right)$$

Before discussing the equations of motion, we remark that one may differentiate the first of Equations [13] once with respect to ξ and substitute in it the second. If the resulting equation is then integrated once with respect to ξ, it is found that

$$\frac{\partial^2 y}{\partial\xi^2}+\alpha^2 y = \frac{1}{2}\beta\xi\left.\frac{\partial^2 y}{\partial t^2}\right|_{\xi=1/2}+f(t) \ldots\ldots [16]$$

where $f(t)$ is an arbitrary function of time.

The boundary conditions are those given by Grammel (4); they are

$$\left.\begin{aligned}y(0,t) &= 0\\ \frac{\partial y}{\partial\xi}\left(\frac{1}{2},t\right) &= 0\end{aligned}\right\} \quad \ldots\ldots [17]$$

Equations [16] and [17] constitute the boundary-value problem.

It may be ascertained readily by a trial that a product solution $y = F(\xi)G(t)$ fails to satisfy the differential equation. The

physical implication of this observation is, of course, that the system does not respond in the form of standing waves. This seems unexpected in a vibration problem which possesses the symmetries of the one in hand. These symmetries are that an examination of the problem in the interval $^1/_2 \leq \xi \leq 1$ would result in the identical formulation as the one in $0 \leq \xi \leq {}^1/_2$, examined here. Moreover, special initial conditions which might destroy standing waves have not entered the problem; in fact, the failure of a product solution is quite independent of boundary or initial conditions and resides altogether in the constitution of the differential equation of motion.

Solution of Boundary-Value Problem

If a solution of the form

$$y = G(t)[\xi/\alpha + A \sin \alpha\xi + B \cos \alpha\xi + f(t)/\alpha^2] \quad [18]$$

is proposed, where A and B are independent of ξ, but not of t, it will be seen that one set satisfying the boundary conditions is

$$\left.\begin{aligned} A &= -\left(\alpha^2 \cos \frac{\alpha}{2}\right)^{-1} \\ B &= 0 \\ f(t) &\equiv 0 \end{aligned}\right\} \quad [19]$$

so that the solution becomes

$$y(\xi, t) = G(t)\left(\frac{\xi}{\alpha} - \frac{\sin \alpha\xi}{\alpha^2 \cos \frac{\alpha}{2}}\right), \quad \alpha \neq 0 \quad [20]$$

and G must satisfy the equation

$$G\,\alpha = \frac{1}{2}\,\beta\,\frac{d^2}{dt^2}\left[G\left(\frac{1}{2\alpha} - \frac{1}{\alpha^2}\tan\frac{\alpha}{2}\right)\right] \quad [21]$$

with α as defined in Equation [15].

It will be remembered that $\alpha(\gamma, t)$ is a function of γ^2 by virtue of ϵ, and that $|\epsilon|$ is small with γ^2. Therefore we may expand α in powers of ϵ and, for sufficiently small γ^2, power of ϵ higher than the first may be ignored.

When Equation [21] is expanded in powers of ϵ and only linear terms are retained, there results

$$G'' - 4\epsilon\omega\,\frac{K_2}{K_1}\sin 2\omega t G' - \frac{4}{\beta}\,\frac{K_2}{K_1}\left[\frac{\rho_0}{K_2} + \epsilon\left(\beta\omega^2 - \frac{\rho_0}{K_1} + \frac{1}{2}\right)\cos 2\omega t\right]G = 0 \quad [22]$$

where primes denote differentiation with respect to time, and

$$K_1 = (\rho_0 - \tan \rho_0)/4\rho_0^2$$

$$K_2 = 1 - \frac{1}{\rho_0}\tan \rho_0 + \frac{1}{2}\tan^2 \rho_0$$

$$\rho_0 = \alpha_0/2$$

This equation can be somewhat simplified by the transformation

$$G(t) = \tau(t) \exp\left(-2\epsilon\,\frac{K_2}{K_1}\cos 2\omega t\right), \quad |K_2/K_1| \neq \infty \quad [23]$$

It goes, then, over into the Mathieu equation

$$\tau'' + 4\omega^2(a + b \cos 2\omega t)\tau = 0 \quad [24]$$

where $4\omega^2 a = -4\rho_0/\beta K_1$

$$4\omega^2 b = -\epsilon\,\frac{4}{\beta}\,\frac{K_2}{K_1}\left(\beta\omega^2 - \frac{\rho_0}{K_1} + \frac{1}{2K_2} - \frac{8\omega^2}{K_1}\right)$$

Before discussing the stability of the system in hand we observe that, by virtue of Equation [23], instability of $\tau(t)$ is identified with that of $G(t)$, and in view of Equation [20], $y(\xi, t)$ becomes unstable with $G(t)$. Therefore instability of $\tau(t)$ implies shaft instability.

The Instabilities

Equation [24] is easily transformed into the standard form of the Mathieu equation

$$\frac{d^2\tau}{du^2} + (a + b \cos u)\tau = 0 \quad [25]$$

with a and b defined as in Equation [24]. The stability of the solution depends on the magnitude of the parameters a and b and is normally found from the set of curves in the ab-plane which divides that plane into stable and unstable regions. If a point (a, b) lies in the interior of a stable region, the solution is stable. If the point (a, b) with $b \neq 0$ falls into the interior or on the boundary of an unstable region, the solution is unstable (5).

Now it is evident from the equations defining a and b that, in general, b is small of order ϵ. Therefore the region of interest in the ab-plane is normally a small strip in the immediate neighborhood of the a-axis. But the only unstable points in the neighborhood of the a-axis occur near the values (5)

$$a = n^2/4, \qquad (n = 1, 2, \ldots) \quad [26]$$

If the value of a as given in Equation [24] is substituted into this equation, and use is made of the fact that the critical speed of the shaft without torque and without shaft angularity is given by

$$\nu^2 = 48EI/ml^3 \quad [27]$$

the unstable points are defined by

$$\left(\frac{\omega}{\nu}\right)^2 = \frac{1}{n^2}\,\frac{\rho_0^3}{3(\tan \rho_0 - \rho_0)} \quad [28]$$

Now, it can be shown (4) that approximately

$$\rho_0^3/[3(\tan \rho_0 - \rho_0)] \cong 1 - \left(\frac{2\rho_0}{\pi}\right)^2 = 1 - (\alpha_0/\pi)^2 \quad [29]$$

and this relation is exact for $\alpha_0 = 0, \pi$. Introducing this approximation into Equation [28], that result becomes

$$\omega = \pm\frac{\nu}{n}\,[1 - (\alpha_0/\pi)^2]^{1/2} = \pm\frac{\nu}{n}\left[1 - \left(T_0\Big/\frac{\pi}{l}\,EI\right)^2\right]^{1/2}, \quad (n = 1, 2, \ldots) \quad [30]$$

For sufficiently small torques, $\alpha_0^2 \ll \pi^2$, one may write

$$\omega = \pm\frac{\nu}{n}\left[1 - \frac{1}{2}\left(\frac{\alpha_0}{\pi}\right)^2\right] = \pm\frac{\nu}{n}\left[1 - \frac{1}{2}\left(T_0\Big/\frac{\pi}{l}\,EI\right)^2\right], \quad (n = 1, 2, \ldots) \quad [31]$$

It is evident from Equation [31] that instabilities occur very near $^1/_2$, $^1/_3$, etc., times the critical speed ν, when a shaft is required to resist moderate torques, transmitted through a universal joint with small angularity.

It also may be concluded from Equations [28] or [30] that no instabilities occur when $\alpha_0 > \pi$ or when $T_0 > (\pi/l)EI$.

A rather curious feature of the solution is that there seems to exist a critical torque of magnitude $(\pi/l)EI$ (when $\alpha_0 = \pi$) sufficient to reduce all critical speeds to zero. This is, however, not

the case. When $\alpha_0 = \pi$, it turns out that $K_1 = K_2 = K_2/K_1 = -\infty$ as may be readily verified from Equation [22]. For this special case the transformation from $G(t)$ to $\tau(t)$ is no longer valid. To find the solution when $\alpha_0 = \pi$, we divide Equation [22] by K_2/K_1, and let K_1, K_2 and K_2/K_1 take on the value $-\infty$. The resulting equation is

$$G' + (\omega + {}^1/_2\beta\omega) \operatorname{ctn} 2\omega t G = 0 \quad \ldots\ldots [32]$$

and its integral is

$$\left.\begin{aligned} G &= C[\sin 2\omega t]^{-(1+1/2\beta\omega^2)} \\ &= C[\sin 2\omega t]^{-\left[1+\left(\frac{\omega}{\nu}\right)^2/96\right]} \end{aligned}\right\} \quad \ldots\ldots [33]$$

where C is a constant of integration. Since Equaton [33] is a periodic solution with finite amplitude we conclude that the shaft is stable for all $\alpha_0 \geqslant \pi$, or for all torques $T_0 \geqslant (\pi/l)EI$.

From the preceding analysis one may deduce that the "violence" of the instabilities decreases with the speeds at which they occur and goes to zero with them as $\alpha_0 \rightarrow \pi$ or as $T_0 \rightarrow (\pi/l)EI$.

It should be observed that our present analysis which includes the effect of nonzero torque cannot be reduced to the case of vanishing torque simply by putting $T_0 = 0$. Such a procedure must fail because $T_0 = 0$ implies $\alpha = 0$, and for vanishing α, the solution given in Equation [20] is not admissible. Thus the presence of nonvanishing torque is intrinsic to this analysis, and the case of zero torque, examined in the first part of this paper, is not merely a special case of the results obtained here.

The quantity $(\pi/l)EI$ is exactly one half as large as the critical torque T_{cr} which is sufficient to cause a uniform shaft to become unstable (by being deflected into a helix). This torque $T_{cr} = 2(\pi/l)EI$ was found by Greenhill (6) who investigated the behavior of a shaft under a combination of a Euler column load and a torque. He found that torque added to column loading always reduces the critical column load, and the critical torque is that sufficient to reduce the critical column load to zero.

The critical torque also was found in two other analyses. Grammel (4) discusses the massless rotating shaft with a single mass at the center, and acted upon by a torque (and also by a column load.) He finds that the torque reduces the critical speed and the Greenhill critical torque is that sufficient to reduce the critical speed to zero. Golomb and Rosenberg (7) examine the uniform rotating shaft with distributed mass and acted upon by a torque. They find that all critical speeds are reduced by the torque, and the Greenhill torque is that sufficient to reduce the first of an infinity of critical speeds to zero.

One may, now, ask why the present investigation has not also yielded the Greenhill torque. Actually, it is not to be expected that our analysis should contain the Greenhill problem. It will be seen that all analyses producing the Greenhill torque are eigenvalue problems with constant coefficients, whereas our problem has periodic coefficients. Thus our problem would produce the critical torque only if a shaft were to become unstable when subjected to a torque which oscillates about the value $2(\pi/l)EI$. This is, however, not an unstable state of a shaft as our analysis has shown.

Summary

The subject of this paper is the influence of Hooke-joint angularity on the critical-speed behavior of a shaft supported by two such joints at the ends. The mechanical model on which this phenomenon is investigated is a massless, uniform shaft having equal bending stiffness in all directions, and carrying a concentrated mass at its mid-point.

It has been shown that this model, when not required to transmit torques, develops mild instabilities at odd-ordered integer submultiples of the critical speed which would occur with a straight Hooke joint, as well as the familiar critical speed which is present in the usual strength.

When the shaft is required to transmit moderate torques through Hooke joints with nonzero angularity, there appear new instabilities near, but below, all integer submultiples of the familiar critical speed. These vanish when the torque becomes sufficiently large. In addition, there exists the familiar critical speed which is also present with the straight Hooke joint, and which does not vanish with joint angularity, or for sufficiently large torques. Its behavior with zero joint angularity and in the presence of torque has been analyzed for a system with one degree of freedom by Grammel (4) and for a system with infinitely many degrees of freedom by Golomb and Rosenberg (7).

The mechanical model chosen is that normally employed when disclosing the mechanism of the critical speed, and it is generally considered adequate for a shaft carrying a single large mass at the mid-point. It possesses the same degree of realism as the single-degree-of-freedom mass-spring system in which the mass of the spring has been ignored.

It is likely that the results presented here can be generalized without further analysis to include systems with infinitely many degrees of freedom. For instance, the investigation of reference (7) has shown that the effect of torque on all critical speeds of a uniform physical shaft is essentially the same as that on the single critical speed of the idealized model considered in reference (4) and here. There is no evident reason why a similar generalization should not be made in the present case.

BIBLIOGRAPHY

1 "Handbook for Machine Designers," by F. A. Halsey, McGraw-Hill Book Company, Inc., New York, N. Y., second edition, 1916, p. 308. (For instance.)

2 "Universal Joints," by L. D. Hagenbook and J. H. Holstein, *Product Engineering*, vol. 13, no. 6, 1942, pp. 334–336. (For instance.)

3 "Technische Dynamik," by C. B. Biezeno and R. Grammel, Julius Springer, Berlin, Germany, 1939, p. 776. (This reference is now available in an English translation under the title "Engineering Dynamics," by C. B. Biezeno and R. Grammel, Blackie and Son Limited, London and Glasgow, 1957.)

4 "Der Einfluss der Wellentorsion auf die kritische Drehzahl," by R. Grammel, Stodola Festschrift, Zurich and Leipzig, 1929, p. 180. (Re-treated in reference (3), pp. 796–800.)

5 "Nonlinear Vibrations," by J. J. Stoker, Interscience Publishers, Inc., New York, N. Y., 1950, pp. 202–208. (For instance.)

6 "A Treatise on the Mathematical Theory of Elasticity," by A. E. H. Love, Dover Publications, New York, N. Y., fourth revised edition, 1955, pp. 417–419.

7 "Critical Speeds of Uniform Shafts Under Axial Torques," by M. Golomb and R. M. Rosenberg, Proceedings of the First U. S. National Congress of Applied Mechanics, ASME, New York, N. Y., 1952, pp. 103–110.

On the Bounds of Eigenvalues of a Clamped Plate in Tension

By R. K. KAUL[1] and S. G. TEWARI,[2] NEW DELHI, INDIA

In this paper, use is made of Temple's generalizations of Kato's theorem for the determination of close lower bounds to the fundamental frequency of oscillation of a clamped square plate subjected to uniform biaxial edge tension. The success of the method depends upon the solution of an auxiliary problem governing the residual mode shape; and in the present case, this mode is determined by using the variational method of Ritz. The principle of computation of the number ϵ_V^2 (which corresponds to the ratio of the elastic energies in the residual and the tentative mode) is explained, and the value of the lower bound is determined by using the inequality $(1 - \rho/\beta)(\rho/\alpha - 1) \leq \epsilon_V^2$. The results are compared with those obtained previously by Weinstein and Chien, and it is shown that the present method leads to much closer bounds.

Introduction

RAYLEIGH'S energy method (1)[3] for the approximate determination of the natural frequencies of an elastic system is quite well known, and problems defying exact solution can be solved easily by using this technique. This principle, however, shows that it always leads to an upper bound to the lowest natural frequency and a lower bound to the highest one, and that first-order errors in the assumed mode shape produce only second-order effects of small quantities in the estimation of the natural frequency. The one major drawback of this principle is that it does not provide any information of the magnitude of error in the estimation of the natural frequency, and therefore the results cannot be considered as completely satisfactory. To perfect this method of calculation, all that is required is a means of calculating an approximation which necessarily should be lower than the true value for the lowest natural frequency and must err on the high side in the case of the highest frequency. Simultaneously, it should yield as accurate a result as Rayleigh's stationary principle.

A formula for obtaining close lower bounds was given by Kato (2) and has been extended recently by Temple (3) to systems with both elastic and inertial couplings. It is found that Temple's theorem yields lower bounds for the natural frequencies to the same degree of accuracy as Rayleigh's method gives upper bounds. As a matter of fact, from an examination of a number of problems which can be solved exactly, it is found that the lower bounds are even closer to the exact eigenvalues than the upper bounds derived by using the Rayleigh-Ritz method.

Except for two recent papers (4, 5) no attempt seems to have been made to apply this theorem to problems in vibration of thin plates. In the present paper, the solution to the auxiliary problem governed by the Euler-Lagrange equation $Vv = R$, representing the elastic mode v corresponding to the residual force R, has been arrived at by using the variational method of Ritz. The results for the lower estimate obtained by using Temple's extension are compared with those obtained by Weinstein and Chien (6), and it is shown that much narrower bounds to this eigenvalue problem can be obtained by using this theorem.

The theory of the principle has been taken *mutatis mutandis* from reference (3), and only relevant portions of the theorem are discussed here.

Temple's theorem for determination of lower bound

Kato's theorem originally applicable to systems with no inertial coupling, was extended by Temple to general Lagrangian systems of the type $Vw = \lambda Tw$ having both elastic and inertial couplings.

Rayleigh's upper estimate ρ to the eigenvalue λ; $(\rho \geq \lambda)$ corresponding to an approximate eigenvector w, is given by

$$\rho(w, Tw) = (w, Vw)$$

where V and T denote the bounded differential operators which specify the potential and kinetic energies and the symbol (v, u) denotes the scalar product of the two vectors.

The use of Temple's theorem for the determination of close lower bounds necessitates the knowledge of two numbers α and β (corresponding to two distinct normal modes of vibration which by convention are normed), selected such that $\alpha < \rho < \beta$; while no eigenvalue λ of the system lies in the interval $\alpha < \lambda < \beta$.

Then the generalization depends upon the lemma, that if the residual forces corresponding to the two eigenvalues α and β be A and B, respectively, such that

$$A = Vw - \alpha Tw$$

and

$$B = Vw - \beta Tw$$

then by using the theory of normal modes, it can be shown that

$$K_T(w) \equiv (A, T^{-1}B) \geq 0$$

and

$$K_V(w) \equiv (A, V^{-1}B) \geq 0$$

where T^{-1} and V^{-1} are the matrices of influence coefficients which specify the mobility and flexibility of the system.

The generalization of Kato's theorem follows from this lemma, for if

$$\text{Rayleigh's ratio } \rho = (w, Vw)/(w, Tw) \quad \ldots\ldots [1]$$

and residual force

---

[1] Junior Scientific Officer, Division of Applied Mechanics, National Physical Laboratory of India; at present, on University Fellowship at Columbia University, New York, N. Y.

[2] Junior Scientific Assistant, Division of Applied Mechanics, National Physical Laboratory of India.

[3] Numbers in parentheses refer to the Bibliography at the end of the paper.

Contributed by the Applied Mechanics Division and presented at the Annual Meeting, New York, N. Y., December 1–6, 1957, of THE AMERICAN SOCIETY OF MECHANICAL ENGINEERS.

Discussion of this paper should be addressed to the Secretary, ASME, 29 West 39th Street, New York, N. Y., and will be accepted until April 10, 1958, for publication at a later date. Discussion received after the closing date will be returned.

NOTE: Statements and opinions advanced in papers are to be understood as individual expressions of their authors and not those of the Society. Manuscript received by ASME Applied Mechanics Division, July 2, 1956. Paper No. 57—A-32.

$$R = Vw - \rho Tw \quad \ldots\ldots [2]$$

then

$$K_T(w) \equiv (A, T^{-1}B) = \tfrac{1}{2}[R + (\rho - \alpha)Tw], \quad [T^{-1}R + (\rho - \beta)w]\}$$

$$K_V(w) \equiv (A, V^{-1}B) = \tfrac{1}{2}\left\{\left[\frac{\alpha}{\rho}R + \left(1 - \frac{\alpha}{\rho}\right)Vw\right], \quad \left[\frac{\beta}{\rho}V^{-1}R + \left(1 - \frac{\beta}{\rho}\right)w\right]\right\}$$

and since external forces do no work on the system, $(R, w) = 0$; it follows

$$K_T(w) \equiv (R, T^{-1}R) + (\rho - \alpha)(\rho - \beta)(w, Tw)$$

and

$$K_V(w) \equiv \frac{\alpha\beta}{\rho^2}(R, V^{-1}R) + \left(1 - \frac{\alpha}{\rho}\right)\left(1 - \frac{\beta}{\rho}\right)(w, Vw)$$

Since $K_T(w)$ and $K_V(w)$ are non-negative, we have the two generalizations in the form

$$(\beta - \rho)(\rho - \alpha) \leqslant \frac{(R, T^{-1}R)}{(w, Tw)} = \epsilon_T^2 \quad \ldots\ldots [3a]$$

$$(\beta - \rho)(\rho - \alpha) \leqslant \alpha\beta\frac{(R, V^{-1}R)}{(w, Vw)} = \alpha\beta\epsilon_V^2 \quad \ldots\ldots [3b]$$

These Inequalities [3*a*, 3*b*] as shown by Washizu (7) can be interpreted geometrically in n-dimensional vector space.

In order to determine a close lower bound to ρ which is Rayleigh's approximation to the smallest eigenvalue λ_1, we select

$$\alpha = \lambda_1 \quad \text{and} \quad \beta = \mu$$

where μ is the smallest eigenvalue greater than λ_1, and a lower bound to the next eigenvalue λ_2. Since, for any reasonably good Rayleigh's approximation $\rho < \mu$, it follows that

$$(\rho - \lambda_1) \leqslant \epsilon_T^2/(\beta - \rho)$$

or

$$(\rho/\lambda_1 - 1) \leqslant \beta\epsilon_V^2/(\beta - \rho)$$

Knowing that $\rho \geqslant \lambda_1$, the bounds to λ_1 are given by the inequalities

$$\rho - \frac{\epsilon_T^2}{\beta - \rho} \leqslant \lambda_1 \leqslant \rho \quad \ldots\ldots [4a]$$

or

$$\frac{\rho(\beta - \rho)}{\beta(1 + \epsilon_V^2) - \rho} \leqslant \lambda_1 \leqslant \rho \quad \ldots\ldots [4b]$$

Determination of upper bound

Let S be the domain of a plate of arbitrary shape and C its boundary. The equation of motion of such a thin plate of thickness $2h$ and under uniform biaxial tension T_0 is governed by the partial differential equation

$$D_0\nabla^4 w_0 - T_0\nabla^2 w_0 - 2h\sigma\frac{\partial^2 w_0}{\partial t^2} = 0 \quad \text{in} \quad S \quad \ldots\ldots [5]$$

In the case of normal mode of free vibration

$$w_0 = w\sin(\bar{\omega}t + \theta)$$

and hence the transverse displacement w satisfies in S the differential equation

$$\nabla^4 w - \tau\nabla^2 w - \lambda w = 0 \quad \ldots\ldots [6]$$

where

$D_0 = 2Eh^3/3(1 - \nu^2)$ = flexural rigidity
$2h$ = thickness of plate
$\tau = T_0/D_0 = (10\pi^2/a^2$, in present example)
σ = density of plate material
$\lambda = 2\sigma h\bar{\omega}^2/D_0$ = eigenvalue
$\bar{\omega} = 2\pi f$ = circular frequency
$\nabla^2 = (\partial^2/\partial x^2 + \partial^2/\partial y^2)$
$\nabla^4 = (\partial^4/\partial x^4 + 2\partial^4/\partial x^2\partial y^2 + \partial^4/\partial y^4)$

Since the plate is rigidly clamped, the boundary conditions for w are

$$\left.\begin{aligned} w &= 0 \\ \text{and} \qquad \frac{\partial w}{\partial n} &= 0 \end{aligned}\right\} \quad \text{on} \quad C \text{ of } S \quad \ldots\ldots [7]$$

A formal solution of the differential eigenvalue problem is quite difficult; however, a close upper bound to the eigenvalues λ can be determined by treating this as a minima problem. In this case, the eigenvalue $\rho \geqslant \lambda$ is given by the variational problem

$$U_{(w)} = \iint_s \left\{(\nabla^2 w)^2 + \tau\left[\left(\frac{\partial w}{\partial x}\right)^2 + \left(\frac{\partial w}{\partial y}\right)^2\right]\right\} dxdy$$

$$= \text{minimum}$$

$$= \rho; \quad (\rho \geqslant \lambda) \quad \ldots\ldots [8]$$

with the auxiliary condition

$$H_{(w)} = \iint_s w^2 dxdy = 1$$

and the boundary conditions

$$w = \partial w/\partial n = 0$$

on C of S.

For minimizing the expression $U(w)$, we assume a tentative mode for the dynamic deflection w. If the location of the origin of the rectangular co-ordinates is such that the lines $x = 0$, $x = a$, and $y = 0$, $y = b$ coincide with the rectilinear edges of the clamped plate, then the most suitable choice for the deflection wave shape is to represent it in the form of a parameter-laden double series

$$w = \sum_{m=1,3,5,\ldots}^{\infty}\sum_{n=1,3,5,\ldots}^{\infty}\alpha_{mn}\varphi_m(x)\psi_n(y) \quad \ldots\ldots [9]$$

where α_{mn} are the arbitrary parameters to be determined later and $\varphi_m(x)$ and $\psi_n(y)$ constitute the set of characteristic functions of a clamped-clamped beam and are the solutions of the differential problem

$$\left.\begin{aligned} \frac{\partial^4\varphi_m}{\partial x^4} &= k_m^4\varphi_m \\ \text{or} \qquad \frac{\partial^4\psi_n}{\partial y^4} &= k_n^4\psi_n \end{aligned}\right\} \quad \ldots\ldots [10a]$$

with

$$\left.\begin{aligned} \varphi_m = \partial\varphi_m/\partial x = 0 \quad &\text{at} \quad x = 0;\ a \\ \text{or} \qquad \psi_n = \partial\psi_n/\partial y = 0 \quad &\text{at} \quad y = 0;\ b \end{aligned}\right\} \quad \ldots\ldots [10b]$$

on each of the two clamped ends of the respective beams.

Owing to the symmetry of the dynamic deflection of the plate with respect to the lines $x = a/2$ and $y = b/2$, for the fundamental mode, only odd values of m and n will occur in series representation for w. Substituting for w in the expression for $U_{(w)}$ and using the properties of these functions we obtain

$$U_{(w)} = \int_0^a \int_0^a \Big\{ \sum_m \sum_n \alpha_{mn}{}^2 [(\varphi_m{}''\psi_n)^2 + (\varphi_m\psi_n{}'')^2 + \tau(\varphi_m{}'\psi_n)^2 + \tau(\varphi_m\psi_n{}')^2 - \rho] + \sum_m{}' \sum_n{}' \sum_r{}' \sum_s{}' \alpha_{mn}\alpha_{rs} [2\varphi_m{}''\varphi_r\psi_n{}''\psi_s + \tau(\varphi_m{}'\varphi_r{}'\psi_n\psi_s + \varphi_m\varphi_r\psi_n{}'\psi_s{}')] \Big\} dxdy \quad \ldots [11]$$

where the symbol Σ' excludes the combinations $mn = rs$. Equating to zero the first variation of $U_{(w)}$ with respect to α_{mn}, we get

$$\frac{\partial U(w)}{\partial \alpha_{mn}} = \alpha_{mn} \left[(k_m{}^4 + k_n{}^4 - \rho) + 2 \int_0^a \int_0^a \varphi_m{}''\varphi_m\psi_n{}''\psi_n dxdy + \tau \left(\int_0^a \varphi_m{}'\varphi_m{}'dx + \int_0^a \psi_n{}'\psi_n{}'dy \right) \right] + \sum_r{}' \sum_s{}' \alpha_{rs} \left[2 \int_0^a \int_0^a \varphi_m{}''\varphi_r\psi_n{}''\psi_s dxdy + \tau \left(\delta_{ns} \int_0^a \varphi_m{}'\varphi_r{}'dx + \delta_{mr} \int_0^a \psi_n{}'\psi_s{}'dy \right) \right] = 0 \quad \ldots [12]$$

where the symbol δ_{pq} denotes the Kronecker delta and is

$$= 0 \quad \text{for} \quad p \neq q$$
$$= 1 \quad \text{for} \quad p = q$$

In the foregoing equation the values of the typical integrals for odd integers m and n are

$$\left. \begin{aligned} \int_0^a \varphi_m\varphi_m{}''dx &= -\frac{k_m a}{a^2} \tan k_m a/2 [2 + k_m a \tan k_m a/2] \\ \int_0^a \varphi_m\varphi_r{}''dx &= \frac{8k_m{}^2k_r{}^2}{a^2(k_r{}^4 - k_m{}^4)} [k_m a \tan k_m a/2 - k_r a \tan k_r a/2] \quad (m \neq r) \end{aligned} \right\} \quad \ldots [13]$$

where $k_m a$ is the mth odd root of the transcendental equation

$$\tan k_m a/2 = (-1)^m \tanh k_m a/2$$

or its equivalent

$$\cosh k_m a = \sec k_m a$$

The successive roots (8) for $m = 1, 3$, and 5 are

$$4.7300408, \quad 10.9956078, \quad 17.2787596$$

and for $m > 5$

$$k_m a \doteq (2m + 1)\pi/2$$

Numerical values of these integrals have been calculated and are given in Table 1.

Table 1 Values of $\int_0^a \varphi_m\varphi_n{}''dx$

m/n	1	3	5
1	−12.30262	9.73079	7.61544
3	9.73079	−92.90480	24.34987
5	7.61544	24.34987	−263.99798

Using these values in Equation [12], a system of simultaneous equations in coefficients α_{mn} and eigenvalues ρ is obtained for each of the r, s-combinations of m, n. The characteristic values

$$\rho_1 \leqslant \rho_2 \leqslant \rho_3 \ldots \leqslant \rho_n$$

are found from the condition of compatibility which requires the evanescence of the determinant of homogeneous equations. In order to compare the results with those obtained by Weinstein and Chien, the present calculations have been carried out for tension

$$T_0 = 10\pi^2 D_0/a^2$$

A six-term series corresponding to the combinations

$$m, n = 1.1;\ 1.3;\ 1.5;\ 3.1;\ 3.3;\ \text{and } 5.1$$

is used; and this in effect leads to a system of only four equations since $\alpha_{mn} = \alpha_{nm}$ for the symmetric fundamental mode. The fundamental eigenvalue calculated on this basis for a square plate $(a \times a)$ is found to be

$$\rho = 3598.20941/a^4$$
$$= 36.9391539\pi^4/a^4$$

and the amplitude coefficients are given in Table 2.

Table 2 Values of coefficients α_{mn}

m/n	1	3	5
1	1.000 000 000	0.048 937 002	0.008 989 801
3	0.048 937 002	0.001 302 435	...
5	0.008 989 801	...	...

Determination of elastic mode

Having estimated the Rayleigh ratio ρ and the amplitude coefficients α_{mn}, it is now possible to determine close lower bounds. The accuracy with which the approximation vector w represents the normal mode of oscillation is measured by the residual frictionless forces R required to maintain oscillation in the trial mode w with eigenvalue ρ. These forces are given by

$$R = \nabla^4 w - \tau\nabla^2 w - \rho w \quad \ldots [14]$$

Corresponding to the residual force R, there is an elastic mode v governed by the differential equation

$$Vv = R$$

where

$$V \equiv (\nabla^4 - \tau\nabla^2)$$

In order to determine the number $\epsilon_1{}^2$ it is necessary to first find the elastic mode v of the clamped plate corresponding to the residual force R. The boundary-value problem, the solution of which is to be found, is therefore

$$\nabla^4 v - \tau\nabla^2 v = R \quad \text{in} \quad S \quad \ldots [15]$$

subject to the restraints that the deflection v and the slope $\partial v/\partial n$ vanish on each of the four clamped-end boundaries of the square plate.

The exact solution of this equation is almost impossible, and therefore use is again made of variational principles. Corresponding to the Euler-Lagrange differential Equation [15], the variational problem is

$$J(v) = \frac{1}{2} \iint_s \Big\{ (\nabla^2 v)^2 + \tau \left[\left(\frac{\partial v}{\partial x} \right)^2 + \left(\frac{\partial v}{\partial y} \right)^2 \right] - 2Rv \Big\} dx\, dy \quad \ldots [16]$$

On similar considerations, it is expedient to use characteristic beam functions and represent the deflection v in the form of a double series.

$$v = \sum_{p=1,3,5,\ldots}^{\infty} \sum_{q=1,3,5,\ldots}^{\infty} \beta_{pq}\varphi_p(x)\psi_q(y) \quad [17]$$

From conditions of symmetry p and q again occur only in odd powers in the foregoing deflection series. Substituting for v in $J(v)$ and using the minimizing conditions

$$\partial J(v)/\partial\beta_{pq} = 0$$

we obtain

$$\frac{\partial J(v)}{\partial \beta_{pq}} = \beta_{pq}\left[(k_p^4 + k_q^4) + 2\int_0^a\int_0^a \varphi_p''\varphi_p\psi_q''\psi_q dx\,dy + \tau\left(\int_0^a \varphi_p'\varphi_p' dx + \int_0^a \psi_q'\psi_q' dy\right)\right] + \sum_r{}' \sum_s{}' \beta_{rs}\left[2\int_0^a\int_0^a \varphi_p''\varphi_r\psi_q''\psi_s dx\,dy + \tau\left(\delta_{qs}\int_0^a \varphi_p'\varphi_r' dx + \delta_{pr}\int_0^a \psi_q'\psi_s' dy\right)\right] - \int_0^a\int_0^a R\varphi_p\psi_q dx\,dy = 0 \quad [18]$$

where the residual load R for the tentative mode w is

$$R = \nabla^4 w - \tau\nabla^2 w - \rho w \quad [19]$$

Since

$$w = \sum_m \sum_n \alpha_{mn}\varphi_m(x)\psi_n(y) \quad [20]$$

we have

$$R = \sum_m \sum_n \alpha_{mn}[(k_m^4 + k_n^4 - \rho)\varphi_m\psi_n + 2\varphi_m''\psi_n'' - \tau(\varphi_m''\psi_n + \varphi_m\psi_n'')] \quad [21]$$

and therefore

$$\int_0^a\int_0^a R\varphi_p\psi_q dx\,dy = \left[\alpha_{mn}(k_m^4 + k_n^4 - \rho)\delta_{mp}\delta_{nq} + 2\sum_m\sum_n \alpha_{mn}\int_0^a\int_0^a \varphi_m'\varphi_p'\psi_n'\psi_q' dx\,dy\right] + \tau\int_0^a\left[\sum_m \alpha_{mn}\delta_{nq}\varphi_m'\varphi_p' dx + \sum_n \alpha_{mn}\delta_{mp}\psi_n'\psi_q' dy\right] \quad [22]$$

The numerical values of this integral have been calculated for the nine combinations corresponding to taking both p and q equal to 1, 3, and 5, with given six variations of m, n. These values are given in Table 3.

Table 3 Values of $a^4\int_0^a\int_0^a R\varphi_p\psi_q dx\,dy$

p/q	1	3	5
1	−0.000 001 652	−0.002 690 490	−0.000 151 759
3	−0.002 690 490	−0.192 407 971	0.007 276 476
5	−0.000 151 759	0.007 276 476	212.613 695 475

The set of linear simultaneous equations given by Equation [18] are solved by using Crout's method. This gives the arbitrary constants β_{pq}, and these coefficients are given in Table 4.

Table 4 Values of coefficients $10^3.\beta_{pq}$

p/q	1	3	5
1	−0.011 229 067	−0.003 101 496	0.024 399 150
3	−0.003 101 496	−0.003 630 348	0.046 428 094
5	0.024 399 150	0.046 428 094	0.579 469 480

Knowing the coefficients β_{pq}, we get the solution of the equation $Vv = R$, and therefore the equation of the mode shape corresponding to residual load R.

Evaluation of lower bound

In order to determine the lower bound to the fundamental eigenvalue λ_1, we now require the knowledge of the number

$$\epsilon_V{}^2 = (R, V^{-1}R)/(w, Vw)$$

(the ratio of the elastic energies in the modes v and w), and also the eigenvalue β for the next symmetrical mode. Now

$$R = \sum_m \sum_n \alpha_{mn}[(k_m^4 + k_n^4 - \rho)\varphi_m\psi_n + 2\varphi_m''\psi_n'' - \tau(\varphi_m''\psi_n + \varphi_m\psi_n'')]$$

and

$$v = \sum_p \sum_q \beta_{pq}\varphi_p(x)\psi_q(y) \quad [23]$$

therefore

$$(R, v) = \left[\sum_m\sum_n \alpha_{mn}\beta_{pq}(k_m^4 + k_n^4 - \rho)\delta_{mp}\delta_{nq} + 2\sum_m\sum_n\sum_p\sum_q \alpha_{mn}\beta_{pq}\int_0^a\int_0^a \varphi_m'\varphi_p'\psi_n'\psi_q' dx\,dy + \tau\sum_m\sum_n\sum_p\sum_q \alpha_{mn}\beta_{pq}\int_0^a (\delta_{nq}\varphi_m'\varphi_p' dx + \delta_{mp}\psi_n'\psi_q' dy)\right] \quad [24]$$

and

$$(w, Vw) = \left[\sum_m\sum_n \alpha_{mn}{}^2(k_m^4 + k_n^4) + 2\sum_m\sum_n\sum_r\sum_s \alpha_{mn}\alpha_{rs}\int_0^a\int_0^a \varphi_m'\varphi_r'\psi_n'\psi_s' dx\,dy + \tau\sum_m\sum_n\sum_r\sum_s \alpha_{mn}\alpha_{rs}\int_0^a (\delta_{ns}\varphi_m'\varphi_r' dx + \delta_{mr}\psi_n'\psi_s' dy)\right] \quad [25]$$

Knowing the coefficients α_{mn}, β_{pq}, k_m^4, k_n^4, and with the help of table of integrals, it is now quite simple to determine the number $\epsilon_V{}^2$. On substituting in the foregoing expressions, we find, for a square plate in tension

$$(R, v) = 0.123\ \ 204\ \ 5341/a^4$$

$$(w, Vw) = 3616.887\ \ 221/a^4$$

and therefore

$$\epsilon_V^2 = (R, v)/(w, Vw) = 0.000\,034\,063\,692$$

In terms of the Inequality [3b] we therefore write

$$(1 - \rho/\beta)(\rho/\alpha - 1) \leqslant 0.000\,034\,063\,692 \ldots\ldots [26]$$

For the eigenvalue β, the next symmetrical mode $(1/3 + 3/1)$ is considered. It is evaluated from the same set of simultaneous Equations [12] from which the fundamental is first eliminated by using the orthogonality relationship. In the present case using the same six term series, we get for the next symmetric mode $\beta = 28339.13776/a^4$. Knowing the values of β and ρ, we get from the Inequality [26] a lower bound

$$\alpha \geqslant 3598.069020/a^4 = 36.9377127\pi^4/a^4$$

Hence, for a plate size $(\pi \times \pi)$ and $\tau = 10\pi^2/a^2$ the brackets to the fundamental eigenvalue are

$$36.93771\ 27 \leqslant \lambda_1 \leqslant 36.93915\ 39$$

This gives a mean as 36.93843 33 which deviates from the lower estimate by 0.00195 per cent only.

Comparative results

Using *modified* minimal principle, Weinstein and Chien determined for the same tension τ, the lower bound $\lambda_1 \geqslant \alpha = 36.862\ \pi^4/a^4$. It is well known that the Rayleigh-Ritz method gives a very close upper bound, and using characteristic beam functions and six-term series the value for

$$\rho \geqslant \lambda_1 = 36.93915\ 39\pi^4/a^4$$

To have an idea of convergence this value also was calculated with a 36-term series (based on taking m and n varying from 1 to 6), and the value is

$$\rho \geqslant \lambda_1 = 36.93902\ 42\pi^4/a^4$$

The comparative results for plate size $(\pi \times \pi)$ are given in Table 5.

It is therefore quite apparent that use of the inequality based on Temple's generalizations leads to much closer lower bounds. In principle, the relative closeness of the lower bound depends primarily on how closely the assumed mode shape approximates the exact mode of vibration, so as to make the components of the residual force R as small as possible. The only difficulty lies in calculating $V^{-1}R$; i.e., in determining the residual mode shape which, however, can be overcome by using the variational approximation as illustrated in this paper.

Table 5 Comparative results of the bounds of eigenvalues of a clamped square plate under tension $\tau = 10$

(π = 3.141 592 654)

	Lower bound	Upper bound (Rayleigh's)	Harmonic mean	Per cent deviation of lower bound from mean
Weinstein and Chien	36.862	36.93902[a]	36.90047	0.10426
Authors	36.93771	36.93915[b]	36.93843	0.00195

[a] Using 36-term series in Ritz method.
[b] Using 6-term series in Ritz method.

Acknowledgment

The work described in this paper forms part of the research program of the Laboratory and the paper is published with the permission of the Director.

Bibliography

1 "Theory of Sound," by Lord Rayleigh, Dover Publications, New York, N. Y., 1945, pp. 109–113.

2 "On the Upper and Lower Bounds of Eigenvalues," by T. Kato, *Journal of the Physical Society of Japan*, vol. 4, no. 1, 1949, pp. 334–339.

3 "The Accuracy of Rayleigh's Method of Calculating the Natural Frequencies of Vibrating Systems," by G. Temple, Proceedings of the Royal Society of London, series A, vol. 211, 1952, pp. 204–224.

4 "The Natural Frequencies of Thin Skew Plates," by R. K. Kaul and V. Cadambe, *The Aeronautical Quarterly*, vol. 7, part 4, 1956, pp. 337–352.

5 "On the Bounds of the Critical Load of a Clamped Plate in Compression," by R. K. Kaul and S. G. Tewari, to be published.

6 "On the Vibration of a Clamped Plate Under Tension," by A. Weinstein and W. Z. Chien, *Quarterly of Applied Mathematics*, vol. 1, 1943, pp. 61–68.

7 "On the Bounds of Eigenvalues," by K. Washizu, *Quarterly Journal of Mechanics and Applied Mathematics*, vol. 8, part 3, 1955, pp. 311–325.

8 "Tables of Characteristic Functions Representing the Normal Modes of Vibration of a Beam," by D. Young and R. P. Felgar, Engineering Research Series, No. 44, University of Texas, Austin, Texas, July, 1949.

Natural Frequencies of Nonuniform Beams on Multiple Elastic Supports

By R. A. DI TARANTO,[1] PHILADELPHIA, PA.

A method is presented for the determination of the natural frequencies of nonuniform beams on two or more torsionally and linearly elastic supports, including the effect of rotary mass moment of inertia. The method employed is an extension of the Myklestad method.[2] The cases of two supports with varied end conditions and three supports with a torsional and linear restraint at each support are formulated. It is indicated how this method may be used for problems concerning forced vibrations of beams on multiple elastic supports and for the determination of critical rotor speeds including gyroscopic effects.

Nomenclature

The following nomenclature is used in the paper:

- n = station number where mass and mass moment of inertia are concentrated
- b = station number of last station to left of beam
- c = station number of center support
- m = concentrated mass
- J = mass moment of inertia
- l_n = length of beam between station n and $n + 1$
- EI_n = average stiffness between station n and $n + 1$
- y_n = deflection of mass n from equilibrium
- α_n = slope of elastic curve at station n
- S_n = shear to left of station n
- M_n = moment to left of station n
- ϕ = slope at station 1
- δ = deflection at station 1
- P_1 = shear at right support
- P_c = shear at center support
- P_b = shear at left support
- f_{in} = slope coefficient of ith unknown at nth station
- g_{in} = deflection coefficient of ith unknown at nth station
- G_{in}' = moment coefficient of ith unknown at nth station
- G_{in} = shear coefficient of ith unknown at nth station
- γ_j = an operator which multiplies the shear and moment reactions at each support. It is zero if station under consideration is to right of jth support, and is 1 if station under consideration is to left of jth support
- J_D = mass moment of inertia about diameter of a disk
- M_1 = external restraining moment at right support
- M_c = external restraining moment at center support
- M_b = external restraining moment at last support

Introduction

The problem of determining the natural frequencies and forced response of nonuniform beams including the effects of rotary mass moments of inertia and elastic supports is a problem in which the idealized picture occurs in many applied situations. The cases of the fuselage of a helicopter or airplane on the ground, or the rotor of a turbine, are examples of this situation.

Myklestad and Prohl have developed methods for determining the natural frequencies of nonuniform beams. These methods are tabular methods well suited for hand or digital-computer machines. Extension of these methods to include elastic supports and results for specific cases form the basis of this paper. The specific cases presented are:

1 Beam on two supports with various end conditions.

2 Beam on three supports with torsional and linear spring at each support.

General Formulation

It is desired to determine the natural frequencies of a nonuniform beam having external reactions (normally at supports), with no damping in the system and having mass moments of inertia along its length. Such a beam is shown in Fig. 1.

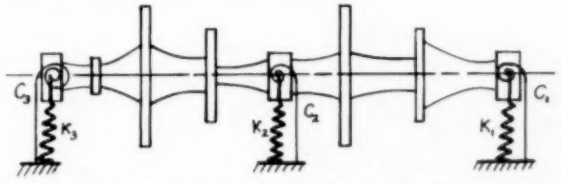

Fig. 1 Nonuniform Beam on Elastic Supports

In order to make this problem amenable to solution, the nonuniform beam is simulated by a beam having N-stations with concentrated masses and $(N - 1)$ uniform weightless beams between the masses.[2,3,4] A suggested procedure for obtaining this simulated beam is as follows: The original beam is divided into $(N - 1)$ sections with stations located at each end and at each support. The mass distribution is carried out so that the simulated beam has the same total mass, and the center of gravity (CG) of each section is the same as the equivalent section of the original beam. A method for obtaining the stiffness EI_n of each uniform section is to average the actual stiffness within each section.

For each of the uniform beam sections, deflection and slope coefficients are obtained considering the beam sections to be cantilevered at one end. These deflection and slope coefficients are defined as follows:

---

[1] Engineer, Defense Electronic Products Division of Radio Corporation of America. Assoc. Mem. ASME.

[2] "A New Method of Calculating Natural Modes of Uncoupled Bending Vibrations of Airplane Wings and Other Types of Beams," by N. O. Myklestad, *Journal of the Aeronautical Sciences*, vol. 11, 1944, p. 153.

Contributed by the Applied Mechanics Division and presented at the Fall Meeting, Hartford, Conn., September 23–25, 1957, of The American Society of Mechanical Engineers.

Discussion of this paper should be addressed to the Secretary, ASME, 29 West 39th Street, New York, N. Y., and will be accepted until April 10, 1958, for publication at a later date. Discussion received after the closing date will be returned.

Note: Statements and opinions advanced in papers are to be understood as individual expressions of their authors and not those of the Society. Manuscript received by ASME Applied Mechanics Division, July 10, 1956. Paper No. 57—F-5.

[3] "A General Method for Calculating Critical Speeds of Flexible Rotors," by M. A. Prohl, Trans. ASME, vol. 67, 1945, p. A-142.

[4] "Matrix Solution for the Vibration of Nonuniform Beams," by W. T. Thomson, Journal of Applied Mechanics, Trans. ASME, vol. 72, 1950, p. 337.

d_F = deflection at tip due to a unit load at tip
d_M = deflection at tip due to a unit moment at tip
v_M = slope at tip due to a unit moment at tip
v_F = slope at tip due to a unit load at tip

These required data may be tabulated as shown in Table 1. The beam of Fig. 1 for only three supports can be simulated by the beam of Fig. 2. If a section of the beam is taken out, and placed in dynamic equilibrium, the forces and moments are as shown in Fig. 3. P_j and M_j are, respectively, the shear and moment reactions to the right of the section. Using the notation of Fig. 3, the deflection, slope, moment, and shear on the left side of the section may be written in terms of these quantities on the right side of the section. These equations lead to a set of recurrence equations. To develop the recurrence equations, a section between stations n and $(n + 1)$ is analyzed. This typical section, with sign convention for the deflections, slopes, moments, and shears, is shown in Fig. 3. The externally applied shears and moments are positive up and counterclockwise, respectively. The beam is assumed vibrating at a frequency ω. From Fig. 3, we may write the deflection, slope, moment, and shear, respectively, as

$$\left.\begin{aligned} y_{(n+1)} &= y_n - l_n\alpha_{(n+1)} - S_n d_{Fn} - M_n d_{Mn} \\ \alpha_{(n+1)} &= \alpha_n - S_n v_{Fn} - M_n v_{Mn} \\ S_n &= \sum_{i=1}^{n} m_i y_i \omega^2 - \gamma_j \sum_{j}^{n} P_j \\ M_n &= \sum_{i=1}^{(n-1)} l_i S_i + \sum_{i=1}^{n} J_i \omega^2 \alpha_i - \gamma_j \sum_{j}^{n} M_j \end{aligned}\right\} \quad \ldots [1]$$

If

$$\left.\begin{aligned} j \leqq n \quad & \gamma_j = 1 \\ j > n \quad & \gamma_j = 0 \\ j = 1, c, b \text{ for 3 supports} \\ j = 1, b \quad \text{for 2 supports} \end{aligned}\right\}$$

The γ_j is an operator which adds in the shear or moment at a support j when station n is at or is to the left of the support j.

If these four quantities are written in terms of the unknown initial slope, initial deflection, and unknown moments and shears

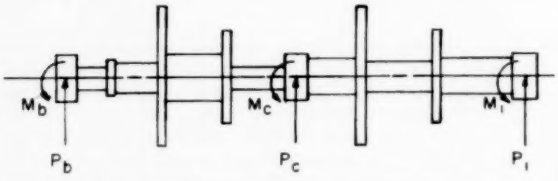

FIG. 2 IDEALIZED NONUNIFORM BEAM ON ELASTIC SUPPORTS

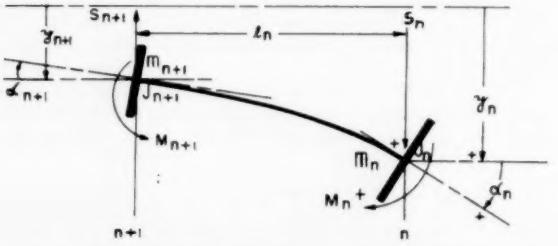

FIG. 3 TYPICAL BEAM SECTION—SHOWING SIGN CONVENTION

TABLE 1
DATA SHEET

n	m	J	EI	ℓ	d_F	$d_M = v_F$	v_M
1							
2							
⋮	⋮	⋮	⋮	⋮	⋮	⋮	⋮
b							

at each support to the right of the section, a set of linear equations in these unknowns may be written as

$$\left.\begin{aligned} y_n &= g_{\phi n}\phi + g_{\delta n}\delta + \gamma_j \sum_{j}^{n} g_{P(j)n} P_j + \gamma_j \sum_{j}^{n} g_{M(j)n} M_j \\ \alpha_n &= f_{\phi n}\phi + f_{\delta n}\delta + \gamma_j \sum_{j}^{n} f_{P(j)n} P_j + \gamma_j \sum_{j}^{n} f_{M(j)n} M_j \\ S_n &= G_{\phi n}\phi + G_{\delta n}\delta + \gamma_j \sum_{j}^{n} G_{P(j)n} P_j + \gamma_j \sum_{j}^{n} G_{M(j)n} M_j \\ M_n &= G_{\phi n}'\phi + G_{\delta n}'\delta + \gamma_j \sum_{j}^{n} G_{P(j)n}' P_j + \gamma_j \sum_{j}^{n} G_{M(j)n}' M_j \end{aligned}\right\} \quad \ldots [2]$$

where

ϕ = unknown slope at station 1
δ = unknown deflection at station 1
P_j = unknown shear at support j
M_j = unknown moment at support j

Placing these last relationships in the original deflection, slope, moment, and shear equations, Equation [1] leads to a set of recurrence equations for the coefficients of the unknown initial deflection, initial slope, and unknown moment and shear reactions. This is explicitly done for the deflection in Equations [3] and [4] as follows:

Inserting the relationships of Equation [2] into the deflection Equation [1] there results

$$\left.\begin{aligned} & g_{\phi(n+1)}\phi + g_{\delta(n+1)}\delta + \gamma_j \sum_{j}^{n} g_{P(j)(n+1)} P_j \\ & \quad + \gamma_j \sum_{j}^{n} g_{M(j)(n+1)} M_j = g_{\phi n}\phi + g_{\delta n}\delta \\ & \quad + \gamma_j \sum_{j}^{n} g_{P(j)n} P_j + \gamma_j \sum_{j}^{n} g_{M(j)n} M_j \\ & - l_n \left[f_{\phi(n+1)}\phi + f_{\delta(n+1)}\delta + \gamma_j \sum_{j}^{n} f_{P(j)(n+1)} P_j \right. \end{aligned}\right\} \quad \ldots [3]$$

$$
\begin{aligned}
&+ \gamma_i \sum_j^n f_{M(j)(n+1)} M_j \Big] \\
&- d_{Fn} \sum_{i=1}^n m_i\omega^2 \Big[g_{\phi i}\phi + g_{\delta i}\delta \\
&+ \gamma_i \sum_j^n g_{P(j)i} P_j + \gamma_i \sum_j^n g_{M(j)i} M_j \Big] \\
&\gamma_i \sum_j^n P_j d_{Fn} - d_{Mn} \sum_{i=1}^{(n-1)} l_i \Big[G_{\phi i}\phi + G_{\delta i}\delta \\
&+ \gamma_i \sum_j^n G_{P(j)i} P_j + \gamma_i \sum_j^n G_{M(j)i} M_j \Big] \\
&+ \gamma_i \sum_j^n M_j d_{Mn} - d_{Mn} \sum_{i=1}^n J_i\omega^2 \Big[f_{\phi i}\phi + f_{\delta i}\delta \\
&+ \gamma_i \sum_j^n f_{P(j)i} P_j + \gamma_i \sum_j^n f_{M(j)i} M_j \Big]
\end{aligned}
\quad \left.\vphantom{\sum}\right\} \ldots [3] \ (cont.)
$$

and equating coefficients of like terms yields deflection coefficients

$$
\left.
\begin{aligned}
g_{\phi(n+1)} &= g_{\phi n} - l_n f_{\phi(n+1)} - \sum_{i=1}^n m_i\omega^2 g_{\phi i} d_{Fn} \\
&\quad - \sum_{i=1}^{(n-1)} l_i G_{\phi i} d_{Mn} - \sum_{i=1}^n J_i\omega^2 f_{\phi i} d_{Mn} \\
g_{\delta(n+1)} &= g_{\delta n} - l_n f_{\delta(n+1)} - \sum_{i=1}^n m_i\omega^2 g_{\delta i} d_{Fn} \\
&\quad - \sum_{i=1}^{(n-1)} l_i G_{\delta i} d_{Mn} - \sum_{i=1}^n J_i\omega^2 f_{\delta i} d_{Mn} \\
g_{P(j)(n+1)} &= g_{P(j)n} - l_n f_{P(j)(n+1)} - \sum_{i=1}^n m_i\omega^2 g_{P(j)i} d_{Fn} \\
&\quad - \sum_{i=1}^{(n-1)} l_i G_{P(j)i} d_{Mn} + d_{Fn} - \sum_{i=1}^n J_i\omega^2 f_{P(j)i} d_{Mn} \\
g_{M(j)(n+1)} &= g_{M(j)n} - l_n f_{M(j)(n+1)} - \sum_{i=1}^n m_i\omega^2 g_{M(j)i} d_{Fn} \\
&\quad - \sum_{i=1}^{(n-1)} l_i G_{M(j)i} d_{Mn} - \sum_{i=1}^n J_i\omega^2 f_{M(j)i} d_{Mn} + d_{Mn}
\end{aligned}
\right\} \ldots [4]
$$

In a like manner, the slope, shear, and moment are rewritten and coefficients of like terms are equated. The resulting recurrence equations are

Slope coefficients

$$
\left.
\begin{aligned}
f_{\phi(n+1)} &= f_{\phi n} - v_{Fn} \sum_{i=1}^n m_i\omega^2 g_{\phi i} \\
&\quad - v_{Mn} \sum_{i=1}^{(n-1)} l_i G_{\phi i} - v_{Mn} \sum_{i=1}^n J_i\omega^2 f_{\phi i} \\
f_{\delta(n+1)} &= f_{\delta n} - v_{Fn} \sum_{i=1}^n m_i\omega^2 g_{\delta i} \\
&\quad - v_{Mn} \sum_{i=1}^{(n-1)} l_i G_{\delta i} - v_{Mn} \sum_{i=1}^n J_i\omega^2 f_{\delta i} \\
f_{P(j)(n+1)} &= f_{P(j)n} + v_{Fn} \Big[1 - \sum_{i=1}^n m_i\omega^2 g_{P(j)i} \\
&\quad - v_{Mn} \sum_{i=1}^{(n-1)} l_i G_{P(j)i} - v_{Mn} \sum_{i=1}^n J_i\omega^2 f_{P(j)i} \\
f_{M(j)(n+1)} &= f_{M(j)n} - v_{Fn} \sum_{i=1}^n m_i\omega^2 g_{M(j)i} + v_{Mn} \\
&\quad \Big[1 - \sum_{i=1}^{(n-1)} l_i G_{M(j)i} \Big] - v_{Mn} \sum_{i=1}^n J_i\omega^2 f_{M(j)i}
\end{aligned}
\right\} \ldots [5] \ (cont.)
$$

Shear coefficients

$$
\left.
\begin{aligned}
G_{\phi n} &= \sum_{i=1}^n m_i\omega^2 g_{\phi i} \\
G_{\delta n} &= \sum_{i=1}^n m_i\omega^2 g_{\delta i} \\
G_{P(j)n} &= \sum_{i=1}^n m_i\omega^2 g_{P(j)i} - 1 \\
G_{M(j)n} &= \sum_{i=1}^n m_i\omega^2 g_{M(j)i}
\end{aligned}
\right\} \ldots\ldots [6]
$$

Moment coefficients

$$
\left.
\begin{aligned}
G_{\phi n}' &= \sum_{i=1}^{(n-1)} l_i G_{\phi i} + \sum_{i=1}^n J_i\omega^2 f_{\phi i} \\
G_{\delta n}' &= \sum_{i=1}^{(n-1)} l_i G_{\delta i} + \sum_{i=1}^n J_i\omega^2 f_{\delta i} \\
G_{P(j)n}' &= \sum_{i=1}^{(n-1)} l_i G_{P(j)i} + \sum_{i=1}^n J_i\omega^2 f_{P(j)i} \\
G_{M(j)n}' &= \sum_{i=1}^{(n-1)} l_i G_{M(j)i} + \sum_{i=1}^n J_i\omega^2 f_{M(j)i} - 1
\end{aligned}
\right\} \ldots [7]
$$

Substituting Equations [6] and [7] into Equations [4] and [5] we obtain

$$
\left.
\begin{aligned}
g_{\phi(n+1)} &= g_{\phi n} - l_n f_{\phi(n+1)} - d_{Fn} G_{\phi n} - d_{Mn} G_{\phi n}' \\
g_{\delta(n+1)} &= g_{\delta n} - l_n f_{\delta(n+1)} - d_{Fn} G_{\delta n} - d_{Mn} G_{\delta n}' \\
g_{P(j)(n+1)} &= g_{P(j)n} - l_n f_{P(j)(n+1)} \\
&\quad - d_{Fn} G_{P(j)n} - d_{Mn} G_{P(j)n}' \\
g_{M(j)(n+1)} &= g_{M(j)n} - l_n f_{M(j)(n+1)} \\
&\quad - d_{Fn} G_{M(j)n} - d_{Mn} G_{M(j)n}'
\end{aligned}
\right\} \ldots [8]
$$

$$
\left.
\begin{aligned}
f_{\phi(n+1)} &= f_{\phi n} - v_{Fn} G_{\phi n} - v_{Mn} G_{\phi n}' \\
f_{\delta(n+1)} &= f_{\delta n} - v_{Fn} G_{\delta n} - v_{Mn} G_{\delta n}' \\
f_{P(j)(n+1)} &= f_{P(j)n} - v_{Fn} G_{P(j)n} - v_{Mn} G_{P(j)n}' \\
f_{M(j)(n+1)} &= f_{M(j)n} - v_{Fn} G_{M(j)n} - v_{Mn} G_{M(j)n}'
\end{aligned}
\right\} \ldots [9]
$$

The set of recurrence equations of the coefficients for each of the unknowns is essentially the same. The general form of the recurrence Equations [6], [7], [8], and [9] has been tabulated in Table 2 (*a*) for all of the unknowns. The specific initial conditions are shown in Table 2 (*b*), (*c*), (*d*), and (*e*). Thus by use of the tables, the coefficients of the unknowns can be computed from station to station until the last station is reached. With these last values, the determinant of the coefficients of a set of linear homogeneous equations may be set up and evaluated. The set of

TABLE 2

GENERAL TABLE

	n	$J\omega^2$	$m\omega^2$	③ g_n = ③ − ⑦	④ G_n = ④ + [3]×[2]	⑤ G'_n = ⑤ + ❶×④ + [1]×[6]	⑥ f_{n+1} = ⑥ − $J\omega^2$×[4] − $m\omega^2$×[5]	⑦ Δg_{n+1} = ❶×[6] + $J\omega^2$×[4] + $m\omega^2$×[5]
(a)								
	b							

○ DENOTES QUANTITY IN PRECEEDING ROW
□ DENOTES QUANTITY IN SAME ROW

Φ-TABLE

	n	$J\omega^2$	$m\omega^2$	$g_{\phi n}$	$G_{\phi n}$ ⑤	$G'_{\phi n}$ ⑤	$f_{\phi\, n+1}$ ⑥	$\Delta g_{\phi\, n+1}$
(b)	1			0	0		1.0000	

δ TABLE

	n	$J\omega^2$	$m\omega^2$	$g_{\delta n}$	$G_{\delta n}$ ⑤	$G'_{\delta n}$	$f_{\delta\, n+1}$ ⑥	$\Delta g_{\delta\, n+1}$
(c)	1			1.0000		0		

P-TABLE

	n	$J\omega^2$	$m\omega$	$g_{P n}$	$G_{P n}$ ⑤	$G'_{P n}$	$f_{P\, n+1}$ ⑥	$\Delta g_{P\, n+1}$
(d)				0	−1.0000	0		

M-TABLE

	n	$J\omega^2$	$m\omega$	$g_{M n}$	$G_{M n}$ ⑤	$G'_{M n}$	$f_{M\, n+1}$ ⑥	$g_{M\, n+1}$
(e)				0	0	−1.0000		

linear homogeneous equations expresses the boundary conditions which must exist when the beam is vibrating at one of its natural frequencies. This set of equations, and so the determinant, varies as the boundary conditions vary. Specific boundary conditions and the determinantal relationship which must exist are given in the following.

It is noted that the ϕ (unknown initial slope) table and δ (unknown initial deflection) table are computed from one end of the beam to the other for all cases when there exists an initial slope or deflection. The M and P tables are carried out for each support where a torsional or linear restraint, respectively, occurs. Each table is started at the support and computed to the end of the beam.

The Two General Cases

Two Supports—Torsional and Linear Spring at Each Support. For this condition the ϕ, δ, P, and M tables are started at Station 1 with the following initial values

$$f_{\phi 1} = g_{\delta 1} = 1$$

$$G_{P(1)1} = G_{P(1)1}' = -1$$

$$f_{\delta 1} = f_{P(1)1} = f_{M(1)1} = 0$$

$$g_{\phi 1} = g_{P(1)1} = g_{M(1)1} = 0$$

$$G_{P(1)1} = G_{M(1)1} = G_{\delta 1}' = G_{P(1)1}' = 0$$

$$G_{\delta 1} = m_1\omega^2 g_{\delta 1}$$

$$G_{\phi 1}' = J_1\omega^2 f_{\phi 1}$$

Complete these tables to Station b.

The other boundary conditions to be satisfied are

$$\left.\begin{aligned} K_1 y_1 &= P_1 \\ K_2 y_b &= P_b \\ C_1\alpha_1 &= M_1 \\ C_2\alpha_b &= M_b \\ P_b &= G_{\phi b}\phi + G_{\delta b}\delta + G_{P(1)b}P_1 + G_{M(1)b}M_1 \\ M_b &= G_{\phi b}'\phi + G_{\delta b}'\delta + G_{P(1)b}'P_1 + G_{M(1)b}'M_1 \end{aligned}\right\} \quad [10]$$

Substituting $y_1 = \delta$; $\alpha_1 = \phi$ and the relations for y_b and α_b we obtain

$$\left.\begin{aligned} K_1\delta &= P_1 \\ C_1\phi &= M_1 \\ K_2[g_{\phi b}\phi + g_{\delta b}\delta + g_{P(1)b}P_1 + g_{M(1)b}M_1] &= G_{\phi b}\phi + G_{\delta b}\delta + G_{P(1)b}P_1 + G_{M(1)b}M_1 \\ C_2[f_{\phi b}\phi + f_{\delta b}\delta + f_{P(1)b}P_1 + f_{M(1)b}M_1] &= G_{\phi b}'\phi + G_{\delta b}'\delta + G_{P(1)b}'P_1 + G_{M(1)b}'M_1 \end{aligned}\right\} \quad [11]$$

Substituting the first two equations [11] into the second two of [11] we obtain

$$\left.\begin{aligned} &\left[g_{M(1)b} - \frac{G_{\phi b}}{C_1K_2} + \frac{g_{\phi b}}{C_1} - \frac{G_{M(1)b}}{K_2}\right]M_1 \\ &\quad + \left[g_{P(1)b} - \frac{G_{\delta b}}{K_1K_2} + \frac{g_{\delta b}}{K_1} - \frac{G_{P(1)b}}{K_2}\right]P_1 = 0 \\ &\left[f_{M(1)b} - \frac{G_{\phi b}'}{C_1C_2} + \frac{f_{\phi b}}{C_1} - \frac{G_{M(1)b}'}{C_2}\right]M_1 \\ &\quad + \left[f_{P(1)b} - \frac{G_{\delta b}'}{K_1C_2} + \frac{f_{\delta b}}{K_1} - \frac{G_{P(1)b}'}{C_2}\right]P_1 = 0 \end{aligned}\right\} \quad [12]$$

If we let

$$\left.\begin{aligned} A &= g_{M(1)b} - \frac{G_{\phi b}}{C_1K_2} + \frac{g_{\phi b}}{C_1} - \frac{G_{M(1)b}}{K_2} \\ B &= g_{P(1)b} - \frac{G_{\delta b}}{K_1K_2} + \frac{g_{\delta b}}{K_1} - \frac{G_{P(1)b}}{K_2} \\ C &= f_{M(1)b} - \frac{G_{\phi b}}{C_1C_2} + \frac{f_{\phi b}}{C_1} - \frac{G_{M(1)b}'}{C_2} \\ D &= f_{P(1)b} - \frac{G_{\delta b}'}{K_1C_2} + \frac{f_{\delta b}}{K_1} - \frac{G_{P(1)b}'}{C_2} \end{aligned}\right\} \quad [13]$$

We then obtain

$$\left.\begin{aligned} AM_1 + BP_1 &= 0 \\ CM_1 + DP_1 &= 0 \end{aligned}\right\} \quad [14]$$

For a nontrivial solution

$$AD - BC = 0 \quad [15]$$

A plot of the value of Equation [15] against assumed values of ω will indicate what values of Equation [15] equal zero. These are the natural frequencies. The mode shape is

$$y_n = g_{\phi n}\phi + g_{\delta n}\delta + g_{P(1)n}P_1 + g_{M(1)n}M_1 \quad [16]$$

where the deflection at Station 1 is normalized to 1. Then

RESULTS OF VARIOUS TWO SUPPORT END CONDITIONS

BEAM	A	B	C	D	P	M	δ	φ	TABLES REQUIRED
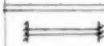	$g_{\alpha_1 a}$	$g_{\beta_1 a}$	$f_{\alpha_1 a}$	$f_{\beta_1 a}$	$-\frac{A}{B}$	1	0	0	M P
	$g_{\alpha_1 b} - \frac{G_{\alpha_1 b}}{K_2}$	$g_{\beta_1 b} - \frac{G_{\beta b}}{K_1 K_2} + \frac{g_{\beta b}}{K_1} - \frac{G_{\beta_1 b}}{K_2}$	$f_{\alpha_1 b}$	$f_{\beta_1 b} + \frac{f_{\beta b}}{K_1}$	K_1	$-\frac{B}{A}K_1$	1	0	M P δ
	$g_{\alpha_1 b} + \frac{g_{\alpha b}}{C_1}$	$g_{\beta_1 b}$	$f_{\alpha_1 b} - \frac{G_{\phi b}}{C_1 C_2} + \frac{f_{\alpha b}}{C_1} - \frac{G'_{\alpha_1 b}}{C_2}$	$f_{\beta_1 b} - \frac{G'_{\beta b}}{C_2}$	$-\frac{A}{B}C_1$	C_1	0	1	M P φ
FREE-FREE	$G_{\phi b}$	$G_{\delta b}$	$G'_{\phi b}$	$G'_{\delta b}$	0	0	1	$-\frac{0}{C}$	δ φ
	$-G_{\phi_1 b} + K_2 g_{\phi b}$	$K_1 K_2 g_{\beta_1 b} - G_{\beta b} + K_2 g_{\beta b} - K_1 G_{\beta_1 b}$	$-G'_{\phi b}$	$-G'_{\delta b} - K_1 G'_{\beta_1 b}$	K_1	0	1	$-\frac{B}{A}$	P δ φ
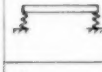	$g_{\phi b}$	$g_{\delta b}$	$f_{\phi b}$	$f_{\delta b}$	0	0	1	$-\frac{B}{A}$	δ φ

NATURAL FREQUENCY CRITERIA~ $AD - BC = 0$

DEFLECTION ~ $y_n = g_{\phi_n}\phi + g_{\beta_n}\delta + g_{P_n}P + g_{M_n}M$

FIG. 4 RESULTS OF VARIOUS TWO-SUPPORT END CONDITIONS

$$\left.\begin{aligned} \delta &= 1 \\ P_1 &= K_1 \\ M_1 &= -\frac{B}{A}K_1 \\ \phi &= -\frac{B}{A}\frac{K_1}{C_1} \end{aligned}\right\} \quad \ldots\ldots\ldots\ldots [17]$$

This general flexible two-support beam can be specialized to a number of normally encountered end fixities for beams. The results are shown in Fig. 4.

Three Supports—Torsional and Linear Springs at Each Support. The ϕ, δ, P_1, and M_1 tables are started at Station 1 with the following initial conditions

$$\begin{aligned} f_{\phi 1} &= g_{\delta 1} = 1 \\ G_{P(1)1} &= G_{M(1)1}{}' = 1 \\ f_{\delta 1} &= f_{P(1)1} = f_{M(1)1} = 0 \\ g_{\phi 1} &= g_{P(1)1} = g_{M(1)1} = 0 \\ G_{\delta 1}{}' &= G_{P(1)1}{}' = 0 \\ G_{\phi 1} &= G_{M(1)1} = 0 \\ G_{\phi 1}{}' &= J_1\omega^2 f_{\phi 1} \\ G_{\delta 1} &= m_1\omega^2 g_{\delta 1} \end{aligned}$$

Complete these tables to Station b. Also start tables P_c and M_c at Station c with the following initial condition

$$f_{P(c)c} = g_{P(c)c} = G_{P(c)c}{}' = 0 \qquad f_{M(c)c} = g_{M(c)c} = G_{M(c)c} = 0$$

$$G_{P(c)c} = -1 \qquad G_{M(c)c}{}' = -1$$

Complete these tables to Station b

The other boundary conditions are

$$\left.\begin{aligned} K_1 y_1 &= P_1 \\ C_1\alpha_1 &= M_1 \\ K_2 y_c &= P_c \\ C_2\alpha_c &= M_c \\ K_3 y_b &= P_b \\ C_3\alpha_b &= M_b \\ M_b &= G_{\phi b}{}'\phi + G_{\delta b}{}'\delta + G_{P(1)b}{}'P_1 + G_{M(1)b}{}'M_1 \\ &\quad + G_{P(c)b}{}'P_c + G_{M(c)b}{}'M_c \\ P_b &= G_{\phi b}\phi + G_{\delta b}\delta + G_{P(1)b}P_1 + G_{M(1)b}M_1 \\ &\quad + G_{P(c)b}P_c + G_{M(c)b}M_c \end{aligned}\right\} \quad \ldots [18]$$

Substituting the last two of Equations [18] into the other six and making use of the initial boundary conditions, Equations [18] may be written as

$$\left.\begin{aligned} &K_2[g_{\phi c}\phi + g_{\delta c}\delta + g_{P(1)c}P_1 + G_{M(1)c}M_1] - P_c = 0 \\ &C_2[f_{\phi c}\phi + f_{\delta c}\delta + f_{P(1)c}P_1 + f_{M(1)c}M_1] - M_c = 0 \\ &K_3[g_{\phi b}\phi + g_{\delta b}\delta + g_{P(1)b}P_1 + g_{M(1)b}M_1 \\ &\quad + g_{P(c)b}P_c + g_{M(c)b}M_c] - G_{\phi b}\phi - G_{\delta b}\delta - G_{P(1)b}P_1 \\ &\quad - G_{M(1)b}M_1 - G_{P(c)b}P_c - G_{M(c)b}M_c = 0 \\ &C_3[f_{\phi b}\phi + f_{\delta b}\delta + f_{P(1)b}P_1 + f_{M(1)b}M_1 + f_{P(c)b}P_c \\ &\quad + f_{M(c)b}M_c] - G_{\phi b}{}'\phi - G_{\delta b}{}'\delta - G_{P(1)b}{}'P_1 - G_{M(1)b}{}'M_1 \\ &\quad - G_{P(c)b}{}'P_c - G_{M(c)b}{}'M_c = 0 \\ &C_1\phi = M_1 \\ &K_1\delta = P_1 \end{aligned}\right\} \quad \ldots [19]$$

Substituting the last two of Equations [19] into the other four, he six equations reduce to

$$\left.\begin{aligned} AM_1 + BP_1 - P_c &= 0 \\ CM_1 + DP_1 - M_c &= 0 \\ EM_1 + FP_1 + HM_c + JP_c &= 0 \\ LM_1 + MP_1 + NM_c + RP_c &= 0 \end{aligned}\right\} \quad \ldots\ldots [20]$$

where

$$\left.\begin{aligned} A &= [C_1 g_{M(1)c} + g_{\phi c}]K_2 \\ B &= \left[C_1 g_{P(1)c} + \frac{C_1 g_{\delta c}}{K_1}\right] K_2 \\ C &= C_2 f_{M(1)c} + \frac{C_2}{C_1} f_{\phi c} \\ D &= C_2 f_{P(1)c} + \frac{C_2}{K_1} f_{\delta c} \\ E &= C_1 g_{M(1)b} - \frac{C_1 G_{M(1)b}}{K_2} + g_{\phi b} - \frac{G_{\phi b}}{K_2} \\ F &= g_{P(1)b} C_1 - \frac{C_1}{K_2} G_{P(1)b} + \frac{C_1}{K_1} g_{\delta b} - \frac{C_1}{K_1 K_2} G_{\delta b} \\ H &= C_1 g_{M(c)b} - \frac{C_1}{K_2} G_{M(c)b} \\ J &= C_1 g_{P(c)b} - \frac{G_{P(c)b}}{K_2} C_1 \\ L &= C_1 C_2 f_{M(1)b} - C_1 G_{M(1)b}' + C_2 f_{\phi b} - G_{\phi b}' \\ M &= C_1 C_2 f_{P(1)b} - C_1 G_{P(1)b}' + \frac{C_1 C_2}{K_1} f_{\delta b} - \frac{C_1 G_{\delta b}'}{K_1} \\ N &= C_1 C_2 f_{M(c)b} - C_1 G_{M(c)b}' \\ R &= C_1 C_2 f_{P(c)b} - C_1 G_{P(c)b}' \end{aligned}\right\} \quad \ldots [21]$$

For a nontrivial solution of Equations [20] the determinant of the coefficients must equal zero.

$$\begin{vmatrix} A & B & 0 & -1 \\ C & D & -1 & 0 \\ E & F & H & J \\ L & M & N & R \end{vmatrix} = 0 \quad \ldots\ldots [22]$$

Thus for a natural frequency to be obtained

$$\left.\begin{aligned} A[DHR - JM + FR - DJN] \\ - B[CHR - JL + ER - CJN] \\ + [CFN + DHL - EM + FL \\ - DEN - CHM] = 0 \end{aligned}\right\} \quad \ldots [23]$$

Special cases of this general case may be obtained by placing limits of 0 or ∞ onto the torsional spring constants C; or linear spring constants K:

1 For no torsional restraint

$$C_1 = C_2 = C_3 = 0$$

Tables M_1 and M_c are not required.

2 For no torsional restraint and linear spring constants infinite (simple supports)

$$C_1 = C_2 = C_3 = 0$$

$$K_1 = K_2 = K_3 = \infty$$

Tables M_1 and M_c are not required.

For the general case, the mode shape is

$$y_n = g_{\phi n}\phi + g_{\delta n}\delta + g_{P(1)n}P_1 + g_{M(1)n}M_1 + g_{P(c)n}P_c + g_{M(c)n}M_c \quad \ldots\ldots [24]$$

where the deflection at Station 1 is normalized to 1. Then

$$\left.\begin{aligned} \delta &= 1 \\ P_c &= \left[\frac{EB + HBC - AF - HAD}{E + HC + JA}\right] K_1 \\ M_1 &= -\left[\frac{F + HD + JB}{E + CH + AJ}\right] K_1 \\ M_c &= DK_1 + CM_1 \\ \phi &= \frac{M_1}{C_1} \end{aligned}\right\} \quad \ldots [25]$$

Additional Uses for the Method

1 *Forced Vibration.* The method presented herein can be used to determine the forced response of a nonuniform beam, with varied end conditions when subjected to a harmonically varying force or harmonically varying moment. The procedure is the same as that used for determining natural frequencies with the following additions and/or exceptions:

(*a*) A station is located at the position of the impressed force or moment.

(*b*) The tables are calculated only once using the frequency of excitation ω.

(*c*) The boundary conditions are set up in a set of r linear equations for r unknowns which can be solved in terms of the magnitude of the exciting force or moment.

(*d*) After solving the equations for the unknown ϕ and/or δ and support reactions, the deflection, slope, moments, and shear may be evaluated at each station.

2 *Determination of Critical Rotor Speeds.* This method also may be applied to determine the critical rotor speeds including the gyroscopic effect of the rotating disks. The method employed is the same as for determining natural frequencies of nonuniform beams except that the actual mass moments of inertia J_D are replaced by:

(*a*) $-J_D$ for forward precession

(*b*) $3J_D$ for backward precession

when disks are being considered.[5]

3 *Determination of Natural Frequencies of Beam With Overhangs.* The natural frequencies of beams with overhangs may be found by completing ϕ and δ tables from end to end, and applicable P and M tables from each support to the end of the beam. The conditions at each support and at the left end of the beam must be satisfied in a set of linear homogeneous equations in a manner similar to that shown above.

[5] "Steam and Gas Turbines," by A. Stodola, P. Smith, New York, N. Y., vol. 1, 1945, p. 434.

4 *Design of a Beam-Support System to a Given Natural Frequency.* The method allows for the design of an elastic beam on elastic supports to a given natural frequency. This is accomplished by inserting the desired frequency for ω in the table and completing the necessary tables once, to obtain the coefficients of the unknowns at Station b.

The spring constants at each support may then be varied to satisfy the determinantal relationship.

Conclusion

An extension of the Myklestad method for calculating natural frequencies of nonuniform beams which have multiple elastic supports has been presented.

The special cases of various end fixities of a two-support beam and a beam on three elastic torsional and linear supports have been formulated. The natural frequencies for these cases may be obtained by computing the applicable ϕ, δ, P, and M tables and satisfying the remaining boundary conditions in the form of a set of linear homogeneous equations.

This systematic procedure for calculating all tables, and then evaluating a determinant, is well suited to computation on an electronic digital computer.

The Pressure for Indenting Material Resting on a Rough Foundation

By W. JOHNSON[1] and D. M. WOO[2]

To indent a material on a rough foundation under conditions of plane strain, a slip-line-field solution is proposed and a general expression obtained for the necessary pressure. For extreme values of friction, calculated values are given.

Introduction

THE indentation of material resting on a plane foundation using a flat punch has long been the subject of many theoretical investigations. When the material is deeper than it is wide it has been treated, principally, by Prandtl (1),[3] Hill (2), and Bishop (3), for the case of plane strain and by Hencky (4), Ishlinsky (5), Shield and Drucker (6), and Shield (7) for the cases in which a circular or a rectangular punch is employed. If the punch is wider than the material is deep then analyses have been made by Prandtl (1), Hill (2), Green (8), and Shield (9). In this paper attention is restricted to the plane strain instance when the supporting plane is rough and the material deeper than the punch is wide.

It is well known that when rigid, perfectly plastic material confined under conditions of plane strain and resting on a smooth foundation is indented by a smooth flat die, the plastic zones originating at the corner of the die fuse and spread through the material, the final plastic zone touching the foundation in one point only (2). While it is easy to calculate the necessary indentation pressure given this condition, it is considerably more laborious and somewhat more devious when the foundation is not smooth. As in Hill's analysis, it is assumed that a false head of metal attaches itself to the punch, but further, that a footing or zone of dead metal is developed in contact with the rough foundation.

With these assumptions the slip-line field may then be constructed as in Fig. 1.

For small values of the coefficient of friction, an approximate method due to Hill (2) may be used. However, when these coefficients are no longer small this modified field must be used for further calculations.

Slip-Line Field

The analysis takes account of all values of friction, and for this reason the slip lines of the field meet the foundation at angles different from 45 deg. In Fig. 1, if ψ is 45 deg, then the coefficient of friction μ is zero and there is no footing; for all other values of μ, ψ is greater than 45 deg and the size of the footing increases as μ increases.

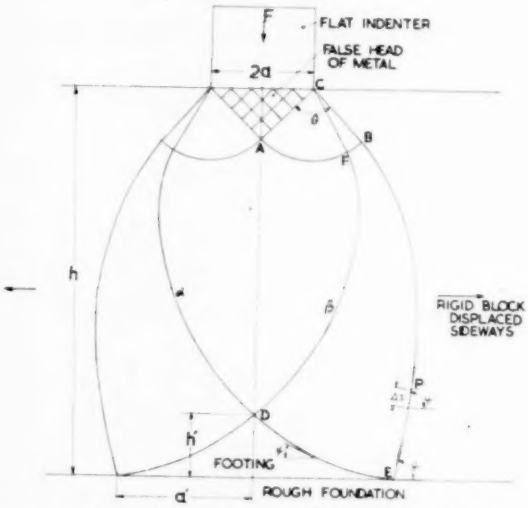

Fig. 1 Slip-Line Field for Plane Strain Indentation of a Block of Material Resting on a Rough Foundation

As noted, the field proposed is an extension of that given by Hill (2) and the method of analysis is substantially the same as his. An account of the theory of slip-line fields is easily available, see (2) and (10). The α and β-lines for use in connection with the Hencky equations are (Hill's convention) as labeled in Fig. 1.

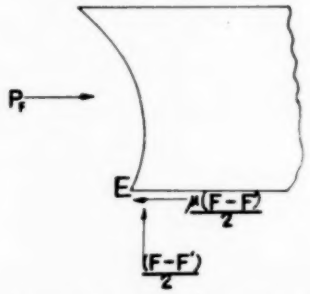

Fig. 2 Forces on a Rigid Block of Material

Referring to Fig. 2, if the indentation force is F, then part F' is carried by the footing and the remainder, $\frac{1}{2}(F - F')$, must be distributed over the foundation on either side of the footing. When indentation occurs, two rigid blocks of material are displaced sideways as indicated, and the force necessary to do this, P_F, must be such as to overcome the frictional force, see Fig. 2; thus

[1] Senior Lecturer in Engineering, Manchester University, Manchester, England.

[2] Lecturer in Mechanical Engineering, Sheffield University, Sheffield, England.

[3] Numbers in parentheses refer to the Bibliography at the end of the paper.

Contributed by the Applied Mechanics Division and presented at the Annual Meeting, New York, N. Y., December 1–6, 1957, of The American Society of Mechanical Engineers.

Discussion of this paper should be addressed to the Secretary, ASME, 29 West 39th Street, New York, N. Y., and will be accepted until April 10, 1958, for publication at a later date. Discussion received after the closing date will be returned.

Note: Statements and opinions advanced in papers are to be understood as individual expressions of their authors and not those of the Society. Manuscript received by ASME Applied Mechanics Division, September 6, 1956. Paper No. 57—A-24.

$$\frac{1}{2}\mu(F - F') = P_F \ldots\ldots\ldots\ldots\ldots [1]$$

By use of the Hencky equations, and in terms of the quantities indicated in Fig. 1, it may be shown that

$$P_F/k = h(p_E/k - 2\psi) + 2I - (a - a') \ldots\ldots [2]$$

where $I = \int \psi' \sin \psi' \, ds$, the integration being performed along line *E-B-C* and where p_E is the hydrostatic pressure at E, and k the yield shear stress of the material in plane strain.

The indentation force is then given by

$$F/4ak = p_E/2k + 2\theta - \psi + \frac{\pi}{4} + \frac{1}{2} \ldots\ldots [3]$$

The force taken by the footing is

$$F'/2k = h' + ap_E/k + 2\left(\psi - \frac{\pi}{2}\right)a' + 2I' \ldots [4]$$

where $I' = \int \psi' \sin \psi' ds$,the integration being performed along line *E-D*.

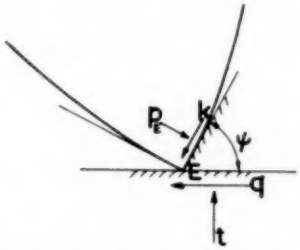

FIG. 3 NOTATION FOR STRESSES AT POINT *E* OF FOOTING

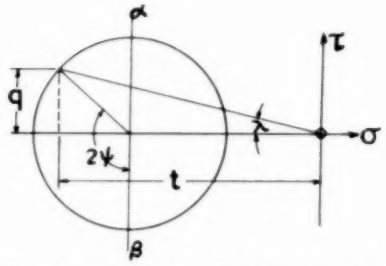

FIG. 4 MOHR-CIRCLE DIAGRAM FOR STRESSES AT POINT *E* OF FOOTING

The stresses at point E in Fig. 1, are shown in Fig. 3 and represented by means of the Mohr-circle diagram in Fig. 4. It is seen that μ and ψ are related thus

$$\mu = \tan \lambda = q/t = -\cos 2\psi/(2x + \sin 2\psi) \ldots\ldots [5]$$

where $p_E/2k$ is denoted by x. In terms of the geometry of the situation it is found that x is the positive radical of the equation

$$x^2 + x\frac{\sin 2\psi}{2} + \frac{2\alpha + 2(a - a')\cos 2\psi}{4h} + \frac{1}{4h}\left\{\alpha \sin 2\psi + \cos 2\psi\left[a\left(4\theta - 2\psi + 1 + \frac{\pi}{2}\right) - h' - 2\left(\psi - \frac{\pi}{2}\right)a' - I'\right]\right\} = 0 \ldots\ldots [6]$$

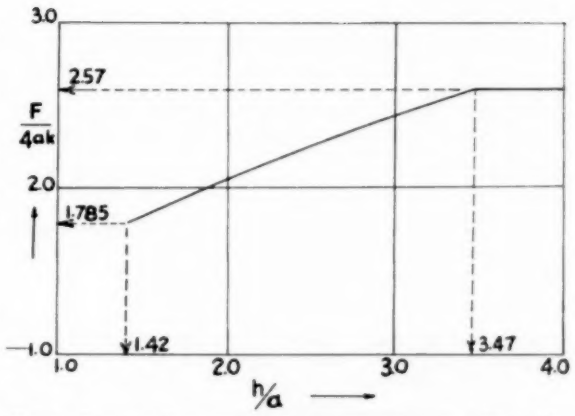

FIG. 5 SHOWING VARIATION OF INDENTATION PRESSURE WITH h/a FOR EXTREME VALUES OF FRICTION

in which $$\alpha = 2I - 2\psi + a' - a$$

If x is determined from Equation [6], indentation pressure $F/4ak$ follows from using Equation [3].

The drawing of a hodograph for this particular type of stress field is not difficult. In Fig. 6(*a*) is shown a scale drawing of one half of the stress field for $h/a = 2$ and in Fig. 6(*b*) the corresponding hodograph, lettered to correspond with Fig. 6(*a*). The graphs are drawn using 5-deg equiangular nets.

RESULTS

When ψ is 45 deg, the foundation is perfectly smooth and the variation of $F/4ak$ with h/a has been calculated and given by Hill (2). For the range of cases in which ψ is 90 deg, the variation of $F/4ak$ with h/a has been calculated by the authors using a 5-deg equiangular net of slip lines drawn out on a large scale; the result is given in Fig. 5.

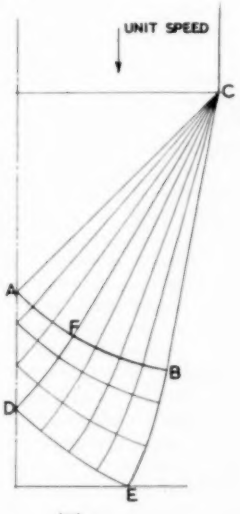

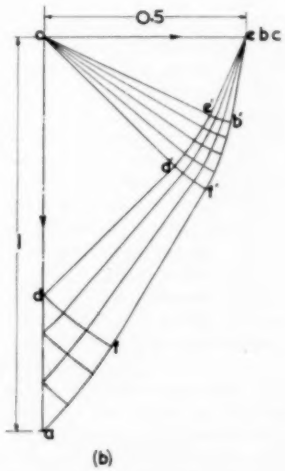

FIG. 6(*a*) ONE HALF OF A 5-DEG EQUIANGULAR NET OF SLIP LINES FOR THE CASE IN WHICH $h/a = 2$

FIG. 6(*b*) ONE HALF OF HODOGRAPH CORRESPONDING TO FIELD IN (*a*)

When the indentation pressure reaches a value of $2k(1 + \pi/2)$ an alternative mode of deformation becomes possible and instead of the rigid blocks of material being forced out sideways, plastic material is forced up at the sides of the punch. From this it appears that the mode of deformation, shown in Fig. 1, which holds for a perfectly rough foundation applies only over the range

$$1.42 < \frac{h}{a} < 3.47$$

The curve Fig. 5 is of course an upper bound for the necessary indentation pressure because no suggestion is made as to how the slip-line field may be extended into the rigid regions.

BIBLIOGRAPHY

1 "Über die Haerte plastischer Körper," by L. Prandtl, Nachrichten von der Koeniglichen Gesellschaft der Wissenschaften zu Goettingen, Mathematisch—Physikalische Klasse, 1920, pp. 74–85.

2 "The Mathematical Theory of Plasticity," by R. Hill, Clarendon Press, Oxford, England, 1950.

3 "On the Complete Solution to Problems of Deformation of a Plastic-Rigid Material," by J. F. W. Bishop, *Journal of the Mechanics and Physics of Solids*, vol. 2, 1954, pp. 43–53.

4 "Über einige statisch bestimmte Faelle des Gleichgewichts in Plastischen Koerpern," by H. Hencky, *Zeitschrift für angewandte Mathematik und Mechanik*, vol. 3, 1923, pp. 241–251.

5 "The Problem of Plasticity with Axial Symmetry and Brinell's Test," by A. Iu Ishlinsky, *Prikladnaia Mathematika i Mekhanika*, vol. 8, 1944, pp. 201–224.

6 "The Application of Limit Analysis to Punch-Indentation Problems," by R. T. Shield and D. C. Drucker, JOURNAL OF APPLIED MECHANICS, Trans. ASME, vol. 75, 1953, pp. 453–460.

7 "The Plastic Indentation of a Layer by a Flat Punch," by R. T. Shield, *Quarterly of Applied Mathematics*, vol. 13, 1955, pp. 27–46.

8 "On the Use of Hodographs in Problems of Plane Plastic Strain," by A. P. Green, *Journal of the Mechanics and Physics of Solids*, vol. 2, 1955, pp. 73–80.

9 "On the Plastic Flow of Metals Under Conditions of Axial Symmetry," by R. T. Shield, Proceedings of the Royal Society of London, England, series A, vol. 233, 1955, pp. 267–287.

10 "Theory of Perfectly Plastic Solids," by W. Prager and P. G. Hodge, John Wiley & Sons, Inc., New York, N. Y., 1951.

The Bending of Pretwisted Thin-Walled Beams of Symmetric Star-Shaped Cross Sections[1]

By L. MAUNDER,[2] EDINBURGH, SCOTLAND

The customary method of determining the elastic bending deflections of pretwisted beams predicts that the deflections of a uniform beam with a cross section having equal principal moments of inertia will be independent of pretwist. Experimental deflections of a thin-walled pretwisted beam with a doubly symmetric cruciform cross section have been found, however, to be significantly larger than those thus predicted. Based on energy methods, an approximate analysis is developed for pretwisted thin-walled beams having symmetric star-shaped cross sections, which takes into account the effect of interactions between pretwist and distortions of cross sections. An equivalent bending stiffness is derived which is a function of pretwist. The principal theoretical and experimental results are shown in Fig. 4.

Nomenclature

The following nomenclature is used in the paper:

A = $(1 - \sin^2 \xi \cos^2 \phi)^{1/2}$
a = $c - b$
b = radius of solid core of cross section
$2c$ = width of beam
ϵ_1, ϵ_2, ϵ_{12} = coefficients of mid-surface strain
E = Young's modulus
F, G = coefficients of variations δK, $\delta \bar{w}$
$2h$ = thickness of helicoidal sheets
I_0 = moment of inertia of cross section of untwisted beam
I_t = effective moment of inertia for pretwisted beam
k_1, k_2, k_{12} = coefficients of bending strain
K_1, K_2, K = component and resultant curvatures of axis of beam
M_1, M_2, M = component and resultant bending moments
m = total number of helicoidal sheets
n = designation of a particular helicoidal sheet
r = distance from axis of beam
t = pretwist per unit axial length
u, v, w = component displacements of mid-surface
v', w' = component displacements of axis of beam
w_n = distortion function for nth sheet
$\bar{w}_c$ = distortion parameter
$\bar{w}$ = 0 for $0 \leq r < b$, and $\bar{w}_c$ for $b \leq r \leq c$
U = strain energy of beam per unit length
V = potential energy per unit length
x, y, z = Cartesian co-ordinates
α_{11}, α_{12}, α_{21}, α_{22} = influence coefficients corresponding to M_1, M_2
β = ct
Δ = deflection of pretwisted beam
Δ_0 = deflection of untwisted beam
ϵ_1', ϵ_2', γ_{12}' = mid-surface strain components
ϵ_1'', ϵ_2'', γ_{12}'' = bending strain components
ϵ_1, ϵ_2, γ_{12} = total strain components
η = distance from mid-surface in w-direction
θ_0 = angle between M-vector and y-axis
λ = $(\bar{w}_c/K)^{1/2}$
ν = Poisson's ratio
ξ = $\tan^{-1}(\partial z/\partial x)$
ϕ = $\tan^{-1}(\partial z/\partial y)$
ρ = b/c
ψ = $\pi(r - b)/2(c - b)$
ω_1, ω_2 = rotations determining bending strains

Introduction

Problems of static bending of pretwisted beams, such as turbine and compressor blades, are often solved by means of conventional beam theory, pretwist being taken into account only in finding the components of bending moment which act about the principal axes of a cross section. Bending stresses and components of centerline curvature then can be determined in a manner similar to that discussed by Timoshenko (1)[3] with reference to unsymmetrical bending. One obvious and interesting consequence of the application of this approach to a pretwisted beam having a cross section with equal principal moments of inertia is that curvatures and hence deflections are predicted which are independent of pretwist. This follows from the consideration that if the two principal moments of inertia of the cross section are equal, then all moments of inertia about centroidal axes are equal. However, in conducting bending tests on the rotor of an Elliot-Lysholm compressor, consisting of a symmetric arrangement of twisted lobes, W. A. Wilson and J. W. Crocker found that the measured deflections were appreciably larger than the predictions. Subsequently (2) similar effects were observed during bending tests on a pretwisted beam of thin-walled cruciform cross section. These results are referred to by den Hartog (3).

In a previous paper (4) an explicit solution was obtained for the bending of pretwisted plates, based on the theory of slightly curved plates as developed by Marguerre (7) and Reissner (8). The analysis shows that the bending stiffness and the stress distributions associated with bending about the shorter principal axis of a cross section are influenced by pretwist in a manner

[1] The research was performed at the Massachusetts Institute of Technology and was sponsored under Contract AF 33(616)-5 by the Aeronautical Research Laboratory, Wright Air Development Center, whose support is gratefully acknowledged.

[2] Postgraduate School of Applied Dynamics, University of Edinburgh.

Contributed by the Applied Mechanics Division and presented at the Annual Meeting, New York, N. Y., December 1–6, 1957, of The American Society of Mechanical Engineers.

Discussion of this paper should be addressed to the Secretary, ASME, 29 West 39th Street, New York, N. Y., and will be accepted until April 10, 1958, for publication at a later date. Discussion received after the closing date will be returned.

Note: Statements and opinions advanced in papers are to be understood as individual expressions of their authors and not those of the Society. Manuscript received by ASME Applied Mechanics Division, January 24, 1956. Paper No. 57—A-84.

[3] Numbers in parentheses refer to the Bibliography at the end of the paper.

which is not predicted by beam theory. The physical cause of this effect is an interaction between pretwist and anticlastic deformations. Effects of a similar nature are discussed in the present paper with reference to pretwisted beams having thin-walled star-shaped cross sections, to which the previous analysis does not appear to be applicable.

Zickel (5, 6) develops a general analysis for bending of thin-walled pretwisted beams and for buckling of thin-walled pretwisted columns which follows an approach similar to that of Love (9) in his "Theory of Naturally Curved Rods." By taking account of the inclinations of helical fibers to the axis of the beam and also of the greater length of those fibers farther away from the axis, the author shows that the bending stiffness about a principal axis of a cross section is not expressed accurately by the product of Young's modulus and the appropriate moment of inertia, but is instead a decreasing function of pretwist. This analysis also points out that the deflections of a beam having a doubly-symmetric cruciform cross section, contrary to the predictions of beam theory, will increase with pretwist.

The experimental results for a beam of this type, Fig. 3, confirm that its deflections increase with pretwist. Quantitatively, however, the experimental deflections are not only appreciably larger than the predictions of beam theory but also are larger than those of the previous analysis. This suggests that there is a further effect of pretwist on the bending characteristics of such beams, and strain measurements, Fig. 5(*b*), show that it is due to the interactions of pretwist with distortions of cross sections. Such distortions include anticlastic effects, but since the beams considered are thin-walled, further distortions are suggested by the stress redistributions thereby produced.

Fig. 1 illustrates that both primary tensile and compressive stresses can be relieved in this way. From an energy standpoint, it can be said that the strain energy associated with the primary bending stresses has been reduced at the expense of adding strain energy associated with the transverse bending of the helicoidal sheets of the beam, and that the latter will occur such that the

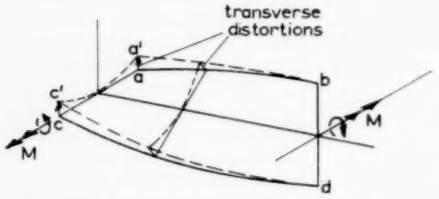

Fig. 1 Distortions of a single sheet of a multisheet beam. Tensile stresses along *ab* and compressive stresses along *cd* can be relieved by distortions of this type.

total potential energy of the system is a minimum. The present analysis assumes a form of transverse distortion governed by a single free parameter, which is then determined by minimum principles. The results may be applied to thin-walled beams of any symmetrical star-shaped cross sections. When compared with experimental results for the beam of cruciform cross section, there is fair agreement up to the largest experimental values of pretwist, where the deflections exceed the predictions of beam theory by 50 per cent.

Analysis for beam of cruciform cross section

(*a*) *Strains and Displacements.* Fixed orthogonal axes are chosen as shown in Fig. 2 with Ox directed along the centerline of the undeformed beam and Oy along the mid-surface of one helicoidal sheet. This sheet is assumed to be represented in the region $(tx) \ll 1$ by the equation

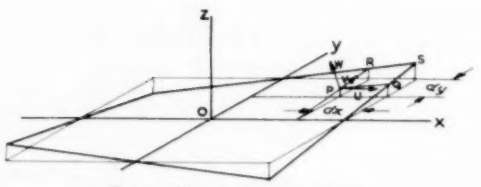

Fig. 2 The co-ordinate system

$$z = txy \qquad [1]$$

where t is the pretwist per unit axial length. Component displacements (u, v, w) of any mid-surface point P are defined to be in the directions Ox, perpendicular to Ox along the mid-surface, and along the mutual perpendicular to these directions, respectively. With the displacements described in this way it will be possible to make use of the known displacement functions for an untwisted beam. The mid-surface strain at a point can be expressed in components having mid-surface directions parallel to the x, z and y, z-planes. These directions are perpendicular when $x = 0$, and it is shown in the Appendix that the corresponding linearized components of strain are expressed by the following

$$\left.\begin{aligned} \epsilon_1' &= (u_x + tyw_x + t^2yv)(1 - t^2y^2) \\ \epsilon_2' &= v_y \\ \gamma_{12}' &= [u_y + v_x + t(yw_y - w)]\left(1 - \frac{1}{2}\,t^2y^2\right) \end{aligned}\right\} \qquad [2]$$

where ϵ_1' and ϵ_2' are extensional strains, γ_{12}' is the shearing strain, $(ty)^4$ and higher powers have been neglected compared with unity, and literal subscripts denote partial differentiation.

The additional bending strain at a point not in the mid-surface is found by consideration of an element which has its corner edges defined by straight lines in the directions of the w-components of mid-surface displacement. The mid-surface of such an element is shown in Fig. 2 as $PQRS$ and projects into the rectangle dx, dy on the x,y-plane. It is assumed that after deformation each corner edge, such as that at P, remains straight and contains the same angles with the corresponding mid-surface lines, such as PQ and PR. The components of bending strain at a point in the cross section $x = 0$, whose distance from the mid-surface measured in the w-direction is η, are shown in the Appendix to be represented by the following

$$\left.\begin{aligned} \epsilon_1'' &= -\eta[w_{xx} - tyu_{xx} + t(1 - t^2y^2)v_x \\ &\qquad + t^4y^2w](1 - 2t^2y^2) \\ \epsilon_2'' &= -\eta w_{yy} \\ \gamma_{12}'' &= -\eta\left[2w_{xy}(1 - t^2y^2) + t(v_y - yu_{xy})\right. \\ &\qquad \left(1 - \frac{3}{2}\,t^2y^2\right) - tu_x\left(1 - \frac{7}{2}\,t^2y^2\right) \\ &\qquad \left. - t^2yv(2 - t^2y^2) - t^2yw_x\right] \end{aligned}\right\} \qquad [3]$$

from which the total strain components at a point are found by the addition of corresponding quantities in Equations [2] and [3].

Let the component curvatures of the center line of the deformed beam be represented by perpendicular vectors of magnitudes K_1 and K_2 directed oppositely to the local v and w-displacement components of the sheet containing the y-axis. This sheet will be counted as the first of the four helicoidal sheets which comprise the cruciform beam. The assumed displacement functions are derived from the corresponding functions for an untwisted beam

(10) except that as described in the foregoing additional w-displacements are introduced and are represented by the function w_n for the nth sheet. In terms of the component curvatures, the assumed displacements for the mid-surface of the first sheet are then expressed as

$$\left.\begin{aligned} u &= \int_0^x K_1 r dx \\ v &= v' - \frac{1}{2}\nu K_1 r^2 \\ w &= w' + \frac{1}{2}\nu K_2 r^2 + w_1 \end{aligned}\right\} \quad \ldots\ldots\ldots\ldots [4]$$

where $r = y(1 + t^2x^2)^{1/2}$

is the distance from the axis of the beam, and v' and w' are the component displacements of the axis. The latter are chosen such that an axial element at $x = 0$ remains fixed, and thus

$$v' = w' = v_x' = w_x' = 0. \quad \ldots\ldots\ldots\ldots [5]$$

when $x = 0$, while from definition it follows that when $x = 0$

$$v_{xx}' = -K_1, \quad w_{xx}' = -K_2 \quad \ldots\ldots\ldots\ldots [6]$$

The mid-surface and bending strains at the cross section $x = 0$ are found by substituting Equations [4] into Equations [2] and [3], with the result that

$$\left.\begin{aligned} \epsilon_1' &= y\left\{K_1\left[1 - \frac{\nu}{2}t^2y^2\right] + t\left[\frac{\nu}{2}y^2(K_2)_x + (w_1)_x\right]\right\}(1 - t^2y^2) \\ \epsilon_2' &= -\nu K_1 y \\ \gamma_{12}' &= \left\{\frac{\nu}{2}y^2[tK_2 - (K_1)_x] + t[y(w_1)_y - w_1]\right\}\left(1 - \frac{1}{2}t^2y^2\right) \\ \epsilon_1'' &= -\eta\left\{(w_1)_{xx} - K_2 + \frac{\nu}{2}y^2[(K_2)_{xx} + 2t^2K_2]\right. \\ &\quad \left. - \frac{1}{2}ty^2[2 + \nu(1 - t^2y^2)](K_1)_x + t^4y^2w_1\right\}(1 - 2t^2y^2) \\ \epsilon_2'' &= -\eta\left\{(w_1)_{yy} + \nu K_2\right\} \\ \gamma_{12}'' &= -\eta\left\{2(w_1)_{xy}(1 - t^2y^2) - t^2y(2 - t^2y^2)(w_1)_x \right. \\ &\quad + \nu y(2 - 3t^2y^2)(K_2)_x \\ &\quad \left. - ty\left[(2 + \nu) - t^2y^2\left(5 + \frac{\nu}{2}\right)\right]K_1\right\} \end{aligned}\right\} \quad \ldots [7]$$

A considerable simplification is obtained by noting that the centerline of the beam bends entirely in the plane of the applied bending moment. This follows from consideration of a horizontal length of the beam, one end of which is supported such that the tangent to the centerline there maintains a fixed direction in space on application of a pure bending moment to the other end. If the applied bending moment has components M_1 and M_2 about horizontal and vertical axes, respectively, then the component rotations of the tangent to the axis at the free end may be written generally as $(\alpha_{11}M_1 + \alpha_{12}M_2)$ and $(\alpha_{21}M_1 + \alpha_{22}M_2)$, respectively, in which it follows from reciprocity that $\alpha_{12} = \alpha_{21}$. Consideration of the separate application of the component bending moments shows, however, that the biaxial symmetry of all cross sections requires that $\alpha_{12} = -\alpha_{21}$. It follows that $\alpha_{12} = \alpha_{21} = 0$, application of which to an infinitesimal length of the beam leads to the conclusion that the curvature of the axis occurs entirely in the plane of the resultant bending moment. If the vector representing the resultant bending moment is inclined at an angle θ_0 counterclockwise round Ox from Oy, the component curvature vectors may therefore be expressed as

$$\left.\begin{aligned} K_1 &= K \sin(\theta_0 + tx) \\ K_2 &= K \cos(\theta_0 + tx) \end{aligned}\right\} \quad \ldots\ldots\ldots\ldots [8]$$

where, in the case of pure bending, K, the magnitude of the resultant curvature vector, is a constant.

The distortion function w_1 is assumed to be represented by

$$\left.\begin{aligned} w_1 &= \bar{w}(1 - \cos\psi)\cos(\theta_0 + tx) \\ \text{where} \\ \bar{w} &= 0 \quad \text{for} \quad 0 \le r < b \\ \bar{w} &= \bar{w}_c \quad \text{for} \quad b \le r \le c \end{aligned}\right\} \quad \ldots\ldots\ldots [9]$$

and $\bar{w}_c$ is a constant, c is the width of a helicoidal sheet ($0 \le r \le c$). b is the radius of the solid core of the cross section in which distortions w_1 are assumed to be zero, and

$$\psi = \pi(r - b)/2(c - b)$$

The variation of w_1 with x is thus such as to satisfy all the requirements imposed by the symmetry of the problem and will provide a maximum relief of strain ϵ_1' at the most highly strained points of a cross section, as will be seen by substitution in the first of Equations [7]. It will be noted from Equations [11] that the variation of w_1 with r will not satisfy exactly the requirements of a stressless boundary at $r = c$; however, the term contributing the major stress at that boundary, namely $(w_1)_{yy}$, does vanish when $r = c$, while the residual nonvanishing stresses involve the small quantity (ty). The selection of a more exact variation with r does not appear warranted at this stage, and thus the form [9] is retained as a reasonable and simple approximation. Substitution of the Equations [8] and [9] into Equations [7] allows the components of total strain at a point in $x = 0$ to be expressed as

$$\left.\begin{aligned} \epsilon_1 &= \epsilon_1' + \epsilon_1'' = e_1 \sin\theta_0 + \eta k_1 \cos\theta_0 \\ \epsilon_2 &= \epsilon_2' + \epsilon_2'' = e_2 \sin\theta_0 + \eta k_2 \cos\theta_0 \\ \gamma_{12} &= \gamma_{12}' + \gamma_{12}'' = e_{12} \cos\theta_0 + \eta k_{12} \sin\theta_0 \end{aligned}\right\} \quad \ldots [10]$$

where

$$\left.\begin{aligned} e_1 &= Ky[1 - (1 + \nu)t^2y^2] - t^2y\bar{w}(1 - \cos\psi) \\ e_2 &= -\nu Ky \\ e_{12} &= -t\bar{w}\left(1 - \cos\psi - \frac{\pi y}{2a}\sin\psi\right) \\ k_1 &= K(1 - t^2y^2) + t^2\bar{w}\left(1 - \cos\psi - \frac{\pi y}{2a}\sin\psi\right) \\ k_2 &= -\left(\nu K + \frac{\pi^2}{4a^2}\bar{w}\cos\psi\right) \\ k_{12} &= t\left[Ky(2 + 3\nu) + \frac{\pi}{a}\bar{w}\sin\psi\right] \end{aligned}\right\} \quad \ldots [11]$$

in which $a = (b - c)$, $(ty)^4$ has been neglected compared with unity, $(ty)^2$ has been neglected compared with unity in the co-

efficients of $\bar{w}$, and Kt^2y^4 has been neglected when compared with $\bar{w}$. It will be seen in what follows that retention of the latter two terms will, within the limits of the analysis, affect the results only by quantities of secondary magnitudes.

The strain functions for the remaining three sheets of the beam of cruciform cross section can be expressed in a similar way. The mid-surface of the second sheet is perpendicular to Oy at $x = 0$, which allows new axes to be defined having a common origin with the first set and derived from them by a clockwise rotation of 90 deg about Ox. The directions of the component displacements (u, v, w) are defined relative to the second sheet in the same way as the corresponding quantities were defined for the first sheet. It follows that the new displacement functions can be derived from the corresponding functions for the first sheet, as given in Equations [4], by the replacement of the angle θ_0 (which determines the magnitudes of K_1 and K_2 according to Equations [8]) by the angle $(\theta_0 + \pi/2)$, and also by the replacement of the distortion function w_1 for the first sheet by w_2 for the second. However, symmetry requires that w_2 be derived from w_1 by the same substitution of $(\theta_0 + \pi/2)$ for θ_0. Hence all components of strain in the second sheet are obtained from the corresponding quantities for the first sheet by the formal replacement of θ_0 in the latter by $(\theta_0 + \pi/2)$. The components of strain for the nth sheet at the cross section $x = 0$ are, similarly, expressed as

$$\left.\begin{aligned}
\epsilon_1 &= e_1 \sin [\theta_0 + (n-1)\pi/2] \\
&\quad + \eta k_1 \cos [\theta_0 + (n-1)\pi/2] \\
\epsilon_2 &= e_2 \sin [\theta_0 + (n-1)\pi/2] \\
&\quad + \eta k_2 \cos [\theta_0 + (n-1)\pi/2] \\
\gamma_{12} &= e_{12} \cos [\theta_0 + (n-1)\pi/2] \\
&\quad + \eta k_{12} \sin [\theta_0 + (n-1)\pi/2]
\end{aligned}\right\} \quad [12]$$

where $e_1 \ldots k_{12}$ are as defined in Equations [11], θ_0 remains defined as the angle between the resultant bending-moment vector and the mid-surface of the first sheet at $x = 0$, and $0 \leq y \leq c$ for all sheets.

(*b*) *Minimum Potential Energy.* Since the state of strain in all sheets is assumed to correspond to a state of plane stress, the total strain energy of the beam per unit axial length at $x = 0$ is obtained from the expression

$$U = \sum_{n=1}^{4} \int_{A_n} \frac{E}{2(1-\nu^2)} \left(\epsilon_1^2 + \epsilon_2^2 + 2\nu\epsilon_1\epsilon_2 + \frac{1-\nu}{2}\gamma_{12}^2 \right) dA_n \quad [13]$$

where dA_n is an element of cross-sectional area of the nth sheet. Insertion of Expressions [10], [11], and [12] gives the results in the form

$$U = \frac{2Eh}{1-\nu^2} \int_0^c \left(e_1^2 + e_2^2 + 2\nu e_1 e_2 + \frac{1-\nu}{2} e_{12}^2 \right) \left(1 + \frac{1}{2} t^2y^2 \right) dy + \frac{2Eh^3}{3(1-\nu^2)} \int_0^c \left(k_1^2 + k_2^2 + 2\nu k_1 k_2 + \frac{1-\nu}{2} k_{12}^2 \right) \left(1 + \frac{3}{2} t^2y^2 \right) dy \quad [14]$$

where $2h$ is the normal thickness of the sheet. The total potential energy of the system per unit axial length is expressed by

$$V = U - MK \quad [15]$$

where M is the applied bending moment.

The principle of minimum potential energy states (10) that the potential energy of the equilibrium configuration of an elastic system under the action of given external loads is less than that of all other geometrically admissible configurations. The variation in potential energy corresponding to small variations of displacement about the equilibrium configuration is therefore zero to terms of the first order. If variations $\delta\bar{w}$ and δK are introduced into the system considered, the resulting first-order variation in potential energy can be expressed from Equations [14] and [15] as

$$\delta V = \frac{4Eh}{1-\nu^2} \int_0^c \left[(e_1 + \nu e_2)\delta e_1 + (e_2 + \nu e_1)\delta e_2 + \frac{1-\nu}{2} e_{12}\delta e_{12} \right] \left(1 + \frac{1}{2} t^2y^2 \right) dy + \frac{4Eh^3}{3(1-\nu^2)} \int_0^c \left[(k_1 + \nu k_2)\delta k_1 + (k_2 + \nu k_1)\delta k_2 + \frac{1-\nu}{2} k_{12}\delta k_{12} \right] \left(1 + \frac{3}{2} t^2y^2 \right) dy - M\delta K \quad [16]$$

where the variations $\delta e_1 \ldots \delta k_{12}$ are found in terms of $\delta\bar{w}$ and δK from Equations [11]. Substitution of the latter in Equation [16] and collection of like terms allows the result to be expressed in the form

$$\delta V = \int_0^c (F\delta K + G\delta\bar{w})dy - M\delta K \quad [17]$$

where

$$\left.\begin{aligned}
F &= 4Eh \left\{ Ky^2 \left[1 - \frac{1}{2} t^2y^2(3+4\nu) \right] - \bar{w}t^2y^2(1-\cos\psi) \right\} \\
&\quad + \frac{4Eh^3}{3(1-\nu^2)} \left\{ \begin{aligned} &K(1-\nu^2)\left(1 + \frac{1}{2} t^2y^2 \frac{3+11\nu+9\nu^2}{1+\nu} \right) \\ &+ \bar{w}t^2 \left[(1-\nu^2)\left(1 - \cos\psi - \frac{\pi y}{2a}\sin\psi \right) + \frac{\nu\pi^2y^2}{4a^2}\cos\psi + (1-\nu)(2+3\nu)\frac{\pi y}{2a}\sin\psi \right] \end{aligned} \right\} \\
G &= 4Eh \left\{ -Kt^2y^2(1-\cos\psi) + \bar{w}t^2 \left(1 - \cos\psi - \frac{\pi y}{2a}\sin\psi \right)^2 \Big/ 2(1+\nu) \right\} + \frac{4Eh^3}{3(1-\nu^2)} \bar{w} \frac{\pi^4\cos^2\psi}{16a^4}
\end{aligned}\right\} \quad [18]$$

and

If, as is now assumed, the sheet is sufficiently thin for $(h/c)^2$ to be neglected compared with unity, Expressions [18] reduce to the following

$$\left.\begin{aligned} F &= 4Eh\left\{Ky^2\left[1-\frac{1}{2}t^2y^2(3+4\nu)\right]\right. \\ &\qquad \left. -\bar{w}t^2y^2(1-\cos\psi)\right\} \\ G &= 4Eh\left\{-Kt^2y^2(1-\cos\psi)\right. \\ &\quad +\bar{w}\left[t^2\left(1-\cos\psi-\frac{\pi y}{2a}\sin\psi\right)^2\Big/2(1+\nu)\right. \\ &\qquad \left.\left.+(\pi^4h^2\cos^2\psi)/48(1-\nu^2)a^4\right]\right\} \end{aligned}\right\} \quad [19]$$

Since the variations δK and $\delta\bar{w}$ are independent and $\delta V = 0$, it follows that

$$\int_0^c G\,dy = 0 \quad \text{and} \quad \int_0^c F\,dy = M \qquad [20]$$

The first of these equations gives the distortion parameter $\bar{w}_c$ in terms of K as

$$\bar{w}_c = Kc^2(tc)^2\left(\frac{c}{h}\right)^2 \frac{0.210(1-\nu^2)(1-3.47\rho+4.08\rho^2-1.57\rho^3)}{1+0.056(1-\nu)(tc)^2\left(\frac{c}{h}\right)^2(1+2.39\rho-2.43\rho^2-6.32\rho^3)} \qquad [21]$$

where $\rho = b/c$, and ρ^4 and higher powers are neglected compared with unity. With the notation $\bar{w}_c = \lambda^2 K$, Expression [21] may now be introduced into the second of Equations [20] to determine the moment-curvature relationship, with the result that

$$M = (EI)_t K \qquad [22]$$

where

$$(EI)_t/(EI)_0 = 1 - 0.9\left(1+\frac{4\nu}{3}\right)t^2c^2 - 0.638\lambda^2t^2(1-0.474\rho-0.344\rho^2-0.182\rho^3) \qquad [23]$$

and

$$(EI)_0 = \frac{4Ehc^3}{3}$$

Thus $(EI)_0$ represents the bending stiffness of the untwisted cross section, and the right-hand side of Equation [23] represents the decrease in bending stiffness associated with pretwist. Substitution of the value of λ from Relation [21] gives the final form of the result as

$$(EI)_t/(EI)_0 = 1 - 0.9\left(1+\frac{4\nu}{3}\right)\beta^2 - 0.134\left(\frac{c\beta^2}{h}\right)^2 \frac{(1-\nu^2)(1-3.95\rho+5.38\rho^2-2.49\rho^3)}{1+0.056(1-\nu)(c\beta/h)^2(1+2.39\rho-2.43\rho^2-6.32\rho^3)} \qquad [24]$$

where $\beta = ct$ is the tangent of the angle contained between the tangent to the extreme helical fiber and the center line of the beam, and is thus a nondimensional measure of the pretwist. If the core of the section is so small that ρ may be neglected compared with unity, the results reduce to

$$\bar{w}_c = Kc^2(c\beta/h)^2\frac{0.210(1-\nu^2)}{1+0.056(1-\nu)(c\beta/h)^2} \qquad [25]$$

$$(EI)_t/(EI)_0 = 1 - 0.9\left(1+\frac{4\nu}{3}\right)\beta^2 - 0.134(c\beta^2/h)^2 \frac{(1-\nu^2)}{1+0.056(1-\nu)(c\beta/h)^2} \qquad [26]$$

(*c*) *Interpretation.* Three separate factors which contribute to the reduction in bending stiffness can be distinguished in Equations [24] and [26]. The first, represented by the term $0.9\beta^2$, is a purely geometrical effect arising from the inclination of the helical line elements of the beam to the beam axis and from the variation in length of the line elements with distance from the axis. The second, represented by the term $1.2\nu\beta^2$, is a consequence of the anticlastic deformations of the helicoidal sheets interacting with the pretwist in such a way as to relieve the main bending stresses. The third, represented by the last term on the right-hand side of Equation [24] is similar in effect to the second, and is due to distortions of the cross sections. Unlike anticlastic effects, however, the magnitude of these distortions is shown by the energy analysis to be substantially proportional to the product of the center-line curvature and the square of the pretwist, and the resulting effect on the bending stiffness varies almost as the fourth power of pretwist.

The approximations made in the analysis restrict the results to cases for which (i) $\beta^4 \ll 1$, (ii) $(b/c)^4 \ll 1$, and (iii) $(h/c)^2 \ll 1$. The last two conditions state in effect that the beam must be thin-walled; the first permits application up to comparatively large values of pretwist. From the result of Equation [21], it is seen that the additional approximation made in the analysis that $Kt^2c^4 \ll \bar{w}$ is justified provided that, with $\nu = 0.3$

$$(h/c)^2 + 0.04\beta^2 \ll 0.2 \qquad [27]$$

which in view of condition (i) has the effect of replacing condition (iii) by the somewhat more restrictive "thin-wall" condition that $(h/c)^2 \ll 0.2$. Although the moment-curvature Relation [22] has been determined at the cross section $x = 0$, the result is independent of the choice of origin and will apply at any cross section.

Extension to multiple-arm cross sections

The previous analysis can be extended to all pretwisted beams which consist of a symmetric star formation of thin-walled sheets. Symmetry again shows that the centerline curvature of such beams will occur in the plane of the applied bending moment. If there are m helicoidal sheets equally spaced at angles $(2\pi/m)$, and if the displacement functions (u, v, w) are assumed to be identical with those previously assumed in Equations [4], then it follows immediately from Equations [13] that the total strain energy per unit length at the cross section $x = 0$ is expressed by

$$U = \frac{Eh}{1-\nu^2}\sum_{n=1}^{m}\int_0^c\left\{(e_1^2+e_2^2+2\nu e_1e_2)\sin^2\left[\theta_0+(n-1)\frac{2\pi}{m}\right]+\frac{1-\nu}{2}e_{12}^2\cos^2\left[\theta_0+(n-1)\frac{2\pi}{m}\right]\right\}\left(1+\frac{1}{2}t^2y^2\right)dy + \frac{Eh^3}{3(1-\nu^2)}\sum_{n=1}^{m}\int_0^c\left\{(k_1^2+k_2^2+2\nu k_1k_2)\cos^2\left[\theta_0+(n-1)\frac{2\pi}{m}\right]+\frac{1-\nu}{2}k_{12}^2\sin^2\left[\theta_0+(n-1)\frac{2\pi}{m}\right]\right\}\left(1+\frac{3}{2}t^2y^2\right)dy \qquad [28]$$

where $e_1 \ldots k_{12}$ are as defined in Equations [11]. The Result [24] for an equivalent bending stiffness $(EI)_e$ therefore follows for the more general case also, where now the conventional bending stiffness is $(mEhc^3)/3$.

Experimental results

Tests were performed on a mild-steel beam, 50 in. long, which had the cruciform cross section shown in Fig. 3. Pure bending tests on the untwisted beam showed that the bending stiffness of the cross section was 0.895×10^6 lb in.^{2} which, with the calculated moment of inertia of 0.0293 in.^{4}, corresponded to a modulus of elasticity of 30.5×10^6 psi. The average value of Poisson's ratio obtained from strain measurements in bending was found to be 0.30.

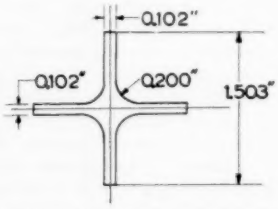

Fig. 3 Cross section of experimental beam

Pretwist was applied with a standard torsion testing machine in steps corresponding to an increase in β of approximately 0.02, and bending tests were conducted after each increase in pretwist. The beam was supported at points equidistant from its ends by two slotted steel rings which were attached to the beam at its core in order that the supported cross sections could distort with a minimum of constraint. Equal loads were applied at the ends of the beam with dead weights suspended from wire loops slung over grooved loading rings, and the deflections were measured with dial gages at three positions, one central and the others equidistant from the center of the beam.

Three bending-deflection tests were performed at each value of pretwist. The rotational position of the beam relative to the plane of bending differed by 120 deg in each of these tests, but no significant differences in deflection were observed as a result of the different positions. Care was taken to insure that the residual stresses introduced by pretwisting did not result in plastic deformations during bending, and to check on the effect of residual stresses on the recorded elastic deflections, some additional bending tests were performed at several fixed values of pretwist. In these tests, the residual stresses were varied by deliberately yielding the beam with high bending loads in between elastic bending tests at the fixed pretwist, and although overloading the beam in this way changed the residual stresses, it was found that the subsequent elastic deflections remained the same. The effect of the recovery of the elastic properties of the steel after cold-working during pretwisting also was investigated. Bending deflections were measured immediately after application of pretwist and again after an interval of several days. No significant differences were noted.

A comparison of predicted and observed deflections is shown in Fig. 4. The deflection Δ of the pretwisted beam refers to the central deflection relative to the deflection at the outer gages. Average experimental values were obtained from linear load-deflection curves, and the results are shown as a ratio of Δ to the corresponding quantity Δ_0 for an identical untwisted beam. The predicted values were calculated from Equation [24]. Since the experimental beam was designed with large fillets at the core in order to reduce stress concentrations during twisting, it is difficult to assign an exact value to the effective core radius as regards

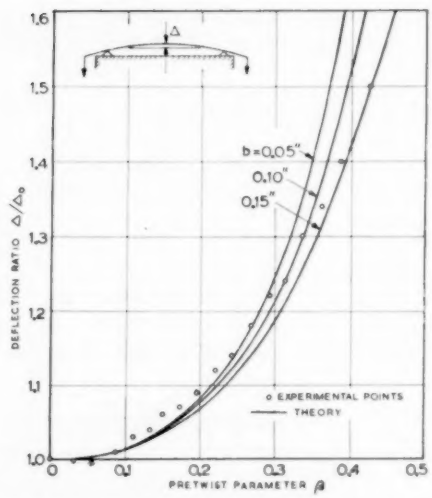

Fig. 4 Variation with pretwist of bending deflections of beam with cruciform cross section

transverse bending of the helicoidal sheets. Accordingly, three predicted curves are shown which correspond to the probable range of effective core radius.

Two principal groups of bending-strain measurements were made. The first group comprised measurement with wire-resistance strain gages of the helical and transverse strains ϵ_1 and ϵ_2 at constant pretwist, as the rotational position of the beam relative to the plane of bending was varied through 180 deg. The results are shown in Fig. 5.

The helical strain varied almost sinusoidally with inclination θ, the average experimental magnitude of 350×10^{-6} in/in. recorded at $\theta = 90$ deg agreeing closely with the calculated value of 346×10^{-6} in/in. for a similar untwisted beam. Of main interest, however, is the variation of the transverse strain ϵ_2. This shows that no transverse bending of the sheet occurred when the arm was vertical, and the strain -72×10^{-6} in/in. recorded at this position for gage 5 represents the maximum anticlastic strain of the mid-surface at the point corresponding to the location of the strain gage. The anticlastic strain at the gage position therefore can be represented by the expression

$$-(72 \sin \theta + 10.9 \cos \theta) \times 10^{-6}$$

in which the second term appears in consequence of the distance of the gage from the mid-surface. Subtraction of this quantity from the total observed strain leaves a remainder which represents the strain associated with the additional distortion of the cross section.

As shown in Fig. 5(*b*), the variation of this additional strain indicates that the distortion takes the form of transverse bending of the sheets towards that side of the cross section which is in tension. It is a maximum at a horizontal arm and zero at a vertical arm, which agrees with the assumptions made regarding the form of w_1 in Equation [9].

In the second group of strain measurements, the variation with pretwist of the transverse strain ϵ_2 at a horizontal arm of a cross section was obtained, also with wire resistance strain gages. The results are compared in Fig. 6 with the predictions of Equation [10], based on a range of possible values of effective core of the beam. Additionally, a few measurements were made of the distribution of helical strain ϵ_1 at a vertical arm, using a Huggen-

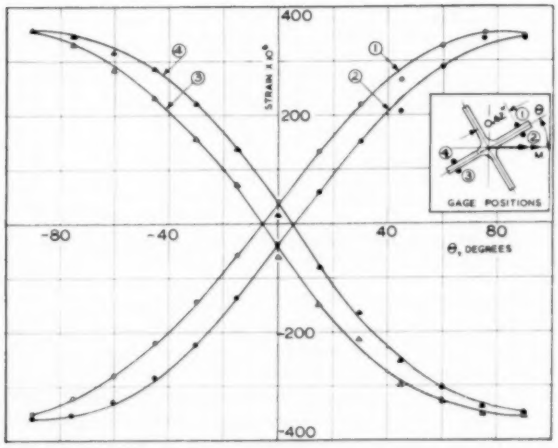

Fig. 5(*a*) Experimental helical strains in bending of pretwisted beam; M = 500 in-lb, β = 0.325

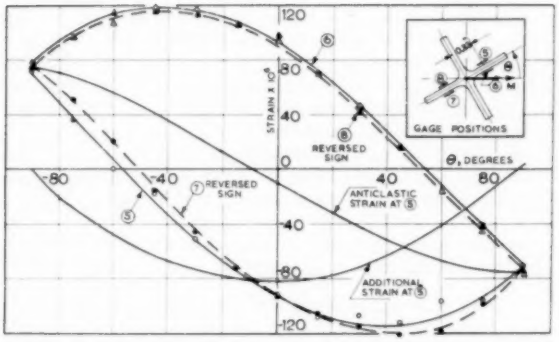

Fig. 5(*b*) Experimental transverse strains in bending of pretwisted beam; M = 500 in-lb, β = 0.325

berger extensometer in order to obtain accurate definitions of gage positions. A typical result is compared in Fig. 7 with the linear distribution for a similar untwisted beam and with the predictions of Equation [10]. While the nonlinearities predicted by the latter are slight, it is believed that definite indications of their presence are shown.

Conclusions

Bending deflections of a thin-walled pretwisted beam of cruciform cross section have been measured which are appreciably larger than those predicted by conventional beam theory. Strain measurements have shown that in-plane distortions of cross sections during bending steadily increase with pretwist, and the way in which such distortions affect the bending stiffness has been outlined. The approximate analysis, applicable to pure bending of pretwisted beams of symmetric star-shaped cross sections, results in an equivalent bending stiffness which decreases with pretwist.

Acknowledgment

The author is indebted to Prof. J. P. den Hartog for his interest in this work and for the valuable advice he gave during the research.

Bibliography

1 "Elements of Strength of Materials," by S. Timoshenko and G. H. MacCullough, D. Van Nostrand Company, Inc., New York, N. Y., third edition, 1949, pp. 198–200.

2 "Experimental Determination of the Bending and Torsional Stiffnesses of a Beam With Rotationally Constant Moment of Inertia With Varying Amounts of Pretwist," by J. Woolston and L. N. Leutz, ME thesis, Massachusetts Institute of Technology, Cambridge, Mass., unpublished.

3 "Advanced Strength of Materials," by J. P. den Hartog, McGraw-Hill Book Company, Inc., New York, N. Y., first edition, 1952, p. 319.

4 "Pure Bending of Pretwisted Rectangular Plates," by L. Maunder and E. Reissner, *Journal of the Mechanics and Physics of Solids*, vol. 5, September, 1957, pp. 261–266.

5 "Bending of Pretwisted Beams," by J. Zickel, JOURNAL OF APPLIED MECHANICS, TRANS. ASME, vol. 77, 1955, pp. 348–352.

6 "Pretwisted Beams and Columns," by J. Zickel, JOURNAL OF APPLIED MECHANICS, TRANS. ASME, vol. 78, 1956, pp. 165–175.

7 "Zur Theorie der Gekrummten Platte Grosser Formanderung," by K. Marguerre, Proceedings of the Fifth International Congress of Applied Mechanics, 1938, pp. 93–101.

8 "On Some Aspects of the Theory of Thin Elastic Shells," by E. Reissner, *Journal of the Boston Society of Civil Engineers*, vol. 42, April, 1955, p. 120.

9 "The Mathematical Theory of Elasticity," by A. E. H. Love, Dover Publications, New York, N. Y., fourth edition, 1944, Chapters 18, 21.

10 "The Theory of Elasticity," by S. Timoshenko and J. N. Goodier, McGraw-Hill Book Company, Inc., New York, N. Y., second edition, 1951, pp. 153 and 253.

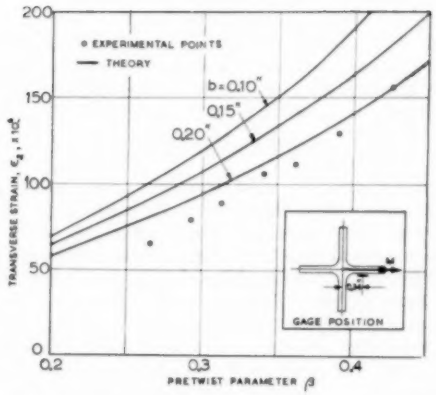

Fig. 6 Variation of transverse strain with pretwist; M = 500 in-lb

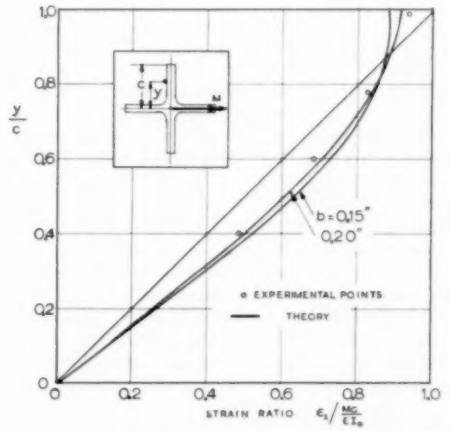

Fig. 7 Distribution of helical strains in bending of pretwisted beam; β = 0.388

APPENDIX

Before deformation, the length of the line-element PQ, Fig. 2, is $dx \sec \xi$, where $\xi = \tan^{-1} z_x$, $\phi = \tan^{-1} z_y$ and subscripts denote partial differentiation. After displacements u at P and $(u + u_x dx)$ at Q, the deformed length $P'Q'$ is

$$dx(1 + 2u_x \cos^2 \xi)^{1/2} \sec \xi$$

and thus the linearized strain component of ϵ_1' corresponding to the u-displacements is $u_x/(1 + z_x^2)$. The strain components of ϵ_1' corresponding to v and w-displacements can be found in a similar way, when addition and substitution of the mid-surface Equation [1] will give the first of Equations [2], provided that $(tx) \ll 1$ and $(ty)^4 \ll 1$.

Similar consideration of the changes in length of the line-element PR gives the second of Equations [2]. The shearing strain is found from the change in angle QPR. After displacements u, the lengths of $P'R'$ and $Q'R'$ are $dy \sec \phi$ and

$$[(dx)^2(2u_x + \cos^2 \xi) + (dy \sec \phi)^2 - 2dx\, dy(u_y + \tan \xi \tan \phi)]^{1/2}$$

respectively. Angle $Q'P'R'$ is therefore less than a right angle by the small amount

$$u_y \cos \xi \cos \phi - u_x \sin \xi \cos^2 \xi \sin \phi + \sin \xi \sin \phi \quad [29]$$

and hence the decrease in angle QPR due to u-displacements is represented by the first two terms of Expression [29].

Similar calculations for the v and w-displacements and addition of results gives the total reduction of angle, which equals the shearing strain at $x = 0$. Substitution of Equation [1] gives the third of Equations [2].

The lines shown in Fig. 8, in addition to the mid-surface lines PQ, PR, are as follows: PN is perpendicular to PR in plane y, z and hence is the direction of w-displacements; PL is perpendicular to PQ and PN, and hence lies in plane RPx; PM is perpendicular to PQ and PL, and hence is coplanar with NPQ. Direction cosines of these lines are

$$\left.\begin{aligned} &PQ(\cos \xi, 0, \sin \xi)\ PR(0, \cos \phi, \sin \phi) \\ &PN(0, -\sin \phi, \cos \phi) \\ &PL(-\sin \xi \sin \phi, \cos \xi \cos \phi, \cos \xi \sin \phi)/A \\ &PM(-\sin \xi \cos \xi \cos \phi, -\sin \phi, \cos^2 \xi \cos \phi)/A \end{aligned}\right\} \quad [30]$$

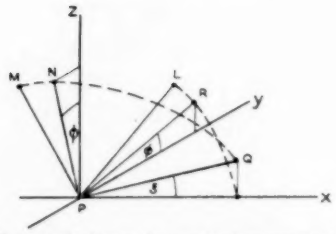

Fig. 8 Geometrical axes for strain-displacement relations

where $A = (1 - \sin^2 \xi \cos^2 \phi)^{1/2}$

To satisfy the requirement that the line PN fixed in the shell shall contain the same angles with lines PQ and PR after deformation, it is necessary that the rotation of PN be such that (i) its resolved part about PL equal the rotation of PQ about PL, and (ii) its resolved part about Px equal the rotation of PR about Px. Calling these small rotations ω_1 and ω_2, respectively, and noting that PL, Px are not perpendicular, it follows that the resultant rotation of PN about an axis in the plane $PLRx$, to which PN is normal, can be expressed as the perpendicular components ω_1 and $(\omega_1 \tan \xi \tan \phi + A\omega_2 \sec \xi)$ about Px and PR, respectively. The additional u and v-components of displacement of a point on PN whose distance from P is η are, therefore, $+\eta(\omega_1 \tan \xi \tan \phi + A\omega_2 \sec \xi)$ and $-\eta\omega_1$, respectively. The additional w-components of displacement are assumed to be zero. Insertion of these quantities in Equation [2] will give the strain components corresponding to bending of the helicoidal sheet. The quantities ω_1 and ω_2 can be found from the displacements of points Q and R relative to P, which are $(u_x, 0, 0)dx$ and $(u_y, 0, 0)dy$, respectively. Resolution of the former in direction PM and division by length PQ gives ω_2, and resolution of the latter in direction PN and division by length PR gives ω_1. Hence

$$\omega_1 = 0, \quad \omega_2 = (u_x \sin \xi \cos^2 \xi \cos \phi)/A \quad [31]$$

Similar calculations performed for v and w-displacement components, and addition of corresponding results, give the total magnitudes of ω_1 and ω_2. Hence the bending displacements (u, v, w) of points not on the mid-surface can be found as noted in the foregoing. Following substitution in Equation [2], the approximation $(ty)^4 \ll 1$ will give Equations [3] for the bending strains at $x = 0$.

Creep Deflections and Stresses of Beam-Columns

By T. H. LIN,[1] LOS ANGELES, CALIF.

A method of calculating the creep deflections and stresses of a beam-column is shown. The differential equation of equilibrium in terms of creep strain is solved by the method of integrating factors with Green's function. For restrained and built-in ends, the end moments are found from the end conditions. An illustrative example is given for a beam-column of an ideal H-section with built-in ends and subjected to uniform lateral load. The deflection-time curve and flange stresses at different instants are shown.

Nomenclature

The following nomenclature is used in the paper:

A = area, a constant
A_f = flange area
B = constant
E = Young's modulus of elasticity
e = strain, compressive strain is considered positive
e_p = creep strain
$\bar{e}_p$ = average creep strain of section
F, f = functions
g = Green's function
h = function, depth of beam-column
I = moment of inertia of column section
$k = \sqrt{\frac{P}{EI}}$, curvature
K = constant
L = column length
M = moment
P = axial load
q = uniform lateral load
t = time
u = nondimensional ratio
y = lateral deflection of column
x = distance along axis of column
η = distance from centroidal axis of cross section
σ = stress; compressive stress is taken to be positive

Subscript o denotes centroidal axis of the section, and subscript b denotes bending.

Introduction

The recent increase in the use of structures at elevated temperatures, as in the case of high-speed aircraft, has made it necessary to consider the creep effect in a number of structures. The growing importance of the creep deflection in columns has been recognized widely. A number of studies have been made by assuming the columns to be viscoelastic (1–5).[2] The stress-strain-time relations of some engineering metallic materials, under constant stress, may be approximated by viscoelastic models (5). However, under varying stress the stress-strain-time relations may deviate considerably from being linearly viscoelastic. The stress variation across the different sections in the column increases with the column deflection. For columns with appreciable deflection, the assumption of linearly viscoelastic creep is rather unrealistic (6).

Studies of pin-ended columns with creep based on empirical stress-strain-time relations, have been made by different investigators (7–11). Hu and Triner (12) have shown a method of calculating the end deflection of a cantilever column under an eccentric load. In the present paper, creep deflections of beam-columns (with both axial and lateral loads) with restrained ends are analyzed. The equilibrium and compatibility conditions are satisfied at all sections. The method given can be applied easily to beam-columns with pin ends.

Theoretical Analysis

The uniaxial strain rate under uniaxial stress at elevated temperature is a function of the stress, time, and total creep strain, and the history of loading. After following a stress-time curve, the material, at some condition of stress and strain, will have a strain rate under constant stress. If the material is given an instantaneous change in stress $\Delta\sigma$, the instantaneous strain increment Δe will be $\Delta\sigma/E$, where E is the elastic modulus of the material at the particular temperature (13). This implies that creep changes the curvature of the member but does not affect the flexural rigidity EI of the column.

For the following analysis, the smooth stress-time curve of different fibers of the column is represented by infinitesimal steps (8). Each step consists of a constant stress period of time dt followed by an instantaneous increment of stress $d\sigma$, Fig. 1.

With the rate of strain under constant stress denoted by ϕ

$$de = \phi dt + \frac{d\sigma}{E} \quad [1]$$

This approximation of a smooth stress history by a series of infinitesimal steps is the same as used in the previous analyses of column deflections [8, 11, 12]

$$\sigma = E(e - e_p)$$

$$\Delta\sigma = E(\Delta e - \Delta e_p) \quad [2]$$

Instead of considering the equilibrium conditions for the total load and total moment at each section, the equilibrium conditions for the incremental load and moment are considered

$$\Delta P = \int \Delta\sigma dA = E \int (\Delta e - \Delta e_p) dA \quad [3]$$

$$\Delta M = \int \Delta\sigma\eta dA = E \int (\Delta e - \Delta e_p)\eta \, dA \quad [4]$$

With the condition that plane section before loading remains plane during loading

---

[1] Professor of Engineering, University of California.

Contributed by the Applied Mechanics Division and presented at the Annual Meeting, New York, N. Y., December 1–6, 1957, of The American Society of Mechanical Engineers.

Discussion of this paper should be addressed to the Secretary, ASME, 29 West 39th Street, New York, N. Y., and will be accepted until April 10, 1958, for publication at a later date. Discussion received after the closing date will be returned.

Note: Statements and opinions advanced in papers are to be understood as individual expressions of their authors and not those of the Society. Manuscript received by ASME Applied Mechanics Division, December 13, 1955. Paper No. 57—A-3.

[2] Numbers in parentheses refer to Bibliography at end of paper.

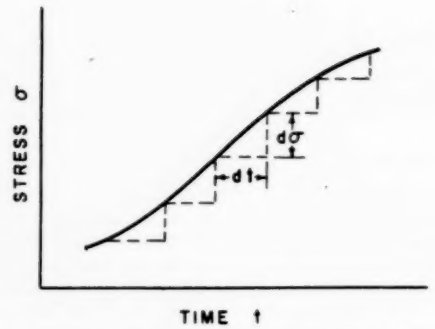

FIG. 1 APPROXIMATION OF A STRESS-TIME CURVE BY A SERIES OF INFINITESIMAL STEPS

$$e = e_o + k\eta$$

$$\Delta e = \Delta e_o + \Delta k\eta \quad [5]$$

Under constant load P

$$\Delta P = 0$$

$$\int (\Delta e - \Delta e_p)dA = \int (\Delta e_o + \eta\Delta k - \Delta e_p)dA = 0$$

$$\Delta e_o A + \Delta k \int \eta dA = \int \Delta e\, dA$$

Let η be zero at the geometrical neutral axis of the section

$$\int \eta dA = 0 \quad [6]$$

$$\Delta e_o = \frac{\int \Delta e_p dA}{A} = \Delta \bar{e}_p \quad [7]$$

$$\Delta M = E \int [(\Delta e_o + \eta\Delta k) - \Delta e_p]\eta dA = EI\Delta k - E \int \eta\, \Delta e_p dA \quad [8]$$

For a beam-column with fixed ends and with uniformly distributed lateral loads, Fig. 2

$$M = M_o + \frac{qL}{2} x - \frac{qx^2}{2} + Py \quad [9]$$

$$\Delta M = \Delta M_o + P\Delta y \quad [10]$$

The curvature is assumed to be small

$$\Delta k = -\frac{d^2\Delta y}{dx^2} \quad [11]$$

From Equations [8], [10], and [11], the condition of equilibrium gives

$$\Delta M_o + P\Delta y = -EI\frac{d^2\Delta y}{dx^2} - E \int \Delta e_p \eta dA \quad [12]$$

where the term on the left-hand side is the external moment increment, and the terms on the right-hand side are the incremental moment due to incremental curvature and the relaxation moment due to creep in a given time interval Δt

$$\frac{d^2\Delta y}{dx^2} + \frac{P}{EI}\Delta y = -\frac{1}{I} \int \Delta e_p \eta dA - \frac{\Delta M_o}{EI} \quad [13]$$

Δe_p varies from one section to another. Hence the right-hand integral is a function of x. With

$$F(x) = -\frac{1}{I} \int \Delta e_p \eta dA$$

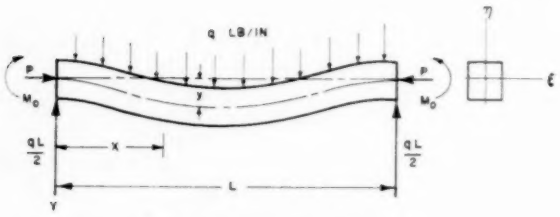

FIG. 2 BEAM-COLUMN NOTATION

the equation of equilibrium, Equation [13], becomes

$$\frac{d^2\Delta y}{dx^2} + \frac{P}{EI}\Delta y = -\frac{\Delta M_o}{EI} + F(x) \quad [14]$$

SOLUTION OF DIFFERENTIAL EQUATION OF EQUILIBRIUM

The differential equation of equilibrium is resolved into two parts

$$\frac{d^2\Delta y_1}{dx^2} + k^2\Delta y_1 = F(x) \quad [15]$$

and

$$\frac{d^2\Delta y_2}{dx^2} + k^2\Delta y_2 = -\frac{\Delta M_o}{EI} \quad [16]$$

where $k^2 = P/EI$

$$\Delta y = \Delta y_1 + \Delta y_2 \quad [17]$$

Equation [15] contains no ΔM_o and is solved as if the beam-column were pin-ended. It has been shown that Equation [15] can be solved by expanding y_1 into sine series [11]. For deflection curves close to half sine wave, as in the case of a pin-ended column with initial deflection of half sine wave, few terms in the sine series will give result close enough for practical purposes. However, for a pin-ended beam-column under arbitrary lateral loads, the deflection curve may deviate considerably from a half sine wave. More terms in the sine series are required and the method of sine series may be very lengthy. Therefore, in the following, the method of integrating operators with Green's function (14, 15) is applied.

$$\Delta y_1 = -\int_0^L g(x, a)F(a)da \quad [18]$$

$$g(x, a) = g_l(x, a) = \frac{\sin kx \sin k(L - a)}{k \sin kL}, \quad 0 \leqslant x \leqslant a$$

$$g(x, a) = g_r(x, a) = \frac{\sin k(L - x) \sin ka}{k \sin kL}, \quad a \leqslant x \leqslant L$$

$$\Delta y_1 = -\int_0^x g_r(x, a)F(a)da - \int_x^L g_l(x, a)F(a)da$$

$$\Delta y_1 = -\sin k(L - x) \int_0^x \frac{\sin ka}{k \sin kL} F(a)da - \sin kx \int_x^L \frac{\sin k(L - a)}{k \sin kL} F(a)da \quad [19]$$

$$\frac{d\Delta y_1}{dx} = -g_r(x, x)F(x) - \int_0^x \frac{dg_r(x, a)}{dx} F(a)da + g_l(x, x)F(x) - \int_x^L \frac{dg_l(x, a)}{dx} F(a)da$$

with $g_r(x, x) = g_l(x, x)$

$$\frac{d\Delta y_1}{dx} = -\int_0^x \frac{dg_r(x, a)}{dx} F(a)da - \int_x^L \frac{dg_l(x, a)}{dx} F(a)da$$

At $x = 0$

$$\left(\frac{d\Delta y_1}{dx}\right)_{x=0} = -\int_0^L \frac{\sin k(L-a)}{\sin kL} F(a)da \ldots\ldots [20]$$

For a beam-column symmetrically loaded, the slopes at both ends are numerically equal. Applying Green's function as a linear integral operator to Equation [16] with equal ΔM_o at both ends, Δy_2 is obtained from Equation [19] with $F(a)$ replaced by $-(\Delta M_o)/(EI)$

$$\left(\frac{d\Delta y_2}{dx}\right)_{x=0} = \frac{\Delta M_o}{EI}\int_0^L \frac{\sin k(L-a)}{\sin kL} da \ldots\ldots [21]$$

$$\left(\frac{d\Delta y}{dx}\right)_{x=0} = \frac{\Delta M_o}{EI}\int_0^L \frac{\sin k(L-a)}{\sin kL} da - \int_0^L \frac{\sin k(L-a)}{\sin kL} F(a)da \ldots\ldots [22]$$

For restrained ends $\Delta M_o = -\beta\Delta\theta$, where

$$\Delta\theta = \left(\frac{d\Delta y}{dx}\right)_{x=0}$$

and β is the moment required at both ends to rotate the restraining structure by one radian. With β known, $\Delta\theta$ and ΔM_o can be found from Equation [22]. For built-in ends

$$\left(\frac{d\Delta y}{dx}\right)_{x=0} = 0$$

Equation [22] reduces to

$$\frac{\Delta M_o}{EIk}\tan\frac{kL}{2} = \int_0^L \frac{\sin k(L-a)}{\sin kL} F(a)da \ldots\ldots [23]$$

The calculation of the elastic deflection and moment at any section of a beam-column at the instant when the loads are applied, is shown in several texts (16, 17). For uniform lateral load, the moment is given by Equation [9]. From the stress-strain-time relationship of the material at the particular temperature, Δe_p for the first time interval Δt are calculated at different points on different sections. The more points and sections calculated, and the smaller the time interval, the more accurate will be the results. Suitable numbers of points and sections and suitable time intervals can be chosen for the desirable degree of accuracy. Then $\Delta\bar{e}_p$ and $F(x)$ for different sections are calculated by graphical integration. The values of ΔM_o and Δy are obtained by the use of Green's function as the integrating factor.

Considering a particular point on a section, in a small time interval Δt, the relaxation stress due to creep is $E\Delta e_p$. Owing to the condition that $\Delta P = 0$, the section has an average incremental axial strain of $\Delta\bar{e}_p$ giving an incremental uniform stress of $E\Delta\bar{e}_p$. This uniform incremental stress produces no incremental moment. However, the relaxation stress causes a loss of resisting moment

$$\int E\Delta e_p \eta dA$$

and hence the equilibrium condition is disturbed. To restore the equilibrium condition, the curvature at the section is increased giving an incremental moment of $EI\Delta k$ to compensate the relaxation moment

$$\int E\Delta e_p \eta dA$$

and to balance the increase of external moment due to ΔM_o and $P\Delta y$. This equilibrium condition is given by Equation [12] as $EI\Delta k = \Delta M_o + P\Delta y + E\int \Delta e_p \eta dA$.

The change of stress at a particular point in this time interval

$$\Delta\sigma = E\eta\Delta k - E\Delta e_p + E\Delta\bar{e}_p$$

$$= E(\Delta\bar{e}_p - \Delta e_p) + \frac{\eta}{I}[\Delta M_o + P\Delta y + E\int \Delta e_p \eta dA] \ldots [24]$$

With the stress and the history of the stress-strain-time path known, the incremental creep strain Δe_p for the next time interval can be obtained either empirically by testing the material following the same stress-time history, or by using some stress-strain-time relationship. With Δe known, the process is repeated. By repeating the same process for successive time intervals, the stress distribution and deflections of the beam-column at different sections at different instants can be calculated.

This method is applied to a 75S-T aluminum-alloy beam-column at 600 F as shown in the Appendix. The calculated deflection-time curve and stresses at different instants are shown in Figs. 3 and 4.

BIBLIOGRAPHY

1 "An Elementary Theory of Creep Buckling of Columns," by D. Rosenthal and H. W. Baer, Proceedings of the First U. S. National Congress of Applied Mechanics, ASME, June, 1951, pp. 603–611.

2 "Creep Collapse of Visco-Elastic Columns With Initial Curvatures," by H. H. Hilton, *Journal of the Aeronautical Sciences*, vol. 19, December, 1952, p. 844.

3 "The Inelastic Behavior of Engineering Materials and Structures," by A. M. Freudenthal, John Wiley & Sons, Inc., New York, N. Y., first edition, 1950, pp. 518–519.

4 "Creep Bending and Buckling of Linearly Visco-Elastic Columns," by J. Kempner, NACA TN 3136, January, 1954.

5 "Stresses in Columns With Time-Dependent Elasticity," by T. H. Lin, Proceedings of the First Mid-Western Conference on Solid Mechanics, 1953, pp. 196–199.

6 "Mechanics of Creep and Design for Members Subjected to Buckling," by F. R. Shanley, Proceedings for Short Course Mechanics of Creep, Department of Engineering Mechanics, The Pennsylvania State University, 1954, pp. 130–131.

7 "Creep Deflections in Columns," by J. Marin, *Journal of Applied Physics*, vol. 18, January, 1947, pp. 103–109.

8 "Creep Buckling of Columns," by C. Libove, *Journal of the Aeronautical Sciences*, vol. 19, July, 1952, p. 459.

9 "Creep Buckling Analysis of Rectangular-Section Columns," by C. Libove, NACA TN 2956, June, 1953.

10 "Effect of Creep on Column Deflections," by T. P. Higgins, Institute of Aeronautical Sciences, Preprint No. 385, 1951.

11 "Creep Stresses and Deflections in Columns," by T. H. Lin, JOURNAL OF APPLIED MECHANICS, Trans. ASME, vol. 78, 1956, pp. 214–218.

12 "Bending Creep and Its Application to Beam-Columns," by L. W. Hu and N. H. Triner, JOURNAL OF APPLIED MECHANICS, Trans. ASME, vol. 78, 1956, pp. 35–42.

13 "Bending of Beams With Creep," by E. P. Popov, *Journal of Applied Physics*, vol. 20, 1949, pp. 251–256.

14 "Partial Differential Equations," by H. Bateman, Dover Publications, New York, N. Y., first American edition, 1944, pp. 65–66.

15 "Introduction to Applied Mathematics," by F. D. Murnaghan, John Wiley & Sons, Inc., New York, N. Y., vol. 2, 1943, chapter 14.

16 "Theory of Elastic Stability," by S. Timoshenko, McGraw-Hill Book Company, Inc., New York, N. Y., first edition, 1936, pp. 8–17.

17 "Airplane Structures," by A. S. Niles and J. S. Newell, John Wiley & Sons, Inc., New York, N. Y., third edition, vol. 2, 1943, chapter 14.

18 "Weight-Strength Analysis of Aircraft Structures," by F. R. Shanley, McGraw-Hill Book Company, Inc., New York, N. Y., first edition, 1952, pp. 271, 315–316, 329, and 350.

Appendix

ILLUSTRATIVE EXAMPLE

A 75S-T aluminum-alloy beam-column at 600 F with built-in ends is subjected to an axial load of 625 lb and a uniform lateral load of 2 lb/in. The column is 16 in. long and has two flanges of 0.125 sq in. each. The distance between the centroids of the flanges is 0.289 in. and the flange area is assumed to be concentrated at its centroid. This gives a moment of inertia equivalent

to a square section of $^1/_2$ in. $\times$ $^1/_2$ in. The deflection of the column is assumed to be due to flanges alone (8). The Young's modulus of elasticity E at 600 F is 5.2×10^6 psi and the stress-strain-time relationship for constant stress is taken to be represented by (18)

$$\epsilon = \frac{\sigma}{E} + Ae^{B\sigma}t^k \quad \ldots\ldots\ldots\ldots\ldots\ldots [25]$$

where $A = 2.64 \times 10^{-7}$
$B = 1.92 \times 10^{-3}$
σ in psi
t in hr
$K = 0.66$

$$I = 2 \times \frac{1}{8} \times 0.1445^3 = \frac{1}{192}$$

$$\frac{\pi^2 EI}{L^2} = 1046 \text{ lb}$$

$$u = \frac{L}{2}\left(\frac{P}{EI}\right)^{1/2} = 1.213 \text{ rad} = 69.5°, \cos u = 0.35$$

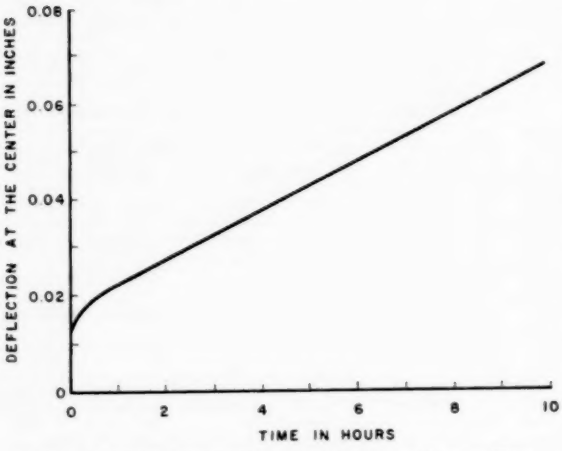

FIG. 3 CENTER DEFLECTION OF BEAM-COLUMN VERSUS TIME

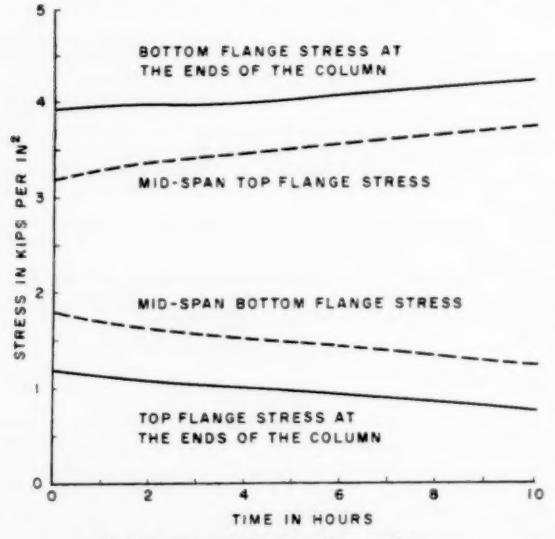

FIG. 4 FLANGE STRESSES VERSUS TIME

For a beam-column with built-in ends subjected to uniform lateral load q (16)

$$M_o = -\frac{qL^2}{12}\frac{3(\tan u - u)}{u^2 \tan u} = -47.6 \text{ in-lb}$$

The lateral deflection of the beam-column (16)

$$y = \frac{L^2}{8EIu^2}\left\{\left(\frac{qL^2}{2u^2 \cos u} + \frac{2M_o}{\cos u}\right)\left[\cos\left(1 - \frac{2x}{L}\right)u - \cos u\right] - qx(L - x)\right\}$$

$$= 0.1798\left\{\left[\cos\left(1 - \frac{2x}{L}\right)u - 0.35\right] - 0.00895 \times (16 - x)\right\}$$

$$M = -47.6 + 16x - x^2 + 625y$$

$$\sigma = \frac{P}{A} + \frac{M}{I}\eta \quad \ldots\ldots\ldots\ldots\ldots [26]$$

Term 'σ' is calculated at different points on a number of sections. With the first time interval Δt, Δe_p is obtained from the empirical relation (18)

$$\Delta e_p = Ae^{B\sigma}(\Delta t)^k$$

The values of $F(x) = -\frac{1}{I}\int \Delta e_p \eta dA$

at different sections, are obtained by graphical integration. ΔM_o is calculated from Equation [23], Δy_1 is obtained from Equation [19], and Δy_2 is found by replacing $F(a)$ by $-(\Delta M_o)/(EI)$ in Equation [19]. Δy is the sum of Δy_1 and Δy_2. $\Delta \bar{e}_p$ is calculated from Equation [7] and $\Delta\sigma$ is obtained from Equation [24]. This gives the stress σ for the subsequent time interval.

In calculating the Δe_p for the next time interval, the beam-column is assumed to follow Shanley's engineering hypothesis of creep (8, 18). This hypothesis assumes mainly that the strain rate under constant stress is a function only of the stress and the strain, and not of the path of attaining this stress and strain. With given creep strain e_p, and stress σ, the time required to obtain this creep strain under constant stress σ

$$t_1 = \left(\frac{e_{p_1}}{Ae^{B\sigma}}\right)^{\frac{1}{k}}$$

The incremental creep strain in a time interval Δt following t_1

$$\Delta e_p = Ae^{B\sigma}\left[\left(\frac{e_{p_1}}{Ae^{B\sigma}}\right)^{\frac{1}{k}} + \Delta t\right]^k - e_{p_1} \quad \ldots\ldots [27]$$

where e_{p_1} is the plastic strain at the start of the time interval Δt. With Δe_p calculated in the subsequent time intervals, $\Delta \bar{e}_p$, $F(x)$, ΔM_o, and Δy are calculated as before. By repeating the same process to successive time intervals, the stresses and deflections at different sections at different instants are calculated. The calculated center deflections versus time curve of the beam-column at different instants are shown in Fig. 3. The variation of flange stresses with time are shown in Fig. 4. This present method can be extended to cases with different lateral loads and different end conditions.

The present method is based on the method of small deflections. It is not applicable when the slope $(dy)/(dx)$ is not negligible as compared to unity. Since excessive deflection is generally undesirable in actual structures, this method of calculating deflections will be able to serve to indicate the practical life of the structure.

Carrying Capacity of an Elastic-Plastic Cylindrical Shell With Linear Strain-Hardening[1]

By P. G. HODGE, JR.,[2] and S. V. NARDO,[3] BROOKLYN, N. Y.

The approximate capacity of a thin-walled closed circular cylindrical shell, simply supported at each end and subjected to a uniform hydrostatic pressure, is determined. Elastic and plastic strains are considered, and the latter are assumed to follow a linear law of isotropic hardening. The principle of minimum potential energy is used to determine an approximate solution for the stress resultants, displacements, and maximum load. In an example, it is found that the carrying capacity is considerably lower than that predicted by either rigid-plastic theory or elasticity theory.

1 Introduction

WHEN a rigid, perfectly plastic circular cylindrical shell is subjected to a combination of end load and radial pressure, the carrying capacity of the shell is its collapse load and may be easily determined (1, 2).[4] If there is no end load, or if the end load is tensile, the collapse load so determined also will be a reasonable approximation to the carrying capacity of an actual shell which exhibits elastic strains and strain-hardening. However, if the end load is compressive, this no longer will be the case. The compressive end load will act on the elastic radial displacement to produce a greatly increased axial bending moment, the so-called beam-column effect. If reasonable answers are to be obtained, the elastic strains must be taken into account in the analysis.

This paper presents an approximate analysis of this problem based on the principle of minimum potential energy. The applicability of this principle to certain elastic-plastic problems has been established recently by Hodge (3, 4, 5).

The following section contains an account of the basic equations available for a circular cylindrical shell with beam-column effect. The next section considers the principle of minimum potential energy as it relates to this problem. The following two sections treat the problem of a simply supported circular cylindrical shell subjected to hydrostatic pressure, with Section 4 containing a general discussion and Section 5 a numerical example. Finally, the conclusions of the paper are summarized in Section 6.

2 Basic Equations

The axially symmetric state of a circular cylindrical shell under end load and axially symmetric pressure is characterized by the axial and circumferential direct stress resultants, the resulting axial bending moment, and the radial and axial displacements. It is convenient to define these in the following dimensionless terms:

$$\left.\begin{aligned} &\text{Axial direct stress: } n_x = N_x/N_0 \\ &\text{Circumferential direct stress: } n_\varphi = N_\varphi/N_0 \\ &\text{Axial bending moment: } m_x = M_x/M_0 \\ &\text{Axial displacement: } U = (E/Y)(u/L) \\ &\text{Radial displacement: } W = (E/Y)(w/a) \end{aligned}\right\} \quad \ldots\ldots [1]$$

Here N_0 and M_0 are the fully plastic direct stress and moment

$$N_0 = 2Yh, \qquad M_0 = Yh^2 \ldots\ldots [2]$$

E is Young's modulus, and Y is the tensile yield stress. The shell dimensions are defined in Fig. 1.

These five unknown quantities are to be determined from the two equilibrium equations

$$n_x' = 0 \ldots\ldots [3]$$

$$m_x''/2c^2 + 2n_x b^2 W'' + n_\varphi + P = 0 \ldots\ldots [4]$$

and three stress-strain relations. In Equations [4], P is the dimensionless pressure

$$P = pa/2Yh \ldots\ldots [5a]$$

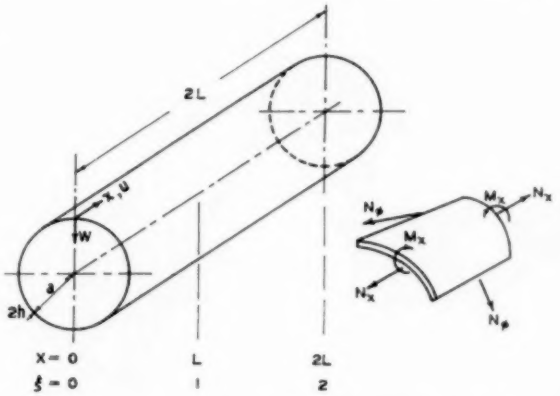

FIG. 1 GEOMETRY OF SHELL. CO-ORDINATE SYSTEM, STRESS RESULTANTS, AND DISPLACEMENTS. HYDROSTATIC LOADING. RINGS AT $x = 0, 2L$

---

[1] The results presented in this paper were obtained in the course of research sponsored by the Office of Naval Research.

[2] Professor of Applied Mechanics, Polytechnic Institute of Brooklyn. Now at Illinois Institute of Technology, Chicago, Ill. Mem. ASME.

[3] Associate Professor of Aeronautical Engineering, Polytechnic Institute of Brooklyn.

[4] Numbers in parentheses refer to Bibliography at end of paper.

Contributed by the Applied Mechanics Division and presented at the Annual Meeting, New York, N. Y., December 1–6, 1957, of THE AMERICAN SOCIETY OF MECHANICAL ENGINEERS.

Discussion of this paper should be addressed to the Secretary, ASME, 29 West 39th Street, New York, N. Y., and will be accepted until April 10, 1958, for publication at a later date. Discussion received after the closing date will be returned.

NOTE: Statements and opinions advanced in papers are to be understood as individual expressions of their authors and not those of the Society. Manuscript received by ASME Applied Mechanics Division, November 14, 1956. Paper No. 57—A-5.

b and c are shell parameters

$$b^2 = Ya^2/2EL^2, \qquad c^2 = L^2/ah \ldots\ldots\ldots [5b]$$

and primes indicate differentiation with respect to the dimensionless distance

$$\xi = x/L \ldots\ldots\ldots [5c]$$

The stress-strain relations are expressed in terms of the dimensionless extensions and curvatures of the middle surface, defined by

$$\left.\begin{aligned} e_x &= \frac{E}{Y}\left[\frac{du}{dx} + \frac{1}{2}\left(\frac{dw}{dx}\right)^2\right] = U' + b^2W'^2 \\ e_\varphi &= \frac{E}{Y}\left[-\frac{w}{a}\right] = -W \\ \kappa_x &= \frac{Eh}{2Y}\left[-\frac{d^2w}{dx^2}\right] = -\frac{W''}{2c^2} \end{aligned}\right\} \ldots [6]$$

Under the assumption that normals to the middle surface remain normal after deformation, the stress and strain resultants may be computed in terms of the component stresses and strains. If these latter are related by Hooke's law, the resultants must satisfy

$$\left.\begin{aligned} e_x^e &= n_x - \nu n_\varphi \\ e_\varphi^e &= n_\varphi - \nu n_x \\ \kappa_x^e &= (3/4)(1 - \nu^2)m_x \end{aligned}\right\} \ldots\ldots\ldots [7]$$

where ν is Poisson's ratio.

In discussing the plastic stress-strain law, the yield condition for initial plastic behavior must first be determined. In the present discussion, it will be assumed that this consists of a collection of twelve linear functions, as determined by Onat (1) and Hodge (2). These may be represented conveniently by a polyhedron in a stress space with co-ordinates n_x, n_φ, and m_x. The quadrant for negative n_x and n_φ of this polyhedron is shown in Fig. 2.

In terms of Fig. 2, a given material particle will behave elastically so long as it remains in the interior of the polyhedron. Once it reaches the polyhedron it must then satisfy a plastic-flow law whose precise form depends upon the face, edge, or vertex of the polyhedron with which it is in contact. As the deformation proceeds, the stress point will move beyond the original polyhedron. According to the theory of isotropic strain-hardening, the polyhedron will expand uniformly about the origin so as to maintain contact with the stress point.[5]

In the problem to be considered here, it turns out that each element of the shell either remains elastic or first encounters face 1 (regime 1)

$$n_\varphi = -1 \ldots\ldots\ldots [8]$$

of the yield surface. As the load increases, it may later move to the intersection of faces 1 and 10 (regime 1–10), originally defined by

$$n_\varphi = -1, \qquad m_x - n_x = 1 \ldots\ldots\ldots [9]$$

A stress point which moves only from the elastic region to a face and thence to an adjacent corner so that it never loses contact with a face once encountered, is said to "progress regularly." Hodge has shown (3, 4, 5) that when the stress point progresses regularly the flow law may be integrated to yield a finite stress relation. In particular, it turns out that in regime 1 the plastic strains are given by the simple relations[6]

[5] Other theories of hardening have been discussed by Batdorf and Budiansky (6), Prager (7), and Hodge (5).

[6] Details leading to the plastic stress-strain laws may be found in references (3, 4, 5, 8).

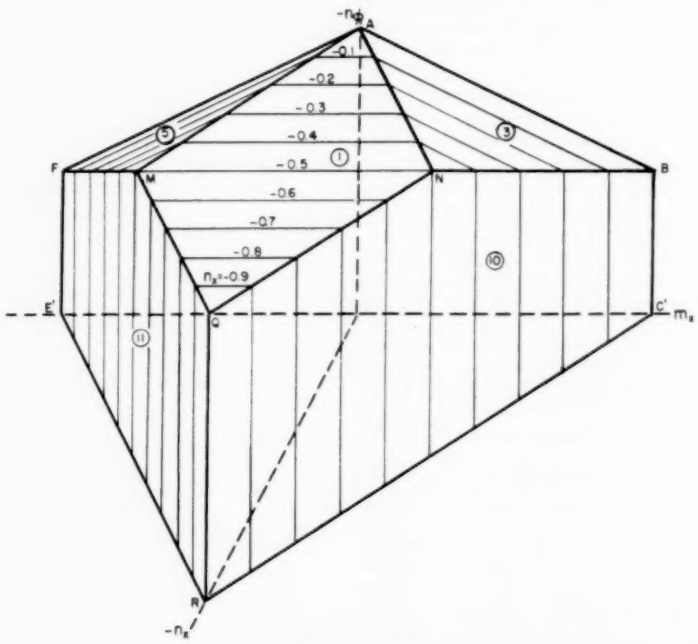

FIG. 2 YIELD POLYHEDRON

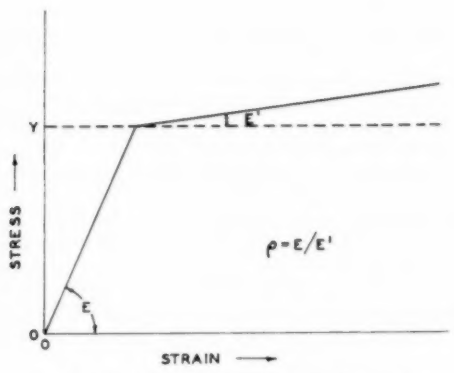

FIG. 3 UNIAXIAL STRESS-STRAIN CURVE

$$e_x^p = 0, \quad e_\varphi^p = (\rho - 1)(n_\varphi + 1), \quad \kappa_x^p = 0 \ldots [10]$$

Here ρ is the ratio of the slopes of the elastic and plastic segments of the stress-strain curve, Fig. 3

$$\rho = E/E'$$

On regime 1-10, one of the stress-strain relations is replaced by a relation stating that the stress point remains at the intersection of the two faces

$$n_\varphi = n_x - m_x \ldots [11a]$$

and the other two equations can be written in the form[6]

$$\left.\begin{aligned} e_x^p + \kappa_x^p &= 0 \\ e_x^p + e_\varphi^p &= (\rho - 1)(n_\varphi + 1) \end{aligned}\right\} \ldots [11b]$$

The total strain of a particle is the sum of an elastic part which continues to be given by Equations [7] and a plastic part given by Equations [10] or [11]. Thus

Regime 1

$$\left.\begin{aligned} e_x &= n_x - \nu n_\varphi \\ e_\varphi &= -\nu n_x + \rho n_\varphi + \rho - 1 \\ \kappa_x &= (3/4)(1 - \nu^2) m_x \end{aligned}\right\} \ldots [12]$$

Regime 1-10

$$\left.\begin{aligned} e_x + \kappa_x &= n_x - \nu n_\varphi + (3/4)(1 - \nu^2) m_x \\ e_x + e_\varphi &= (1 - \nu) n_x + (\rho - \nu) n_\varphi + \rho - 1 \\ n_\varphi &= n_x - m_x \end{aligned}\right\} \ldots [13]$$

3 POTENTIAL ENERGY

The principle of minimum potential energy is well known in elasticity, and Hodge has shown (4, 5) that for problems where the stress points all progress regularly it is also valid for piecewise linear plasticity. In the problem to be considered the artificial stress distributions always satisfy this restriction and it will be assumed that the actual state does so also. The significance of this assumption will be discussed in the final section.

Expressed in terms of the dimensionless resultants of the shell, the strain energy of the shell is equal to

$$V_i = (2\pi a h L Y^2/E) \int_0^1 [2 \int (n_x de_x + n_\varphi de_\varphi + m_x d\kappa_x)] d\xi \ldots [14]$$

Similarly, the external energy is given by

$$\left.\begin{aligned} V_e &= \int_{\text{end}} [pdAu]_L^0 + \int_{\text{cylinder}} pwdS \\ &= (2\pi a h L Y^2/E) \int_0^1 P(2W - U') d\xi \end{aligned}\right\} \ldots [15]$$

The total potential energy is the difference between these two quantities. Therefore, it is proportional to

$$I = \int_0^1 (\varphi + \psi) d\xi \ldots [16]$$

where

$$\varphi = 2 \int (n_x de_x + n_\varphi de_\varphi + m_x d\kappa_x) \ldots [17]$$

and

$$\psi = P(2W - U') \ldots [18]$$

The quantity φ must be evaluated from the appropriate stress-strain law. The following results are easily obtained from Equations [7], [12], and [13]

$$\left.\begin{aligned} &\text{Elastic} \\ &\quad \varphi = [n_x e_x + n_\varphi e_\varphi + m_x \kappa_x] \\ &\text{Regime 1} \\ &\quad \varphi = [n_x e_x + n_\varphi e_\varphi + m_x \kappa_x - (\rho - 1)(n_\varphi + 1)] \\ &\text{Regime 1-10} \\ &\quad \varphi = [n_x e_x + n_\varphi e_\varphi + m_x \kappa_x - (\rho - 1)(n_\varphi + 1)] \end{aligned}\right\} \ldots [19]$$

Obviously, the appropriate stress-strain law must be used to write the expression for U entirely in terms of strains and, hence, displacements.

The principle of minimum potential energy states that among all displacement fields satisfying the boundary conditions on displacements, the actual field will minimize the quantity I. As used to obtain an approximate solution to a problem, a displacement field containing one or more parameters is chosen, and these parameters are then determined so as to minimize I. This procedure will be illustrated in the next section.

4 SIMPLY SUPPORTED SHELL UNDER HYDROSTATIC PRESSURE

Equation [3] states that the axial force n_x is constant along the shell. If this force is caused by a hydrostatic pressure p, then, in terms of the dimensionless quantities, Equations [5]

$$n_x = -P/2 \ldots [20]$$

If this value of n_x is substituted into the various stress-strain laws, along with the values of e_x, e_φ, and κ_x from Equations [6], the resulting expressions may be solved for the resultants n_φ and m_x, and the axial displacement U in terms of the radial displacement W. In view of Equations [7], [12], and [13], the resulting expressions are

$$\left.\begin{aligned} &\text{Elastic} \\ &\quad U' = -(1/2)(1 - \nu^2) P + \nu W - b^2 W'^2 \\ &\quad n_\varphi = -W - \nu P/2 \\ &\quad m_x = -2W''/[3(1 - \nu^2)c^2] \end{aligned}\right\} \ldots [21a]$$

$$\left.\begin{aligned} &\text{Regime 1} \\ &U' = -(1/2)(1 - \nu^2/\rho) P \\ &\qquad + (\nu/\rho) W - b^2 W'^2 + \nu(1 - 1/\rho) \\ &n_\varphi = -(1/\rho)(W + \nu P/2) - (1 - 1/\rho) \\ &m_x = -2W''/[3(1 - \nu^2)c^2] \end{aligned}\right\} \ldots [21b]$$

Regime 1–10

$$\left.\begin{aligned} U' &= [(3/4)(1-\nu^2)+\rho]^{-1} \\ &\{[(3/4)(1-\nu^2)+\nu][W+\rho-1]+(\rho-\nu)W''/2c^2 \\ &-[(3/4)(1-\nu^2)+\rho]b^2W'^2+(P/2)[(3\nu/2)(1-\nu^2) \\ &-(3/4)(\rho+1)(1-\nu^2)+\nu^2-\rho]\} \\ n_\varphi &= -[(3/4)(1-\nu^2)+\rho]^{-1} \\ &\{(W+\rho-1)-W''/2c^2 \\ &+(P/2)[(3/4)(1-\nu^2+\nu]\} \\ m_s &= [(3/4)(1-\nu^2)+\rho]^{-1}[W+\rho-1\,W''/2c^2 \\ &+(P/2)(\nu-\rho)] \end{aligned}\right\} \quad [21c]$$

Next, these expressions, together with the appropriate stress-strain laws, are substituted into Equations [18] and [19] in order to obtain the potential-energy kernel as a function of W and the load P only. After some computation this leads to

Elastic

$$\varphi+\psi=K_e \quad [22a]$$

Regime 1

$$\varphi+\psi=K_e-K_1 \quad [22b]$$

Regime 1–10

$$\varphi+\psi=K_e-K_1-K_2 \quad [22c]$$

where

$$K_e=W^2-Pb^2W'^2+W''^2/[3c^4(1-\nu^2)] -(2-\nu)PW-(1-\nu^2)P^2/4 \quad [23a]$$

$$K_1=(1-1/\rho)[W-1+\nu P/2]^2 \quad [23b]$$

$$K_2=\frac{(3/4\rho)(1-\nu^2)}{(3/4)(1-\nu^2)+\rho}[(P/2)(\rho-\nu) -(W+\rho-1)-(2\rho/3c^2)W''/(1-\nu^2)]^2 \quad [23c]$$

For P sufficiently small, it is expected that the shell will be entirely elastic, hence the usual elastic analysis is used. Let W be any function which satisfies the displacement boundary conditions on the shell and depends upon n-parameters. Thus

$$W=W(\alpha,\beta,\gamma,\ldots,P,\xi) \quad [24]$$

When the shell is everywhere elastic, Equation [22a] is applicable and Equation [16] becomes

$$I=\int_0^1 K_e d\xi \quad [25]$$

where K_e is given by Equation [23]. Next, Equation [24] is substituted into Equation [25] and the derivatives of I with respect to $\alpha, \beta, \gamma, \ldots$ set equal to zero

$$\partial I/\partial\alpha=0, \qquad \partial I/\partial\beta=0, \qquad \partial I/\partial\gamma=0, \ldots \quad [26]$$

The n Equations [26] determine the n constants $\alpha, \beta, \gamma, \ldots$, so that the approximate elastic solution can be obtained. In particular, if W is linear in $\alpha, \beta, \gamma, \ldots$, Equations [26] are linear and easily solved.

With $\alpha, \beta, \gamma, \ldots$ known, Equations [24], [21a], and [20] determine the solution for any value of P. In particular

$$n_s=-P/2, \qquad n_\varphi=n_\varphi(\xi), \qquad m_s=m_s(\xi) \quad [27]$$

are all known. Equations [27] determine a curve in the stress-resultant space of Fig. 2, known as the "stress profile." In particular, since n_s is constant, the stress profile lies everywhere in the plane $n_s=-P/2$. Now, for each value of P the stress profile can be plotted, as can the intersection of the yield polyhedron with the plane $n_s=-P/2$. As long as the elastic stress profile is wholly within the resulting yield curve, the elastic solution is valid. However, when part of the elastic stress profile extends beyond the yield curve, the correct approximate solution is partially plastic and must be modified.

In the example to be considered in the next section, it is found that the stress profile first touches the yield curve on face 1 at the center of the shell $\xi=1$, for some value P_1 of the load. Therefore, for $P>P_1$ it is assumed that the shell is elastic for $0<\xi<\eta$, and is plastic in regime 1 for $\eta<\xi<1$. The value of η is determined so that the elastic solution just touches regime 1 at $\xi=\eta$, hence, in view of Equations [6], [7], and [8]

$$W(\alpha,\beta,\gamma,\ldots,P,\eta)=1-\nu P/2 \quad [28]$$

In view of Equations [22a, b], Equation [16] may now be written in the form

$$I=\int_0^1 K_e d\xi-\int_\eta^1 K_1 d\xi \quad [29]$$

In taking the partial derivatives with respect to $\alpha, \beta, \gamma, \ldots$, it will be observed that η is a function of these quantities defined implicitly by Equation [28]. Thus, for example

$$\partial I/\partial\alpha=\int_0^1(\partial K_e/\partial\alpha)d\xi-\int_\eta^1(\partial K_1/\partial\alpha)d\xi + K_{1(\xi=\eta)}(\partial\eta/\partial\alpha)$$

However, in view of Equations [23b] and [28], K_1 vanishes at $\xi=\eta$. Therefore η can be treated as a constant in taking the partial derivatives of Equation [29].

In this elastic-plastic state, η is an additional unknown; hence the total problem is to determine the $n+1$ quantities $\alpha, \beta, \gamma, \ldots$, and η from Equation [28] and the n Equations [26]. A difficulty is encountered here in that the equations are highly nonlinear in terms of η. This may be partially resolved by regarding η as independent and P as dependent. The entire solution, including the load, is then obtained as functions of the parameter η by the solution of linear and quadratic equations.

The solution so obtained will be valid so long as the stress profile does not exceed the initial yield curve for $0<\xi<\eta$, and does not extend beyond the limits on face 1 which are set by the other faces. It turns out that for a value P_2 of the load the stress point at $\xi=1$ reaches the intersection of faces 1 and 10. For loads greater than P_2, there are three possibilities to consider. The center of the shell may pass over to face 10, it may remain in the intersection of faces 1 and 10, or it may return to face 1. For the example considered, the second possibility is the actual one, so that for $P>P_2$ it is necessary to postulate three regimes

$$\left.\begin{aligned} &0<\xi<\eta && \text{elastic} \\ &\eta<\xi<\zeta && \text{plastic, regime 1} \\ &\zeta<\xi<1 && \text{plastic, regime 1–10} \end{aligned}\right\} \quad [30]$$

Here η is still given by Equation [28] while ζ is determined from Equation [11a]. In view of Equations [12] and [6] this latter relation becomes

$$W(\zeta)+[(2\rho/3c^2)/(1-\nu^2)]W''(\zeta) -(P/2)(\rho-\nu)+(\rho-1)=0 \quad [31]$$

The proper energy integral is now given by

$$I=\int_0^1 K_e d\xi-\int_\eta^1 K_1 d\xi-\int_\zeta^1 K_2 d\xi \quad [32]$$

Here, again η and ζ are functions of $\alpha, \beta, \gamma, \ldots$, but by reasoning

similar to that employed following Equation [29], it is easily shown that they may be regarded as constants for the purpose of taking partial derivatives. Therefore, Equations [31], [28], and the n Equations [26] are available for determining $\alpha, \beta, \gamma, \ldots, \eta$, and ζ. In practice, the best method found was to solve Equations [31], [28], and $n-1$ of Equations [26] for $\alpha, \beta, \gamma, \ldots$, and P, regarding η and ζ both as known. These values were then substituted into the remaining Equation [26] to obtain a compatibility equation between η and ζ. Taking, say, η as the independent parameter, this equation could then be solved numerically or graphically for ζ.

5 Example

As a particular numerical example, the shell dimensions and stress-strain characteristics were chosen so that

$$\left.\begin{aligned} c^2 = L^2/ah = 3, \qquad b^2 = Ya^2/2EL^2 = 0.1 \\ \nu = 0.3, \qquad \rho = E/E' = 400 \end{aligned}\right\} \quad \ldots [33]$$

For simplicity of computation a deflected shape of the form

$$W = \alpha \sin(\pi\xi/2) \quad \ldots [34]$$

was chosen. The possible accuracy of such a simple approximation will be discussed in the concluding section.

The elastic solution is easily obtained in this case. Some typical stress profiles are shown in Fig. 4(a), and some typical values

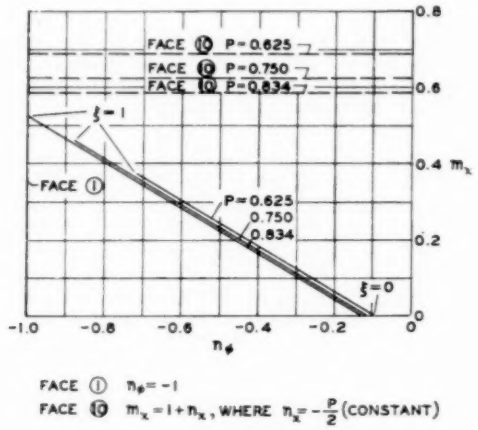

Fig. 4(a) Typical Stress Profiles for Various P. Elastic Solution.

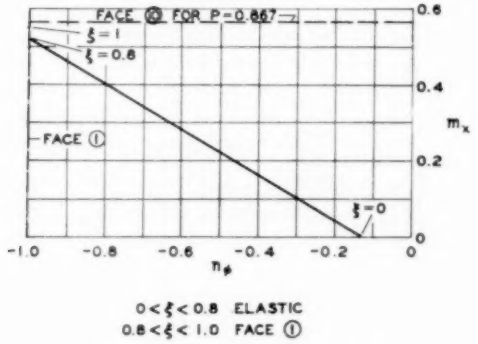

Fig. 4(b) Stress Profile for $P = 0.867$

Table 1 Stresses and Displacements for Various Loads

P	η	ζ	α = W_max	η_x	η_φ(1)	ε_x(1)	Regimes
0.2	–	–	0.181	-0.1	-0.211	0.109	Elastic only
0.4	–	–	0.377	-0.2	-0.437	0.227	
0.6	–	–	0.591	-0.3	-0.681	0.356	
0.625*	–	–	0.619	-0.312	-0.713	0.373	
0.75*	–	–	0.762	-0.375	-0.874	0.460	
0.834*	–	–	0.875	-0.417	-1.000	0.527	
0.867**	0.80	–	0.915	-0.433	-1.0000	0.551	Elastic and 1
0.870	0.76	–	0.930	-0.435	-1.0000	0.565	
0.871	0.7	0.815	0.976	-0.436	-1.0003	0.565	Elastic, 1, and 1-10
0.887***	0.6	0.660	1.070	-0.444	-1.006	0.559	
0.873	0.4	0.435	1.480	-0.437	-1.002	0.566	
0.868	0.3	0.327	1.920	-0.434	-1.004	0.570	

Stress profiles plotted:
*Fig. 4(a) **Fig. 4(b) ***Fig. 4(c)

are given in Table 1. From Fig. 4(a) it is evident that the stress profile first touches face 1 for

$$P = P_1 = 0.834 \quad \ldots [35]$$

For $P > P_1$, the stress profile is partly elastic and partly plastic in regime 1 as suggested in the previous section. Typical values are given in Table 1, and the corresponding stress profiles are shown in Fig. 4(b). It will be observed that the amount of strain-hardening occurring in this phase is so small as to be imperceptible in the scale of Fig. 4.

At a value of the load given by

$$P = P_2 = 0.870 \quad \ldots [36]$$

the center of the shell goes into the edge regime 1–10, and for all greater values of P the scheme of Equations [30] must be used. Stress profiles for this case are shown in Fig. 4(c) and typical values are again given in Table 1. Here again the amount of strain-hardening is insignificant.

Fig. 5 shows the three stress resultants and the regime boundaries η and ζ as functions of the maximum displacement

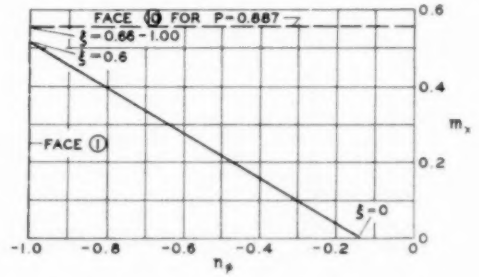

Fig. 4(c) Stress Profile for $P = 0.887$

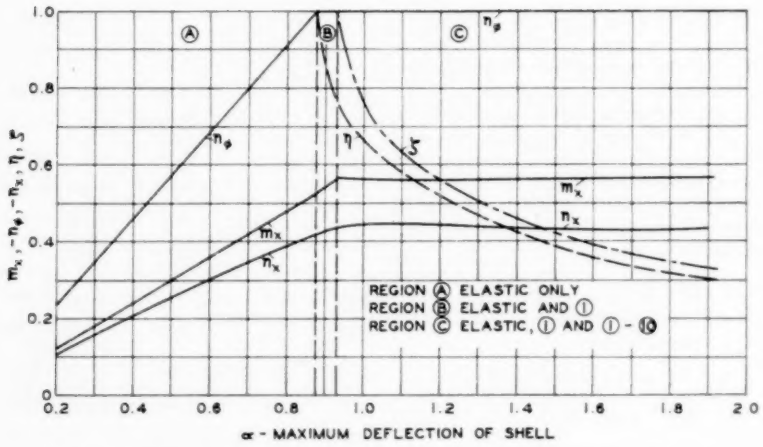

FIG. 5 VARIATION OF n_φ, m_x, n_x, η, AND ζ WITH MAXIMUM DEFLECTION OF SHELL

$$W_{max} = W(1) = \alpha \quad [37]$$

at the center of the shell, and Fig. 6 shows the load P as a function of W_{max}. It will be observed that P reaches a maximum value of 0.887, and then decreases. This phenomenon is due to the beam-column effect caused by the presence of end pressure. Its significance will be commented upon further in the final section.

6 CONCLUSIONS

The discussion of the conclusions available from the preceding paper is conveniently divided into two parts; namely, the physical significance of the solution and the accuracy of the methods used. In order to separate these two viewpoints, it first will be assumed that the approximate solution based upon a sinusoidal displacement does, in fact, reasonably represent the physical behavior of the shell.

Under this assumption, it is evident from Fig. 6 that the most significant point is the maximum in the $P - W_{max}$ curve. If, by some mechanism, it were possible to carry out a test in which the displacement W was controlled and P was measured then the curve shown in Fig. 6 would be obtained. However, in the more usual situation P is given and W is measured. Here it is evident that once P reached the value 0.887, the deformation would continue and there would be no further equilibrium position for that load. In other words

$$P_{max} = 0.887 \quad [38]$$

is truly the maximum carrying capacity of the shell according to the present theory.

It is of some interest to compare this value with other criteria.[7] For a rigid-plastic material, there can be no straining, and hence no beam-column effect, until the collapse load is reached. The collapse load in this case is easily computed and turns out to be

$$P_c = 1 + 1/(1 + 2c^2) = 1.143 \quad [39]$$

A comparison with Equation [38] shows that this theory which ignores elastic strains is completely unrealistic in this problem.

If elastic strains only were to be considered, the shell would still have a maximum carrying capacity, which can be computed according to various assumptions. The simplest approach is to assume an axially symmetric mode of deformation; i.e., to continue the elastic analysis described in the previous section without

[7] The authors wish to thank Prof. J. Kempner for his help in preparing this part of the discussion.

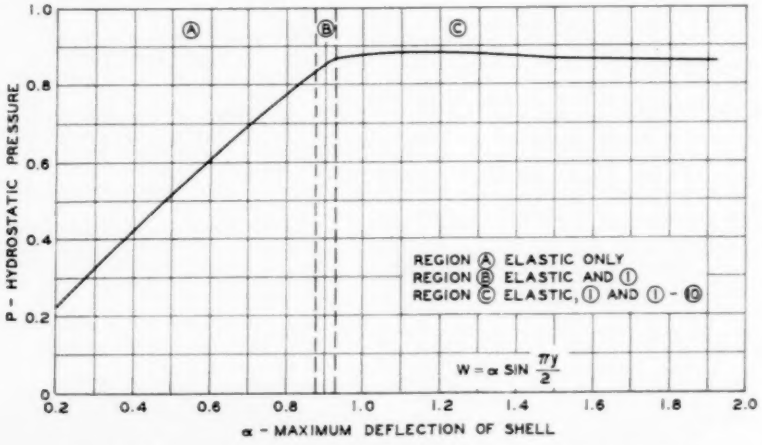
Ⓐ
Ⓑ
Ⓒ
REGION Ⓐ ELASTIC ONLY
REGION Ⓑ ELASTIC AND ①
REGION Ⓒ ELASTIC, ① AND ① - ⑩
$W = \alpha \sin \frac{\pi y}{2}$
P - HYDROSTATIC PRESSURE
α - MAXIMUM DEFLECTION OF SHELL

FIG. 6 HYDROSTATIC PRESSURE VERSUS MAXIMUM DEFLECTION OF SHELL

regard to the yield limit. In this case the shell deformations become infinite as P approaches the value

$$P_{cla} = 5.05 \quad [40]$$

asymptotically.

However, nonsymmetric buckling modes are also available, although the associated computations are more difficult. Using a linear theory based on Love's equations, Timoshenko (9) obtains a buckling pressure

$$P_T = 1.68 \quad [41]$$

for the present problem. Batdorf (10) gives buckling curves based on Donnell's equations which result in a value

$$P_B = 1.56 \quad [42]$$

Kempner (11) has shown that the inclusion of certain nonlinear terms modifies Batdorf's result by less than 3 per cent. All of these values are considerably higher than the value P_{max} obtained in the present analysis, which indicates that the assumed elastic buckling modes involve stresses well above the yield limit, and hence they are unrealistic.

Other authors (12, 13) have approached the shell-buckling problem from the viewpoint of assumed initial eccentricities. As far as initial deviation in the axial direction is concerned, such eccentricities are not particularly important since the lateral pressure produces radial displacements anyhow. However, initial circumferential eccentricities have a more profound effect. In the first place, the concept of carrying capacity is not well defined in this case. In addition, if a definition related to the maximum stress in the shell is adopted, it is found that the carrying capacity depends upon the magnitude of the eccentricities. Therefore, by suitable choice of such eccentricities it is possible to obtain almost any value of P.

With regard to the reliability of the results here obtained, the situation is not entirely clear. In the first place, there is no guarantee that the minimum principle used is, in fact, valid for this particular problem. As shown in (4) and (5), the principle of minimum potential energy is valid provided both the actual and assumed stress points progress regularly. In the present example, the assumed stress point certainly satisfies this condition. However, since the actual solution is unknown, no such statement can be made for the actual stress point. It follows that the mathematical validity of the proposed solution has not been established.

However, lacking any information to the contrary, the principle of minimum potential energy appears to be the most reasonable method of determining the coefficients to be associated with an assumed deflection shape. This leads to the next question; namely, the suitability of assuming a single half-sine wave. For the fully elastic shell, this is known to lead to reasonable results, but there is not sufficient evidence available to indicate whether or not it is also reasonable for the partially plastic case. Some computations were made using an assumed shape with two sinusoidal terms

$$W = \alpha \sin \pi\xi/2 + \beta \sin 3\pi\xi/2 \quad [43]$$

For the fully elastic case and the partially plastic case involving only regime 1, the effect of the second term on the stress profile did not appear to be significant. However, the computations became too laborious for the case defined by Equations [30], and it was not feasible to continue them.

As an alternative approach to the problem, an approximate solution was obtained using the principle of complementary energy. However, even when rather complex functions were used to approximate the stress resultants, the results did not appear particularly significant and have not been recorded. The one fact in which the two approximate solutions do appear to agree is that the carrying capacity of the shell is achieved at rather small strains, so that strain-hardening is not particularly significant.

Finally, then, it appears that for the particular shell investigated, plastic behavior and elastic strains are both vital in determining the carrying capacity of the shell, so that neither the rigid-plastic collapse load nor the classical buckling load is a reasonable approximation to the true maximum load. This conclusion is further reinforced by the fact that consideration of more general modes of axial deformation or even nonsymmetric deformation modes will probably serve to reduce Equation [38] and hence further increase the discrepancies.

A second conclusion is that the effect of strain-hardening is negligible. Therefore, in future investigations it might be well to consider the simplifications available in dealing with an elastic, perfectly plastic material. Such a simplification must be made cautiously, however, since the assumed hardening ratio of $E'/E = 1/400$ was certainly not large.

BIBLIOGRAPHY

1 "The Plastic Collapse of Cylindrical Shells Under Axially Symmetrical Loading," by E. T. Onat, *Quarterly of Applied Mathematics*, vol. 13, 1955, pp. 63–72.

2 "Rigid-Plastic Analysis of Symmetrically Loaded Cylindrical Shells," by P. G. Hodge, Jr., JOURNAL OF APPLIED MECHANICS, Trans. ASME, vol. 76, 1954, pp. 336–342.

3 "Piecewise Linear Isotropic Plasticity Applied to a Circular Cylindrical Shell With Symmetrical Radial Loading," by P. G. Hodge, Jr., *Journal of the Franklin Institute*, vol. 263, 1957, pp. 13–34.

4 "Minimum Principles of Piecewise Linear Isotropic Plasticity," by P. G. Hodge, Jr., *Journal of Rational Mechanics and Analysis*, vol. 5, 1956, pp. 917–938.

5 "The Mathematical Theory of Plasticity," by P. G. Hodge, Jr., in "Elasticity and Plasticity," by J. N. Goodier and P. G. Hodge, Jr., John Wiley & Sons, Inc., New York, N. Y., 1957.

6 "A Mathematical Theory of Plasticity Based on the Concept of Slip," by S. B. Batdorf and B. Budiansky, NACA TN 1871, 1949.

7 "The Theory of Plasticity—A Survey of Recent Achievements," by W. Prager, The Institution of Mechanical Engineers, James Clayton Lecture, London, England, 1955.

8 "The Theory of Piecewise Linear Isotropic Plasticity," by P. G. Hodge, Jr., "Deformation and Flow of Solids," R. Grammel, Editor, Julius Springer, Berlin, Germany, 1956, pp. 147–168.

9 "Theory of Elastic Stability," by S. Timoshenko, McGraw-Hill Book Company, Inc., New York, N. Y., 1956.

10 "A Simplified Method of Elastic-Stability Analysis for Thin Cylindrical Shells. I. Donnell's Equations," by S. B. Batdorf, NACA TN 1341, 1947.

11 "Postbuckling Behavior of Circular Cylindrical Shells," by J. Kempner, K. A. V. Pandalai, S. A. Patel, and Jacques Crouzet-Pascal, *Journal of the Aeronautical Sciences*, vol. 24, 1957, pp. 253–264.

12 "The Effect of Imperfections on the Stresses in a Circular Cylindrical Shell Under Hydrostatic Pressure," by S. R. Bodner and William Berks, PIBAL Report 210, Polytechnic Institute of Brooklyn, Brooklyn, N. Y., 1952.

13 "Effects of Boundary Conditions and Initial Out-of-Roundness on the Strength of Thin-Walled Cylinders Subject to External Hydrostatic Pressure," by G. D. Galletly and R. Bart, JOURNAL OF APPLIED MECHANICS, Trans. ASME, vol. 78, 1956, pp. 351–358.

Thermal Stresses in Transversely Isotropic Semi-Infinite Elastic Solids

By BRAHMADEV SHARMA,[1] MADHYA-PRADESH, INDIA

A general method of solution of the steady-state thermal-stress problem of a transversely isotropic semi-infinite elastic solid is given in this paper.

Nomenclature

The following nomenclature is used in the paper:

$\sigma_x, \sigma_y, \sigma_z$ = Cartesian components of stress
$\tau_{xy}, \tau_{yz}, \tau_{zx}$
u, v, w = Cartesian components of displacement
$c_{11}, c_{12}, \ldots$ = elastic constants
$\epsilon_x, \epsilon_y, \epsilon_z$ = unit elongation in x, y, z-directions
$\gamma_{xy}, \gamma_{yz}, \gamma_{zx}$ = shearing-strain components in Cartesian coordinates
α_1 = coefficient of linear expansion in z-plane
α_2 = coefficient of linear expansion along z-axis
k^2 = ratio of coefficients of conductivity along z-axis and in z-plane

Introduction

While the solution of problems of thermal stress in two dimensions has been considered in great detail, comparatively little work has been done on similar problems in three dimensions. The aeolotropic media have attracted even less attention because of greater difficulty of problems involving more than two elastic constants. Recently the solution of some such problems has been discussed by Nowacki (1)[2] and Nowinski (2, 3). In this paper, following the general analysis developed by Elliott (4), a general solution of the thermal-stress problem of a transversely isotropic semi-infinite elastic solid is developed. The method can be extended easily to solve the problem of an infinite elastic disk of similar medium.

Solution

We take the origin on the plane boundary of the semi-infinite solid and the axis z is drawn into the body. Assuming the axis z as the axis of elastic symmetry, we obtain the stress-strain relations as

$$\left.\begin{aligned}\sigma_x &= c_{11}\epsilon_x + c_{12}\epsilon_y + c_{13}\epsilon_z - b_1T\\ \sigma_y &= c_{12}\epsilon_x + c_{11}\epsilon_y + c_{13}\epsilon_z - b_1T\\ \sigma_z &= c_{13}\epsilon_x + c_{13}\epsilon_y + c_{33}\epsilon_z - b_2T\end{aligned}\right\} \quad \ldots\ldots\ldots [1]$$

$$\left.\begin{aligned}\tau_{yz} &= c_{44}\gamma_{yz}\\ \tau_{zx} &= c_{44}\gamma_{zx}\\ \tau_{xy} &= \frac{1}{2}(c_{11} - c_{12})\gamma_{xy}\end{aligned}\right\} \quad \ldots\ldots\ldots [2]$$

where

$$b_1 = (c_{11} + c_{12})\alpha_1 + c_{13}\alpha_2, \qquad b_2 = 2c_{13}\alpha_1 + c_{33}\alpha_2$$

In steady state T, the temperature at any point in the body, satisfies the differential equation

$$\frac{\partial^2 T}{\partial x^2} + \frac{\partial^2 T}{\partial y^2} + k^2\frac{\partial^2 T}{\partial z^2} = 0 \quad \ldots\ldots\ldots [3]$$

A general solution of Equation [3] appropriate to our problem is

$$T = \int_{-\infty}^{+\infty}\int A(p, q)\exp\left\{ipx + iqy - \frac{(p^2 + q^2)^{1/2}}{k}z\right\}dp\,dq \quad \ldots [4]$$

In the usual notation, writing $\epsilon_x, \epsilon_y, \ldots$ in terms of displacement components, and substituting stress components from Equations [1] and [2] in the equations of equilibrium in the absense of body forces

$$\left.\begin{aligned}&\frac{\partial \sigma_x}{\partial x} + \frac{\partial \tau_{xy}}{\partial y} + \frac{\partial \tau_{zx}}{\partial z} = 0\\ &\ldots\ldots\ldots\ldots\\ &\ldots\ldots\ldots\ldots\end{aligned}\right\} \quad \ldots\ldots\ldots [5]$$

we get

$$c_{11}\frac{\partial^2 u}{\partial x^2} + \frac{1}{2}(c_{11} - c_{12})\frac{\partial^2 u}{\partial y^2} + c_{44}\frac{\partial^2 u}{\partial z^2} + \frac{\partial}{\partial x}\left[\frac{1}{2}(c_{11} + c_{12})\frac{\partial v}{\partial y} + (c_{12} + c_{44})\frac{\partial w}{\partial z}\right] - b_1\frac{\partial T}{\partial x} = 0 \ldots [6]$$

$$\frac{1}{2}(c_{11} - c_{12})\frac{\partial^2 v}{\partial x^2} + c_{11}\frac{\partial^2 v}{\partial y^2} + c_{44}\frac{\partial^2 v}{\partial z^2} + \frac{\partial}{\partial y}\left[\frac{1}{2}(c_{11} + c_{12})\frac{\partial u}{\partial x} + (c_{12} + c_{44})\frac{\partial w}{\partial z}\right] - b_1\frac{\partial T}{\partial y} = 0 \ldots [7]$$

$$c_{44}\left(\frac{\partial^2 w}{\partial x^2} + \frac{\partial^2 w}{\partial y^2}\right) + c_{33}\frac{\partial^2 w}{\partial z^2} + (c_{13} + c_{44})\frac{\partial}{\partial z}\left(\frac{\partial u}{\partial x} + \frac{\partial v}{\partial y}\right) - b_2\frac{\partial T}{\partial z} = 0 \ldots [8]$$

---

[1] Assistant Commissioner, Saugor.

[2] Numbers in parentheses refer to the Bibliography at the end of the paper.

Contributed by the Applied Mechanics Division and presented at the Annual Meeting, New York, N. Y., December 1–6, 1957, of The American Society of Mechanical Engineers.

Discussion of this paper should be addressed to the Secretary, ASME, 29 West 39th Street, New York, N. Y., and will be accepted until April 10, 1958, for publication at a later date. Discussion received after the closing date will be returned.

Note: Statements and opinions advanced in papers are to be understood as individual expressions of their authors and not those of the Society. Manuscript received by ASME Applied Mechanics Division, July 26, 1956. Paper No. 57—A-22.

We assume that the solution may be found in the form

$$u = \frac{\partial \phi}{\partial x} + \frac{\partial \bar{T}}{\partial x}, \quad v = \frac{\partial \phi}{\partial y} + \frac{\partial \bar{T}}{\partial y},$$
$$w = \lambda \frac{\partial \phi}{\partial z} + \mu \frac{\partial \bar{T}}{\partial z} \ldots [9]$$

where λ and μ are constants and

$$\bar{T} = \int_{-\infty}^{+\infty}\int A(p, q)B(p, q) \exp\left\{ipx + iqy - \frac{(p^2 + q^2)^{1/2}}{k} z\right\} dp\, dq \ldots [10]$$

Then Equations [6] and [7] are satisfied if

$$c_{11}\left(\frac{\partial^2 \phi}{\partial x^2} + \frac{\partial^2 \phi}{\partial y^2}\right) + [c_{44} + \lambda(c_{13} + c_{44})]\frac{\partial^2 \phi}{\partial z^2} = 0 \ldots [11]$$

and

$$B(p^2 + q^2)[\mu(c_{13} + c_{44}) + c_{44} - k^2 c_{11}] - b_1 k^2 = 0 \ldots [12]$$

and Equation [8] is satisfied if

$$[(c_{13} + c_{44}) + \lambda c_{44}]\left(\frac{\partial^2 \phi}{\partial x^2} + \frac{\partial^2 \phi}{\partial y^2}\right) + \lambda c_{33}\frac{\partial^2 \phi}{\partial z^2} = 0 \ldots [13]$$

and

$$B(p^2 + q^2)[\mu c_{33} - k^2\{(c_{13} + c_{44}) + \mu c_{44}\}] - b_2 k^2 = 0 \ldots [14]$$

Both Equations [12] and [14] are satisfied if

$$\mu = \frac{b_1 k^2(c_{13} + c_{44}) + b_2(c_{44} - k^2 c_{11})}{b_1(c_{33} - k^2 c_{44}) - b_2(c_{13} + c_{44})} \ldots [15]$$

$$(p^2 + q^2)B = k^2 \frac{b_1(c_{33} - k^2 c_{44}) - b_2(c_{13} + c_{44})^2}{(c_{44} - c_{11}k^2)(c_{33} - k^2 c_{44}) + k^2(c_{13} + c_{44})^2} = E \text{ (a constant)} \ldots [16]$$

A nonzero solution of Equations [11] and [13] can be found only if they are identical; this occurs if

$$\frac{\lambda(c_{13} + c_{44}) + c_{44}}{c_{11}} = \frac{\lambda c_{33}}{\lambda c_{44} + (c_{13} + c_{44})} = \nu^2 \ldots [17]$$

Then, ϕ_1 and ϕ_2 are solutions of

$$\left(\frac{\partial^2}{\partial x^2} + \frac{\partial^2}{\partial y^2} + \nu_i^2 \frac{\partial^2}{\partial z^2}\right)\phi_i = 0 \qquad (i = 1, 2) \ldots [18]$$

where ν_1^2 and ν_2^2 are the roots of

$$c_{11}c_{44}\nu^4 + (2c_{13}c_{44} - c_{11}c_{33} + c_{13}^2)\nu^2 + c_{33}c_{44} = 0 \ldots [19]$$

So

$$u = \frac{\partial}{\partial x}(\phi_1 + \phi_2 + \bar{T}), \qquad v = \frac{\partial}{\partial y}(\phi_1 + \phi_2 + \bar{T}),$$
$$w = \frac{\partial}{\partial z}(\lambda_1 \phi_1 + \lambda_2 \phi_2 + \mu \bar{T}) \ldots [20]$$

where λ_1 and λ_2 are the two values of λ corresponding to ν_1^2 and ν_2^2, respectively. The stresses are obtained as

$$\sigma_x = \left(c_{11}\frac{\partial^2}{\partial x^2} + c_{12}\frac{\partial^2}{\partial y^2}\right)(\phi_1 + \phi_2 + \bar{T}) + c_{12}\frac{\partial^2}{\partial z^2}(\lambda_1 \phi_1 + \lambda_2 \phi_2 + \mu \bar{T}) - b_1 T \ldots [21]$$

$$\sigma_y = \left(c_{12}\frac{\partial^2}{\partial x^2} + c_{11}\frac{\partial^2}{\partial y^2}\right)(\phi_1 + \phi_2 + \bar{T}) + c_{13}\frac{\partial^2}{\partial z^2}(\lambda_1 \phi_1 + \lambda_2 \phi_2 + \mu \bar{T}) - b_1 T \ldots [22]$$

$$\sigma_z = c_{13}\left(\frac{\partial^2}{\partial x^2} + \frac{\partial^2}{\partial y^2}\right)(\phi_1 + \phi_2 + \bar{T}) + c_{33}\frac{\partial^2}{\partial z^2}(\lambda_1 \phi_1 + \lambda_2 \phi_2 + \mu \bar{T}) - b_2 T \ldots [23]$$

$$\tau_{xy} = (c_{11} - c_{12})\frac{\partial^2}{\partial x \partial y}(\phi_1 + \phi_2 + \bar{T}) \ldots [24]$$

$$\tau_{yz} = c_{44}\frac{\partial^2}{\partial y \partial z}[(1 + \lambda_1)\phi_1 + (1 + \lambda_2)\phi_2 + (1 + \mu)\bar{T}] \ldots [25]$$

$$\tau_{xz} = c_{44}\frac{\partial^2}{\partial z \partial x}[(1 + \lambda_1)\phi_1 + (1 + \lambda_2)\phi_2 + (1 + \mu)\bar{T}] \ldots [26]$$

Now, to determine the stresses due to temperature in the semi-infinite solid we have to free the plane surface, that is

$$\tau_{xz} = \tau_{yz} = \sigma_z = 0 \qquad \text{when } z = 0 \ldots [27]$$

To this end, as all the stress and displacement components vanish at infinity, assume

$$\phi_1 = \int_{-\infty}^{+\infty}\int C(p, q) \exp\left(ipx + iqy - \frac{(p^2 + q^2)^{1/2}}{\nu_1} z\right) dp\, dq \ldots [28]$$

$$\phi_2 = \int_{-\infty}^{+\infty}\int D(p, q) \exp\left(ipx + iqy - \frac{(p^2 + q^2)^{1/2}}{\nu_2} z\right) dp\, dq \ldots [29]$$

Substituting for T, $\bar{T}$, ϕ_1, and ϕ_2 in the expressions of the stress components, Condition [27] is satisfied if

$$C\left(\frac{\lambda_1}{\nu_1^2} c_{33} - c_{13}\right) + D\left(\frac{\lambda_2}{\nu_2^2} c_{33} - c_{13}\right) + \frac{A}{p^2 + q^2}\left\{E\left(\frac{c_{33}}{k^2} - c_{13}\right) - b_2\right\} = 0 \ldots [30]$$

$$C\frac{1 + \lambda_1}{\nu_1} + D\frac{1 + \lambda_2}{\nu_2} + \frac{AE}{(p^2 + q^2)k}(1 + \mu) = 0$$

If the temperature distribution on the plane surface is known, say

$$T = f(x, y) \qquad z = 0$$

by Fourier's integral formula (5)

$$[T]_{z=0} = \frac{1}{4\pi^2}\int_{-\infty}^{+\infty}\int dp\, dq \int_{-\infty}^{+\infty}\int f(\xi, \eta) \exp\{ip(x - \xi) + iq(y - \eta)\} d\xi d\eta$$

or

$$T = \frac{1}{4\pi^2}\int_{-\infty}^{+\infty}\int \exp\left(-\frac{(p^2 + q^2)^{1/2}}{k} z\right) d\eta\, dq \int_{-\infty}^{+\infty}\int f(\xi, \eta) \exp\{ip(x - \xi) + iq(y - \eta)\} d\xi d\eta \ldots [31]$$

By comparing Equation [31] with Equation [3] A is determined as a function of p and q and hence all the unknowns are defined. This completes the solution of the problem in the general case.

In the case of axisymmetric temperature distribution, we can solve the problem as a special case of the foregoing by transforming to polar co-ordinates. But the problem is simplified if we proceed from the beginning, taking an appropriate form of T. We take T as

$$T = \int_0^\infty A(m) \exp\left(-\frac{mz}{k}\right) J_0(mr)dm \quad \ldots\ldots [32]$$

and

$$\bar{T} = \int_0^\infty A(m)B(m) \exp\left(-\frac{mz}{k}\right) J_0(mr)dm \quad \ldots\ldots [33]$$

Equations [11] to [27] remain unchanged except that we replace $(p^2 + q^2)$ by m^2 whenever it occurs. We assume

$$\left.\begin{aligned} \phi_1 &= \int_0^\infty C(m) \exp\left(-\frac{mz}{\nu_1}\right) J_0(mr)dm \\ \phi_2 &= \int_0^\infty D(m) \exp\left(-\frac{mz}{\nu_2}\right) J_0(mr)dm \end{aligned}\right\} \quad \ldots\ldots [34]$$

The Condition [27] is satisfied if

$$\left.\begin{aligned} &C\left(\frac{\lambda_1}{\nu_1^2} c_{33} + c_{13}\right) + D\left(\frac{\lambda_2}{\nu_2^2} c_{33} - c_{13}\right) \\ &\qquad + \frac{A}{m^2}\left\{E\left(\frac{c_{33}}{k^2} - c_{13}\right) - b_3\right\} = 0 \\ &C\,\frac{1+\lambda_1}{\nu_1} + D\,\frac{1+\lambda_2}{\nu_2} + \frac{AE}{m^2k}(1+\mu) = 0 \end{aligned}\right\} \quad \ldots [35]$$

As a particular case, suppose a circular area of the plane surface is kept at a uniform temperature V while the rest of the surface is at zero temperature. That is

$$\left.\begin{aligned} z &= 0 \\ T &= V \qquad r \le a \\ &= 0 \qquad r > a \end{aligned}\right\} \quad \ldots\ldots [36]$$

By Fourier-Bessel representation

$$[T]_{z=0} = Va \int_0^\infty J_1(ma)J_0(mr)dm$$

Hence

$$T = Va \int_0^\infty \exp\left(-\frac{mz}{k}\right) J_1(ma)J_0(mr)dm \quad \ldots\ldots [37]$$

Comparing Equation [32] with Equation [37]

$$A = Va\,J_1(ma) \quad \ldots\ldots [38]$$

Hence from Equation [35]

$$\left.\begin{aligned} C &= \frac{L}{m^2} J_1(ma) \\ D &= \frac{M}{m^2} J_1(ma) \end{aligned}\right\} \quad \ldots\ldots [39]$$

where L and M are constants independent of m.

With these values of C and D it will be seen that ϕ_1 and ϕ_2 are divergent at the lower limit. This can be avoided if we modify the functions as

$$\left.\begin{aligned} \phi_1 &= \int_0^\infty \frac{L}{m^2} [e^{-mz/\nu_1} J_0(mr) - 1]J_1(ma)dm \\ \phi_2 &= \int_0^\infty \frac{M}{m^2} [e^{-mz/\nu_2} J_0(mr) - 1]J_1(ma)dm \end{aligned}\right\} \quad \ldots [40]$$

With this modification no change is brought about in the expressions of displacement components as the additional term does not give any derivatives. Thus all the integrals used are convergent and the stress and displacement components are uniquely determined.

In the case of an infinite elastic disk of finite thickness we can introduce four arbitrary constants through ϕ_1 and ϕ_2. Hence the stress distribution will be completely determined as we can satisfy four boundary conditions involving stresses and/or displacements at both the surfaces.

ACKNOWLEDGMENT

The author offers his grateful thanks to Dr. B. Sen for his kind help in the preparation of this paper.

BIBLIOGRAPHY

1 "Thermal Stresses in Anisotropic Bodies," by Witold Nowacki, I, *Arch. Mech. Stos.*, vol. 6, 1954, pp. 481–492.

2 "Thermal Stresses in a Thick-Walled Spherical Vessel of Transversely Isotropic Material," by J. Nowinski, *Arch. Mech. Stos.*, vol. 7, no. 3, 1955, pp. 363–374.

3 "On Thermo-Elastic Problems in the Case of a Body with Arbitrary Type of Curvilinear Orthotropy," by J. Nowinski, W. Olszak, and W. Urbanowski, *Arch. Mech. Stos.*, vol. 7, no. 2, 1955, pp. 247–264.

4 "Three-Dimensional Stress Distribution in Hexagonal Aeotropic Crystals," by H. A. Elliott, Proceedings of the Cambridge Philosophical Society, vol. 44, 1948, pp. 522–533.

5 "Partial Differential Equations," by A. Sommerfeld, Academic Press, Inc., New York, N. Y., 1949, p. 59.

The Bursting Pressure of Cylindrical and Spherical Vessels

By N. L. SVENSSON,[1] LONDON, ENGLAND

The relationship between pressure and change of dimensions for cylindrical and spherical vessels subjected to internal pressure is considered for a material having a stress-strain curve of the form $\sigma = \sigma_0 \epsilon^n$. The equations obtained are analyzed further to obtain expressions for the bursting pressure for these vessels. From these results simplified expressions are obtained for the calculation of the bursting pressure for any vessel. Comparison with one set of experimental results shows excellent agreement.

Nomenclature

The following nomenclature is used in the paper:

K = ratio (outer radius)/(inner radius)
p = pressure
$\bar{p}$ = bursting pressure
R = radius
S = stress ratio (σ/σ_0)
t = wall thickness
u = radial displacement
x = ratio (displaced radius)/(original radius)
y = ratio (current wall thickness)/(original wall thickness)
ϵ = natural strain
ϵ' = engineering strain
σ = true stress
σ' = nominal stress
σ_0, n = parameters to define stress-strain curve

Subscripts

c = referring to cylinder
i = initial conditions
r = radial component
s = referring to sphere
t = tangential component
u = at ultimate
y = at yield
1 = inner radius
2 = outer radius

Introduction

The rational design of vessels subjected to internal pressure requires the study of two modes of failure. The first possibility of failure occurs when the deformation becomes excessive and there is a possibility of permanent deformation. The second type of failure occurs at a higher pressure and takes the form of bursting of the vessel. It is the purpose of this paper to derive an expression for the bursting pressure of cylindrical and spherical vessels manufactured from work-hardening materials.

The pressure which causes permanent deformation to begin is that which is sufficient to initiate a yield zone at the inner surface. If it is considered that yielding begins when the octahedral shear stress reaches a limiting value the appropriate pressures for a long cylindrical vessel and a spherical vessel, respectively, are (1)[2]

$$p_y = \frac{\sigma_y}{\sqrt{3}} \left(\frac{K^2 - 1}{K^2} \right) \quad [1]$$

$$p_y = \frac{2\sigma_y}{3} \left(\frac{K^3 - 1}{K^3} \right) \quad [2]$$

Subsequent plastic deformation depends upon the variation of the octahedral shear stress over the thickness of the vessel wall. For ideally plastic materials, this stress remains constant and bursting occurs when the plastic zone spreads to the outer surface. For work-hardening materials, on the other hand, the octahedral shear stress rises as the octahedral shear strain increases and bursting may not occur until well after the entire vessel wall has become plastic. While the problem of predicting bursting pressures has been solved for ideally plastic materials (1), only numerical methods have been developed for work-hardening materials (2). In this paper, the relationship between internal pressure and the increase in internal surface radius is derived for a material having a stress-strain curve of the Ludwik type, defined by $\sigma = \sigma_0 \epsilon^n$. From this relationship the maximum, or bursting, pressure is obtained and expressed as a function of the common strength properties of the material.

Derivation of Pressure-Deformation Equations

(*a*) *Thick-Walled Cylindrical Vessel.* For any element of the tube wall initially at radius R but instantaneously at radius $(R + u)$, the equation of equilibrium is

$$(R + u) \frac{d\sigma_r}{d(R + u)} = (\sigma_t - \sigma_r) \quad [3]$$

Since large displacements are involved, the radial and tangential strains are defined as

$$\epsilon_r = \log_e \left(1 + \frac{du}{dR} \right) \quad [4a]$$

$$\epsilon_t = \log_e \left(1 + \frac{u}{R} \right) \quad [4b]$$

By eliminating the displacement u from these equations the strain compatibility equation is obtained. When written in terms of the instantaneous radius this becomes

$$(R + u) \frac{d\epsilon_t}{d(R + u)} = 1 - e^{\epsilon_t - \epsilon_r} \quad [5]$$

---

[1] Lecturer in Mechanical Engineering, Imperial College of Science and Technology.

Contributed by the Applied Mechanics Division and presented at the Annual Meeting, New York, N. Y., December 1–6, 1957, of The American Society of Mechanical Engineers.

Discussion of this paper should be addressed to the Secretary, ASME, 29 West 39th Street, New York, N. Y., and will be accepted until April 10, 1958, for publication at a later date. Discussion received after the closing date will be returned.

Note: Statements and opinions advanced in papers are to be understood as individual expressions of their authors and not those of the Society. Manuscript received by ASME Applied Mechanics Division, September 24, 1956. Paper No. 57—A-15.

[2] Numbers in parentheses refer to the Bibliography at the end of the paper.

For convenience, effective stress and strain proportional to the octahedral shear values are defined as

$$\sigma = \frac{\sqrt{2}}{2}\left[(\sigma_1 - \sigma_2)^2 + (\sigma_2 - \sigma_3)^2 + (\sigma_3 - \sigma_1)^2\right]^{1/2} \quad [6]$$

$$\epsilon = \frac{\sqrt{2}}{3}\left[(\epsilon_1 - \epsilon_2)^2 + (\epsilon_2 - \epsilon_3)^2 + (\epsilon_3 - \epsilon_1)^2\right]^{1/2} \quad [7]$$

It will be observed that σ and ϵ are also the true stress and natural strain as determined in a simpler tensile test.

In this problem the principal axes of stress and strain remain fixed and coincident. Thus a deformation law of plastic flow can be employed and σ expressed as a function of ϵ. One form of equation which has been employed to represent the stress-strain law for many materials is

$$\sigma = \sigma_0 \epsilon^n \quad [8]$$

A family of curves of this power-law function is shown in Fig. 1 while in Fig. 2 is shown the corresponding family of nominal stress-engineering strain curves. A suitable method for determining the constants σ_0 and n is given in the Appendix.

Crossland and Bones (3) in a series of bursting tests on small

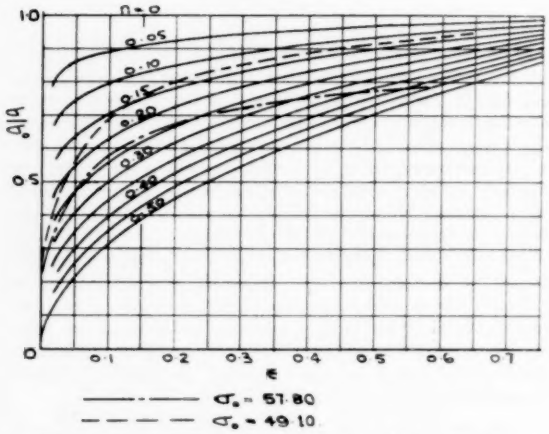

FIG. 1 FAMILY OF TRUE STRESS-NATURAL STRAIN CURVES
(Stress-strain curve for 0.28 per cent C steel used by Crossland and Bones (3) is shown for two different values of n.)

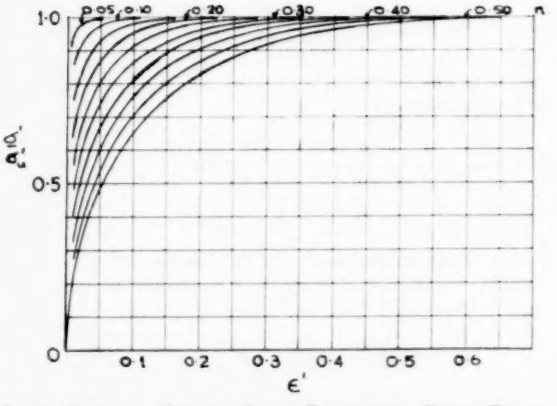

FIG. 2 FAMILY OF NOMINAL STRESS-ENGINEERING STRAIN CURVES
(Plotted until onset of necking.)

pressure vessels found that the axial strain in a closed-end vessel was small. If this component of strain is assumed to be zero, then since the material is incompressible we have

$$\epsilon_r = -\epsilon_t \quad [9a]$$

$$\sigma_a = \frac{1}{2}(\sigma_r + \sigma_t) \quad [9b]$$

Therefore

$$\sigma = \frac{\sqrt{3}}{2}(\sigma_t - \sigma_r) \quad [10a]$$

$$\epsilon = \frac{2}{\sqrt{3}}\epsilon_t \quad [10b]$$

If the dimensionless numbers x and S are defined as

$$x = \frac{R + u}{R_1}, \quad S = \frac{\sigma}{\sigma_0} \quad [11]$$

then Equations [3] and [5] become

$$x\frac{dS_r}{dx} = \frac{2}{\sqrt{3}}S \quad [12]$$

$$x\frac{d\epsilon_t}{dx} = 1 - e^{2\epsilon_t} \quad [13]$$

This equation may be integrated and substituting Equation [10b] leads to an equation giving the effective strain distribution over the wall thickness

$$\epsilon = \frac{1}{\sqrt{3}}\log_e\left(\frac{x^2}{c + x^2}\right) \quad [14]$$

At the inner bore

$$\epsilon_1 = \frac{1}{\sqrt{3}}\log_e x_1^2 \quad [15]$$

Therefore

$$\epsilon = \frac{1}{\sqrt{3}}\log_e\left(\frac{x^2}{1 - x_1^2 + x^2}\right) \quad [16]$$

The strain at the outer radius is then

$$\epsilon_2 = \frac{1}{\sqrt{3}}\log_e\left(\frac{K^2 - 1 + x_1^2}{K^2}\right) \quad [17]$$

By eliminating x_1 between Equations [15] and [17], the effective strain at the outer surface can be expressed as a function of ϵ_1 as

$$\epsilon_2 = \frac{1}{\sqrt{3}}\log_e\left[1 - \left(\frac{1 - e^{\sqrt{3}\epsilon_1}}{K^2}\right)\right] \quad [18]$$

Having thus determined the variation of effective strain with radius, Equation [12] may now be integrated to determine the variation of radial stress. By making use of the boundary conditions that

$$S_r = 0 \quad \text{at} \quad x = x_2 \quad [19a]$$

$$S_r = \frac{-p}{\sigma_0} \quad \text{at} \quad x = x_1 \quad [19b]$$

the internal pressure producing the inner bore strain is given by

$$p = \frac{2\sigma_0}{\sqrt{3}}\int_{x_1}^{x_2} S\frac{dx}{x} \quad [20]$$

By using Equation [16], this integral can be transformed to an integral in the strain plane; viz.

$$p = \sigma_0 \int_{\epsilon_1}^{\epsilon_2} \frac{\epsilon^n}{1 - e^{\sqrt{3}\epsilon}} d\epsilon \quad [21]$$

The solution of this integral is

$$p = \frac{\sigma_0}{\sqrt{3}} \left[\epsilon^n \left\{ -\frac{1}{n} + \frac{\sqrt{3}\epsilon}{2(n+1)} - \sum_{m=1}^{\infty} (-1)^{m-1} \frac{B_m}{(2m)!} \frac{(\sqrt{3}\epsilon)^{2m}}{(2m+n)} \right\} \right]_{\epsilon_1}^{\epsilon_2} \quad [22]$$

where B_m are the Bernoulli numbers (4) defined as

$$B_m = \frac{2(2m)!}{(2\pi)^{2m}} \sum_{n=1}^{\infty} \frac{1}{n^{2m}} \quad [23]$$

NOTE: $B_1 = 1/6$, $B_2 = 1/30$, $B_3 = 1/42$, $B_4 = 1/30$

(b) Thick-Walled Spherical Vessel. In the case of a spherical vessel, the tangential stress is independent of the orientation of the tangent and the equation of equilibrium is

$$\left(\frac{R+u}{2}\right) \frac{d\sigma_r}{d(R+u)} = (\sigma_t - \sigma_r) \quad [24]$$

On the other hand, the expressions for the radial and tangential strains hold as before and the strain compatibility Equation [5] is still valid

$$(R+u)\frac{d\epsilon_t}{d(R+u)} = 1 - e^{\epsilon_t - \epsilon_r} \quad [5]$$

Assuming constancy of volume during plastic deformation it is found that

$$\epsilon_r = -2\epsilon_t \quad [25]$$

Therefore

$$\sigma = (\sigma_t - \sigma_r) \quad [26a]$$

$$\epsilon = 2\epsilon_t \quad [26b]$$

By following through an analysis which is similar to that carried out previously, the expressions for the various strains become

$$\epsilon_1 = \frac{2}{3} \log_e x_1^3 \quad [27]$$

and

$$\epsilon = \frac{2}{3} \log_e \left(\frac{x^3}{1 - x_1^3 + x^3} \right) \quad [28]$$

Therefore

$$\epsilon_2 = \frac{2}{3} \log_e \left(\frac{K^3 - 1 + x_1^3}{K^3} \right) \quad [29]$$

Whence, by eliminating x_1 between Equations [27] and [29]

$$\epsilon_2 = \frac{2}{3} \log_e \left[1 - \left(\frac{1 - e^{3\epsilon_1/2}}{K^3} \right) \right] \quad [30]$$

The integration of Equation [24] with substitution of appropriate limits leads to

$$p = \sigma_0 \int_{\epsilon_1}^{\epsilon_2} \frac{\epsilon^n d\epsilon}{1 - e^{3\epsilon/2}} \quad [31]$$

whence

$$p = \frac{2}{3} \sigma_0 \left[\epsilon^n \left\{ -\frac{1}{n} + \frac{3\epsilon}{4(n+1)} - \sum_{m=1}^{\infty} (-1)^{m-1} \frac{B_m}{(2m)!} \frac{(3\epsilon/2)^{2m}}{(2m+n)} \right\} \right]_{\epsilon_1}^{\epsilon_2} \quad [32]$$

(c) Thin-Walled Cylindrical Vessel. Although the foregoing analysis applies to any possible (wall-thickness)/(vessel diameter) ratio, the computations tend to become exacting when this ratio becomes less than approximately 0.05. It is thus convenient to consider the analysis of the simpler thin-walled-vessel problem.

In this case the equilibrium equations lead to

$$\sigma_t = \frac{pR}{t} \quad [33a]$$

$$\sigma_a = \frac{pR}{2t} \quad [33b]$$

If the dimensionless number $y = t/t_i$ is used to express the current wall-thickness ratio, then these equilibrium equations become

$$\sigma_t = \frac{pR_i}{t_i} \left(\frac{x}{y} \right) \quad [34a]$$

$$\sigma_a = \frac{pR_i}{2t_i} \left(\frac{x}{y} \right) \quad [34b]$$

If it is assumed that the radial stress is zero, then the axial strain is zero so the expressions for effective stress and strain become

$$\sigma = \frac{\sqrt{3}}{2} \sigma_t = \frac{\sqrt{3}}{2} p \frac{R_i}{t_i} x^2 \quad [35]$$

$$\epsilon = \frac{2}{\sqrt{3}} \epsilon_t = \frac{2}{\sqrt{3}} \log_e x \quad [36]$$

Then from Equation [8], the pressure may be expressed in terms of x as

$$p = \left(\frac{2}{\sqrt{3}} \right)^{n+1} \frac{\sigma_0 t_i}{R_i} \frac{(\log_e x)^n}{x^2} \quad [37]$$

(d) Thin-Walled Spherical Vessel. By carrying out an analysis similar to the previous case

$$\sigma = \frac{pR_i}{2t_i} x^2 \quad [38]$$

$$\epsilon = 2 \log_e x \quad [39]$$

Then, making use of Equation [8], the pressure may again be expressed in terms of x as

$$p = (2)^{n+1} \frac{\sigma_0 t_i}{R_i} \frac{(\log_e x)^n}{x^2} \quad [40]$$

DETERMINATION OF BURSTING PRESSURE

(a) Thick-Walled Cylindrical Vessel. By substituting Equation [18] in [22], it is possible to express the internal pressure as a function of the effective strain at the inner bore (ϵ_1). The manner in which p varies with ϵ_1 is shown for a number of values of K and n in Fig. 3. In this, it is noticed that the pressure required to strain the vessel increases to a maximum and then begins to diminish as the strain increases. The nature of this variation depends upon the relative rates of work-hardening and reduction in cylinder-wall thickness as the vessel deforms. In this respect, the behavior is similar to that of the simple tension test where

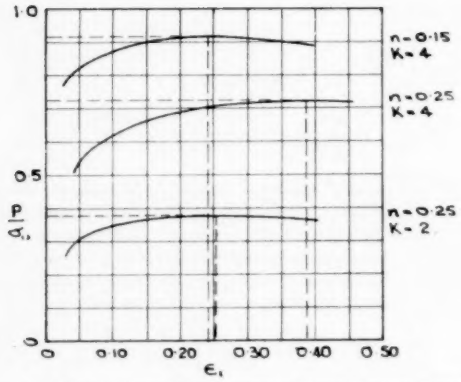

FIG. 3 TYPICAL PRESSURE-INTERNAL BORE STRAIN CURVES

TABLE 1 INNER AND OUTER DIAMETER STRAINS CORRESPONDING TO BURSTING PRESSURE

n	Radius ratio K					
	1.5	2.0	2.5	3.0	3.5	4.0
0.05	0.0419 0.0190	0.0596 0.0236	0.0619 0.0204	0.0701 0.0068	0.0772 0.0067	0.0837 0.0056
0.10	0.0830 0.0369	0.1040 0.0478	0.1220 0.0213	0.1377 0.0170	0.1516 0.0140	0.1640 0.0117
0.15	0.1233 0.0580	0.1541 0.0426	0.1801 0.0329	0.2071 0.0264	0.2231 0.0218	0.2411 0.0184
0.20	0.1670 0.0782	0.2028 0.0577	0.2367 0.0450	0.2662 0.0364	0.2921 0.0303	0.3153 0.0256
0.25	0.2023 0.0987	0.2505 0.0736	0.2915 0.0577	0.3272 0.0409	0.3586 0.0392	0.3866 0.0334
0.30	0.2409 0.1196	0.2970 0.0898	0.3448 0.0709	0.3861 0.0560	0.4229 0.0468	0.4555 0.0418
0.35	0.2790 0.1408	0.3426 0.1065	0.3967 0.0846	0.4435 0.0697	0.4849 0.0569	0.5218 0.0507
0.40	0.3166 0.1623	0.3873 0.1237	0.4472 0.0990	0.4991 0.0820	0.5448 0.0696	0.5857 0.0602
0.45	0.3537 0.1842	0.4310 0.1413	0.4964 0.1139	0.5530 0.0948	0.6029 0.0808	0.6473 0.0702
0.50	0.3905 0.2063	0.4739 0.1595	0.5444 0.1299	0.6054 0.1081	0.6591 0.0926	0.7070 0.0808

Note: Upper figures refer to the inner diameter, lower figures to the outer diameter.

the load-extension curve shows a similar maximum. In both cases the maximum corresponds to an unstable condition beyond which it is not possible to maintain uniformity of deformation. In the tension test, the maximum load corresponds with the formation of a neck in which all subsequent deformation is confined. In the case of the pressure vessel, this instability takes the form of the development of a localized bulge which grows until cracks form and the vessel ultimately bursts.

The bursting, or ultimate, pressure may be calculated from Equation [22] if the two strains ϵ_1 and ϵ_2 corresponding to this maximum pressure are known. By investigating Equation [21], the necessary condition that

$$\left(\frac{dp}{d\epsilon_1}\right)_{\epsilon_1=\bar{\epsilon}_1} = 0$$

is that $\bar{\epsilon}_1$ should satisfy the equation

$$\left(\frac{\bar{\epsilon}_1}{\bar{\epsilon}_2}\right)^n = \frac{e^{\sqrt{3}\bar{\epsilon}_1}}{\left[1 - \left(\frac{1 - e^{\sqrt{3}\bar{\epsilon}_1}}{K^2}\right)\right]} \quad \ldots\ldots [41]$$

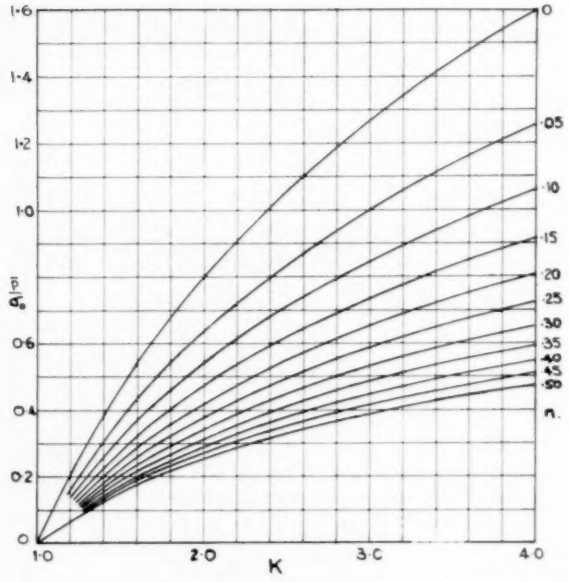

FIG. 4 VARIATION OF BURSTING-PRESSURE RATIO WITH RADIUS RATIO

where $\bar{\epsilon}_2$ is defined as a function of $\bar{\epsilon}_1$ in Equation [18].

Values of $\bar{\epsilon}_1$ and $\bar{\epsilon}_2$ which satisfy this equation are listed in Table 1. In computing these tables it was found simpler to assume $\bar{\epsilon}_1$ and calculate $\bar{\epsilon}_2$ for the given value of K from Equation [18]. These values were then substituted in Equation [41] and the required n determined. The values shown in the table were then obtained by interpolation. The values of $\bar{\epsilon}_1$ and $\bar{\epsilon}_2$ so determined were then substituted in Equation [22] to obtain the bursting pressure ratio ($\bar{p}/\sigma_0$). Values of this ratio for various values of K and n are listed in Table 2 and shown graphically in Fig. 4.

(*b*) *Thick-Walled Spherical Vessel.* In this case the necessary condition that

$$\left(\frac{dp}{d\epsilon_1}\right)_{\epsilon_1=\bar{\epsilon}_1} = 0$$

is that ϵ_1 must satisfy

$$\left(\frac{\bar{\epsilon}_1}{\bar{\epsilon}_2}\right)^n = \frac{e^{3\bar{\epsilon}_1/2}}{\left[1 - \left(\frac{1 - e^{3\bar{\epsilon}_1/2}}{K^3}\right)\right]} \quad \ldots\ldots [42]$$

where ϵ_2 is given in terms of $\bar{\epsilon}_1$ in Equation [30]. The bursting pressure ratio ($\bar{p}/\sigma_0$) is then given by

$$\frac{\bar{p}}{\sigma_0} = \frac{2}{3}\left[\epsilon^n\left\{-\frac{1}{n} + \frac{3\epsilon}{4(n+1)} - \sum_{m=1}^{\infty}(-1)^{m-1}\frac{B_m}{(2m)!}\frac{(3\epsilon/2)^{2m}}{(2m+n)}\right\}\right]_{\epsilon_1}^{\bar{\epsilon}_2} \quad \ldots\ldots [43]$$

(*c*) *Thin-Walled Cylindrical Vessel.* After equating the differential of p with respect to x to zero it is found that the critical value of x is

$$\bar{x} = e^{n/2} \quad \ldots\ldots [44]$$

Substituting this value in Equation [37] leads to the bursting-pressure ratio

TABLE 2 BURSTING PRESSURE RATIO p/σ_0

n	Radius ratio K					
	1.5	2.0	2.5	3.0	3.5	4.0
0.05	0.3706	0.6355	0.8359	1.0029	1.1393	1.2579
0.10	0.3180	0.5409	0.7126	0.8487	0.9619	1.0608
0.15	0.2756	0.4720	0.6203	0.7383	0.8356	0.9185
0.20	0.2481	0.4204	0.5502	0.6535	0.7379	0.8107
0.25	0.2236	0.3784	0.4946	0.5866	0.6618	0.7252
0.30	0.2037	0.3421	0.4495	0.5322	0.5993	0.6556
0.35	0.1879	0.3160	0.4117	0.4871	0.5480	0.5986
0.40	0.1733	0.2909	0.3805	0.4491	0.5047	0.5508
0.45	0.1614	0.2721	0.3536	0.4171	0.4683	0.5105
0.50	0.1514	0.2548	0.3307	0.3897	0.4370	0.4760

$$\frac{p}{\sigma_0} = \frac{t_i}{R_i}\left(\frac{n}{e}\right)^n \frac{2}{(\sqrt{3})^{n+1}} \quad \ldots\ldots [45]$$

(*d*) *Thin-Walled Spherical Vessel.* In a similar manner the bursting-pressure ratio is given by

$$\frac{p}{\sigma_0} = \frac{t_i}{R_i}\left(\frac{n}{e}\right)^n \frac{2^{n+1}}{3^n} \quad \ldots\ldots [46]$$

Simplified Design Formulas

(*a*) *Thick-Walled Cylindrical Vessel.* In the form so far derived, the results are not suitable for design calculations except when purely numerical results are required. By making some simplifying approximations, however, the results may be expressed as relatively simple formulas which are much easier to handle in calculations.

If the value $n = 0$ is considered (ideally plastic material) the stress ratio $S = 1$ so that, for a thick-walled cylinder, the integration of Equation [20] leads to the result

$$\frac{p}{\sigma_0} = \frac{2}{\sqrt{3}} \log_e K \quad \ldots\ldots [47]$$

This suggests that the bursting-pressure ratio for all values of n may approximate to a logarithmic function of K. In order to investigate this, the values given in Table 2 were replotted as a function of $\log_e K$ in Fig. 5. From this graph it will be observed that, using the calculated values at $K = 1$ and 4, the logarithmic approximation slightly underestimates the bursting pressure, the error becoming worse as n increases. Since the error is on the "safe" side for design purposes it may be concluded that $p/\sigma_0 \propto \log_e K$ for all values of n.

Furthermore, if the ratio of the bursting pressure, at $K = 4$, for $n = 0$ to that for any n is plotted against n, Fig. 6, it is found that this ratio shows a linear variation. Thus for values of $K < 4$, the results obtained for the thick-walled cylinder may be approximated by the expression

$$\frac{p}{\sigma_0} = \left(\frac{0.25}{n + 0.227}\right) \log_e K \quad \ldots\ldots [48]$$

It is shown in the Appendix that the constant σ_0 may be related to the ultimate tensile strength σ_u' by the equation

$$\sigma_0 = \left(\frac{e}{n}\right)^n \sigma_u' \quad \ldots\ldots [49]$$

Thus the bursting pressure may be expressed in terms of σ_u'

$$\frac{p}{\sigma_u'} = \left[\frac{0.25}{n + 0.227}\right]\left(\frac{e}{n}\right)^n \log_e K \quad \ldots\ldots [50]$$

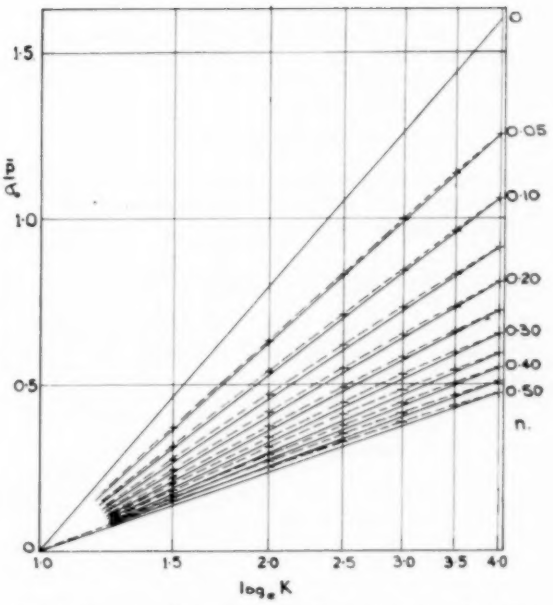

Fig. 5 Bursting-Pressure Ratio Plotted Against Log$_e$ K

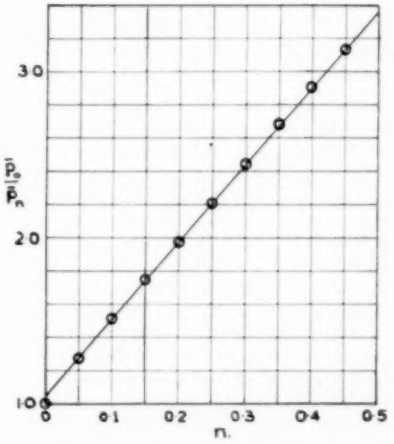

Fig. 6 Variation of Bursting Ratio With n at $K = 4$
($\bar{p}_0$ is bursting pressure at $K = 4$, $n = 0$;
$\bar{p}_n$ is bursting pressure at $K = 4$, $n = n$.)

(*b*) *Thick-Walled Spherical Vessel.* It will be observed from Equations [22] and [43] that the bursting pressure for thick-walled cylindrical and spherical vessels can be expressed as

$$\frac{\bar{p}_c}{\sigma_0} = \left(\frac{1}{\sqrt{3}}\right)^{n+1} f(\sqrt{3}\bar{\imath}_1) \quad \ldots\ldots [51a]$$

and

$$\frac{\bar{p}_s}{\sigma_0} = \left(\frac{2}{3}\right)^{n+1} f\left(\frac{3}{2}\,\bar{\imath}_1\right) \quad \ldots\ldots [51b]$$

respectively.

Also by comparing Equations [41] and [42] it is found that, if $K_c^3 = K_s^3$, then $\sqrt{3}\epsilon_e = 3\bar{\epsilon}_e/2$, where the subscripts c and s refer to the cylinder and sphere, respectively. Thus, for this condition only

$$\bar{p}_s = \left(\frac{2}{\sqrt{3}}\right)^{n+1} \bar{p}_c \quad [52]$$

Thus Equation [50] can be transformed to produce the following approximate equation for determining the bursting pressure of thick-walled spherical vessels

$$\frac{\bar{p}}{\sigma_u'} = \left[\frac{0.433}{n + 0.227}\right]\left(\frac{2}{\sqrt{3}}\,\frac{e}{n}\right)^n \log_e K \quad [53]$$

(*c*) *Thin-Walled Vessels.* The corresponding equations for the bursting pressure of thin-walled vessels are

$$\frac{\bar{p}}{\sigma_u'} = \frac{2}{(\sqrt{3})^{n+1}}\,\frac{t_i}{R_i} \quad [54]$$

for cylindrical vessels, and

$$\frac{\bar{p}}{\sigma_u'} = \frac{2^{n+1}}{3^n}\,\frac{t_i}{R_i} \quad [55]$$

for spherical vessels.

Discussion

The accuracy with which the derived expressions will predict the bursting pressure of the vessels considered depends largely on the validity of two assumptions:

(*a*) That elastic deformations can be entirely neglected.

(*b*) That the Ludwik law expresses the stress-strain relationship to a sufficient degree of accuracy.

That the first assumption is valid can be proved by the following argument: Equation [21] shows that the pressure corresponding with any degree of deformation depends only on an integral in the strain plane between two definite limits. Since this integral is not dependent on prior straining, it is only necessary that the law should fit the experimental data over the range between $\bar{\epsilon}_2$ and $\bar{\epsilon}_1$. If then $\bar{\epsilon}_2$ is greater than the elastic strain at yield, no account need be taken of elastic-stress distributions.

The second assumption, however, is the one most likely to lead to errors in the prediction. A first essential, common to most methods of theoretical analysis, is that the material should be isotropic and homogeneous. Departures from these conditions will have some indeterminate influence on the correlation obtainable. In so far as anisotropy is concerned, it is likely that errors would be reduced if the stress-strain data are obtained from tensile tests on specimens whose axes are tangential. Crossland and Bones made use of torsion tests where the axis of the specimen was parallel to the axis of the vessel.

Of greater importance is the accuracy with which the Ludwik law defines the stress-strain curve for the material. As shown previously, it is only necessary that this agreement extend over the strain range between $\bar{\epsilon}_2$ and $\bar{\epsilon}_1$. In the Appendix, two methods for determining the parameters σ_0 and n are given. When applied to the published stress-strain curve for the material used by Crossland and Bones, the two methods produce the following laws:

The nominal stress-engineering strain curve for the material shows an ultimate tensile strength of 32 tons per sq in. (tsi) with the maximum load occurring at a strain of 0.16.

$$\therefore n = \epsilon_u = \log_e (1 + 0.16) = 0.148$$

$$\sigma_0 = \left(\frac{e}{n}\right)^n \sigma_u' = 49.1 \text{ tsi}$$

Thus using the first method given in the Appendix, the Ludwik law takes the form

$$\sigma = 49.1\epsilon^{0.148} \quad [56a]$$

Using the least-squares technique of curve fitting, as shown in the Appendix, between the limits $0.02 < \epsilon < 0.35$, the law is

$$\sigma = 57.80\epsilon^{0.341} \quad [56b]$$

Hence the ultimate tensile strength, if the material obeys this law, is 32.2 tsi. Using these two values of σ_0 the stress-strain curve for the material is shown in Fig. 1, where the agreement with the theoretical curves for the appropriate value of n can be seen. It is observed readily that the second method produces a much closer agreement between experimental data and the power-law function.

Using the two values of n so obtained, Equation [50] may be used to predict the (bursting pressure)/(ultimate tensile strength) ratio as a function of K. For the law defined by Equation [56*a*], this ratio becomes

$$\frac{\bar{p}}{\sigma_u'} = 1.022 \log_e K \quad [57a]$$

while Equation [56*b*] leads to

$$\frac{\bar{p}}{\sigma_u'} = 0.958 \log_e K \quad [57b]$$

These curves are plotted, together with the experimental results, in Fig. 7 where the good correlation with Equation [57*b*] is readily noted. Comparison of the experimental data with the predicted results shows the effect of the accuracy achieved in fitting the Ludwik law to the stress-strain curve for the material. This may be regarded as evidence of the fact that if the stress-strain curve for the material is represented by this law without error, then the bursting pressure may also be predicted without error.

Further comparison can be made with the results of experiments carried out by Faupel and Furbeck (5). In these tests a range of materials was tested but the radius ratio was not varied appreciably. Since the stress-strain curves for the material were not published, it is not possible to make an accurate comparison. However, values of the proof stress at two offsets were quoted for each material in addition to the ultimate tensile strength. By considering the stress at 0.2 per cent offset and the ultimate tensile strength it was possible to obtain a value for the exponent n; thus

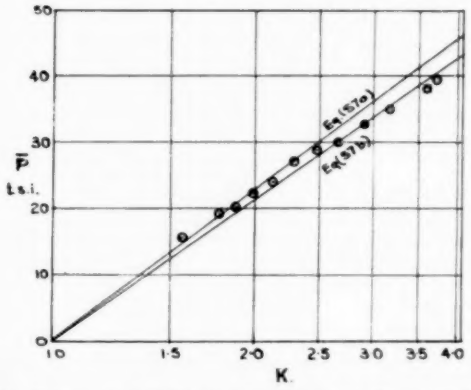

Fig. 7 Comparison of Calculated Bursting Pressure With Experimental Results (3)

$$\frac{\sigma_{\epsilon,2}}{\sigma_u'} = \left(\frac{0.002e}{n}\right)^n$$

When the value of n so obtained was substituted in Equation [50] and the appropriate value of σ_u' employed, the calculated results shown in Table 3 were obtained. It has been shown already that the manner of obtaining n has a considerable effect on the accuracy of the results. In this particular case then, the agreement between the calculated and measured bursting pressures further supports the accuracy of the analysis.

Equation [50] shows that the ratio of bursting pressure to ultimate tensile strength is proportional to $\log_e K$ where the constant of proportionality is a function of n only. Since for the ideally plastic material this constant is 1.155, it is of interest to observe the variation with n. Table 4 shows how the multiplying factor $p/(\sigma_u' \log_e K)$ varies with n. It is of interest to note that for a given vessel made from materials having the same ultimate tensile strength, the bursting pressure decreases as the work-hardening capacity increases (i.e., as n increases). This decrease in bursting pressure is due to the greater amount of deformation leading to a greater reduction in the vessel wall thickness before the bursting pressure is reached. One perhaps obvious conclusion which can be drawn from this comparison is that for vessels subjected to slowly varying pressures a material with a low value of n should be chosen for economy in material utilization. Such a material is one in which the ratio of yield to ultimate strengths approaches unity.

Conclusions

Expressions have been derived for the calculation of bursting pressures for thin and thick-walled cylindrical and spherical pressure vessels by making use of an idealized stress-strain curve. By relating this ideal case to the results of a simple tension test on the material, the bursting pressure may be calculated from a simple design formula. If the stress-strain curve for the material is of suitable form, it is only necessary to know the ultimate tensile strength and the strain at the onset of necking in order to calculate the bursting pressure for any vessel. A more accurate method for determining the parameters of the stress-strain law from the experimental data is given in the Appendix.

It is shown that, provided the material characteristics can be adequately represented by the assumed law, the theoretical predictions show excellent agreement with experimental results.

Bibliography

1 "Mathematical Theory of Plasticity," by R. Hill, Clarendon Press, Oxford, England, 1950, pp. 98–109.

2 "The Overstrain of Tubes by Internal Pressure," by W. R. D. Manning, *Engineering* (London), vol. 159, 1945, pp. 101–102, 183–184.

3 "The Ultimate Strength of Thick Walled Cylinders Subjected to Internal Pressure," by B. Crossland and J. A. Bones, *Engineering* (London), vol. 179, 1955, pp. 80–83, 114–117.

4 "Differential and Integral Calculus," by R. Courant, Blackie and Son, London, England, vol. 1, 1934, p. 422.

5 "Influence of Residual Stress on Behavior of Thick-Wall Closed-End Cylinders," by J. H. Faupel and A. R. Furbeck, Trans. ASME, vol. 75, 1953, pp. 345–354.

Table 3

Cylinder	K	Material[a]	Proof stress 0.01% psi	Proof stress 0.20% psi	Ultimate tensile strength, psi	n	Bursting pressure Calculated psi	Bursting pressure Measured psi	Error (based on measured) %
1	2.74	Cr, Ni, Mo, V	47000	47800	93100	0.188	93400	100000	−6.6
2	2.74	Cr, Ni, Mo, V	141200	159800	177500	0.047	197300	>200000	=
3	2.74	SAE 3320	74300	79500	105400	0.099	113000	106000	6.6
4	2.75	SAE 4340	99400	103900	124100	0.070	136500	133000	2.6
5	2.75	SAE 4340	83400	86500	115300	0.100	124200	120000	3.5
6	2.50	SAE 4340	119600	115600	124600	0.038	127200	117000	8.7
7	2.75	SAE 1045	57500	60900	101800	0.154	105300	107000	−1.6
8	2.75	SAE 1045[b]	76800	81600	122200	0.128	128400	119000	6.2

[a] See Ref. (5) for details of heat-treatment.
[b] Material subjected to bore quench during heat-treatment.

Table 4

n	0	0.05	0.10	0.15	0.20	0.25	0.30	0.35	0.40	0.50
$\frac{p}{\sigma_u' \log_e K}$	1.155	1.101	1.062	1.023	0.986	0.948	0.915	0.885	0.854	0.801

Appendix

Determination of Parameters of Stress-Strain Law

The stress-strain law $\sigma = \sigma_0 \epsilon^n$ relates true stress with the natural strain. In simple tension tests, however, the stress-strain curve for the material is generally given in terms of nominal stress and engineering strain. If the engineering strain is denoted by ϵ' and the nominal stress by σ' then

$$\epsilon = \log_e (1 + \epsilon') \quad [58]$$

and

$$\sigma = \sigma'(1 + \epsilon') \quad [59]$$

(It is assumed that deformation takes place at constant volume.)

For ductile materials, the nominal stress reaches a maximum (the ultimate strength) when[3]

[3] Reference (1), pp. 11–12.

$$\left(\frac{d\sigma}{d\epsilon'}\right)_{\epsilon'=\epsilon_u'} = \left(\frac{\sigma}{1+\epsilon'}\right)_{\epsilon'=\epsilon_u'} \quad [60]$$

where ϵ_u' is the engineering strain corresponding to the ultimate strength. If, in this equation, the engineering strain is replaced by the natural strain, and if the material obeys the assumed stress-strain law

$$n = \epsilon_u = \log_e(1+\epsilon_u') \quad [61]$$

and

$$\sigma_0 = \left(\frac{e}{n}\right)^n \sigma_u' \quad [62]$$

The method just derived agrees with the experimental data at one point and possesses the same slope at that point. Often, however, the stress-strain curve for the material does not bend so sharply as does the power-law function. This means that the two curves may be out of agreement by a considerable amount at some points. This position can be improved by a better method of curve fitting. It is usually regarded that the curve of best fit to agree with experimental data is obtained by the method of least squares.[4] In order to make use of this method the stress-strain law must be written as

$$\sigma = f(\epsilon, \bar{\sigma}_0, \bar{n}) + \left[\frac{\partial f}{\partial \bar{\sigma}_0}(\Delta\sigma_0) + \frac{\partial f}{\partial n}(\Delta n)\right] + \ldots$$

where $\bar{\sigma}_0$ and $\bar{n}$ are approximate values of σ_0 and n obtained from a previous estimate, and $\Delta\sigma_0$ and Δn are corrections to these values. When the appropriate differentials are evaluated, the equation takes the form

$$\sigma = \bar{\sigma}_0\epsilon^{\bar{n}} + \epsilon^{\bar{n}}(\Delta\sigma_0) + \bar{\sigma}_0\epsilon^{\bar{n}}\log_e\epsilon(\Delta n) \quad [63]$$

If, at a number of points i, the corresponding values of ϵ_i and σ_i are read off from the stress-strain curve, then the residual is defined as

$$v_i = \bar{\sigma}_0\epsilon_i^{\bar{n}} + \epsilon_i^{\bar{n}}(\Delta\sigma_0) + \bar{\sigma}_0\epsilon_i^{\bar{n}}\log_e\epsilon_i(\Delta n) - \sigma_i$$

The curve of best fit will be the one which is such that $\sum_{i=1}^{m} v_i^2$ is a minimum; i.e.

$$\frac{\partial(\Sigma v_i^2)}{\partial(\Delta\sigma_0)} = 0 = \frac{\partial(\Sigma v_i^2)}{\partial(\Delta n)}$$

From these two conditions, two equations are obtained which enable the corrections $(\Delta\sigma)$ and (Δn) to be calculated; viz

$$\sum_{i=1}^{m}(\bar{\sigma}_0\epsilon_i^{\bar{n}} - \sigma_i)\epsilon_i^{\bar{n}} + \sum_{i=1}^{m}\epsilon_i^{2\bar{n}}(\Delta\sigma_0) + \sum_{i=1}^{m}\sigma_0\epsilon_i^{2\bar{n}}\log_e\epsilon_i(\Delta n) = 0 \quad [64]$$

$$\sum_{i=1}^{m}(\bar{\sigma}_0\epsilon_i^{\bar{n}} - \sigma_i)\bar{\sigma}_0\epsilon_i^{\bar{n}}\log_e\epsilon_i + \sum_{i=1}^{m}\bar{\sigma}_0\epsilon_i^{2\bar{n}}\log_e\epsilon_i(\Delta\sigma_0) + \sum_{i=1}^{m}\bar{\sigma}_0\epsilon_i^{2\bar{n}}(\log_e\epsilon_i)^2(\Delta n) = 0 \quad [65]$$

For correlation with the experimental tests cited in the paper it was decided to attempt to fit the Ludwik law to the stress-strain curve over the range $0.02 < \epsilon < 0.35$. From the simple tensile-stress curve, starting values for n and σ_0 were chosen to be $\bar{n} = 0.148$, $\bar{\sigma}_0 = 49.1$. Six points were chosen such that $\epsilon_i = 0.02, 0.05, 0.08, 0.15, 0.25, 0.35$. Substitution of these values in Equations [64] and [65] lead to the values for the corrections; viz.

$$\Delta\sigma_0 = 8.49 \text{ and } \Delta n = 0.100$$

A second approximation was determined using the new values $\bar{\sigma}_0 = 57.59$, $\bar{n} = 0.248$. These corrections were then evaluated as; $\Delta\sigma_0 = 0.21$, $\Delta n = -0.007$. Thus the Ludwik law of best fit to the experimental data over the range considered is

$$\sigma = 57.80\epsilon^{0.241} \quad [56b]$$

[4] "Higher Mathematics for Engineers and Physicists," by I. S. and E. S. Sokolnikoff, McGraw-Hill Book Company, Inc., New York, N. Y., 1941, pp. 536–544.

Axially Symmetric Motions of Thick Cylindrical Shells[1]

By I. MIRSKY[2] and G. HERRMANN,[3] NEW YORK, N. Y.

An approximate theory of axially symmetric motions of thick, elastic, cylindrical shells, in which the effect of transverse normal stress is retained, is deduced from the three-dimensional theory of elasticity. The present theory contains, in addition to the usual membrane and bending terms, also the influence of rotatory inertia and transverse shear deformation. Thus it may be specialized to a variety of shell, plate, and solid-cylinder equations. The propagation of free harmonic waves in an infinite shell is studied on the basis of the present theory and the three-dimensional theory of elasticity. Excellent agreement is obtained for the phase velocity of the lowest mode of motion for a wide range of the parameters involved.

Introduction

VARIOUS theories have been established to describe motions of shells, which include, such as the one of Love (1),[4] membrane and bending effects, and, more recently, such as the one of the authors (2), rotatory inertia and shear-deformation effects. However, these theories cannot be expected to hold for shells, whose thicknesses are large with respect to the mean radius of curvature. This is owing to the underlying assumption of all these theories; namely, that the average normal stress through the thickness is negligible.

Previous work on thick shells, by Hildebrand, Reissner, and Thomas (3), and by Vlasov (4), dealt only with the derivation of the various sets of equations of equilibrium, and no solution of these equations was sought.

The present theory of motion retains the effect of average normal stress, and is thus valid for thick shells. Attention is restricted to axially-symmetric motions of cylindrical shells.

The development begins as in (2), with the specification of the dependence of the displacement components on the co-ordinate in the direction of the normal to the middle surface. The stress equations of motion and the appropriate boundary and initial conditions are obtained by application of Hamilton's principle, and Neumann's uniqueness theorem. The stress-displacement relations are deduced from Hooke's law for a three-dimensional, elastic, isotropic continuum, making use of the standard strain-displacement relations.

It is shown that the proposed theory can be reduced (*a*) to less inclusive equilibrium equations for thick shells established by Vlasov (4), (*b*) to Mindlin plate theory (5), and (*c*) to Mindlin-Herrmann rod theory (6).

Calculation of the phase velocity of the fundamental (lowest) mode of motion on the basis of the proposed theory and the three-dimensional theory of linear elasticity, reveals that even for a cylinder whose thickness equals the mean radius, the approximate theory predicts practically the same velocities as the exact theory. In the extreme case of a solid cylinder, the discrepancy still does not exceed 15–20 per cent.

Deformations

A cylindrical shell of inner radius a and outer radius b is considered. The thickness of the shell, $b - a$, is designated by h and the mean radius, $(a + b)/2$, by R. The shell is referred to a co-ordinate system x, θ, z; x being taken in axial direction of the shell, θ in the circumferential, and z in the direction of the normal to the middle surface, measured positive outward from the middle surface of the shell.

The components of the displacement in this co-ordinate system are designated by u_x, u_θ, u_z. Considering axially symmetric motions only, $u_\theta = \partial/\partial\theta = 0$, the displacements will be approximated by $\tilde{u}_x$, $\tilde{u}_z$, which are taken as

$$\left.\begin{aligned} \tilde{u}_x &= u(x, t) + z\psi_x(x, t) \\ \tilde{u}_z &= w(x, t) + z\psi_z(x, t) \end{aligned}\right\} \quad \ldots\ldots\ldots\ldots [1]$$

u and w are seen to be the displacement components of a particle on the middle surface ($z = 0$), ψ_x is the angle of rotation of a cross section in the x-z-plane, ψ_z is the transverse normal strain. The elongations and shears

$$\left.\begin{aligned} e_{xx} &= \frac{\partial u_x}{\partial x} & \gamma_{x\theta} &= 0 \\ e_{\theta\theta} &= \frac{u_z}{R + z} & \gamma_{xz} &= \frac{\partial u_z}{\partial x} + \frac{\partial u_x}{\partial z} \\ e_{zz} &= \frac{\partial u_z}{\partial z} & \gamma_{z\theta} &= 0 \end{aligned}\right\} \quad \ldots\ldots\ldots [2]$$

are then approximated by

$$\left.\begin{aligned} \tilde{e}_{xx} &= \frac{\partial u}{\partial x} + z\frac{\partial \psi_x}{\partial x} & \tilde{\gamma}_{x\theta} &= 0 \\ \tilde{e}_{\theta\theta} &= \frac{w}{R + z} + \frac{z}{R + z}\psi_z & & \\ & & \tilde{\gamma}_{xz} &= \left(\frac{\partial w}{\partial x} + \psi_x\right) + z\frac{\partial \psi_z}{\partial x} \\ \tilde{e}_{zz} &= \psi_z & \tilde{\gamma}_{z\theta} &= 0 \end{aligned}\right\} \quad \ldots [3]$$

[1] This investigation was supported by the United States Air Force, through the Office of Scientific Research of the Air Research and Development Command, under Contract AF 18(600)-1247.

[2] Development Engineer, Foster Wheeler Corporation.

[3] Associate Professor of Civil Engineering, Institute of Flight Structures, Columbia University. Mem. ASME.

[4] Numbers in parentheses refer to the Bibliography at the end of the paper.

Contributed by the Applied Mechanics Division and presented at the Annual Meeting, New York, N. Y., December 1–6, 1957, of The American Society of Mechanical Engineers.

Discussion of this paper should be addressed to the Secretary, ASME, 29 West 39th Street, New York, N. Y., and will be accepted until April 10, 1958, for publication at a later date. Discussion received after the closing date will be returned.

Note: Statements and opinions advanced in papers are to be understood as individual expressions of their authors and not those of the Society. Manuscript received by ASME Applied Mechanics Division, March 5, 1956. Paper No. 57—A-19.

Energy Considerations

The strain-energy density

$$2W^* = \sigma_{xx}e_{xx} + \sigma_{\theta\theta}e_{\theta\theta} + \sigma_{zz}e_{zz} + \sigma_{xz}\gamma_{xz} \quad [4]$$

will therefore be approximated by

$$2W^* = \sigma_{xx}\left(\frac{\partial u}{\partial x} + z\frac{\partial \psi_x}{\partial x}\right) + \sigma_{\theta\theta}\left(\frac{w}{R+z} + \frac{z}{R+z}\psi_z\right) + \sigma_{zz}\psi_z + \sigma_{xz}\left(\psi_x + \frac{\partial w}{\partial x} + z\frac{\partial \psi_z}{\partial x}\right) \quad [5]$$

The strain energy of the shell is obtained by integration over the cross-sectional area, the element of area being $d\theta(R + z)dz$, and over the length l of the shell, say from $-l/2$ to $l/2$, with the result

$$\frac{W}{\pi} = \int_{-l/2}^{l/2}\left[RN_{xx}\frac{\partial u}{\partial x} + RM_{xx}\frac{\partial \psi_x}{\partial x} + N_{\theta\theta}w + M_{\theta\theta}\psi_z + RN_{zz}\psi_z + RQ_x\left(\psi_x + \frac{\partial w}{\partial x}\right) + RM_{xz}\frac{\partial \psi_z}{\partial x}\right]dx \quad [6]$$

The variation of this expression is

$$\frac{\delta W}{2\pi} = \int_{-l/2}^{l/2}\left[RN_{xx}\delta\frac{\partial u}{\partial x} + RM_{xx}\delta\frac{\partial \psi_x}{\partial x} + N_{\theta\theta}\delta w + M_{\theta\theta}\delta\psi_z + RN_{zz}\delta\psi_z + RQ_x\delta\left(\psi_x + \frac{\partial w}{\partial x}\right) + RM_{xz}\delta\frac{\partial \psi_z}{\partial x}\right]dx \quad [7]$$

where

$$\left.\begin{aligned} N_{xx} &= \int_{-h/2}^{h/2}\sigma_{xx}\left(1+\frac{z}{R}\right)dz \\ M_{xx} &= \int_{-h/2}^{h/2}\sigma_{xx}\left(1+\frac{z}{R}\right)z\,dz \\ N_{\theta\theta} &= \int_{-h/2}^{h/2}\sigma_{\theta\theta}\,dz \\ M_{\theta\theta} &= \int_{-h/2}^{h/2}\sigma_{\theta\theta}\,z\,dz \\ N_{zz} &= \int_{-h/2}^{h/2}\sigma_{zz}\left(1+\frac{z}{R}\right)dz \\ Q_x &= \int_{-h/2}^{h/2}\sigma_{xz}\left(1+\frac{z}{R}\right)dz \\ M_{xz} &= \int_{-h/2}^{h/2}\sigma_{xz}\left(1+\frac{z}{R}\right)z\,dz \end{aligned}\right\} \quad [8]$$

The expression for the kinetic energy density T^*, according to the general linear theory, is

$$T^* = \frac{1}{2}\rho\left[\left(\frac{\partial u_x}{\partial t}\right)^2 + \left(\frac{\partial u_z}{\partial t}\right)^2\right] \quad [9]$$

ρ being the mass density. It is used to obtain an approximate expression for the kinetic energy $\bar{T}$ of the shell, employing forms, Equations [1], for the displacements with the result

$$\frac{\bar{T}}{\pi} = \int_{-l/2}^{l/2}\rho\left[Rh\left(\frac{\partial u}{\partial t}\right)^2 + Rh\left(\frac{\partial w}{\partial t}\right)^2 + \frac{h^3}{6}\left(\frac{\partial u}{\partial t}\right)\left(\frac{\partial \psi_z}{\partial t}\right) + \frac{h^3}{6}\left(\frac{\partial w}{\partial t}\right)\left(\frac{\partial \psi_z}{\partial t}\right) + \frac{Rh^3}{12}\left(\frac{\partial \psi_x}{\partial t}\right)^2 + \frac{Rh^3}{12}\left(\frac{\partial \psi_z}{\partial t}\right)^2\right]dx \quad [10]$$

The variation of this expression is

$$\frac{\delta\bar{T}}{2\pi} = \int_{-l/2}^{l/2}\rho\left[Rh\frac{\partial u}{\partial t}\delta\frac{\partial u}{\partial t} + Rh\frac{\partial w}{\partial t}\delta\frac{\partial w}{\partial t} + \frac{h^3}{12}\frac{\partial u}{\partial t}\delta\frac{\partial \psi_x}{\partial t} + \frac{h^3}{12}\frac{\partial \psi_x}{\partial t}\delta\frac{\partial u}{\partial t} + \frac{h^3}{12}\frac{\partial w}{\partial t}\delta\frac{\partial \psi_z}{\partial t} + \frac{h^3}{12}\frac{\partial \psi_z}{\partial t}\delta\frac{\partial w}{\partial t} + \frac{Rh^3}{12}\frac{\partial \psi_x}{\partial t}\delta\frac{\partial \psi_x}{\partial t} + \frac{Rh^3}{12}\frac{\partial \psi_z}{\partial t}\delta\frac{\partial \psi_z}{\partial t}\right]dx \quad [11]$$

Let f_x, f_z denote the x and z-components, respectively, of the external force per unit area acting at the boundary of the shell. The increment (or variation) of work done by these forces will be

$$\delta W_e = \iint_S (f_x\delta u_x + f_z\delta u_z)dS \quad [12]$$

the integration being extended over the whole surface of the shell. This surface consists of the two cylindrical boundaries $z = \pm h/2$ and the two end cross sections, $x = \pm l/2$. Using the form of the displacements Equations [1], the approximate expression δW_e may be written therefore as

$$\delta W_e = 2\pi R\int_{-l/2}^{l/2}(F_x\delta u + m_x\delta\psi_x + q\delta w + m_z\delta\psi_z)dx + 2\pi R[N_{xx}^*\delta u + M_{xx}^*\delta\psi_x + Q_x^*\delta w + M_{xz}^*\delta\psi_z]_{x=-l/2}^{x=l/2} \quad [13]$$

where

$$\left.\begin{aligned} F_x &= f_x\left(1+\frac{z}{R}\right)\Big]_{z=-h/2}^{z=h/2} \\ m_x &= f_x z\left(1+\frac{z}{R}\right)\Big]_{z=-h/2}^{z=h/2} \\ q &= f_z\left(1+\frac{z}{R}\right)\Big]_{z=-h/2}^{z=h/2} \\ m_z &= f_z z\left(1+\frac{z}{R}\right)\Big]_{z=-h/2}^{z=h/2} \\ N_{xx}^* &= \int_{-h/2}^{h/2}f_x\left(1+\frac{z}{R}\right)dz \\ M_{xx}^* &= \int_{-h/2}^{h/2}f_x z\left(1+\frac{z}{R}\right)dz \\ Q_x^* &= \int_{-h/2}^{h/2}f_z\left(1+\frac{z}{R}\right)dz \\ M_{xz}^* &= \int_{-h/2}^{h/2}f_z z\left(1+\frac{z}{R}\right)dz \end{aligned}\right\} \quad [14]$$

Stress Equations of Motion

Hamilton's principle

$$\delta\int_{t_1}^{t_2}L\,dt = 0 \quad [15]$$

is now applied to deduce the equations of motion, as well as the appropriate boundary and initial conditions.

The variation of the approximate expression for the kinetic potential

$$\delta L = \delta T - \delta W + \delta W_e \quad \ldots\ldots [16]$$

after partial integration of all terms in δT with respect to time, and of some terms in δW with respect to x, may be put into the form

$$\left.\begin{aligned}\delta \bar{L} = \int_{-l/2}^{l/2}\int_{t_1}^{t_2} 2\pi \Big[\Big(&-Rh\rho\ddot{u} - \frac{\rho h^3}{12}\ddot{\psi}_x \\ &+ RN_{xx}' + RF_x \Big)\delta u + \Big(-\frac{\rho h^3}{12}\ddot{u} - R\,\frac{\rho h^3}{12}\ddot{\psi}_x \\ &- RQ_x + RM_{xx}' + Rm_x \Big)\delta\psi_x + \Big(-Rh\rho\ddot{w} \\ &- \frac{\rho h^3}{12}\ddot{\psi}_x - N_{\theta\theta} + RQ_x' + Rq \Big)\delta w + \Big(-R\,\frac{\rho h^3}{12}\ddot{\psi}_x \\ &- \frac{\rho h^3}{12}\ddot{w} - M_{\theta\theta} - RN_{xx} + RM_{xx}' + Rm_x \Big)\delta\psi_x \Big]\, dx \\ &+ 2\pi R\,[(N_{xx}^* - N_{xx})\delta u + (M_{xx}^* - M_{xx})\delta\psi_x \\ &+ (Q_x^* - Q_x)\delta w + (M_{xx}^* - M_{xx})\delta\psi_x]_{x=-l/2}^{x=l/2} = 0\end{aligned}\right\} \quad \ldots [17]$$

where primes and dots denote differentiation with respect to x and t, respectively.

This variation of the kinetic potential $\delta\bar{L}$ must be equal to zero for arbitrary values of δu, $\delta\psi_x$, and so on. We thus obtain the four stress equations of motion from the integrand of the preceding expression

$$\left.\begin{aligned} N_{xx}' + F_x &= \rho h\left(\ddot{u} + \frac{h^2}{12R}\ddot{\psi}_x\right) \\ M_{xx}' - Q_x + m_x &= \frac{\rho h^3}{12}\left(\ddot{\psi}_x + \frac{1}{R}\ddot{u}\right) \\ Q_x' - N_{\theta\theta}/R + q &= \rho h\left(\ddot{w} + \frac{h^2}{12R}\ddot{\psi}_x\right) \\ M_{xx}' - N_{xx} - M_{\theta\theta}/R + m_x &= \frac{\rho h^3}{12}\left(\ddot{\psi}_x + \frac{1}{R}\ddot{w}\right)\end{aligned}\right\} \quad \ldots [18]$$

and from the integrated part we identify the starred quantities with the corresponding unstarred quantities.

An application of F, Neumann's uniqueness theorem,[6] leads to the appropriate boundary and initial conditions, which are as follows:

1 At each end of the shell one member of each of the products $N_{xx}u$, $M_{xx}\psi_x$, Q_xw, $M_{xx}\psi_x$, must be specified.

2 The initial displacements and velocities must be specified.

Stress-Displacement Relations

Just as in (2), the relation between the shell stresses defined by the Set [8] and shell displacements introduced by Equations [1], will be derived, starting from the stress-strain relations of an isotropic three-dimensional solid obeying Hooke's law. It appears at present, that the use of Lamé's constants of elasticity, λ and μ, is more convenient than that of Young's modulus E and Poisson's ratio ν. The relations of the three-dimensional theory

$$\left.\begin{aligned}\sigma_{xx} &= (\lambda + 2\mu)e_{xx} + \lambda(e_{\theta\theta} + e_{zz}) \\ \sigma_{\theta\theta} &= (\lambda + 2\mu)e_{\theta\theta} + \lambda(e_{xx} + e_{zz}) \\ \sigma_{zz} &= (\lambda + 2\mu)e_{zz} + \lambda(e_{xx} + e_{\theta\theta}) \\ \sigma_{xz} &= \mu\gamma_{xz}\end{aligned}\right\} \quad \ldots\ldots [19]$$

become those of the present shell theory by using the forms for the Displacements [1] and the definitions for shell Stresses [8], with the result

$$\left.\begin{aligned} N_{xx} &= (\lambda + 2\mu)h\left(u' + \frac{h^2}{12R}\psi_x'\right) + \lambda h\left(\psi_x + \frac{w}{R}\right) \\ M_{xx} &= \frac{(\lambda + 2\mu)h^3}{12R}(u' + R\psi_x') + \frac{\lambda h^3}{6R}\psi_x \\ N_{\theta\theta} &= (\lambda + 2\mu)(\alpha w + \beta\psi_x) + \lambda h(u' + \psi_x) \\ M_{\theta\theta} &= (\lambda + 2\mu)(\beta w + \eta\psi_x) + \frac{\lambda h^3}{12}\psi_x' \\ N_{zz} &= (\lambda + 2\mu)h\psi_x + \lambda h\left(u' + \frac{w}{R} + \frac{h^2}{12R}\psi_x'\right) \\ Q_x &= \kappa^2\mu h\left(\psi_x + w' + \frac{h^2}{12R}\psi_x'\right) \\ M_{xz} &= \kappa^2\frac{\mu h^3}{12R}(\psi_x + w' + R\psi_x')\end{aligned}\right\} \quad \ldots [20]$$

where

$$\left.\begin{aligned}\alpha &= \int_{-h/2}^{h/2}\frac{dz}{R+z} = \log\frac{1 + h/2R}{1 - h/2R} \\ \beta &= \int_{-h/2}^{h/2}\frac{z\,dz}{R+z} = h - R\alpha \\ \eta &= \int_{-h/2}^{h/2}\frac{z^2 dz}{R+z} = \alpha R^2 - Rh\end{aligned}\right\} \quad \ldots\ldots [21]$$

κ is a constant to be determined, as in Mindlin's plate theory (5) and as in the authors' previous work on shells (2).

Displacement Equations of Motion

Substituting the stress displacement Relations [20] into the stress Equations of Motion [18], displacement Equations of Motion [22] are obtained, which may be put in the form of Table 1. This proposed shell theory contains thus, aside from the usual membrane and bending effects, and in addition to the influence of rotatory inertia and transverse-shear deformation, considered by the authors in (2), also the effect of transverse normal stress.

The set of four Equations [22] may be reduced readily to the three equations of (2). This has to be done by keeping in mind that in (2) transverse normal stress has been neglected both in the equations of motion and in the stress-strain relations, while the transverse normal strain, presently ψ_z, was neglected in the equations of motion only, but not in the stress-strain relations for N_{xx}, $N_{\theta\theta}$, and M_{xx}. This was done to let Poisson's ratio effect take place in an unrestrained manner in the z-direction. The proper process of reduction is thus effected by neglecting both N_{zz} and ψ_z in the stress equations of motion, ψ_z in the stress-strain relations, and, in addition, replacing

[6] Reference (1), p. 176.

TABLE 1 EQUATIONS [22]

$u(x,t)$	$\psi_x(x,t)$	$w(x,t)$	$\psi_z(x,t)$	
$(\lambda+2\mu)\frac{\partial^2}{\partial x^2} - \rho\frac{\partial^2}{\partial t^2}$	$\left[(\lambda+2\mu)\frac{\partial^2}{\partial x^2} - \rho\frac{\partial^2}{\partial t^2}\right]\frac{h^2}{12R}$	$\frac{\lambda}{R}\frac{\partial}{\partial x}$	$\lambda\frac{\partial}{\partial x}$	F_x/h
$\left[(\lambda+2\mu)\frac{\partial^2}{\partial x^2} - \rho\frac{\partial^2}{\partial t^2}\right]\frac{h^2}{12R}$	$\left[(\lambda+2\mu)\frac{h^2\partial^2}{12\partial x^2} - \kappa^2\mu - \rho\frac{h^2\partial^2}{12\partial t^2}\right]$	$-\kappa^2\mu\frac{\partial}{\partial x}$	$(2\lambda-\kappa^2\mu)\frac{h^2}{12R}\frac{\partial}{\partial x}$	m_x/h
$-\frac{\lambda}{R}\frac{\partial}{\partial x}$	$\kappa^2\mu\frac{\partial}{\partial x}$	$\left[\kappa^2\mu\frac{\partial^2}{\partial x^2} - \frac{(\lambda+2\mu)\alpha}{Rh} - \rho\frac{\partial^2}{\partial t^2}\right]$	$\left[\frac{\kappa^2\mu h^2}{12R}\frac{\partial^2}{\partial x^2} - \frac{(\lambda+2\mu)\beta}{Rh} - \frac{\lambda}{R} - \rho\frac{h^2}{12R}\frac{\partial^2}{\partial t^2}\right]$	q/h
$-\lambda\frac{\partial}{\partial x}$	$-(2\lambda-\kappa^2\mu)\frac{h^2}{12R}\frac{\partial}{\partial x}$	$\left[\frac{\kappa^2\mu h^2}{12R}\frac{\partial^2}{\partial x^2} - \frac{(\lambda+2\mu)\beta}{Rh} - \frac{\lambda}{R} - \frac{\rho h^2}{12R}\frac{\partial^2}{\partial t^2}\right]$	$\left[\frac{\kappa^2\mu h^2}{12}\frac{\partial^2}{\partial x^2} - (\lambda+2\mu)(1+\frac{\eta}{Rh}) - \frac{\rho h^2}{12}\frac{\partial^2}{\partial t^2}\right]$	m_z/h

$$\lambda + 2\mu = \frac{E(1-\nu)}{(1+\nu)(1-2\nu)} \quad \ldots\ldots\ldots\ldots [23]$$

by

$$\frac{E}{(1-\nu^2)}$$

and

$$\lambda = \frac{E\nu}{(1+\nu)(1-2\nu)}$$

by

$$\frac{E\nu}{(1-\nu^2)}$$

in the stress-strain relations for N_{xx}, $N_{\theta\theta}$, M_{xx}.

It does not appear possible to eliminate ψ_z from the stress-strain relation for, say, N_{xx} directly, by using the stress-strain relation for N_{zz}, as this was done with three-dimensional stresses σ_{xx} and σ_{zz}, because of the factor $(1 + z/R)$ in the defining integral of N_{zz}.

With the foregoing alterations, the first three equations of the Set [22] become identical with the three equations of the Set [42] in (2). The fourth equation of the Set [22], or rather of the Set [18], remains no longer an equation of motion. Since the shell stress M_{zz} does work in ψ_z, as is seen from the expression for the strain energy, Equation [6], M_{zz} can no longer be determined from a stress-strain relation, if ψ_z is neglected. Thus the fourth equation of the Set [18] becomes a relation expressing M_{zz} in terms of other shell stresses and may be disregarded in the solution of problems.

Equations [22] also may be reduced to the more elementary equations of equilibrium of thick shells, advanced by Vlasov (4). If in the present theory the assumption is made, that the cross sections of the shell remain perpendicular to the middle surface, that is

$$\psi_z = -w'$$

and the quantities α, β, η are expanded, to give

$$\alpha = \frac{h}{R} + \frac{h^3}{12R^3}$$

$$\beta = -\frac{h^3}{12R^2}$$

$$\frac{\eta}{Rh} = 0$$

Equations [8.2] of (4) specialized to the case of axial symmetry, are found to be identical to the ones discussed here.

Considering the limiting case of a solid cylinder, the proposed Equations [22] also may be specialized to the ones deduced by Mindlin and Herrmann (6). For a solid cylinder $h = 2R$, and letting $\psi_z = 0$ as was done in (6), the first equation of the Set [22] becomes identical to the first equation of the Set [20] in (6), provided $\kappa_1 = 1$. The third and fourth equations of the Set [22], if added, become identical to the second equation of the Set [20] in (6). The second equation of the Set [22], or rather of Equations [18], becomes an equation relating M_{zz} to other stresses.

WAVE SOLUTIONS

The propagation of free harmonic waves in an infinite cylinder will be studied again to compare solutions of a problem on the basis of the exact three-dimensional theory and the present theory. The solution of the shell equations will be sought in the form

$$\left.\begin{aligned} u(x,t) &= Ue^{i(\omega t-\alpha x)} \\ \psi_x(x,t) &= \Psi e^{i(\omega t-\alpha x)} \\ w(x,t) &= We^{i(\omega t-\alpha x)} \\ \psi_z(x,t) &= \Phi e^{i(\omega t-\alpha x)} \end{aligned}\right\} \quad \ldots\ldots\ldots\ldots [24]$$

Designating by L the wave length, the natural frequency ω and the wave number α are related to the phase velocity c by

$$\omega = \frac{2\pi c}{L}, \quad \alpha = \frac{2\pi}{L} \quad \ldots\ldots\ldots\ldots [25]$$

Introducing further the notations

$$\left.\begin{aligned} m &= h/R \\ s &= c/c_s, \quad c_s^2 = \frac{\mu}{\rho} \\ \delta &= h/L \\ M &= 2(1-\nu)/(1-2\nu) \\ P &= 1/(1-2\nu) \\ A &= 1 - m^2/12 \\ B &= 1 - m^2/6 \\ C &= 1 - m^2/12 + m^4/36 \end{aligned}\right\} \quad \ldots\ldots\ldots [26]$$

and substituting Forms [24] into the set of Equations [22], omitting any external loading, the characteristic equation is calculated to be

Frequency Equation

$$\begin{aligned} F(\delta, s) = \frac{16}{9} A^2(s^2 - M)^2(s^2 - \kappa^2)^2[\pi^8\delta^8] \\ - \left[\left[\left\{\frac{4}{3} A\left(M\alpha m + 4\frac{M\alpha}{m} - \frac{4}{3} m^2P + 4\kappa^2\right)\right\} s^6\right.\right. \\ - \left\{\frac{8}{3} AM\left(M\alpha m + 4\frac{M\alpha}{m} - \frac{4}{3} m^2P\right) - \frac{64}{3} P^2\nu^2C\right. \\ + \frac{16}{3}\kappa^2A\left(M + \frac{M\alpha}{m} + \frac{1}{4} M\alpha m - \frac{m^2}{3}(1+\nu)P\right) \\ \left.\left. + \frac{16}{3} A\kappa^4\right\} s^4 + \left\{\frac{4}{3} M^2A\left(Mm\alpha + 4\frac{M\alpha}{m} - \frac{4}{3} m^2P\right)\right. \\ - \frac{64}{3} P^2M\nu^2C + \kappa^2\left[\frac{8}{3} MA\left(Mm\alpha + 4\frac{M\alpha}{m} - \frac{4}{3} m^2P\right)\right. \\ \left.\left.\left. - \frac{64}{3} P^2\nu^2C - \frac{16}{9} m^2APM\nu\right] + \kappa^4\left[\frac{16}{3} MA - \frac{16}{9} m^2AP\nu\right]\right\} s^2 \\ - \left\{\frac{4}{3} AM^2\kappa^2\left(Mm\alpha + 4\frac{M\alpha}{m} - \frac{4}{3} m^2P\right)\right. \\ \left.\left. - \frac{64}{3} MP^2\nu^2C\kappa^2 - \frac{16}{9} MP\nu m^2A\kappa^4\right\}\right] [\pi^4\delta^4] \\ + \left[\left[\left\{\frac{16}{3} mAP(M\alpha - Pm) + 4\kappa^2\left(Mam + 4\frac{M\alpha}{m}\right.\right.\right. \\ \left.\left.\left. - \frac{4}{3} m^2P\right)\right\} s^4 - \left\{\frac{64}{3} m^2P^2\nu^2B - \frac{64}{3} M\alpha mP^2\nu^2A\right. \\ + \frac{32}{3} MPAm(M\alpha - Pm) + \kappa^2\left[16M^2\frac{\alpha}{m}\right. \\ + 4M^2m\alpha - 64AP^2\nu^2 - \frac{32}{3} m^2P^2\nu A - \frac{16}{3} m^2MP\Big] \\ \left. + \frac{4}{3} Mm\alpha A\kappa^4\right\} s^2 + \left\{\frac{16}{3} M^2PAm(M\alpha - Pm)\right. \\ + \frac{32}{3} MP^2\nu^2(2PBm^2 - 2Mm\alpha A) + \frac{64}{9} m^4P^4\nu^4 \\ + \frac{32}{3} P^2\nu m^2A(4P\nu^2 - M)\kappa^2 + \kappa^4\left(\frac{4}{3} M^2m\alpha A\right. \\ \left.\left.\left. - \frac{16}{3} P^2\nu^2m^2A\right)\right\}\Big] [\pi^4\delta^4] \\ - [s^2 - (M - 4P\nu^2)]\, 16mP\kappa^2(M\alpha - Pm)[\pi^2\delta^2] = 0. \quad [27] \end{aligned}$$

where

$$m = \frac{h}{R} \qquad \alpha = \log_e\left(\frac{1 + \frac{m}{2}}{1 - \frac{m}{2}}\right)$$

$$A = 1 - \frac{m^2}{12}$$

$$B = 1 - \frac{m^2}{6} \qquad M = \frac{2(1-\nu)}{(1-2\nu)}$$

$$C = 1 - \frac{m^2}{12} + \frac{m^4}{36} \qquad P = \frac{1}{(1-2\nu)}$$

There are four roots for s^2, corresponding to the four modes of motion contained in the theory. As in previous work (2), attention will be given only to the fundamental mode, corresponding to the lowest root of s^2. The phase velocity of the fundamental mode, based on the solution of Equation [27], is plotted in Fig. 1. The calculations were carried out with Poisson's ratio $\nu = 0.3$. The coefficient $\kappa^2 = 0.86$ is the same as in the preceding work (2). The ratio m of shell thickness h to mean radius R was taken as 0 (flat plate), $1/20$, $1/4$, $2/3$, 1, and 2 (solid cylinder).

Similarly as in (2), the limiting velocities may be evaluated directly from Equation [27]. For very long waves, $\delta \to 0$, the limiting velocity is

$$s^2 = 2(1 + \nu) \ldots\ldots\ldots\ldots\ldots\ldots [28]$$

which coincides with the exact solution, as discussed in (2). For very short waves, $\delta \to \infty$, Equation [27] reduces to

$$(s^2 - \kappa^2)^2(s^2 - M)^2 = 0 \ldots\ldots\ldots\ldots\ldots [29]$$

and has thus a double root $s^2 = M$ belonging to the two higher modes and a double root $s^2 = \kappa^2$ belonging to the two lower modes.

It may appear surprising, at first sight, that the two lower modes approach the same limiting velocity for short wave lengths. However, as may be seen from the equations of motion, Equations [22], for very short wave lengths (or for a flat plate) the motion in u and ψ_z, which are coupled through Poisson's ratio, becomes independent of the motion in ψ_z and w, which remains coupled through the shear modulus. The phase velocity of each of these two independent motions will be the one of Rayleigh surface waves, ($s = \kappa$), as the wave length approaches zero.

Letting $m \to 0$, the shell approaches a flat plate and it would be possible to reduce the frequency Equation [27] to this special case. The predicted phase velocities would be closer to the exact values than those predicted by the Mindlin plate theory (5). However, since both the exact solution and the solution based on Mindlin plate theory predict practically the same values, the foregoing reduction would have no practical significance.

The opposite limiting case of a solid cylinder is of greater interest. Letting $m = 2$, it is noted that the integral α, defined by Equation [21], approaches infinity. The frequency Equation [27] reduces to

$$\begin{aligned} -\frac{1}{3} A\left(1 + \frac{4}{m^2}\right)(s^2 - \kappa^2)(s^2 - M)^2[\pi^6\delta^6] \\ + \left[\left\{\frac{4}{3} PA + \kappa^2\left(1 + \frac{4}{m^2}\right)\right\} s^4 - \left\{\frac{8}{3} A(MP - 2P^2\nu^2)\right. \\ \left. + M\kappa^2\left(1 + \frac{4}{m^2}\right) + \frac{1}{3} A\kappa^4\right\} s^2 \\ + \frac{1}{3} MA(4MP - 16P^2\nu^2 + \kappa^4)\Big][\pi^4\delta^4] \\ - 4P\kappa^2[s^2 - (M - 4P\nu^2)][\pi^2\delta^2] = 0. \ldots\ldots [30] \end{aligned}$$

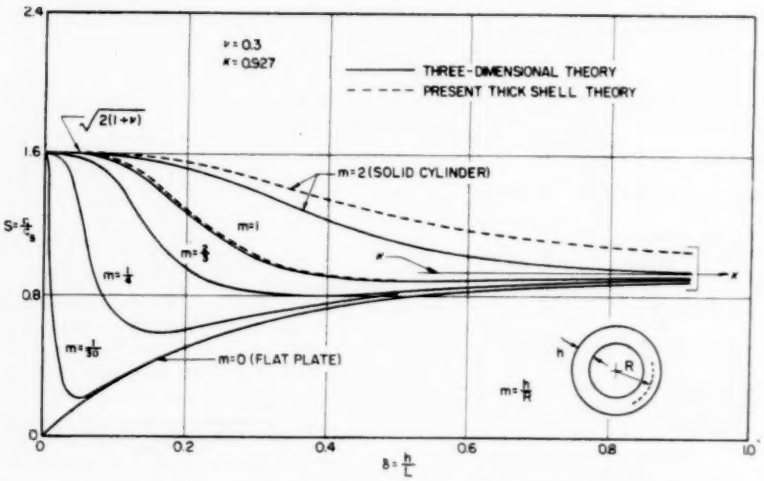

FIG. 1 AXIAL-PHASE VELOCITY (LOWEST MODE) AS A FUNCTION OF WAVE LENGTH

The limiting velocities for both short and long waves reduce to the previous results, Equations [28] and [29]. The phase velocity of the lowest mode calculated from Equation [30] yields values which are closer to the exact ones, than those calculated from the Mindlin-Herrmann theory (6), (with $\kappa_1 = 1$). This is obviously due to the fact that in the present theory the axial displacement is composed of two terms, while in (6) only one term was considered.

SOLUTION BY THREE-DIMENSIONAL THEORY

The frequency equation of axially symmetric harmonic motions in an infinite cylinder has been derived and discussed by the authors in (2), where a numerical evaluation has been carried out for a thickness to mean radius ratio of $m = 1/10$. Results of calculations for $m = 1/4$, $3/4$, and 1 are given here, and, in addition, those of the two limiting cases of a flat plate ($m = 0$) and of a solid cylinder ($m = 2$). The phase velocity $s = c/c_s$ versus $\delta = h/L$ is plotted for these values of m, and is indicated by the solid curves in Fig. 1. The two limiting cases were considered, by specializing first the general frequency equation as derived in (2).

For a flat plate, both $a \to \infty$ and $b \to \infty$, but $b - a = h$ remains constant. The frequency equation in the form of Equation [20] of (2) reduces then to

$$2[1 - \cosh \bar{\beta}h \cosh \bar{\gamma}h] + \left(\bar{F} + \frac{1}{\bar{F}}\right) \sinh \bar{\beta}h \sinh \bar{\gamma}h = 0 \quad \ldots\ldots [31]$$

which represents the Rayleigh-Lamb frequency equation for free motions of an infinite plate (7, 8). The notation is that of (2). For a solid cylinder, the inner radius $a \to 0$. Employing the relations

$$\left.\begin{aligned} K_{10}(\beta) &\sim \frac{2}{\pi} J_1(\beta b) \log\left(\frac{1}{2}\beta a\right) \\ K_{01}(\beta) &\sim -\frac{2}{\pi\beta a} J_0(\beta b) \\ K_{11}(\beta) &\sim -\frac{2}{\pi\beta a} J_1(\beta b) \\ K_{00}(\beta) &\sim \frac{2}{\pi} J_0(\beta b) \log\left(\frac{1}{2}\beta a\right) \end{aligned}\right\} \quad \ldots\ldots [32]$$

the frequency equation in the Form [14] of (2) reduces to

$$(1 + \bar{B})J_1(\beta b)J_1(\gamma b) + F\gamma b J_0(\beta b)J_1(\gamma b) + \gamma b J_0(\gamma b)J_1(\beta b) = 0 \quad \ldots\ldots [33]$$

which represents the Pochhammer frequency equation (9).

A comparison of the curves plotted in Fig. 1, indicates that up to $m = 3/4$ the approximate thick-shell theory of this paper predicts practically the same phase velocities of the lowest mode of motion as the three-dimensional theory. For $m = 1$ the discrepancy does not exceed a few per cent and even in the extreme case of $m = 2$ (solid cylinder), the discrepancy is still not larger than 15–20 per cent.

BIBLIOGRAPHY

1 "A Treatise on the Mathematical Theory of Elasticity," by A. E. H. Love, Dover Publications, New York, N. Y., fourth edition, 1944, Chapter 24.

2 "Three-Dimensional and Shell-Theory Analysis of Axially Symmetric Motions of Cylinders," by G. Herrmann and I. Mirsky, Contract AF 18(600)-1247 of Office of Scientific Research, Air Research and Development Command, United States Air Force, Technical Note No. 1, April, 1955; JOURNAL OF APPLIED MECHANICS, Trans. ASME, vol. 78, 1956, pp. 563–568.

3 "Notes on the Foundations of the Theory of Small Displacements of Orthotropic Shells," by F. B. Hildebrand, E. Reissner, and G. B. Thomas, NACA TN 1833, 1949.

4 "Basic Differential Equations in General Theory of Elastic Shells," by V. Z. Vlasov, NACA TM 1241 Translation, 1951.

5 "Influence of Rotatory Inertia and Shear on Flexural Motions of Isotropic, Elastic Plates," by R. D. Mindlin, JOURNAL OF APPLIED MECHANICS, Trans. ASME, vol. 73, 1951, pp. 31–38.

6 "A One-Dimensional Theory of Compressional Waves in an Elastic Rod," by R. D. Mindlin and G. Herrmann, Proceedings of the First National Congress of Applied Mechanics, ASME, 1952.

7 "On the Free Vibrations of an Infinite Plate of Homogeneous Isotropic Elastic Matter," by Lord Rayleigh, Proceedings of the London Mathematical Society, London, England, vol. 10, 1889, pp. 225–234.

8 "On Waves in an Elastic Plate," by H. Lamb, Proceedings of the Royal Society of London, England, series A, vol. 93, 1917, pp. 114–128.

9 "Über die Fortpflanzungsgeschwindigkeiten kleiner Schwingungen in einem unbegrenzten isotropen Kreiscylinder," by L. Pochhammer, *Journal für Mathematik* (Crelle), vol. 81, 1876, p. 324.

Reflection of an Acoustic Step Wave From an Elastic Cylinder[1]

By RICHARD SKALAK[2] AND M. B. FRIEDMAN,[3] NEW YORK, N. Y.

An elastic cylinder, circular in section and infinite in length, is considered in an infinite acoustic fluid. The object of this paper is the determination of the reflected and diffracted pressure fields at large distances resulting from a plane step wave of pressure impinging on the cylinder and moving in a direction normal to the axis of the cylinder. A formal solution is obtained for the general case of an elastic cylinder. Numerical results are computed for rigid, fixed cylinders, and for rigid, floating cylinders. Two different methods are used to achieve results in the different ranges of time which are of interest. A short time approximation is developed by the use of a double integral-transform method. A mode approach and a single integral transform are used for later times. The results show that the reflected pulse decays quickly, within a time on the order of the transit time of the original wave across the cylinder.

1 Equations for an Elastic Floating Cylinder by Modes

Consider an elastic shell, circular in cross section, homogeneous, and infinitely long, under the action of a plane step wave as shown in Fig. 1. Taking only the dilatational-flexural modes into account[4] and following (1),[5] the simultaneous equations which couple the generalized co-ordinates of the shell and the fluid are

$$\ddot{q}_n + \omega_n^2 q_n = \frac{P_n + \rho \dot{\Psi}_n(a, t)}{m_n} \quad \ldots\ldots [1]$$

$$\dot{q}_n = \frac{V_n}{\rho c} + \frac{\partial \Psi_n}{\partial a} \quad \ldots\ldots [2]$$

ω_n are the natural frequencies of the cylindrical vibrations of the shell in vacuo; q_n and Ψ_n are the generalized co-ordinates of the shell and the fluid-velocity potential, respectively. The radial deflections w of the cylinder and the potential of the reflected waves are

$$\left.\begin{aligned} w &= \sum_{n=0}^{\infty} q_n(t) \cos n\theta \\ \phi(r, \theta, t) &= \sum_{n=0}^{\infty} \Psi_n(r, t) \cos n\theta \end{aligned}\right\} \quad \ldots\ldots [3]$$

The generalized masses are

$$m_n = m \frac{(n^2 + 1)}{n} \quad \text{for} \quad n > 0$$

while $m_0 = 0$, m is the mass of the shell per unit area; p_n, V_n are the time-dependent expansion coefficients of the pressure and velocity of the shock wave. For a step wave of magnitude p_*

$$P_n(r, t) = \left\{\begin{array}{ll} \dfrac{p_* \beta}{\pi}, & n = 0 \\ \dfrac{2p_*}{n\pi} \sin n\beta, & n > 0 \end{array}\right\} \quad t \leq \frac{r + a}{c};$$

$$P_n(r, t) = \left\{\begin{array}{ll} p_*, & n = 0 \\ 0, & n > 0 \end{array}\right\} \quad t > \frac{r + a}{c} \quad \ldots\ldots [4]$$

$$V_n = \left\{\begin{array}{ll} \dfrac{p_*}{\pi} \sin \alpha & n = 0 \\ \dfrac{p_*}{\pi} (\alpha + \sin \alpha \cos \alpha) & n = 1 \\ \dfrac{p_*}{\pi} \left[\dfrac{\sin (n-1)\alpha}{n-1} + \dfrac{\sin (n+1)\alpha}{n+1}\right], & n > 1 \end{array}\right\} 0 \leq t \leq \frac{2a}{c}$$

$$V_n = \left\{\begin{array}{ll} 0, & n = 0 \\ p_*, & n = 1 \\ 0, & n > 1 \end{array}\right\} \quad t \geq \frac{2a}{c} \quad \ldots\ldots [5]$$

where

$$\beta = \arccos\left(\frac{a - ct}{r}\right), \quad \alpha = \arccos\left(1 - \frac{ct}{a}\right)$$

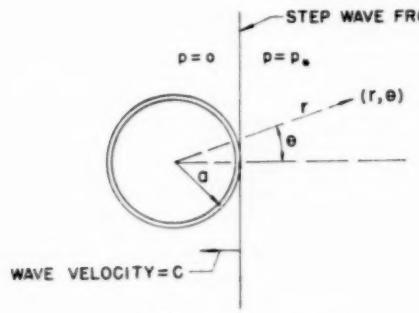

Fig. 1 Initial Conditions

[1] This research was supported by the Office of Naval Research, Contract Nonr 266(27).

[2] Associate Professor, Department of Civil Engineering and Engineering Mechanics, Columbia University.

[3] Assistant Professor, Department of Civil Engineering and Engineering Mechanics, Columbia University.

[4] It is possible to take the extensional modes into account also, using the equations given by Baron (2).

[5] Numbers in parentheses refer to the Bibliography at the end of the paper.

Contributed by the Applied Mechanics Division and presented at the Annual Meeting, New York, N. Y., December 1–6, 1957, of The American Society of Mechanical Engineers.

Discussion of this paper should be addressed to the Secretary, ASME, 29 West 39th Street, New York, N. Y., and will be accepted until April 10, 1958, for publication at a later date. Discussion received after the closing date will be returned.

Note: Statements and opinions advanced in papers are to be understood as individual expressions of their authors and not those of the Society. Manuscript received by ASME Applied Mechanics Division, February 20, 1956. Paper No. 57—A-7.

In order to eliminate the velocity potential between Equations [1] and [2] a transformation with respect to time is applied. Let the transform of $f(r, \theta, t)$ be

$$\bar{f}(r, \theta, \Omega) = \frac{1}{2\pi} \int_0^\infty f(r, \theta, t) e^{-i\Omega t} dt \quad \ldots\ldots [6]$$

Then

$$f(r, \theta, t) = \int_{-\infty - i\gamma}^{\infty - i\gamma} \bar{f}(r, \theta, \Omega) e^{i\Omega t} d\Omega \quad \ldots\ldots [7]$$

It follows by separation of variables that the Ψ_n satisfy Bessel's equation of order n and hence may be written in the form

$$\bar{\Psi}_n(r, \Omega) = A_n H_n^{(2)}\left(\frac{\Omega r}{c}\right) \quad \ldots\ldots [8]$$

considering only diverging waves. A_n is an arbitrary function of Ω and $H_n^{(2)}$ is the Hankel function of order n. If Equation [8] is inverted through [7] and the result substituted into Equations [1] and [2], there results for $\bar{\Psi}_n$ and $\bar{q}_n$ the solutions

$$\bar{q}_n = \frac{\bar{P}_n H_n^{(2)\prime}\left(\frac{\Omega a}{c}\right) - i\bar{\Gamma}_n H_n^{(2)}\left(\frac{\Omega a}{c}\right)}{m_n(\omega_n^2 - \Omega^2) H_n^{(2)\prime}\left(\frac{\Omega a}{c}\right) + \rho\Omega c H_n^{(2)}\left(\frac{\Omega a}{c}\right)} \quad \ldots [9]$$

$$\bar{\Psi}_n = \left[ic\bar{q}_n - \frac{\bar{\Gamma}_n}{\rho\Omega}\right] \frac{H_n^{(2)}\left(\frac{\Omega r}{c}\right)}{H_n^{(2)\prime}\left(\frac{\Omega a}{c}\right)} \quad \ldots\ldots [10]$$

where

$$\left.\begin{aligned} \bar{\Gamma}_n &= -\frac{p_* i^n \epsilon_n}{2\pi\Omega} e^{-i\frac{\Omega a}{c}} J_n'\left(\frac{\Omega a}{c}\right) \\ \bar{P}_n(r, \Omega) &= -\frac{p_* i^{(n+1)} \epsilon_n}{2\pi\Omega} e^{-i\frac{\Omega a}{c}} J_n\left(\frac{\Omega r}{c}\right) \end{aligned}\right\} \quad \ldots [11]$$

and

$$\epsilon_n = 1 \quad \text{for} \quad n = 0 \quad \text{and} \quad \epsilon_n = 2 \quad \text{for} \quad n > 0$$

The total pressure $p(r, \theta, t)$ at any point is the sum of the incident wave pressure whose expansion coefficients are P_n plus the reflected and radiated pressures represented by $\rho\dot{\Psi}_n$; i.e.

$$p(r, \theta, t) = \sum_{n=0}^{\infty} \{P_n(r, t) + \rho\dot{\Psi}_n(r, t)\} \cos n\theta \quad \ldots [12]$$

and in the transformed system

$$\bar{p}(r, \theta, \Omega) = \sum_{n=0}^{\infty} \{\bar{P}_n(r, \Omega) + i\rho\Omega\bar{\Psi}_n(r, \Omega)\} \cos n\theta \quad \ldots [13]$$

Substitution of Equation [9] into [13] and the application of Equation [7] leads to the expression for the total pressure:

$$p(r, \theta, t) = \sum_{n=0}^{\infty} \int_{-\infty - i\gamma}^{\infty - i\gamma} \left[\bar{P}_n - \left(\frac{\bar{\Gamma}_n}{\rho\Omega} - ic\bar{q}_n\right) \frac{H_n^{(2)}\left(\frac{\Omega r}{c}\right)}{H_n^{(2)\prime}\left(\frac{\Omega a}{c}\right)}\right] e^{i\Omega t} d\Omega \cos n\theta \quad \ldots\ldots [14]$$

The three terms in the integrand represent the original step-wave pressure, the reflection from a rigid fixed cylinder, and the pressure due to the motion of the cylinder.

2 Solution for Fixed, Rigid Cylinder by Modes

For a rigid, fixed cylinder, all the q_n describing the motion of the cylinder are zero. The same transformations and manipulations as before lead to an equation for the total pressure which is identical to Equation [14] with $q_n = 0$, all other terms having the same significance as before. This procedure identifies the $\bar{\Gamma}_n$ terms of Equation [14] as the reflection from a rigid, fixed cylinder.

With $q_n = 0$, Equation [14] may be put in the following form which will be used in the numerical computations

$$p(r, \theta, t) = \frac{p_*}{2\pi} \sum_{n=0}^{\infty} i^{(n+1)} \epsilon_n \int_{-\infty - i\gamma}^{\infty - i\gamma} \frac{J_n'\left(\frac{\Omega a}{c}\right) H_n^{(2)}\left(\frac{\Omega r}{c}\right) - J_n\left(\frac{\Omega r}{c}\right) H_n^{(2)\prime}\left(\frac{\Omega a}{c}\right)}{\Omega H_n^{(2)\prime}\left(\frac{\Omega a}{c}\right)} e^{i\Omega\left(t - \frac{\Omega a}{c}\right)} d\Omega \cos n\theta \quad \ldots\ldots [15]$$

where $\bar{\Gamma}_n$ and $\bar{P}_n$ have been replaced according to Equation [11].

3 Solution for Floating, Rigid Cylinders by Modes

Any motion of a floating, rigid cylinder under a step wave will be a translation perpendicular to the wave front. Such a motion is described by q_1 in Equation [15], all other q_n being zero. The results are the same as for a rigid, fixed cylinder, Equation [1], except for the $n = 1$ mode.

For $n = 1$, $m_1 = 2m = \rho a$, since for a neutrally buoyant shell $m = \rho a/2$.

The natural frequency ω_1 of the $n = 1$ mode is zero. Using these results in Equation [10]

$$\bar{q}_1 = \frac{\bar{P}_1 H_1^{(2)\prime}\left(\frac{\Omega a}{c}\right) - i\bar{\Gamma}_1 H_1^{(2)}\left(\frac{\Omega a}{c}\right)}{-\rho a\Omega^2 H_1^{(2)\prime}\left(\frac{\Omega a}{c}\right) + \rho\Omega c H_1^{(2)}\left(\frac{\Omega a}{c}\right)} \quad \ldots\ldots [16]$$

Substituting Equation [16] in the $n = 1$ term of Equation [14] and using Equation [11] for $\bar{P}_1$ and $\bar{\Gamma}_1$, there results after some rearrangement

$$p_1 = \frac{-p_*}{\pi} \int_{-\infty - i\gamma}^{\infty - i\gamma} \frac{J_2\left(\frac{\Omega a}{c}\right) H_1^{(2)}\left(\frac{\Omega r}{c}\right) - J_1\left(\frac{\Omega r}{c}\right) H_2^{(2)}\left(\frac{\Omega a}{c}\right)}{\Omega H_2^{(2)}\left(\frac{\Omega a}{c}\right)} e^{i\Omega\left(t - \frac{a}{c}\right)} d\Omega \quad \ldots\ldots [17]$$

where p_1 is the component of the total pressure in the $n = 1$ mode for a rigid floating cylinder. The pressures for the modes $n \neq 1$ are given again by Equation [15].

4 Numerical Results by Modes

(*a*) *Rigid Fixed Cylinders.* The integral in the nth mode for the total pressure, Equation [15], is evaluated by using the path of integration shown in Fig. 2. The Hankel functions require a

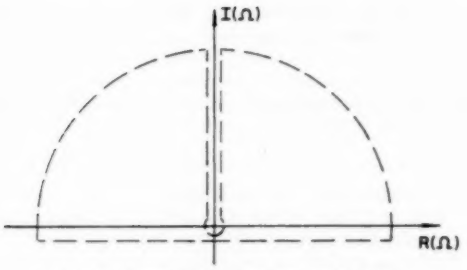

FIG. 2 PATH OF INTEGRATION IN Ω-PLANE

branch cut along the positive imaginary axis. The original integral, Equation [15], is then equal to the integral around the branch cut plus $2\pi i$ times the residues at the poles enclosed by the contour. The poles of the integrand are located using Newton's method in the complex plane and tables of values of J_0, J_1, Y_0, Y_1 for complex arguments (3). The values of the roots are shown in Table 1. These roots occur in pairs and their total number N is given by the formula

$$N = n - \frac{1}{2} + (-1)^n \frac{1}{2} \quad \ldots\ldots\ldots\ldots [18]$$

This formula was derived by the procedure given by Watson (4) for the number of zeros of $K_n(z)$.

TABLE 1 ROOTS OF $\frac{d}{dz} H_n^{(2)}(z) = 0$

n	$z_{1,2}$	$z_{3,4}$
0	No roots	.....
1	$\pm 0.501 + 0.644i$	.....
2	$\pm 1.434 + 0.834i$	.....
3	$\pm 2.637 + 0.970i$	$\pm 0.439 + 1.975i$
4	$\pm 3.289 + 1.197i$	$\pm 1.400 + 2.425i$

In all the numerical evaluations only points far from the cylinder are considered and the values of n used were 0, 1, 2, 3, and 4. This permitted replacement of the Bessel functions involving r by asymptotic formulas for small order and large arguments. The contribution to p_n, the pressure in the nth mode, due to the residues at the poles may be then written

$$[p_n]_{\text{Res}} = \sum_m -p_*(-1)^n \left(\frac{a}{\pi r}\right)^{1/2} (1+i)\epsilon_n \left[\frac{J_n'(z)e^{iz(\tau-2)}}{z^{3/2}\frac{d}{dz}[H_n^{(2)\prime}(z)]}\right]_{z=z_m} \quad \ldots\ldots [19]$$

where z stands for $\Omega a/c$, and z_m are the values at which the poles occur, given in Table 1. The nondimensional time τ is defined by $\tau = (1/a)(ct + a - r)$

It can be shown that when $\tau < 0$, the path of integration of Equation [15] may be closed by a semicircle in the lower half of the Ω-plane, Fig. 2, the integral over the semicircle being zero. Then, by Cauchy's residue theorem, the original integral is zero. Hence τ is a dimensionless "delay time." The value $\tau = 0$ corresponds to the time it takes a wave starting at the cylinder surface at $t = 0$ to reach a radius r traveling at the sound velocity c.

The Integrand [15] has a pole for $n = 0$ at $\Omega = 0$; but not for $n > 0$. The pole at $\Omega = 0$ leads to a contribution which is simply p_*. This may be interpreted as the long-time solution for the total pressure since all other portions decay in time. This assures that the reflected pressure is a pulse of finite duration, as

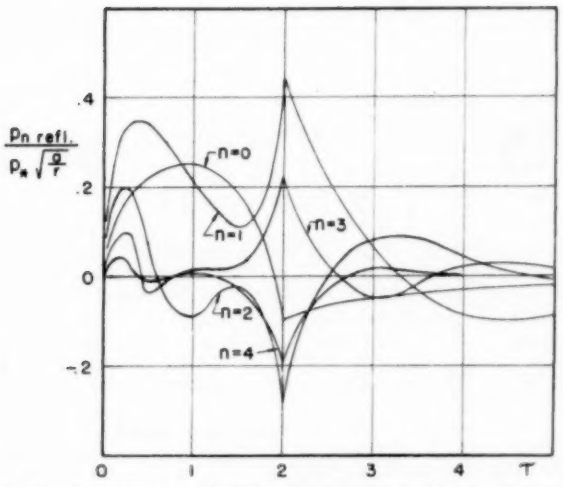

FIG. 3 REFLECTED AND DIFFRACTED PRESSURE BY MODES; RIGID, FIXED CYLINDER

may be expected. Considering only points distant from the cylinder the contribution to p_n due to the branch integrals is

$$[p_n]_{Br} = -p_*\epsilon_n \left(\frac{a}{2\pi r}\right)^{1/2} \int_0^\infty \frac{[I_{n-1}(x) + I_{n+1}(x)][K_{n-1}(x) + K_{n+1}(x)]}{x^{3/2}\{\pi^2[I_{n-1}(x) + I_{n+1}(x)]^2 + [K_{n-1}(x) + K_{n+1}(x)]^2\}} e^{-x(\tau-2)}dx \quad \ldots\ldots [20]$$

where x is real and equal to the absolute values of $(\Omega a)/c$ along the branch cut. I_n and K_n are the modified Bessel functions. Their values were taken from Watson (4) and the Integrals [20] were evaluated numerically.

The sum of Equations [19] and [20] (plus p_* for $n = 0$) for a given n is the pressure $p_n(r, \tau)$ in the nth mode.

The numerical computations were carried through for the first five modes, $n = 0, 1, 2, 3, 4$. It was found that the convergence of the series in θ is very slow for the total pressure which was computed as described in the foregoing. Part of the difficulty may be attributed to the fact that Equation [15] contains the incident pressure which has a slowly convergent series representation in θ. By subtracting the components of the incident pressure, Equation [4], from the respective components of the total pressure (considering large radii) yields values of the reflected pressure components in each mode which converge more rapidly. For $\tau \geq 2$ the incident wave components are constant and the convergence of the reflected pressure components is no better than for the total pressure.

The values of the pressure at the leading edge of the reflected wave ($\tau = 0$) is derived by another method discussed in later sections. Fig. 3 shows the final results for the reflected wave at $\theta = 0$. The total pressure for $\theta = 0$ is equal to these values plus the incident pressure which is simply p_*. The discontinuity of slope at $\tau = 2$ in the components of the reflected pressure arises when the incident pressure is subtracted from the total pressure componentwise because the incident pressure components have a discontinuity in slope.

(*b*) *Rigid, Floating Cylinder.* The total pressure for a rigid floating cylinder is the same as for a rigid, fixed cylinder except for the mode $n = 1$, for which case it is given by Equation [17]. The Integral [17] is evaluated in similar fashion to the rigid case.

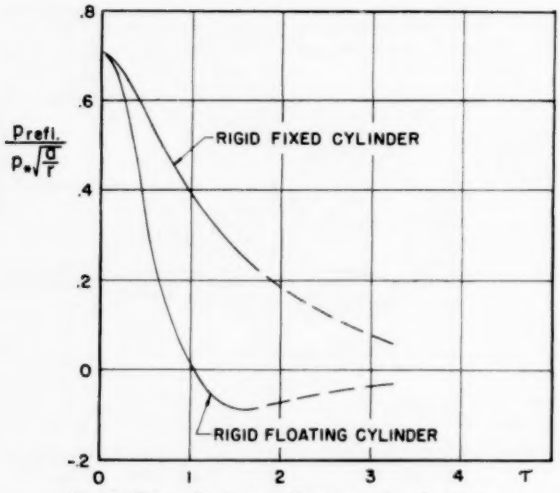

FIG. 4 TOTAL REFLECTED PRESSURE, $\theta = 0$, $r \gg a$

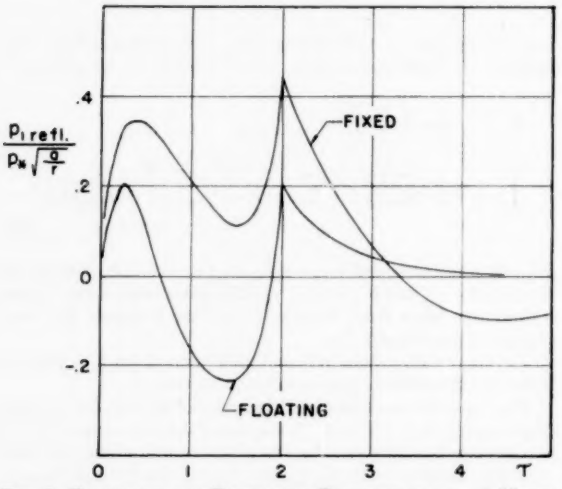

FIG. 5 REFLECTED AND DIFFRACTED PRESSURE IN $n = 1$ MODE; RIGID FIXED AND RIGID FLOATING CYLINDERS

The zeros of $H_2^{(2)}(z)$ are given approximately by Watson,[6] and were refined by computations using tables of Bessel functions of complex arguments (2). The values derived are $z_{1,2} = \pm 0.429 + 1.279i$. As in the case of the rigid, fixed cylinder, only large values of r are considered. The contributions from the poles are

$$[p_1]_{\text{Res}} = \sum_{1,2} 2p_* \left(\frac{2a}{\pi r}\right)^{1/2} e^{i\frac{\pi}{4}} \left[\frac{J_2(z)e^{iz\tau}}{z^{2/3}\dfrac{d}{dz}\,[H_2^{(2)}(z)]}\right]_{z=z_{1,2}} \quad [21]$$

where z stands for $(\Omega a)/c$.

The branch integral in this case is

$$[p_1]_{\text{Br}} = -p_* \left(\frac{2a}{\pi r}\right)^{1/2} \int_0^\infty \frac{K_2(x)I_2(x)e^{-x\tau}}{x^{3/2}[K_2^2(x) + \pi^2 I_2^2(x)]}\,dx \quad [22]$$

where x is real and equal to the absolute value of $(\Omega a)/c$ along the branch cut.

The sum of Equations [21] and [27] is the total pressure in the $n = 1$ mode for a rigid floating cylinder. Subtracting the incident shock-wave pressure in the $n = 1$ mode, the reflected pressure is obtained. A comparison of the reflected pressure in the $n = 1$ mode for the fixed and floating cylinders is shown in Fig. 5.

The reflected pressure, summed for all modes, for the floating cylinder $0 = \theta$, $r \gg a$ is shown in Fig. 4.

5 SOLUTION FOR FIXED, RIGID CYLINDER BY POISSON'S FORMULA

As the convergence of the mode approach is slow in certain regions of interest, it is desirable to convert the Infinite Series [15] into some more amenable form.

For this purpose Poisson's summation formula (5)

$$\sum_{m=-\infty}^{\infty} f(2\pi m) = \frac{1}{2\pi} \sum_{\nu=-\infty}^{\infty} \int_{-\infty}^{\infty} f(\tau)e^{-i\nu\tau}d\tau \quad [23]$$

is appropriate.

By means of Equation [23] the expression for the reflected pressure for the rigid cylinder, which is contained in Equation [15] as

$$p_{\text{refl}}(r, \theta, t) = \frac{p_*}{2\pi} \sum_{n=0}^{\infty} i^{(n+1)}\epsilon_n \int_{-\infty - i\gamma}^{\infty - i\gamma} \frac{J_n'\left(\frac{\Omega a}{c}\right) H_n^{(2)}\left(\frac{\Omega r}{c}\right)}{\Omega H_n^{(2)\prime}\left(\frac{\Omega a}{c}\right)} e^{i\Omega\left(t - \frac{a}{c}\right)} d\Omega \cos n\theta \quad [24]$$

can be transformed to

$$p_{\text{refl}} = \sum_{m=-\infty}^{\infty} \int_{-i\infty+\gamma'}^{i\infty+\gamma'} \int_{-\infty}^{\infty} \frac{ip_* I_n'(s)K_n(s\bar{r})e^{in(\theta+2\pi m)+s(\bar{l}-1)}}{2\pi s K_n'(s)}\,ds\,dn - \int_{-i\infty+\gamma'}^{i\infty+\gamma'} \frac{ip_* I_0'(s)K_0(s\bar{r})e^{s(\bar{l}-1)}}{2\pi s K_0'(s)}\,ds \quad [25]$$

where $\bar{l} = ct/a$ and $\bar{r} = r/a$ and $-\pi \leq \theta \leq \pi$, as p_{refl} has a period of 2π with respect to θ. This result can be obtained formally by calculating the Fourier coefficients of the right-hand side of Equation [24]. Although Equation [25] appears more complicated than the original, important qualitative and quantitative results can be obtained from it.

Consider the integration over n, for a typical term of the m-series

$$F(\bar{r}, \theta, s) = \int_{-\infty}^{\infty} \frac{I_n'(s)K_n(s\bar{r})}{K_n'(s)} e^{in\theta}\,dn \quad [26]$$

The integrand is a single-valued function of n considered as a complex variable for fixed $s \neq 0$. Hence the integral can be evaluated by the method of residues. The location of the poles of the integrand are given by the zeros of $K_n(s)$. These zeros have been shown by Friedlander (6) to be the pure imaginaries $n = i\mu_j$, $(j = 1, 2, \ldots)$ in the upper half plane and $n = -i\mu_j$, $(j = 1, 2, \ldots)$ in the lower half plane for s real and positive. A contour may be chosen in the n-plane consisting of the real axis and a circular arc about the origin resulting in

$$F(\bar{r}, \theta, s) = 2\pi \sum_{j=1}^{\infty} \frac{I_{i\mu_j}'(s)K_{i\mu_j}(s\bar{r})}{\left[\dfrac{\partial}{\partial\mu} K_{i\mu}(s)\right]_{\mu=\mu_j}} e^{[\mp\mu_j(\theta+2m\pi)]} \quad -\pi \leq \theta \leq \pi \quad [27]$$

for $m > 0$ and $m < 0$ while for $m = 0$, the exponential in Equation [27] becomes

[6] Reference (4), p. 512.

$$e^{(-\mu_j|\theta|)}, \quad 0 \leq |\theta| \leq \pi \ldots\ldots\ldots\ldots\ldots [28]$$

Substitution of Expression [27], [28] into [23] yields for the reflected pressure

$$p_{refl} = p_s \int_{-\infty - i\gamma}^{\infty - i\gamma} 2\pi \sum_{j=1}^{\infty} \frac{I_{i\mu_j}'(s)K_{i\mu_j}(s\bar{r})}{\left[\frac{\partial}{\partial\mu} K_{i\mu}(s)\right]_{\mu=\mu_j}} e^{-\mu_j|\theta|}\, ds$$

$$+ p_s \sum_{m=-\infty}^{\infty} (\lambda_m)^2 \int_{-\infty - i\gamma}^{\infty - i\gamma} 2\pi \sum_{j=1}^{\infty} \frac{I_{i\mu_j}'(s)K_{i\mu_j}(s\bar{r})}{\left[\frac{\partial}{\partial\mu} K_{i\mu}(s)\right]_{\mu=\mu_j}} e^{\mu_j(\theta+2m\pi)\lambda_m}\, ds \ldots\ldots [29]$$

where
$$\lambda_m = +1 \quad \text{for} \quad m < 0$$
$$= 0 \quad \text{for} \quad m = 0$$
$$= -1 \quad \text{for} \quad m > 0$$

6 Identification of Reflected and Diffracted Pulses

In the form of Equation [29] the equation for p_{refl} lends itself to an approximation valid just after the reflected wave arrives at a given point. Solutions for large values of s correspond to small values of delay time. Under the assumption s is large, asymptotic expansions of the Bessel functions may be utilized. The appropriate expansions have been derived by Friedlander (6) and lead to an approximation for a typical term of the j-series of Equation [29] in the form

$$c_j \exp\left\{-s\tau_m - s^{1/3} a_j \delta_m\right\} \ldots\ldots\ldots\ldots [30]$$

where, for $m = 0$

$$\tau_0 = \delta_0 + (\bar{r}^2 - 1)^{1/2} + 1,$$
$$\delta_0 = -\frac{\pi}{2} + |\theta| - \cos^{-1}\frac{1}{\bar{r}}, \quad -\pi \leq \theta \leq \pi$$

for $m > 0$

$$\tau_m = \delta_m + (\bar{r}^2 - 1)^{1/2} + 1,$$
$$\delta_m = -\frac{\pi}{2} + \theta + 2m\pi - \cos^{-1}\frac{1}{\bar{r}}, \quad -\pi \leq \theta \leq \pi$$

for $m < 0$

$$\tau_m = \delta_m + (\bar{r}^2 - 1) + 1,$$
$$\delta_m = -\frac{\pi}{2} - \theta - 2m\pi - \cos^{-1}\frac{1}{\bar{r}}, \quad -\pi \leq \theta \leq \pi \quad \ldots [31]$$

and the a_j are positive constants arising in the asymptotic representations of the Bessel functions (5). Each term of the j-series contains a complete series in m, the terms of which have an interesting interpretation. The presence of τ_m in the exponential implies that the Laplace transform corresponding to the mth term, has an original of the form

$$F_m(r, \theta, t)H(t - \tau_m)$$

where H is the Heaviside step function

$$H(t - \tau_m) = \left\{\begin{array}{ll} 0 & \text{for} \quad t < \tau_m \\ 1 & \text{for} \quad t \geq \tau_m \end{array}\right\}$$

Now for $\begin{matrix} m > 0 \\ m < 0 \end{matrix}$, by Equations [31]

$$\tau_{m+1} - \tau_m = 2\pi > 0$$

and also

$$\left.\begin{array}{ll} \text{for } m > 0 & \\ & \tau_m - \tau_0 = 2m\pi + \theta - |\theta| \geq 0 \\ \text{for } m < 0 & \\ & \tau_m - \tau_0 = -2m\pi - 2\theta \geq 0 \end{array}\right\} \ldots\ldots [32]$$

so that
$$\tau_0 \leq \tau_m < \tau_m + 1, \quad \begin{matrix} m > 0 \\ m < 0 \end{matrix} \Big\} \ldots\ldots [33]$$

Each term of the m-series is thus "triggered" at some later time than the preceding term. The $m = 0$ term can be identified as the direct reflection from the cylinder since its time of arrival τ_0 is exactly the time of arrival of the reflected wave computed by ray acoustics as shown in the next section, Fig. 6. The successive terms of the m-series may be considered as diffraction effects, which appear at a finite time after direct reflection has occurred at any point.

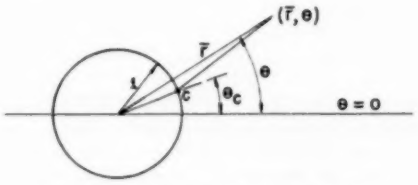

Fig. 6 Geometry of Reflected Front

Friedlander (6) has interpreted this behavior of the individual terms of the m-series as representing diffracted pulses which have encircled the cylinder m times in the direction of increasing θ, and $-m$ times in the direction of decreasing θ. Then τ_m denotes the arrival time of a diffracted front, and the disturbance due to this diffracted pulse starts at τ_m.

As the residue method discussed previously fails when $\delta < 0$, and for $m = 0$, δ is < 0 in the pure reflection region, the term $m = 0$ will be evaluated in a totally different manner.

7 Short-Time Approximation of Reflected Pulse From Poisson's Formula

Consider the integral over n in Equation [25]; i.e.

$$F(\bar{r}, \theta, s) = \int_{-\infty}^{\infty} \frac{I_n'(s)K_n(s\bar{r})}{K_n'(s)} e^{in\theta}\, dn \ldots\ldots [34]$$

For s large, real, and positive, the ratio of the Bessel functions in the integrand is approximately independent of n for $|n/s|$ small. The principal contribution to the integral then arises from large values of n. By applying the WKB method to the differential equation for $K_n(s)$ Friedlander (6) obtained asymptotic expansions valid for s and n both large. These expansions may be used to reduce the n integration of Equation [25] to the asymptotic representation

$$F(\bar{r}, \theta, s) \cong \int_{-\infty}^{\infty} g(n)e^{h(n)}dn \ldots\ldots [35]$$

where

$$h(n) = in\theta - n \sinh^{-1}\frac{n}{s} + (s^2 + n^2)^{1/2}$$

$$g(n) = \left(\frac{1}{2\pi}\right)^{1/2} (s^2 + n^2)^{-1/4}$$

The Integral [35] can be evaluated approximately by the

saddle-point method for both $\bar{r} = 1, \bar{r} \gg 1$. On the surface, i.e., $\bar{r} = 1$, this yields

$$F(1, \theta, s) = \left(- \frac{2\pi}{h''(n_0)} \right)^{1/2} g(n_0) e^{h(n_0)} = -e^{s \cos \theta} \ldots [36]$$

Substitution of Equation [36] into [25], for p_{refl} yields

$$p_{refl} = p_0 H(t - \tau_R) \ldots [37]$$

(The integral in Equation [25] independent of n can be evaluated by the usual asymptotic expansions for Bessel functions of small order and is seen to be of higher order in $[t - \tau_0]\{[t - \tau_0]^{1/2}\}$ with respect to the integral over n.)

For the surface of the cylinder, $\tau_0 = 1 - \cos \theta$ is the time of arrival of the original step wave and the beginning of the reflected pulse at a point $(1, \theta)$ on the cylinder.

Equation [37] implies the usual acoustic doubling of the pressure at any point on the forward surface of the cylinder for small values of $(t - \tau_R)$; i.e., for short times after the passage of the original shock wave over the point.

For $\bar{r} \gg 1$, the saddle-point method applied to [35] yields

$$p_{refl} = p_0 \left[\frac{\cos \theta/2}{2\bar{r}} \right]^{1/2} H(t - \tau_R) \ldots [38]$$

where for distant points $\tau_R = 1 + \bar{r} - 2 \cos \theta/2$ is the time at which the reflected wave is first felt. The fact that τ_R is the arrival time of the earliest reflected wave is shown as follows: From ray acoustics, the time required for a wave originating at any point $(1, \theta_C)$ on the cylinder to reach the point $(\bar{r}, \theta)$ is given by

$$t_R = 1 - \cos \theta_e + [1 + \bar{r}^2 - 2\bar{r} \cos (\theta_e - \theta)]^{1/2} \ldots [39]$$

which for large $\bar{r}$ has a minimum

$$(t_R)_{min} \cong 1 + \bar{r} - 2 \cos \frac{\theta}{2} \ldots [40]$$

confirming the identity mentioned

$$\tau_0 = (\tau_R)_{min} \ldots [41]$$

8 Summary of Results

The total pressure field due to a plane step wave impinging on a cylinder is expressed by Equation [14]. The three terms are, respectively, the pressure of the original wave, a reflection and diffraction corresponding to a fixed rigid cylinder, and the pressure due to the motion of cylinder under the impact.

The numerical results for a rigid, fixed cylinder are shown in Fig. 4. The difference between this case and that of a rigid, but neutrally buoyant, freely floating cylinder is shown in Fig. 5. The difference is due to the translation suffered by the freely floating cylinder. For freely floating but elastic cylinder this translation and the corresponding pressure component will be the same. However, an elastic cylinder will have additional deflections in higher modes of motion causing additional radiated pressures.

The numerical results show that the reflected pulse is of comparatively short duration. For a rigid, fixed cylinder the reflected pressure decays to about 20 per cent of its initial value in a time equal to the transit time of the step wave across the cylinder. For a floating cylinder the decay is even more rapid.

The variation of the initial pressure of the reflected pulse at large distances is given by Equation [38] which shows it varies as $(r)^{-1/2}$ and is a maximum in the direction from which the step wave originated, as may be expected.

BIBLIOGRAPHY

1 "Response of an Elastic Cylindrical Shell to a Transverse Step Shock Wave," by R. D. Mindlin and H. H. Bleich, Journal of Applied Mechanics, Trans. ASME, vol. 75, 1953, pp. 189–195.

2 "A Further Study of the Response of an Elastic Cylindrical Shell to a Transverse Shock Wave," by M. L. Baron, Proceedings of the Second U. S. National Congress of Applied Mechanics, June, 1954, p. 201.

3 "Table of the Bessel Functions $Y(z)$ and $Y_1(z)$ for Complex Arguments," National Bureau of Standards, Columbia University Press, New York, N. Y., 1950. Also—"Table of Bessel Functions $J(z)$ and $J_1(z)$ for Complex Arguments," Works Projects Administration, Columbia University Press, New York, N. Y., 1950.

4 "A Treatise on the Theory of Bessel Functions," by G. N. Watson, Cambridge University Press, New York, N. Y., second edition, 1948.

5 "Methods of Mathematical Physics," by R. Courant and D. Hilbert, Interscience Publishers, New York, N. Y., vol. 1, 1953, p. 73.

6 "Diffraction of Pulses by a Circular Cylinder," by F. G. Friedlander, Institute of Mathematical Sciences, New York, N. Y., Research Report No. EM-64, April, 1954.

Axial-Temperature-Gradient Bending Stresses in Tubes

By F. G. HAMMITT,[1] ANN ARBOR, MICH.

A study is conducted of the bending stresses induced in a thin-walled tube adjacent to a joint between the tube and a heavier section by an axial temperature gradient imposed across the assembly. A solution is shown utilizing basic relations taken from the existing literature for a tube of uniform wall thickness attached at either end to a flange of infinite stiffness. Both long and short tubes are considered. The possibility of substantial reductions of stress through the use of a tapered wall thickness is discussed. Approximate methods are developed for the calculation of stress and wall thickness under conditions in which the wall thickness is varied in each instance to give (*a*) constant radius of curvature (or arbitrary radii of curvature), (*b*) constant stress, and (*c*) arbitrary stress distribution.

Nomenclature

The following nomenclature is used in the paper:

D = plate-stiffness factor
E, μ = modulus of elasticity, Poisson's ratio
h, r = tube-wall thickness and average radius (Fig. 2)
x, y = dimensions measured approximately parallel and normal to tube center line (Figs. 1 and 3)
R = radius of curvature of deflected element of tube wall
A—D, = constants of integration
C_2—C_6 = constants of integration
β = $(Eh/4Dr^2)^{1/4}$
l = tube length
σ = bending stress
Q = heat flow
k = thermal conductivity
A = area
ΔT = temperature difference between ends of tube
d = tube diameter
r = tube radius
α = temperature coefficient of expansion
C_1, K_1, K_2 = constants defined in Equations [10], [13], [18]
p = slope dy/dx
e = base of natural logarithms

Introduction

A major problem in the design of high-temperature equipment is the provision for and analysis of thermal stresses. This problem is of especial importance in heat-exchange equipment, certain types of turbomachinery (as turbines, compressors, and pumps handling high-temperature fluids), in nuclear reactors, furnaces, and numerous other equipment items.

The thermal-stress problems which must be considered involve (*a*) a radial-temperature gradient across a tube wall as in a heat exchanger or across the disk of a rotating machine, and (*b*) an axial-temperature gradient which may be encountered in certain types of heat-exchange equipment, in the support casings of pumps and turbines, and in various other applications.

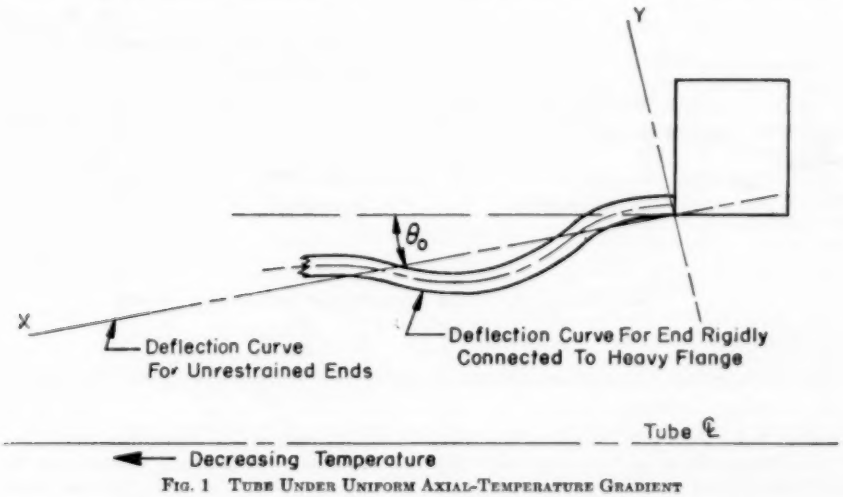

Fig. 1 Tube Under Uniform Axial-Temperature Gradient

[1] Associate Research Engineer, Engineering Research Institute, Lecturer, Mechanical Engineering Department, University of Michigan. Mem. ASME.

Contributed by the Applied Mechanics Division and presented at the Annual Meeting, New York, N. Y., December 1–6, 1957, of The American Society of Mechanical Engineers.

Discussion of this paper should be addressed to the Secretary, ASME, 29 West 39th Street, New York, N. Y., and will be accepted until April 10, 1958, for publication at a later date. Discussion received after the closing date will be returned.

Note: Statements and opinions advanced in papers are to be understood as individual expressions of their authors and not those of the Society. Manuscript received by ASME Applied Mechanics Division, August 6, 1956. Paper No. 57—A-13.

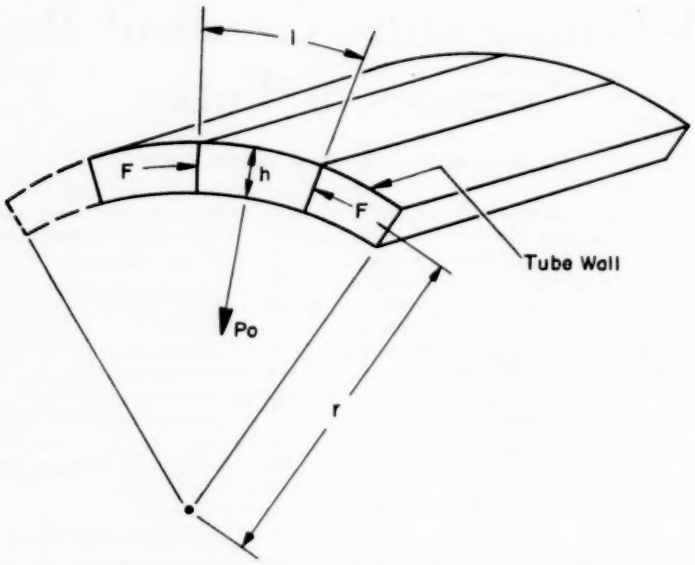

FIG. 2 CYLINDER SEGMENT AS BEAM ON ELASTIC FOUNDATION

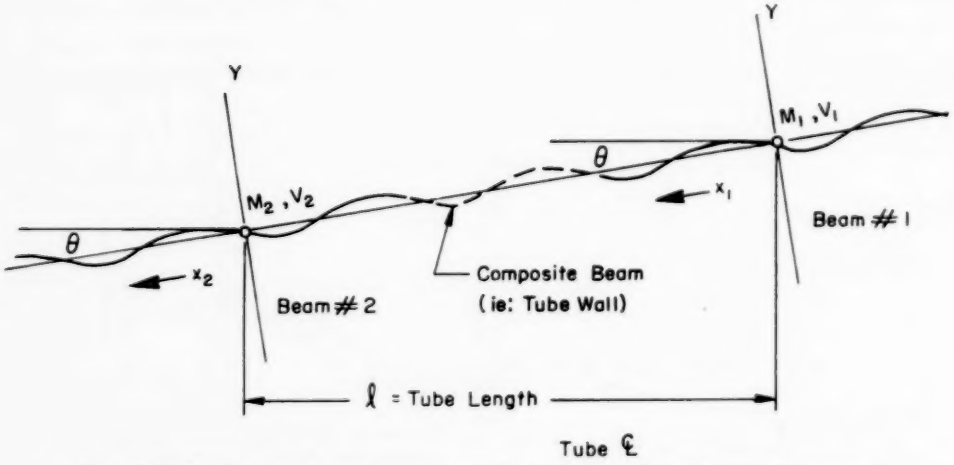

FIG. 3 TUBE UNDER AXIAL-TEMPERATURE GRADIENT AS COMPOSITE BEAM ON ELASTIC FOUNDATION

The present treatment is concerned with stresses resulting from the existence of an axial-temperature gradient in a tube, which may be either a portion of a heat exchanger or of the casing or rotor of a turbomachine. In general, stresses of this sort will exist in combination with other types of stresses, as, for example, the direct stress due to pressure loading of a pipe. The total stress and deflection at a point are the result of a summation of their individual components.

This paper considers only the components resulting from the thermal conditions.

General Situation

A thin-walled tube under a uniform axial-temperature gradient, with unrestrained ends, is not thermally stressed, since it is free to assume the deflection curve dictated by the axial-temperature distribution (it is assumed that the axial gradient is symmetrical about the center line). Under these conditions the deflected tube will become a straight cone. However, if the tube is joined at the ends to members of increased cross section, i.e., flanges, the situation is basically altered. In general, the axial-temperature gradient in the flanges will be less than that in the tube, in many cases approximately zero, considering the larger cross-sectional area available to a constant heat flux. Consequently, the angle of deflection assumed by the flange will be less than that of the tube. Since tube and flange are joined securely, the deflection curve and its slope must be continuous at this point, and the tube will be forced to accommodate itself approximately to the slope and deflection which would be assumed by the flange in the absence of the tube (due to the presumably much greater stiffness of the flange). Thus as shown in Fig. 1, there will be bending stresses induced in the tube which are at a maximum at the joint and extend a considerable axial distance into the tube.

Constant-Wall-Thickness Case

If a tube of constant wall thickness is joined to a flange of relatively large stiffness, the tube being subjected to a uniform axial-temperature gradient and the flange to zero axial gradient (assuming that a constant heat flux is conducted axially through the flange and tube), longitudinal elements of the wall will be under the condition of beams with bending stiffness

$$D = \frac{Eh^3}{12(1 - \mu^2)} \quad [1]$$

on an elastic foundation exerting a force of Eh/r^2 per unit length and width, per unit deflection.[2]

The deflection curve for a semi-infinite, thin-walled tube, built into a flanged end, and under axial-temperature gradient is shown in Fig. 1. It is assumed that the axis coincides with the deflected position of the tube wall for the case of unrestrained ends. Then for restrained ends, the tube-wall deflection at the end is zero (since the flange and tube are assumed at equal temperature at the joint), but the slope is equal to tan θ, where θ is the angle of deflection of the unrestrained tube wall. Using the beam on an elastic-foundation analysis, the basic differential equation is

$$D \frac{d^4y}{dx^4} = \frac{Eh}{r^2} y \quad [2]$$

The deflection curve (and the bending stress) from this analysis is a damped harmonic curve. For most metallic structural materials, the stress will be reduced to about 15 per cent of the maximum value at a distance from the tube end equal to about one third of the square root of the product of tube diameter and wall thickness, while the deflection is reduced to this value at a distance from the end equal to the square root of this product. Thus if the tube is quite short, it will be necessary to consider both ends. The general solution for the differential Equation [2] is

$$y = e^{\beta x}(A \cos \beta x + B \sin \beta x) + e^{-\beta x}(C \cos \beta x + D \sin \beta x) \quad [3]$$

where

$$\beta = (Eh/4Dr^2)^{1/4}$$

This expression contains four arbitrary constants and is subject to four boundary conditions; i.e., the deflection must be zero and the angle of deflection that of an unrestrained beam at each tube end. Thus four equations can be set up for determining the four constants. The moment can be calculated from the second derivative of y and, from it, the bending stress at any point.

[2] "Strength of Materials," by S. Timoshenko, D. Van Nostrand and Company, Inc., New York, N. Y., second edition, vol. 2, 1956, pp. 2 and 126.

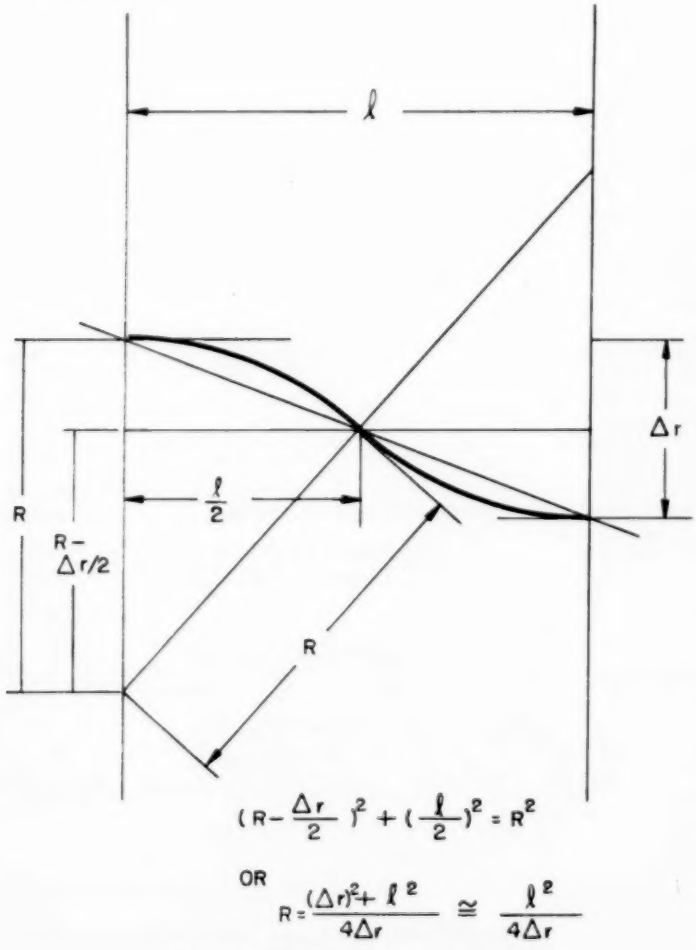

Fig. 4 Constant-Radius-of-Curvature Case

Design Methods for Reducing Stress

Where the axial-temperature gradient is severe and the material is weakened seriously by elevated temperature, it may be found that the bending stresses, as calculated in the foregoing, for the case of constant wall thickness, are too great for a successful design. Several possible approaches have been considered for designing and calculating structures consistent with reasonable stresses under the most stringent conditions. These methods involve a variable tube-wall thickness.

Constant Radius of Curvature and Possible Variations. The maximum bending stress in an element of the tube wall can be reduced if its radius of curvature is maximized at all points (if the resultant benefits are not sacrificed by too great an increase in wall thickness). Consider a tube built into a much heavier section, with consequent reduced axial-temperature gradient and slope of deflection curve in the heavier section, so that the wall exhibits virtually zero slope of the deflection curve at each end. As shown in Fig. 4, a maximum radius of curvature may be obtained at all points if the deflection curve is caused to follow a constant radius in each half, changing sign at mid-span. To calculate this radius, it is first necessary to compute the change in tube radius Δr from the known temperatures at the tube ends and the properties of the material. The radius of curvature then may be found easily from geometric considerations, Fig. 4. If it is desired that the stress level be

higher at one end of the tube than at the other, because of a difference in allowable stress because of different temperatures, it is possible in the same way to use a shorter radius at the high-stress end.

One possibility is to design the tube-wall thickness in such a way that the deflection curve, which would be produced by the temperature variations alone if the wall were perfectly free to move radially, will follow the assumed constant-radius curves. A rough estimate shows that very little deviation from this "temperature-controlled" deflection curve actually will occur because of the large restoring hoop stresses that would result. The necessary wall thickness to produce this result may be calculated for each point from the consideration of continuity of heat flow. This may be accomplished graphically, using the standard procedure of a heat-flow net. It also may be approximated by dividing the tube length into a number of segments and calculating the required mean thickness of each segment to pass the total heat flow, considering the temperature drop between segment medians as approximated from the desired deflection curve, assuming the deflection to be directly proportional to the temperature. If desired, corrections for radiation and convection losses from the wall may be included. Then if the deflection curve follows the assumed curve, the bending stress would be

$$\sigma = \frac{Eh}{2R(1 - \mu^2)} \quad [4]$$

If the wall thicknesses are computed as suggested, the actual deflection curve will not follow the assumed curve exactly since there are bending stresses which are in a direction to reduce the curvature. Thus the actual stresses will be slightly less than those calculated from this method. The wall thickness resulting from calculations of this type will form a double taper with the minimum thickness at the center. Therefore the stresses will be a maximum at the ends and minimum at the mid-point (where a weld might be located advantageously). It may not be useful in some cases to utilize as thick a section at the ends as the foregoing method would indicate because of the increase of stress with thickness.

If it is desired to change the stress distribution, the following procedure might be used: A new deflection curve can be assumed deviating in the desired direction. If this curve can be expressed as an equation, the radius of curvature can be calculated at any point from the second derivative. Otherwise the curve can be plotted to enlarged vertical scale, and the local radius of curvature found in any region from consideration of three points in the close vicinity, and the application of the relations shown in Fig. 5. Once the deflection curve is assumed, the wall thicknesses can be computed as suggested for the constant-radius case. Then it is possible to calculate the bending stresses by Equation [4]. To achieve the desired stress distribution in this way is a trial-and-error process. It is also possible to assume a wall-thickness distribution, compute deflection from temperature, and then check stresses by the method outlined above.

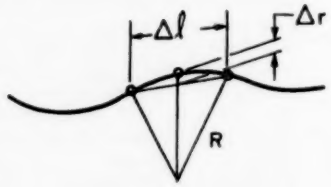

$$R^2 = \left(\frac{\Delta l}{2}\right)^2 + (R - \Delta r)^2$$

$$\text{OR} \quad R = \frac{(\Delta l)^2 + 4(\Delta r)^2}{8\Delta r} \cong \frac{(\Delta l)^2}{8\Delta r}$$

FIG. 5 LOCAL RADIUS OF CURVATURE

Constant-Stress Design and Variations. Consider again the case of a tube under axial-temperature gradient built into relatively heavy-end sections, where the temperature gradient is controlled by heat conduction axially through the wall.

For a given minimum and/or maximum wall thickness, that distribution of wall thickness which gives a constant stress throughout, or over a reasonable portion of the length, may be desired. On the other hand, it may be desirable in some cases to allow a higher stress at one end than the other because of temperature-weakening effects on the material. Considering the first alternative, it will be noted from Equation [4] that the stress (based on the approximate assumption that the actual deflection curve is the same as the "temperature-controlled" deflection curve) is constant if h/R is constant. This condition leads to the following differential equation and solution

$$\sigma = \frac{Eh}{2R(1 - \mu^2)} = \frac{Eh}{2(1 - \mu^2)} \frac{d^2y}{dx^2} \quad [5]$$

where σ is a constant.

From the heat-flow equation

$$Q = kA\, dT/dx \text{ and } A = \pi d h \quad [6]$$

Then

$$\frac{dx}{dT} = \frac{k\pi dh}{Q} \quad [7]$$

and

$$\frac{dy}{dT} = \alpha \frac{d}{2}, \quad \text{so that} \quad \frac{dx}{dy} = \frac{2}{\alpha d} \frac{k\pi d}{Q} h \quad [8]$$

or

$$h = \frac{dx}{dy} \Big/ \frac{2k\pi}{\alpha Q} \quad [9]$$

Let

$$C_1 = \frac{2k\pi}{\alpha Q}, \quad \text{so} \quad h = \frac{1}{C_1} \frac{dx}{dy} \quad [10]$$

Substitute Equation [10] into [5] to give

$$\frac{1}{C_1} \left(\frac{d^2y}{dx^2}\right) \left(\frac{dx}{dy}\right) \frac{E}{2(1 - \mu^2)} = \sigma \quad [11]$$

or

$$\frac{d^2y}{dx^2} - \frac{2\sigma C_1(1 - \mu^2)}{E} \frac{dy}{dx} = 0 \quad [12]$$

Letting

$$K_1 = \frac{2\sigma(1 - \mu^2)C_1}{E} \quad [13]$$

we have

$$\frac{d^2y}{dx^2} - K_1 \frac{dy}{dx} = 0 \quad [14]$$

The solution to this second-order, linear, homogeneous, constant-coefficient, differential equation may be written

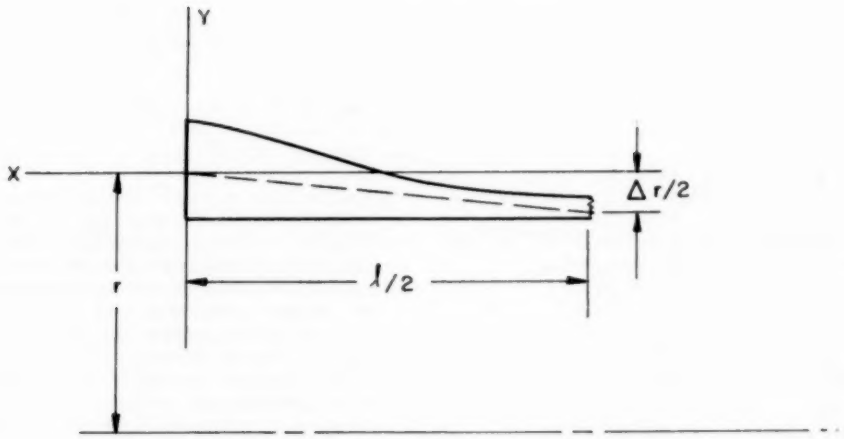

FIG. 6 SCHEMATIC REPRESENTATION OF CONSTANT-STRESS SOLUTION

$$y = C_2 e^{K_1 x} + C_3 \quad \ldots\ldots [15]$$

Assume, for example, the following boundary conditions:

$$(a) \text{ at } x = 0 \qquad (b) \text{ at } x = l/2$$
$$y = 0 \qquad\qquad y = \Delta r/2$$

The x-axis is considered to be parallel to the center line of the tube and to pass through the tube wall at one end, Fig 6. The second boundary condition implies that the deflection curve is to be symmetrical about the mid-span point which is then a point of inflection. However, the equation here considered covers only half the length. For the total solution, a similar equation with the origin at the opposite end would be considered.

If these boundary conditions are applied, Equation [15] becomes

$$y = \frac{\Delta r[\exp(K_1 x) - 1]}{2[\exp(K_1 l/2) - 1]} \quad \ldots\ldots [16]$$

where

$$\Delta r = \alpha \frac{d}{2} \Delta T$$

Substitute this and Equation [13] into Equation [16]; substituting also for C_1

$$y = \frac{\alpha d \Delta T\{\exp[4\sigma(1-\mu^2)k\pi x/\alpha QE] - 1\}}{4\{\exp[2\sigma(1-\mu^2)k\pi l/\alpha QE] - 1\}} \quad \ldots\ldots [17]$$

Letting

$$K_2 = 2(1-\mu^2)k\pi/\alpha E \quad \ldots\ldots [18]$$

Equation [17] becomes

$$y = \frac{\alpha d \Delta T[\exp(2K_2\sigma x/Q) - 1]}{4[\exp(K_2\sigma l/Q) - 1]} \quad \ldots\ldots [19]$$

Differentiating Equation [19] we may write

$$\frac{dy}{dx} = \frac{\alpha d \Delta T K_2 \sigma \exp(2K_2\sigma x/Q)}{2[\exp(K_2\sigma l/Q) - 1]} \quad \ldots\ldots [20]$$

and then substituting Equation [20] into [10]

$$h = \frac{Q[\exp(K_2\sigma l/Q) - 1]\exp(-2K_2\sigma x/Q)}{k\pi d \Delta T K_2 \sigma} \quad \ldots\ldots [21]$$

Thus we have a solution showing an exponentially decreasing wall thickness up to the mid-point. Considering the other half of the tube length as a mirror image, the wall thickness will then increase in the same way.

To solve any particular case, consider Equations [18] and [22]. The steps in the solution are as follows:

(*a*) Evaluate K_2 from Equation [18] from the material characteristics.

(*b*) Select an allowable stress limit σ and evaluate h from Equation [22] as a function of Q.

(*c*) From physical conditions related either to the required thickness at the flange end for bolting, and the like, or to the minimum allowable thickness at mid-span governed by fabrication, pressure, and so on, select h. Solve for Q.

(*d*) If h at any point or Q is unacceptable for other reasons, re-examine σ and repeat.

In this way it will become apparent whether or not a constant-stress solution is possibly consistent with the other requirements.

VARYING STRESS

Rather than having a constant stress, it may be desirable that the stress vary in a predetermined manner along the tube axis. For example, it may be required that stress should increase as some function $f(x)$ of distance x from the high-temperature end (since allowable stress is an inverse function of the temperature). In that case, it is necessary to substitute $f(x)$ for σ in Equation [5]

$$\frac{Eh}{2(1-\mu^2)} \frac{d^2y}{dx^2} = f(x) \quad \ldots\ldots [22]$$

and Equation [12] can be written

$$\frac{d^2y}{dx^2} - \frac{2f(x)C_1(1-\mu^2)}{E} \frac{dy}{dx} = 0 \quad \ldots\ldots [23]$$

or

$$\frac{d^2y}{dx^2} - \frac{2K_2}{Q} f(x) \frac{dy}{dx} = 0 \quad \ldots\ldots [24]$$

Setting $dy/dx = p$

$$\frac{dp}{dx} - \frac{2K_2}{Q} p f(x) = 0 \quad \ldots\ldots [25]$$

and
$$\frac{dp}{p} = \frac{2K_2}{Q} f(x)dx \quad [26]$$

so
$$C_4 \exp\left(\frac{2K_2}{Q}\int_0^x f(x)dx\right) = dy/dx \quad [27]$$

or
$$y = C_4 \int \exp\left[\frac{2K_2}{Q}\int_0^x f(x)dx\right] dx + C_5 \quad [28]$$

If the boundary conditions used in the case of constant stress are assumed again, the condition that for $x = 0$, $y = 0$ gives $C_5 = 0$.

C_4 must be evaluated after integration. Depending on the desired stress function $f(x)$, this integration may or may not be graphical. With C_4 evaluated it is possible to substitute Equation [28] into [10] to give the necessary expressions for h

$$h = \alpha Q \left[\exp\left(\frac{-2K_2}{Q}\int_0^x f(x)dx\right)\right] \Big/ 2k\pi C_4 \quad [29]$$

If, for example, $f(x) = \sigma_0 + \beta x$

$$h = \alpha Q \exp\left[\frac{-2K_2}{Q}\left(\sigma_0 x + \beta\frac{x^2}{2}\right)\right] \Big/ 2k\pi C_4 \quad [30]$$

Equation [29] or [30] is analogous to [21] in the constant-stress case. For a given solution it is necessary only to consider Equations [18] and [29], and proceed in the manner previously outlined.

Whatever design method is used, it is always possible to use "locked-up" residual stresses to prevent excessive stresses (or plastic deformation) in the operating condition. In other words, if the component is prestressed to give a residual stress near yield in the direction opposite to that expected upon heating, bending stresses of approximately the sum of the yield stresses in the normal and elevated-temperature conditions may be allowed without plastic deformation. This may be accomplished by proper application of a weld, by mechanical stressing, or simply by subjecting the component to conditions more severe than the normal operating condition and relying upon the resultant plastic deformation on this first cycle.

Torsion and Flexure of Slender Solid Sections[1]

By W. J. CARTER,[2] AUSTIN, TEXAS

The solution of the torsion problem for a slender rectangular section has been made previously by approximate methods based on the Prandtl membrane analogy. In this paper approximate methods are employed in the solution of both the torsion and flexural shear problem for slender sections having a variety of shapes, most of them being doubly symmetric. Solutions obtained in this manner are compared with exact solutions, when these are available, and otherwise with solutions obtained by relaxation. It is shown that approximate methods provide an adequate solution for elements such as compressor-turbine blades when pretwist and taper can be neglected. Some attention is given to the problem of elastic-plastic torsion and elastic-plastic flexural shear of slender sections.

Nomenclature

The following nomenclature is used in the paper:

- σ = normal stress, tension or compression
- τ = shear stress, with subscripts such as τ_{xz} and τ_{yz} to indicate directions of the components
- τ_B = boundary-directed shear stress
- G = shear modulus
- θ = angular twist per unit length, radians
- I = second moment of area of cross section
- M_t = torsional stiffness of bar
- P = bending load on beam
- x, y, z = rectangular Cartesian co-ordinates
- x_B = value of x on boundary of cross section
- ϕ = Prandtl stress function
- ϕ_B = boundary values of stress function
- ν = Poisson's ratio
- A = area of bar cross section
- b = long axis of doubly symmetric section
- a = short axis of doubly symmetric section
- b/a = slenderness ratio of doubly symmetric section

Approximate Method of Solution of Torsion Problem of a Slender Section

When applied to the problem of torsional shear stress and torsional-stiffness determination for slender sections, such as is illustrated in Fig. 1, the membrane analogy as developed by Prandtl[3] suggests that fairly good approximate solutions may be obtained by using stress functions of the form

$$\phi = G\theta(x_B^2 - x^2) \quad [1]$$

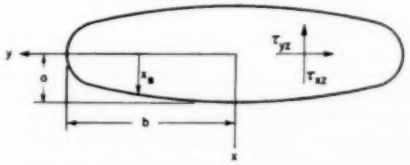

Fig. 1 Slender Doubly Symmetric Cross Section

This is equivalent to assuming that the ϕ-surface is the same as that which would be obtained for a slender rectangular section of the same width.

The shear stresses are given by the expressions

$$\tau_{xz} = \frac{\partial \phi}{\partial y} \quad [2]$$

$$\tau_{yz} = -\frac{\partial \phi}{\partial x} \quad [3]$$

and the torsional stiffness is given by twice the integral of ϕ over the cross section

$$M_t = 2 \int\int \phi \, dx \, dy \quad [4]$$

Approximate Solution for Torsion of Slender Ellipse

For the slender ellipse whose semi-axes along the x and y-axes are a and b, respectively, the value of x at the boundary is given by

$$x_B^2 = a^2 - \frac{a^2}{b^2} y^2$$

and Equation [1] becomes

$$\phi = G\theta \left[a^2 \left(1 - \frac{y^2}{b^2} \right) - x^2 \right] \quad [5]$$

The stress components are found by substitution of the partial derivatives of ϕ in Equations [2] and [3]. The maximum shear stress occurs where x_B is maximum.

Table 1 shows the values of τ_{max} and M_t as computed from the approximate stress function, Equation [5], together with the values given by the known exact solution for the ellipse. It may be seen that the agreement is quite good for ratios of b/a greater than 3.

Approximate Solution for Torsion of Slender Diamond Section

For the diamond section

$$x_B = a \left(1 - \frac{y}{b} \right) \quad \text{for} \quad y > 0$$

[1] The results presented in this paper are based on a dissertation submitted by the author in partial fulfillment of the requirements for the degree of Doctor of Philosophy in Engineering Mechanics at Stanford University, Stanford, Calif., June, 1952. The investigation was made when the author was research assistant under a grant from the Office of Naval Research. The work reported here was directed by Prof. J. N. Goodier of the Department of Engineering Mechanics, Stanford University.

[2] Associate Professor of Mechanical Engineering, The University of Texas. Mem. ASME.

Contributed by the Applied Mechanics Division and presented at the Fall Meeting, Hartford, Conn., Sept. 23–25, 1957, of The American Society of Mechanical Engineers.

Discussion of this paper should be addressed to the Secretary, ASME, 29 West 39th Street, New York, N. Y., and will be accepted until April 10, 1958, for publication at a later date. Discussion received after the closing date will be returned.

Note: Statements and opinions advanced in papers are to be understood as individual expressions of their authors and not those of the Society. Manuscript received by ASME Applied Mechanics Division, August 24, 1956. Paper No. 57—F-4.

[3] "Zur Torsion von prismatischen Staben," by L. Prandtl, *Zeitschrift für Physik*, vol. 4, 1903, p. 758.

TABLE 1 VALUES OF τ_{max} AND M_t

b/a	τ_{max} Approximate	τ_{max} Exact	M_t Approximate	M_t Exact
3	$2\ G\theta a$	$1.800\ G\theta a$	$3\ \pi G\theta a^4$	$2.700\ \pi G\theta a^4$
5	$2\ G\theta a$	$1.922\ G\theta a$	$5\ \pi G\theta a^4$	$4.808\ \pi G\theta a^4$
8	$2\ G\theta a$	$1.970\ G\theta a$	$8\ \pi G\theta a^4$	$7.877\ \pi G\theta a^4$
20	$2\ G\theta a$	$1.995\ G\theta a$	$20\ \pi G\theta a^4$	$19.95\ \pi G\theta a^4$

and the approximate stress function becomes

$$\phi = G\theta\left(a^2 - 2a^2\frac{y}{b} + a^2\frac{y^2}{b^2} - x^2\right) \quad [6]$$

According to this equation the maximum stress has the value

$$\tau_{max} = 2G\theta a \quad [7]$$

and

$$M_t = \frac{4}{3}\,G\theta a^3 b \quad [8]$$

The torsion problem for the diamond section has been solved by the relaxation method for ratios of $b/a = 5$ and 10. The exact solution for $b/a = 1$ may be obtained from the known exact solution for the square section. A comparison of the results obtained by the approximate solution and by the relaxation solution, Fig. 2, reveals that the agreement is quite good for large values of b/a, especially for M_t.

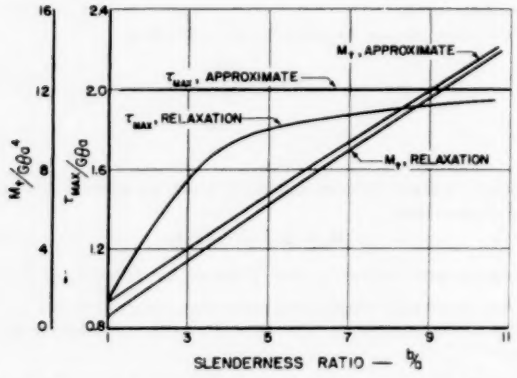

FIG. 2 TORSION STRESS AND TORSIONAL STIFFNESS FOR SLENDER DIAMOND SECTION

It also should be noted that the approximate solution gives the maximum stress at the point of maximum thickness and that, in the case of the diamond section which has an outstanding corner at this point, the solution is seriously in error. Actually the shear stress is zero at the outstanding corner. The area of low shear stress at the corner is quite small. The maximum stress point as determined by the relaxation solution is quite near the point of maximum thickness and, as a result, the magnitude of the maximum shear as given by Equation [7] is not seriously in error for reasonably large values of b/a.

APPROXIMATE SOLUTION FOR TORSION OF PARABOLIC SECTION

For the section whose boundaries are formed by two parabolas

$$x_b = \pm a\left(1 - \frac{y^2}{b^2}\right)$$

and

$$\phi = G\theta\left(a^2 - 2a^2\frac{y^2}{b^2} + a^2\frac{y^4}{b^4} - x^2\right) \quad [9]$$

which gives

$$\tau_{max} = 2G\theta a \quad [10]$$

and

$$M_t = \frac{256}{105}\,G\theta a^3 b \quad [11]$$

The torsion problem for the parabolic section has been solved by relaxation for ratios of $b/a = 3$, 6, and 9. A comparison of the approximate solution and the results obtained by relaxation is

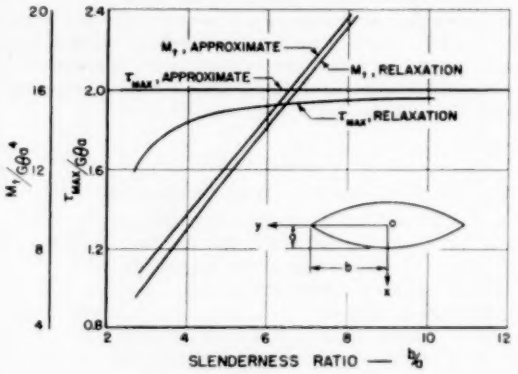

FIG. 3 TORSION STRESS AND TORSIONAL STIFFNESS FOR SLENDER PARABOLIC SECTION

shown in the curves of Fig. 3. It may be seen that the agreement is quite good, especially for ratios of b/a greater than 3.

ELASTIC-PLASTIC TORSION OF BARS OF SLENDER SECTION

A very simple approximate solution of the problem of elastic-plastic torsion of slender sections may be obtained by a combination of the techniques which have been demonstrated in this paper with the familiar sand-heap analogy for plastic torsion due to Nadai.[4] Nadai has considered the torsion of bars for which the material has an idealized stress-strain diagram like that in Fig. 4. He has shown that the completely plastic torsion of a bar of such material has a simple nature. The shear-stress function which corresponds to this condition represents a surface of constant maximum slope. For example, if a model of the contour of the cross section is cut out of some material and is then covered with sand while lying horizontally, the resulting sand heap will give a picture of the plastic-stress function.

The Nadai analogy can be extended to cover the case of elastic-plastic torsion of bars. A plastic roof, conforming to the sand heap, is imagined to be erected over the model of the bar section, and under this roof a membrane having the same boundary is formed. As the membrane is raised it gradually will come in contact with more and more of the plastic-roof area. At any given elastic-plastic condition, the zone of plastic behavior will be that over which the membrane and the plastic roof are in contact; the remainder of the cross section will have elastic behavior.

[4] "Theory of Flow and Fracture of Solids," by A. Nadai, McGraw-Hill Book Company, Inc., New York, N. Y., second edition, vol. 1, 1950.

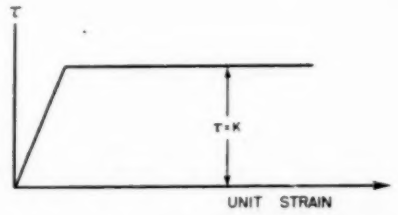

FIG. 4 IDEALIZED STRESS-STRAIN DIAGRAM

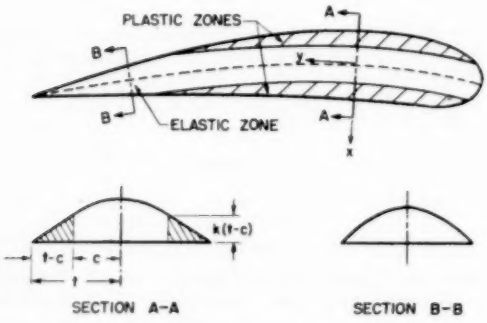

FIG. 5 ELASTIC-PLASTIC TORSION OF SLENDER SECTION

This analogy may now be applied to a bar of slender section. The bar cross section shown in Fig. 5 is first visualized as having a roof placed over it of the shape that would be formed by a sand heap. The roof will have a slope k, normal to the boundary cross section. Section A-A represents a cross section normal to the bar center line at which the slender bar has partially plastic behavior. Owing to the slenderness, the elastic membrane may be regarded as having a slope k in the x-direction where it leaves the plastic roof. For the elastic region a parabola is taken

$$\phi = C_1x^2 + C_2 \quad \ldots\ldots\ldots\ldots\ldots\ldots [12]$$

to satisfy $(d^2\phi)/(dx^2) = -2G\theta$, and C_1 and C_2 are chosen so that the slope is $-k$, and the ordinate is $k(t - c)$ at $x = c$. Thus it becomes evident

$$C_1 = -G\theta = -\frac{k}{2c}$$

$$C_2 = k\left(t - \frac{c}{2}\right)$$

and

$$c = \frac{k}{2G\theta} \quad \ldots\ldots\ldots\ldots\ldots\ldots [13]$$

Equation [13] illustrates that the elastic zone has a constant width c. This fact brings great simplicity to the problem of elastic-plastic torsion for slender bars.

The torsional stiffness of the bar in the elastic-plastic zone is found in the usual way as twice the volume under the stress-function surface. The stress-function surface has a constant slope k over the regions of plastic yielding and is described by Equation [12] in the region of elastic behavior. The curves of Figs. 6 and 7 show the elastic-plastic-torsion behavior for a slender rectangle and a slender diamond section, respectively.

The simplified method presented here obviously may be used to describe the elastic-plastic-torsion behavior of any slender open section such as an I-beam or channel section.

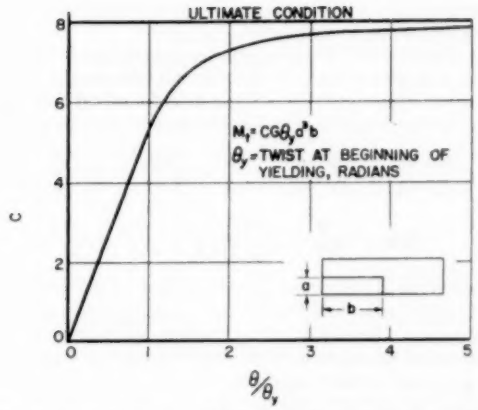

FIG. 6 ELASTIC-PLASTIC TORSION OF SLENDER RECTANGLE

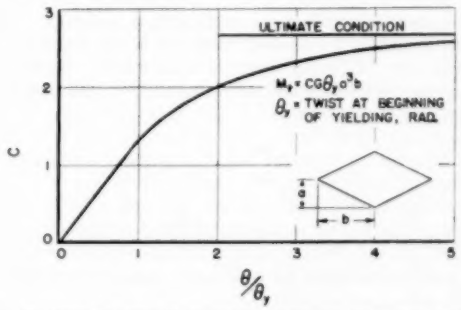

FIG. 7 ELASTIC-PLASTIC TORSION OF SLENDER DIAMOND SECTION

INTRODUCTION TO PROBLEM OF SHEAR DUE TO FLEXURE

In this part of the paper a study is made of the Saint Venant flexural shear stress on the transverse section of a cantilever beam loaded by a force at its free end. Elasticity theory shows that the solution of such a problem requires the determination of functions which satisfy a special form of Poisson's equation, $\nabla^2\phi = \varphi(y)$. For slender solid sections it is shown that approximate solutions inferred from the membrane analogy give reasonably accurate results.

For a cantilever beam like that shown in Fig. 8, it may be

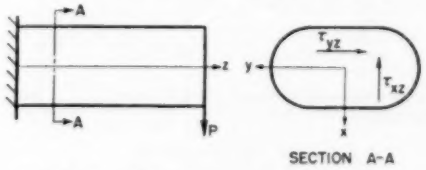

FIG. 8 SIGN CONVENTION FOR BEAM FLEXURE

shown in a simple manner that the conditions of equilibrium are satisfied when τ_{zz} is given by the expression

$$\tau_{zz} = \frac{PQ}{Iw} \quad \ldots\ldots\ldots\ldots\ldots\ldots [14]$$

where Q is the first moment of the beam cross-section area above the level at which τ_{zz} is evaluated, I is the moment of inertia of the beam cross section, and w is the width of the beam section where the shear stress is determined. This solution does not satisfy all of the equations of elasticity; and, in some cases, such

as the types of cross sections considered in this paper, it will give results that are seriously in error.

For a beam which carries a load normal to the y-axis of its cross section, as shown in Fig. 8, the Saint Venant flexure analysis leads to the following equations. These must be solved if the shear-stress distribution on the cross section is to be determined

$$\frac{\partial \phi}{\partial y}\frac{dy}{ds} + \frac{\partial \phi}{\partial x}\frac{dx}{ds} = \frac{\partial \phi}{\partial s} = \left[\frac{Px^2}{2I} - f(y)\right]\frac{dy}{ds} \quad [15]$$

$$\nabla^2\phi = \frac{\partial^2\phi}{\partial x^2} + \frac{\partial^2\phi}{\partial y^2} = \frac{\nu}{1+\nu}\frac{Py}{I} - \frac{df}{dy} \quad [16]$$

where s is the arc length along the boundary of the cross section, ν is Poisson's ratio, and P is the load normal to the y-axis of the cross section. Equation [16] is the differential equation of the stress distribution in terms of the stress function ϕ, and Equation [15] gives the boundary condition for ϕ.

Approximate Solution of Flexural Shear Problem

Term $f(y)$ in Equation [15] is chosen so as to have $(\partial\phi)/(\partial s)$ equal to zero everywhere, thus making ϕ constant along the boundary. There is no loss of generality in making the constant equal to zero. With $f(y)$ chosen in this manner, Equation [16] must be solved for ϕ. With ϕ determined, the stress components are given by the expressions

$$\tau_{zx} = \frac{\partial \phi}{\partial y} - \frac{Px^2}{2I} + f(y) \quad [17]$$

$$\tau_{yz} = -\frac{\partial \phi}{\partial x} \quad [18]$$

The positive directions for the stress components are shown in Fig. 8.

In order that $(\partial\phi)/(\partial s)$ be zero along the boundary, it is necessary that

$$f(y) = \frac{Px_B^2}{2I}$$

where x_B is the value of x along the boundary of the cross section (x_B is a known function of y). Equation [16] now becomes

$$\nabla^2\phi = \frac{\nu}{1+\nu}\frac{Py}{I} - \frac{P}{2I}\frac{d}{dy}(x_B)^2 = g(y) \quad [19]$$

For slender sections it may be assumed that the variation of ϕ with y is small compared with the variation in x, thus

$$\frac{d^2\phi}{dx^2} = \frac{\nu}{1+\nu}\frac{Py}{I} - \frac{P}{2I}\frac{d}{dy}(x_B)^2 = g(y) \quad [20]$$

For sections having symmetry with respect to the y-axis it may be shown that

$$\phi = \frac{g(y)}{2}[x^2 - x_B^2] \quad [21]$$

Approximate Solution of Flexural Shear Problem for Ellipse

For the ellipse

$$x_B^2 = a^2 - \frac{a^2}{b^2}y^2$$

and

$$f(y) = \frac{P}{2I}\left(a^2 - \frac{a^2}{b^2}y^2\right)$$

from which

$$\frac{df}{dy} = -\frac{P}{I}\frac{a^2}{b^2}y$$

thus

$$g(y) = \frac{Py}{I}\left[\frac{a^2}{b^2} + \frac{\nu}{1+\nu}\right] \quad [22]$$

Equation [21] now becomes

$$\phi = \frac{Py}{I}\left[\frac{a^2}{b^2} + \frac{\nu}{1+\nu}\right]\left(x^2 - a^2 + \frac{a^2}{b^2}y^2\right) \quad [23]$$

When the derivatives of ϕ with respect to x and y are computed and substituted in Equations [17] and [18], the result is

$$\tau_{zx} = \frac{P}{2I}\left[\left(\frac{a^2}{b^2} + \frac{\nu}{1+\nu}\right)\left(x^2 - a^2 + 3\frac{a^2}{b^2}y^2\right) - x^2 + a^2 - \frac{a^2}{b^2}y^2\right] \quad [24]$$

$$\tau_{yz} = -\frac{Pxy}{I}\left[\frac{a^2}{b^2} + \frac{\nu}{1+\nu}\right] \quad [25]$$

Usually the τ_{zx} component is of greatest interest. The value of τ_{zx} at the center of the cross section is given by the expression

$$(\tau_{zx})_{x=y=0} = \frac{2P}{A}\left[-\frac{\nu}{1+\nu} - \frac{a^2}{b^2} + 1\right] \quad [26]$$

(In Equation [26] the proper value for the ellipse ($Aa^2/4$) has been substituted for I.)

The exact solution of the flexural shear problem for the ellipse is known. For the τ_{zx} component at the center, the exact solution gives

$$(\tau_{zx})_{x=y=0} = \frac{2P}{A}\left[\frac{2(1+\nu)a^2 + b^2}{(1+\nu)(3a^2 + b^2)}\right] \quad [27]$$

It will be seen that, as might be expected, Equations [26] and [27] reduce to the same value for large values of b/a.

A comparison of the results obtained by the approximate solution and by the known exact solution for the ellipse is given in Fig. 9. The agreement for the stress component τ_{zx} is fairly good for ratios of b/a greater than 7, and even for ratios lower than 7, the approximate solution is nearer the exact result than the elementary solution. The agreement shown indicates that the approximate method of solution of the flexural shear problem for thin sections such as propeller and turbine blades is accurate enough to be adequate for engineering work.

The direction of the resultant shear stress on the boundary of any section is parallel to the boundary. The value of the boundary-directed shear stress is of greater interest than either τ_{zx} or τ_{yz} at the boundary. The magnitude of the boundary-directed shear stress may be found by adding vectorially the τ_{zx} and τ_{yz} components along the boundary. The magnitude of the boundary-directed stress also may be expressed in terms of the angle that the boundary makes with the y-axis

$$\tau_B = \tau_{zx}\csc\alpha = \tau_{yz}\sec\alpha$$

The results shown in Fig. 10 are of particular significance. Here the maximum value of the boundary-directed stress $(\tau_B)_{max}$ has been plotted as computed from the approximate solution and from the known exact solution. By the approximate method, $(\tau_B)_{max}$ occurs at a value of y very slightly greater than $b/\sqrt{2}$. The agreement is quite good for fairly large values of b/a. The fact that $(\tau_B)_{max}$ reaches quite large values for large ratios of b/a

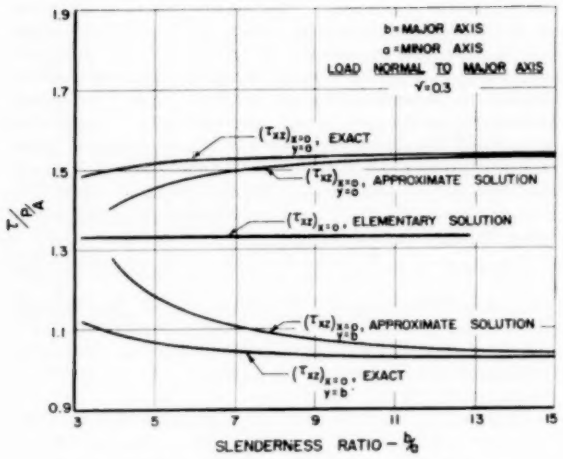

FIG. 9 SHEAR DUE TO FLEXURE OF SLENDER ELLIPSE

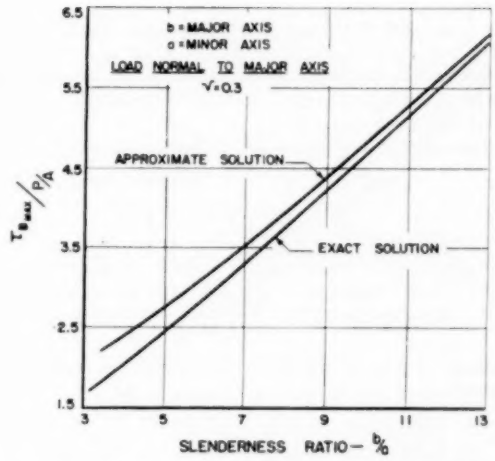

FIG. 10 BOUNDARY DIRECTED SHEAR STRESS DUE TO FLEXURE OF SLENDER ELLIPSE

should be noted. For $b/a = 50$ this stress is approximately 23 P/A. Another noteworthy point is that a longitudinal notch in the region of $(\tau_B)_{max}$ will have the same stress-raising effect as in the case of shear due to torsion.

It is generally recognized that stress-raising surface grooves and notches should always be avoided on structural elements like turbine blades and propeller blades; and, if the shear stresses are produced by twisting, the reason why high level shear stresses may develop on the surface can easily be seen. It is not generally recognized that flexure of thin sections also may produce large magnitude surface shear stresses.

APPROXIMATE SOLUTION OF FLEXURAL SHEAR PROBLEM OF PARABOLIC SECTION AND COMPARISON WITH RESULTS OBTAINED BY RELAXATION

For the section formed by two parabolas

$$x_B^2 = a^2\left(1 - \frac{2y^2}{b^2} + \frac{y^4}{b^4}\right)$$

and

$$f(y) = \frac{Pa^2}{2I}\left(1 - \frac{2y^2}{b^2} + \frac{y^4}{b^4}\right)$$

from which

$$\frac{df}{dy} = \frac{2Pa^2}{I}\left(\frac{y^3}{b^4} - \frac{y}{b^2}\right)$$

thus

$$\phi = \frac{Py}{2I}\left[\frac{\nu}{1+\nu} - 2a^2\left(\frac{y^2}{b^4} - \frac{1}{b^2}\right)\right]\left(x^2 - a^2 + 2\frac{a^2}{b^2}y^2 - a^2\frac{y^4}{b^4}\right) \quad \ldots\ldots [28]$$

The derivatives of ϕ with respect to x and y may be computed and substituted in Equations [17] and [18] to obtain the equations of the stress components. The algebraic detail incident to this solution is lengthy, and only the result for the stress at the center will be given here

$$(\tau_{xz})_{x=y=0} = \frac{P}{A}\left[\frac{35}{16} - \frac{35}{8}\frac{a^2}{b^2} - \frac{35\nu}{16(1+\nu)}\right] \quad \ldots\ldots [29]$$

(In Equation [29] $[8/35]Aa^2$ has been substituted for I). At the ends of the section, $x = 0$, $y = \pm b$; $\tau_{xz} = 0$.

Since the exact solution for the flexural shear of a parabolic section is not known, a relaxational solution has been made for ratios of $b/a = 4$, 7, and 10. The approximate-solution results are compared with the relaxation results in Fig. 11. It may be seen that the agreement is fairly good for ratios of b/a greater than 3 or 4, and in almost all cases the approximate solution is much better than the elementary solution.

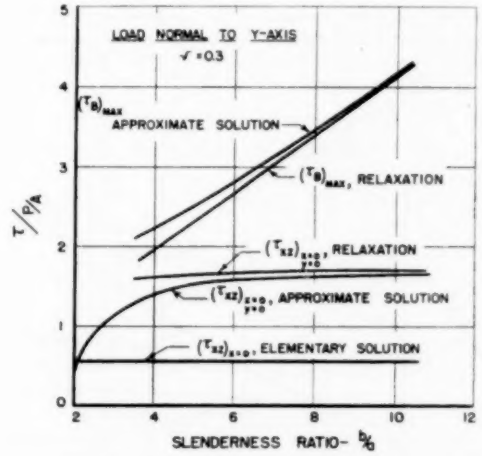

FIG. 11 SHEAR DUE TO FLEXURE OF SLENDER PARABOLIC SECTION

The maximum value of the boundary-directed shear stress is found very near $y = b/2$. The values of this maximum are shown in the curves of Fig. 11. It is important to note that the boundary-directed shear is again the most significant stress and that it reaches fairly high values for b/a greater than 10.

APPROXIMATE SOLUTION OF FLEXURAL SHEAR PROBLEM OF DIAMOND SECTION AND COMPARISON WITH RESULTS OBTAINED BY RELAXATION

For the diamond section

$$x_B^2 = a^2\left(1 - \frac{2y}{b} + \frac{y^2}{b^2}\right), \quad y \geqq 0$$

and to make the right-hand side of Equation [15] zero there also must be

$$f(y) = \frac{Pa^2}{2I}\left(1 - \frac{2y}{b} + \frac{y^2}{b^2}\right), \quad y \geqq 0$$

thus

$$\frac{df}{dy} = \frac{Pa^2}{I}\left[\frac{y}{b^2} - \frac{1}{b}\right]$$

from which

$$g(y) = \frac{\nu}{1+\nu}\frac{Py}{I} - \frac{Pa^2}{I}\left[\frac{y}{b^2} - \frac{1}{b}\right], \quad y \geqq 0$$

and since $I = (Aa^2/6)$, substitution of this value in Equation [21] results in

$$\phi = \frac{P}{2A}\left\{\left[\frac{6\nu}{a^2(1+\nu)} - \frac{6}{b^2}\right]y + \frac{6}{b}\right\}\left(x^2 - a^2 + 2a^2\frac{y}{b} - a^2\frac{y^2}{b^2}\right) \quad [30]$$

The partial derivatives of ϕ when substituted in Equations [17] and [18] give the shear-stress components. At the center of the section

$$(\tau_{xz})_{x=y=0} = \frac{P}{A}\left[3 + \frac{9a^2}{b^2} - \frac{3\nu}{(1+\nu)}\right] \quad [31]$$

At the ends of the section, $x = 0$, $y = \pm b$, $\tau_{xz} = 0$. The boundary-directed shear stress is found by dividing the τ_{ys} component along the boundary by $\cos^{-1}(a/b)$. The maximum value of τ_B occurs at y slightly less than $b/2$.

The flexural shear problem of the diamond section has been solved by relaxation for ratios of $b/a = 4$, 7, and 10. A comparison of the values obtained by this method and the results of the approximate solution is shown in Fig. 12.

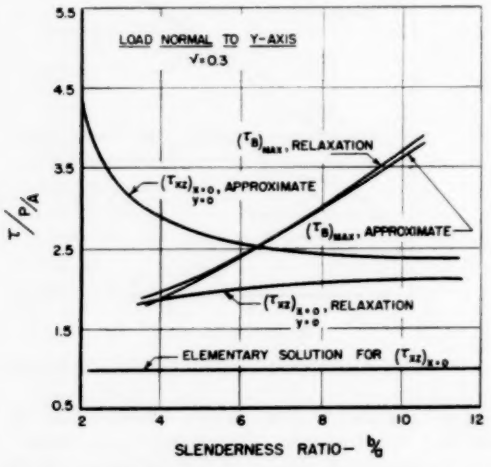

FIG. 12 SHEAR DUE TO FLEXURE OF SLENDER DIAMOND SECTION

It should be noted that the expressions for $(df)/(dy)$ and $g(y)$ for the diamond section contain a constant term. If $(df)/(dy)$ and $g(y)$ are evaluated for $y < 0$, the sign of the constant term changes. Interpreted in terms of the membrane analogy, this constant means that there is a discontinuity in the pressure at $y = 0$. In the approximate solution, this change of sign gives rise to a ϕ-function which is also discontinuous at $y = 0$. From the requirements of symmetry, the exact stress function must be zero along $y = 0$. This inherent discrepancy in the stress function for the diamond section would suggest that the value obtained for τ_{xz} at the center should have a greater percentage error than should the approximate solutions for the ellipse and parabolic sections in which this discrepancy does not arise. An examination of the results shows the discrepancy to be greater. Even so, the results are better than the elementary solution for ratios of b/a greater than 3 or 4.

SHEAR WITH PLASTIC BENDING OF BARS OF SYMMETRIC SECTION

The approximate method of solution to the flexural shear problem may be extended easily to treat some problems of flexural shear associated with partially plastic bending. Here it will be assumed that the stress-strain diagram of the bar material is like that shown in Fig. 13.

Consider a cantilever beam whose cross section is symmetrical about the axis normal to the load. If the applied load is large enough, there will be plastic behavior of a portion of the beam cross section, Fig. 14. The strain variation at Section A-A has a simple nature; and, if the beam cross section is known, the relations between e, the maximum strain, and the bending moment

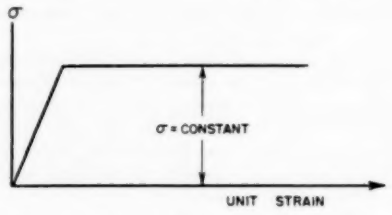

FIG. 13 IDEALIZED STRESS-STRAIN DIAGRAM

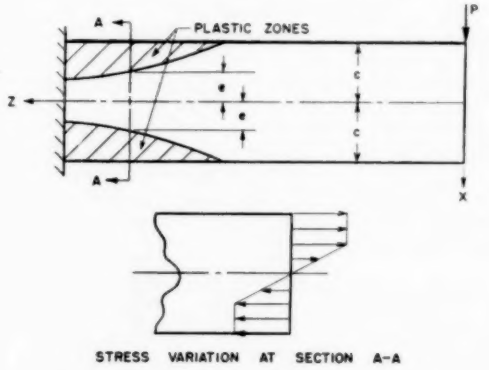

FIG. 14 ELASTIC-PLASTIC BENDING OF BEAM

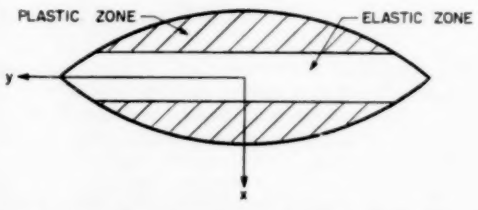

FIG. 15 BEAM CROSS SECTION IN ELASTIC-PLASTIC BENDING

may be found easily. Prager and Hodge[5] have shown that, if the beam cross section is symmetric (like that of Fig. 15), the depth of the zone of plastic bending may be computed readily.

If the usual assumptions of beam theory are made—plane sections remain plane, and so on—it may be shown that there is no shear stress in the plastic section of the beam.[6] Thus the shear necessary to resist P must be taken entirely by the elastic center portion of the beam cross section. The elastic part of the beam cross section will always have a portion in the middle part which is rectangular. The elastic part of the cross section shown in Fig. 15 has tapering end portions in addition to the rectangular part. If the elastic core is slender, it is evident that the approximate method can be used in determining the shear due to flexure.

There is some question as to the validity of solving the flexural shear problem in the manner indicated for a beam which is in a partially plastic state. Although it is true that the elastic core carries all the shear, the Saint Venant flexure theory assumes that the anticlastic curvature of the shear-carrying member is free to develop. In the plastic bending of a cross section, the anticlastic curvature will be partially constrained.

[6] "Theory of Perfectly Plastic Solids," by W. Prager and P. G. Hodge, Jr., John Wiley & Sons, Inc., New York, N. Y., 1951, p. 51.

Acknowledgment

The author wishes to make known his indebtedness to Prof. J. N. Goodier of the Engineering Mechanics Department, Stanford University. Most of the problems considered here were suggested by him, and his aid in their solution was very great.

Effect of Curvature on the Hertz Theory for Two Circular Cylinders in Contact

By TSU-TAO LOO,[1] TROY, N. Y.

The effect of curvature on the Hertz theory for the case of two circular cylinders in line contact is studied, and a correction term due to consideration of this curvature is found. An expression for the relative normal approach of two cylinders is also obtained, a result which heretofore has not been formulated.

Nomenclature

The following nomenclature is used in the paper:

$x, y; r, \theta$ = Cartesian and polar co-ordinates
u, v = displacements in x and y-directions
R_1, R_2 = radii of circular cylinders
E, G, μ, λ = elastic modulus, modulus of rigidity, Poisson's ratio, Lamé constant of material
$2s_0; 2\varphi_1, 2\varphi_2$ = arc length and angles of contact
$2a$ = amplitude of contact in y-direction
P = total normal load per unit longitudinal length
β = normal approach of the two cylinders
s, t = circumferential distance measured from initial point of contact
ξ_1, ξ_2 = angle parameters
$r_1, \alpha_1; r_2, \alpha_2$ = position co-ordinates of any point in reference to the loading points (see Fig. 1)

Introduction

Contact problems are essentially nonlinear; nevertheless, the only approach to these problems has been through Hertz's approximate theory (1)[2] which is based upon linear theory of elasticity. In general, this theory has been substantiated satisfactorily by tests and practical applications. It has been found, however, in some problems such as the loading of ball and roller bearings that a more refined theory is desirable.

In an earlier paper (2) the author obtained a second approximation theory of three-dimensional elastic contact, in which the Taylor series used in describing the contacting surfaces was truncated at the fourth power rather than at the second-power terms as done by Hertz. Through this refinement, an additional term in the expression of the pressure distribution was found and was shown to be appreciable as the eccentricity of the contact ellipse increases. However, Hertz's approximation in considering both contacting bodies as elastic half-spaces was still retained; i.e., the Boussinesq solution of a force on the half-space was used for the displacements of the points in the contact region.

In the present paper, the effect of curvature on the two-dimensional plane Hertz theory is discussed. The problem is the line contact of two infinitely long circular cylinders of dissimilar materials and radii. The solution is achieved by using the displacement field of an infinitely long circular cylinder under nondiametrical, equal, and opposite concentrated forces. The usual attack on the two-dimensional contact problems is through the two-dimensional analog of the Boussinesq problem (3, 4). This suffers the same objection as in the three-dimensional problem; i.e., approximating cylinders by half-spaces, thus neglecting the effect of curvature.

A second defect is that, unlike the three-dimensional problem, the normal approach is unobtainable. In the three-dimensional Boussinesq problem the displacements vanish at infinity and hence the normal approach can be computed. However, in the two-dimensional Boussinesq problem the displacements do not tend to zero at infinity (5); and therefore, while the results of this displacement field may be used in the neighborhood of contact, they cannot be used to compute the normal approach of two distant points. Both these objections are eliminated in this paper. The effect of curvature is found to depend on the dimensionless parameters, P/E_1R_1 and P/E_2R_2, where P is the normal load per unit longitudinal length, R_1, R_2 are the radii of cylinders, and E_1, E_2 are their moduli of elasticity. If these parameters are much smaller than unity, then the effect is negligible. An expression for relative normal approach also is obtained, a result which heretofore has not been possible.

Analysis of problem

In the case of two circular cylinders in contact under load, Hertz's hypothesis treating both bodies as half-spaces is unnecessary, since the displacement field of a circular cylinder under two equal and opposite nondiametrical colinear forces is known (6).

Consider now a homogeneous, isotropic, elastic circular cylinder of radius R under the action of two equal and opposite compressive forces P (per unit longitudinal length) at the points $M(R, \theta)$ and $N(R, \pi-\theta)$ along the chord of a circular section, parallel to a diametric axis, the x-axis as shown in Fig. 1. The

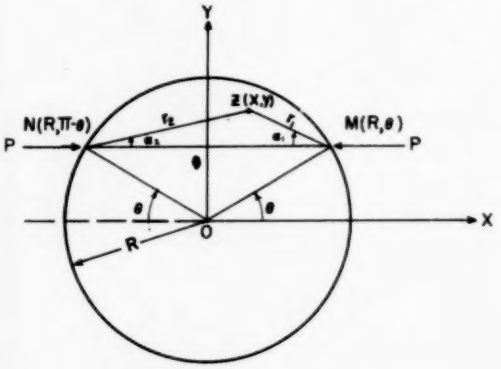

Fig. 1

---

[1] Associate Professor of Mechanics, Rensselaer Polytechnic Institute.

[2] Numbers in parentheses refer to the Bibliography at the end of the paper.

Contributed by the Applied Mechanics Division and presented at the Annual Meeting, New York, N. Y., December 1–6, 1957, of THE AMERICAN SOCIETY OF MECHANICAL ENGINEERS.

Discussion of this paper should be addressed to the Secretary, ASME, 29 West 39th Street, New York, N. Y., and will be accepted until April 10, 1958, for publication at a later date. Discussion received after the closing date will be returned.

NOTE: Statements and opinions advanced in papers are to be understood as individual expressions of their authors and not those of the Society. Manuscript received by ASME Applied Mechanics Division, April 6, 1956. Paper No. 57—A-33.

displacements u and v in the directions of the x and y-axes are as follows (6) (see Fig. 1)

$$u(x, y) = \frac{-P}{4\pi G}\left[\frac{2(\lambda + 2G)}{\lambda + G}\ln\frac{r_2}{r_1} + (\cos 2\alpha_1 - \cos 2\alpha_2) - \frac{2G\cos\theta}{\lambda + G}\frac{x}{R}\right] \quad [1]$$

$$v(x, y) = \frac{-P}{4\pi G}\left[\frac{2G}{\lambda + G}(\alpha_1 + \alpha_2) - (\sin 2\alpha_1 + \sin 2\alpha_2) - \frac{2G\cos\theta}{\lambda + G}\frac{y}{R}\right] \quad [2]$$

With reference to Figs. 1, 2, and 3 for the points on the circumference of the circular section $Q(x, y)$ or in polar co-ordinates $Q(R, \xi)$, the following relations hold

$$\frac{r_2}{r_1} = \frac{\cos\frac{1}{2}(\theta + \xi)}{\sin\frac{1}{2}(\theta - \xi)} \quad [3]$$

$$\cos 2\alpha_1 - \cos 2\alpha_2 = -2\cos\theta\cos\xi \quad [4]$$

for $\xi < \theta$, and

$$\frac{r_2}{r_1} = \frac{\cos\frac{1}{2}(\xi + \theta)}{\sin\frac{1}{2}(\xi - \theta)} \quad [5]$$

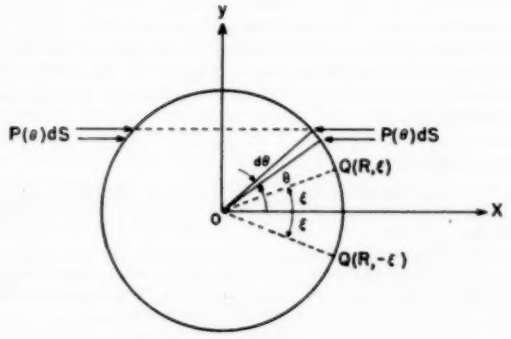

Fig. 2

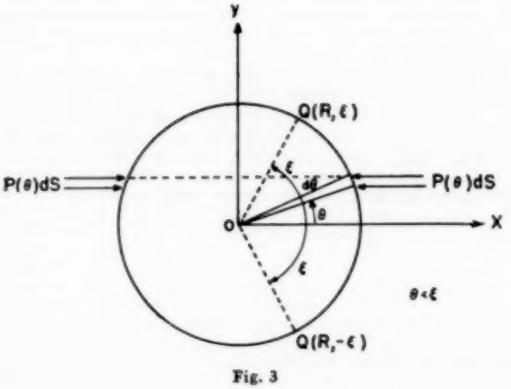

Fig. 3

$$\cos 2\alpha_1 - \cos 2\alpha_2 = -2\cos\theta\cos\xi \quad [6]$$

for $\xi > \theta$. Consequently, for the case of a distributed load $p(\theta)$ symmetrical with respect to the x-axis, the corresponding displacement for circumferential points in the x-direction can be obtained by substituting from Equations [3], [4], [5], and [6] in Equation [1], yielding

$$u(R, \xi) = K\int_0^{\varphi} p(\theta)\, Rd\theta\left[\ln\tan\frac{|\xi - \theta|}{2} + \ln\tan\frac{|\xi + \theta|}{2} + 2\cos\theta\cos\xi\right] \quad [7]$$

By symmetry, $p(\theta) = p(-\theta)$, so that

$$u(R, \xi) = KR\int_{-\varphi}^{\varphi} p(\theta)\left[\ln\tan\frac{|\xi - \theta|}{2} + \cos\theta\cos\xi\right]d\theta \quad [8]$$

where we define

$$K = \frac{\lambda + 2G}{2\pi G(\lambda + G)} = \frac{2(1 - \mu^2)}{\pi E} \quad [9]$$

Let subscript 1 denote the first cylinder and subscript 2 denote the second cylinder; then the respective displacements for their surface points will be

$$u_1(R_1, \xi_1) = K_1R_1\int_{-\varphi_1}^{\varphi_1} p_1(\theta_1)\left[\ln\tan\frac{|\xi_1 - \theta_1|}{2} + \cos\theta_1\cos\xi_1\right]d\theta_1 \quad [10]$$

$$u_2(R_2, \xi_2) = K_2R_2\int_{-\varphi_2}^{\varphi_2} p_2(\theta_2)\left[\ln\tan\frac{|\xi_2 - \theta_2|}{2} + \cos\theta_2\cos\xi_2\right]d\theta_2 \quad [11]$$

Let s (or t) be the circumferential distance measured from the initial point of contact between the two cylinders, and assume the points at the same s (or t) on each cylinder will be in contact after deformation, i.e.

$$\left.\begin{aligned} s &= R_1\theta_1 = R_2\theta_2 \\ t &= R_1\xi_1 = R_2\xi_2 \\ s_0 &= R_1\varphi_1 = R_2\varphi_2 \end{aligned}\right\} \quad [12]$$

and hence

$$\left.\begin{aligned} p_1(\theta_1) &= p_1(s/R_1) = p(s) \\ p_2(\theta_2) &= p_2(s/R_2) = p(s) \end{aligned}\right\} \quad [13]$$

According to the criterion of contact, we must have, at all points of the compressed area

$$u_1(t) + u_2(t) + \beta = [R_1 - x_1(t)] + [R_2 - x_2(t)] \quad [14]$$

where β, which is a constant, is defined as the normal approach of the two cylinders or $|u_1 + u_2|_{s=0}$ (i.e., at initial point of contact). Substituting for u_1 from Equation [10] and for u_2 from Equation [11] in Equation [14], and with the help of Equations [12] and [13], we obtain

$$K_1\int_{-s_0}^{s_0} p(s)\left[\ln\tan\frac{|t-s|}{2R_1}+\cos\frac{s}{R_1}\cos\frac{t}{R_1}\right]ds + K_2\int_{-s_0}^{s_0} p(s)\left[\ln\tan\frac{|t-s|}{2R_2}+\cos\frac{s}{R_2}\cos\frac{t}{R_2}\right]ds+\beta = R_1\left(1-\cos\frac{t}{R_1}\right)+R_2\left(1-\cos\frac{t}{R_2}\right)\quad[15]$$

This equation cannot be solved easily. However, if the arc of contact is very small ($s_0 \ll R_1, R_2$) the trignometric functions may be represented by power series. By neglecting second-order small terms and the small quantities compared with unity, Equation [15] can be reduced to the simple form

$$-(K_1+K_2)\int_{-s_0}^{s_0} p(s)\ln\frac{1}{|t-s|}\,ds - P(K_1\ln 2R_1+K_2\ln 2R_2)+(K_1+K_2)P - \left(\frac{K_1}{2R_1^2}+\frac{K_2}{2R_2^2}\right)Pt^2+\beta=\frac{1}{2}\left(\frac{1}{R_1}+\frac{1}{R_2}\right)t^2\quad[16]$$

Rearranging Equation [16] we have

$$\int_{-s_0}^{s_0} p(s)\ln\frac{1}{|t-s|}\,ds = A - Bt^2\quad[17]$$

where

$$A = P\left(1-\frac{K_1}{K_1+K_2}\ln 2R_1-\frac{K_2}{K_1+K_2}\ln 2R_2\right)+\frac{\beta}{K_1+K_2}\quad[18]$$

$$B=\frac{1}{2(K_1+K_2)}\left[\left(\frac{1}{R_1}+\frac{1}{R_2}\right)+\left(\frac{K_1}{R_1^2}+\frac{K_2}{R_2^2}\right)P\right]\quad[19]$$

$$P=\int_{-s_0}^{s_0} p(s)\,ds\quad[20]$$

Equation [17], except with different constants involved, is the same type of integral equation as found in Hertz's half-space theory, the solution of which has been found by Shtaerman (7)

$$p(t)=\frac{2P}{\pi s_0^2}(s_0^2-t^2)^{1/2}\quad[21]$$

$$s_0=(P/B)^{1/3}\quad[22]$$

and

$$P=\frac{A-\frac{1}{2}Bs_0^2}{\ln\frac{2}{s_0}}\quad[23]$$

Substituting from Equations [22] and [23] in Equation [18], we find the normal approach

$$\beta = P\left[K_1\ln 2R_1+K_2\ln 2R_2+(K_1+K_2)\ln\left(\frac{4\beta}{P}\right)^{1/3}-\frac{1}{2}(K_1+K_2)\right]\quad[24]$$

It is interesting to note that if as a first approximation we let $s \cong y$ (Fig. 4) and the amplitude of contact $s_0 \cong a$, then the present theory differs from the Hertz theory only by the values of two constants A and B. The constant A here will yield the value of relative normal approach of the two cylinders. Equation [19]

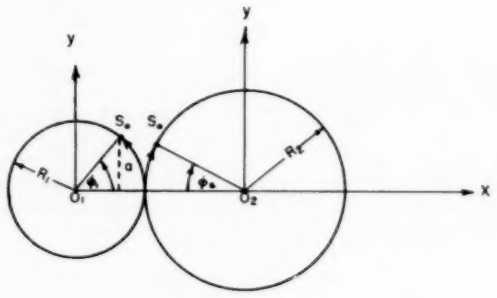

Fig. 4

shows an extra term in the value of B. This is due to considering the bodies as cylinders rather than half-spaces and can be considered as a curvature correction term, which depends on the material constants, radii of curvature, and the total normal load.

Acknowledgment

The author wishes to express his appreciation to the New Departure Division of the General Motors Corporation for making possible the research reported in this paper. The work reported here is from a portion of a research project currently in progress in the Department of Mechanics at Rensselaer Polytechnic Institute under the sponsorship of the New Departure Division of the General Motors Corporation. Thanks are also due to Dr. H. Bückner, Dr. J. L. Krahula, and Prof. E. A. Fox for their valuable help.

Bibliography

1 "Contact of Elastic Solids," by H. Hertz, English translation in "Miscellaneous Papers," Macmillan Company, London, England, 1896, pp. 146–183.

2 "A Second Approximation Solution for the Pressure Between Two Elastic Bodies in Contact," by T. T. Loo, Rensselaer Research Report, LRR No. 13A3C-3(A-5), submitted to New Departure Division of General Motors Corporation, January, 1954.

3 "Neue Ableitung der Hertzschen Härteformeln für die Walze," by L. Föppl, *Zeitschrift für angewandte Mathematik und Mechanik*, vol. 16, 1936, pp. 165–170.

4 "Stresses and Deflections of Cylindrical Bodies in Contact With Application to Contact of Gears and of Locomotive Wheels," by H. Poritsky, JOURNAL OF APPLIED MECHANICS, TRANS. ASME, vol. 72, 1950, pp. 191–201.

5 "A Treatise on the Mathematical Theory of Elasticity," by A. E. H. Love, Dover Publications, New York, N. Y., 1944, p. 211.

6 "Some Basic Problems of the Mathematical Theory of Elasticity," by N. I. Muskhelishvili, translated by J. R. M. Radok, P. Noordhoof Ltd., Groningen-Holland, 1953, pp. 324–328.

7 "The Contact Problems of the Theory of Elasticity," by I. Ya. Shtaerman (Russian), Moscow, Russia, 1949, pp. 97–98.

Displacement Discontinuity in the Elastic Half-Space

By LEIF RONGVED[1] and J. T. FRASIER[2]

The displacement generated by an arbitrary displacement discontinuity over a plane bounded area in a semi-infinite, isotropic, elastic solid is determined. The solution is given in terms of integrals over the area of discontinuity. As an example, the case of a constant displacement discontinuity over a rectangular area parallel to the boundary is worked out in closed form.

Introduction

THE Papkovitch functions for an arbitrary displacement discontinuity over a plane bounded area in an infinite solid have been determined by Rongved.[3] In this paper, the Papkovitch functions are determined for the same type of dislocation in a semi-infinite solid, where the plane of discontinuity has an arbitrary orientation with respect to the free boundary. As in the previous paper[3] the solution is given in terms of integrals containing the displacement discontinuity.

The solution is obtained by superposition. Starting with the solution for the infinite solid with a dislocation in the region $z > 0$ an appropriate state of stress is added to it such that the traction on the plane $z = 0$ vanishes. The state of stress added and the corresponding displacement must be continuous in the region $z \geq 0$ and must vanish at infinity.

The co-ordinate system used in Rongved's paper[3] is oriented such that the displacement discontinuity is over an area in the $z = 0$ plane. In Section 1, this solution is given in a new co-ordinate system oriented such that the dislocation has an arbitrary position with respect to the $z = 0$ plane. The Papkovitch functions for two such solutions are given, the first for a dislocation in the region $z > 0$, and the second for a dislocation in $z < 0$. The two dislocations are assumed to be identical except that one is located at the image of the other with respect to the $z = 0$ plane. It is to the first solution that we wish to add a state of stress such that the traction vanishes on the $z = 0$ plane. The Papkovitch functions for the second solution are used here since it turns out that the Papkovitch functions for the state of stress to be added can be expressed conveniently in terms of them. This is shown in Section 2.

In Section 3 the displacement is determined in closed form for the case of a constant displacement discontinuity over a rectangular area parallel to the boundary.

[1] Member of Technical Staff, Bell Telephone Laboratories, Inc., Murray Hill, N. J.; formerly, Assistant Professor of Engineering Mechanics, The Pennsylvania State University, University Park, Pa.

[2] Graduate Assistant in Engineering Mechanics, The Pennsylvania State University, University Park, Pa.

[3] "Dislocation Over a Bounded Plane Area in an Infinite Solid," by L. Rongved, Journal of Applied Mechanics, Trans. ASME, vol. 79, 1957, pp. 252–254.

Contributed by the Applied Mechanics Division and presented at the Annual Meeting, New York, N. Y., December 1–6, 1957, of The American Society of Mechanical Engineers.

Discussion of this paper should be addressed to the Secretary, ASME, 29 West 39th Street, New York, N. Y., and will be accepted until April 10, 1958, for publication at a later date. Discussion received after the closing date will be returned.

Note: Statements and opinions advanced in papers are to be understood as individual expressions of their authors and not those of the Society. Manuscript received by ASME Applied Mechanics Division, October 1, 1956. Paper No. 57—A-23.

1—The Papkovitch Functions for a Plane Dislocation in an Infinite Solid

Let the normal to the plane of dislocation have the direction cosines $(l, 0, n)$. Let ξ, η, ζ be a Cartesian co-ordinate system whose origin is at the intersection of the z-axis with the plane of dislocation, and with the ζ-axis perpendicular to this plane, and with the η axis parallel to the y-axis, Fig. 1.

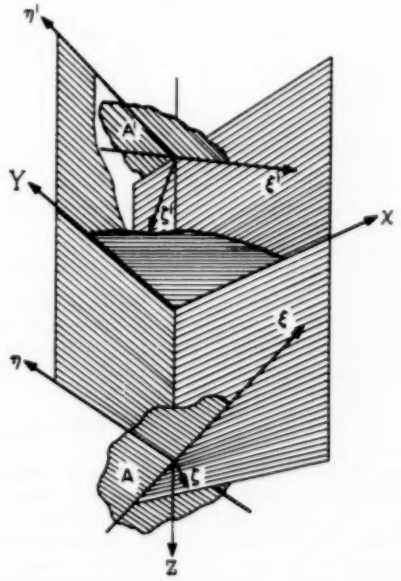

Fig. 1 Three Cartesian Co-Ordinate Systems Used, and Areas A and A' Over Which There Is a Discontinuity in the Displacement. A' Is the Image of A Reflected in the $z = 0$ Plane

The Papkovitch functions for this dislocation in terms of the independent variables x, y, z are:

1 For a discontinuity, $\hat{u}_\zeta$, in the ζ-component of the displacement

$$\bar{B}_x = l^2 \frac{\partial I}{\partial x} + \ln \frac{\partial I}{\partial z} \quad [1]$$

$$\bar{B}_y = 0 \quad [2]$$

$$\bar{B}_z = \ln \frac{\partial I}{\partial x} + n^2 \frac{\partial I}{\partial z} \quad [3]$$

$$\bar{\beta} = (1 - 2\nu)I - cn\left(l \frac{\partial I}{\partial x} + n \frac{\partial I}{\partial z}\right) \quad [4]$$

2 For a discontinuity, $\hat{u}_\xi$, in the ξ-component of the displacement

$$\bar{B}_x = 2nl \frac{\partial J}{\partial x} + (n^2 - l^2) \frac{\partial J}{\partial z} \quad [5]$$

$$\bar{B}_y = 0 \quad [6]$$

$$\bar{B}_z = (n^2 - l^2)\frac{\partial J}{\partial x} - 2nl\frac{\partial J}{\partial z} \quad [7]$$

$$\bar{\beta} = (z - 2cn^2)\frac{\partial J}{\partial x} - (x - 2cnl)\frac{\partial J}{\partial z} \quad [8]$$

3 For a discontinuity, $\hat{u}_\eta$, in the η-component of the displacement

$$\bar{B}_x = l\frac{\partial K}{\partial y} \quad [9]$$

$$\bar{B}_y = l\frac{\partial K}{\partial x} + n\frac{\partial K}{\partial z} \quad [10]$$

$$\bar{B}_z = n\frac{\partial K}{\partial y} \quad [11]$$

$$\bar{\beta} = l\left[x\frac{\partial K}{\partial y} - y\frac{\partial K}{\partial x}\right] + n\left[(z - 2c)\frac{\partial K}{\partial y} - y\frac{\partial K}{\partial z}\right] \quad [12]$$

where

$$[I, J, K] = \frac{1}{4\pi}\int_A [2\hat{u}_\zeta, \hat{u}_\xi, \hat{u}_\eta]\frac{d\xi\, d\eta}{\bar{r}_0}, \quad [13]$$

A is the area over which there is a discontinuity in the displacement and

$$\bar{r}_0 = [(x - n\xi)^2 + (y - \eta)^2 + (z - c + l\xi)^2]^{1/2}$$

The quantity $\bar{r}_0$ is the distance from the point $(\xi, \eta, 0)$ to the point (x, y, z). These solutions are obtained from Rongved's solution[3] for the infinite solid by a simple co-ordinate transformation. The displacement in each case is given by

$$\bar{u}_i = \bar{B}_i - \frac{1}{4(1-\nu)}[x_i\bar{B}_j + \bar{\beta}]_{,i} \quad [14]$$

For later use we write down also the solution for three more dislocations which are identical to the previous ones, except that they are located at the image of the former reflected in the $z = 0$ plane. Let ξ', η', and ζ' be a Cartesian co-ordinate system shown in Fig. 1. The normal to the plane of discontinuity is now $(-l, 0, n)$. One obtains the following solutions for discontinuities over an area A' in the $\xi'\eta'$-plane:

1(a) for a discontinuity, $\hat{u}_{\zeta'}$, in the ζ' component of the displacement

$$\bar{B}_x = l^2\frac{\partial \bar{I}}{\partial x} - \ln\frac{\partial \bar{I}}{\partial z} \quad [15]$$

$$\bar{B}_y = 0 \quad [16]$$

$$\bar{B}_z = -ln\frac{\partial \bar{I}}{\partial x} + n^2\frac{\partial \bar{I}}{\partial z} \quad [17]$$

$$\bar{\beta} = (1 - 2\nu)\bar{I} - cn\left(l\frac{\partial \bar{I}}{\partial x} - n\frac{\partial \bar{I}}{\partial z}\right) \quad [18]$$

2(a) for a discontinuity, $\hat{u}_{\xi'}$, in the ξ'-component of the displacement

$$\bar{B}_x = -2nl\frac{\partial J}{\partial x} + (n^2 - l^2)\frac{\partial J}{\partial z} \quad [19]$$

$$\bar{B}_y = 0 \quad [20]$$

$$\bar{B}_z = (n^2 - l^2)\frac{\partial J}{\partial x} + 2nl\frac{\partial J}{\partial z} \quad [21]$$

$$\bar{\beta} = (z + 2cn^2)\frac{\partial J}{\partial x} - (x - 2cnl)\frac{\partial J}{\partial z} \quad [22]$$

3(a) For a discontinuity, $\hat{u}_{\eta'}$, in the η'-component of the displacement

$$\bar{B}_x = -l\frac{\partial \bar{K}}{\partial y} \quad [23]$$

$$\bar{B}_y = -l\frac{\partial \bar{K}}{\partial x} + n\frac{\partial \bar{K}}{\partial z} \quad [24]$$

$$\bar{B}_z = n\frac{\partial \bar{K}}{\partial y} \quad [25]$$

$$\bar{\beta} = -l\left[x\frac{\partial \bar{K}}{\partial y} - y\frac{\partial \bar{K}}{\partial x}\right] + n\left[(z + 2c)\frac{\partial \bar{K}}{\partial y} - y\frac{\partial \bar{K}}{\partial z}\right] \quad [26]$$

where

$$[\bar{I}, \bar{J}, \bar{K}] = \frac{1}{4\pi}\int_{A'} [2\hat{u}_{\xi'}, \hat{u}_{\xi'}, \hat{u}_{\eta'}]\frac{d\xi' d\eta'}{\bar{r}_0} \quad [27]$$

and

$$\bar{r}_0 = [(x - n\xi')^2 + (y - \eta')^2 + (z + c - l\xi')^2]^{1/2}$$

The quantity $\bar{r}_0$ is the distance from the point $(\xi', \eta', 0)$ to the point (x, y, z).

2—Determination of Solution to Be Added to Yield Zero Traction on Boundary

By symmetry or inspection, it can be seen that the corresponding bar and double-bar solutions given in the previous section produce tractions on the boundary of the region $z > 0$ that are equal with opposite sign in shear components, and identical in the normal components. In view of this fact and using Equation [13] and the generalized Hooke's law

$$\sigma_{ij} = \lambda u_{l,l}\delta_{ij} + \mu(u_{i,j} + u_{j,i}) \quad [28]$$

the boundary conditions for the solution to be added, here denoted by an asterisk, can be written as follows, after arbitrarily setting $B_y^* = 0$

$$2(1-\nu)\frac{\partial B_x^*}{\partial z} + 2\nu\frac{\partial B_z^*}{\partial x} - x\frac{\partial^2 B_x^*}{\partial z^2} - \frac{\partial^2 \beta^*}{\partial z^2} = -\left[2(1-\nu)\frac{\partial \bar{B}_x}{\partial z} + 2\nu\frac{\partial \bar{B}_z}{\partial x} + 2\nu\frac{\partial \bar{B}_y}{\partial y} - x\frac{\partial^2 \bar{B}_x}{\partial z^2} - y\frac{\partial^2 \bar{B}_y}{\partial z^2} - \frac{\partial^2 \bar{\beta}}{\partial z^2}\right] \quad [29]$$

$$(1-2\nu)\left(\frac{\partial B_x^*}{\partial x} + \frac{\partial B_z^*}{\partial z}\right) - x\frac{\partial^2 B_x^*}{\partial x \partial z} - \frac{\partial^2 \beta^*}{\partial x \partial z} = (1-2\nu)\left(\frac{\partial \bar{B}_x}{\partial x} + \frac{\partial \bar{B}_z}{\partial z}\right) - x\frac{\partial^2 \bar{B}_x}{\partial x \partial z} - y\frac{\partial^2 \bar{B}_y}{\partial x \partial z} - \frac{\partial^2 \bar{\beta}}{\partial x \partial z} \quad [30]$$

$$(1-2\nu)\frac{\partial B_x^*}{\partial y} - x\frac{\partial^2 B_x^*}{\partial y \partial z} - \frac{\partial^2 \beta^*}{\partial y \partial z} = (1-2\nu)\left(\frac{\partial \bar{B}_y}{\partial z} + \frac{\partial \bar{B}_z}{\partial y}\right) - x\frac{\partial^2 \bar{B}_x}{\partial y \partial z} - y\frac{\partial^2 \bar{B}_y}{\partial y \partial z} - \frac{\partial^2 \bar{\beta}}{\partial y \partial z} \quad [31]$$

The double-bar functions now stand for any one of the Solutions 1(a), 2(a), and 3(a) of the previous section. These are known functions and they are finite, continuous, and harmonic in the re-

gion $z \geq 0$. The functions with an asterisk are to be finite and continuous in the region $z \geq 0$, and in the same region we have

$$\nabla^2 B_i^* = 0 \quad [32]$$

$$\nabla^2 \beta^* = 0 \quad [33]$$

The last five equations constitute our mathematical problem.

Taking the derivative of Equations [30] and [31] with respect to y and x, respectively, and subtracting the results, one obtains

$$\frac{\partial^2 B_z^*}{\partial y \partial z} = \frac{\partial^2 \bar{B}_x}{\partial y \partial z} - \frac{\partial^2 \bar{B}_y}{\partial x \partial z} \quad [34]$$

It follows by the uniqueness theorem of the Dirichlet problem that, since the right side is harmonic in $z \geq 0$, Equation [34] is valid in $z \geq 0$. One then obtains the result

$$B_z^* = \bar{B}_z - \int \frac{\partial \bar{B}_y}{\partial x}\, dy \quad [35]$$

With this result the boundary conditions may be reduced to the following two equations

$$2(1-\nu)\frac{\partial B_x^*}{\partial z} - \frac{\partial^2 \beta^*}{\partial z^2} = -2(1-\nu)\frac{\partial \bar{B}_z}{\partial z} - 4\nu \frac{\partial \bar{B}_z}{\partial x} + 2x\frac{\partial^2 \bar{B}_z}{\partial z^2} - 2\nu \frac{\partial \bar{B}_y}{\partial y} + y\frac{\partial^2 \bar{B}_y}{\partial z^2} + \frac{\partial^2 \bar{\beta}}{\partial z^2} - x\int \frac{\partial^3 \bar{B}_y}{\partial x \partial z^2}\, dy + 2\nu \int \frac{\partial^2 \bar{B}_y}{\partial z^2}\, dy \quad [36]$$

$$(1-2\nu)\frac{\partial B_x^*}{\partial x} - \frac{\partial^2 \beta^*}{\partial x \partial z} = (1-2\nu)\frac{\partial \bar{B}_z}{\partial x} - y\frac{\partial^2 \bar{B}_y}{\partial x \partial z} - \frac{\partial^2 \bar{\beta}}{\partial x \partial z} + (1-2\nu)\int \frac{\partial^2 \bar{B}_y}{\partial x \partial z}\, dy - x\int \frac{\partial^3 \bar{B}_y}{\partial x^2 \partial z} dy \quad [37]$$

Now it can be shown that if

$$\nabla^2 \varphi = 0$$

then

$$\nabla^2 \left(x_i \frac{\partial \varphi}{\partial x_j} - x_j \frac{\partial \varphi}{\partial x_i} \right) = 0 \quad [38]$$

where $i \neq j$

Using this result, the right sides of Equations [36] and [37] may be made harmonic without changing their value on $z = 0$. To the right side of Equation [36] one adds

$$-2z\frac{\partial^2 \bar{B}_z}{\partial x \partial z} - z\frac{\partial^2 \bar{B}_y}{\partial y \partial z} + z\int \frac{\partial^3 \bar{B}_y}{\partial x^2 \partial z}\, dy$$

and to the right side of Equation [37] one adds

$$z\frac{\partial^2 \bar{B}_y}{\partial x \partial y} + z\int \frac{\partial^3 \bar{B}_y}{\partial x^3}\, dy$$

Again by the uniqueness theorem of the Dirichlet problem the resulting equations must be valid in the region $z \geq 0$. One then obtains without difficulty the results

$$B_x^* = -(3-4\nu)\bar{B}_x + 2(1-2\nu)\int \left(\frac{\partial \bar{B}_z}{\partial x} + \frac{\partial \bar{B}_y}{\partial y} \right) dz + 2\left(x\frac{\partial}{\partial z} - z\frac{\partial}{\partial x} \right)\bar{B}_x + 2\left(y\frac{\partial}{\partial z} - z\frac{\partial}{\partial y} \right)\bar{B}_y + 2\frac{\partial \bar{\beta}}{\partial z} - \int \frac{\partial \bar{B}_y}{\partial z}\, dy \quad [39]$$

$$\beta^* = -4(1-\nu)(1-2\nu)\left[\int \bar{B}_z dz - \iint \left(\frac{\partial \bar{B}_x}{\partial x} + \frac{\partial \bar{B}_y}{\partial y} \right)(dz)^2 \right] + (3-4\nu)(\bar{\beta} + y\bar{B}_y) + 2(1-2\nu)x\bar{B}_x - 4(1-\nu)\int \bar{B}_y\, dy - 2(1-2\nu)z\int \left(\frac{\partial \bar{B}_z}{\partial x} + \frac{\partial \bar{B}_y}{\partial y} \right) dz + \int \left(x\frac{\partial \bar{B}_y}{\partial x} + z\frac{\partial \bar{B}_y}{\partial z} \right) dy \quad [40]$$

It is easy to show that the corresponding displacement is given by

$$\left.\begin{aligned} u_x^* &= \bar{B}_x - \frac{1}{4(1-\nu)}\frac{\partial}{\partial x}(x\bar{B}_x + zB_z' + \beta') \\ u_y^* &= \bar{B}_y - \frac{1}{4(1-\nu)}\frac{\partial}{\partial y}(x\bar{B}_x + zB_z' + \beta') \\ u_z^* &= B_z' - \frac{1}{4(1-\nu)}\frac{\partial}{\partial z}(x\bar{B}_x + zB_z' + \beta') \end{aligned}\right\} \quad [41]$$

where

$$B_z' = -(3-4\nu)\bar{B}_z + 2(1-2\nu)\varphi + 2\left(x\frac{\partial}{\partial z} - z\frac{\partial}{\partial x} \right)\bar{B}_x + 2\left(y\frac{\partial}{\partial z} - z\frac{\partial}{\partial y} \right)\bar{B}_y + 2\frac{\partial \bar{\beta}}{\partial z} \quad [42]$$

$$\beta' = -4(1-\nu)(1-2\nu)\psi + 2(1-2\nu)x\bar{B}_x + (3-4\nu)(\bar{\beta} + y\bar{B}_y) - 2(1-2\nu)z\varphi \quad [43]$$

and where in B_z' and β'

$$\varphi = \int \left(\frac{\partial \bar{B}_x}{\partial x} + \frac{\partial \bar{B}_y}{\partial y} \right) dz$$

$$\psi = \int (\bar{B}_z - \varphi) dz$$

The arbitrary functions of integration in φ and ψ must be so determined that the displacement u_i^* is zero at infinity in the region $z \geq 0$. With this restriction we obtain the following expressions for φ and ψ corresponding to displacement discontinuities in the ζ, ξ, and η-component of the displacement, respectively

(1) $$\varphi = l^2 \frac{\partial^2 L}{\partial x^2} - ln\frac{\partial \bar{l}}{\partial x} \quad [44]$$

(2) $$\varphi = -2nl\frac{\partial^2 M}{\partial x \partial y} + (n^2 - l^2)\frac{\partial \bar{J}}{\partial x} \quad [45]$$

(3) $$\varphi = -2l\frac{\partial^2 N}{\partial x \partial y} + n\frac{\partial \bar{K}}{\partial y} \quad [46]$$

(1) $$\psi = n^2 \bar{I} + l^2 \frac{\partial P}{\partial x} \quad [47]$$

(2) $$\psi = 2nl\left(J - \frac{\partial Q}{\partial x} \right) \quad [48]$$

(3) $$\psi = 2l\frac{\partial R}{\partial y} \quad [49]$$

where in φ and ψ

$$[L, M, N] = \frac{1}{4\pi}\int_{A'} [2\hat{u}_\xi', \hat{u}_\xi', \hat{u}_\eta'] \log (\bar{r}_0 + z + c - l\xi')d\xi'd\eta' \quad \ldots\ldots [50]$$

$$[P, Q, R] = \frac{1}{4\pi}\int_{A'} [2\hat{u}_\xi', \hat{u}_\xi', \hat{u}_\eta'] \frac{x - n\xi'}{\bar{r}_0 + z + c - l\xi'} d\xi'd\eta' \quad \ldots\ldots [51]$$

The displacement generated by a displacement discontinuity in the elastic half-space, given by

$$u_i = \bar{u}_i + u_i^* \quad \ldots\ldots [52]$$

is now expressed in terms of integrals of the form of Equations [13], [27], [50], and [51]. One obtains the solutions for discontinuities in the ξ, η, and ζ-component of the displacement separately, and the general case is then obtained by superposition of these solutions.

3—Constant-Displacement Discontinuity Over a Rectangular Area

As an example we work out the displacement generated by a constant displacement discontinuity over a rectangular area parallel to the boundary. The direction cosines l and n have the values zero and unity, respectively. We work out two cases: (a) a discontinuity in the displacement component normal to the boundary, and (b) a discontinuity in the displacement parallel to the boundary. For case (a) we obtain from Equations [1], [2], [3], [4], and [14]

$$[\bar{u}_x, \bar{u}_y, \bar{u}_z] = \left[0, 0, \frac{\partial \bar{I}}{\partial z}\right] - \frac{1}{4(1-\nu)}\frac{\partial}{\partial[x, y, z]}\left[(z - c)\frac{\partial \bar{I}}{\partial z} + (1 - 2\nu)\bar{I}\right] \quad \ldots\ldots [53]$$

and from Equations [15], [16], [17], [18], [41], [42], [43], [44], and [47] we obtain

$$[u_x^*, u_y^*] = \frac{1}{4(1-\nu)}\frac{\partial}{\partial[x, y]}\left\{[z - c(3 - 4\nu)]\frac{\partial \bar{I}}{\partial z} - 2zc\frac{\partial^2 \bar{I}}{\partial z^2} + (1 - 2\nu)\bar{I}\right\}$$

$$u_z^* = \frac{1}{4(1-\nu)}\frac{\partial}{\partial z}\left\{[z + c(3 - 4\nu)]\frac{\partial \bar{I}}{\partial z} - 2cz\frac{\partial^2 \bar{I}}{\partial z^2} - 2(1 - \nu)\bar{I}\right\} \quad \ldots\ldots [54]$$

where

$$2\pi\frac{\partial \bar{I}}{\partial x} = \hat{u}_x \log\frac{(\bar{r}_1 - y + b)(\bar{r}_3 - y - b)}{(\bar{r}_2 - y + b)(\bar{r}_4 - y - b)}$$

$$2\pi\frac{\partial \bar{I}}{\partial y} = \hat{u}_x \log\frac{(\bar{r}_1 - x + a)(\bar{r}_3 - x - a)}{(\bar{r}_4 - x + a)(\bar{r}_2 - x - a)}$$

$$2\pi\frac{\partial \bar{I}}{\partial z} = -\hat{u}_x\left[\tan^{-1}\frac{(a - x)(b - y)}{(z - c)\bar{r}_1} + \tan^{-1}\frac{(a + x)(b - y)}{(z - c)\bar{r}_2} + \tan^{-1}\frac{(a + x)(b + y)}{(z - c)\bar{r}_3} + \tan^{-1}\frac{(a - x)(b + y)}{(z - c)\bar{r}_4}\right]$$

$$2\pi\frac{\partial \bar{I}}{\partial x} = \hat{u}_z \log\frac{(\bar{r}_1 - y + b)(\bar{r}_2 - y - b)}{(\bar{r}_2 - y + b)(\bar{r}_4 - y - b)}$$

$$2\pi\frac{\partial \bar{I}}{\partial y} = \hat{u}_z \log\frac{(\bar{r}_1 - x + a)(\bar{r}_3 - x - a)}{(\bar{r}_4 - x + a)(\bar{r}_2 - x - a)}$$

$$2\pi\frac{\partial \bar{I}}{\partial z} = -\hat{u}_z\left[\tan^{-1}\frac{(a - x)(b - y)}{(z + c)\bar{r}_1} + \tan^{-1}\frac{(a + x)(b - y)}{(z + c)\bar{r}_2} + \tan^{-1}\frac{(a + x)(b + y)}{(z + c)\bar{r}_3} + \tan^{-1}\frac{(a - x)(b + y)}{(z + c)\bar{r}_4}\right]$$

where

$$\bar{r}_1^2 = (a - x)^2 + (b - y)^2 + (z - c)^2$$
$$\bar{r}_2^2 = (a + x)^2 + (b - y)^2 + (z - c)^2$$
$$\bar{r}_3^2 = (a + x)^2 + (b + y)^2 + (z - c)^2$$
$$\bar{r}_4^2 = (a - x)^2 + (b + y)^2 + (z - c)^2$$
$$\bar{r}_1^2 = (a - x)^2 + (b - y)^2 + (z + c)^2$$
$$\bar{r}_2^2 = (a + x)^2 + (b - y)^2 + (z + c)^2$$
$$\bar{r}_3^2 = (a + x)^2 + (b + y)^2 + (z + c)^2$$
$$\bar{r}_4^2 = (a - x)^2 + (b + y)^2 + (z + c)^2$$

This completes the case of a discontinuity in the z-component of the displacement.

We turn now to case (b) with a discontinuity in the displacement component parallel to the boundary. From Equations [5], [6], [7], [8], and [14] one obtains

$$[\bar{u}_x, \bar{u}_y, \bar{u}_z] = \left[\frac{\partial \bar{J}}{\partial z}, 0, \frac{\partial \bar{J}}{\partial x}\right] - \frac{1}{2(1-\nu)}\frac{\partial}{\partial[x, y, z]}\left[(z - c)\frac{\partial \bar{J}}{\partial x}\right]$$

and from Equations [19], [20], [21], [22], [41], [42], [43], [45], and [48]

$$[u_x^*, u_y^*, u_z^*] = \left[\frac{\partial \bar{J}}{\partial z}, 0, \frac{\partial \bar{J}}{\partial x} + 4c\frac{\partial^2 \bar{J}}{\partial x \partial z}\right] - \frac{1}{4(1-\nu)}\frac{\partial}{\partial[x, y, z]}\left\{2[z + (3 - 4\nu)c]\frac{\partial \bar{J}}{\partial x} + 4cz\frac{\partial^2 \bar{J}}{\partial x \partial z}\right\}$$

where J and $\bar{J}$ are the same as I and $\bar{I}$ given previously except that $\hat{u}_x$ is replaced by $\frac{1}{2}(\hat{u}_x)$. This completes the case of a discontinuity in the x-component of the displacement.

Stress Distribution Around a Circular Inclusion in a Semi-Infinite Elastic Plate

By E. M. SALEME,[1] TUCUMAN, ARGENTINA

This paper contains an exact two-dimensional solution in series form for the stresses and displacements around a circular inclusion perfectly bonded to a semi-infinite elastic plate. At infinity the plate is assumed to be in a state of uniform tension parallel to the straight boundary. It should be emphasized, however, that the method of solution presented may be applied to other types of loading. Numerical results are given for the variation along the axis of symmetry of the normal stress which is parallel to the straight boundary, for a given geometry, and various ratios of the elastic moduli of the plate and the inclusion. Finally, the known solutions corresponding to an infinite plate with a circular inclusion and to a semi-infinite plate with a circular hole are obtained as limiting cases.

Introduction

THE problem of a circular hole in a semi-infinite elastic plate was first studied by Jeffery (1)[2] as an application of his general solution of the two-dimensional field equations of elasticity theory referred to bipolar co-ordinates. Mindlin (2) noticed and corrected an error in Jeffery's paper, as a consequence of which the straight boundary was not free of tractions. The stress distribution in an infinite plate with an elliptical inclusion was determined by Donnell (3) who used elliptical co-ordinates.[3]

In what follows, we make use of bipolar co-ordinates to obtain the generalized plane-stress solution for a semi-infinite elastic plate with a perfectly bonded circular inclusion of a different elastic material. The body forces are assumed to vanish and, so far as the loading is concerned, we confine ourselves to the uniaxial case in which the tractions at infinity reduce to a uniform tension parallel to the straight boundary. The problem is solved by extending the uniform stress field at infinity throughout the region occupied by the medium, and superimposing on this uniaxial field two sequences of solutions of the field equations, one regular for the domain exterior to the inclusion and the other regular inside the inclusion, such that the resultant stress and displacement fields satisfy all the boundary and bond conditions. It should be noted, moreover, that the plane-strain solution associated with this problem is reached from the generalized plane-stress solution by applying the well-known transformation of elastic constants.

The solution presented here may prove useful in the analysis of such technical problems as the determination of the stresses in the neighborhood of a reinforcing bar in reinforced-concrete construction, effects of reinforcement of the edge of a circular opening in a plate, and terrain stresses around underground tunnels or pipes.

General Solution of Two-Dimensional Field Equations in Bipolar Co-Ordinates

In this section we recall briefly Jeffery's (1) general solution of the two-dimensional field equations referred to bipolar co-ordinates[4] as defined by the mapping

$$x + iy = c \operatorname{cotanh} \frac{\alpha + i\beta}{2}, \qquad (-\infty < \alpha < \infty,\ -\pi < \beta \leq \pi) \quad [1]$$

where $c > 0$ is the abscissa of one of the poles, Fig. 1. Equivalently, we have

$$x = J \sinh \alpha, \quad y = -J \sin \beta \quad [2]$$

where

$$J = \left[\left(\frac{\partial x}{\partial \alpha}\right)^2 + \left(\frac{\partial y}{\partial \alpha}\right)^2\right]^{1/2} = \frac{c}{\cosh \alpha - \cos \beta} \quad [3]$$

is the "stretch ratio" of the Transformation [1].

Referring to Fig. 1, the curves α = const are circles of radii c cosech α, centered at the points (c cotanh α, 0). The pole $C(c, 0)$ is the limiting point to which these circles shrink as $\alpha \to \infty$. The curves β = const are circular arcs passing through the pole and centered at the points $(0, -c \operatorname{cotan} \beta)$.

In the absence of body forces the Airy stress function $\chi(\alpha, \beta)$ must satisfy the biharmonic equation in bipolar co-ordinates

$$\nabla^4 \chi(\alpha, \beta) = \left[\frac{1}{J^2}\left(\frac{\partial^2}{\partial \alpha^2} + \frac{\partial^2}{\partial \beta^2}\right)\right]^2 \chi(\alpha, \beta) = 0 \quad [4]$$

Following Jeffery (1), we consider the function

$$\chi^*(\alpha, \beta) = \frac{\chi(\alpha, \beta)}{J} \quad [5]$$

instead of $\chi(\alpha, \beta)$. Substituting into Equation [4], there results

$$\nabla^4 J\chi^* = \frac{1}{J^4}\left[\frac{\partial^4}{\partial \alpha^4} + 2\frac{\partial^4}{\partial \alpha^2 \partial \beta^2} + \frac{\partial^4}{\partial \beta^4} - 2\frac{\partial^2}{\partial \alpha^2} + 2\frac{\partial^2}{\partial \beta^2} + 1\right]\chi^* = 0 \quad [6]$$

In terms of $\chi^*(\alpha, \beta)$, the bipolar components of stress are given by

[1] Professor, Facultad de Ciencias Exactas y Tecnologia, Universidad Nacional de Tucuman.

[2] Numbers in parentheses refer to the Bibliography at the end of the paper.

[3] See chapter 7 of (4) for a rather extensive bibliography of related problems.

Contributed by the Applied Mechanics Division and presented at the Annual Meeting, New York, N. Y., December 1–6, 1957, of The American Society of Mechanical Engineers.

Discussion of this paper should be addressed to the Secretary, ASME, 29 West 39th Street, New York, N. Y., and will be accepted until April 10, 1958, for publication at a later date. Discussion received after the closing date will be returned.

Note: Statements and opinions advanced in papers are to be understood as individual expressions of their authors and not those of the Society. Manuscript received by ASME Applied Mechanics Division, June 11, 1956. Paper No. 57—A-18.

[4] For a comprehensive account of the plane problem in orthogonal curvilinear co-ordinates see chapter 2 of (5).

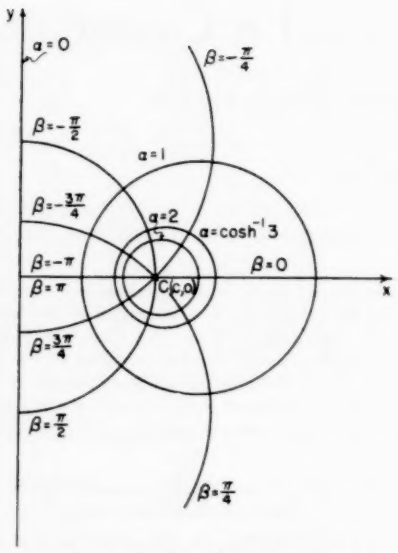

FIG. 1 BIPOLAR CO-ORDINATES

$$
\left.\begin{aligned}
c\tau_{\alpha\alpha} &= \left[(\cosh\alpha - \cos\beta)\frac{\partial^2}{\partial\beta^2} - \sinh\alpha\frac{\partial}{\partial\alpha} - \sin\beta\frac{\partial}{\partial\beta} + \cosh\alpha\right]\chi^*(\alpha,\beta)\\
c\tau_{\beta\beta} &= \left[(\cosh\alpha - \cos\beta)\frac{\partial^2}{\partial\alpha^2} - \sinh\alpha\frac{\partial}{\partial\alpha} - \sin\beta\frac{\partial}{\partial\beta} + \cos\beta\right]\chi^*(\alpha,\beta)\\
c\tau_{\alpha\beta} &= -(\cosh\alpha - \cos\beta)\frac{\partial^2}{\partial\alpha\partial\beta}\chi^*(\alpha,\beta)
\end{aligned}\right\} \quad \ldots[7]
$$

and the components of displacement are

$$
\left.\begin{aligned}
EU_\alpha &= \frac{1-\nu}{J}\frac{\partial\chi(\alpha,\beta)}{\partial\alpha} - \frac{1}{J}\frac{\partial Q(\alpha,\beta)}{\partial\beta}\\
&= (1-\nu)\left[\frac{\partial}{\partial\alpha} - \frac{\sinh\alpha}{\cosh\alpha - \cos\beta}\right]\chi^*(\alpha,\beta)\\
&\quad - \left[\frac{\partial}{\partial\beta} - \frac{\sin\beta}{\cosh\alpha - \cos\beta}\right]Q^*(\alpha,\beta)\\
EU_\beta &= \frac{1-\nu}{J}\frac{\partial\chi(\alpha,\beta)}{\partial\beta} + \frac{1}{J}\frac{\partial Q(\alpha,\beta)}{\partial\alpha}\\
&= (1-\nu)\left[\frac{\partial}{\partial\beta} - \frac{\sin\beta}{\cosh\alpha - \cos\beta}\right]\chi^*(\alpha,\beta)\\
&\quad + \left[\frac{\partial}{\partial\alpha} - \frac{\sinh\alpha}{\cosh\alpha - \cos\beta}\right]Q^*(\alpha,\beta)
\end{aligned}\right\} \quad \ldots[8]
$$

where the associated displacement function

$$
Q^*(\alpha,\beta) = \frac{1}{J}Q(\alpha,\beta)
$$

satisfies the differential equations

$$
\frac{\partial^2}{\partial\alpha\partial\beta}Q^* = \left[\frac{\partial^2}{\partial\alpha^2} - \frac{\partial^2}{\partial\beta^2} - 1\right]\chi^*,
$$

$$
\left[\frac{\partial^2}{\partial\alpha^2} - \frac{\partial^2}{\partial\beta^2} - 1\right]Q^* = -4\frac{\partial^2}{\partial\alpha\partial\beta}\chi^* \quad \ldots[9]
$$

For continuity, the stress and displacement components must be periodic in β, of period 2π. This leads us to consider solutions of the form

$$
\chi^*(\alpha,\beta) = \sum_{k=0}^{\infty}\varphi_k(\alpha)[a_k\cos k\beta + b_k\sin k\beta] \quad \ldots[10]
$$

In the following we shall restrict ourselves to the symmetric case ($b_k = 0$) and, without loss of generality,[5] set $a_k = 1$.

Jeffery (1, 2) has shown that the solutions of Equations [6] and [9] that give a single-valued displacement field, can be written

$$
\chi^*(\alpha,\beta) = B_0\alpha(\cosh\alpha - \cos\beta) + [A_1 + C_1\cosh 2\alpha + D_1\sinh 2\alpha]\cos\beta + \sum_{k=2}^{\infty}\varphi_k(\alpha)\cos k\beta \quad \ldots[11]
$$

$$
\left.\begin{aligned}
Q^*(\alpha,\beta) &= 2B_0\beta(\cosh\alpha - \cos\beta)\\
&\quad + 2[C_1\sinh 2\alpha + D_1\cosh 2\alpha]\sin\beta\\
&\quad + \sum_{k=2}^{\infty}\psi_k(\alpha)\sin k\beta
\end{aligned}\right\} \quad \ldots[12]
$$

where

$$
\varphi_k(\alpha) = A_k\cosh(k-1)\alpha + B_k\sinh(k-1)\alpha + C_k\cosh(k+1)\alpha + D_k\sinh(k+1)\alpha, \quad (k \geq 2) \quad \ldots[13]
$$

$$
\psi_k(\alpha) = 2[A_k\sinh(k-1)\alpha + B_k\cosh(k-1)\alpha + C_k\sinh(k+1)\alpha + D_k\cosh(k+1)\alpha], \quad (k \geq 2) \quad \ldots[14]
$$

CIRCULAR INCLUSION IN A SEMI-INFINITE PLATE UNDER UNIFORM TENSION AT INFINITY

We are concerned with an elastic plate extending over the half-plane $x \geq 0$, subjected to a uniform tension at infinity $\tau_{yy} = \tau_0$, in a direction parallel to the straight edge. Let the plate have a circular hole of radius r_0, centered at the point $C_0(x, 0)$, which is filled by an elastic inclusion of another material, perfectly bonded to the plate.

Without loss of generality, let $\tau_0 = 1$ and consider the Airy stress function

$$
\chi_0(x,y) = \frac{x^2}{2} - cx \quad \ldots[15]
$$

together with the associated displacement function

$$
Q_0(x,y) = xy - cy \quad \ldots[16]
$$

which satisfies the relations

$$
\frac{\partial^2 Q_0}{\partial x\partial y} = \nabla^2\chi_0 = 1, \quad \nabla^2 Q_0 = 0 \quad \ldots[17]
$$

The functions χ_0 and Q_0 generate the solution

$$
\tau_{xx} = \tau_{xy} = 0, \quad \tau_{yy} = 1,
$$

$$
U_x = -\frac{\nu}{E}(x - c), \quad U_y = \frac{1}{E}y \quad \ldots[18]
$$

which thus corresponds to a homogeneous uniaxial stress field throughout the region $x \geq 0$.

[5] The coefficients a_k may be absorbed in $\varphi_k(\alpha)$.

We note that the arbitrary additive rigid-displacement field in Equations [18] has been chosen in such a way that the point $C(c, 0)$ has zero displacement. By Equations [2], the functions χ_0 and Q_0 admit the representation

$$\chi_0(\alpha, \beta) = \frac{1}{2} J^2 \sinh^2 \alpha - cJ \sinh \alpha \quad \ldots\ldots [19]$$

$$Q_0(\alpha, \beta) = -J^2 \sinh \alpha \sin \beta + cJ \sin \beta \quad \ldots\ldots [20]$$

Hence

$$\left.\begin{aligned} \chi_0^*(\alpha, \beta) &= \frac{1}{J} \chi_0(\alpha, \beta) \\ &= \frac{c}{2}\left[\frac{\sinh \alpha}{\cosh \alpha - \cos \beta} - 2\right] \sinh \alpha \\ &= \frac{c}{2}\left[-\sinh \alpha + 2 \sum_{k=1}^{\infty} e^{-k\alpha} \sinh \alpha \cos k\beta\right] \end{aligned}\right\} \ldots [21]$$

$$\left.\begin{aligned} Q_0^*(\alpha, \beta) &= \frac{1}{J} Q_0(\alpha, \beta) \\ &= c\left[1 - \frac{\sinh \alpha}{\cosh \alpha - \cos \beta} \sin \beta\right] \\ &= c\left[e^{-2\alpha} \sin \beta - 2 \sum_{k=2}^{\infty} e^{-k\alpha} \sinh \alpha \sin k\beta\right] \end{aligned}\right\} \ldots [22]$$

where the series expansion is valid for $\alpha > 0$

A more general stress function generating uniform tension at infinity, while maintaining the straight boundary free from tractions, is obtained by adding to Equation [21] a function of the form represented by Equation [11] subject to the conditions

$$\tau_{\alpha\alpha}(0, \beta) = \tau_{\alpha\beta}(0, \beta) = \tau_{\beta\beta}(0, 0) = 0 \quad \ldots\ldots [23]$$

Substituting Equations [23] and [11] into Equation [7] we obtain

$$\left.\begin{aligned} &A_1 + C_1 = 0, \quad B_0 + 2D_1 = 0 \\ &A_k + C_k = 0, \quad (k-1)B_k + (k+1)D_k = 0, \quad (k \geq 2) \end{aligned}\right\} \ldots [24]$$

The required stress function can then be written in the form

$$\chi_1^* = \chi_0^* + \chi^* = -\frac{c}{2} \sinh \alpha + B_0 \alpha (\cosh \alpha - \cos \beta) + \sum_{k=1}^{\infty} \phi_k(\alpha) \cos k\beta \quad \ldots\ldots [25]$$

where

$$\left.\begin{aligned} \phi_1(\alpha) &= ce^{-\alpha} \sinh \alpha + A_1(1 - \cosh 2\alpha) + \frac{B_0}{2} \sinh 2\alpha \\ \phi_k(\alpha) &= ce^{-k\alpha} \sinh \alpha + A_k [\cosh (k-1)\alpha - \cosh (k+1)\alpha] \\ &\quad + (k-1)B_k \left[\frac{\sinh (k-1)\alpha}{k-1} - \frac{\sinh (k+1)\alpha}{k+1}\right] (k \geq 2) \end{aligned}\right\} \ldots [26]$$

The associated displacement function is given by

$$Q_1^* = Q_0^* + Q^* = 2B_0\beta(\cosh \alpha - \cos \beta) + \sum_{k=1}^{\infty} \psi_k(\alpha) \sin k\beta \quad \ldots\ldots [27]$$

with

$$\left.\begin{aligned} \psi_1(\alpha) &= ce^{-2\alpha} - 2A_1 \sinh 2\alpha + B_0 \cosh 2\alpha \\ \psi_k(\alpha) &= -2ce^{-k\alpha} \sinh \alpha + 2A_k [\sinh (k-1)\alpha - \sinh (k+1)\alpha] \\ &\quad + (k-1)B_k \left[\frac{\cosh (k-1)\alpha}{k-1} - \frac{\cosh (k+1)\alpha}{k+1}\right] (k \geq 2) \end{aligned}\right\} \ldots [28]$$

Considerations, analogous to those introduced earlier regarding the single-valuedness of the displacement field, lead us to take the stress and displacement functions for the inclusion in the form

$$\left.\begin{aligned} \bar{\chi}^*(\alpha, \beta) &= \bar{C}_0 \sinh \alpha + \bar{B}_0 \alpha (\cosh \alpha - \cos \beta) \\ &\quad + [\bar{A}_1 + \bar{C}_1 \cosh 2\alpha + \bar{D}_1 \sinh 2\alpha] \cos \beta \\ &\quad + \sum_{k=2}^{\infty} \bar{\varphi}_k(\alpha) \cos k\beta \end{aligned}\right\} \ldots [29]$$

$$\left.\begin{aligned} Q^*(\alpha, \beta) &= 2\bar{B}_0 \beta (\cosh \alpha - \cos \beta) \\ &\quad + 2[\bar{C}_1 \sinh 2\alpha + \bar{D}_1 \cosh 2\alpha] \sin \beta \\ &\quad + \sum_{k=2}^{\infty} \bar{\psi}_k(\alpha) \sin k\beta \end{aligned}\right\} \ldots [30]$$

where

$$\left.\begin{aligned} \bar{\varphi}_k(\alpha) &= \bar{A}_k \cosh (k-1)\alpha + \bar{B}_k \sinh (k-1)\alpha \\ &\quad + \bar{C}_k \cosh (k+1)\alpha + \bar{D}_k \sinh (k+1)\alpha, \quad (k \geq 2) \end{aligned}\right\} \ldots [31]$$

$$\left.\begin{aligned} \bar{\psi}_k(\alpha) &= 2\bar{A}_k \sinh (k-1)\alpha + 2\bar{B}_k \cosh (k-1)\alpha \\ &\quad + 2\bar{C}_k \sinh (k+1)\alpha + 2\bar{D}_k \cosh (k+1)\alpha, \quad k(\geq 2) \end{aligned}\right\} \ldots [32]$$

In Equations [29] to [32], as well as throughout the remainder of this paper, letters carrying bars refer to the inclusion.

The condition of regularity of the stress and displacement fields at the pole C, i.e., as $\alpha \to \infty$, requires

$$\left.\begin{aligned} &\bar{B}_0 = 0, \qquad \bar{C}_0 + \bar{A}_1 = 0 \\ &\bar{A}_k + \bar{B}_k = 0, \quad \bar{C}_k + \bar{D}_k = 0, \quad (k \geq 2) \end{aligned}\right\} \ldots [33]$$

Hence

$$\bar{\chi}^*(\alpha, \beta) = -\bar{A}_1 \sinh \alpha + \sum_{k=1}^{\infty} \bar{\phi}_k(\alpha) \cos k\beta \quad \ldots\ldots [34]$$

$$\bar{Q}^*(\alpha, \beta) = \sum_{k=1}^{\infty} \bar{\psi}_k(\alpha) \sin k\beta \quad \ldots\ldots [35]$$

in which

$$\bar{\phi}_1(\alpha) = \bar{A}_1 + \bar{C}_1 e^{-2\alpha}, \quad \bar{\phi}_k(\alpha) = \bar{A}_k e^{-(k-1)\alpha} + \bar{C}_k e^{-(k+1)\alpha}, \quad (k \geq 2) \quad \ldots\ldots [36]$$

$$\bar{\psi}_1(\alpha) = -2\bar{C}_1 e^{-2\alpha}, \quad \bar{\psi}_k(\alpha) = -2\bar{A}_k e^{-(k-1)\alpha} - 2\bar{C}_k e^{-(k+1)\alpha}, \quad (k \geq 2) \quad \ldots\ldots [37]$$

In the case of perfect bond between the plate and the inclusion, the following conditions must be satisfied by the stresses and displacements at the common boundary $\alpha = \alpha_0$

$$\tau_{\alpha\alpha} = \bar{\tau}_{\alpha\alpha}, \quad \tau_{\alpha\beta} = \bar{\tau}_{\alpha\beta} \quad \ldots\ldots [38]$$

$$U_\alpha = \bar{U}_\alpha, \quad U_\beta = \bar{U}_\beta \quad \ldots\ldots [39]$$

From Equations [7], [25], [34], and [38], we obtain

$$-\frac{B_0}{2}\sinh 2\alpha_0 + \phi_1(\alpha_0) = \bar{\phi}_1(\alpha_0) \quad \ldots\ldots [40]$$

$$-B_0 + \phi_1'(\alpha_0) = \bar{\phi}_1'(\alpha_0) \quad \ldots\ldots [41]$$

$$\phi_k(\alpha_0) = \bar{\phi}_k(\alpha_0), \quad (k \geq 2) \quad \ldots\ldots [42]$$

$$\phi_k'(\alpha_0) = \bar{\phi}_k'(\alpha_0), \quad (k \geq 2) \quad \ldots\ldots [43]$$

By Equations [36], [37], [42], and [43], we have

$$\left.\begin{aligned} \bar{\psi}_k(\alpha_0) &= -2\bar{\phi}_k(\alpha_0) = -2\phi_k(\alpha_0), \quad (k \geq 2) \\ \bar{\psi}_k'(\alpha_0) &= -2\bar{\phi}_k(\alpha_0) = -2\phi_k'(\alpha_0), \quad (k \geq 2) \end{aligned}\right\} \quad \ldots [44]$$

Equations [39] finally yield

$$\begin{aligned} &\frac{1-\nu}{E}\left[-\frac{c}{2} + \frac{B_0}{2}(2 + \cosh 2\alpha_0) - \frac{1}{2}\phi'_1\right] \\ &\qquad - \frac{1}{E}\left[B_0(2 + \cosh 2\alpha_0) - \psi_1\right] \\ &\qquad = \frac{1-\bar{\nu}}{\bar{E}}\left[-\bar{A}_1 - \frac{1}{2}\phi_1'\right] - \frac{1}{\bar{E}}\left[-\bar{\psi}_1\right] \quad \ldots\ldots [45] \end{aligned}$$

$$\left.\begin{aligned} L = &-\left[\frac{3-\nu}{E} + \frac{1+\bar{\nu}}{\bar{E}}\right] \\ &\Big\{-4c\lambda e^{-(2k+1)\alpha_0}\sinh\alpha_0 - A_k\left[1 - \lambda e^{-2k\alpha_0}\right. \\ &- 2k\lambda e^{-(2k+1)\alpha_0}\sinh\alpha_0] + A_{k+1}\left[1 - \lambda e^{-2(k+1)\alpha_0}\right. \\ &- 2(k+1)\lambda e^{-(2k+1)\alpha_0}\sinh\alpha_0] - \frac{B^*_{k,k+1}}{k(k+1)} \\ &[1 + \lambda e^{-2k\alpha_0} + 2k\lambda e^{-(2k+1)\alpha_0}\sinh\alpha_0]\Big\}, \quad (k \geq 1) \end{aligned}\right\} \quad \ldots [46]$$

$$\left.\begin{aligned} L = &-\left[\frac{1+\nu}{E} + \frac{3-\bar{\nu}}{\bar{E}}\right] \\ &\Big\{A_k[\mu + e^{2k\alpha_0} + 2ke^{(2k+1)\alpha_0}\sinh\alpha_0] \\ &- A_{k+1}[\mu + e^{2(k+1)\alpha_0} + 2(k+1)e^{(2k+1)\alpha_0}\sinh\alpha_0] \\ &- \frac{B^*_{k,k+1}}{k(k+1)}[\mu + e^{2k\alpha_0} - 2ke^{(2k+1)\alpha_0}\sinh\alpha_0]\Big\}, \\ &(k \geq 1) \end{aligned}\right\} \quad \ldots [47]$$

where

$$\left.\begin{aligned} L = &-\frac{1-\nu}{E}\left[\phi_1 - \frac{B_0}{2}\sinh 2\alpha_0\right] \\ &+ \frac{1}{E}\left[\frac{1}{2}\psi_1' - B_0\sinh 2\alpha_0\right] + \frac{1-\bar{\nu}}{\bar{E}}\bar{\phi}_1 - \frac{1}{2\bar{E}}\bar{\psi}_1' \\ &= -\frac{c}{2}\left[\frac{1-\nu}{E} + \frac{1+\nu}{E}e^{-2\alpha_0}\right] \\ &- A_1\left[\frac{1-\nu}{E} + \frac{1+\nu}{E}\cosh 2\alpha_0\right] \\ &+ \frac{1-\bar{\nu}}{\bar{E}}\bar{A}_1 - \frac{1+\bar{\nu}}{\bar{E}}\bar{C}_1 e^{-2\alpha_0} \end{aligned}\right\} \quad \ldots [48]$$

$$\lambda = \frac{\dfrac{1+\nu}{E} - \dfrac{1+\bar{\nu}}{\bar{E}}}{\dfrac{3-\nu}{E} + \dfrac{1+\bar{\nu}}{\bar{E}}}, \quad \mu = \frac{\dfrac{3-\nu}{E} - \dfrac{3-\bar{\nu}}{\bar{E}}}{\dfrac{1+\nu}{E} + \dfrac{3-\bar{\nu}}{\bar{E}}} \quad \ldots\ldots [49]$$

$$\left.\begin{aligned} B^*_{1,2} &= -B_0 - 2B_2 \\ B^*_{k,k+1} &= (k-1)kB_k - k(k+1)B_{k+1}, \quad (k \geq 2) \end{aligned}\right\} \quad \ldots [50]$$

By taking the limit of Equations [46] and [47] as $k \to \infty$, it can be shown that $L = 0$. Finally, the coefficients of the stress and displacement functions for the plate are given by

$$\left.\begin{aligned} A_1 = &-c\frac{e^{-2\alpha_0}}{\Delta}\{\bar{\epsilon}(\gamma - \bar{\gamma}) + (\epsilon - \bar{\epsilon})(2\gamma - 3\bar{\gamma})e^{-2\alpha_0} \\ &+ [2(\epsilon - \bar{\epsilon})(\epsilon + \bar{\gamma}) + \bar{\epsilon}(\gamma - \bar{\gamma})]e^{-4\alpha_0} \\ &- \bar{\gamma}(\epsilon - \bar{\epsilon})e^{-6\alpha_0}\} \\ B_0 = &-2c\frac{e^{-2\alpha_0}}{\Delta}\{\bar{\epsilon}(\gamma - \bar{\gamma}) + [\gamma(\gamma - \bar{\gamma}) \\ &- (\epsilon - \bar{\epsilon})(\epsilon + 2\bar{\gamma})]e^{-2\alpha_0} + \bar{\gamma}(\epsilon - \bar{\epsilon})e^{-4\alpha_0}\} \end{aligned}\right\} \quad \ldots [51]$$

where

$$\left.\begin{aligned} &\gamma = \frac{1-\nu}{E}, \quad \bar{\gamma} = \frac{1-\bar{\nu}}{\bar{E}}, \quad \epsilon = \frac{1+\nu}{E}, \quad \bar{\epsilon} = \frac{1+\bar{\nu}}{\bar{E}} \\ &\Delta = \bar{\epsilon}(\epsilon + \bar{\gamma}) + [2(\epsilon - \bar{\epsilon})(\epsilon + 2\bar{\gamma}) \\ &\quad + \bar{\epsilon}(\gamma + 2\epsilon) - \gamma\bar{\gamma}]e^{-2\alpha_0} + [(\epsilon - \bar{\epsilon})(2\gamma - 5\bar{\gamma}) \\ &\quad + (\epsilon + \bar{\gamma})(2\gamma + \bar{\epsilon})]e^{-4\alpha_0} + [2(\epsilon - \bar{\epsilon})(\epsilon + \bar{\gamma}) \\ &\quad + \bar{\epsilon}(\gamma - 2\bar{\gamma}) - \gamma\bar{\gamma}]e^{-6\alpha_0} + \bar{\gamma}(\epsilon - \bar{\epsilon})e^{-8\alpha_0} \end{aligned}\right\} \quad \ldots [52]$$

$$A_k = \frac{A_1 f_1 e^{2\alpha_0} + c(h_1 - h_k)}{f_k}e^{-2k\alpha_0}, \quad (k \geq 1) \quad \ldots [53]$$

$$\begin{aligned} B^*_{k,k+1}\left[4\lambda\sinh^2\alpha_0 + \frac{\mu - \lambda}{k(k+1)}\right] &= A_k d_k e^{2k\alpha_0} + cg_k \\ &- [A_{k+1}d_{k+1}e^{2(k+1)\alpha_0} + cg_{k+1}] \quad \ldots [54] \end{aligned}$$

in which

$$\left.\begin{aligned} f_k &= (1 + \lambda e^{-2k\alpha_0})(1 + \mu e^{-2k\alpha_0}) \\ &\quad + 4k^2\lambda e^{-2k\alpha_0}\sinh^2\alpha_0, \quad (k \geq 1) \\ h_k &= 2k\lambda\sinh\alpha_0(k\sinh\alpha_0 - \cosh\alpha_0) \\ &\quad + \lambda\mu e^{-2k\alpha_0}, \quad (k \geq 1) \\ d_k &= 1 - 2k\lambda e^{-2k\alpha_0}\sinh 2\alpha_0 - \lambda\mu e^{-4k\alpha_0}, \quad (k \geq 1) \\ g_k &= 2k\lambda\sinh\alpha_0(k\sinh\alpha_0 - \cosh\alpha_0) \\ &\quad - \lambda\mu e^{-2k\alpha_0}, \quad (k \geq 1) \end{aligned}\right\} \quad \ldots [55]$$

The coefficients for the inclusion are, on account of Equations [40] to [43]

$$\left.\begin{aligned} \bar{A}_1 &= \frac{1}{2}[c + 2A_1(1 - e^{2\alpha_0}) + 2B_0\sinh^2\alpha_0] \\ \bar{C}_1 &= -\frac{1}{2}[c - 2A_1e^{2\alpha_0}\sinh 2\alpha_0 + 2B_0e^{2\alpha_0}\sinh^2\alpha_0] \\ \bar{A}_k &= \frac{1}{2}\{c + A_k[1 + ke^{2(k-1)\alpha_0} - (k+1)e^{2k\alpha_0}] \\ &\quad - B_k[1 - ke^{2(k-1)\alpha_0} + (k-1)e^{2k\alpha_0}]\}, \quad (k \geq 2) \\ \bar{C}_k &= -\frac{1}{2}\{c + A_k[1 + (k-1)e^{2k\alpha_0} - ke^{2(k+1)\alpha_0}] \\ &\quad + \frac{k-1}{k+1}B_k[1 + (k+1)e^{2k\alpha_0} - ke^{2(k+1)\alpha_0}]\}, \\ &\quad (k \geq 2) \end{aligned}\right\} \quad \ldots [56]$$

Finally, the stresses in the plate become

$$\tau_{\alpha\alpha} = e^{-\alpha}\sinh\alpha + \frac{A_1}{c}(1-\cosh 2\alpha) + \frac{1}{2c}\sum_{k=1}^{\infty}\Big\{-4ce^{-k\alpha}\sinh\alpha\,(k\sinh\alpha - \cosh\alpha) + [(k-2)(k-1)A_{k-1} - (k-1)kA_k]\cosh(k-2)\alpha + B^*_{k-1,k}\sinh(k-2)\alpha - [(k-2)(k-1)A_{k-1} + 2kA_k - (k+1)(k+2)A_{k+1}]\cosh k\alpha - [(k-2)B^*_{k-1,k} + (k+2)B^*_{k,k+1}]\frac{\sinh k\alpha}{k} + [k(k+1)A_k - (k+1)(k+2)A_{k+1}]\cosh(k+2)\alpha + B^*_{k,k+1}\sinh(k+2)\alpha\Big\}\cos k\beta$$

$$\tau_{\beta\beta} = e^{-\alpha}\cosh\alpha + \frac{A_1}{c}(1+\cosh 2\alpha) + \frac{1}{2c}\sum_{k=1}^{\infty}\Big\{4ce^{-k\alpha}\sinh\alpha\,(k\sinh\alpha - \cosh\alpha) - [(k-2)(k-1)A_{k-1} - (k-1)kA_k]\cosh(k-2)\alpha - B^*_{k-1,k}\sinh(k-2)\alpha + [(k-1)(k+2)A_{k-1} - 6kA_k - (k-2)(k+1)A_{k+1}]\cosh k\alpha + [(k+2)B^*_{k-1,k} + (k-2)B^*_{k,k+1}]\frac{\sinh k\alpha}{k} - [k(k+1)A_k + (k+1)(k+2)A_{k+1}]\cosh(k+2)\alpha - B^*_{k,k+1}\sinh(k+2)\alpha\Big\}\cos k\beta \quad \text{..[57]}$$

$$\tau_{\alpha\beta} = \frac{1}{2c}\sum_{k=1}^{\infty}\{-4ce^{-k\alpha}\sinh\alpha(k\sinh\alpha - \cosh\alpha) - [(k-2)(k-1)A_{k-1} - (k-1)kA_k]\sinh(k-2)\alpha + [(k-1)kA_{k-1} - 2kA_k - k(k+1)A_{k+1}]\sinh k\alpha - [k(k+1)A_k - (k+1)(k+2)A_{k+1}]\sinh(k+2)\alpha - B^*_{k-1,k}[\cosh(k-2)\alpha - \cosh k\alpha] + B^*_{k,k+1}[\cosh k\alpha - \cosh(k+2)\alpha]\}\sin k\beta$$

while the stresses in the inclusion take the form

$$\bar{\tau}_{\alpha\alpha} = \frac{1}{c}(\bar{A}_1 + \bar{C}_1 e^{-2\alpha}) + \frac{1}{2c}\sum_{k=1}^{\infty}\{[(k-2)(k-1)\bar{A}_{k-1} - (k-1)k\bar{A}_k]e^{-(k-2)\alpha} + [(k-2)(k-1)\bar{C}_{k-1} - (k-1)(k+2)\bar{A}_k - (k-2)(k+1)\bar{C}_k + (k+1)(k+2)\bar{A}_{k+1}]e^{-k\alpha} - [k(k+1)\bar{C}_k - (k+1)(k+2)\bar{C}_{k+1}]e^{-(k+2)\alpha}\}\cos k\beta$$

$$\bar{\tau}_{\beta\beta} = \frac{1}{c}(\bar{A}_1 - \bar{C}_1 e^{-2\alpha}) - \frac{1}{2c}\sum_{k=1}^{\infty}\{[(k-2)(k+1)\bar{A}_{k-1} - (k-1)k\bar{A}_k]e^{-(k-2)\alpha} + [(k-1)(k+2)\bar{C}_{k-1} - (k-2)(k-1)\bar{A}_k - (k+1)(k+2)\bar{C}_k + (k-2)(k+1)\bar{A}_{k+1}]e^{-k\alpha} - [k(k+1)\bar{C}_k - (k+1)(k+2)\bar{C}_{k+1}]e^{-(k+2)\alpha}\}\cos k\beta \quad \text{..[58]}$$

$$\bar{\tau}_{\alpha\beta} = \frac{1}{2c}\sum_{k=1}^{\infty}\{[(k-2)(k-1)\bar{A}_{k-1} - (k-1)k\bar{A}_k]e^{-(k-2)\alpha} + [(k-1)k(\bar{C}_k - \bar{A}_k) - k(k+1)(\bar{C}_{k+1} - \bar{A}_{k+1})]e^{-k\alpha} - [k(k+1)\bar{C}_k - (k+1)(k+2)\bar{C}_{k+1}]e^{-(k+2)\alpha}\}\sin k\beta \quad \text{..[58] (Cont.)}$$

Limiting Cases

(*a*) *Circular Hole in a Semi-Infinite Plate.* If the modulus of elasticity $\bar{E}$ of the inclusion is zero, we have the case of a circular hole in a semi-infinite elastic plate.

Proceeding to the limit in Equations [51] as $\bar{E} \to 0$, we obtain

$$A_1 = -ce^{-2\alpha_0}\frac{-1+3e^{-2\alpha_0}-3e^{-4\alpha_0}+e^{-6\alpha_0}}{1-4e^{-2\alpha_0}+6e^{-4\alpha_0}-4e^{-6\alpha_0}+e^{-8\alpha_0}} = c\frac{e^{-2\alpha_0}}{1-e^{-2\alpha_0}} \quad \text{.....[59a]}$$

$$B_2 = -2ce^{-2\alpha_0}\frac{-1+2e^{-2\alpha_0}-e^{-4\alpha_0}}{1-4e^{-2\alpha_0}+6e^{-4\alpha_0}-4e^{-6\alpha_0}+e^{-8\alpha_0}} = 2c\frac{e^{-2\alpha_0}}{(1-e^{-2\alpha_0})^2} \quad \text{.....[59b]}$$

Equations [49] give

$$\lim_{\bar{E}\to 0}\lambda = \lim_{\bar{E}\to 0}\mu = -1 \quad \text{.....[60]}$$

By Equations [60], Equations [55] become

$$\left.\begin{aligned} &f_1 = 0,\quad f_k = 4[\sinh^2 k\alpha_0 - k^2\sinh^2\alpha_0],\quad (k\geq 2)\\ &h_1 = 1,\quad h_k = -2k\sinh\alpha_0(k\sinh\alpha_0 - \cosh\alpha_0) + e^{-2k\alpha_0},\quad (k\geq 2)\\ &d_1 = 2(1-e^{-4\alpha_0}),\quad d_k = 2[\sinh 2k\alpha_0 + k\sinh 2\alpha_0]e^{-2k\alpha_0},\quad (k\geq 2)\\ &g_1 = 1-2e^{-2\alpha_0},\quad g_k = -2k\sinh\alpha_0(k\sinh\alpha_0 - \cosh\alpha_0) - e^{-2k\alpha_0},\quad (k\geq 2)\end{aligned}\right\} \quad \text{..[61]}$$

Hence

$$\left.\begin{aligned} A_k &= c\frac{1+2k\sinh\alpha_0(k\sinh\alpha_0-\cosh\alpha_0)-e^{-2k\alpha_0}}{4[\sinh^2 k\alpha_0 - k^2\sinh^2\alpha_0]}\\ &= c\frac{k\sinh\alpha_0(k\sinh\alpha_0-\cosh\alpha_0)+e^{-k\alpha_0}\sinh k\alpha_0}{2[\sinh^2 k\alpha_0 - k^2\sinh^2\alpha_0]},\\ &\qquad (k\geq 2)\end{aligned}\right\} \quad \text{..[62]}$$

$$B_k = -\frac{c}{2}\frac{k(k+1)\sinh^2\alpha_0}{\sinh^2 k\alpha_0 - k^2\sinh^2\alpha_0)^2},\quad (k\geq 2) \quad \text{.....[63]}$$

This limit solution is in agreement with Jeffery's solution (1) as corrected by Mindlin (6).

(*b*) *Circular Inclusion in an Infinite Plate.* The solution for the case of a circular inclusion in an infinite plate can be obtained from the present solution by taking the limit as the "shape ratio," that is, the ratio of the distance x_0 from the center of the inclusion to the straight boundary, to the radius r_0 of the inclusion, approaches infinity.

This shape ratio, henceforth designed by ρ, is

$$\rho = \frac{x_0}{r_0} = \frac{c\operatorname{cotanh}\alpha_0}{c\operatorname{cosech}\alpha_0} = \cosh\alpha_0 \quad \text{.....[64]}$$

hence

$$\lim_{\rho \to \infty} \alpha_0 = \infty \quad \ldots\ldots\ldots\ldots\ldots\ldots [65]$$

Expanding Equations [51], [53], and [54] in power series with respect to $e^{-\alpha_0}$ and subsequently letting $\alpha_0 \to \infty$, we obtain[6]

$$\left.\begin{aligned}
A_1 &= -c\,\frac{\gamma - \tilde{\gamma}}{\epsilon + \tilde{\gamma}}\,[1 - p_1 e^{-2\alpha_0} + O(e^{-4\alpha_0})]e^{-2\alpha_0} \\
A_k &= -c\,\frac{\epsilon - \tilde{\epsilon}}{2\gamma + \epsilon + \tilde{\epsilon}}\left[\frac{(k-1)k}{2} - p_k e^{-2\alpha_0} \right. \\
&\qquad \left. + O(e^{-4\alpha_0})\right] e^{-2(k-1)\alpha_0}, \quad (k \geq 2) \\
B^*_{1,2} &= -2c\,\frac{\epsilon - \tilde{\epsilon}}{2\gamma + \epsilon + \tilde{\epsilon}}\left[3 - \frac{\gamma - \tilde{\gamma}}{\epsilon - \tilde{\epsilon}}\,\frac{2\gamma + \epsilon + \tilde{\epsilon}}{\epsilon + \tilde{\gamma}} \right. \\
&\qquad \left. - q_{1,2} e^{-2\alpha_0} + O(e^{-4\alpha_0})\right] e^{-2\alpha_0} \\
B^*_{k,k+1} &= k(k+1)c\,\frac{\epsilon - \tilde{\epsilon}}{2\gamma + \epsilon + \tilde{\epsilon}}\left[\frac{(k-1)k}{2} \right. \\
&\qquad \left. - q_{k,k+1} e^{-2\alpha_0} + O(e^{-4\alpha_0})\right] e^{-2(k-1)\alpha_0}, \quad (k \geq 2)
\end{aligned}\right\} \ldots [66]$$

where

$$\left.\begin{aligned}
p_1 &= 1 + \frac{\tilde{\gamma}}{\tilde{\epsilon}}\,\frac{\epsilon + \tilde{\epsilon}}{\gamma + \tilde{\gamma}}\,\frac{\gamma + \epsilon}{\epsilon + \tilde{\gamma}} \\
&\qquad + \frac{\tilde{\gamma}(\epsilon - \tilde{\epsilon}) + \tilde{\epsilon}(\gamma - \tilde{\gamma}) + \epsilon\tilde{\epsilon} - \gamma\tilde{\gamma}}{\tilde{\epsilon}(\epsilon + \tilde{\gamma})} \\
p_k &= k^2 - 1 + 4\,\frac{\epsilon - \tilde{\epsilon}}{2\gamma + \epsilon + \tilde{\epsilon}}\,\delta_{2,k} \\
&\qquad - 2\,\frac{\gamma - \tilde{\gamma}}{\epsilon - \tilde{\epsilon}}\,\frac{\gamma + \epsilon}{\epsilon + \tilde{\gamma}}, \quad (k \geq 2) \\
q_{1,2} &= 6 - 4\,\frac{\gamma - \tilde{\gamma}}{\epsilon - \tilde{\epsilon}}\,\frac{\gamma + \epsilon}{\epsilon + \tilde{\gamma}}\,\frac{\tilde{\gamma} + \tilde{\epsilon}}{\epsilon + 2\tilde{\gamma} + \tilde{\epsilon}} \\
&\quad + 12\,\frac{\epsilon - \tilde{\epsilon}}{2\gamma + \epsilon + \tilde{\epsilon}} - \frac{\gamma - \tilde{\gamma}}{\epsilon - \tilde{\epsilon}}\,\frac{2\gamma + \epsilon + \tilde{\epsilon}}{\epsilon + \tilde{\gamma}}\,p_1 \\
&\qquad + 2\,\frac{\gamma - \tilde{\gamma}}{\epsilon + \tilde{\epsilon}}\,\frac{\tilde{\gamma} + \tilde{\epsilon}}{\tilde{\epsilon} + \tilde{\gamma}}\left[\frac{2\gamma + \epsilon + \tilde{\epsilon}}{\epsilon + 2\tilde{\gamma} + \tilde{\epsilon}} \right. \\
&\qquad \left. - \frac{\gamma + \epsilon}{\tilde{\gamma} + \tilde{\epsilon}}\right] - \frac{2\gamma + \epsilon + \tilde{\epsilon}}{\epsilon + 2\tilde{\gamma} + \tilde{\epsilon}} \\
q_{k,k+1} &= \frac{k(k+1)}{2} + k^2 + 1 + 4\,\frac{\epsilon - \tilde{\epsilon}}{2\gamma + \epsilon + \tilde{\epsilon}}\,\delta_{2,k} \\
&\qquad - 2\,\frac{\gamma - \tilde{\gamma}}{\epsilon + \tilde{\epsilon}}\,\frac{\gamma + \epsilon}{\epsilon - \tilde{\gamma}}, \quad (k \geq 2)
\end{aligned}\right\} \ldots [67]'$$

Substituting into Equations [57] and [58] we obtain for the boundary of the inclusion ($\alpha = \alpha_0 \to \infty$)

$$\left.\begin{aligned}
\tau_{\alpha\alpha} &= \frac{\gamma + \epsilon}{2(\epsilon + \tilde{\gamma})} - \frac{\gamma + \epsilon}{2\gamma + \epsilon + \tilde{\epsilon}}\cos 2\beta = \tilde{\tau}_{\alpha\alpha} \\
\tau_{\beta\beta} &= \frac{\epsilon - \gamma + 2\tilde{\gamma}}{2(\epsilon + \tilde{\gamma})} + \frac{\gamma - \epsilon + 2\tilde{\epsilon}}{2\gamma + \epsilon + \tilde{\epsilon}}\cos 2\beta \\
\tau_{\alpha\beta} &= -\frac{\gamma + \epsilon}{2\gamma + \epsilon + \tilde{\epsilon}}\sin 2\beta = \tilde{\tau}_{\alpha\beta} \\
\tilde{\tau}_{\beta\beta} &= \frac{\gamma + \epsilon}{2(\epsilon + \tilde{\gamma})} + \frac{\gamma + \epsilon}{2\gamma + \epsilon + \tilde{\epsilon}}\cos 2\beta
\end{aligned}\right\} \ldots [68]$$

These formulas are in accordance with the results obtained directly by applying polar co-ordinates[8] to the problem of a circular inclusion in an infinite plate.

Numerical Results—Discussion

Numerical computations were carried out to determine the stress distribution along the axis of symmetry for a shape ratio $\rho = x_0/r_0 = 3$ and different values of the stiffness ratio $E/\bar{E}$, while keeping $\nu = \bar{\nu} = 1/3$. The results of these computations are summarized in Figs. 2 and 3.

Fig. 2 shows that, for a value of the stiffness ratio $E/\bar{E} = 1/2$, the maximum values of τ_{yy} occur at the free edge in the plate and at the pole in the inclusion, and the minimum values occur at the common boundary in both. Moreover, the stresses τ_{yy} in the inclusion are greater than in the plate. The reverse applies for $E/\bar{E} = 2$.

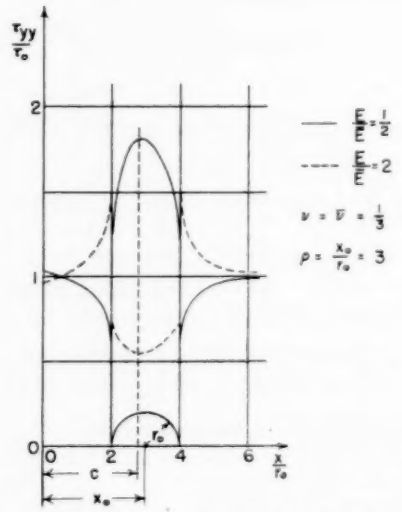

Fig. 2 Distribution of τ_{yy} Along the Axis of Symmetry

Fig. 3 depicts[9] the variation of normal stress τ_{yy} at various points along the axis of symmetry in terms of the stiffness ratio. It is seen that the stress at the common edge of the plate and the inclusion increases in the plate, and decreases in the inclusion as the stiffness ratio increases, while for the shape ratio selected, the stress at the free edge is relatively insensitive to changes in $E/\bar{E}$. We observe also that τ_{yy} is practically the same at opposite end

[6] In what follows, the symbol $O(e^{-n\alpha_0})$ is used in its standard mathematical connotation. Thus $f(x) = O[g(x)]$ as $x \to \infty$ if $\left|\frac{f(x)}{g(x)}\right|$ remains bounded as $x \to \infty$.

[7] $\delta_{2,k}$ (Kronecker's delta) has the value one for $k = 2$ and zero for $k \neq 2$.

[8] See, for instance, chapter 4 of (4).

[9] The method of plotting used in Fig. 3 is due to Donnell (7).

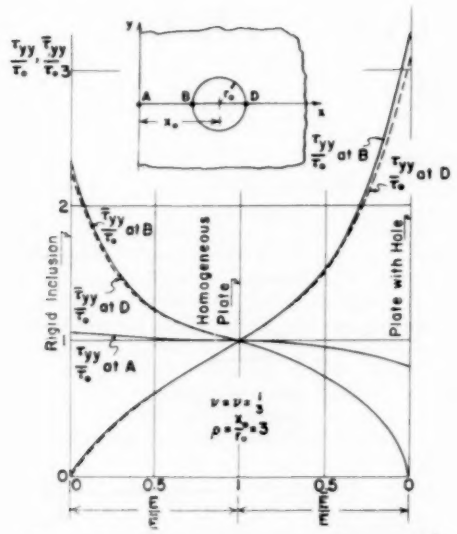

FIG. 3 DEPENDENCE OF τ_{yy} ON THE RATIO E/E

points of the transverse diameter of the inclusion. The same is true of $\bar{\tau}_{yy}$.

In the course of the numerical work, the values of the normal stress τ_{xx} along the axis of symmetry also were determined and were found to be comparatively small (less than 0.05 τ_0 for the cases considered).

ACKNOWLEDGMENT

The author is greatly indebted to Dr. E. Sternberg for invaluable advice and criticism in this investigation.

BIBLIOGRAPHY

1 "Plane Stress and Plane Strain in Bipolar Coordinates," by G. B. Jeffery, Transactions of the Royal Society of London, series A, vol. 221, 1920, p. 265.

2 "Stress Distribution Around a Tunnel," by R. D. Mindlin, Proceedings of the American Society of Civil Engineers, vol. 65, no. 4, 1939, p. 619; also, Trans. ASCE, vol. 105, 1941, p. 1117.

3 "Stress Concentration Due to Elliptical Discontinuities in Plates Under Edge Forces," by L. H. Donnell, Theodore von Kármán Anniversary Volume, California Institute of Technology, Pasadena, Calif., 1941, p. 293.

4 "Theory of Elasticity," by S. Timoshenko and J. N. Goodier, McGraw-Hill Book Company, Inc., New York, N. Y., second edition, 1951.

5 "A Treatise on Photoelasticity," by E. G. Coker and L. N. G. Filon, Cambridge University Press, Cambridge, England, 1931.

6 "Stress Distribution Around a Hole Near the Edge of a Plate Under Tension," by R. D. Mindlin, Proceedings of the Society for Experimental Stress Analysis, vol. 5, no. 2, 1948, p. 56.

7 "A Chart for Plotting Relations Between Variables Over Their Entire Real Range," by L. H. Donnell, *Quarterly of Applied Mathematics*, vol. 1, no. 10, 1943, p. 276.

Spherical Symmetry in the Theory of Elasticity

By F. GODED,[1] MADRID, SPAIN

Part 1 of the paper presents a study of the common characteristics of both plane symmetry and axial symmetry in the theory of elasticity; viz., the form of the stress tensor and the existence of further analogous symmetries. In Part 2, the subject deals with the possibility of the existence of further analogous symmetries which are found to be possible only in some specific cases. In particular, spherical symmetry is treated. The method of obtaining the stress function of this new symmetry and the equation which this function must satisfy also are discussed, together with the stresses expressed by means of this stress function. The paper ends with a brief review of a general solution of the stress function and an example of the application of this stress function to a given problem.

Introduction

For the general treatment of orthogonal curvilinear co-ordinate problems the notation follows that adopted by I. S. Sokolnikoff (1).[2] The notation followed in the specific treatment of the spherical symmetry problem is that used by S. Timoshenko and J. N. Goodier (2).

In Part 1 of this paper, the following orthogonal co-ordinate system is used

$$\alpha_i = \alpha_i(x, y, z); \; i = 1, 2, 3$$

The element of arc is given by

$$ds^2 = \sum_{i=1}^{3} g_{ii} d\alpha_i^2$$

Additional required notation follows

$$g = (g_{11}g_{22}g_{33})^{1/2}$$

u_i = displacement in direction normal to the co-ordinate surface α_i = const

e_{ij} = components of strain tensor

τ_{ij} = components of stress tensor; first subscript indicates direction of perpendicular to plane in question, whereas second subscript indicates direction of component of stress tensor.

In the case of spherical symmetry the notation becomes

u = displacement in direction of radius

v = displacement normal to radius plane

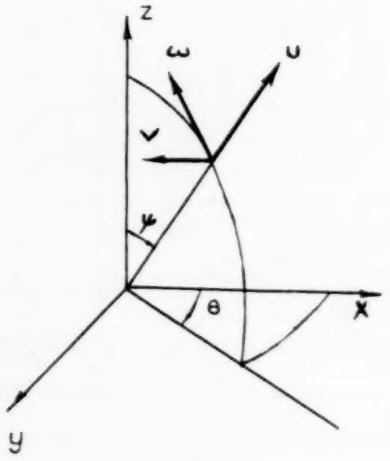

Fig. 1

w = displacement normal to uv-plane, Fig. 1

The components of the stress tensor in the u, v, w-directions are σ_R, σ_θ, σ_ψ, respectively. The meanings of $\tau_{R\theta}$, $\tau_{R\psi}$, $\tau_{\psi\theta}$ and of strain-tensor components ϵ_R, ϵ_θ, ϵ_ψ, $\gamma_{R\theta}$, $\gamma_{R\psi}$, $\gamma_{\psi\theta}$ are self-explanatory.

PART 1

Symmetries with respect to surface $\alpha_3 = K$ (const)

Two symmetries have been used widely in the theory of elasticity; namely, symmetry with respect to a plane $z = k$ (k arbitrary), and symmetry with respect to an axis. In both cases all the stresses can be expressed by means of a single stress function: Airy's function in the first case; Love's, Weber's, or Neuber's functions in the second case. It should be pointed out that these functions are not independent (3, 4, 5).

For all points of space the elastic stress tensor in both symmetries has the following form

$$\begin{pmatrix} \tau_{11} & \tau_{12} & 0 \\ \tau_{12} & \tau_{22} & 0 \\ 0 & 0 & \tau_{33} \end{pmatrix} \quad \ldots\ldots\ldots\ldots\ldots\ldots [1]$$

in either the rectangular Cartesian or the polar cylindrical co-ordinate system. The usual notation for Cartesian co-ordinates is

$$\left.\begin{aligned} \tau_{11} &= \sigma_x \\ \tau_{22} &= \sigma_y \\ \tau_{12} &= \tau_{xy} \\ \tau_{33} &= \sigma_z = 0 \quad \text{plane stress} \\ u_3 &= 0 \quad\quad\quad\; \text{plane strain} \end{aligned}\right\} \quad \ldots\ldots\ldots [2]$$

In axisymmetric problems the notation is

---

[1] Ingeniero de Caminos, General Eléctrica Espanola.

[2] Numbers in parentheses refer to the Bibliography at the end of the paper.

Contributed by the Applied Mechanics Division and presented at the Annual Meeting, New York, N. Y., December 1–6, 1957, of The American Society of Mechanical Engineers.

Discussion of this paper should be addressed to the Secretary, ASME, 29 West 39th Street, New York, N. Y., and will be accepted until April 10, 1958, for publication at a later date. Discussion received after the closing date will be returned.

Note: Statements and opinions advanced in papers are to be understood as individual expressions of their authors and not those of the Society. Manuscript received by ASME Applied Mechanics Division, September 15, 1954. Paper No. 57—A-119.

$$\left.\begin{aligned} \tau_{1_1} &= \sigma_r \\ \tau_{22} &= \sigma_z \\ \tau_{12} &= \tau_{r_z} \\ \tau_{33} &= \sigma_\theta \\ u_3 &= 0 \end{aligned}\right\} \quad \ldots\ldots [3]$$

The question may be raised as to whether a suitable curvilinear orthogonal co-ordinate system can be found such that the stress tensor has the same form as [1], and such that its components are expressible in terms of a single stress function. An affirmative answer is provided by the spherical co-ordinate system in which symmetry will refer to a sphere with an arbitrary radius.

Before a demonstration is given of how to obtain a stress function corresponding to a spherical symmetry, the problem will be stated in the most general case in which $\tau_{13} = \tau_{23} = 0$ and $U_3 = 0$. These conditions imply symmetry in the displacements and stresses with reference to the $\alpha_3 = K$ surface.

The equilibrium equations in this general case are (6)

$$\frac{\partial(g\tau_{ii})}{\partial\alpha_i} - \frac{1}{2}\sum_{j=1}^{3}\frac{g\tau_{jj}}{g_{jj}}\frac{\partial g_{jj}}{\partial\alpha_i} + \sum_{j\neq i}\frac{\partial}{\partial\alpha_j}\left(\frac{gg_{ii}\tau_{ij}}{\sqrt{g_{ii}g_{jj}}}\right) + F_i g\sqrt{g_{ii}} = 0 \quad (i = 1, 2, 3) \ldots\ldots [4]$$

The strains, as functions of the displacements, are as follows

$$e_{ii} = \frac{\partial}{\partial\alpha_i}\left(\frac{u_i}{\sqrt{g_{ii}}}\right) + \frac{1}{2g_{ii}}\sum_{K=1}^{3}\frac{\partial g_{ii}}{\partial\alpha_K}\frac{u_K}{\sqrt{g_{KK}}} \ldots\ldots [5]$$

$$e_{ij} = \frac{1}{2(g_{ii}g_{jj})^{3/4}}\left[g_{ii}\frac{\partial}{\partial\alpha_j}\left(\frac{u_i}{\sqrt{g_{ii}}}\right) + g_{jj}\frac{\partial}{\partial\alpha_i}\left(\frac{u_j}{\sqrt{g_{jj}}}\right)\right], \quad i \neq j \ldots\ldots [6]$$

Since the displacement of the solid is symmetrical with respect to the surface $\alpha_3 = K$, both stresses τ_{13} and τ_{23} can be eliminated if the displacement functions have the following form

$$\left.\begin{aligned} u_2 &= \sqrt{(g_{22})}f_2(\alpha_1, \alpha_2) \\ u_3 &= 0 \\ u_1 &= \sqrt{(g_{11})}f_1(\alpha_1, \alpha_2) \end{aligned}\right\} \quad \ldots\ldots [7]$$

From Functions [5] and [6] it is possible to obtain e_{ii} and e_{12} as functions of f_1 and f_2. Then employing τ_{ii} and τ_{ij} can be expressed in terms of f_1 and f_2 with the use of Lamé's equations. The equations which f_1 and f_2 must satisfy will be obtained by replacing these stress values in the equilibrium Equations [4].

Hence when there is symmetry in the displacements, that is, when the solid slides between the surfaces $\alpha_3 = K_1$, and $\alpha_3 = K_2$, the two functions f_1 and f_2 must satisfy three equations.

The solution of this problem is possible only in those particular cases, which lead to compatible systems. In the foregoing case which involves symmetry with respect to a sphere of arbitrary radius, this symmetry is double, since it applies both to displacements and strains.

PART 2

Spherical symmetry

The simultaneous cancellation of the two sheer components leads to three possible combinations

$$\left.\begin{aligned} \tau_{11} &= \sigma_\theta \\ \tau_{22} &= \sigma_\psi \\ \tau_{33} &= \sigma_R \\ \tau_{12} &= \tau_{\theta\psi} \\ \tau_{13} &= \tau_{\theta R} = 0 \\ \tau_{23} &= \tau_{\psi R} = 0 \end{aligned}\right\} \quad \ldots\ldots [8a] \qquad \left.\begin{aligned} \tau_{11} &= \sigma_R \\ \tau_{22} &= \sigma_\psi \\ \tau_{33} &= \sigma_\theta \\ \tau_{12} &= \tau_{R\psi} \\ \tau_{13} &= \tau_{R\theta} = 0 \\ \tau_{23} &= \tau_{\psi\theta} = 0 \end{aligned}\right\} \quad \ldots\ldots [8b]$$

$$\left.\begin{aligned} \tau_{11} &= \sigma_R \\ \tau_{22} &= \sigma_\theta \\ \tau_{33} &= \sigma_\psi \\ \tau_{12} &= \tau_{R\theta} \\ \tau_{13} &= \tau_{R\psi} = 0 \\ \tau_{23} &= \tau_{\psi\theta} = 0 \end{aligned}\right\} \quad \ldots\ldots [8c]$$

The set of Equations [8b] again leads to the axial symmetry previously considered. The set [8c] is not important because the number of solutions is finite and, therefore, there is no stress function. The general solution which corresponds to [8c] is as follows

$$u = A_0R^{-2} + B_0R$$
$$v = (A_1R^{-2} + B_1R)\sin\psi$$
$$w = 0$$

The particular spherical symmetry which will be discussed later refers to Equations [8a] and its corresponding stress function can be found according to the following procedure:

The equilibrium equations and the elementary strains are given by (7)

$$\frac{\partial\sigma_R}{\partial R} + \frac{1}{R\sin\psi}\frac{\partial\tau_{R\theta}}{\partial\theta} + \frac{1}{R}\frac{\partial\tau_{R\psi}}{\partial\psi} + \frac{2\sigma_R - \sigma_\theta - \sigma_\psi + \tau_{R\psi}\cot\psi}{R} = 0 \ldots\ldots [9a]$$

$$\frac{\partial\tau_{R\theta}}{\partial R} + \frac{1}{R\sin\psi}\frac{\partial\sigma_\theta}{\partial\theta} + \frac{1}{R}\frac{\partial\tau_{\theta\psi}}{\partial\psi} + \frac{3\tau_{R\theta} + 2\tau_{\theta\psi}\cot\psi}{R} = 0 \ldots\ldots [9b]$$

$$\frac{\partial\tau_{R\psi}}{\partial R} + \frac{1}{R\sin\psi}\frac{\partial\tau_{\theta\psi}}{\partial\theta} + \frac{1}{R}\frac{\partial\sigma_\psi}{\partial\psi} + \frac{(\sigma_\psi - \sigma_\theta)\cot\psi + 3\tau_{R\psi}}{R} = 0 \ldots\ldots [9c]$$

$$\epsilon_R = \frac{\partial u}{\partial R} \ldots\ldots [9d]$$

$$\epsilon_\psi = \frac{1}{R}\frac{\partial w}{\partial\psi} + \frac{u}{R} \ldots\ldots [9e]$$

$$\epsilon_\theta = \frac{1}{R\sin\psi}\frac{\partial v}{\partial\theta} + \frac{u}{R} + \frac{w}{R}\cot\psi \ldots\ldots [9f]$$

$$\gamma_{\psi\theta} = \frac{1}{R\sin\psi}\frac{\partial w}{\partial\theta} + \frac{1}{R}\frac{\partial v}{\partial\psi} - \frac{v}{R}\cot\psi \ldots\ldots [9g]$$

$$\gamma_{R\theta} = \frac{1}{R \sin \psi} \frac{\partial u}{\partial \theta} + \frac{\partial v}{\partial R} - \frac{v}{R} \quad [9h]$$

$$\gamma_{R\psi} = \frac{1}{R} \frac{\partial u}{\partial \psi} + \frac{\partial w}{\partial R} - \frac{w}{R} \quad [9i]$$

If $\tau_{R\psi} = \tau_{R\theta} = 0$ and either $\sigma_R = \nu(\sigma_\theta + \sigma_\psi)$ or $\sigma_R = 0$ are assumed in the equilibrium equations, one obtains the same result shown in the following. If, for example

$$\sigma_R = \nu(\sigma_\theta + \sigma_\psi)$$

is assumed, then Equation [9a] becomes

$$R \frac{\partial \sigma_R}{\partial R} + 2\sigma_R = \frac{1}{R} \frac{\partial}{\partial R}(R^2 \sigma_R) = \sigma_\theta + \sigma_\psi = \frac{\sigma_R}{\nu}$$

which has the solution

$$\sigma_R = CR^{\frac{1-2\nu}{\nu}} \quad [10]$$

It can be seen that the assumption $\tau_{R\theta} = \tau_{R\psi} = 0$ is fulfilled by displacement functions of the form

$$\left.\begin{aligned} u &= \Phi_1(R) \\ v &= R\Phi_2(\theta, \psi) \\ w &= R\Phi_3(\theta, \psi) \end{aligned}\right\} \quad [11]$$

which are more general than the functions in [7].

Now, since $\epsilon_R = 0$, the first displacement Equation [9d] gives $u = K$ (constant). For $K = 0$, Equations [9e] and [9f] become

$$\left.\begin{aligned} \epsilon_\psi &= \frac{\partial \Phi_3}{\partial \psi} = F_1(\theta, \psi) \\ \epsilon_\theta &= \frac{1}{\sin \psi} \frac{\partial \Phi_2}{\partial \theta} + \Phi_3 \cot \psi = F_2(\theta, \psi) \end{aligned}\right\} \quad [12]$$

One also may write

$$\left.\begin{aligned} E\epsilon_\psi = \sigma_\psi - \nu(\sigma_R + \sigma_\theta) &= \sigma_\psi(1+\nu) - C(1+\nu)R^{\frac{1-2\nu}{\nu}} \\ &= EF_1(\theta, \psi) \\ E\epsilon_\theta = \sigma_\theta - \nu(\sigma_R + \sigma_\psi) &= C\frac{1-\nu^2}{\nu} R^{\frac{1-2\nu}{\nu}} \\ &\quad - (1+\nu)\sigma_\psi = EF_2(\theta, \psi) \end{aligned}\right\} \quad [13]$$

These equations are compatible only when $C = 0$ and hence $\sigma_R = 0$. Therefore when the displacements are of the form of Equations [11], the condition $\epsilon_R = 0$ leads to the same result as the condition $\sigma_R = 0$.

When σ_R and ϵ_R are zero, it is also necessary that $\sigma_\theta = -\sigma_\psi$. If now the values $\tau_{R\theta} = \tau_{R\psi} = \sigma_R = 0$ and $\sigma_\theta = -\sigma_\psi$ are inserted in Equilibrium Equations [9b] and [9c], they become

$$\frac{\partial \sigma_\theta}{\partial \theta} + \frac{1}{\sin \psi} \frac{\partial}{\partial \psi}(\tau_{\theta\psi} \sin^2 \psi) = 0 \quad [14a]$$

$$\frac{\partial \tau_{\theta\psi}}{\partial \theta} - \frac{1}{\sin \psi} \frac{\partial}{\partial \psi}(\sigma_\theta \sin^2 \psi) = 0 \quad [14b]$$

Furthermore by virtue of Equations [11], the six displacement Equations [9d] through [9i] are reduced to

$$\epsilon_R = 0 \quad [15a]$$

$$\epsilon_\theta = \frac{1}{R \sin \psi} \frac{\partial v}{\partial \theta} + \frac{w}{R} \cot \psi \quad [15b]$$

$$\epsilon_\psi = \frac{1}{R} \frac{\partial w}{\partial \psi} \quad [15c]$$

$$\gamma_{\psi\theta} = \frac{1}{R} \frac{\partial v}{\partial \psi} + \frac{1}{R \sin \psi} \frac{\partial w}{\partial \theta} - \frac{v}{R} \cot \psi = \frac{2(1+\nu)}{E} \tau_{\psi\theta} \quad [15d]$$

$$\gamma_{R\psi} = 0 \quad [15e]$$

$$\gamma_{R\theta} = 0 \quad [15f]$$

If one adopts a stress function of the form

$$\sigma_\theta = \frac{\partial^2 \varphi(\psi, \theta)}{\partial \psi \partial \theta} \quad [16]$$

then Equation [14b] gives

$$\tau_{\psi\theta} = \frac{1}{\sin \psi} \frac{\partial}{\partial \psi}\left(\frac{\partial \varphi}{\partial \psi} \sin^2 \psi\right) \quad [17]$$

If this stress function satisfies the single equation

$$\sin^2 \psi \frac{\partial^2 \varphi}{\partial \psi^2} + 3 \sin \psi \cos \psi \frac{\partial \varphi}{\partial \psi} + \frac{\partial^2 \varphi}{\partial \theta^2} + \varphi = 0 \quad [18]$$

it will be shown that all equations in both Systems [14] and [15] are satisfied.

Equation [15a] gives

$$\frac{\partial w}{\partial \psi} = \frac{R}{E}(\sigma_\psi - \nu\sigma_\theta) = -\frac{1+\nu}{E} R\sigma_\theta$$

so that

$$w = -\frac{1+\nu}{E} R \frac{\partial \varphi}{\partial \theta} \quad [19]$$

inasmuch as an arbitrary function of θ is included in φ.

Similarly, Equation [15b] leads to

$$\frac{1}{R \sin \psi} \frac{\partial v}{\partial \theta} = \frac{1}{E}(\sigma_\theta - \nu\sigma_\psi) - \frac{w}{R} \cot \psi = \sigma_\theta \frac{1+\nu}{E} + \frac{1+\nu}{E} \frac{\partial \varphi}{\partial \theta} \cot \psi$$

which can be integrated to give

$$v = \frac{1+\nu}{E} R\left[\sin \psi \frac{\partial \varphi}{\partial \psi} + \varphi \cos \psi\right] = \frac{1+\nu}{E} R \frac{\partial}{\partial \psi}(\varphi \sin \psi) \quad [20]$$

Here also it is not necessary to add any arbitrary function of ψ.

The values of v and w in Equations [19] and [20] and σ_θ and $\tau_{\psi\theta}$ in Equations [16] and [17] must satisfy Equations [14a] and [15d], which are the only ones which have not been used so far in the Systems [14] and [15].

If v from Equations [20], w from Equation [19], and $\tau_{\psi\theta}$ from Equations [17] are substituted in Equation [15d], the result is Equation [18], after simplification. This equation must be satisfied by the stress function.

If σ_θ from Equation [16] and $\tau_{\psi\theta}$ from Equation [17] are substituted in Equation [14a], the resulting equation is

$$\sin \psi \frac{\partial^3 \varphi}{\partial \psi \partial \theta^2} + \frac{\partial}{\partial \psi}\left[\sin \psi \frac{\partial}{\partial \psi}\left(\sin^2 \psi \frac{\partial \varphi}{\partial \psi}\right)\right] = 0$$

After expansion and simplification, this equation becomes

$$\frac{\partial^3\varphi}{\partial\psi\partial\theta^2} + (6\cos^2\psi - 2)\frac{\partial\varphi}{\partial\psi} + 5\sin\psi\cos\psi\frac{\partial^2\varphi}{\partial\psi^2} + \sin^2\psi\frac{\partial^3\varphi}{\partial\psi^3} = 0 \quad [21]$$

Since this same equation also can be obtained by partial differentiation of Equation [18] with respect to ψ; it is apparent that stress-function solution of [18] also will satisfy Equation [21].

Stresses [16] and [17] satisfy the compatibility equations, provided the stress function is a solution of Equation [18]. It will now be seen that the resulting symmetry is similar to the two afore-mentioned symmetries. Since the stresses are independent of R, they will have the same value throughout the radii, and, since $\tau_{R\psi} = \tau_{R\theta} = 0$ the forces will always set in directions perpendicular to the radii.

The background is now complete for the study of the distribution of stresses in a body which is bounded by two concentric spheres of arbitrary radius and a cone with its vertex at the origin, Fig. 2. The thickness $d = R_2 - R_1$ of the enclosed body can have any given value.

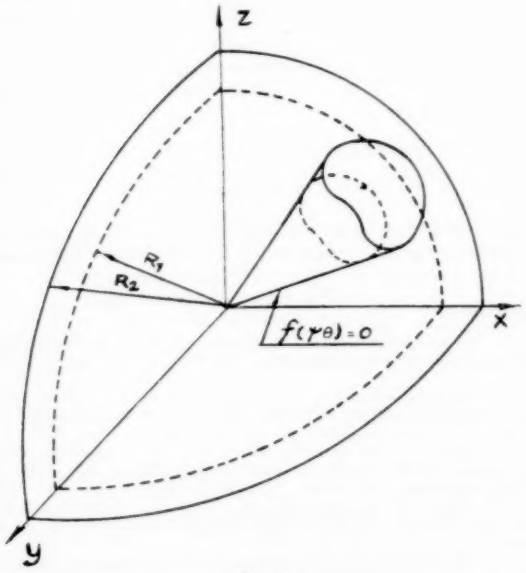

Fig. 2

Since $\sigma_R = \tau_{R\psi} = \tau_{R\theta} = 0$, both boundary spheres are free from any stresses, the thickness of the body is arbitrary, and, since $u = 0$, the body is strained when it slides between the two spheres. Therefore the analogy between the present symmetry and the previously mentioned two symmetries is clear.

Practical problems

Since Equation [18] is a separable equation, its solutions may be found by assuming

$$\varphi = \Theta(\theta)\Psi(\psi) \quad [22]$$

which leads to the two ordinary differential equations

$$\left.\begin{aligned}\Psi''\sin^2\psi + 3\Psi'\sin\psi\cos\psi + \Psi(1 - K^2) &= 0\\ \Theta'' + K^2\Theta &= 0\end{aligned}\right\} \quad [23]$$

The general integral of the second of these equations is

$$\Theta = A_k\cos K\Theta + B_k\sin K\Theta \quad [24]$$

The substitution of

$$X = \frac{1}{\sin^2\psi} \quad [25]$$

in the first of Equations [23] converts it into the following hypergeometrical equation

$$X(1 - X)\Psi'' - \frac{1}{2}\Psi' - \frac{1 - K^2}{4}\Psi = 0 \quad [26]$$

The adoption of the usual notation (8) gives

$$\left.\begin{aligned}c &= -\frac{1}{2}\\ a + b &= -1\\ ab &= \frac{1 - K^2}{4}\end{aligned}\right\} \quad [27]$$

from which it follows that

$$\left.\begin{aligned}a &= \frac{-1 \pm K}{2}\\ b &= \frac{-1 \pm K}{2}\end{aligned}\right\} \quad [28]$$

Since $X > 1$ from the definition of X in Equation [25], the two significant solutions in this case are the ones that converge for X in the indicated range. The solution of Equation [26] is obtained through the substitution (9)

$$X = \xi^{-1} \qquad \Psi = \xi^a z \quad [29]$$

The general solution which results and which is valid for the range $X > 1$ is given by

$$\left.\begin{aligned}\Psi = {} & CX^{-a}F(a, a - c + 1, a - b + 1, X^{-1})\\ & + DX^{-b}F(b, b - c + 1, b - a + 1, X^{-1})\end{aligned}\right\} \quad [30]$$

Taking into account Equations [25], [27], and [28], Expression [30] can be written as follows

$$\begin{aligned}\Psi = {} & C(\sin\psi)^{-1\pm K}\left[1 + \frac{(-1 \pm K)(2 \pm K)}{2^2(1 \pm K)}\sin^2\psi + \frac{(-1 \pm K)(4 \pm K)}{2^5}\sin^4\psi + \cdots\cdots\right]\\ & + D(\sin\psi)^{-1\pm K}\left[1 + \frac{(-1 \pm K)(2 \pm K)}{2^2(1 \pm K)}\sin^2\psi + \frac{(-1 \pm K)(4 \pm K)}{2^5}\sin^4\psi + \cdots\cdots\right]\\ & = CF_1(\psi) + DF_2(\psi) \quad [31]\end{aligned}$$

Where $F_1(\psi)$ and $F_2(\psi)$ refer to the two series which are enclosed within brackets.

Hence the general solution of Equations [18] which have the form [22] will be

$$\varphi = \sum_K (A_K\cos K\theta + B_K\sin K\theta)[CF_1(\psi) + DF_2(\psi)] \quad [32]$$

The expressions for the stresses are now obtainable through the substitution of Equation [32] in [17] and [16]. The resulting expressions will be very valuable in the solution of several problems of practical interest. The solution of Equation [18] will be completed by looking for the solution of the form

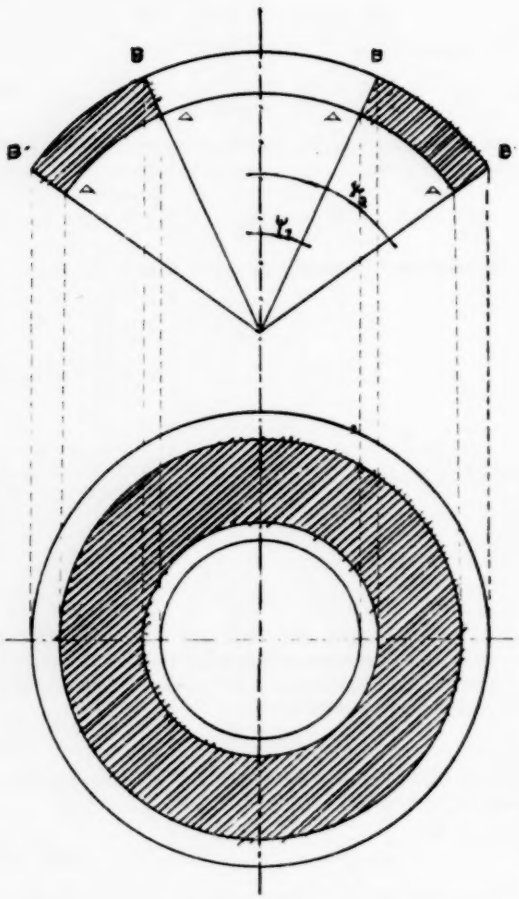

Fig. 3

$$\varphi = \Psi(\psi) \quad [33]$$

If this value of φ is inserted in Equations [18] through [25], one obtains the following differential equation

$$X(1 - X)\Psi'' - \frac{1}{2}\Psi' - \frac{1}{4}\Psi = 0 \quad [34]$$

This is a special case of Equation [26], obtained for $K = 0$, in which case the two Solutions [31] coincide and yield the single solution

$$\Psi_1(\psi) = (\sin\psi)^{-1} F\left(-\frac{1}{2}, 1, 1, \sin^2\psi\right) \quad [35]$$

The second solution of Equations [34] which is convergent for $X > 1$ is found at once by applying Frobenius' method to the equation obtained from Equation [34] through the change of variables indicated in Equations [29]. Since the indicial equation has a double root $\rho = 0$, the second solution of Equation [34] becomes (9)

$$\Psi_2(\psi) = (\sin\psi)^{-1}\left\{\frac{3}{2}\sin^2\psi + \frac{3}{2^4}\sin^4\psi + 2F\left(-\frac{1}{2}, 1, 1, \sin^2\psi\right)\log\sin\psi\right\} \quad [36]$$

The general solution of Equation [18] which has the form indicated in Equation [33] will be

$$\varphi = A_1\Psi_1(\psi) + B_1\Psi_2(\psi) \quad [37]$$

The stresses due to this last stress function are as follows

$$\left.\begin{aligned} \sigma_R = \sigma_\theta = \sigma_\psi = \tau_{R\psi} = \tau_{R\theta} = 0 \\ \tau_{\psi\theta} = Af_1(\psi) + Bf_2(\psi) \end{aligned}\right\} \quad [38]$$

If one considers the spherical ring which is bounded by the coordinates $\psi = \psi_1$, $\psi = \psi_2$, $\theta = 0$, $\theta = 2\pi$, Fig. 3, it will be seen that the foregoing solution corresponds to the action of constant tangential stresses τ_1 and τ_2 on the faces AB and $A'B'$. The constants A and B in Equations [38] are determined by the two following equations

$$\left.\begin{aligned} \tau_1 = Af_1(\psi_1) + Bf_2(\psi_1) \\ \tau_2 = Af_1(\psi_2) + Bf_2(\psi_2) \end{aligned}\right\} \quad [39]$$

In view of the theoretical nature of this paper, no numerical solutions or further applications of the foregoing stress function will be mentioned.

Bibliography

1 "Mathematical Theory of Elasticity," by I. S. Sokolnikoff, McGraw-Hill Book Company, Inc., New York, N. Y., second edition, 1956.

2 "Theory of Elasticity," by S. Timoshenko and J. N. Goodier, McGraw-Hill Book Company, Inc., New York, N. Y., second edition, 1951.

3 "Tratado de Elasticidad Teórico-Técnica," by E. Butty, Tomo I. Centro de Estudiantes de Ingeniería de Buenos Aires, Buenos Aires, Argentina, first edition, 1946, pp. 619–620.

4 "Notes on the Galerkin and Papkovich Stress Functions," by R. D. Mindlin, *Bulletin of American Mathematical Society*, vol. 32, 1936.

5 "On the Stress Function Approaches of Boussinesq and Timpe to the Axisymmetric Problem of Elasticity Theory," by E. Sternberg, R. A. Eubank, and M. A. Sadowsky, *Journal of Applied Physics*, vol. 22, September, 1951, p. 1121.

6 Reference (1), pp. 177–181.

7 Reference (3), pp. 737–738.

8 "A Course of Modern Analysis," by E. T. Whittaker and G. N. Watson, Cambridge University Press, second edition, 1915, p. 283.

9 "Ecuaciones Diferenciales," by D. Marin Toyos, third edition, Librería General Victoriano Suárez, Madrid, Spain, 1950, pp. 260–261.

10 "A Treatise on Differential Equations," by A. R. Forsyth, Macmillan and Company, Ltd., London, England, sixth edition, 1933, pp. 251–252.

Design Data and Methods

It is important that the data contained in technical papers be made readily available to design engineers. In order to satisfy these needs of industry, this section of the Journal includes a concise presentation of data and information drawn chiefly from papers previously published by the Applied Mechanics Division of The American Society of Mechanical Engineers.

Elastic and Damping Properties of Oil-Film Journal Bearings for Application to Unbalance Vibration Calculations

By A. C. HAGG[1] and G. O. SANKEY,[2] PITTSBURGH, PA.

Nomenclature

The following nomenclature is used in the paper:

W = static load, lb
N = journal speed, rpm
ω = vibration frequency, rad/sec, $\omega = \pi N/30$
R = journal radius, in.
D = journal diameter, in.
A = projected bearing area, sq in.
C = radial bearing clearance, in.
L = axial bearing length, in.
a = length of tilting pad in direction of journal motion, in.
μ = viscosity of the lubricant in reyns, lb sec/in.[2]
P = static load per unit projected bearing area, psi
$S = \left(\frac{R}{C}\right)^2 \frac{\mu N}{P}$ sec/min
K_1 = minimum film elasticity, lb per in.
K_2 = maximum film elasticity, lb per in.
$B_1\omega$ = minimum film damping, lb per in.
$B_2\omega$ = maximum film damping, lb per in.
$\left(\frac{C}{W}\right)K$ = dimensionless film elasticity
$\left(\frac{C}{W}\right)B\omega$ = dimensionless film damping

Introduction

Oil films lower the values of rotor critical speeds under those determined on the basis of simple support at the bearings, and account for low and practical vibration magnification. This has been discussed previously.[3,4] In the interest of more realistic calculations of unbalance vibration and critical speeds of machines such as turbines and generators, design data are given on the elastic and damping properties of several representative jour-

[3] "Some Dynamic Properties of Oil-Film Journal Bearings With Reference to the Unbalance Vibration of Rotors," by A. C. Hagg and G. O. Sankey, Journal of Applied Mechanics, Trans. ASME, vol. 78, 1956, pp. 302–306.

[4] "Forced Lateral Vibration of Beams on Damped Flexible End Supports," by D. F. Miller, Journal of Applied Mechanics, Trans. ASME, vol. 75, 1953, pp. 167–172.

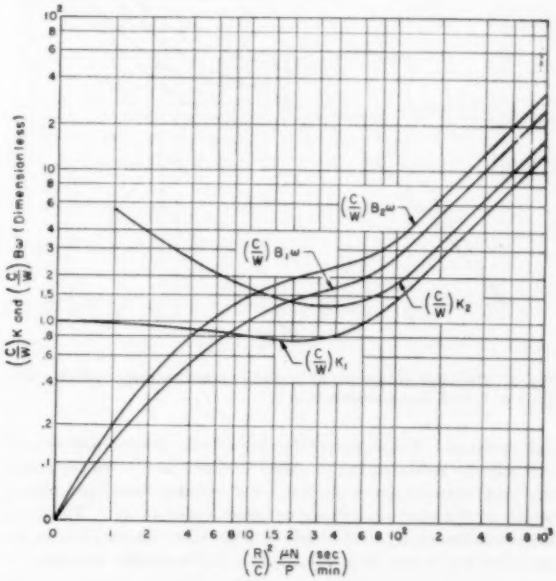

Fig. 1 Dynamic properties of partial journal bearing; 150-deg arc, $L/D = 1$, central load

[1] Manager, Dynamics Section, Mechanics Department, Westinghouse Research Laboratories, Pittsburgh, Pa. Mem. ASME.

[2] Research Engineer, Mechanics Department, Westinghouse Research Laboratories.

Discussion of this paper should be addressed to the Secretary, ASME, 29 West 39th Street, New York, N. Y., and will be accepted until April 10, 1958, for publication at a later date. Discussion received after the closing date will be returned.

Note: Statements and opinions advanced in papers are to be understood as individual expressions of their authors and not those of the Society. Manuscript received by ASME Applied Mechanics Division, July 1, 1957.

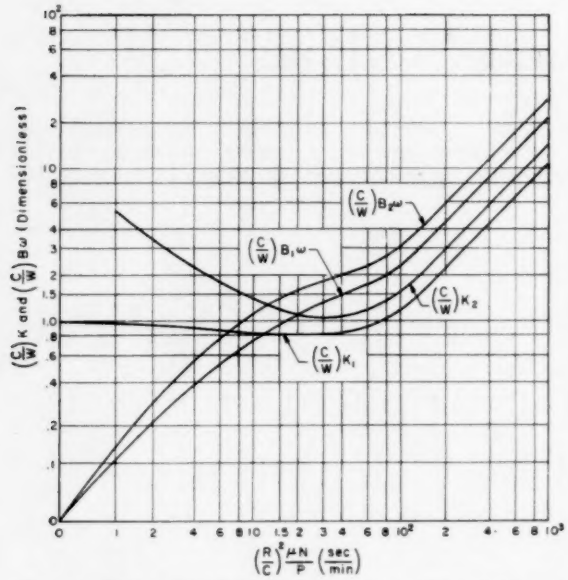

Fig. 2 Dynamic properties of partial journal bearing; 125-deg arc, L/D = 1, central load

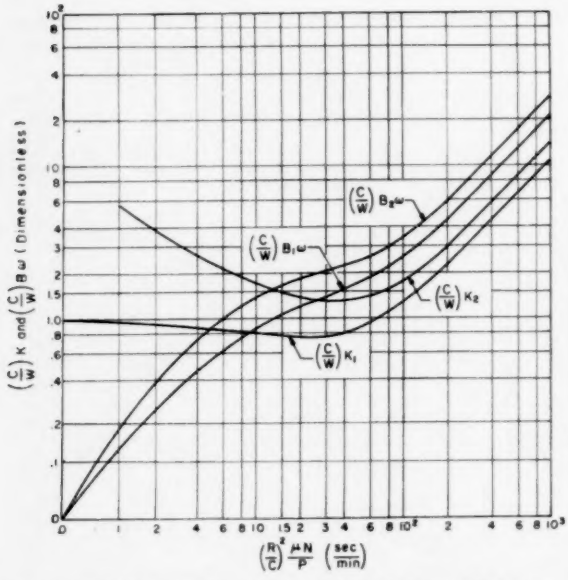

Fig. 3 Dynamic properties of partial journal bearing; 125-deg arc, L/D = 1, 17.5-deg eccentric load

nal bearings. These properties have been determined experimentally by resolving the dynamic oil-film reaction (of the rotating load) into displacement-force and velocity-force components which are the elastic and damping forces, respectively.[3] The properties are linearized on the basis that the vibration amplitudes are assumed not to exceed about one half of the oil-film thickness.

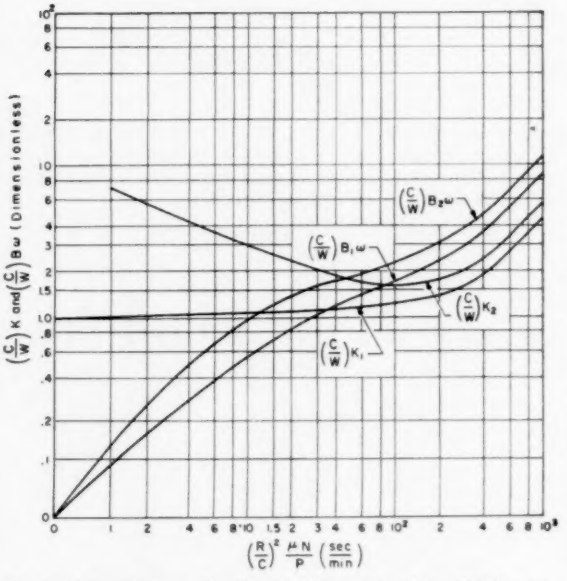

Fig. 4 Dynamic properties of partial journal bearing; 125-deg arc, L/D = 0.4, central load

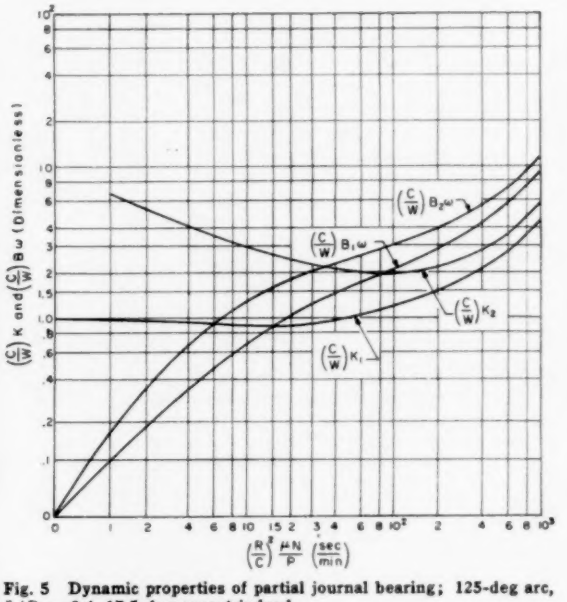

Fig. 5 Dynamic properties of partial journal bearing; 125-deg arc, L/D = 0.4, 17.5-deg eccentric load

Notes on Design Curves

The journal motion for a partial bearing is noncircular, and maximum and minimum values for elasticity and for damping are obtained. The maximum values are in the direction of the minor axis of the journal path, and the minimum values are in the direction of the major axis. The partial bearings of Figs. 1 through 5 show this characteristic.

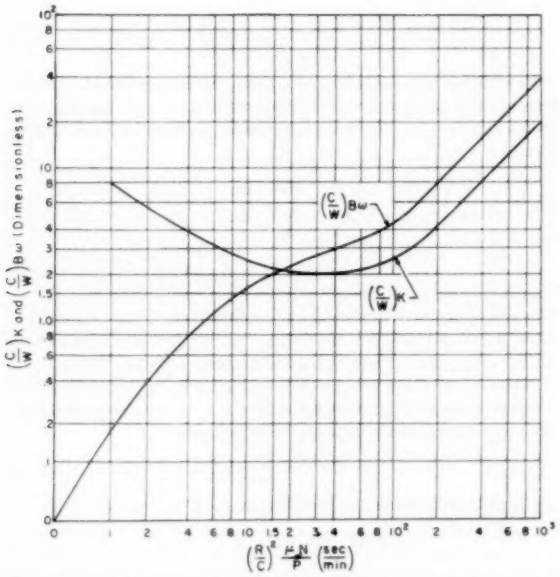

Fig. 6 Dynamic properties of tilting-pad bearing; 4 pads, a/L = 0.8, load between pads

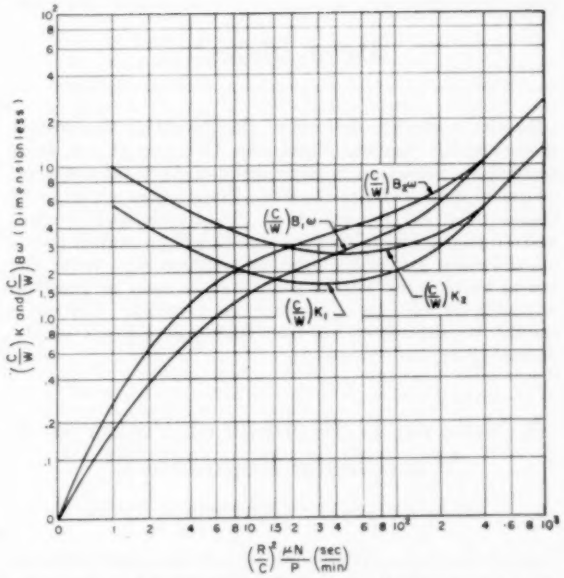

Fig. 7 Dynamic properties of tilting-pad journal bearing; 6 pads, a/L = 0.5, load between pads

A single set of values for elasticity and for damping occurs when the journal path is a circle for the applied rotating load. Circular journal motion occurs at the higher values of $(R/C)^2$ $(\mu N/P)$ for bearings surrounding the journal. The tilting-pad bearings, Figs. 6 and 7, and the full bearing, Fig. 8, are in this category. In addition, it can be noted that the 4-pad bearing, Fig. 6, has single values over the complete range in S; this is caused apparently by the oil-film reactions at 45 deg with respect to the static load which is directed midway between the pads.

Properties at Zero Static Load

At high values of S the elasticity and damping are linear with S, hence

$$\left(\frac{C}{W}\right)K = \left(\frac{C}{PA}\right)K = \varphi_K\left(\frac{R}{C}\right)^2\frac{\mu N}{P}$$

Eliminating P

$$K = \varphi_K\left(\frac{R}{C}\right)^2\left(\frac{1}{C}\right)\mu NA$$

where the coefficient φ_K is the slope of the elasticity curve in the linear region. If $(C/W)K^*$ is the value of $(C/W)K$ at $S = 10^3$

$$\varphi_K = \left(\frac{C}{W}\right)K^* \times 10^{-3}$$

Similarly

$$B\omega = \varphi_{B\omega}\left(\frac{R}{C}\right)^2\left(\frac{1}{C}\right)\mu NA$$

where

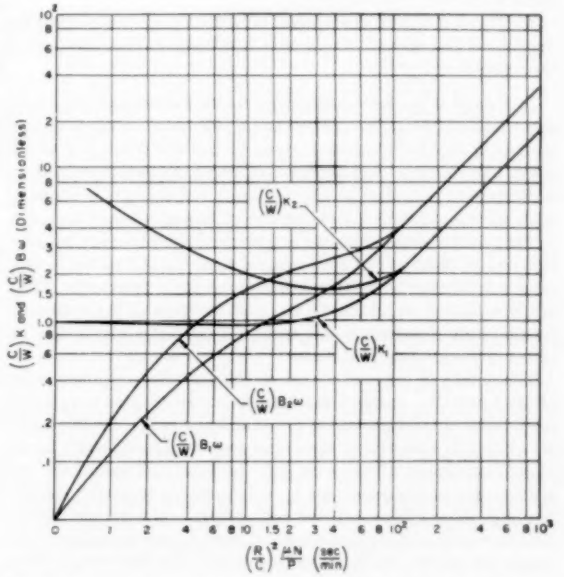

Fig. 8 Dynamic properties of full journal bearing; L/D = 0.44

$$\varphi_{B\omega} = \left(\frac{C}{W}\right)B\omega^* \times 10^{-3}$$

and $(C/W)\ B\omega^*$ is the value of $(C/W)\ B\omega$ at $S = 10^3$.

Brief Notes*

On the recommendations of the Executive Committee of the ASME Applied Mechanics Division, it has been decided to initiate a section devoted to brief notes on technical matters in mechanics. These notes must not be longer than 750 words (about 2½ double-spaced typewritten pages, including figures) and will be subject to the usual review procedure prior to publication. After approval such notes will be published as soon as possible, normally in the next issue of the Journal. The notes should be submitted to the Technical Editors of the *Journal of Applied Mechanics*.

A Note on Deflections of Plates on a Viscoelastic Foundation[1]

By E. REISSNER,[2] CAMBRIDGE, MASS.

In the analysis of plates and beams on an elastic foundation, one generally describes the foundation by one of the following two assumptions:

1 The foundation is a three-dimensional continuum for which linear stress-strain relations hold.

2 The foundation is a system of continuously distributed independent coil springs which offer resistance in the direction of their axes only.

In the use of the first assumption, the Boussinesq solution for a point load on the surface of an elastic half space serves to obtain a singular integrodifferential equation for the deflection of the plate. With the second assumption, one reduces the problem to a differential equation which, for linear coil springs, is identical with the equation for a plate on the surface of a heavy liquid.

The present note has as its purpose the description of a foundation model which, while more general than the coil-spring model, retains in essence the mathematical simplicity of this model. This is accomplished by adding to the axial stiffness of the system of continuously distributed coil springs a property which may be called differential shear stiffness.

The details of the analysis are as follows: We consider a layer of thickness H. Introducing Cartesian co-ordinates x, y, z, the boundaries of the layer are at $z = 0$ and at $z = H$. In this layer, we allow the existence of normal stresses σ perpendicular to the plane boundaries, which represent the axial stiffness of the coil springs, and of shear stresses τ_x and τ_y, which represent the differential shear stiffness of the coil springs. We assume further that normal and shear stresses σ_x, σ_y, and τ_{xy} are negligible. The remaining stress system must then satisfy the following system of equilibrium differential equations

$$\frac{\partial \tau_x}{\partial z} = 0, \quad \frac{\partial \tau_y}{\partial z} = 0, \quad \frac{\partial \tau_x}{\partial x} + \frac{\partial \tau_y}{\partial y} + \frac{\partial \sigma}{\partial z} = 0 \quad \text{.....[1]}$$

In addition to equilibrium equations, we have relations between stresses and components of displacement u, v, w in the direction of the axes x, y, z. We here take these relations in the following form

$$\left(1 + \lambda \frac{\partial}{\partial t}\right)\left(\frac{\partial w}{\partial x}, \frac{\partial u}{\partial z} + \frac{\partial w}{\partial x}, \frac{\partial v}{\partial z} + \frac{\partial w}{\partial y}\right) = \left(\frac{\sigma}{E}, \frac{\tau_x}{G}, \frac{\tau_y}{G}\right) \quad \text{.....[2]}$$

When $\lambda = 0$ we have the case of an elastic medium. When $E = G = 0$ but $E\lambda$ and $G\lambda$ are finite, we have the case of a viscous fluid. The general case is that of a viscoelastic medium.

The system of Differential Equations [1] and [2] is to be solved subject to suitable boundary conditions. As such boundary conditions we take, at the base of the foundation

$$z = 0: \; u = v = w = 0 \quad \text{.....[3]}$$

while at the surface of the foundation

$$z = H: \; u = v = 0, \quad \sigma = p \quad \text{.....[4]}$$

The load intensity p is also acting on the plate which is supported by the foundation. If we designate the deflection of this plate by W and the external load intensity by q, and if we assume that this plate is of uniform thickness and that its deflection is governed by classical theory, then we have the following further relation

$$D\nabla^2\nabla^2 W = q - p \quad \text{.....[5]}$$

In Equation [5], D is the bending stiffness factor of the plate, ∇^2 is the Laplace operator, and, furthermore, W is related to w, as follows

$$W(x, y, t) = w(x, y, H, t) \quad \text{.....[6]}$$

Equations [1] to [6] allow a reduction of the problem to two simultaneous differential equations for the deflection W and for the foundation pressure p, together with an appropriate number of boundary conditions. One of the two differential equations is given by Equation [5]. The other is obtained as follows:

Equations [1] show that τ_x and τ_y are independent of z, and that σ varies linearly with z. In view of Equation [4]

$$\sigma = p + (H - z)\left(\frac{\partial \tau_x}{\partial x} + \frac{\partial \tau_y}{\partial y}\right) \quad \text{.....[7]}$$

Equations [2] and [3] lead to the following formulas for w, u, v

$$E\left(1 + \lambda \frac{\partial}{\partial t}\right) w = pz + \left(Hz - \frac{1}{2} z^2\right)\left(\frac{\partial \tau_x}{\partial x} + \frac{\partial \tau_y}{\partial y}\right) \quad \text{....[8]}$$

$$G\left(1 + \lambda \frac{\partial}{\partial t}\right) u = \tau_x z - \frac{G}{E}\left[\frac{z^2}{2}\frac{\partial p}{\partial x} + \left(H\frac{z^2}{2} - \frac{z^3}{6}\right)\frac{\partial}{\partial x}\left(\frac{\partial \tau_x}{\partial x} + \frac{\partial \tau_y}{\partial y}\right)\right] \quad \text{...[9]}$$

$$G\left(1 + \lambda \frac{\partial}{\partial t}\right) v = \tau_y z - \frac{G}{E}\left[\frac{z^2}{2}\frac{\partial p}{\partial y} + \left(H\frac{z^2}{2} - \frac{z^3}{6}\right)\frac{\partial}{\partial y}\left(\frac{\partial \tau_x}{\partial x} + \frac{\partial \tau_y}{\partial y}\right)\right] \quad \text{...[10]}$$

There remain the first two of the boundary condition Equations [4], and these lead to relations between τ_x, τ_y, and p of the form

[1] Work supported by the Office of Naval Research under a contract with Massachusetts Institute of Technology.

[2] Department of Mathematics, Massachusetts Institute of Technology.

* Discussion of papers in Brief Notes should be addressed to the Secretary, ASME, 29 West 39th Street, New York, N. Y., and will be accepted until April 10, 1958, for publication at a later date. Discussion received after the closing date will be returned.

Note: Statements and opinions advanced in papers are to be understood as individual expressions of their authors and not those of the Society. Manuscript received by Applied Mechanics Division, April 29, 1957.

$$\tau_x = \frac{G}{E}\left[\frac{H}{2}\frac{\partial p}{\partial x} + \frac{H^3}{3}\frac{\partial}{\partial x}\left(\frac{\partial \tau_x}{\partial x} + \frac{\partial \tau_y}{\partial y}\right)\right] \quad [11]$$

$$\tau_y = \frac{G}{E}\left[\frac{H}{2}\frac{\partial p}{\partial y} + \frac{H^3}{3}\frac{\partial}{\partial y}\left(\frac{\partial \tau_x}{\partial x} + \frac{\partial \tau_y}{\partial y}\right)\right] \quad [12]$$

A further relation which is needed follows by combining Equations [6] and [8]

$$E\left(1 + \lambda\frac{\partial}{\partial t}\right)W = Hp + \frac{H^3}{2}\left(\frac{\partial \tau_x}{\partial x} + \frac{\partial \tau_y}{\partial y}\right) \quad [13]$$

We now eliminate τ_x and τ_y from Equations [11] to [13] and obtain as the second of the two differential equations relating W and p

$$\left(1 + \lambda\frac{\partial}{\partial t}\right)\left(W - \frac{H^2}{3}\frac{G}{E}\nabla^2 W\right) = \frac{H}{E}\left(p - \frac{H^2}{12}\frac{G}{E}\nabla^2 p\right) \quad [14]$$

The system of Equations [5] and [14] is of the sixth order. Accordingly, in addition to the two boundary conditions at the edge of the plate which are associated with Equation [5] when the foundation pressure p is a given function, a third boundary condition is needed which describes what occurs at the cylindrical boundary position of the foundation. In view of the assumptions made for the physical properties of the foundation, this condition cannot involve either one of the displacement components u, v. A simple and reasonable condition is that of vanishing edge shear τ_n, where n is the normal direction to the cylindrical boundary. Equations [11] to [13] indicate that in terms of p and W this condition takes on the following form

$$G\frac{\partial}{\partial n}\left[\left(1 + \lambda\frac{\partial}{\partial t}\right)W - \frac{1}{4}\frac{H}{E}p\right]_B = 0 \quad [15]$$

We note that when $G = 0$ then the System [5] and [14] reduces to the single equation

$$D\nabla^2\nabla^2 W + \frac{E}{H}\left(1 + \lambda\frac{\partial}{\partial t}\right)W = q \quad [16]$$

while the Boundary Condition [15] disappears. When $\lambda = 0$ then Equation [16] becomes the known differential equation of the elementary theory of plates on an elastic foundation, with foundation modulus E/H.

The presence of the additional parameter H^2G/E in the differential Equation [14] offers the possibility of obtaining a closer agreement between actual foundation behavior and model behavior than otherwise would be possible.

A Theorem in Plane Kinematics

By J. S. BEGGS,[1] PACIFIC PALISADES, CALIF.

This theorem relates the curvature of the paths of momentarily coincident points fixed in each of two bodies to the instant center of these bodies as they undergo plane motion.

Referring to Fig. 1, the plane motion of bodies 1 and 2 is determined by their centrodes rolling on each other without slipping. P_1 is a point fixed in body 1 and traces out a path C_1 in body 2. P_2 is fixed in body 2 and traces out the path C_2 in body 1 during the motion. P_1 and P_2 are momentarily coincident. ρ_1 is the radius of curvature of C_1 at P_1 and ρ_2 is the radius of curvature of C_2 at P_2. O_{12} is the instant center of bodies 1 and 2. b is the distance of O_{12} from P_1 and P_2; b is always positive. ρ_1 is positive when C_1 is concave toward O_{12}.

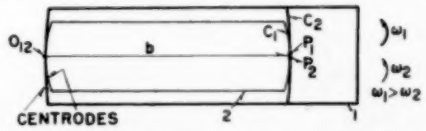

Fig. 1 The relative plane motion of bodies 1 and 2 described in terms of their centrodes rolling on each other without slipping. ω_1 and ω_2 are measured relative to the paper.

The theorem may be stated as follows

$$\frac{1}{\rho_1} + \frac{1}{\rho_2} = \frac{2}{b} \quad [1]$$

Although this theorem was discovered by comparing the Coriolis and normal accelerations of points P_1 and P_2 as measured in bodies 2 and 1, it may be derived readily from geometrical considerations as depicted in Fig. 2. In order to readily check the

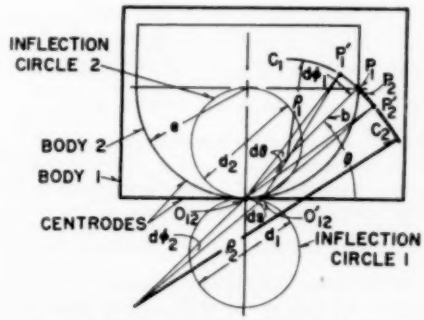

Fig. 2 A specific example of plane motion in which the centrodes are a straight line and a circle

theorem analytically, a straight line was chosen for the centrode of body 1 and a circle of radius e for the centrode of body 2. P_1 and P_2 were chosen arbitrarily on the circle at a distance e from the straight line at the instant considered. C_2 is therefore a cycloid. C_1 appears to be nameless, although it is intimately related to the involute of a circle. The following results are derived by means of analytical geometry and the calculus

$$b = \sqrt{2}e,\ \rho_1 = \frac{2\sqrt{2e}}{3},\ \text{and}\ \rho_2 = 2\sqrt{2e} \quad [2]$$

These values satisfy Equation [1].

Assume that in Fig. 2 body 1 rotates in a counterclockwise direction relative to body 2 through an angle $d\theta$. As the centrodes roll without slipping, the instant center moves from O_{12} to O_{12}', P_1 moves to P_1', and P_2 moves to P_2'. From Fig. 2

$$P_1P_1' = P_2P_2' = bd\theta = \rho_2 d\varphi_2 = \rho_1 d\varphi_1 \quad [3]$$

and

$$ds\sin\theta = (\rho_2 - b)d\varphi_2 = (b - \rho_1)d\varphi_1 \quad [4]$$

---

[1] Professor of Engineering, University of California, Los Angeles, Calif.; formerly member of the technical staff, The Ramo-Wooldridge Corp. Mem. ASME.

Note: Statements and opinions advanced in papers are to be understood as individual expressions of their authors and not those of the Society. Manuscript received by Applied Mechanics Division, May 15, 1957.

Equations [3] and [4] may be combined to yield Equation [1].

It is of interest to derive Equation [1] from considerations of accelerations because the theorem finds its principal use in determining normal accelerations. In Fig. 3 the X_0Y_0 co-ordinate system is fixed in the paper but the XY system is free to move in

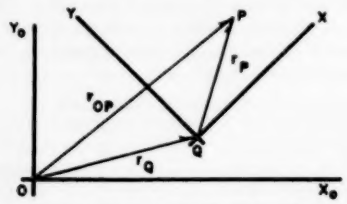

Fig. 3 The motion of P relative to X_0Y_0 is described in terms of P's motion relative to XY, and the motion of XY relative to X_0Y_0

the X_0Y_0 system. The acceleration of any point P moving in the plane of the paper relative to X_0Y_0 is given by

$$\underline{a}_{0P} = \underline{a}_Q + \dot{\underline{\omega}} \times \underline{r}_P - \omega^2 \underline{r}_P + 2\underline{\omega} \times \underline{V}_P + \underline{a}_P \quad [5]$$

where $\underline{a}_Q$ is the acceleration of Q, $\underline{\omega}$ and $\dot{\underline{\omega}}$ are the angular velocity and angular acceleration of XY (all relative to X_0Y_0), and $\underline{V}_P$ and $\underline{a}_P$ are the velocity and acceleration of P relative to XY. Equation [5] is used first to determine the acceleration $\underline{a}_{0P_1}$, of P_1 relative to X_0Y_0 by referring its motion to XY fixed in body 2. Q is chosen fixed at P_2 so that $\underline{r}_{P_1}$ is momentarily zero and $\underline{a}_Q = \underline{a}_{0P_2}$, thus simplifying the equation

$$\underline{a}_{0P_1} = \underline{a}_{0P_2} + 2\underline{\omega}_2 \times \underline{V}_{P_1} + \underline{a}_{P_1} \quad [6]$$

In a similar manner the acceleration of P_2 relative to X_0Y_0 is determined by referring its motion to XY fixed in body 1

$$\underline{a}_{0P_2} = \underline{a}_{0P_1} + 2\underline{\omega}_1 \times \underline{V}_{P_2} + \underline{a}_{P_2} \quad [7]$$

Breaking $\underline{a}_{0P_1}$ and $\underline{a}_{0P_2}$ down into their normal and tangential components, noting that $\underline{V}_{P_1} = -\underline{V}_{P_2}$, and that the tangential components of acceleration, $\underline{a}^T_{P_1}$ and $\underline{a}^T_{P_2}$ are equal and opposite, and adding Equations [5] and [6], we have

$$2(\underline{\omega}_1 - \underline{\omega}_2) \times V_{P_2} + \underline{a}^N_{P_1} + a^N_{P_2} = 0 \quad [8]$$

Expressing the normal accelerations in terms of the velocities of the points and the radii of curvature of their paths, and noting that $(\omega_1 - \omega_2)b = V_{P_2}$ ($\hat{\underline{b}}$ is the unit vector in the $\underline{b}$-direction) we have

$$\frac{2V^2_{P_2}}{b}\hat{\underline{b}} - \frac{V^2_{P_2}}{\rho_1}\hat{\underline{b}} - \frac{V^2_{P_2}}{\rho_2}\hat{\underline{b}} = 0 \quad [9]$$

which reduces to Equation [1].

The present theorem is useful when analyzing a mechanism graphically by means of Equation [5],[2] when ρ_1 can only be determined approximately from the drawing but ρ_2 is known accurately from the dimensions of the mechanism. For example, C_2 may be the center line of a circular slot. It often happens that a small error in ρ_1 will produce a large error in the determination of the acceleration of the output of the mechanism.

The Euler-Savary equation for P_2 in Fig. 2 is

$$1/b + 1/(\rho_2 - b) = d\theta/(\sin\theta ds) = 1/(|d_2| \sin\theta) \quad [10]$$

where d_2 is the diameter of the inflection circle[3,4] of body 2. This inflection circle is the locus of all points fixed in body 2 which at the instant are at a point of inflection of their path in body 1. Equation [10] holds for all positions of P_2 fixed in body 2, when the centrodes are in the position illustrated. The same equation for P_1 is

$$-1/b - 1/(\rho_1 - b) = d\theta/(\sin\theta\, ds) = 1/(|d_1| \sin\theta) \quad [11]$$

(The minus signs appear before the first two terms because P_1 lies on the opposite side of O_{12} from inflection circle 1.)[5] The inflection circles of the two bodies always lie on the opposite sides of their instant center. The centrode with the highest curvature has its inflection circle on its concave side.

If R_1 and R_2 are the radii of curvature of the centrodes at O_{12} then

$$d_1 = \frac{R_2R_1}{R_2 - R_1} \quad [12]$$

R_1 is arbitrarily taken as positive and R_2 is taken as positive or negative according as the centrodes are concave in the same or opposite directions. The subscripts are interchanged throughout Equation [11] and the instructions for its use, in order to obtain d_2.

Equating first the left sides and then the right sides of Equations [10] and [11] we obtain Equation [1] and the fact that

$$|d_1| = |d_2| \quad [13]$$

From Fig. 2, $R_1 = \infty$, $R_2 = e$ and $\theta = 45$ deg. From Equation [12] $|d_1| = |d_2| = e$. Equations [10] and [11] give the same values for ρ_1 and ρ_2 as are given in Equations [2].

[2] "Mechanism," by J. S. Beggs, McGraw-Hill Book Company, Inc., New York, N. Y., 1955, p. 22.

[3] "Kinematics of Mechanisms," by N. Rosenauer and A. H. Willis, Associated General Publications, Sidney, Australia, 1953, p. 56.

[4] "Kinematische Getriebesynthese," by R. Beyer, Springer-Verlag, Berlin, 1953, p. 39.

[5] See footnote 3, p. 47.

Transient Conduction in a Semi Infinite Solid With Variable Thermal Conductivity

By KWANG-TZU YANG,[1] NOTRE DAME, IND.

In dealing with analytical solutions of the transient-conduction equation, it is generally assumed that the thermal conductivity remains constant throughout the solid. The results are applicable to those cases where the temperature variation is relatively small or within the range of temperature variation the thermal conductivity is nearly independent of temperature. However, when the temperature change is large or the thermal conductivity varies greatly with temperature, the assumption of constant thermal conductivity may lead to significant errors. In steady heat-conduction problems, the variation of thermal conductivity may be handled generally by the well-known Kirchhoff transformation; and also, this variation does not present any additional difficulty in most of the numerical methods in dealing with transient-conduction problems. Unfortunately, when the latter problem is treated analytically, the partial differential equation becomes nonlinear, and consequently solutions cannot be obtained readily.

It is the purpose of this note to present a solution to the well-

[1] Assistant Professor, Department of Mechanical Engineering, University of Notre Dame, Notre Dame, Ind. Assoc. Mem. ASME.

Note: Statements and opinions advanced in papers are to be understood as individual expressions of their authors and not those of the Society. Manuscript received by Applied Mechanics Division, June 6, 1957.

known classical problem of transient conduction in a semi-infinite solid when its surface undergoes a stepwise temperature change, and it will be shown that the variation of thermal conductivity with temperature can be allowed in the solution.

The differential equation for the temperature variation $t(x, \tau)$, together with the pertinent initial and boundary conditions for this problem, may be written as

$$\frac{\partial t}{\partial \tau} = \frac{1}{\rho c} \frac{\partial}{\partial x}\left(k \frac{\partial t}{\partial x}\right) \quad \ldots\ldots [1]$$

$$\left.\begin{aligned} t(x, 0) &= t_i \text{ (const)} \quad x \geqslant 0 \\ t(0, \tau) &= t_0 \text{ (const)} \quad \tau > 0 \\ t(\infty, \tau) &= t_i \qquad\quad \tau \geqslant 0 \end{aligned}\right\} \quad \ldots\ldots [2]$$

where x is the distance into the solid as measured from the surface, τ the time variable, ρ the density, c the specific heat, k the thermal conductivity, t_i the initial temperature throughout the solid, and t_0 the constant surface temperature after the stepwise change. After introducing a dimensionless dependent variable θ^* defined by

$$\theta^* = \frac{\theta}{\theta_0} = \frac{t - t_i}{t_0 - t_i}$$

Equation [1] reduces to

$$\frac{\partial \theta^*}{\partial \tau} = a \frac{\partial}{\partial x}\left(k^* \frac{\partial \theta^*}{\partial x}\right) \quad \ldots\ldots [3]$$

where the dimensionless thermal conductivity k^* is defined as k/k_0, a the thermal diffusivity based on k_0, and k_0 the thermal conductivity corresponding to a constant reference temperature. Note that k^* may now be considered as a function of θ^* only. The appropriate initial and boundary conditions then become

$$\theta^*(x, 0) = 0, \qquad \theta^*(0, \tau) = 1, \qquad \theta^*(\infty, \tau) = 0 \quad \ldots [4]$$

Now if it is assumed that θ^* is only a function of a dimensionless independent variable y defined by

$$y = \frac{x}{2\sqrt{(a\tau)}} \quad \ldots\ldots [5]$$

Equation [3] may be readily transformed into a second-order nonlinear ordinary differential equation

$$\frac{d^2\theta^*}{dy^2} + \frac{1}{k^*}\left(\frac{dk^*}{d\theta^*}\right)\left(\frac{d\theta^*}{dy}\right)^2 + \frac{2y}{k^*}\left(\frac{d\theta^*}{dy}\right) = 0 \quad \ldots\ldots [6]$$

with the boundary conditions

$$\theta^*(0) = 1, \qquad \theta^*(\infty) = 0 \quad \ldots\ldots [7]$$

according to Equations [4].

For the classical problem where thermal conductivity is assumed to be constant, i.e., $k^* = 1$, Equation [6] reduces to a linear equation

$$\frac{d^2\theta^*}{dy^2} + 2y \frac{d\theta^*}{dy} = 0 \quad \ldots\ldots [8]$$

which, together with the boundary conditions in Equation [7], may be simply solved, resulting in

$$\theta^* = 1 - \text{erf}\left[\frac{x}{2\sqrt{(a\tau)}}\right] \quad \ldots\ldots [9]$$

which is identical with the classical solution. In the general case where thermal conductivity varies with temperature, Equation [6] may be solved numerically by the method of successive approximation. One way of carrying out the calculation is to assume a starting temperature distribution $\theta_1^*(y)$, for which the classical solution in Equation [9] may be conveniently used. Then the second approximation is obtained in treating Equation [6] as though it were a linear equation as follows

$$\theta^* = 1 - \frac{\int_0^y e^{-\int_0^y \left[\frac{1}{k_1^*}\left(\frac{dk^*}{d\theta^*}\right)_1\left(\frac{d\theta^*}{dy}\right)_1 + \frac{2}{k_1^*}y\right]dy} dy}{\int_0^\infty e^{-\int_0^y \left[\frac{1}{k_1^*}\left(\frac{dk^*}{d\theta^*}\right)_1\left(\frac{d\theta^*}{dy}\right)_1 + \frac{2}{k_1^*}y\right]dy} dy} \quad \ldots [10]$$

where the subscript 1 indicates values corresponding to the starting temperature distribution. Next, a third approximation may be evaluated by using the second approximation as θ_1^* in Equation [10]. This procedure is then to be repeated until desired accuracy is obtained. It may be pointed out that, even though the partial differential Equation [3] is always reducible to a total differential Equation [6] by means of the Transformation [5], the present solution, however, is only possible because of the fact that the initial and boundary conditions of the present problem can be reduced to proper boundary conditions with respect to the independent variable y. This is the very reason that the present solution cannot be generalized readily to other physical problems.

Two numerical examples have been calculated on the basis of the following linear thermal conductivity-temperature variation

$$k^* = 1 + \alpha\theta^* \quad \ldots\ldots [11]$$

where α assumes a value of 0.5 in one example and -0.5 in the other. Fig. 1 shows the results of these calculations. Also indicated is a curve for $\alpha = 0$, which corresponds to the classical solution. Furthermore, the heat flow into the solid at the surface at any instant τ is directly proportional to the quantity $-(d\theta^*/dy)_{y=0}$, the values of which are also indicated in Fig. 1 for different α-values. Even though these α-values may not be too realistic, the results, however, do demonstrate the extent to which both the temperature distribution and heat flow at the surface could be affected by the variation of thermal conductivity with temperature. Recently the classical solution, Equation [9], has been used in conjunction with thermal-conductivity measurement under transient conditions,[2] and it is believed that the present solution could serve as useful information for interpreting test results.

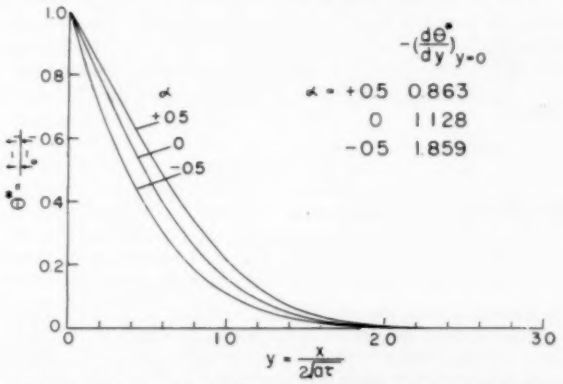

Fig. 1 Effect of varying thermal conductivity on temperature distribution

[2] "Determination of Thermal Conductivities of Metals by Measuring Transient Temperatures in Semi-Infinite Solids," by S. T. Hsu, TRANS. ASME, vol. 79, 1957, pp. 1197–1201.

Discussion

New Approach to the Theory of Thin, Slightly Cambered Profiles[1]

M. J. Schilhansl.[2] This paper offers a promising possibility of expanding and deepening the knowledge about two-dimensional flow around single airfoil sections and past cascades.

So long as single airfoil sections are referred to, there is no doubt that the small deviations u parallel to the velocity U_0 of the main flow from this velocity U_0 can be neglected if the section is sufficiently thin. This means that the slope of the mean camber line dy/dx can be equated to v/U_0 without appreciable error instead of being equated to $v/(U_0 + u)$.

This approximation—tacitly made in the tangency condition [7]—is questionable if a flow past cascades is involved. Here the components u depend not only upon the thickness of the one profile at which the analysis is made but also upon the camber and thickness of all the other profiles of the cascade. The decision as to how thin an airfoil section must be to be estimated as "thin" should not be based on a comparison of the maximum thickness with the length of the chord l but on a comparison of the maximum thickness with the width of a passage between adjacent blades, which is approximated by $t \cos \gamma$. The effect of the thickness can be eliminated if it is assumed that the airfoil sections are infinitely thin. In this case, the velocity components u depend solely upon the camber of all the other profiles of the cascade. The effect may be illustrated by the following example:

A single, infinitely thin, slightly cambered, circular-arc profile has a lift coefficient $c_{L,s} = 2\pi\theta/4$ (see Equation [27] of the paper) at an angle of attack $\alpha = 0$ deg. If this airfoil section is an element of a cascade specified by a solidity $l/t = 1.0$ and a stagger angle $\gamma = \pm 60$ deg, its lift coefficient is changed. If the tangency condition

$$\frac{dy}{dx} = \frac{v}{U_0 + u}$$

is replaced by the approximation

$$\frac{dy}{dx} = \frac{v}{U_0}$$

in this calculation, the result is $C_{L,C} = 2.208\pi\ \theta/4$ at $\alpha = 0$ deg and that independent of the sign of the stagger angle γ. If, however, the small velocity component u is not neglected in the tangency condition, the result is at $\alpha = 0$ deg

$$C_{L,C} = 2.787\pi\ \theta/4 \text{ for } \gamma = -60 \text{ deg (accelerated flow)}$$

and

$$C_{L,C} = 2.050\pi\ \theta/4 \text{ for } \gamma = +60 \text{ deg (decelerated flow)}$$

If the effect of an angle of attack $\alpha \neq 0$ deg is added, the lift coefficients shown in Fig. 1 of this discussion are obtained for $\theta/4 = 0.2$. The straight line a represents the lift coefficient of the single airfoil; the line b represents the lift coefficient of the airfoil section in cascade $l/t = 1.0$ and $\gamma = \pm 60$ deg based on the approximation

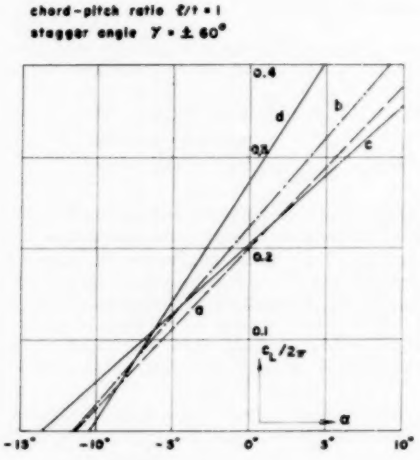

a Single Airfoil
b Induced Horizontal Components
c Decelerated Flow Cascade
d Accelerated Flow Cascade

Fig. 1

$$\frac{dy}{dx} = \frac{v}{U_0}$$

lines c and d represent the c_L for $\gamma = +60$ deg and $\gamma = -60$ deg, respectively, with the correct tangency condition. The latter are taken from a paper of H. Schlichting.[3]

It can be clearly seen that adding the velocity component u due to the remainder of the cascade to the mean velocity U_0 in the tangency condition changes the lift coefficient by the same order of magnitude as replacing the value of the velocity component v perpendicular to U_0 in the case of a single airfoil section by the value of v in the case of a cascade and, simultaneously, applying the approximate tangency condition.

It might be objectionable to demonstrate the fact that the component u should not be neglected in the tangency condition merely by an example. It is possible to prove this generally. For this reason, let us assume that the difference of the velocity U_s at the suction side of the airfoil section and of the velocity U_p at the pressure side is given as a function of the chordwise abscissa x, and that the components v and u are found depending upon $U_s - U_p$. So long as a single airfoil of infinitesimal thickness is involved, $v = v_i$ and, at least in a linearized theory, $u = 0$. If an airfoil section in a cascade is involved, $v = v_e$ and $u = u_e$, Fig. 2 of this discussion. In this figure, the letters a, b, c, and d have the same meaning as in Fig. 1. From Fig. 2, it can be seen that the true criterion for dropping u_e in the tangency condition should be whether or not u_e is small in comparison to the difference $v_e - v_i$.

The velocity $U_0 + u$ approaches at the leading edge the relative

[1] By F. S. Weinig, published in the June, 1957, issue of the JOURNAL OF APPLIED MECHANICS, TRANS. ASME, vol. 79, pp. 177–182.

[2] Professor of Engineering, Brown University, Providence, R. I.

[3] "Berechnung der reibungslosen inkompressiblen Strömung für ein vorgegebenes ebenes Schaufelgitter," by H. Schlichting, *VDI-Forschungsheft*, no. 447, 1955.

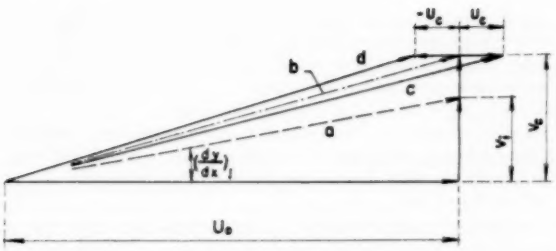

Fig. 2

velocity w_1 of the flow entering the cascade and at the trailing edge the relative velocity w_2 of the flow, leaving the cascade closer the higher the solidity of the cascade l/t. Since the velocity of reference U_0 equals the mean vector sum of w_1 and w_2, the component u is negative at the leading edge and positive at the trailing edge in an accelerated flow and is positive at the leading edge and negative at the trailing edge in a decelerated flow. If the extreme values are approximately calculated from $w_1 - U_0$ and $U_0 - w_2$, respectively, and the difference $v_e - v_i$ approximately from

$$v_e - v_i = \frac{1 - \mu}{\mu} v_i$$

where μ can be taken from Fig. 9 of the paper, a quick estimate can be made whether or not the component u can be dropped in the tangency condition of a given cascade configuration specified by the stagger angle γ and solidity l/t.

Apparently, the author neglected the component u in the tangency condition; otherwise, the curves of Fig. 9 of the coefficients μ of angular exaggeration would not show horizontal tangents at stagger angle $\gamma = 0$ (impulse-type cascade), indicating that

$$(\mu)_{+\gamma} = (\mu)_{-\gamma}$$

It might be that the effect of the component u is larger at higher-order profiles; it might even be that this effect depends upon whether the order n of the polynomials $y = P_n(x)$ is an even or an odd number.

Thus it seems to be recommendable to study, first, how the described method can be adapted to the complete tangency condition

$$\frac{dy}{dx} = \frac{v}{U_0 + u}$$

and then to go ahead with investigations of higher-order profiles.

Author's Closure

The author fully agrees with M. J. Schilhansl on the need of theoretical treatment of cascade flow beyond the level of linearization. He elsewhere contributed his own share to this. But linearization is expedient for many practical purposes, and the presented paper had only the objective of showing a new approach to it. The components u and v of the perturbance are real and imaginary parts of the same function of the complex variable. Hence they are of the same order of magnitude, and if $|v| \ll |U_0|$, also $|u| \ll |U_0|$, and

$$\frac{dy}{dx} = \tan \imath = \frac{v}{U_0 + u} = \frac{v}{U_0} \cdot \frac{U_0}{U_0 + u} = \frac{v}{U_0} - \frac{vu}{U_0^2} + \frac{vu^2}{U_0^3}$$

Of this

$$\frac{dy}{dx} = \frac{v}{U_0}$$

is the linear or first-order approximation. The same order of approximation is obtained by linearization when considering that also $\log w/U_0$ and ν are real and imaginary parts of the same function of the complex variable. This tangency condition has been utilized elsewhere by the author. But the results of linearization are identical in both approaches. Also the linearization holds independent of the "order" of the profile except in case of blunt profiles in the immediate environment of the leading edges.

With respect to differences, depending whether the same cascade is accelerating or decelerating, the author disagrees with M. J. Schilhansl. If a cascade consisting of profiles having cusped or wedge-shaped leading and trailing edges is considered under conditions of smooth approach flow, the shape of the flow pattern and the pressure distribution depend only on the magnitude of the reference velocity but not on the direction of the flow through the cascade, though the role of leading and trailing edge are exchanged. Hence the lift and, when referred to the same reference velocity $|W_\infty| = \frac{1}{2}|W_1 + W_2| = |U_0|$, the lift coefficients are equal, independent of the condition of acceleration or deceleration. The predicted numerical value will still depend, of course, on the degree of approximation and, for the sake of accuracy, more may be needed than linearization.

Two-Dimensional Inflow Conditions for a Supersonic Compressor With Curved Blades[1]

R. D. Buhler.[2] The author is to be commended for having carried out these calculations. In the past few years so much emphasis has been placed on the very difficult three-dimensional turbomachine flow analysis that many important two-dimensional flow problems have been rather neglected, at least in the published literature, though these can be treated fairly readily with existing methods. Certainly the flow regime covered in this paper (subsonic axial and supersonic relative flow) will remain one of great importance in the foreseeable future.

Within the region of validity and the accuracy of the assumed flow pattern the paper establishes the important result that (for curved blades) the Mach number at upstream infinity must be roughly half way between the Mach numbers ahead of and behind the (right-hand) leading-edge shock. It gives an immediate estimate of the incidence angle and the strength of the wave(s) near the leading edge. These results have not always been understood properly.

However, certain important questions concerning the range of applicability and the approximate accuracy of these calculations remain unanswered. First, if one wishes to use the results presented here, one needs to know the lowest Mach number $\mathbf{M}_\infty$ for which these results are still applicable. Certainly, for any given cascade (S/R, β_1) there must exist a value of $\mathbf{M}_\infty$ (or of $\mathbf{M}_1$) at which the flow just after the shock becomes sonic. At Mach numbers below this value the flow pattern must change. Using the results of this paper (θ_1, $\mathbf{M}_1$) together with shock charts, one can enter the lower limit of applicability as a curve on each of the charts (Figs. 4, 5, and 6 of the paper). At Mach numbers below this "validity curve" the results might still be roughly correct, but they certainly should be interpreted with caution.

Then, too, there are some important unanswered questions concerning the basic assumptions of this calculation method. The

[1] By Philip Levine, published in the June, 1957, issue of the JOURNAL OF APPLIED MECHANICS, TRANS. ASME, vol. 79, pp. 165–169.

[2] Propulsion Research Corporation, Santa Monica, Calif.

method used is the direct parallel of the "shock-expansion" method for isolated airfoils, where reflected waves and vorticity are likewise neglected. In applying this to an infinite two-dimensional cascade, difficulties arise from the fact that each blade is preceded by an infinite number of (progressively weaker) shocks and expansion regions. Thus, for the cascade, there is no region in the flow field near the blade which is unaffected by the cumulative effect of many wave reflections and by shed vorticity. That there are entropy gradients in the flow can be seen readily by considering two streamlines very close together, which go, respectively, to the upper and the lower surface of the same blade; i.e., to points e and L. The upper streamline passes through one additional shock wave than the lower one; consequently, there is a higher entropy at point e than at point L.

It would be valuable to know to what extent the reflected waves and the entropy gradients (vorticity) affect the flow solution, particularly the local blade-surface Mach numbers. Furthermore, since each streamline coming from infinity passes through an infinite number of (weak) waves, it is not immediately evident how large the average entropy increase up to the cascade entrance will be for a given wave strength at the leading edge. Obviously this entropy increase affects the accuracy of the calculated Mach number $\mathbf{M}_\infty$.

This paper, based on the assumptions of isentropic flow and of "simple wave" (i.e., Prandtl-Meyer) expansion, certainly constitutes the logical first approximation to the given flow problem, and quite probably also a good one. The foregoing questions are raised in the hope of stimulating further work which will put all cascade calculations in the "subsonic axial-supersonic relative" flow regime on a firmer theoretical basis.

Point Source and Point Vortex in the Hodograph Plane[1]

T. M. Cherry.[2] The writer finds the paper of considerable interest. The work as it stands at present is essentially mathematical. It would be valuable if a sketch were to be given of the contemplated application to the physical problem of cascade design. In fact, further mathematical investigation probably will be required if the range of speeds that is of physical interest straddles the critical speed called q_0 in the paper (Equation [48]); so one will need to know the range of speeds that is of physical interest.

The mathematical investigation here referred to is to determine whether or not the two solutions [53] — and similarly the two solutions [61] — are in fact analytical continuations of each other. It is doubtful whether the argument given in the paper is conclusive on this point; the vital point of logic is whether a series such as [50] is adequate to represent a stream function which (apart from obvious restrictions as to symmetry, and so on) is completely arbitrary. The writer has not examined this question, but from analogy with cases examined by Lighthill and the writer (references 2 and 9 of the paper), formulas [53] and [61] look rather too simple; but it is of course possible that the analogy is false and that the correct formulas have this simplicity. The question could be examined by the method used by Lighthill and the writer, or by that of Goldstein, Lighthill, and Craggs.[3]

J. E. Fowler.[4] The writer wishes to thank the authors for their contribution to the theory of compressible flow about cascades. This is a field in which usable rigorous solutions are almost unknown, and the designer must rely on approximate theories, corrections to incompressible-flow theories, or tests. No one of these is satisfactory when dealing with cascades characterized by large deflection angles and operating at relatively high subsonic Mach numbers; thus rigorous methods of design will prove welcome.

As one faced with the task of cascade design, the writer wishes to ask the authors if they can give an estimate of the amount of computation necessary to evaluate Equations [53] and [61], by either the exact or asymptotic series, over a region which would be of practical interest; that is, a region including all of the hodograph plane except a small area about the source or vortex.

It would appear possible, by matching the streamline patterns of compressible cascade flows in the hodograph plane to that of a known incompressible case, to establish compressibility corrections for incompressible blade shapes. Do the authors believe that such an approach holds any promise?

One difficulty associated with hodograph methods in cascade design is the fact that the hodograph of a blunt-nosed blade often involves a doubly covered surface, i.e., the streamlines $\psi =$ const may cross themselves, forming loops in the hodograph mapping. Do the authors consider that a solution to this problem is feasible in the compressible case?

The writer will await with interest further work in this field by the authors.

F. S. Weinig.[5] Although the hodograph of a cascade flow only exceptionally is single-valued, there exists a large and quite useful class of cascades where at least, at a certain Mach number for one angle of attack, the hodograph is single-valued. For these conditions the point vortex and point source, as they are the subject of the paper, are the valid basis of possible solutions. If the solution has to be determined for other angles of incidence, one may attempt to treat this problem in the physical plane, starting from the obtained solution by linearization with respect to the change of the angle of incidence.

Even the case of the double-valued hodograph itself is not at all the most general. But if restricting to the class of the cascade flows which correspond to double-valued hodographs, it should not be too difficult to find also point-source and point-vortex solutions in these cases, which, of course, besides the parameter τ_0, also the parameters τ_∞ and ϑ_∞ which may characterize the winding point of the double-valued hodograph would have to appear in the solution.

Considering the practical needs, however, to solve the direct problem of a given cascade at variable angle of incidence and variable Mach number, which arise immediately, if once by the inverse method of a given hodograph a cascade is determined, the writer is very doubtful if there will be a pay-off for all the efforts put in the hodograph method. These doubts have been the reason, with some regrets, he remembers that once[6] he proposed to use the hodograph as a means to obtain favorable turbine profiles. In his opinion there exist quite promising other ways to solve the proper indirect problem of velocity distribution given as a function of the curvature length of the profile, not only for incompressible but also for a compressible flow.

---

[1] By H. Poritsky and R. A. Powell, published in the June, 1957, issue of the JOURNAL OF APPLIED MECHANICS, TRANS. ASME, vol. 79, pp. 183–190.

[2] University of Melbourne, Victoria, Australia.

[3] "On the Hodograph Transformation for High-Speed Flow. I—A Flow Without Circulation," by S. Goldstein, M. J. Lighthill, and J. W. Craggs, *Quarterly Journal of Mechanics and Applied Mathematics*, vol. 1, 1948, pp. 344–357.

[4] Supervisor, Turbine Fluid Mechanics Research, General Electric Company, Schenectady, N. Y. Mem. ASME.

[5] Consultant, Aerodynamics, Aircraft Gas Turbine Development Department, General Electric Company, Cincinnati, Ohio. Mem. ASME.

[6] Third International Congress on Applied Mechanics, Stockholm, Sweden, 1930.

Nevertheless, the writer wishes to applaud the authors for their fine approach and he will certainly not be the only one to apply their results when they are made available in the form of handy tables.

Authors' Closure

The authors wish to thank the discussers for their interesting comments and will attempt to reply to their questions within the space available.

When the flow through a cascade with subsonic velocities at infinity is mapped on the hodograph plane, the flow at infinity on the inlet side is mapped into the neighborhood of a point vortex-source; the flow at infinity on the exit side is mapped into the neighborhood of a point vortex-sink. This is in contrast to the flow around a single cylinder, where the image of the flow at infinity may be a branch point. Thus the point-source and point-vortex singularities form an integral part of cascade flow studies by the hodograph method.

The velocities of physical interest near the point vortex-source and vortex-sink straddle the velocity of that point. Moreover, since the velocity at infinity on the inlet side is generally different from the velocity at infinity on the exit side, it is evident that at least one of the point vortex-source, point vortex-sink flows will have to be used considerably beyond the circle of convergence of the first series in Equations [50], [53]. The question of analytic continuation of the series is thus of real, not merely academic, interest.

Dr. Cherry states that "the vital point of logic is whether a series such as [50] is adequate to represent a stream function which (apart from obvious restrictions as to symmetry, and so on) is completely arbitrary." But he doubts whether an adequate proof of this point has been given.

However, the authors make no such broad claims for the proposed series. Thus for the point-vortex solution, the representation given by the series [53] plus the added series

$$\Sigma C_n \cos n\tau \psi_n(\tau), \text{ convergent for } \tau < \tau_1, \tau_1 > \tau_0 \ldots [91]$$

is proposed *only* when ψ is *single-valued* in the *larger* region $\tau < \tau_1$, enclosing the point vortex, even about $\theta = 0$, and satisfies Equation [2], except at $\tau = \tau_0, \theta = \theta_0$, where it possesses a logarithmic singularity described by Equation [47].

Similar statements apply to the point-source solution, where the representation given by the series [49], [50], with the added series

$$\Sigma C_n \sin n\tau \ \psi_n(\tau), \text{ convergent for } \tau < \tau_1, \tau_1 > \tau_0 \ldots [92]$$

is proposed for solutions of Equation [2] which are single-valued on a Riemann surface with a logarithmic branch point at $\tau = \tau_0$, $\theta = 0$ (i.e., for which $\psi - \tan^{-1}[\theta/(\lambda - \lambda_0)]$ is single-valued), and for which a proper determination is odd in θ for $\tau > \tau_0$.

Turning to the point-vortex solution, let its Fourier cosine series in θ be

$$\psi = \Sigma f_n(\tau) \cos n\theta \ldots [93]$$

Consider the functional operation 0_n leading from a function $f(\tau, \theta)$ to any term of its Fourier series in θ. It may be shown that 0_n is permutable with the differential operator L on the left side of Equation [2]

$$L[0_n(f)] = 0_n[L(f)] \ldots [94]$$

provided f is of class $C^{(2)}$ in the circular region $\tau < \tau_1$ or in the region bounded by two circles $\tau = \tau_1, \tau = \tau_2$. It follows that when 0_n is applied to the point-vortex function ψ satisfying Equation [2] (and restricted as described above), the resulting function $f_n(\tau) \cos n\tau$ will satisfy Equation [2] both for $\tau < \tau_0$ and for $\tau > \tau_0$. Hence f_n must reduce to a multiple of $\psi_n(\tau)$ for $\tau < \tau_0$ and to a linear combination of ψ_n, $\psi_{-n}{}^*$ for $\tau > \tau_0$. Examination of the continuity, discontinuity of $f_n(\tau)$, $f_n'(\tau)$ at $\tau = \tau_0$, based on the nature of the singularity [47] at $\tau = \tau_0$, $\theta = 0$ then leads to two linear equations in the three coefficients of ψ_n, $\psi_{-n}{}^*$ for $\tau < \tau_0$, $\tau > \tau_0$.

The authors do not wish to leave the impression that point vortex-source and vortex-sinks are the only singularities that may be encountered in cascade flows, nor that for cascade flows ψ is always single-valued in the hodograph plane. It is true that examples may be constructed in which, by adding flows of proper point source, sinks, and vortexes (and no other singularities), desirable cascade blade shapes are obtained. Yet branch-point singularities, which often occur in the hodograph plane for flows around single cylinders (or airfoils), may also occur in cascade flows. If the branch point is at $\tau = \tau_b, \theta = \theta_b$, then the representations [50], [53] (with the additions of [91], [93]) can be used in that branch of the Reimann surface which contains the point vortex-source or vortex-sink, provided $\tau_b > \tau_0$. In the contrary case, if $\tau_b < \tau_0$, and if the branch point is of the second order, i.e., if ψ is double-valued, the series [93] are inadequate altogether. The Fourier series [93] for a point vortex must now be replaced by

$$\psi = \sum_{n=0}^{\infty} f_{n/2}(\tau) \cos n\theta/2 \ldots [95]$$

where $f_{n/2}(\tau)$ to each side of τ_0 are solutions of Equation [10], for $\nu = n/2$, that is, for half-integer and integer orders. The continuity, discontinuity of $f_{n/2}$, $f'_{n/2}$ at τ_0 are determined in a similar manner.

In their profound studies of analytical continuation of series such as [91], [93], in references (2) and (9), both Cherry and Lighthill develop a method based essentially on the analytic continuation across its circle of convergence of the function

$$g(\zeta) = \Sigma C_n \zeta^n, \ \zeta = e^{\lambda + i\theta} \ldots [96]$$

as well as of certain other functions $g_m(\zeta)$ which are obtained from $g(\zeta)$ by means of the following integral operations

$$g_m(\zeta) = \zeta^{-m} \int_0^{\zeta} z^{m-1} g(z) dz \ldots [97]$$

Here λ is a proper function of τ (see Equations [66], [67]). If $g(\zeta)$ represents a function whose analytic continuation across its circle of convergence is well-known, then the analytic continuation of the functions [95] is available from the expansions given by Cherry and Lighthill.

To test the first series [53], [61] by this method, it would be necessary to form a proper power series [95] for $g(\zeta)$ corresponding to these series, and study its analytic continuation beyond its circle of convergence. It is evident that, due to the occurrence of $\psi_{-n}{}^*(\tau_0)$, $\psi_{-n}{}^{*\prime}(\tau_0)$ in the coefficients, the precise decision in regard to analytic continuation of $g(\zeta)$ would be difficult to reach.

Actually, the aforesaid method of Cherry and Lighthill is closely related to the Bergman solution which is briefly discussed in Section 8. An application of the Bergman method (as described by Equations [77] to [83] which are taken from reference (11)) to point source and vortex solutions is made in Equations [86] and [87]. By choosing the function $\varphi_0(\xi)$ as $\log(\xi - \xi_0)$, ($\varphi_0(\xi)$ is analogous to the function $g(\zeta)$), the stream-functions ψ for the point-source and point-vortex solutions are obtained as the imaginary and real parts of the right-hand member of Equation [87]. It will be seen, however, that the real part of the solution [87] is not single-valued near ξ_0; nor does its imaginary part have the proper multiple-valuedness. Therefore the use of the series [87] is not recommended.

In regard to the comments by Mr. Fowler, we feel that if proper

use is made of the published tables by Lighthill, Cherry, and others, and of the asymptotic representations, the cost of these calculations would not be excessive.

The convergence of the series [50], [53], or [61] for $\tau \neq \tau_0$ is essentially like that of a geometric series. For $\tau = \tau_0$ the series, if convergent at all, converges very poorly. It is, therefore, advisable to evaluate ψ by means of these series for a grid of points *not including* τ_0, and obtain ψ for $\tau = \tau_0$ by interpolation in τ.

In regard to the question of approaching the compressible hodograph solution by starting with a hodograph solution for the incompressible cascade flow, this, of course, forms the very basis of most compressible hodograph approaches. Indeed, in the work of Cherry and Lighthill the function $g(\zeta)$ is generally chosen from considerations of the incompressible hodograph case. Likewise, the logarithmic singularities of the present paper are based on the analogy to the incompressible case. However, the question probably pertains to successive correction methods which start with the incompressible flow and then correct successively for the effects of compressibility. Such a method could be based upon expansions of the solutions of [2] in powers of β. For $\beta = 0$, Equation [2] reduces to the Laplace equation with $(\sqrt{\tau}, \theta)$ as polar co-ordinates, while the solutions [6] become the familiar incompressible-flow product solutions $q^r e^{ri\theta}$. Presumably, the first few terms of these expansions would yield the corrections for the compressibility of the flow. The authors believe that the application of this method to the point-source and point-vortex solutions would be very laborious unless τ_0 is quite small.

General Instability of a Ring-Stiffened, Circular Cylindrical Shell Under Hydrostatic Pressure[1]

S. B. Batdorf.[2] The writer wishes to make one comment on the interesting paper by the author which may serve to codify and extend the range of his results.

In my referenced paper on cylinder theory, it is shown that the buckling of cylindrical shells generally can be described by very simple equations in the dimensional ranges of greatest practical interest. For example, the unstiffened shell corresponding to the curve $F = 0$ in Fig. 5 of the paper, buckles according to the formula

$$C_p = 1.04\, z^{0.5} \qquad 100 < z < 4.5 \left(\frac{R}{t}\right)^2$$

A logarithmic plot of the ratio of C_p for a stiffened cylinder to C_p for the unstiffened cylinder against the parameter $F + 1$ (the stiffness ratio for the two cases), results in a straight line of slope 0.75. This means that all the numerical results in Fig. 5 for $z > 100$ can be represented by the formula

$$C_p = 1.04\, z^{0.5} (1 + F)^{0.75}$$

This gratifyingly simple result is probably valid to substantially higher values of z and F than appear in the paper.

Author's Closure

The author is very grateful to Dr. Batdorf for his important contribution to the paper.

[1] By S. R. Bodner, published in the June, 1957, issue of the JOURNAL OF APPLIED MECHANICS, TRANS. ASME, vol. 79, pp. 269–277.

[2] Assistant Director of Research, Missile Systems Division, Lockheed Aircraft Corporation, Sunnyvale, Calif. Mem. ASME.

The Specific Damping Energy of Fixed-Fixed Beam Specimens[1]

A. W. Cochardt.[2] The writer wishes to congratulate the authors on a very interesting paper which, in general, substantiates the results of his work. However, a few points require clarification.

It seems that the authors have overemphasized the effect of static stress on the magnetomechanical part of the damping by only giving the results of those measurements which were obtained on their softest specimens, and for which this effect is greatest. It would have been more realistic if the authors had measured the effect of static stress—or presented their data—on their specimen 403-3.

The writer cannot agree with the authors' statement, "the presence of static tension nullifies any gains obtained by magnetomechanical damping," although it is true that static tension generally reduces this effect. Even using their softest specimen and a static stress of 11,000 psi, the authors (Fig. 2) report damping values which are considerably higher—probably higher by a factor of 5—than those that would have been obtained if the magnetomechanical effect had been nullified.

A small static stress or static magnetic field (stress and field are equivalent in this respect) may increase the magnetomechanical damping. This does not seem to be inconsistent with theory, as the authors suggest, as long as the stress or field is very small compared to the critical stress or field at which the ferromagnetic domain walls become fixed. It appears that the authors themselves must have observed this effect, since they state, "there is a small initial damping increase at low oersted values."

Authors' Closure

We wish to thank Dr. Cochardt for contributing a somewhat different, if not indisputable, interpretation of our results.

The data for specimen 403-3 are presented in Fig. 1 of this closure; this family of curves shows a damping decrease, caused by increasing static stress from zero to 19,000 psi, similar to that plotted in Fig. 2 in the paper for specimen 403-6. It was already shown in Fig. 5 that increased specimen hardness (in the range of 225 to 388 Bhn) causes the logarithmic decrement at a maximum normal stress of 30,000 psi to decrease from 0.028 to 0.001 when $\sigma_T = 0$ psi, and from 0.004 to 0.003 when $\sigma_T = 19{,}000$ psi.

If an AISI-403 turbine blade is longer than about 7 in., its root—under normal large-steam-turbine operating conditions—undergoes a centrifugal stress in excess of 19,000 psi; the statement with which Dr. Cochardt disagrees was directed at and is valid for such an application. Of course, the root of a blade shorter than 7 in. would be centrifugally stressed as a function of blade mass, radius of gyration, and rotational velocity; there is also a centrifugal-stress gradient out to the tip of the blade. Without undertaking a more precise stress analysis not in the scope of this investigation, it does appear that those who use the damping data of ferromagnetic materials obtained when static stress is zero are greatly overestimating the internal energy dissipated.

Although d-c magnetic field could be increased continuously from zero to more than 500 oersteds to uncover an initial damping increase, a static stress of less than 5600 psi was not applied to determine whether an equivalent damping increase occurs. However, the inconsistency of Dr. Cochardt's data in reference (9) is that he observed a damping increase when static stress equaled

[1] By W. C. Hagel and J. W. Clark, published in the September, 1957, issue of the JOURNAL OF APPLIED MECHANICS, TRANS. ASME, vol. 79, pp. 426–430.

[2] Advisory Engineer, Research Laboratories, Westinghouse Electric Corp., East Pittsburgh, Pa.

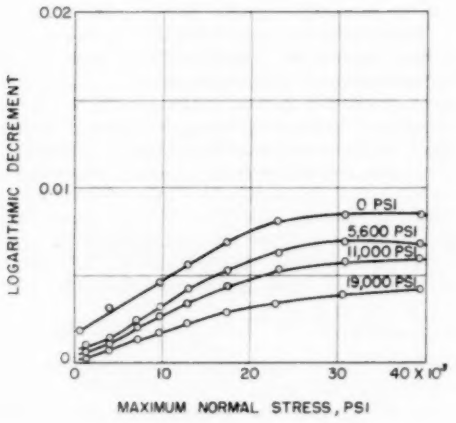

Fig. 1

9800 psi, since such a high value would not be "very small compared to the critical stress at which the ferromagnetic domain walls become fixed." When static stress equaled or exceeded 5600 psi, all of our data for AISI-403 specimens softer than 335 Bhn showed a damping decrease.

A Study of the Propagation of Flexural Waves in Elastic Beams[1]

E. Volterra.[2] The authors should be congratulated for their excellent paper on the propagation of flexural waves in elastic bars. In fact, this paper, based on experiments, answers the important question of the validity of the classical Timoshenko theory of flexural-wave propagation for the case of very short pulses. In recent years many authors have presented approximate engineering theories for studying the problem of wave propagation in elastic rods. In a recent OOR Report,[3] E. C. Zachmanoglou and the writer discussed a more accurate engineering approach of the method of internal constraints. The application of this method to the case of flexural wave propagation in a long elastic rod will be outlined briefly in the following:

Consider a bar of rectangular cross section, Fig. 1 of this discussion; let the components of the displacement in the directions of the x, y, z-axes (the x-axis coinciding with the axis of the bar, the y and z-axes coinciding with the principal axes of inertia of the cross section of the bar) be

$$\left.\begin{aligned} u(x, y, z; t) &= y\lambda_x(x; t) \\ v(x, y, z; t) &= \nu_y(x; t) + \frac{1}{2} y^2 f_1(x; t) \\ w(x, y, z; t) &= yz f_2(x; t) \end{aligned}\right\} \quad \ldots\ldots [1]$$

In order to comply with the condition that the normal components of stress σ_y and σ_z be zero throughout the bar, the following condition must be satisfied

$$f_1(x; t) = f_2(x; t) = -\sigma \frac{\partial \lambda_x(x; t)}{\partial x} \quad \ldots\ldots [2]$$

σ being Poisson's ratio of the material of the bar. By neglecting the terms y^2 and yz in the expressions for the components of strain and particle velocities in comparison with linear terms, the following expression for the potential energy is obtained

$$U = -\int_0^L \left\{ \frac{E}{2} I_z \left[1 + \frac{K\sigma^2}{2(1+\sigma)} \frac{I_y}{I_z} \right] \left(\frac{\partial \lambda_x}{\partial x} \right)^2 + K \frac{G}{2} A \left[(\lambda_x)^2 + \left(\frac{\partial \nu_y}{\partial x} \right)^2 + 2\lambda_x \frac{\partial \nu_y}{\partial x} \right] \right\} dx \quad \ldots\ldots [3]$$

The kinetic energy is expressed by

$$T = \frac{\rho}{2} \int_0^L \left[I_z \left(\frac{\partial \lambda_x}{\partial t} \right)^2 + A \left(\frac{\partial \nu_y}{\partial t} \right)^2 \right] dx \quad \ldots\ldots [4]$$

In Equations [3] and [4] ρ represents the density, E Young's modulus, G the shear modulus of the material of the bar, A the cross-sectional area, I_y and I_z the moments of inertia of the cross section of the bar with respect to the y and z-axes, respectively. The factor K is introduced to take into account the nonuniform distribution of shear over the cross section of the bar and has the same significance as the well-known Timoshenko shear coefficient. The application of Hamilton's principle gives the following equations of motion

$$\left.\begin{aligned} EI_z(1+\epsilon) \frac{\partial^2 \lambda_x}{\partial x^2} - KGA\lambda_x - KGA \frac{\partial \nu_y}{\partial x} &= \rho I_z \frac{\partial^2 \lambda_x}{\partial t^2} \\ KG \frac{\partial^2 \nu_y}{\partial x^2} + KG \frac{\partial \lambda_x}{\partial x} &= \rho \frac{\partial^2 \nu_y}{\partial t^2} \end{aligned}\right\} \quad \ldots [5]$$

where

$$\epsilon = \frac{K\sigma^2}{2(1+\sigma)} \frac{I_y}{I_z}$$

and boundary conditions at $x = 0;\ x = L$

$$\left.\begin{aligned} \left[\frac{\partial \lambda_x}{\partial x} \right] \delta\lambda_x &= 0 \\ \left[\frac{\partial \nu_y}{\partial x} + \lambda_x \right] \delta\nu_y &= 0 \end{aligned}\right\} \quad \ldots\ldots [6]$$

It should be pointed out that the validity of Equations [5] and [6] is not limited to a bar of rectangular cross section. In fact, the only parameter related to the shape of the cross section is the ratio of the moments of inertia I_y/I_z so that Equations [5] and [6] can be used for a bar of any cross section so long as the assumptions on which the foregoing derivation is based are considered satisfactory.

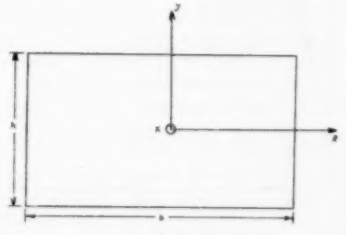

Fig. 1

[1] By E. A. Ripperger and H. N. Abramson, published in the September, 1957, issue of the JOURNAL OF APPLIED MECHANICS, TRANS. ASME, vol. 79, pp. 431–434.

[2] Professor of Engineering Mechanics, The University of Texas, Austin, Texas.

[3] "A Second Approximation of the Method of Internal Constraints as Applied to Dynamic Problems," by E. C. Zachmanoglou and E. Volterra, Office of Ordnance Research, Technical Report No. 6, May 20, 1957. Contract No. DA-30-155-ORD-709. Project No. 454.13 Rensselaer Polytechnic Institute, Troy, N. Y.

In the case of plane stress, the ratio I_y/I_z tends toward zero and Equations [5] reduce to the classical Timoshenko equations[4]

$$\left.\begin{aligned} EI_z \frac{\partial^2 \lambda_z}{\partial x^2} - KGA\lambda_z - KGA \frac{\partial \nu_y}{\partial x} &= \rho I_z \frac{\partial^2 \lambda_z}{\partial t^2} \\ KG \frac{\partial^2 \nu_y}{\partial x^2} + KG \frac{\partial \lambda_z}{\partial x} &= \rho \frac{\partial^2 \nu_y}{\partial t^2} \end{aligned}\right\} \quad \ldots [7]$$

The boundary conditions here are the same as in Equations [6].

To study the dispersion of waves in a rod of infinite length let

$$\left.\begin{aligned} \lambda_z &= Ae^{i\gamma(x-ct)} \\ \nu_y &= Be^{i\gamma(x-ct)} \end{aligned}\right\} \quad \ldots [8]$$

where A and B are two constants, $\gamma = 2\pi/L$ the wave number, and L the wave length. Substituting Equations [8] into Equations [5], a system of two homogeneous algebraic equations in A and B is obtained. Expressing the determinant of the coefficients of A and B equal to zero, the following dispersion equation is obtained

$$\left(\frac{r_z}{L}\right)^2 = \frac{1}{4\pi^2} \frac{K}{2(1+\sigma)} \frac{\left(\frac{c}{c_0}\right)^2}{\left[\left(\frac{c}{c_0}\right)^2 - \frac{K}{2(1+\sigma)}\right]\left[\left(\frac{c}{c_0}\right)^2 - (1+\epsilon)\right]} \quad \ldots [9]$$

By letting $\epsilon \to 0$ in Equation [9] one gets

$$\left(\frac{r_z}{L}\right)^2 = \frac{1}{4\pi^2} \frac{K}{2(1+\sigma)} \frac{\left(\frac{c}{c_0}\right)^2}{\left[\left(\frac{c}{c_0}\right)^2 - \frac{K}{2(1+\sigma)}\right]\left[\left(\frac{c}{c_0}\right)^2 - 1\right]} \quad \ldots [10]$$

which is the dispersion equation in the classical Timoshenko theory. The quantity ϵ is the correction of the Timoshenko theory, taking into account the effects of the dimensions of the bar in the z-direction. In Equations [9] and [10], c is the phase velocity, $c_0 = (E/\rho)^{1/2}$ the bar velocity, and r_z is the radius of gyration of the cross section of the bar with respect to the z-axis.

In Fig. 2 dispersion curves for flexural waves in cylindrical bars are presented. The values of the exact Pochhammer theory[5] as given by Davies[6] are compared with the results obtained from the elementary theory,[7] from the Rayleigh theory, from the Timoshenko theory, and from the method of internal constraints in the cases of first and second approximation. The value for the Timoshenko shear coefficient was assumed $K = 0.9$.

[4] "On the Correction for Shear of the Differential Equations for Transverse Vibrations of Prismatic Bars," by S. P. Timoshenko, *Philosophical Magazine*, vol. 41, 6th series, 1921, pp. 742–746.

Authors' Closure

The authors wish to thank Professor Volterra for his kind comment concerning their paper.

The analysis presented by Professor Volterra is very interesting and offers the possibility of further refinement in the solution of the problem of bending wave propagation. However, such refinement appears to be unnecessary at present in view of the excellent agreement which has been obtained between theoretical calculations based on the Timoshenko equation and experimental results. The degree to which wave form can be predicted is demonstrated by the work of Dengler, Goland, and Wickersham, and Plass and Steyer,[8] while the paper under discussion shows that propagational velocities are also accurately predicted. These comparisons are completely summarized also in another paper.[9]

[5] "Über die Fortpflanzungsgeshwindigkeiten Kleiner Schwingungen in einem unbegrenzten isotropes Kreiszylinder," by L. Pochhammer *Journal für die reine und angewandte Mathematik*, Crelle, vol. 81 1876, p. 324.

[6] "A Critical Study of the Hopkinson Pressure Bar," by R. M. Davies, *Philosophical Transactions of the Royal Society of London*, series A, vol. 240, 1948, pp. 375–457.

[7] "Stress Waves in Solids," by H. Kolsky, Clarendon Press, Oxford, 1953.

[8] Plass, H. J. and Steyer, C. C., "Studies of Longitudinal and Bending Waves in Long Elastic Rods," Univ. Texas, DRL Rept. DRL-376, CM-860 (1956).

[9] Abramson, H. N., Plass, H. J., and Ripperger, E. A., "Stress Wave Propagation in Rods and Beams," in *Advances in Applied Mechanics*, Academic Press, Inc., vol. 5, 1958, pp. 111–194.

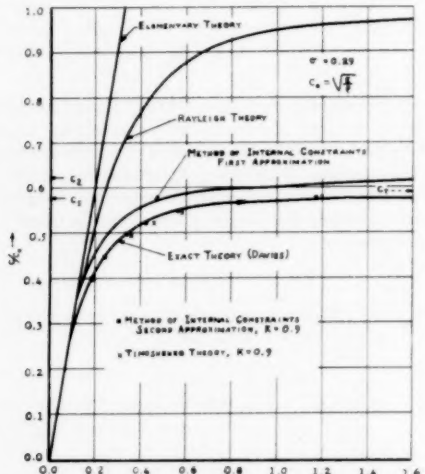

Fig. 2 Phase velocity of flexural waves in cylindrical bars

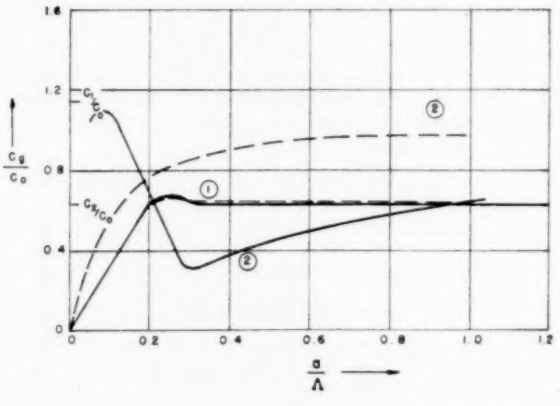

Fig. 3

The authors would like to take this opportunity to correct an error which appeared in Fig. 2.[10] In this figure the second mode of the Timoshenko beam (dashed curve No. 2) is shown as having a maximum and a minimum whereas it should in fact be monotone. A corrected curve is shown here in Fig. 3. This correction displaces the corresponding curve in Fig. 3 of the paper slightly to the right at the higher values of T_p/T_a, but does not affect any of the conclusions reached regarding arrival times.

Two-Dimensional, Steady, Cavity Flow About Slender Bodies in Channels of Finite Breadth[1]

W. G. Cornell.[2] The authors are to be congratulated on an excellent and interesting paper. In addition to the considered case of a body in cavitating flow and symmetrically placed in a plane-walled channel, the results are applicable to the case of zero incidence flow over an unstaggered cascade of bodies of arbitrary shape, assuming a perfect fluid, so that solid walls may be replaced by streamlines, and conversely. The cascade of bodies is a useful model in the analysis of the flow in bluff-body flameholders of afterburners for aircraft gas-turbine engines and of ramjet combustors. The writer's investigation[3] of the Helmholtz-Kirchhoff flow in a vee-gutter cascade corresponds to the authors' case of a wedge with a cavity of infinite length, subject to the effect of the authors' linearizing assumptions.

R. Timman.[4] Mr. J. A. Geurst, of our Institute for Applied Mathematics, has given the following derivation of Formulas [17] and [24] of the paper. The discussed problem can be formulated as a mixed boundary-value problem for the analytic function $w = u - iv$ in an infinite strip with cut corresponding to the body plus cavity. (In contrast with the paper, U_∞ is used as a nondimensionalizing factor throughout, because only a first-order approximation is considered.) With the aid of the conformal transformation

$$z = \xi + i\eta = e^{\frac{2\pi}{h}z} = e^{\frac{2\pi}{h}(x+iy)}$$

the original problem in the z-plane is transformed into a mixed boundary-value problem for the entire z-plane with cut along the real axis. Because of the symmetry of the problem with respect to the x-axis, the problem can be reduced to a mixed boundary-value problem for the upper or lower half-plane, which can be solved by the method of Muskhelishvili.[5] The solution is

$$w = -\frac{1}{2\pi i}\left(\frac{z-1}{z-e^{\frac{2\pi l}{h}}}\right)^{1/2}\int_{e^{-\frac{2\pi l}{h}}}^{1}\frac{2i\,\frac{dy_0}{dx}\left(\frac{\xi-e^{\frac{2\pi l}{h}}}{\xi-1}\right)^{1/2}}{\xi-\zeta}\,d\xi+\frac{\sigma}{2}+C\left(\frac{z-1}{z-e^{\frac{2\pi l}{h}}}\right)^{1/2}$$

where C is an arbitrary real constant. (In this expression the juncture condition has been taken into account.) C and the relation between σ and l are determined from the conditions, that $w = 0$ at $z = 0$ and $z = \infty$. The closure condition is automatically satisfied.

As a result, the following connection between σ and l is found.

$$\frac{\sigma h}{2}\sinh\frac{\pi l}{2h} = \int_{-e}^{0}\frac{dY_0}{dx}\left(\frac{\sinh\pi\left(\frac{x-l}{h}\right)}{\sinh\frac{\pi x}{h}}\right)^{1/2}dx$$

which is equivalent to Equation [17] of the paper in first-order approximation.

The drag D is calculated as follows

$$D = \int_{-e}^{0}(p_+ - p_-)\frac{dY_0}{dx}\,dx = -\sigma U_\infty^2\int_{\text{body}}u\frac{dY_0}{dx}\,dx$$

$$= -\rho U_\infty^2\int_{\text{body}}uv\,dx = -\rho U_\infty^2\int_{\text{body+cavity}}uv\,dx$$

$$= \text{Im}\,\frac{\rho U_\infty^2}{2}\int_{\text{body+cavity}}w^2dz = \pi\rho U_\infty^2\,\text{Re}\,\{\text{res}\,w^2\text{ at }z=l\}$$

This yields

$$C_D = \frac{D}{\frac{1}{2}\rho U_\infty^2} = h\,\frac{e^{\frac{2\pi l}{h}}-1}{e^{\frac{2\pi l}{h}}}\left[\frac{4}{h^2}I^2+\frac{\sigma^2}{4}+\frac{2\sigma}{h}I\right]$$

where

$$I = \int_{-e}^{0}\frac{dY_0}{dx}\frac{e^{\frac{2\pi x}{h}}}{\left[\left(e^{\frac{2\pi x}{h}}-1\right)\left(e^{\frac{2\pi x}{h}}-e^{\frac{2\pi l}{h}}\right)\right]^{1/2}}dx$$

In combination with Equation [17], this expression for C_D can be proved to be equivalent to Equation [24] in a first-order approximation. *Remark:* The integral in the third term in the right-hand side of Equation [24] should be squared. For further details the reader is referred to report 11.[6]

T. Y. Wu.[7] The authors are to be complimented on their elegant work in extending Tulin's linear theory to include the wall effect on the two-dimensional cavity flow about slender bodies. The results of this paper are not only of academic interest but also of value in practical application, for they immediately provide means of estimating the wall effect which can be used to correct the water-tunnel test data of some typical cavity flows where the linear theory is valid. As this paper is presented in an orderly manner, the writer has but a few remarks to make.

First, he would like to present an alternative derivation of Equation [23] and the last equation of the paper. If the limiting case where the cavity length tends to infinity as $\sigma \to \sigma_\infty$ (for $h/c<\infty$) is assumed to exist (the existence was actually shown in the paper), then the asymptotic cavity width and the correspond-

[10] This error was pointed out by Dr. E. E. Zajac and John A. Lewis of Bell Telephone Laboratories in a private communication. Dr. Zajac has also very kindly made the necessary calculations, using a digital computer, to provide us with the corrected curve.

[1] By Hirsh Cohen and Robert Gilbert, published in the June, 1957, issue of the JOURNAL OF APPLIED MECHANICS, TRANS. ASME, vol. 79, pp. 170–176.

[2] Engineering Consultant—Aerodynamics, Systems Analysis Section, General Electric Company, Cincinnati, Ohio. Mem. ASME.

[3] "The Flow in a Vee-Gutter Cascade," by W. G. Cornell, TRANS. ASME, vol. 78, 1956, pp. 573–580.

[4] Delft, Holland.

[5] "Singular Integral Equations," by N. I. Muskhelishvili, Groningen, 1953.

[6] Report 11, Instituut voor Toegepaste Wiskunde, Technische Hogeschool, Delft, Holland.

[7] California Institute of Technology, Pasadena, Calif.

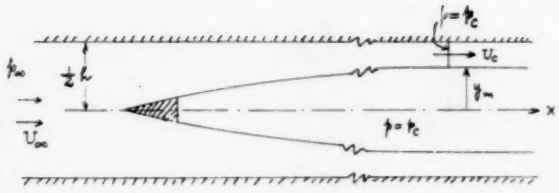

Fig. 1

ing limit of the drag can be obtained directly from a simple consideration of continuity and conservation of momentum. Suppose that, as $\sigma \to \sigma_\infty$

$$\lim_{x \to \infty} Y_s(x) = \text{const} = y_m$$

say, the flow then approaches a uniform state as $x \to \infty$, Fig. 1 of this discussion. The continuity equation of such flow is

$$U_\infty h = U_s(h - 2y_m) \quad \ldots\ldots\ldots\ldots\ldots [1]$$

Applying the definition of σ, as given in this paper, to the Bernoulli equation

$$\tfrac{1}{2}\rho U_\infty^2 + p_\infty = \tfrac{1}{2}\rho U_s^2 + p_s \quad \ldots\ldots\ldots\ldots [2]$$

one obtains

$$U_s = U_\infty(1 + \sigma_\infty)^{1/2} \quad \ldots\ldots\ldots\ldots\ldots [3]$$

Hence, from Equations [1] and [3] of this discussion, one has

$$\frac{y_m}{h} = \tfrac{1}{2}[1 - (1 + \sigma_\infty)^{-1/2}] \quad \ldots\ldots\ldots\ldots [4]$$

which reduces, for small values of σ_∞, to Equation [23] of the paper.

The law of conservation of momentum, when applied to this case, asserts

$$D = \rho U_\infty^2 h - \rho U_s^2(h - 2y_m) + (p_\infty - p_s)h$$

Again using Equations [1] and [3], one has

$$\frac{D}{\frac{1}{2}\rho U_\infty^2} = h\left[2\left(1 - \frac{U_s}{U_\infty}\right) + \sigma_\infty\right]$$

$$= h\left[\sigma_\infty + 2[1 - (1 + \sigma_\infty)^{1/2}]\right] \ldots\ldots [5]$$

which reduces to the last two equations of the paper for small σ_∞. Thus the foregoing simple derivation serves as an alternative to check some of the results of the theory. Furthermore, Equations [4] and [5] herewith, not being subject to linearization, apply to nonlinear theory as well. Along this line of argument, one would have a good reason to wonder whether Equation [26] of the paper could be simplified further. However, for a given geometry of the body and given $\alpha = c/h$, the value of σ_∞, for which these relations are valid, must be calculated from some theory, such as given by Equation [27] of this linear theory.

In order to avoid the flow configuration in which the cavity starts at some point on the solid body upstream of its base, it seems necessary to impose some condition or conditions on $Y_0(x)$, for otherwise one would again have to face the indeterminacy of the separation point of the cavity boundary from the solid body. Without imposing such condition, while still assuming that the cavity starts from the base, it would not be difficult to construct a $Y_0(x)$ such that the right-hand side of Equation [17] or of Equation [18] becomes negative.

Authors' Closure

The authors are very happy to have the comments and additions provided in the discussion. It is certainly gratifying to find, as Mr. Cornell suggests, that there is application of this work to flow behind flameholders. It is probably of interest to mention that one of the authors and his associates, in continuing these studies, have discussed cascades of foils with finite cavities, a generalization of Mr. Cornell's work.[8]

Professors Timman and Wu both discuss methods of obtaining the results of the paper in a far more elegant manner than has been used. The use of the function-theoretic methods by Dr. Geurst and Professor Timman is indeed illuminating. The authors believe that a study of such methods applied to the mixed boundary-value problems of free streamline and cavity theory will yield information on the nature of the linearization and its relation to the "nonexistence" theorems for finite cavity flow in classical free-streamline theory. Application of the Muskhelishvili notions to unsymmetric cavity flows have proved quite successful.[9]

Since the preparation and presentation of the paper under discussion, Professor Wu has made extremely valuable contributions to the understanding and the working out of the linearized theory of finite cavity flows.[10] It should be emphasized, however, that at some time during the analysis of these flows the relation between the cavitation number and the cavity length must be given explicitly. Only then can one go on to compute other characteristics of the flows.

Statistical Appraisal of Prot Method for Determination of Fatigue Endurance Limit[1]

E. L. Dunn.[2] The paper is well written and, it is believed, states the case against using the Prot method quite well.

The writer's comments on the positive side of this question are as follows:

1 We were interested in using the Prot fatigue method in our work, primarily for reduction in the amount of time required for a test rather than in the number of tests required. We realize the number of tests required probably would be increased, but we feel that, timewise, it would be advantageous to use this method.

2 We feel that the linear relationships of rate of increase should be expressed as rate of increase to the nth power rather than rate of increase to the $\frac{1}{2}$ power. This follows the Appendix of the report fairly well. The questions raised about the assumptions are very good, but we feel that proper determination of the correct nth would possibly agree with a more fundamental theory than the rigorous mathematical derivation set forward in the paper.

[8] "The Stall Performance of Cascades," by W. G. Cornell, Proceedings of Second U. S. National Congress of Applied Mechanics, ASME, 1955, pp. 705–713.

[9] "Wall Effects in Cavitating Hydrofoil Flow," by Hirsh Cohen, C. D. Sutherland, and Yih-O Tu, *Journal of Ship Research*, vol. 1, Nov., 1957, pp. 31–39.

[10] "A Simple Method for Calculating the Drag in the Linear Theory of Cavity Flows," by T. Y. Wu, Report No. 85-5, Engr. Div., Cal. Inst. Tech., August, 1957. Also "A Note on the Linear and Nonlinear Theories for Fully Cavitated Hydrofoils," by T. Y. Wu, Report No. 21-22, Hydro. Lab. Cal. Inst. of Tech., August, 1956.

[1] By W. A. Hijab, published in the June, 1957, issue of the JOURNAL OF APPLIED MECHANICS, TRANS. ASME, vol. 79, pp. 214–218.

[2] Design Criteria, General Electric Company, Cincinnati, Ohio.

3 We feel that precision from short tests, where there is less likelihood of extraneous variation entering in, would compensate partially for the precision lost from extrapolation. From the results the writer has seen from Prot tests, this is substantiated. The narrowness of scatter as compared to the scatter of the standard fatigue tests is rather marked.

Author's Closure

The author thanks the writer for his comments and briefly answers them as follows:

1 It is agreed that there is some saving in the time required for the testing of a given number of specimens. However, in the author's opinion, this is not of a magnitude that will appreciably affect the strength of the case against using the Prot method.

2 In giving a rigorous mathematical derivation for the $^1/_2$ power, the author intended to bring out explicitly a possible set of assumptions of the Prot method and not to defend the $^1/_2$ power formula against other possible fractional powers. However, the paper points out *additional* difficulties arising from the use of an n^{th} power determinable from the experimental data.

3 Whether the shortness of the duration of a test contributes to its precision is a matter that is open to question and concerning which the author is not able to form a final opinion.

Uniformly Loaded Circular Plates With a Central Hole and Both Edges Supported[1]

H. A. Eagle[2] and A. L. Ross.[3] The types of problems analyzed by the author have been of interest to the engineers in the writers' department for quite some time, and the author is to be congratulated on having presented the results of this analysis in a very clear and concise manner. The writers apologize for not having published the results of their similar analyses[4,5] at an earlier date. It was intended that the results of the latest report,[5] which covers all four combinations of fixed and simply supported inner and outer edges, would be presented in the near future.

In both the reports mentioned, the analysis was carried out by the method of superposition, and the results of the analysis evaluated by IBM calculation and presented in a form similar to that shown in Fig. 1 of this discussion, in which the b/a ratio was used as the design parameter. The entire stress and deflection distribution, rather than maximum values only, was presented in order to allow these solutions to be used in further superposition as required. The maximum stresses taken from the figures similar to those shown in Fig. 1 were summarized in figures similar to that shown as Fig. 2 here.

An examination of the figures indicates an interesting characteristic of the stress distribution that appears to have been over-

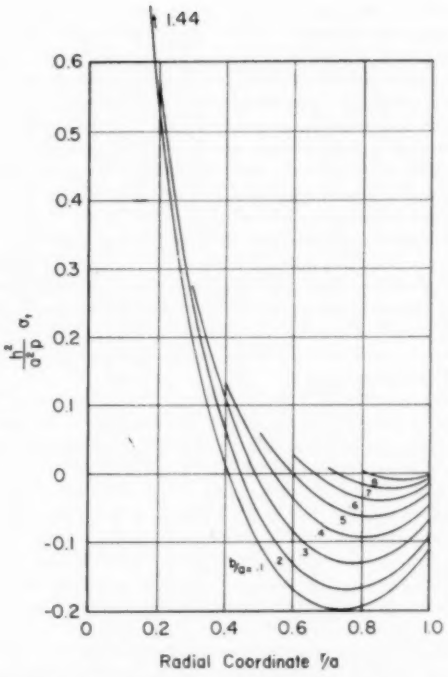

Fig. 1 Tangential stress, simply supported edges

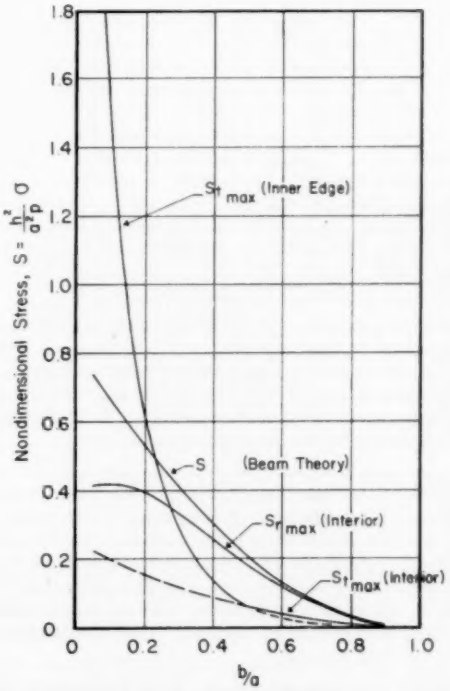

Fig. 2 Summary of maximum stresses, simply supported edges

[1] By J. C. Georgian, published in the June, 1957, issue of the JOURNAL OF APPLIED MECHANICS, TRANS. ASME, vol. 79, pp. 306–310.

[2] Technical Engineer, Aircraft Nuclear Propulsion Department, General Electric Company, Cincinnati, Ohio.

[3] Principal Engineer, Aircraft Nuclear Propulsion Department, General Electric Company, Cincinnati, Ohio.

[4] "Internal Memorandum on Stresses in a Circular Plate With a Central Hole When Loaded by Uniform Pressure and Simply Supported at Both Inner and Outer Edges," by A. L. Ross and G. McClure, February, 1955.

[5] "Design Charts for Analysis of Circular Plates With Central Holes," by H. A. Eagle, ANPD-G.E. Report No. XDC 57-4-97, April, 1957.

looked by the author. In Fig. 6 of the paper the author presents the tangential moments at the inner and outer edges of the plates, possibly implying these to be the maximum tangential moments present. From Fig. 2 of this discussion it can be seen that the maximum tangential stresses occur at the inner edge of the plate only when the b/a ratio is less than 0.49, while for b/a greater than 0.49 the maximum tangential stress occurs within the interior of the plate. This type of behavior occurs when the inner edge is simply supported and the outer edge either simply supported or clamped.

Although the author states, "Poisson's ratio = 0.3 was used in all the computations for the curves. . .," the unwary reader might be misled in using Figs. 3, 6, 7 by the fact that the ordinate of the curves (stress parameter) contains Poisson's ratio μ. These curves are correct only if $\mu = 0.3$ and would have been clarified if the curves had been plotted so that their ordinates did not contain Poisson's ratio μ.

In doing problems of the sort analyzed by the author, designers are sorely tempted to approximate the problem by analyzing beams, of unit width and length of $(a - b)$, supported at the ends. In the case of a plate element the moment of inertia should be used as $h^3/12(1 - \nu^2)$ rather than $h^3/12$, commonly used in the analysis of beams. In Fig. 2 the results of the beam analysis for the nondimensional radial stress (the beam analogy does not yield the tangential stress) are compared with the exact solution. Fig. 2 shows that the maximum stresses can be found, for this problem (and other similar ones), to a satisfactory degree of accuracy for values of $b/a > 0.5$.

The writers' analyses[4,5] have been extended to include the effect of torsional and lateral spring supports at the inner and outer edges and were recently programmed for solution by IBM Type 704 digital computer.

Author's Closure

The author is gratified that Mr. Eagle and Mr. Ross have independently analyzed and checked the results of his analysis of uniformly loaded circular plates by an entirely different procedure, i.e., by the method of superposition and the use of IBM calculating equipment. The author did not have IBM equipment available and calculated his results with a ten-place electric desk calculator. The discussers' Fig. 1 and Fig. 2 are welcome additions to the paper. The author too must apologize for not having published the results of his analysis at an earlier date. He first became interested in this problem while associated with the Nordberg Manufacturing Company, and analyzed the uniformly loaded circular plate with a central hole, edges simply supported, in Nordberg's Technical Memorandum.[6]

While the author has also determined the equations for all four combinations of fixed and simply supported inner and outer edges, he has to date not completed computations for the remaining two cases due to the press of time. It would be of value and interest to have these two cases presented in the Design Data and Methods section of this Journal in the near future.

The discussers are entirely correct in pointing out that the author overlooked the maximum in the tangential moment distribution for Case II plate. Solving equations [16] and [17], in the paper, simultaneously for the tangential bending moment and then differentiating with respect to r/a and setting the result equal to zero, we find the maximum tangential moment is at r/a values as shown in the discussers' Fig. 1. Substituting these r/a values in the foregoing equation yields the maximum tangential bending moment.

[6] "Design of Compressor Valves," by J. C. Georgian, Nordberg Technical Memorandum 620, July, 1949.

$$\left[\frac{M_t}{\frac{qa^2}{8}(1-\mu)}\right]_{\max} = \frac{3+\mu}{2(1-\mu)} + \left[\frac{1-3\mu}{1-\mu}\right]\frac{K_4}{4} - \frac{1+3\mu}{1-\mu} \times \left(\frac{r}{a}\right)^2 - \left[\frac{1+\mu}{1-\mu}\right]\frac{K_4}{2}\log_e\frac{r}{a} + \frac{1}{2}\frac{\frac{5+\mu}{1+\mu}\left[1-\left(\frac{b}{a}\right)^4\right] + \frac{3+\mu}{1+\mu}K_4\left[1-\left(\frac{b}{a}\right)^2\right]}{4\log_e\frac{b}{a}} \quad [1]$$

Where r/a is the maximum value found by the foregoing differentiation, Equation [1] is plotted in Fig. 3 of this closure.

While the curves presented in the paper are correct only if $\mu = 0.3$ as mentioned by the discussers, it can be seen, however, that for Case I the equations are independent of Poisson's ratio, and hence our Figs. 2 and 3 may be used for any values of Poisson's ratio. Though the curves for Case II depend on Poisson's

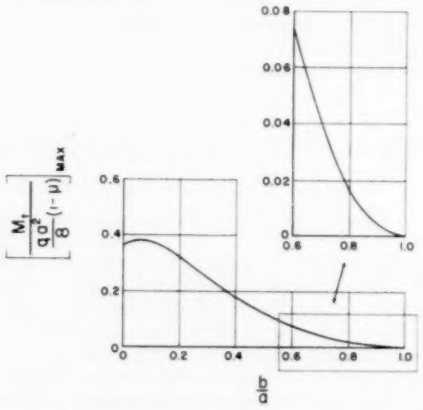

Fig. 3 Maximum tangential bending moment for Case II plate

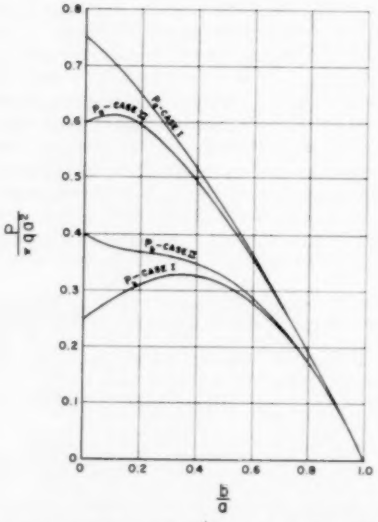

Fig. 4 Reactions at edges for Case I and Case II plate

ratio, it may be noted that Poisson's ratio enters the equations in terms of ratios and sums and differences of these ratios, and hence the curves will be insensitive to variations in Poisson's ratio. Therefore, curves for Case II may be also used for the usual values of Poisson's ratio, say between 0.25 and 0.35.

The question of the distribution of the load on the supports has been raised. If we let P_b and P_a equal the total load on the inner and outer edges, respectively, these loads are presented in Fig. 4 of this closure for Cases I and II of the paper.

Effect of Adverse Pressure Gradients on Turbulent Boundary Layers in Axisymmetric Conduits[1]

H. R. Fraser.[2] Since a completely rational approach to the solution of boundary-layer problems has not yet presented itself, it would appear that mean flow analyses using semiempirical methods are destined to be used in solving practical engineering problems for some time. The paper is certainly a noteworthy attempt to extend a rather new two-dimensional method to axisymmetric flows under an adverse pressure gradient. In addition, it presents some new and quite complete data in an area where reliable data are scanty, to say the least.

During the past year and a half the writer has been working at the axisymmetric boundary layer in a diffuser under the direction of Dr. Robertson at the University of Illinois. His analytic efforts indicate a reasonably plausible, if not rigorous justification, for the use of a flow parameter of the form

$$\frac{\delta}{D}\frac{U_{10}}{U_1}R$$

This is the same parameter used by the authors except for division by the constant R_0, the radius at entrance to the diffuser. Furthermore, it was found that this parameter varied parabolically with x, the distance from the geometrical start of the diffuser. It also was found that δ/θ was not a unique function of D, as suggested by the authors of this paper, but was instead a function of θ/R and D. In fact, for any given value of D, δ/θ appears to be a linear function of θ/R. This ratio of θ/R is really a manifestation of the difference in geometry between the two and three-dimensional flows. For small values of the ratio θ/R (i.e., $R \to \infty$) the value of δ/θ approaches the two-dimensional value as would be expected. With these changes and additions to the results of the authors, the writer has been able to propose a step-by-step method for predicting the rate of growth (and the separation) of the boundary layer in an axisymmetric diffuser. The calculations require that the pressure distribution in the diffuser and the entrance values of U_1, θ, δ, and D be known. The results have been verified with additional data taken on a 10-deg (total angle) conical diffuser.

E. M. Uram.[3] It is always gratifying to see extension and confirmation of one's experiments, and the writer is grateful for the opportunity to discuss this paper.

It is surprising that the shape of the velocity profiles as indicated by either H or D responds almost immediately to the change in local geometry; i.e., pressure gradient. From the generally accepted concept that the condition of the larger outer region of the layer is a consequence of the integrated upstream-flow characteristics (the history concept of Prandtl), one might expect a longer reponse time than the flow exhibits. Although it is heartening to see that taking into account geometry changes produces correlations of the outer flow parameter (for constant initial conditions at least), Figs. 5 and 6 of the paper, along with other information (Ross)[4] infer that there exists no single law governing the outer boundary-layer region when represented by Equation [2] for either the two-dimensional or axisymmetric case.

In view of the generally observed behavior of boundary layers, one intuitively suspects the existence of a universality in the outer region analogous to that found in the inner region. Motivated by the work of Rotta[5] and Coles,[6] the following point of view is proposed. Boundary-layer profiles in general are of the form

$$u/u^* = F\left(\frac{yu^*}{\nu}, y/\delta\right)$$

Accepting the universality of the law of the wall we may write

$$\frac{u}{u^*} = A + B\log\frac{yu^*}{\nu} + \varphi(y/\delta)$$

or, expressed as a deficiency law

$$\frac{u_1 - u}{u^*} = \varphi(1) - \varphi(y/\delta) - B\log y/\delta$$

In either case, $\varphi(y/\delta)$ is the deviation from the logarithmic behavior of the profile. For flat-plate boundary layers Coles[6] has found that $\varphi(1)$ is a constant. This is also obviously true for other "equilibrium" boundary layers (reference 5 of present paper). It is also evident that for any equilibrium boundary layer a single $\varphi(y/\delta)$ must be unique to all the velocity profiles. Under these circumstances one cannot escape the thought that if $\varphi(y/\delta)$ is able to exhibit a universality for certain families of boundary layers, there might exist a much wider universality for $\varphi(y/\delta)$ encompassing all boundary layers. Study of the deviation curves for numerous two-dimensional boundary layers under various conditions show $\varphi(y/\delta)$ to be a unique family of curves approximately described by the function

$$\varphi(y/\delta) = ay/\delta + be^{100c(y/\delta - 1)^2}$$

for $0.1 \lesssim y/\delta \leqslant 1.0$. As yet, correlations leading to the determination of a, b, and c for an arbitrary case have not been found.

Just recently, Coles,[7] quite independently taking the same point of view, has shown that, when subjected to certain normalizing conditions, the deviation curves (called the "law of the wake" by Coles) do indeed form a near universal family. His data include separated flows that have reattached.

The velocity profiles of phases I, II, and III (those for phases IV and V not being immediately available) of the axisymmetric flow described in the present paper exhibit the behavior described.

Authors' Closure

Since one of the authors has been closely connected with the

[1] By J. M. Robertson and J. W. Holl, published in the June, 1957, issue of the JOURNAL OF APPLIED MECHANICS, TRANS. ASME, vol. 79, pp. 191–196.

[2] Colonel, U. S. Army, and Professor of Mechanics, U. S. Military Academy, West Point, N. Y.

[3] Research Engineer, United Aircraft Corporation, East Hartford, Conn.

[4] "A Study of Incompressible Turbulent Boundary Layer," by Donald Ross, PhD thesis, Harvard University, June, 1953.

[5] "On the Theory of the Turbulent Boundary Layer," by J. Rotta, Mitteilungen aus dem Max Planck Institut für Stromungsforschung, Gottingen, No. 1, 1950. Translated as NACA TM 1344.

[6] "The Problem of the Turbulent Boundary Layer," by D. Coles, *Zeitschrift für angewandte Mathematik und Physik*, vol. 5, 1954, pp. 181–203.

[7] "The Law of the Wake in the Turbulent Boundary Layer," by D. Coles, *Journal of Fluid Mechanics*, vol. 1, part 2, July, 1956, pp. 191–226.

researches of Dr. Fraser, his comments are not unexpected. It is encouraging that he has been able to extend the Ross analysis method for plane two-dimensional flows to the axisymmetric case, since this was the unachieved objective of the authors' work. The indication that $\frac{\delta}{D}\frac{U_{10}}{U_1}R$ rather than $\frac{\delta}{D}\frac{U_{10}}{U_1}\frac{R}{R_0}$ is the proper outer-flow parameter emphasizes the need for experiments in diffusers of other initial radii. Work in this direction is currently under way in England at the Mechanical Engineering Research Laboratory, as evidenced by a recent paper of Winternitz and Ramsay.[8] It is hoped that this research will soon yield us the needed experimental information.

Mr. Uram's remarks concerning the surprisingly short response time of the outer flow to changes in geometry, or pressure gradient, are concurred in. One wonders which of the two changes, geometry or pressure, induces the change. The outer-flow parameter indicates that both R and U_1 enter in, but it does not tell us why. It is hoped that Mr. Uram will continue his study of velocity profiles and attempt to tie down the factors a, b, and c. The results indicated are very suggestive but require a more detailed study for adequate comment. There may be some question as to what kind of progress we are making if we substitute a relation involving three empirically determined factors (a, b, and c) for one involving one empirically determined factor (D). Equation [2] does have some rational basis and works reasonably well. It may be that for other reasons such as consideration of the "equilibrium" boundary layers [cf. reference (5) of paper], other relations for the velocity are desirable.

The authors wish to thank Messrs. Fraser and Uram for their interesting discussions.

Improvement of Holzer Table Based on a Suggestion of Rayleigh's[1]

N. O. Myklestad.[2] In this paper a method is developed by which the time involved in finding a natural frequency of torsional vibration by means of the Holzer table can be reduced; but in general this requires judgment on the part of the computer.

Since the task of obtaining a natural torsional mode is an easy one in either case, the method of this paper becomes advantageous only when such calculations must be performed frequently. When this is the case, the Holzer calculations are now nearly always programmed for a high-speed digital computing machine so that any just comparison should be made on this basis.

The usual way of finding natural modes then is to program the calculations so that the machine automatically calculates the shaking torque for regular intervals of ω^2, and every time a reversal of sign is obtained it backtracks and proceeds with smaller intervals of ω^2 until a reversal is again obtained; and this is kept up until the shaking torque is smaller than some predetermined value.

In the method of this paper the value of ω_{Ray}^2 could be calculated every time there was a reversal of sign of the shaking torque; but whether or not this is an advantage probably can be determined only by experience.

E. W. Gaylord.[3] Convergence of successive trials would be assured for any mode if, as in Stodola's method for higher modes,[4] the value of the maximum deflection β, found in the Holzer table, were purified of all the lower modes including the mode for $\omega = 0$.

In terms of the orthogonal eigenfunctions X the β column of the Holzer table may be expressed as

$$V = \Sigma a_j X_j \quad [1]$$

The Rayleigh method reduces to

$$\omega_{\text{Ray}}^2 = \frac{\Sigma \omega_j^2 a_j^2 X_j \cdot BX_j}{\Sigma a_j^2 X_j \cdot BX_j} \quad [2]$$

or with X normalized to

$$\omega_{\text{Ray}}^2 = \frac{\Sigma \omega_j^2 a_j^2}{\Sigma a_j^2} \quad [3]$$

In terms of ω_k

$$\omega_{\text{Ray}}^2 = \omega_k^2 \frac{\Sigma \frac{\omega_j^2}{\omega_k^2} a_j^2}{\Sigma a_j^2} \quad [4]$$

Since $\frac{\omega_j}{\omega_k} > 1$ for all $j > k$

the Rayleigh method gives an upper bound for ω_k^2 if all a_j for $j < k$ are made zero in Equation [4].

This may be readily done if all the lower mode eigenfunctions are known, as would be the case when one successively used the Holzer method to evaluate the preceding modes of vibration.

The purified shape will be $V' = V - \Sigma a_j X_j$; $j < k$

or

$$\beta' = \beta - \Sigma a_j \beta_j \quad [5]$$

To evaluate the a_s form the orthogonal product

$$\sum_{n \neq j} a_j X_j \cdot BX_n = V \cdot BX_n - a_n X_n B \cdot X_n = 0 \quad [6]$$

giving

$$a_n = \frac{V \cdot BX_n}{X_n \cdot BX_n} \quad [7]$$

For the zeroth mode $X_0 = 1, 1, 1 \ldots 1$

$$a_0 = \frac{\Sigma I \beta}{\Sigma I} \quad [8]$$

For purification of the first mode it would be

$$a_1 = \frac{\Sigma I \beta \beta_1}{\Sigma I \beta_1^2}$$

where β_1 is found from the Holzer table for the correct value of ω_1.

Purification of the zeroth and first mode from column 3 of den Hartog's example gave purified values of β as follows

β	$a_0\beta_0$	$a_1\beta_1$	$\beta' = \beta - a_0\beta_0 - a_1\beta_1$
1.00	−2.20	2.42	0.78
−26.78	−2.20	−0.64	−23.94
19.16	−2.20	−0.65	22.01
63.97	−2.20	−0.66	66.83
104.99	−2.20	−0.67	107.86
139.78	−2.20	−0.67	142.65
166.29	−2.20	−0.67	169.16
182.95	−2.20	−0.68	185.83

[8] "Effects of Inlet Boundary Layer on Pressure Recovery, Energy Conversion and Losses in Conical Diffusers," by F.A.L. Winternitz and W. J. Ramsay, *Journal of the Royal Aeronautical Society*, vol. 61, Feb. 1957, pp. 116–124.

[1] By S. H. Crandall and W. G. Strang, published in the June, 1957, issue of the JOURNAL OF APPLIED MECHANICS, TRANS. ASME, vol. 79, pp. 228–230.

[2] Senior Engineer, Specialist, Phoenix Division, AiResearch Manufacturing Company, Phoenix, Ariz. Mem. ASME.

[3] Assistant Professor of Mechanical Engineering, Carnegie Institute of Technology, Pittsburgh, Pa.

[4] "Mechanical Vibrations," by J. P. den Hartog, McGraw-Hill Book Company, Inc., New York, N. Y., fourth edition, 1956, p. 162.

The purified values of β resulted in $\omega_{Ray}^2 = 18{,}332$ which, being an upper bound, is somewhat higher than the value $\omega^2 = 18{,}000$, given by den Hartog.

The authors are fortunate in getting so close to the correct frequency. This is due to the corrections for the first and zeroth mode having a small net effect on the value of β.

F. Söchting.[8] In this valuable paper the authors derive a method to shorten the necessary time to calculate the torsional natural frequencies by using a suggestion of Rayleigh. The authors are inclined to assume that the suggestion of Rayleigh was never used before. The writer thinks it may be of interest to say that this method was used two times before, to calculate the torsional frequency based on Holzer's equation[6] and to determine the frequencies of strings and beams.[7]

Authors' Closure

The suggestion is made by Professor Gaylord that the approximate mode shape obtained in a Holzer table should be orthogonalized with respect to all known modes before computing Rayleigh's quotient. This would insure that ω_{Ray} would be an upper bound for the next natural frequency. Furthermore, the quadratic convergence in the neighborhood of the true mode would still be retained. The authors are in complete agreement so far as the mathematical principles involved are concerned. They are somewhat in doubt, however, as to the practical wisdom of such a procedure. One of the advantages cited[8] for the method as given in the paper was that orthogonalization was *not* required. Systematic orthogonalization of every trial mode entails considerable computational labor, more than the Holzer table itself, for the higher modes.

Dr. Myklestad suggests that a procedure requiring judgment from the computer may not be desirable when a program for a high-speed digital computer is being set up. There is considerable validity in this viewpoint. Unsubtle, overly repetitious procedures are often the easiest to program and trouble shoot, and give the most reliable operation. Furthermore, the present high computing speeds in comparison with set-up and input-output times means that often there is no appreciable penalty involved in using nonoptimum procedures. As for the particular procedure described in the paper, it must be admitted that it was originally designed for hand computation using a desk calculator. The sign pattern criteria which can be evaluated almost instantaneously by eye would require fairly elaborate programming to insure foolproof operation in a digital computer.

It is a pleasure to acknowledge the prior claim of F. Söchting to the process we have called "the Rayleigh-Kohn-Holzer Method." After the publication of our paper we were informed[9] that this method was known in the German literature[10] as Söchting's method. There is a remark in Klotter's paper[10] that the convergence of Söchting's method may be doubtful. An attempt to

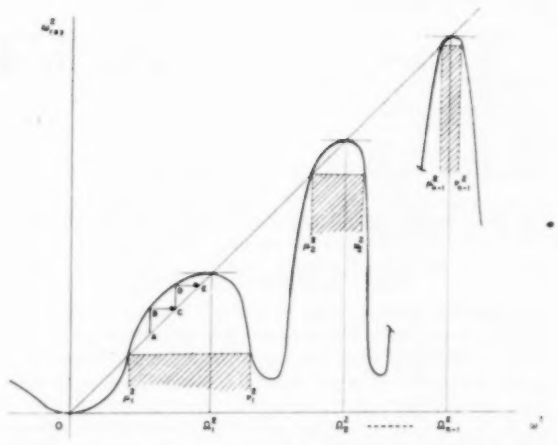

Fig. 1 The curve gives the Rayleigh quotient corresponding to the trial value of ω^2 used in the Holzer table

clarify this was made by Schaefer.[11] In view of this, perhaps the principal contribution of our paper has been in supplying a more complete picture of the convergence of the method. The main features are illustrated[12] in Fig. 1 of this discussion. The Rayleigh quotients of the Söchting process are plotted against the trial values of ω^2. The properties of the curve shown may be deduced from Equation [9] of the paper. The curve crosses the 45-deg line at the Ω_j^2 and the μ_j^2. Strict iteration with the Söchting process can be represented by paths such as ABCDE. The quadratic convergence in the neighborhood of an Ω_j^2 is indicated by the horizontal tangent at $\omega^2 = \Omega_j^2$. The μ_j^2 are unstable foci for the process. The curve crosses the 45-deg line with a slope of 2 at each μ_j^2. At the eigenvalue Ω_p^2 the second derivative of the curve is

$$\frac{d^2\omega_{Ray}^2}{d(\omega^2)^2} = 2\sum_j{}' \frac{h_j^2/h_p^2}{\Omega_j^2 - \Omega_p^2}$$

in the notation of the paper, which implies that the general tendency is for the curve to be concave down at the large eigenvalues and concave up at the small eigenvalues. This general tendency may be ineffective, however, in regions where two or more eigenvalues are very close together. We have been unable to obtain a criterion for predicting the sign of the local curvature. In our experience with practical torsional systems, the curve has been concave down at all natural frequencies except the trivial zero frequency. When the curve is concave down in the neighborhood of the eigenvalue Ω_j^2, as shown in Fig. 1, the Söchting process is sure to converge to Ω_j^2 when $\mu_j^2 < \omega^2 < \nu_j^2$, where ν_j^2 is the smallest value of $\omega^2 > \Omega_j^2$ for which $\omega_{Ray}^2(\nu_j^2) = \mu_j^2$. However, only when $\mu_j^2 < \omega^2 < \Omega_j^2$ is it readily apparent from the sign pattern in the Holzer table that the trial ω^2 is actually in this range. This was the basis for our recommendation to compute ω_{Ray}^2 only when it is indicated that ω_{Ray}^2 will be higher than the trial ω^2.

[8] Curtiss-Wright Corporation, Wright Aeronautical Division, Wood-Ridge, N. J.

[6] "Zur Berechnung der Eigenschwingungszahlen von Wellenleitungen," by F. Söchting, ATZ, vol. 40, 1937, p. 259; also Berechnungen Mechanischer Schwingungen, 1951, p. 234.

[7] "Zur Berechnung von Eigenschwingungszahlen," by F. Söchting, Federhofer-Girkmann Festschrift, 952, p. 365.

[8] "Iterative Procedures Related to Relaxation Methods for Eigenvalue Problems," by S. H. Crandall, Proceedings of the Royal Society of London, series A, vol. 207, 1951, pp. 416–423.

[9] Private communication from Professor H. Schaefer, Technischen Hochschule, Braunschweig.

[10] See, for example, "Analyze der verscheidenen Verfahren zur Berechnung der Torsionseigenschwingungen von Maschinenwellen," by K. Klotter, *Ingenieur Archiv*, vol. 17, 1949, pp. 1–60.

[11] "Das Restmoment der Torsions schwingungen von Maschinenwellen," by H. Schaefer, Abh. Braunschweigischen Wiss. Ges., 6, 1954, pp. 243–254.

[12] This figure was used in the oral presentation of the paper, Nov. 27, 1956. Similar figures appear in the reference of footnote (11) and in the reference of footnote (8). The fallacy in Schaefer's work results from the assumption that the curve is monotonically increasing between $\omega^2 = 0$ and $\omega^2 = \Omega_{n-1}^2$.

Book Reviews

Turbomachinery

Stromungsmachinen. By Carl Pfleiderer. Second Edition, Springer-Verlag, Berlin, Göttingen, Heidelberg, 1957. Cloth. $9^{9}/_{16} \times 6^{1}/_{2}$ in., xiv and 421 pp., illus. DM 36.

Reviewed by Max J. Schilhansl[1]

ACCORDING to the preface to the first edition, "It cannot be the goal of education to train specialists who are interested only in one subject and who do not care about the associations with related subjects." The very general title (which might be translated "Turbomachinery") promises a very broad view of all types of turbomachines and of all problems associated with theory and design (or analysis and synthesis) of turbomachines. The reader looks in vain for the discussion of propellers, windmills, torque converters, and fluid couplings; he also looks in vain for chapters on stress analysis and on vibrations of the essential component parts. It is a very significant experience of the reviewer that sufficient knowledge of flow problems, elastic and vibration problems, and of strength of materials is needed for the design of a machine satisfactory in every respect.

It is evident that a book containing information on all these subjects—of course, so far as it is pertinent to turbomachines—will be quite voluminous. Thus it is natural to omit some subjects; each step in this direction, however, is a step toward specialization and away from the goal so strongly advocated by Pfleiderer. Five pages, out of 421, are devoted to stress analysis, partly containing merely references. Nothing is said about vibrations.

The hydrodynamical problem of blade design is treated in much detail. The treatment follows very closely the pattern of the first edition (1952); the reviewer again quotes the preface of the second edition: "Changes are made only in so far as to account for the scientific progress." It will be admitted that a book does not need to contain new problems, concepts, and solutions before they are confirmed and accepted by a large group of scientists and engineers, in contrast to a journal in which the latest ideas are put up for discussion.

Sometimes it is difficult to find out which theory or method has been generally accepted as an addition to or as a substitute for an existing one. Pfleiderer's approach to the design of an axial-flow water turbine, for instance (Sect. 45–47), is no longer up to date, as it is known that the magnitude of the angle of attack at which the drag-lift ratio is a minimum depends on solidity and stagger angle and as the mutual interference should not be brushed aside "because it would lead to a negative angular exaggeration."

The treatment of the radial and mixed flow turbomachines is based on the one-dimensional theory in which the blade spacing is assumed to be infinitisimal. The effect of the finite spacing in pumps is accounted for by a head ratio which is termed "power diminution"; empirical values of the head ratio are given (p. 38), holding apparently for a very limited range of blade shapes (backwards curved) and of radii ratios (entrance radius $\propto {}^{1}/_{2}$ exit radius). As Pfleiderer used the one-dimensional approach, he faced the difficulty of explaining the flow at "off design" points of operation. He still applies the concept of a "shock." The Fig. 85 on page 179 supposed to illustrate the shock is very wrong; there can never be a discontinuity of the velocity along a stagnation streamline.

The recommendation to arrange ineffective portions at the leading edge as well as at the trailing edge of the blade is also quite obsolete; a blade portion is "ineffective" if it does not create a change of the moment of momentum or, in other words, if the static pressures at both sides are the same. Pfleiderer admits that there is a trend to abandon this idea, at least so far as the entrance portion of a pump blade is concerned.

[1] Professor of Engineering, Brown University, Providence, R. I.

Mathematics

Praktische Mathematik für Ingenieure und Physiker. Second, revised edition. By R. Zurmühl. Springer-Verlag, Berlin, Göttingen, Heidelberg, 1957. Cloth, 6 × 9 in., xii and 524 pp., illus. DM 28.50.

Reviewed by J. Kestin[2]

THIS is a very useful volume whose purpose, admirably achieved, it is to describe comprehensively the methods available for the numerical solutions of mathematical problems which occur in engineering applications. In every case, in addition to the theoretical background, practical methods of actually handling the process of solution are given. But, the book is not a mere collection of formulas and algorithms. It combines clarity and rigor with a real understanding of the details of involved computations.

The book deals with the solution of equations in general, linear equations and matrices, interpolation and integration, statistical treatment of experimental data, the approximate representation of arbitrary functions, initial-value problems, boundary-value and eigenvalue problems.

Rheology

Rheology Theory and Applications, Volume I. Edited by Frederick R. Eirich. Academic Press Inc., Publishers, New York, N. Y. 1956. Cloth, $9^{1}/_{4} \times 6^{1}/_{4}$ in., xiv and 761 pp., illus. $20.

Reviewed by A. M. Freudenthal[3]

THE very wide and not too well defined scope of rheology is one of the main difficulties necessarily facing the editor of a reference work in this field; the other is the heterogeneity of the educational background of those interested in or actually working in rheology. This heterogeneity is reflected not only in an extremely wide divergence of interests but also, and this appears to be more critical, in a wide difference of approach and of methodology. To produce a reference work that would be of equal interest and use to workers in organic chemistry concerned with rheological methods but with little or no mathematical background on the one hand, and to applied mathematicians or theoretical physicists interested in continuum mechanics on the other, appears therefore to be a formidable task. It must be said that, in spite of the imposing array of contributors which he has assembled, the editor has not quite succeeded in this attempt to provide a well-balanced reference

[2] Professor of Engineering, Brown University, Providence, R. I.

[3] Professor of Civil Engineering, Columbia University, New York, N. Y.

work. Nevertheless, the book is an important contribution containing, as it does, a series of mostly well-written up-to-date reviews of various fields of, or at least related to, rheology.

The editor has decided to delimit the scope of rheology in the broadest possible sense, including a substantial part of what would normally be considered solid-state or crystal physics and physical metallurgy. As this field is covered by numerous excellent reference works and reviews, it does not seem that a useful purpose is served by devoting to it more than 20 per cent of a reference work on rheology, necessarily to be paid for by a certain lack of depth in the treatment of some of the fundamental aspects of rheology proper that cannot easily be found anywhere else, such as a consistent continuum-mechanical treatment of complex rheological bodies as a theoretical basis for the chapters in subsequent volumes on the rheology of specific materials.

Of the chapters dealing with this aspect, which are undoubtedly the chapters of principal interest to workers in applied mechanics and which take up roughly one quarter of the book, Chapters 3 and 16 dealing with plastic and viscoplastic flow, Chapter 10 dealing with finite elastic strains, and Chapter 13 on the statistical theory of irreversible processes are examples of conciseness and lucidity; one might perhaps have wished for a more extensive treatment of plastic deformation in the continuum. The masterly presentation of the basis of dislocation theory in Chapter 6 makes the fact, that the subject matter itself can hardly be considered as part of "rheology," seem irrelevant.

Chapter headings and authors are as follows: 1 Introduction (Eirich). 2 Phenomenological Macrorheology (Reiner). 3 Finite Plastic Deformation (Prager). 4 Stress-Strain Relations in the Plastic Range of Metals (Drucker). 5 Mechanical Properties and Imperfections in Crystals (Dienes). 6 Dislocations in Crystal Lattices (J. M. and W. G. Burgers). 7 Mechanical Properties of Metals (Fleeman and Dienes). 8 Some Rheological Properties Under High Pressure (Dow). 9 Theory of Viscosity (Bondi). 10 Large Elastic Deformations (Rivlin). 11 Dynamics of Viscoelastic Behavior (Alfrey). 12 Viscosity Relationship for Polymers in Bulk and in Concentrated Solution (Fox, Gratch, and Loshaek). 13 Statistical Mechanical Theory of Irreversible Processes in Solutions of Macromolecules (Riseman and Kirkwood). 14 Viscosity of Colloidal Suspensions and Macromolecular Solutions (Frisch and Simha). 15 Streaming and Stress Birefringence (Peterlin). 16 Non-Newtonian Flow of Liquids and Solids (Oldroyd). 17 Acoustics and the Liquid State (Lindsay).

Failure of Structural Units

Technical Report, New Series, vol. 3, May 1957, British Engine Boiler & Electrical Insurance Co., Ltd., Manchester, England. Paper, 9½ × 7 in., illus., 222 pp. 15s0d.

Reviewed by John M. Lessells[4]

THE above report, constituting Volume 3 of the New Series of Technical Reports of the British Engine Boiler and Electrical Insurance Co., Ltd., like all previous issues, by the discussion of failures of structural elements, provides useful information for design engineers. Attention was drawn to Volume 1 and Volume 2 of this Series in the JOURNAL OF APPLIED MECHANICS for September, 1953, and June, 1955.

The report discusses various failures of boilers and emphasizes the importance of guarding against the possibility of caustic embrittlement and corrosion fatigue. The conditions which might promote such modes of failure are discussed in some detail. No new evidence is presented to refute the generally accepted belief that corrosion-fatigue cracks are always transcrystalline and caustic-embrittlement cracks intercrystalline.

The importance of high set-up stresses in bolted assemblies subjected to cyclic loading, previously demonstrated by aircraft-engine developments, is clearly indicated. An excellent discussion is made of stress-concentration effects, and many interesting photographs are included in the report of failed parts where stress-concentration factors have been disregarded.

The possible deleterious effect of chromium plating on the fatigue properties of crankshafts is demonstrated by a particular failure. It should be pointed out that it is now well established that the reclaiming of worn crankshafts by chromium plating is quite sound, but regard must be given for adequate control during the plating operation to minimize the reduction in fatigue strength. There is considerable evidence that shot-peening of the surface prior to plating eliminates any harmful effects due to the plating.

A very interesting section discusses in some detail the steps taken by the Insurance Company's Research Department in the examination of service failures.

[4] President, Lessells and Associates, Inc., Boston, Mass. Hon. Mem. ASME.

Nuclear Engineering

Nuclear Engineering. Edited by Charles F. Bonilla. McGraw-Hill Publishing Co., Inc., New York, N. Y., 1957. Cloth, 6¼ × 9¼ in., xi and 850 pp. $12.50.

Reviewed by Samuel Glasstone[5]

"NUCLEAR ENGINEERING" represents a co-operative effort to which thirteen scientists and engineers, with extensive experience in their respective fields, have contributed chapters on various aspects of nuclear physics and nuclear engineering. The general scope of the book can best be indicated by giving the titles of the chapters, the names of their authors, and the numbers of pages. They are as follows: Introduction, by J. R. Dunning and R. W. Houston (16 pp.); Nuclear Particles (34 pp.), and Nuclear Physics (49 pp.), by W. W. Havens, Jr.; Particle Detection, by C-S. Wu (33 pp.); Basic Concepts of Radiation Protection, by G. Failla (37 pp.); Elementary Reactor Physics, by R. W. Houston (79 pp.); Shielding of Power Reactors, by D. C. Peaslee (35 pp.); The Flow of Liquids (86 pp.), and Heat Removal (159 pp.), by C. F. Bonilla; Metallurgy of Uranium and Uranium Alloys, by G. L. Kehl (19 pp.); Thermal-Stress Analysis and Mechanical Design, by A. M. Freudenthal (72 pp.); Instrumentation and Control, by J. W. Hoopes, Jr. (65 pp.); Power Generation, by T. Baumeister (56 pp.); Nuclear-Reactor Types, by J. W. Landis (52 pp.); and Legal Aspects of Nuclear Power, by J. G. Palfrey (20 pp.). In addition, there are 17 appendixes, with a total length of 40 pages, covering topics ranging from physical properties of materials to a summary of the principal characteristics of existing reactors.

It is inevitable that, in a book of this kind compiled from the contributions of a number of individuals, there should be differences both in depth and breadth of the treatment of various topics. Thus the two chapters by Bonilla and the one by Freudenthal, comprising nearly 320 pages, make a complete textbook on what might be called the strictly engineering aspects of nuclear reactor design. On the other hand, the treatment of reactor materials, design of fuel elements, and radiation damage is somewhat more superficial. Such matters as the processing of spent fuel elements, the recovery of fissionable materials, and the concentration and disposal of radioactive fission products are

[5] Consultant, Atomic Energy Commission and Los Alamos Scientific Laboratory, Los Alamos, N. Mex.

not discussed at all. While admitting their importance to a reactor system as an integrated operation, the preface explains their omission on the grounds that these "problems are usually not handled by the same team that designs the reactor and associated equipment." This is, of course, true, but might not the same be said about the legal aspects of nuclear power? However, in all fairness to the editor, who has done an excellent job, it should be pointed out that the book already contains a vast amount of material, and it was a physical necessity to draw the line somewhere.

In describing the purpose of the book, Professor Bonilla states that " 'Nuclear Engineering' is intended to be suitable as a text for a graduate course for engineers and physics majors. . .It is also intended to serve as a single compact reference volume to those employed in this field on the detailed work or supervisory levels." So far as the textbook aspects of the work are concerned, experience alone can tell. This book is not like a pill that can be swallowed with a little water. It is, in large part, solid meat which must be well chewed before it can be digested. However, as a work of reference, there is no question as to the merits of the book. It contains much information, not easily available elsewhere, which both students and practitioners of nuclear reactor engineering will find invaluable.

Centrifugal Pumps

Centrifugal and Axial Flow Pumps. Second Edition. By A. J. Stepanoff. John Wiley and Sons, Inc., New York, N. Y. 1957. Cloth, 9¼ × 6¼ in., vii and 462 pp., illus. $12.

Reviewed by Max J. Schilhansl[6]

A PUMP designer certainly will appreciate the fact that Stepanoff's book on centrifugal and axial-flow pumps contains some information on the subject of the application of pumps which is widely scattered over the technical literature as, for instance, on water hammer, on centrifugal-jet pump systems, on problems of operation, and so on. He will also appreciate that a list of references is added at the end of each chapter. He might, however, disagree with some chapters on theory and the design of blading.

In the field of axial-flow pumps, the design can be based on the requirement that the head should be constant across the radius or that it should vary with the radius; it can be based also on the requirement that the flow through the impeller should have the pattern of a free vortex or that of a forced vortex. Stepanoff very ardently advocates the forced-vortex pattern. The truth is that both patterns constitute a sound foundation for the blade design; it is just necessary to adhere to the initial selection in every respect, such as radial equilibrium or matching of the diffuser vanes. The author's arguments *pro* and *contra* forced vortex or free vortex, respectively, are not convincing; he even admits that "the use of a free vortex theoretical treatment of operation of axial-flow water turbines is the only one possible." This is also not true; some very successful Kaplan turbine designs which came to the knowledge of the reviewer clearly deviate from the free vortex pattern in order to have the required cavitation characteristics.

The statement on page 151, "It is only natural that after sufficient experience was accumulated on efficient axial flow fans, blowers and pumps, the interest in the airfoil theory subsided," is apt to discourage future efforts to improve the theory of cascades of airfoil sections. It certainly is not justified at a time at which the literature on this subject consists of more than one hundred papers, at which it is possible to explain the different performances of cascades for accelerated and for decelerated flow by means of calculating the boundary layer growth, and at which blade sections have been developed for prescribed pressure distributions at given cascade configurations with respect to required cavitation characteristics.

The argument on page 156, "The airfoil theory method of axial impeller design is invariably associated with a free vortex energy distribution along the radius," is also incorrect because the fundamental relation between lift and head still holds when the head is varied along the radius.

The treatment of the centrifugal and mixed-flow pumps follows very closely the one-dimensional Eulerian theory after the ratio of the theoretical head of an impeller with a finite blade spacing to the theoretical head of an impeller with infinitely closely spaced blades having the same mean surface has been introduced. Stepanoff calls this ratio "vane efficiency" and admits in a footnote (p. 37) that it is not really an "efficiency." No numerical values of this vane efficiency are given in Stepanoff's book. In a one-dimensional treatment, the misconception of "shock losses" is inevitable.

These are the essential problems in theory and in the design of pumps in which the reviewer disagrees with the author. It is beyond the scope of this review to discuss all points of disagreement; some additional ones, however, will be briefly enumerated.

"Liquid flow in a pump tends to avoid shock by acquiring prerotation at the impeller" (p. 164). On p. 38, there is a somewhat contradictory statement: "Note that the rotation of the liquid in the impeller approach is not derived from the impeller." How can it be derived from "a tendency of the liquid to follow a path of least resistance on its way to enter an impeller channel" (p. 10)? As long as this minimum principle is not expressed in mathematical terms, the reader will find it difficult to obtain the path of least resistance by any sort of variational calculus.

"Variation of pressure across a channel can occur in such a manner that some streamlines will increase their pressure without decreasing their velocities, thus increasing their total energy, or the constant in Bernoulli's equation" (p. 9). On p. 18, the quantity v^2/R is a centripetal acceleration, not a centrifugal force. "No diffusion (deceleration?) can take place in a curved channel, stationary or moving" (p. 32). The moment diagram (Fig. 7.8, p. 118) must have a change in slope at the support B.

"Piston area (diameter?) of de Haller's pressure measuring device was 1.5 mm" (p. 232).

"Time is necessary for the shaft to develop its maximum deflection which may not be available when the critical speed is passed rapidly" (p. 327). How rapidly it must be passed can be taken from the calculation of C. Biezeno and R. Grammel, "Technische Dynamik," first edition, p. 778. "It has been found that axial forces tend to increase the critical speed" (pp. 347, 348). This is true only if the axial force produces tensile stresses in the shaft; if it produces compression stresses, the critical speed is lowered.

[6] Professor of Engineering, Brown University, Providence, R. I.

Information for Authors

• Manuscripts should be submitted in final form to the Technical Editors. Each manuscript must be accompanied by a statement that it has not been published elsewhere nor has it been submitted for publication elsewhere. A paper which would occupy more than five pages of the Journal may be returned to the author for abridgment.

• The author should state his business connection, the title of his position, and his mailing address. A short abstract (50 to 100 words) should be included on the first page immediately preceding the introductory paragraph of the paper.

• Three copies of the manuscript are required. One of these must be a carefully prepared printer's copy, typed in double spacing, on one side of the page only, with wide margins, on 8½ by 11-in. opaque white paper. Mimeographed manuscripts, if prepared with exceptionally clear copy, can be accepted provided they are completely edited.

• All mathematical expressions should be written by hand in ink or set out by typewriter in a way which would define each symbol unambiguously. Care should be taken to distinguish between capital and lower-case letters, between (0) and the letter (*O*), between the numeral (1) and the letter (*l*), etc. A list of symbols carefully marked, if it has not been included in the body of the paper, should accompany the manuscript on a separate page.

• Before preparing a manuscript the author should study printed articles in the Journal, with special attention to the form and style of mathematical expressions, tables, footnotes, references, and abstract. Care should be taken to arrange all tables and mathematical expressions in such a way that they will fit into a single column when set in type. Equations that might extend beyond the width of one column (fractions that should not be broken or long expressions enclosed in parentheses) should be rephrased to go on two or more lines within column width. Fractional powers are preferred to root signs and should always be used in more elaborate formulas.

• A normal paper should not exceed five pages in the Journal. It is about 6000 words or twenty to twenty-five double-spaced typewritten pages inclusive of drawings. A Brief Note should not exceed 750 words or about one column in the Journal inclusive of drawings.

• Originals and two copies of figures must accompany the manuscript. Line drawings should not be larger than 9 in. × 11 inches, and should be planned for reduction to column width. Lettering should be large enough to be clearly legible when the illustration is reduced. The originals of line drawings must be in India ink on white or pale blue vellum paper or tracing cloth. Photographs of equipment or test specimens must be glossy prints and should be used sparingly. Captions for figures should be typed, double-spaced and included on the last page of the manuscript. The figure number and author's name should be written in the margin or on the back of each illustration.

• Titles of papers should be brief. If an adequate description of the subject requires a title which, along with the author's name, would occupy more than one line on the cover of the Journal, a separate descriptive title should be submitted.

• Authors can obtain copies of the ASME Manual, Bulletin 4, "An ASME Paper," from the Technical Editors and are urged to do so before finishing their papers in final form.

• Papers published in the Journal of Applied Mechanics must be presented at a Meeting, either in person or by title. Submitting of papers is in the hands of the Secretary of the Applied Mechanics Division. Authors should indicate their preference in this respect to the Technical Editors when submitting a paper.

• An author is entitled to 25 printed copies of his paper free of charge (in the case of two authors, 15 each; three or more authors, 10 each). Larger quantities of preprints or reprints can be ordered from Editorial Department, The American Society of Mechanical Engineers, 29 West 39th Street, New York 18, N. Y. Quotations will be sent on request.

S. Kaplan and S. Kaplan, Technical Editors

Please address all correspondence to: Technical Editors,
Journal of Applied Mechanics, ASME
Division of Engineering
Brown University
Providence 12, R. I.

THIRD U. S. NATIONAL CONGRESS OF APPLIED MECHANICS

Brown University, June 11–14, 1958

Final Announcement